# Effects of Nucleoside and PNA Conjugation on Self-assembly of Diphenylalanine (Phe-Phe)

**A thesis**

**submitted in partial fulfillment of the requirements of the degree of**

**Doctor of Philosophy**

**By**

**Om Shanker Tiwari**

**ID: 20142013**

**Research Supervisor: Prof. Krishna N. Ganesh**

**IISER PUNE**

*This Thesis is Dedicated to…..*

*My Family*

## CERTIFICATE

I certify that the work incorporated in the thesis entitled **"Effects of Nucleoside and PNA Conjugation on Self-assembly of Diphenylalanine (Phe-Phe)"** submitted by **Mr. Om Shanker Tiwari** was carried out by the candidate, under my supervision. The work presented here or any part of it has not been included in any other thesis submitted previously for the award of any degree or diploma from any other university or institution.

**Date**: 10th January 2020

**Prof. Krishna N. Ganesh**
**(Research Supervisor)**
FNA, FASc, FTWAS
Director. IISER Tirupati
Co-Editor: ACS Omega
Honorary Faculty, IISER Pune

# DECLARATION

I declare that, this written submission represents my ideas in my own words and where others' ideas have been included, I have adequately cited and referenced the original sources. I also declare that I have adhered to all principles of academic honesty and integrity and have not misrepresented or fabricated or falsified any idea / data / fact / source in my submission. I understand that violation of the above will be cause for disciplinary action by the Institute and can also evoke penal action from the sources which have thus not been properly cited or from whom proper permission has not been taken when needed.

**Date:** 10<sup>th</sup> January 2020, IISER Pune

**Om Shanker Tiwari**
**ID: 20142013**

# Acknowledgements

# Table of Contents

## Chapter 2: Self-assembly of Diphenylalanine (Phe-Phe)-Nucleoside Conjugates

## Chapter 3: Effect of Stereochemistry and Hydrophobicity on Self-assembly of Phe-Phe-Nucleoside Conjugates

## Chapter 4: Self-assembly of Diphenylalanine (Phe-Phe)-Peptide Nucleic Acid (PNA) Conjugates

## Chapter 5: Self-assembly and Biophysical Studies of Diphenylalanine (Phe-Phe)-Peptide Nucleic Acid-$G_n$ Conjugates (Tetraplex Studies)

## Chapter 6: Capacitance and Redox Properties of Self-assembled Phe-Phe with PNA and Ferrocene Conjugates

# Abbreviations

| | |
|---|---|
| A | Adenine |
| Abs. | Absorbance |
| Ac | Acetyl |
| ACN | Acetonitrile |
| $Ac_2O$ | Acetic anhydride |
| *aeg* | Aminoethylglycine |
| ADNS | Aromatic dipeptide nanostructures |
| AIE | Aggregation induced emission |
| Ala | Alanine |
| AFM | Atomic force microscopy |
| anhyd | Anhydrous |
| aq | Aqueous |
| Arg | Arginine |
| Bn | Benzyl |
| BPI | Benzoperylene monoimide |
| $(Boc)_2O$ | Boc anhydride |
| C | Cytosine |
| ºC | Degree Celsius |
| CA | Contact angle |
| CAC | Critical aggregation concentration |
| Calcd | Calculated |
| Cbz | Benzyloxycarbonyl |
| CD | Circular Dichroism |
| cDNA | Complementary DNA |
| CDPNT | Cationic dipeptide nanotube |
| CF | Carboxyfluorescein |
| CHCA | α-cyano-4-hydroxycinnamic acid |
| CT | Charge transfer |
| CuAAC | Copper(I)-catalyzed azide-alkyne cycloaddition |
| CV | Cyclic Voltammetry |
| Cys | Cysteine |
| DCC | Dicyclohexylcarbodiimide |
| DCM | Dichloromethane |
| $\Delta Tm$ | Difference in melting temperature |
| DHB | 2,5-dihydroxybenzoic acid |
| DHBtOH | 3-Hydroxy-1,2,3-benzotriazin-4(3H)-one |
| DIPEA | *N,N*- Diisopropylethylamine |
| DLS | Dynamic light scattering |
| DMAP | *N,N*-Dimethyl-4-aminopyridine |
| DMF | *N,N*-Dimethylformamide |
| DMSO | *N,N*-Dimethyl sulfoxide |
| DX | DNA double crossover |
| DNA | Deoxyribonucleic acid |
| eq | Equivalents |
| ESI-MS | Electro Spray Ionization Mass Spectrometry |
| EBA | Ethylbromo acetate |

| | |
|---|---|
| ECM | Extracellular matrix |
| EDX | Energy dispersive X-ray |
| EDC.HCl | 1-Ethyl-3-(3-dimethylaminopropyl)carbodiimide.HCl |
| ex | Example |
| Et | Ethyl |
| EtOAc | Ethyl acetate |
| FESEM | Field Emission Scanning Electron Microscopy |
| FET | Field effect transistor |
| Fmoc | 9-Fluorenylmethoxycaronyl |
| FTIR | Fourier transform Infra-Red |
| g | gram |
| G | Guanine |
| Gly | Glycine |
| hrs | Hours |
| HBTU | [2-(1H-Benzotriazole-1 -yl)-1,1,3,3-tetramethyl-uronium hexafluorophosphate] |
| HFIP | 1,1,1,3,3,3-hexafluoro-2-propanol |
| HOBt | N- Hydroxybenzotriazole |
| HPLC | High Performance Liquid Chromatography |
| HRMS | High Resolution Mass Spectrometry |
| HRTEM | High Resolution Transmission Electron Microscope |
| Hz | Hertz |
| *in situ* | In the reaction mixture |
| *in vivo* | Within the living organism |
| *in vitro* | Outside the living organism |
| $^i$Bu | Isobutyl |
| IBCF | Isobutyl chloroformate |
| IR | Infra-Red |
| Ile | Isoleucine |
| kV | Kilovolt |
| Leu | Leucine |
| Lys | Lysine |
| M | Molar |
| MHz | Megahertz |
| MALDI-TOF | Matrix Assisted Laser Desorption Ionization-Time of Flight |
| MBHA | p-methoxybenzhydrylamine |
| MeCN | Acetonitrile |
| MeOH | Methanol |
| mg | milligram |
| mL | millilitre |
| MPTTF | Monopyrrolotetrathiafulvalene |
| min | minutes |
| μ | Micron |
| μL | Microliter |

| | |
|---|---|
| μM | Micromolar |
| mmol | millimoles |
| mM | millimolar |
| m.p. | Melting point |
| MS | Mass spectrometry |
| MsCl | Methanesulfonylchloride |
| mV | millivolt |
| Mw | Molecular weight |
| N | Normal |
| NaN$_3$ | Sodium azide |
| nm | Nanometer |
| NMM | N-methylmorpholine |
| NMR | Nuclear Magnetic Resonance |
| NPs | Nucleopeptides |
| Obsvd | Observed |
| OEG | Oligoethylene glycol |
| ONs | Oligonucleotides |
| Pd-C | Palladium on carbon |
| PDA | Photodiode array detector |
| PDI | Polydispersive index |
| Phe | Phenylalanine |
| Phe-Phe | Diphenylalanine |
| Phg | Phenylglycine |
| PNA | Peptide Nucleic Acid |
| ppm | Parts per million |
| PTFE | Polytetrafluoroethylene |
| PXRD | Powder X-ray diffraction |
| Q-PNA | Quadruplex-PNA |
| RP | Reverse phase |
| rpm | Revolution per minute |
| R$_f$ | Retention factor |
| RNA | Ribonucleic acid |
| RT | Retention time |
| rt | Room temperature |
| s | Second |
| ss | Single strand/single stranded |
| Satd | Saturated |
| SPPS | Solid Phase Peptide Synthesis |
| t-Boc | tert-butyloxycarbonyl |
| TFA | Trifluoroacetic acid |
| T | Thymine |
| TBAB | Tetra-n-butylammonim bromide |
| TFMSA | Trifluoromethane sulfonic acid |
| TFE | 2,2,2-Trifluoroethanol |
| THF | Tetrahedrofuran |
| Tf$_2$O | Triflicanhydride |
| TfN$_3$ | Trifluoromethanesulfonyl azide |
| TGA | Thermo gravimetric analysis |
| TLC | Thin layer chromatography |
| $T_m$ | Melting temperature |

| | |
|---|---|
| Trp | Tryptophan |
| Tyr | Tyrosine |
| V | Volt |
| Val | Valine |
| v/v | Volume to volume ratio |
| U | Uridine |
| UV-Vis | Ultraviolet-Visible |

# Abstract

## Effects of Nucleoside and PNA Conjugation on Self-assembly of Diphenylalanine (Phe-Phe)

The thesis entitled "**Effects of Nucleoside and PNA Conjugation on Self-assembly of Diphenylalanine (Phe-Phe)**" is comprised of studies on design, synthesis of peptide Phe-Phe (Diphenylalanine) conjugated with nucleosides, peptide nucleic acid (PNA) and ferrocene and their characterization. The dipeptide Phe-Phe is well known to self-assemble into nanostructures, which have relevance to many disease causing situations (Alzheimer, Parkinson etc.). In order to understand molecular determinants of its self-assembly, the work presented in thesis explores their conjugation with other self-assembling components such as nucleosides and PNA to modulate their inherent self-assembly. The consequences of these modifications on the morphology of the peptide assemblies are probed. As Phe-Phe conjugates form porous nanostructures, their potential for encapsulating small molecules (dyes) and electrochemical properties such as capacitance and redox properties are investigated.

This thesis is presented in six chapters:

**Chapter 1: Introduction to Diphenylalanine (Phe-Phe) and Peptide Nucleic Acid (PNA)**

This chapter gives an overview of the background literature for undertaking the research work in the field of self-assembly of Phe-Phe peptides and peptide nucleic acids. Molecules endowed with special structural features undergo self-assembly spontaneously leading to hierarchical structures at nanoscale under kinetic and/or thermodynamic control.[1,2] Such self-assembly process are mediated through non-covalent, ionic, H-bonding and hydrophobic interactions. Self-assembly plays a crucial role in several biological systems, either to achieve specific biological function or as part of a pathological process. Examples include the self-assembly of phospholipids to form biological membranes, double helix formation through Watson-Crick hydrogen bonding interactions in DNA, polymerization and depolymerization in microtubules and microfilaments, as well as the formation of amyloid fibrils involved in various neurological disorders. Peptide-based building blocks, such as cyclic peptides, amphiphilic peptides, surfactant like oligopeptides, dendritic peptides and aromatic dipeptides have been well known to self-assemble into functional supramolecular assemblies. Diphenylalanine (Phe-Phe) peptide (Figure 1), extracted from Alzheimer's β-amyloid polypeptide as the core motif formation of undesirable fibrils responsible for the disease.[3]
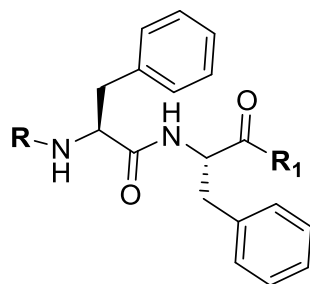
**Figure 1**: Dipeptide Phe-Phe (R = Boc, H etc. and $R_1$ = OMe, OH etc., R, $R_1$ – other amino acids).

Peptide nucleic acids (PNAs) are a class of oligonucleotide (DNA) modifications that contain a peptide bond instead of phosphate link.[4] Because of several favorable properties such as low mismatch tolerance, resistance to proteases and nucleases, and better stability, PNA has wide ranging applications in therapeutics, biosensors, and bioengineering. The advantages of PNA over the conventional antisense oligonucleotides are numerous, partially due to the high flexibility and the absence of charge in the backbone. *In the present thesis, investigation of the self-assembly of Phe-Phe superimposed on self-assembly of the conjugate nucleic acid components is explored further.*

## Chapter 2: Self-assembly of Diphenylalanine (Phe-Phe)-Nucleoside Conjugates

The molecular self-assembly of dipeptide diphenylalanine (Phe-Phe) motif has attracted focus due to its unique morphological structure and utility for potential applications in biomaterial chemistry, sensors and bioelectronics. The ease of their synthesis and a plethora of available experimental tools, the self-assembly of free and protected diphenylalanine scaffolds has unfurled interesting tubular, vesicular or fibrillar morphologies. Developing on this theme, here we attempt to examine the effect of structure and properties (hydrophobic and H-bonding) modifying the functional C-terminus conjugated substituents on Boc-Phe-Phe on its self-assembly process (Figure 2).
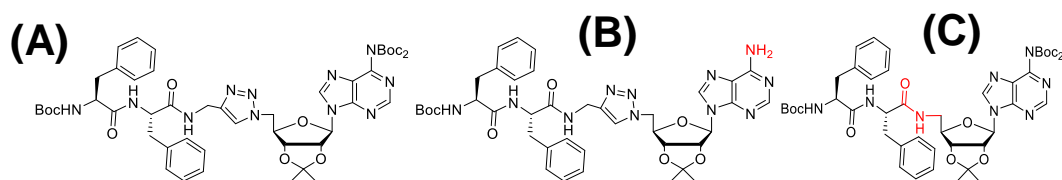


**Figure 2**: Structures of (A) Boc-Phe-Phe-*tz*-A$^{N(Boc)2}$ **(7)**; (B) Boc-Phe-Phe-*tz*-A$^{NH2}$ **(8)** and (C) Boc-Phe-Phe-*am*-A$^{N(Boc)2}$ **(12)**.

This chapter describes the design and synthesis of the conjugation of the Phe-Phe peptides with the nucleosides which contains the different purines as well as the pyrimidine

nucleobases used in the present work. All the peptides were prepared through the solution phase synthesis and characterized by the standard characterization techniques. Further it was observed the effect of protecting group to study the effect of the hydrophobicity as well the hydrophilicity in the different solvents on their self-assembling properties and it was found that only protected [Boc-Phe-Phe-$tz$-A$^{N(Boc)_2}$] **(7)** or partially protected conjugates gave well defined morphology (Figure 3A) and completely/partially deprotected peptide conjugates (H-Phe-Phe-$tz$-A$^{NH_2}$) **(9)** of the peptide conjugates gave sticky aggregates particles (Figure 3B).
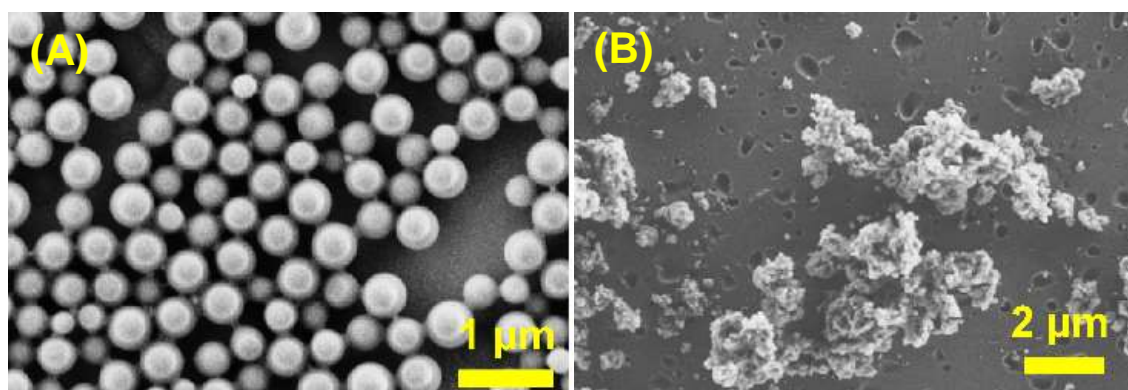


**Figure 3**: FESEM images of (A) Boc-Phe-Phe-$tz$-A$^{N(Boc)_2}$ **(7)** and (B) H-Phe-Phe-$tz$-A$^{NH_2}$ **(9)**.[5]

The molecular hydrophobicity / hydrophilicity were evaluated through the contact angle measurement and the dye encapsulation and release from porous nanostructures demonstrated. The role of amide / triazole linkers are also examined and found that triazole moieties offer better propensity for self-assembly than amide linkage.

## Chapter 3: Effect of Stereochemistry and Hydrophobicity on Self-assembly of Phe-Phe-Nucleoside Conjugates

The self-assembly of homo chiral $L$-dipeptides are well known and since stereochemistry determines conformation which also governs self-assembly through molecular packing effects, studies were done with all 4 diastereomers of Phe-Phe conjugates. It was found that the homochiral peptides ($L$-Phe-$L$-Phe) and ($D$-Phe-$D$-Phe) gave defined nanostructures (nanorods) and while heterochiral dipeptides ($L$-Phe-$D$-Phe and $D$-Phe-$L$-Phe) assembled poorly and did not result in any regular structures.[6,7] Since heterocyclic purines and pyrimidine nucleobases can self-assemble through hydrogen bonded complementary base pairs, the self-assembly of chiral Phe-Phe peptides conjugated with nucleoside was examined. All homo chiral as well as the hetero chiral conjugated Phe-Phe peptides gave perfectly spherical particles (Figure 4).
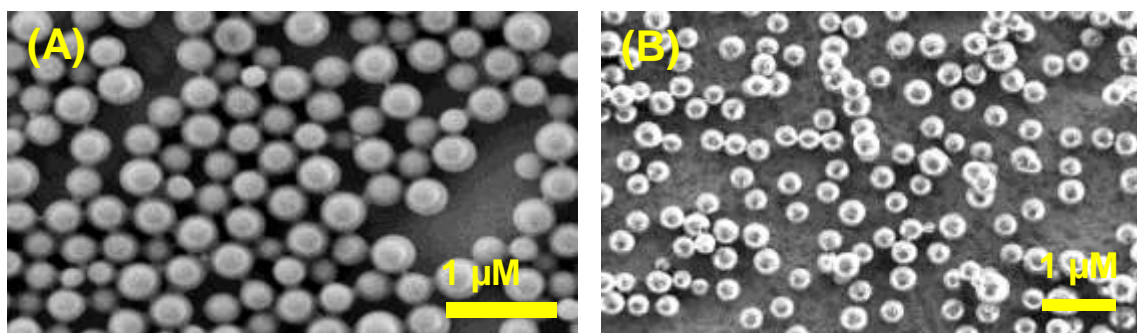
**Figure 4**: FESEM images of (A) Boc-(*L*)Phe-(*L*)Phe-*tz*-A$^{N(Boc)2}$ (**10**) and (B) Boc-(*D*)Phe-(*D*)Phe-*tz*-A$^{N(Boc)2}$ (**11**).

The completely or partially deprotected peptides did not give any defined nanostructures suggesting that self-assembly is governed by careful hydrophobic / hydrophilic balance in the structure. The contact angle measurements of diastereomeric peptides revealed a subtle difference in stereochemistry dependent molecular hydrophobicity.

## Chapter 4: Self-assembly of Diphenylalanine (Phe-Phe)-Peptide Nucleic Acid (PNA) Conjugates

Peptide nucleic acid[4] is a mimic of oligonucleotides that bind to complementary nucleic acids with same H-bonding base specificity as in DNA. PNA hybridizes with complementary DNA/RNA with thermal stability superior to DNA:DNA or DNA:RNA duplex. The synthesis of nucleopeptides, derived from the dipeptide Phe-Phe and PNA unit that are covalently attached through amide or triazole linker are described (Figure 5).
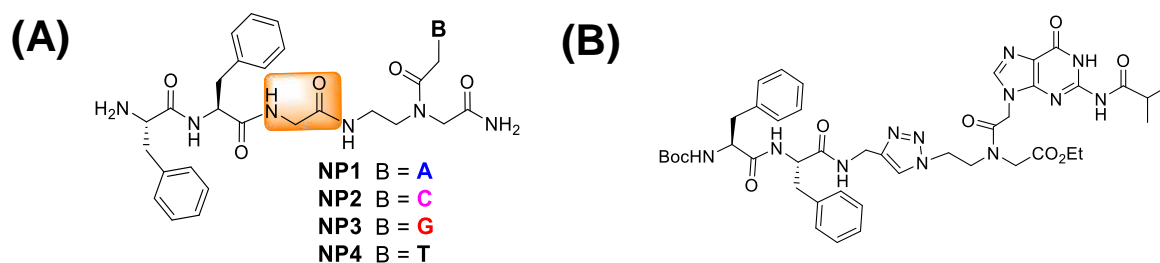


**Figure 5**: Structures of (A) nucleopeptides **NP1**-**NP4** with amide linker and (B) nucleopeptides **6c** with triazole linker.

The self-assembled nanostructures of these conjugates as examined through the FESEM, HRTEM images indicated them to be porous in nature. The stability of nanoparticles was also probed under external stimuli such as pH, temperature and enzymatic hydrolysis using proteolytic enzymes. Hydrophobic substituents on different sites of nucleopeptides and

solvents employed for peptide self-assembly played a crucial role for corresponding morphologies.
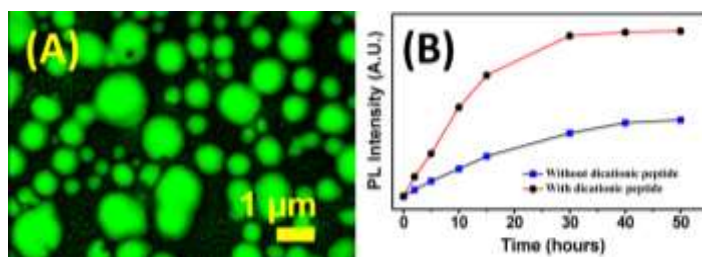


**Figure 6**: (A) Confocal microscope images of fluorescent dye encapsulated [Boc-Phe-Phe-*tz-aeg*{A$^{N(Boc)2}$}-OEt)] and (B) Release of encapsulated CF with and without addition of dicationic peptide from peptide nanoparticles.

## Chapter 5: Self-assembly and Biophysical Studies of Diphenylalanine (Phe-Phe)-Peptide Nucleic Acid-G$_n$ Conjugates (Tetraplex Studies)

It is well known that guanine containing sequences of nucleic acids can self-recognize via cyclic interactions at their Hoogsteen sites to form G-tetraplex structures.[6] The pseudopeptide backbone of PNA[7] is a good structural mimic of the sugar-phosphate backbone forming duplexes[8] and triplex structures.[9] PNA can also form hybrid quadruplexes.[10] In this Chapter PNA-G$_n$ (n = 1-4) oligomers were conjugated with the dipeptide Phe-Phe through glycyl linker to examine Phe-Phe induced G-tetraplex formation. It is seen that only peptides PNA-G$_3$ **(P3)** (with $T_m$ = 40.7 °C) and PNA-G$_4$ **(P4)** (with $T_m$ = 46.6 °C) forms G$_4$-tetraplex structure as evidenced from 290 nm band in UV spectra, characteristic of tetraplexes and the band decreased with increase in temperature, with $T_m$ of 40.7 °C (Figure 7A). Peptide conjugates with Phe-Phe did not exhibit the tetraplex formation perhaps due to steric inhibition from Phe-Phe structure in G$_4$-tetraplex formation (Figure 7B).
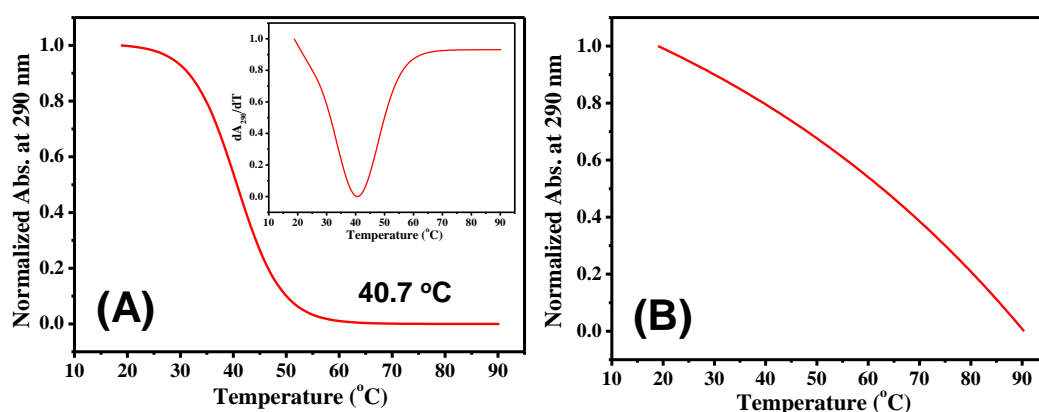


**Figure 7**: UV-$T_m$ plots of (A) PNA-G$_3$ **(P3)**; inset is its derivative cure and (B) Phe-Phe-*gly*-PNA-G$_3$ **(P7)** at 290 nm in Potassium Phosphate buffer 10 mM, (pH 7.24), KCl (100 mM), 50 μM concentration and 1 °C/min temperature.

Morphology of all the deprotected peptides were studied through the FESEM (Figure 8). Formation of tetraplex did not led to formation of well-defined spherical nanoparticles. Only Phe-Phe-*gly*-PNA-G **(P5)** and Phe-Phe-*gly*-PNA-G$_2$ **(P6)** gave spherical particles (diameter around 15 nm – 150 nm) among all Phe-Phe conjugated peptides (Figure 8B).
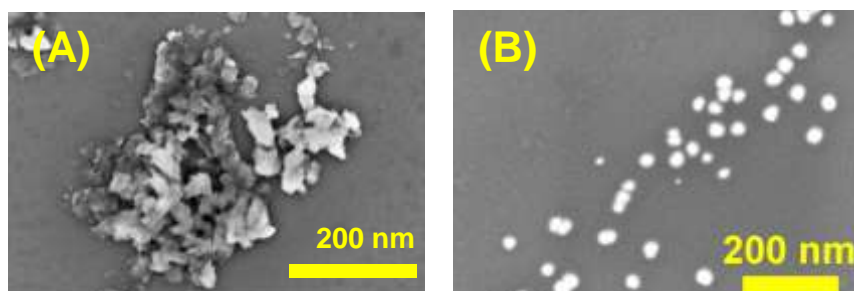


**Figure 8**: FESEM images of (A) PNA-G **(P1)** and (B) Phe-Phe-*gly*-PNA-G **(P5)**.

## Chapter 6: Capacitance and Redox Properties of Self-assembled Phe-Phe with PNA and Ferrocene Conjugates

Self-assembled spherical and tubular mesoscopic morphologies of C- and N- termini protected diphenylalanine (Phe-Phe) result from H-bonding, π-π stacking and Van der Waals interactions. Attachment of electroactive alkyne (propyne) at C-termini of Boc-Phe-Phe and Ferrocene (Fc-Phe-Phe) resulted in nanotube / nanorod structures which transformed into spherical nanoparticles upon conjugation with nucleosides and PNA. The nanoarchitectures aromatic phenylalanine (Phe), tyrosine (Tyr), tryptophan (Trp), phenylglycine (Phg) produce a plethora of peptides as self-assembled biomaterials[11-13] and these have perceived applications in nanophotonics,[14] optoelectronics,[15] biosensing,[16,17] and in electrochemistry as supercapacitor.[18-20] The semiconducting nature of the nucleopeptide modified carbon electrodes suggested their potential use as new capacitor material. In this chapter synthesis and electrochemical properties ferrocene conjugated at C-and N-terminii of Phe-Phe peptides (Figure 9) are reported. These structures exhibited porous nature as seen from FESEM images and entrapment of fluorescent dye.[21]
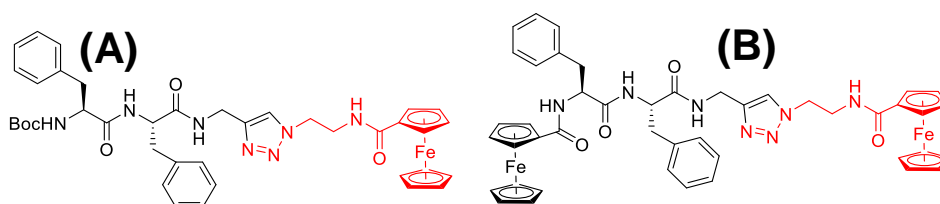


**Figure 9**: Structure of (A) Boc-Phe-Phe-*tz*-Fc and (B) Fc-Phe-Phe-*tz*-Fc.

All ferrocene conjugated peptides gave the spherical particles as seen from FESEM, AFM and HRTEM techniques. The capacitance and the redox properties of all the Phe-Phe conjugated peptides with and without ferrocene using cyclic voltammetry were measured and found that Phe-Phe peptides gave highest capacitance (Figure 10). This is perhaps due to higher surface area on electrodes provided by the coated nanoporous peptides.
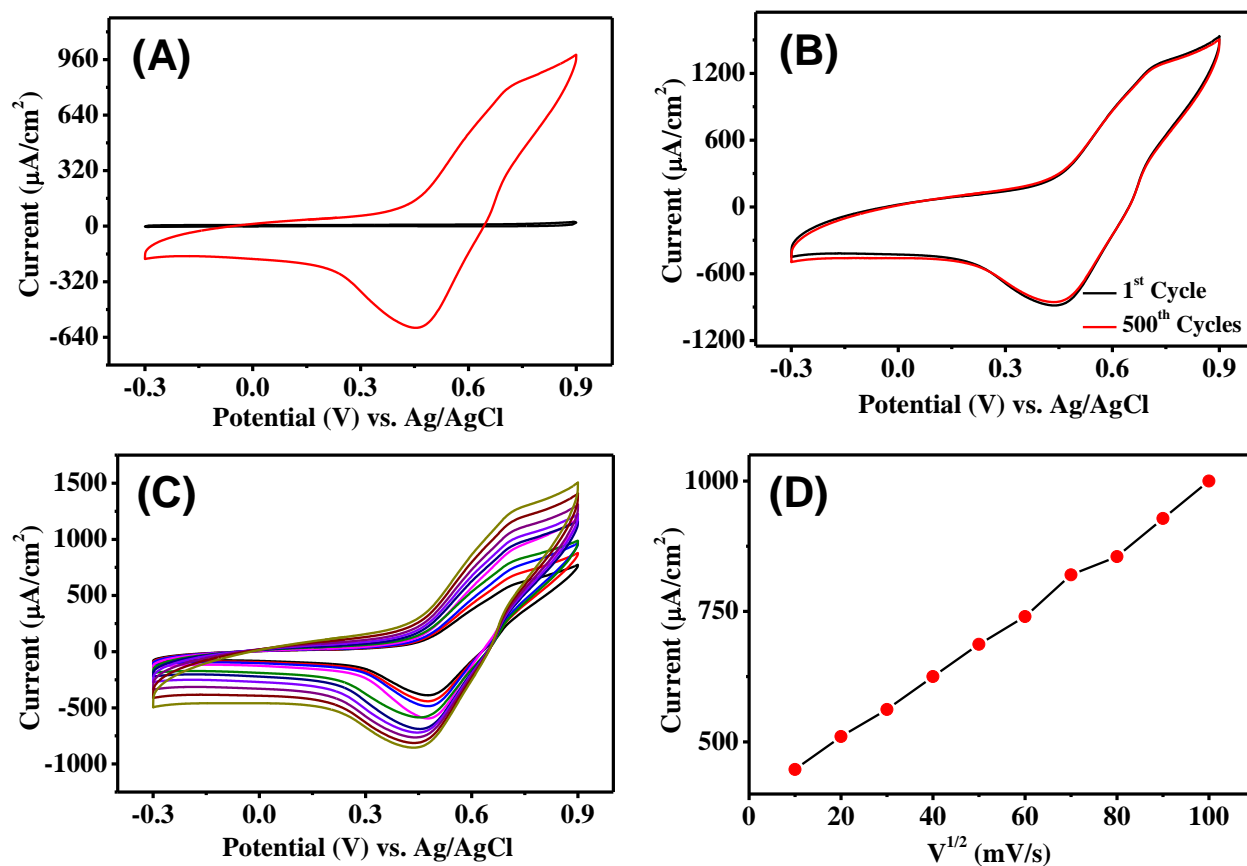


**Figure 10**: Cyclic voltammograms of Fc-Phe-Phe-*tz*-Fc (**11**) supported on Toray Carbon electrode in 0.1 M potassium phosphate buffer electrolytes at pH = 7.4 and 0.1 M KCl (A) at a scan rate of 50 mV/s; (B) at a scan rate of 100 mV/s of 1st and 500th cycles; (C) and (D) scan rate effect at different scan rate from 10 mV/s to 100 mV/s.

The work presented in this thesis have been published in the following research papers.

**1.** Datta, D.[#]; **Tiwari, O.**[#]; Ganesh, K. N. *Nanoscale* **2018**, *10*, 3212-3224.

**2.** Datta, D.[#]; **Tiwari, O.**[#]; Gupta, M. K. *ACS Omega* **2019**, *4*, 10715-10728.

**3.** Datta, D.; Jana, S.[#]; **Tiwari, O.**[#] *Peptide Science* **2019**, e24134.

[#]Contributed equally

# Summary of thesis

> Phe-Phe conjugated with the nucleoside (containing purine and pyrimidine nucleobases) through the triazole and amide linker were synthesized to examine the effects of C-terminus substituents with hydrophobic or H-bonding groups on the self-assembly of Phe-Phe motif.

> Phe-Phe conjugated with the peptide nucleic acid (PNA) through the triazole and amide linker were synthesized on the solution phase and the characterized by the HRMS, $^1$H NMR and $^{13}$C NMR spectroscopy.

> The nature of the linker (triazole / amide) did not have any significant effect on the self-assembled microscopic structures for the conjugation of Phe-Phe with the nucleoside but linker has greater effect in case of the PNA conjugation.

> Peptide Boc-Phe-Phe-*tz*-A$^{N(Boc)_2}$ is stable to external changes such as pH and solvent. Long term storage of spherical particles of peptide **7** (>72 hrs) lead to formation of molecular necklace perhaps through hydrogen bonded nanospheres, since peptide Boc-Phe-Phe-*tz*-A$^{N(Boc)_2}$ has lower tendency to aggregate.

> Nanospheres of peptide Boc-Phe-Phe-*tz*-A$^{N(Boc)_2}$ is thermally stable up to 200 °C and capable of encapsulating dye within the nanosphere which can be released by addition of cationic peptide and amino acids.

> Chiral (homo chiral as well as hetero chiral) Phe-Phe-Nucleoside conjugate peptides were synthesized.

> All the protected and partially protected peptides gave regular spherical structures which were confirm from the FESEM, AFM and HRTEM images.

> The deprotected peptides did not give any regular structures. It gave the sticky aggregates particles which was confirm from the FESEM image.

> The homo chiral *D-D* analogues of the Phe-Phe-Nucleoside conjugates peptide has shown most hydrophobic among all the peptides which was confirmed by the contact angle measurement.

> All the chiral peptides showed the distinct spectra from circular dichroism (CD) spectra. So, there is no any regular conformation.

> Encapsulation of dye and release of that dye from the spherical particles were studied from the confocal microscopy and the fluorescence spectroscopy.

> Adenine containing Phe-Phe peptide gave better self-assembly when compare to others.

- Hydrophobic Phe-Phe conjugated with the nucleoside peptide was found stable under wide range of pH, high temperature and proteolytic enzymes which showed ability of these NPs to behave as stable biocompatible templates.
- PNA-$G_n$ (where n = 1-4) oligomers with and the without Phe-Phe were synthesized, characterized and their self-assembled morphologies were monitored systematically.
- Nucleopeptides without C-/N-termini capping and free nucleobases did not show very good self-assembled morphologies.
- Oligomers PNA-$G_3$ and PNA-$G_4$ forms the G-quadruplex.
- Temperature dependent UV-$T_m$ study shows that Phe-Phe disrupt the G-quadruplex.
- Oligomers PNA-$G_2$, PNA-$G_3$ and Phe-Phe-*gly*-PNA-G form the duplex structure.
- Guanine containing protected Phe-Phe-Nucleoside conjugates peptides shows the highest capacitance value among other peptides.
- Morphological structures remain same before and after cyclic voltammetry experiment.
- The guanine nucleobase containing nucleopeptide furnished the best result with seven fold increment of the capacitance value compared to the bare, unmodified electrode.
- Change in morphology takes place from needle to sphere after conjugating with the Fc-Phe-Phe-Propyne with the nucleoside.
- Both side ferrocene conjugated with the Phe-Phe peptides furnished the best result with 30 fold increment of the capacitance value compared to the bare, unmodified electrode.

This thesis open a new series of the Phe-Phe conjugated peptides which can be used in the drug delivery, supercapacitor, biosensor etc. The results indicated the ability of this new class of peptides to change nanostructures rationally, balancing hydrophobic / hydrophilic nature.

## References

1. Lehn, M. *Proc. Natl. Acad. Sci. U. S. A.* **2002**, *99*, 4763-4768.
2. Whitesides, G. M.; Grzybowski, B. *Science* **2002**, *295*, 2418-2421.
3. Reches, M.; Gazit, E. *Science* **2003**, *300*, 625-627.
4. (a) Egholm, M.; Buchardt, O.; Nielsen, P. E.; Berg, R. H. *J. Am. Chem. Soc.* **1992**, *114,* 1895-1897; (b) Lundin, K. E.; Good, L.; Strömberg, R.; Gräslund, A.; Smith, C. I. *Adv. Genet.* **2006**, *56,* 1-51.
5. Datta, D.; Tiwari, O.; Ganesh, K. N. *Nanoscale* **2018**, *10*, 3212-3224.
6. Williamson, R.; Raghuraman, M. K.; Cech, T. R. *Cell* **1989**, *59*, 871- 880.
7. Nielsen, P. E.; Egholm, M.; Berg, R. M.; Buchardt, O. *Science* **1991**, *254*, 1497.

8. (a) Egholm, M.; Buchardt, O.; Christensen, L.; Behrens, C.; Freier, S. M.; Driver, D. A.; Berg, R. H.; Kim, S. K.; Norden, B.; Nielsen, P. E. *Nature* **1993**, *365*, 566-568; (b) Wittung, P.; Nielsen, P. E.; Buchardt, O.; Egholm, M.; Norden, B. *Nature* **1994**, *368*, 561-563.

9. (a) Uhlmann, E.; Peyman, A.; Breipohl, G.; Will, D. W. *Angew. Chem. Int. Ed.* **1998**, *37*, 2796-2823; (b) Knudsen, H.; Nielsen, P. E. *Nucleic Acids Res.* **1996**, *24*, 494-500; (c) Wittung, P.; Nielsen, P. E.; Norden, B. *Biochemistry* **1997**, *36*, 7973-7979; (d) Wittung, P.; Nielsen, P. E.; Norden, B. *J. Am. Chem. Soc.* **1997**, *119*, 3189.

10. Ghosh, Y. K.; Stephens, E.; Balasubramanian, S. *J. Am. Chem. Soc.* **2004**, *126*, 5944-5945.

11. Hartgerink, J. D.; Beniash, E.; Stupp, S. I. *Science* **2001**, *294*, 1684-1688.

12. Aggeli, A.; Fytas, G.; Vlassopoulos, D.; McLeish, T. C. B.; Mawer, P. J.; Boden, N. *Biomacromolecules* **2001**, *2*, 378-388.

13. Lee, S. W.; Mao, C.; Flynn, C. E.; Belcher, A. M. *Science* **2002**, *296*, 892-895.

14. Zhang, S. *Nature Biotechnol.* **2003**, *21*, 1171-1178.

15. Reches, M.; Gazit, E. *Science* **2003**, *300*, 625-627.

16. Reches, M.; Gazit, E. *Nano Lett.* **2004**, *4*, 581-585.

17. Reches, M.; Gazit, E. *Nat. Nanotechnol.* **2006**, *1*, 195-200.

18. Abramovich, L. A.; Reches, M.; Sedman, V. L.; Allen, S.; Tendler, S. J. B.; Gazit, E. *Langmuir* **2006**, *22*, 1313-1320.

19. Tamamis, P.; Abramovich, L. A.; Reches, M.; Marshall, K.; Sikorski, P.; Serpell, L.; Gazit E.; Archontis, G. *Biophys. J.* **2009**, *96*, 5020-5029.

20. Azuri, I.; Abramovich, L. A.; Gazit, E.; Hod, O.; Kronik, L. *J. Am. Chem. Soc.* **2014**, *136*, 963-969.

21. Datta, D.; Tiwari, O.; Gupta, M. K. *ACS Omega* **2019**, *4*, 10715-10728.

(https://pubs.acs.org/doi/abs/10.1021/acsomega.9b00047)

# Chapter 1

# Introduction to Diphenylalanine (Phe-Phe) and Peptide Nucleic Acid (PNA)

## 1.1 Introduction

Molecular self-assembly can be defined as a spontaneous process by which ordered structures are formed under kinetic and thermodynamic conditions as a consequence of specific and local interactions of molecules themselves.[1,2] Typically, the molecules undergo self-assembly by forming hierarchical structures either at the nanoscale or at the macroscale. In biological systems, self-assembly is an essential feature that often enables a biological function. Assembly of phospholipids into membrane bilayers, formation of DNA double helix through specific complementary hydrogen bonding interactions, and so on are some of the examples of self-assembly of biomolecules. Inspired by the biological systems, a variety of biological and biomimetic materials have been constructed via molecular self-assembly through a ''bottom-up'' approach.[3-9] The self-organization of building blocks into nanostructures relies on specific molecular recognition principles. The interactions between molecules in these systems usually include a combination of non-covalent interactions, namely hydrogen bonds, electrostatic interactions, π-π stacking, hydrophobic forces, non-specific Van der Waals forces, and dipole-dipole interactions. These forces are relatively weak in isolation, however, in combination, they can could direct the self-assembly of molecular building blocks into complex and ordered structures. The individual forces are also not large as compared to the thermal forces. Because they are of a similar magnitude, the structures and properties of the nanostructures can be affected by small variations in the parameters.

The nanostructures prepared from biomolecules, such as DNA, proteins and lipids, are attracting increasing attention due to their biocompatibility, their ability to form specific molecular recognition, simple chemical and biological modification and easy access to bottom up fabrication. These biomolecules, can interact and self-assemble into highly ordered supramolecular architectures.[9-13] Among them, peptides are a class of versatile building blocks.[13-15] The biological origin of peptides may make them favorable for medical and biological applications. In some cases, they can also imitate the behavior and function of proteins, offering an alternative model for gaining insight into self-assembly and protein function. The self-assembling capability of designed or extracted peptide building blocks enables them to be readily manipulated into well-defined nanostructures with various functions. Over the past few decades, researchers have made significant progress in this field.[16-20]

Numerous peptide-based materials, including cyclic peptides, dendritic peptides, amphiphile peptides, surfactant-like oligopeptides, co-polypeptides, and aromatic dipeptides, have been designed and developed for the creation of functional supramolecular architectures. They have been explored for their possible applications in biology, medicine, and nanotechnology.

Some peptide building blocks that display self-assembly are derived from pathogenic protein assemblies. A well-known example is diphenylalanine (Phe-Phe) peptide, which is the key element of Alzheimer's β-amyloid polypeptide, the core recognition motif for molecular self-assembly.[21] Since its emergence, several studies have reported the self-organization of Phe-Phe based building blocks into various functional nanostructures, such as nanotubes, spherical vesicles, nanofibrils, nanowires, and ordered molecular chains (Figure 1.1). Various potential applications of self-assembled Phe-Phe nanomaterials have also been demonstrated. The accelerating pace of this field has considerably improved the properties and functions of Phe-Phe based nanomaterials. However, further developments in the application of Phe-Phe based building blocks are limited by the lack of structure-morphology correlations.

This thesis focuses on the self-assembly of Phe-Phe based building blocks into various nanostructures, and the fabrication of functional inorganic hybrids. Such self-assembled materials have potential applications as functional materials in biological and non-biological areas, including 3D cell culture, drug delivery, bioimaging, biosensors and guest encapsulation as well as templates for nanofabrication.

Nanostructures are ordered clusters with nanoscopic dimensions (10 nm - 200 nm). At this scale, materials tend to acquire physical, chemical, and biological properties, and functions that are remarkably distinct compared to those observed at the macro scale. Hence, in nanostructures constructed by molecular self-association, wherein basic building blocks are easily organized by non-covalent interactions to create ordered supramolecular assemblies. Self-assembly enables synthesis of architectures in stepwise processes with control over the installation of structures. The physical properties of assemblies may be tuned effectively by fine adjustment of the assembly method by physical and chemical means. Moreover, self-assembly progressively permits the co-assembly of two or more kinds of building blocks, allowing fabrication of structurally advanced nano-assemblies with complex physical and chemical properties that are distinct from those of the building blocks.[23-25]
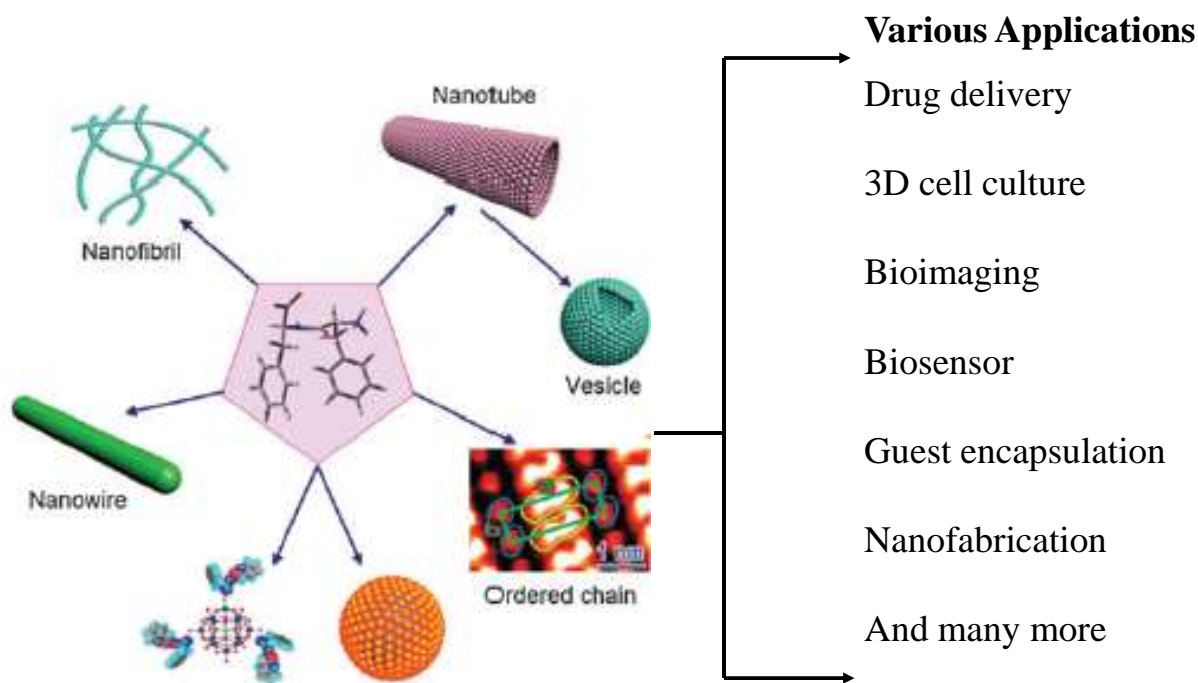
**Figure 1.1**: Structural representation of various nanostructures formed by self-assembly of Phe-Phe based building blocks and their potential applications.[22]

The designed nano-assemblies can be considered to be supramolecular polymers, in which the covalent bonds between building blocks are replaced by non-covalent interactions.[26] These include H bonds, aromatic interactions, and Van der Waals interactions. This permits intensive degree of flexibility within the spatial organization. The smallest self-assembled peptide sequence identified is the diphenylalanine (Phe-Phe). Derived from the core recognition motif of Alzheimer's disease β-amyloid polypeptide, this aromatic dipeptide self-assembles into discrete elongated tubular assemblies (Figure 1.2).[22]
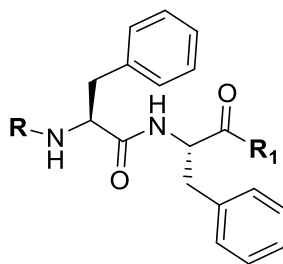


Structure of Phe-Phe dipeptide (where, R = Boc, H etc. and $R_1$ = OMe, OH etc.).

Subsequently, many derivatives of diphenylalanine peptide have been shown to self-assemble to form ordered aromatic dipeptide nanostructures [ADNS] that range from tubes, and spheres to plates and hydrogels (Table 1.1).[27,28] Using single crystal X-ray diffraction studies, Gorbitz *et. al.,*[29] showed that in Phe-Phe peptide, the phenyl rings generated a striking three-dimensional aromatic stacking arrangement, in which it serves as glue between the H-bonded main chains to promote fiber formation. It has been shown that even a single phenylalanine can form ordered fibrillar assemblies with a distinct electron diffraction pattern. Molecular dynamics simulations suggest tight packing of the aromatic moieties, which could stabilize these supramolecular fibrils.[30] These findings highlight the importance of aromatic residues in the accelerated formation and stabilization of ordered amyloid fibrils. The phenylalanine nanostructures are shown to play an important role in neurological damage observed in non-treated phenylketonuria patients.[30] The simplicity of ADNS system and its facile molecular self-assembly, as well as its water solubility has attracted attention in the recent years, motivating characterization and utilization of ADNS in various applications that are discussed in this chapter.
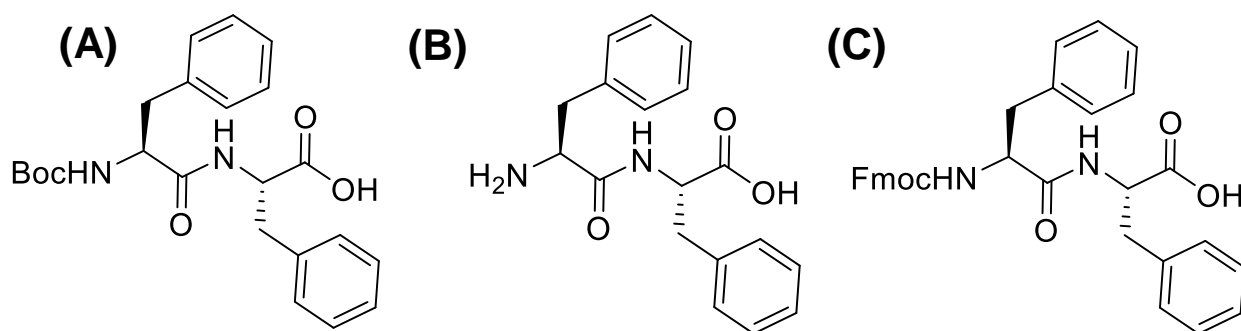


**Figure 1.2**: Aromatic dipeptide structures of (A) Boc-Phe-Phe; (B) H-Phe-Phe and (C) Fmoc-Phe-Phe peptides.[22]

**Table 1.1**: The aromatic peptide nanostructures from diphenylalanine peptide and its derivatives.[27,28]

| Homo-aromatic dipeptide | Assemblies morphology |
|---|---|
| $NH_2$-Phe-Phe-COOH | Nanotubes |
| Ac-Phe-Phe-$NH_2$ | Nanotubes |
| $NH_2$-Phe-Phe-$NH_2$ | Tubular structures |
| Boc-Phe-Phe-COOH | Tubular structures |
| $NH_2$-(*D*-1-Nal)-(*D*-1-Nal)-COOH | Tubular structures |
| $NH_2$-(*D*-2-Nal)-(*D*-2-Nal)-COOH | Tubular structures |
| $NH_2$-(pentafluoro-Phe)-(pentafluoro-Phe)-COOH | Tubular structures |
| $NH_2$-(p-fluoro-Phe)-(p-fluoro-Phe)-COOH | Tubular structures |
| $NH_2$-(p-iodo-Phe)-(p-iodo-Phe)-COOH | Fibrillar structures |
| $NH_2$-(p-nitro-Phe)-(p-nitro-Phe)-COOH | Fibrillar structures and spheres |
| $NH_2$-Phg-Phg-COOH | Nano spheres |
| $NH_2$-(4-phenyl-Phe)-(4-phenyl-Phe)-COOH | Squared plates |
| Fmoc-Phe-Phe-COOH | Amyloid structures |
| Cbz-Phe-Phe-COOH | Amyloid structures |

## 1.2 Self-assembly of Phe-Phe into nanostructures

The following sections describe the versatility of Phe-Phe peptides into a wide variety of self-assembled nanostructures.

**1.2.1 Nanotubes and their transition into vesicle-like structures**: For the fabrication of tubular nanostructures, proteins and peptides are useful as potential building blocks.[31] The simplest peptide building block is the self-assembly of diphenylalanine peptide (*L*-Phe-*L*-Phe and Phe-Phe). The well-ordered tubular structures exhibit a long persistence length (~ 100 μm) due to a combination of hydrogen bonding and π-π stacking of aromatic Phe residues.[22] A recent X-ray diffraction (XRD) study has revealed the molecular organization of the peptides in the nanotubes.[32] The ordered molecular organization of Phe-Phe nanotubes originates from a three dimensional aromatic stacking alignment glues the molecules together into a cylinder using hydrogen bonds along the peptide main chain.[29] Interestingly, the introduction of a thiol group into Phe-Phe peptide alters the self-assembly properties. Cysteine-diphenylalanine tripeptide (C-Phe-Phe) self-assembles into spherical vesicles, rather than nanotubes. This was ascribed to the energetic contribution of the disulfide cross-links, bending the peptide structure and bringing the stacking layer along two axes closer.[33] For the development of newer applications, a better understanding of physical and chemical properties of peptide nanotubes.

As shown with atomic force microscope (AFM) measurements, phenylalanine nanotubes exhibit a thermal stability up to 100 °C. However, they lose their structural integrity beyond 150 °C undergoes degradation.[34] The tubular nanostructures of PheNTs are rigid entities with a high Young's modulus of around 19 GPa [35] (27 GPa seen from a bending beam model in AFM images[31]). This makes them among the stiffest biomolecule-based materials presently known. These unique properties enable the application of such peptide nanotubes for the fabrication of biocompatible nanodevices.[36]

Macroscopic organization or alignment of self-assembled peptide nanotubes are needed for the various nanotechnological applications. A vertically aligned array of PheNTs are fabricated by unidirectional growth of nanotubes.[37] In this method, growth occurs due to the evaporation initiated self-assembly process. The Phe-Phe solution in 1,1,1,3,3,3 hexafluoro-2-propanol (HFIP)

is spread over a glass substrate and the thin layer obtained is composed of nanotube arrays formed upon rapid evaporation of HFIP.

Perhaps, the well-ordered organization of nanotubes are most likely controlled by a nucleation growth mechanism in the vapor-liquid-solid system during the rapid evaporation of solvent. The ordered array or the controlled alignment of PheNTs allows their integration into multi array sensitive sensors and nanodevices. Recently, a cationic dipeptide (CDPNT and H-Phe-Phe-NH$_2$·HCl) derived from Phe-Phe was shown to self-assemble into nanotubes at physiological pH.[38,39] TEM image showed a typical tubular structure with adequate contrast to distinguish the inner part and the periphery of the nanotube. The circular dichroism (CD) signature obtained on the CDPNTs has certain similarities with that of α-helical polypeptides, with the observed extreme corresponding to α-helical π-π* and n-π* transitions. The transition between CDPNTs and vesicle like structures are reversibly dependent on the concentration of the peptide building blocks. This plays a critical role in determining the final morphology of the nanostructure. The conversion between tubular and spherical structures are modulated by varying the concentration of peptide building blocks. The conjoined spheres in a necklace like structure is an intermediate state of the transition of CDPNTs into vesicle like structures, as observed directly by using TEM and fluorescence microscopy (Figure 1.3).
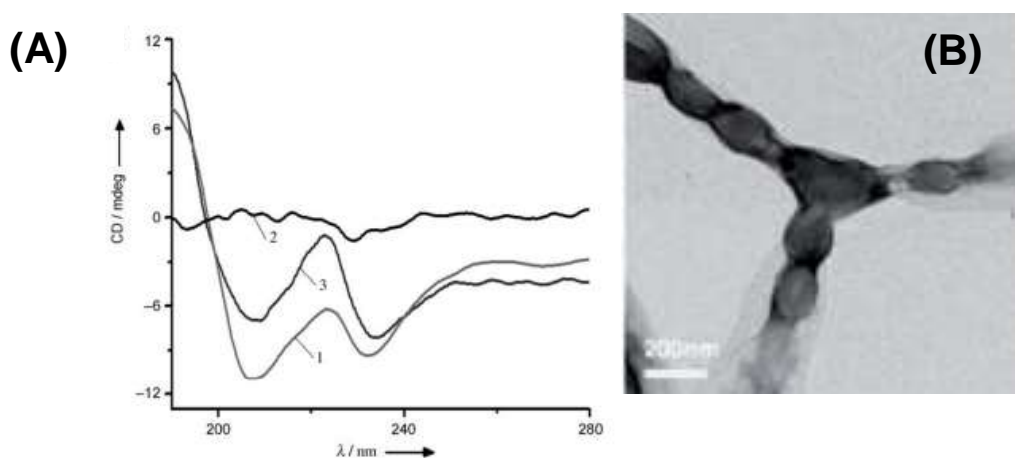


**Figure 1.3**: (A) CD spectra of the cationic DPNTs and vesicle-like structures. 1- the self-assembled nanotubes at 10 mg/mL, 2- vesicle-like structures at 1 mg/mL, 3- the nanotubes after concentration of the diluted solution and (B) TEM image of CDPNTs at a concentration of 7 and 5 mg/mL.[38,39]

Self-assembly of peptides and proteins into fibrils are ubiquitous in biology. In particular, peptide fibrillization is relevant to a number of diseases, including Alzheimer's, Parkinson's, Huntington disease, type II diabetes, and prion disorders with the characteristic of deposition of amyloid fibrils in various tissues and organs.[40,41] These peptide nanofibrils constitute one of the most abundant and important naturally occurring self-assembled materials. It is Phe-Phe, as the shortest structural recognition motif, which plays a decisive role in the fibril formation of the Alzheimer's β-amyloid polypeptide,[40] Thus, Phe-Phe affords the structural communication for molecular self-assembly.

Meanwhile, 9-fluorenylmethoxycarbonyl (Fmoc) protected diphenylalanine (Fmoc-Phe-Phe) has been shown to self-assemble into nanofibrils in water resulting in a hydrogel which is held together in a network of hydrogen bonds and π-π interaction between the moleucles.[42,43] Fmoc-Phe-Phe hydrogel is considerably stronger and stiffer than other hydrogels of biological materials. Their stability can be controlled at a wide range of temperatures and pH, including extreme acidic conditions. Thus Fmoc-Phe-Phe hydrogels has shown advantages for certain applications, such as controlled drug release and 3D cell culture. The molecular stacking mode in the self-assembling fibrous structures has been proposed, according to which the peptides are aligned in an antiparallel β-sheet fashion and adjacent sheets are interlocked via lateral π-π interactions. This led to the formation of a cylindrical structure (Figure 1.4).[44] Since Phe-Phe based peptides can be designed to be responsive to enzymes, their activity and assembly can be regulated and the molecular self-assembly can be controlled for hydrogelation.
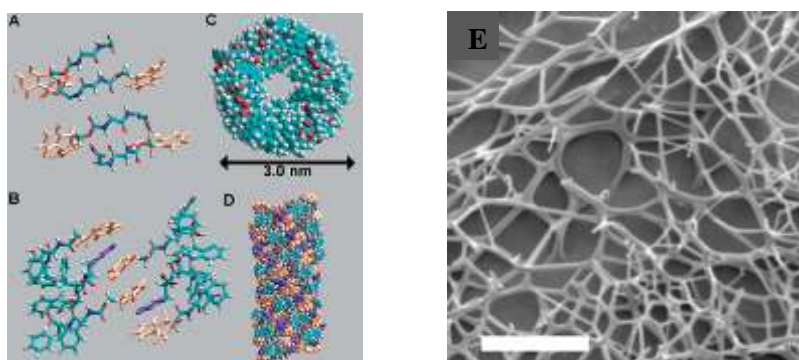


**Figure 1.4**: Molecular models illustrating self-assembly of Fmoc-Phe-Phe dipeptides as stacks of a few molecules (A-B), the top view and side view of the overall architecture (C-D). (E) Cryo SEM images of bundles of fibers formed by Fmoc-Phe-Phe. Scale bar: 500 nm.[44]

The Phe-Phe motif is an extremely versatile self-assembling building block. Subtle changes introduced to the chemical structure of the Phe-Phe derivative produces different morphologies (Figure 1.5).
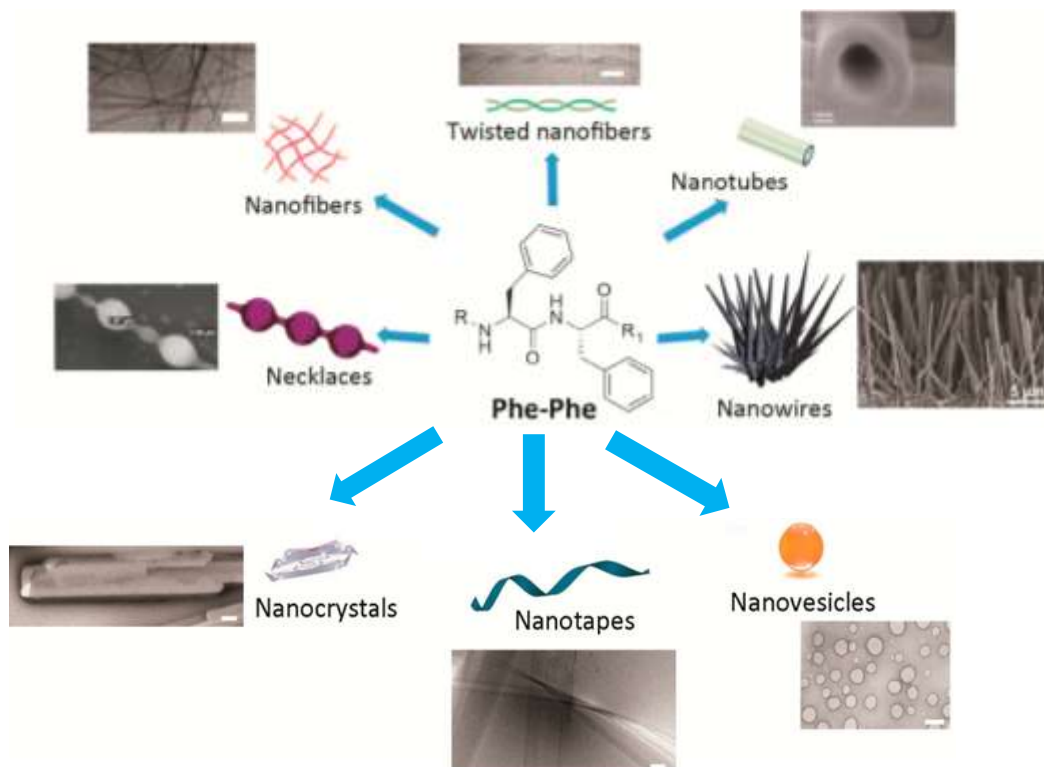


**Figure 1.5**: Phe-Phe motif self-assemble into diverse nanomorphologies. Scale bars = 100 nm, unless otherwise stated on the image diphenylalanine (Phe-Phe).[45]

## 1.3 Applications of Phe-Phe based nanomaterials

The self-assembling properties of Phe-Phe based motifs can be modulated using functional inorganic components to obtain various functional nanostructures. Phe-Phe nanotubes, nanoribbons and nanowires can be suitable templates for the fabrication of functional polymer nanotubes, metal nanowires, and metal oxide nanoribbons. Therefore, we focus on these points to summarize the applications involving the Phe-Phe based nanostructures.

**1.3.1 Applications in biology**: The fibrous hydrogel networks have been used as mimic of extracellular matrix (ECM) for the 3D culture of cells. Chondrocyte cells incorporated into hydrogels by mixing them with Fmoc-Phe-Phe gel. Two photon fluorescence microscopy and environmental scanning electron microscopy (ESEM) studies revealed the growth and proliferation of chondrocytes in the 3D fibrous networks.[43] Thus, Phe-Phe based fibrous scaffolds are promising for applications in tissue engineering and can function analogously to the natural ECM. The Phe-Phe based nanostructures hold potential in the delivery of drugs or genes. Spontaneous transition of self-assembled cationic dipeptide nanotubes (CDPNTs) into vesicles by varying the concentration of Phe-Phe units, oligonucleotides were delivered into the cells through endocytosis.[38]

Establishing a repertoire of organic bio-inspired building blocks for molecular self-assembly is an important task in the nanotechnology. Li *et. al*.,[38] reported that as a cationic dipeptide, H-Phe-Phe-NH$_2$ assembles into nanotubes at physiological pH. However, upon dilution, the cationic dipeptide nanotubes (CDPNTs) can be rearranged into vesicles. This morphological switch can be reversible by changing the peptide concentration. The self-assembled positively charged nanotubes are electrostatically bound to fluorescently labeled ssDNA and could enter cells readily, perhaps by conversion into vesicles. The ssDNA was found to accumulate in the cytoplasm of the cells after internalization.[38]

**1.3.2 Energy storage applications**: The peptide nanostructures can also be organized into arrays, which can be used in the formation of sensitive electrochemical sensors for enzymatic reactions. The peptide nanotubes serve as part of an electrochemical biosensor platform to improve the electrochemical measurement. Covalent immobilization of modified peptide nanotubes to gold electrodes improves the molecular recognition properties and higher electrochemical sensitivity of a biosensor that detects glucose and ethanol using enzymes.[46] Cyclic voltammetric and time based amperometric techniques has been used to show that the integration of peptide nanotubes of dinaphthylalanine or nanospheres from peptide Boc-Phe-Phe onto biosensor electrodes increased the sensitivity of the electrochemical measurements.[47] Notably, electrodes, coated with nanoforest made of vertical arrays of aligned peptide nanotubes were 17 times more sensitive at phenol detection than bare electrode. The deposition of peptide nanostructures on electrodes produces remarkable effects on the cyclic voltammetry parameters.[47]

The study of electrode modification with arrays of peptide nanotubes and the increased functional surface area has enabled formation of peptide nanostructures with energy storage applications. The increased functional surface area of the electrodes significantly enhances its capacitance. The carbon electrodes that were modified by the vertically aligned arrays of peptide nanotubes by vapor deposition method were used to develop electrostatic ultracapacitors.[48] In peptide nanotube-modified ultracapacitor electrodes, the current response was 30 times higher than that in the unmodified carbon electrode and 4 times higher than carbon nanotube modified electrodes. Thus, modification of carbon electrodes leads to significant growth in the electrical double layer capacitance density.[48]

## 1.4 Structure of the peptides and self-assembly

The hierarchical self-assembly is an overarching feature that underlies the organized structure of complex cellular organelles and their functions.[49,50] The hallmarks of these biomolecular architectures are their molecular recognition and reproducibility. The nano-assemblies such as viral capsids,[51] amyloid fibres,[52] flagella,[53] and ribosomes,[54] etc., involve periodic arrangement of biopolymers such as proteins and nucleic acids. Their formation is dependent on the conformation of individual macromolecule as much as it depends on the ensemble of weak interactions holding them together. Our ability to emulate nature to generate sophisticated supramolecular assemblies with an excellent degree of control and predictability over specific molecular interactions and the overall architecture of the complexes are greatly limited by gaps in our understanding of the process of molecular self-assembly. A lack of detailed understanding of general principles outlining the interconnection between the structure and morphology of the self-assembled structure is one of the major impediments in the rational design of synthetic biomolecular nanoassembly and fabrication of artificial nanodevices inspired by them.

**1.4.1 Peptide based self-assembly**: In nature, several molecular machines and supramolecular architectures are made out of proteins. Peptides which are shorter than natural proteins, are easier to synthesize in relatively large amounts, and simpler to handle as compared to many delicate proteins. Unlike large proteins which may have many domains with multiple secondary structural elements and various flexible regions such as loops and turns in their native structure, short

peptides generally contain only one (or a few) conformation. This offers an added advantage of better predictability in terms of their conformational and self-assembling behavior as compared to more complex proteins. The diversity of amino acids in peptide based self-assembled structures also offers similar functional diversity. Due to these reasons, peptide based self-assembly has yielded nanoscale materials of a large variety of morphologies and functions.[55-57] Insights gained from investigations into protein folding and conformational properties of peptide chains become the foundation for the rational self-assembly with synthetic peptides. The ability of certain amino acids to chemically respond to their environmental changes such as pH, ionic strength, presence of specific metals etc., can be exploited for developing stimuli induced responsive nanostructures.

**1.4.2 Designing peptides for the self-assembly**: In order to create supramolecular architectures, ability of simple peptide blocks acting as template must be made to hierarchically assemble through prescribed intermolecular associations mediated by various non-covalent, weak interactions. Rational design of self-assembling peptides involves application of our understanding of the propensity for different amino acids and sequences to adopt specific secondary structures. Suitable designs of self-assembling peptides may also lead to programming spontaneous assembly into specific patterns. Our inadequate understanding of protein folding limits the design of large proteins for functions based on self-assembly. However, the progress in the area of self-assembly of shorter peptide has resulted in the generation of a wide variety of peptide-based materials with excellent control over their morphological features and tunable functional properties.[55]

**1.4.3 Interaction involved in the peptide self-assembly**

An ensemble of specific, but weak interactions hold together the self-assembled peptides. Such programmable interactions to generate stable supramolecular peptide assemblies include ionic/electrostatic, and hydrogen bonding interactions, in addition to even weaker π-π stacking and Van der Waals interactions.

**1.4.3a Ionic interactions**: Ionic/charge complementary peptides were designed to introduce differential charge distribution patterns along the peptide chain by placing positively and negatively charged amino acids in appropriate positions in the β-sheet forming peptide sequence. Electrostatic interactions between the side chains of these peptides lead to their organization into

ordered supramolecular structures (Figure 1.6). Interactions between peptide molecules can be controlled by pH and concentration of salt in the solution. A similar strategy was adopted to self-assemble collagen mimetic peptides into ordered nanosheets and nanofibers.[58,59]
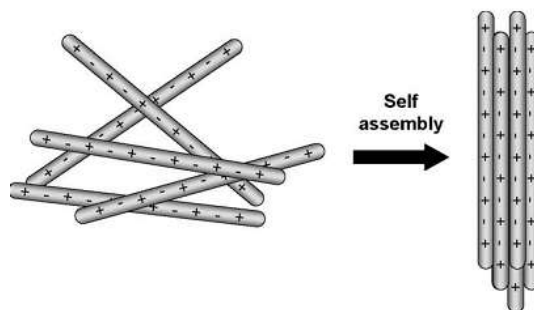


**Figure 1.6**: Schematic representation of self-assembly of peptides through ionic complementarity.[58]

**1.4.3b Hydrophobicity**: Many natural self-assembled structures such as cell membranes exhibit a balance between hydrophilic and hydrophobic properties. Use of hydrophobic amino acid residues in the peptides to drive self-assembly is a common strategy. In peptides that form β-sheet, designing the sequence to have alternating hydrophilic and hydrophobic amino acids leads to β-sheet with two distinct surfaces; the hydrophilic side chains project on one face of the sheet, the hydrophobic side chains form the other face. Increasing hydrophobicity in peptides are found to increase driving force for their self-assembly. Further, it was shown that by increasing the hydrophobicity in self-assembling ionic/charge complementary peptides, the critical aggregation concentration (CAC) for the peptide can be lowered. Increasing hydrophobicity also triggers self-assembly at a lower temperature. Lipidation of the peptides by conjugation with one or more fatty acids are another common approach used to influence the self-assembling properties by altering the hydrophilic / hydrophobic balance in the peptide.[60]

**1.4.3c Aromatic peptide systems**: Among weak interactions other than hydrogen bonds, electrostatic and Van der Waal forces that cause self-assembly are π-π stacking interactions from aromatic residues.[61] Inspired by the self-assembly of amyloid fibers, Reches *et. al*.,[44] identified the core diphenylalanine (Phe-Phe) motif and showed that even the dipeptide alone was able to form regular supramolecular assemblies. The dipeptide formed nanotubes in hydrophobic solvent such as solvent HFIP, facilitated by π- π stacking and hydrogen bonding interactions.

## 1.5 Peptide Nucleic Acids

Nucleic acids (DNA and RNA) are important biological macromolecules present in all forms of life.[62] Their important functions include storage, transmission and expression of the genetic information within the biological systems. Key to their function is the presence of purines (A, G) and pyrimidines (C, T and U) that are endowed with specific and complementary base pairing properties through H-bonding. Nucleic acids thus represent the nature's most versatile molecules for information transfer through base-pairing and molecular assembly.[63] Apart from their biological role which is not discussed here, several chemical modifications have emerged in the context of their applications as antisense therapeutic agents.[64] Among these an important class of analogues is "Peptide Nucleic Acid" (PNA) designed and studied by Nielsen *et. al.*,[65] as a mimic of oligonucleotides. PNA is a composite structure of peptides and nucleic acids, composed of a backbone with repeating N-(2-aminoethyl) glycine units linked by amide bonds (Figure 1.7). The nucleobases are attached to the backbone through a tertiary amide bond via a methylene carbonyl linker. It is a pseudopeptide (amide) backbone that is neutral compared to the negatively charged phosphodiester backbone of nucleic acids. PNAs bind to cDNA through specific purine:pyrimidine base pairing, just as in DNA duplex and with high fidelity. This has made PNA as very versatile probe in diagnostics.[66] Being neither a protein or a nucleic acid, PNAs are highly resistant to degrading enzymes like proteases and nucleases, do not activate RNase H and have been used primarily in translation inhibition and splicing modulation antisense mechanisms. PNA was originally designed and developed as a mimic of a DNA recognizing, major groove binding, triplex-forming oligonucleotide.[67,68] Because of several favorable properties such as low mismatch tolerance, resistance to proteases, nucleases and better stability, PNA has wide ranging applications in therapeutics, biosensors and bioengineering.[69]
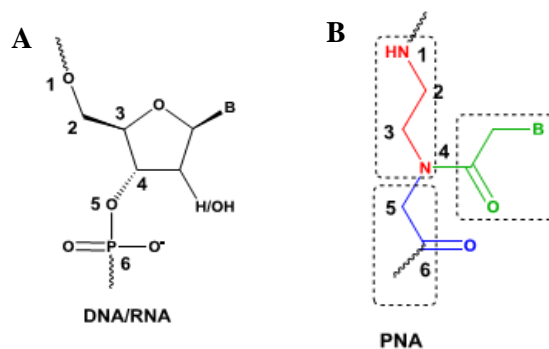


**Figure 1.7**: Comparison between structures of DNA/RNA (A) and PNA (B).

## 1.6 Physicochemical properties of PNA

PNA has proved itself a promising antisense or antigene agent on the basis of its superior properties, such as highly sequence-specific binding to the complementary DNA/RNA targets, high biological and chemical stability, high mismatch discrimination etc.

**1.6.1 Duplex formation with complementary oligonucleotides**: PNA hybridizes to complementary oligonucleotides obeying Watson-Crick base pairing rule. In DNA:DNA duplexes, the two strands are always in antiparallel orientation (with the 5'-end of one strand opposite to the 3'-end of the other). However PNA:DNA hybrids can be formed in two different orientations, arbitrarily termed *parallel* and *antiparallel* (Figure 1.8). Both duplexes are formed at room temperature, with the antiparallel orientation showing higher stability.[70] This creates the possibility for PNAs to bind two DNA tracts of opposite sequence.



**Figure 1.8**: Antiparallel and parallel modes of PNA:DNA duplex formation.

**1.6.2 Triplex properties of PNA**: It is well known that PNAs can easily form the stable structure with complementary DNA, through the formation of $PNA_2$:DNA triplexes.[71] The base pairing in these complexes occurs via Watson-Crick and Hoogsteen hydrogen bonding. In case of one PNA hairpin strand is used to form a $PNA_2$:DNA triplex, both strands are necessarily either antiparallel or parallel to DNA strand. When two PNA sequences are used, Watson-Crick PNA strand is oriented in antiparallel and the Hoogsteen strand is in parallel orientation to form a stable triplex with the strand of DNA.[72] The sequence specificity of triple helix formation is based on the selectivity of formation of the intermediate PNA:DNA duplex, whereas binding of the third strand contributes only slightly to selectivity. The stability of structures enables PNA to perform strand invasion,[71,73] which is an unique property shown by PNAs.

**1.6.3 G-Quadruplex formation by PNA**: DNA and RNA oligomers that contain multiple stretches of consecutive guanine (G) nucleotides are able to fold into a stable secondary structures known as G-quadruplex[74,75] that is gaining increasing attention due to its implication in regulation of gene expression.[76] Balasubramanian *et al.*,[77] have shown the formation of quadruplex composed entirely of PNA (Q-PNA). A homologous PNA (i.e. a PNA having the same sequence as the target) forms a stable PNA$_2$:DNA$_2$/RNA$_2$ hybrid quadruplex by disrupting a bimolecular DNA/RNA G-quadruplex.[78,79]

**1.6.4 Cellular uptake of the PNA**: Although PNA binds to complementary DNA/RNA with high affinity, specificity and stability in biological fluids, the progress of PNA as antisense and antigene agents for inhibition or regulation gene expression has been hampered by their poor cellular uptake. Thus, efficient cellular delivery systems for PNAs are required if these are to be developed into antisense and antigene agents. However, a number of transfection protocols for PNA have been established like micro injection, electroporation, co-transfection with DNA, conjugation to lipophilic moieties, conjugation to cell penetrating peptides etc.[80] To address the issues like poor cell penetration, solubility and ambiguity in binding orientation, various chemical modifications of PNA are known in literature[81] which are not discussed here.

**1.6.5 PNA based self-assembly**: As evidenced by the burgeoning field of DNA nanotechnology, the control of supramolecular assembly of a large number of molecules are possible with high degree of precision and predictability when the oligonucleotides are programmed using simple rules of Watson-Crick base pairing and duplex geometry. As PNA shares its informational blocks, the nucleobases with DNA, PNA can also be used in the same manner. With a peptide backbone, the PNA offers versatility, flexibility and structural complexity.

**1.6.6 PNA amphiphiles**: Similar to peptides, PNA were also conjugated to alkyl chains to induce self-assembly in aqueous solvents. Schneider *et. al.*,[80] prepared amphiphiles of 10-mer PNA and showed that it still retained its DNA hybridizing capacity. Stupp *et. al.*,[82] reported the self-assembly of peptide PNA conjugate into nanofibers. Ganesh *et. al.*,[83] showed that fluorinated chain in the PNA structure thus caused compaction of the assembled particles. PNA strands conjugated to a

perfluoroalkyl chain formed particles that were smaller by 2-3 fold than the PNA amphiphiles conjugated to hydrocarbon tail.

**1.6.7 PNA-DNA hybrid tiles**: DNA double crossover (DX) molecules contain two double helical domains and two crossovers that link the two duplexes. They act as rigid tiles useful for two-dimensional assembly of DNA into different periodic patterns. Seeman *et. al.*,[84] incorporated PNA into the DX tiles to produce heteroduplex DX. Such a strategy allows PNAs to be used readily into the well-studied DNA nanostructures.

**1.6.8 di-PNAs**: Gazit *et. al.*,[85] showed that dimers of PNA containing guanines self-assembled into ordered architectures. Supramolecular organization of the di-PNAs was sustained by the usual Watson-Crick interactions between guanines and cytosines.[86] Several inter- and intra-molecular aromatic π-π stacking interactions between neighboring bases were also involved. The assemblies of PNA exhibited excitation dependent emission over the entire visible spectrum. When GC di-PNAs assembly were deposited on a simple field effect transistor (FET) device, in the gap between source and drain, and potential difference was applied across the device, the PNA assemblies produced electroluminescence at -5V and +5V.

These interesting optical properties of the diPNA assemblies have opened up new avenues for their application in organic optical devices.

## 1.7 Scope of the present thesis

As enumerated in previous section, dipeptide diphenylalanine has gathered interest due to its significant role played in many biological processes. Self-assembly being key to its properties, the work presented here aims to examine the role of hydrophobicity in influencing its assembling properties. There are very few reports that have examined about the role of substituents on the C- or N-terminus of the peptides in self-assembly process.

Since self-assembly processes are dependent on the non-covalent interactions like ionic, covalent, hydrogen bonding, solvation, pH, time (kinetic vs. thermodynamic), temperature etc. study on systematic variation of these properties on self-assembly of peptides are necessary. This thesis is presented as 5 chapters (excluding introduction chapter).

**Chapter 2** explores the effects of the substituents at the C-terminus and the N-terminus of the diphenylalanine peptide backbone on molecular hydrophobicity. The dipeptide is conjugated to nucleosides to influence its self-assembly process with superposition of H-bonding and base pairing properties of nucleobases. The synthesis and characterization of a series of the Phe-Phe conjugates with the nucleoside through either amide or triazole linker (Figure 1.9), R being a protecting group and nucleoside can be free or N-protected adenosine (A), thymidine (T), guanosine (G) and cytidine (C) is described.
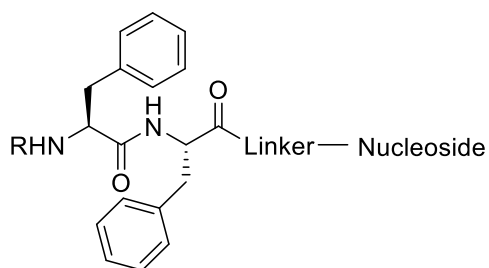


**Figure 1.9**: Phe-Phe-Nucleoside conjugate used in the study. Linker = amide or triazole; nucleoside = Adenosine, thymidine, cytidine and guanosine

Morphological structures which arise from self-assembly at molecular levels were examined through microscopic images from FESEM, AFM and HRTEM techniques (Figure 1.10). Comparative studies are done as a function of temperature, pH, solvent and concentration. Contact angle measurements that measures molecular hydrophobicity were done on various peptide modifications. Thermal stability of the all the peptides also studied through the TGA. Many nanostructures from dipeptides were found to be hollow spheres which may have utility for applications of these peptides for drug delivery. To explore these attributes, encapsulation of fluorescent dye carboxyfluorycien and its release by the cationic peptides was studied.
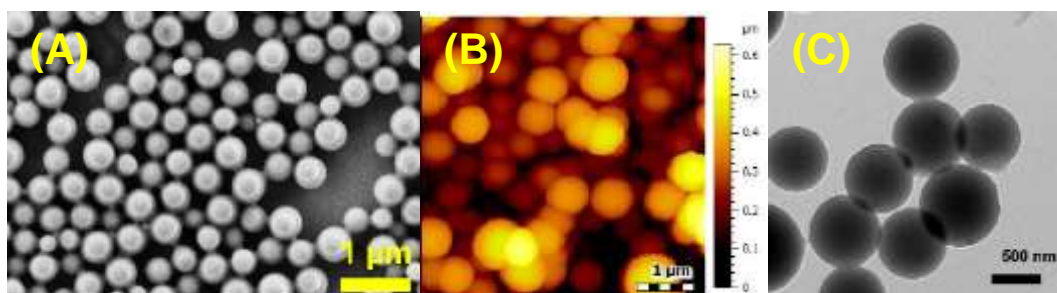


**Figure 1.10**: (A) FESEM image; (B) AFM image and (C) HRTEM image of Boc-Phe-Phe-*tz*-A$^{N(Boc)2}$ (**7**).[86]

Further, **Chapter 3** explores the study of stereochemistry dependent conformations which also affect the self-assembled process. All diastereomeric dipeptides (*LL*, *DD*, *LD* and *DL* peptides) were examined.

**Chapter 4** examines the self-assembly of diphenylalanine (Phe-Phe) conjugated with peptide nucleic acid (PNA) via amide and triazole linker. A series of conjugated nucleopeptides were synthesized (Figure 1.11) and self-assembling abilities investigated by FESEM, HRTEM and AFM imaging techniques. The results suggested that well defined self-assembly forced nanostructures are obtained only in case of the protected or partially protected peptide conjugates. Base pairing of peptide-nucleoside conjugates driven by complementary base pairing of adenine to thymine (A:T) and guanine to cytosine (G:C) was examined both by microscopy and the ESI-MS of the complexes. The base paired conjugates did not give good morphological structures.



**B = A, C, G and T**
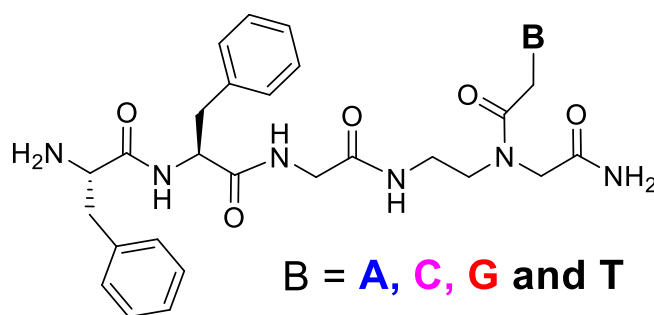
**Figure 1.11**: Structure of Phe-Phe-PNA conjugates.

The nature of peptide-PNA linker (triazole or amide) has an effect on self-assembly, with triazole linked peptides exhibiting the hollow or porous spherical particles. One such hydrophobic nucleopeptide was found to be stable to wide range of pHs, temperature and proteolytic enzymes indicating these nucleopeptides as stable biocompatible templates. Noncovalent encapsulation of fluorescent (CF) dye inside the porous nanospheres and its slow release of dye upon treatment of dicationic dipeptide (Figure 1.12) was demonstrated.
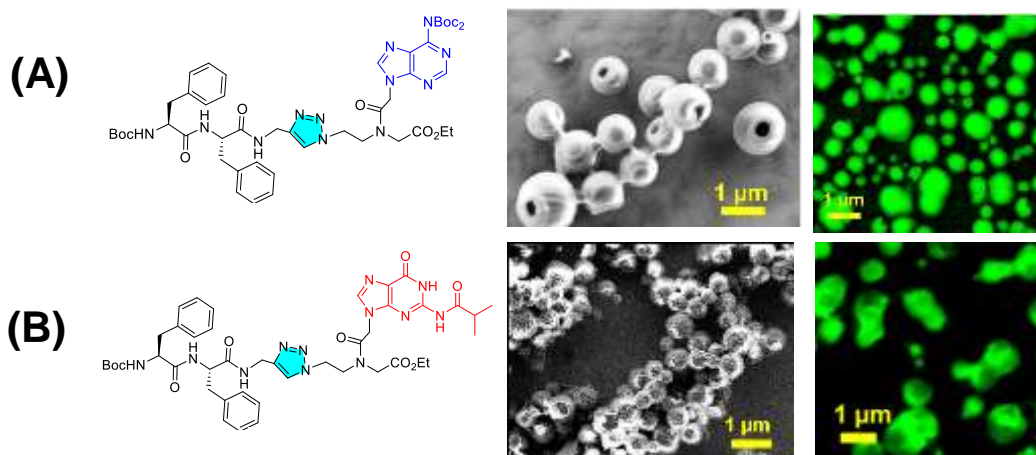
**Figure 1.12**: Confocal microscope images of fluorescent dye encapsulated (A) [Boc-Phe-Phe-*tz-aeg*{A$^{N(Boc)_2}$}-OEt] **(6a)** and (B) [Boc-Phe-Phe-*tz-aeg*(G$^{NHiBu}$)-OEt] **(6c)**.[87]

**Chapter 5** investigates the formation of G-tetraplex in a series of dipeptide-G$_n$ (n=1-4) conjuagtes by UV-$T_m$ and morphological images. The results suggested that G$_4$-tetrad formation was possible only with trimeric and tetrameric G-conjugate. The dipeptide (Phe-Phe) moiety disrupts the formation of G$_4$-tetraplex after conjugation. This is perhaps due to steric reasons where Phe-Phe overlaps prevent assembly of G-tetrads. However, no ordered self-assembly were seen in FESEM imaging and mostly the conjugates exhibited sticky particles. The results clearly point to a fine balance required in competitive constructive and destructive factors that decide the fate of self-assembly in peptide conjugates that have one or more components that assemble by one or more different mechanisms (π-π interaction, H-bonding etc).

**Chapter 6** deals with electrochemical properties of self-assembling Phe-Phe conjugates with ferrocene. Since, diphenylalanine peptides are known for the supercapacitor properties due to their porous particle nature, they were conjugated to an electroactive ligand ferrocene to increase its response. Ferrocene was attached to both sides that is C-terminus as well N-terminus also (Figure 1.13). The electrochemical properties such as capacitance and redox potential were studied using cyclic voltammetry (Figure 1.14). The results indicated enormous increase in the capacitance of ferrocene conjugated nucleopeptides. Morphological structures of the ferrocene conjugated Phe-Phe were studied which gave the hollow spherical particles.
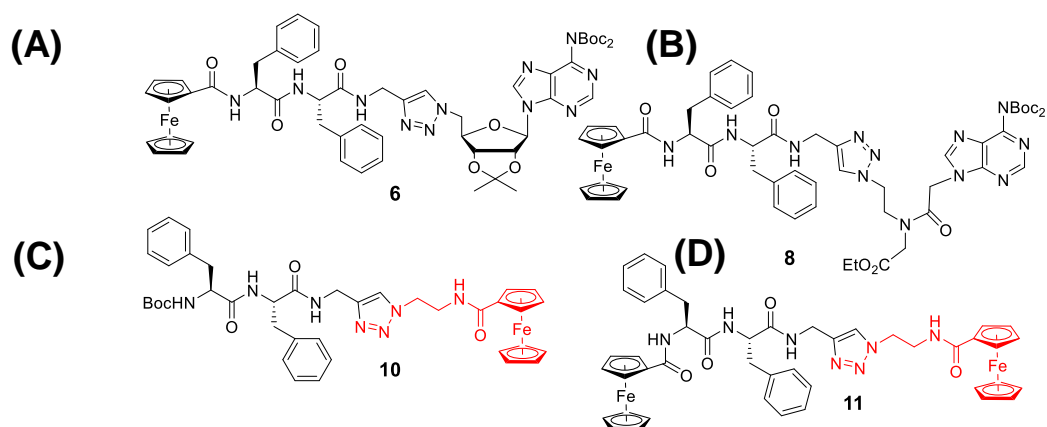
**Figure 1.13**: Structures of (A) [Fc-Phe-Phe-*tz*-A^N(Boc)2] **(6)**; (B) [Fc-Phe-Phe-*tz*-*aeg*{A^(Boc)2}-OEt] **(8)**; (C) Boc-Phe-Phe-*tz*-Fc **(10)** and (D) Fc-Phe-Phe-*tz*-Fc **(11)**.
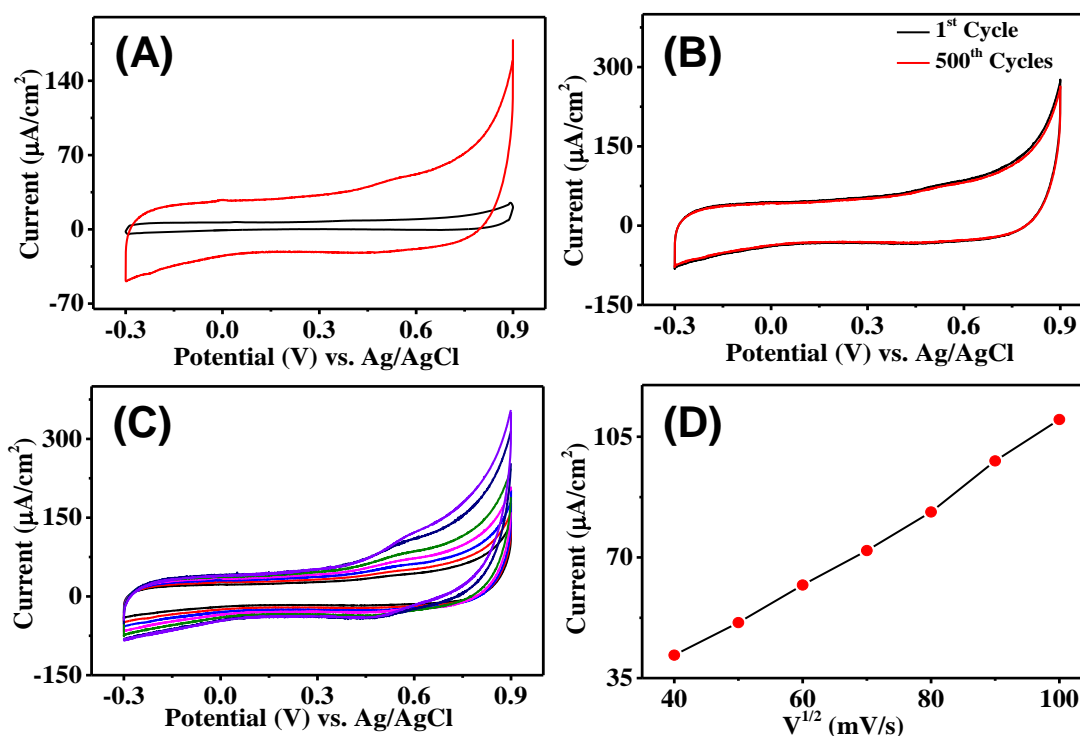


**Figure 1.14**: Cyclic voltammograms of [Boc-Phe-Phe-*tz*-*aeg*(G^NHiBu)-OEt] **(P4)** supported on Toray Carbon electrode in 0.1 M potassium phosphate buffer electrolytes at pH = 7.4 and 0.1 M KCl (A) at a scan rate of 50 mV/s; (B) at a scan rate of 100 mV/s of 1st and 500th cycles; (C) and (D) scan rate effect at different scan rate from 40 mV/s to 100 mV/s.[87]

## 1.8 References

1. Lehn, M. *Proc. Natl. Acad. Sci. U. S. A.* **2002**, *99*, 4763-4768.

2. Whitesides, G. M.; Grzybowski, B. *Science* **2002**, *295*, 2418-2421.

3. Aizenberg, J.; Fratzl, P. *Adv. Mater.* **2009**, *21*, 387-388.

4. Sanchez, C.; Arribart, H.; Madeleine, M.; Guille, G. *Nat. Mater.* **2005**, *4*, 277-288.

5. Palmer, L. C.; Newcomb, C. J.; Kaltz, S. R.; Spoerke, E. D.; Stupp, S. I. *Chem. Rev.* **2008**, *108*, 4754-4783.

6. Ariga, K.; Hill, J. P.; Lee, M. V.; Vinu, A.; Charvet, R.; Acharya, S. *Sci. Technol. Adv. Mater.* **2008**, *9*, 1-96.

7. Nie, Z. H.; Kumacheva, E. *Nat. Mater.* **2008**, *7*, 277-290.

8. Ajayaghosh, A.; Praveen, V. K.; Vijayakumar, C. *Chem. Soc. Rev.* **2008**, *37*, 109-122.

9. He, Q.; Duan, L.; Qi, W.; Wang, K. W.; Cui, Y.; Yan, X. H.; Li, J. B. *Adv. Mater.* **2008**, *20*, 2933-2937.

10. Li, J. B.; Chen, Z. J.; Wang, X. L.; Brezesinski, G.; Hwald, H. M. *Angew. Chem. Int. Ed.* **2000**, *39*, 3059-3062.

11. Wang, K. W.; Yan, X. H.; Cui, Y.; He, Q.; Li, J. B. *Bioconjugate Chem.* **2007**, *18*, 1735-1738.

12. Yamada, N.; Ariga, K.; Naito, M.; Matsubara, K.; Koyama, E. *J. Am. Chem. Soc.* **1998**, *120*, 12192-12199.

13. Zhang, S. G. *Nat. Biotechnol.* **2003**, *21*, 1171-1178.

14. Gazit, E. *Chem. Soc. Rev.* **2007**, *36*, 1263-1269.

15. Ulijn, R. V.; Smith, A. M. *Chem. Soc. Rev.* **2008**, *37*, 664-675.

16. Cui, H.; Webber, M. J.; Stupp, S. I. *Biopolymers (Peptide Science)* DOI 10.1002/bip.

17. Zhao, X.; Pan, F.; Xu, H.; Yaseen, M.; Shan, H.; Hauser, C. A. E.; Zhang, S.; Lu, J. R. *Chem. Soc. Rev.* **2010**, *39*, 3480-3498.

18. Gazit, E. *Chem. Soc. Rev.* **2007**, *36*, 1263-1269.

19. Wang, J.; Liu, K.; Xing, R.; Yan, X. *Chem. Soc. Rev.* **2016**, *45*, 5589-5604.

20. Hamley, I. W. *Soft Matter* **2011**, *7*, 4122-4138.

21. Reches, M.; Gazit, E. *Science* **2003**, *300*, 625-627.

22. Yan. X.; Zhu, P.; Li, J. *Chem. Soc. Rev.* **2010**, *39*, 1877-1890.

23. Sedman, V. L.; Chen, X.; Allen, S.; Roberts, C. J.; Korolkov, V. V.; and Tendler, S. J. B. *J. Microsc.* **2013**, *249*, 165-172.

24. Yuran, S.; Razvag, Y.; Reches, M. *ACS Nano* **2012**, *6*, 9559-9566.

25. Orbach, R.; Harpaz, I. M.; Abramovich, L. A.; Mossou, E.; Mitchell, E. P.; Forsyth, V. T.; Gazit, E.; Seliktar, D. *Langmuir* **2012**, *28*, 2015-2022.

26. Aida, T.; Meijer, E. W.; Stupp, S. I. *Science* **2012**, *335*, 813-817.

27. Reches, M.; Gazit, E. *Phys. Biol.* **2006**, *3*, S10-S19.

28. Reches, M.; Gazit, E. *Isr. J. Chem.* **2005**, *45*, 363-371.

29. Gorbitz, C. H. Chem. Commun. 2006, 2332-2334.

30. Abramovich, L. A.; Vaks, L.; Carny, O.; Trudler, D.; Magno, A.; Caflisch, A.; Frenkel, D.; Gazit, E. *Nat. Chem. Biol.* **2012**, *8*, 701-706.

31. Gao, X. Y.; Matsui, H. *Adv. Mater.* **2005**, *17*, 2037-2050.

32. Gorbitz, C. H. *Chem. Eur. J.* **2007**, *13*, 1022-1031.

33. Reches, M.; Gazit, E. *Nano Lett*. **2004**, *4*, 581-585.

34. Sedman, V. L.; Abramovich, L. A.; Allen, S.; Gazit, E.; Tendler, S. J. B.; *J. Am. Chem. Soc*. **2006**, *128*, 6903-6908.

35. Kol, N.; Abramovich, L. A.; Barlam, D.; Shneck, R. Z.; E. Gazit, E.; Rousso, I. *Nano Lett.* **2005**, *5*, 1343-1346.

36. Niu, L. J.; Chen, X. Y.; Allen, S.; Tendler, S. J. B. *Langmuir* **2007**, *23*, 7443-7446.

37. Reches, M.; Gazit, E. *Nat. Nanotechnol.* **2006**, *1*, 195-200.

38. Yan, X. H.; He, Q.; Wang, K. W.; Duan, L.; Cui, Y.; Li, J. B. *Angew. Chem. Int. Ed.* **2007**, *46*, 2431-2434.

39. Yan, X. H.; Cui, Y.; He, Q.; Wang, K. W.; Li, J. B.; Mu, W. H.; Wang, B. L.; Yang, Z. C. O. *Chem. Eur. J.* **2008**, *14*, 5974-5980.

40. Cherny, I.; Gazit, E. *Angew. Chem. Int. Ed*. **2008**, *47*, 4062-4069.

41. Hamley, I. W. *Angew. Chem. Int. Ed.* **2007**, *46*, 8128-8147.

42. Jayawarna, V.; Ali, M.; Jowitt, T. A.; Miller, A. E.; Saiani, A.; Gough, J. E.; Ulijn, R. V. *Adv. Mater*. **2006**, *18*, 611-614.

43. Mahler, A.; Reches, M.; Rechter, M.; Cohen, S.; Gazit, E. *Adv. Mater.* **2006**, *18*, 1365-1370.

44. Smith, A. M.; Williams, R. J.; Tang, C.; Coppo, P.; Collins, R. F.; Turner, M. L.; Saiani, A.; Ulijn, R. V. *Adv. Mater*. **2008**, *20*, 37-41.

45. Marchesan, S.; Vargiu, A. V.; Styan, K. E. *Molecules* **2015**, *20*, 19775-19788.

46. Yan, X.; Zhu, P.; Li, J. *Chem. Soc. Rev*. **2010**, *39*, 1877-1890.

47. Abramovich, L. A.; Mossberg, M. B.; Gazit, E.; Rishpon, J. *Small* **2010**, *6*, 825-831.

48. Abramovich, L. A.; Aronov, D.; Beker, P.; Yevnin, M.; Stempler, S.; Buzhansky, L.; Rosenman, G.; Gazit, E. *Nat. Nanotechnol*. **2009**, *4*, 849-854.

49. Whitesides, G. M.; Mathias, J. P.; Seto, C. T. *Science* **1991**, *254*, 1312-1319.

50. Whitesides, G. M.; Grzybowski, B. *Science* **2002**, *295*, 2418-2421.

51. (a) Liu, Z.; Qiao, J.; Niu, Z.; Wang, Q. *Chem. Soc. Rev.* **2012**, *41*, 6178-6194; (b) Namba, K.; Stubbs, G. *Science* **1986**, *231*, 1401-1406.

52. Ow, S. Y.; Dunstan, D. E. *Protein Sci*. **2014**, *10*, 1315-1331.

53. (a) Minamino, T.; Imada, K.; Namba, K. *Curr. Opin. Struct. Biol.* **2008**, *18*, 693-701; (b) Evans, L. D. B.; Hughes, C.; Fraser, G. M. *Trends Microbiol.* **2014**, *22*, 566-572.

54. Staley, J. P.; Jr, J. L. W. *Curr. Opin. Cell Biol.* **2009**, *21*, 109-118.

55. (a) Tao, K.; Makam, P; Aizen, R.; Gazit, E. *Science* **2017**, *358*, eaam9756; (b) Basak, S.; Nanda, J.; Banerjee, A. *Chem. Commun.* **2014**, *50,* 18, 2356-2359; (c) Adhikari, B.; Palui, G.; Banerjee, A. *Soft Matter* **2009**, *5*, 3452-3460.

56. Gazit, E. *Chem. Soc. Rev.* **2007**, *36*, 1263-1269.

57. Jiang, T.; Xu, C.; Liu, Y.; Liu, Z.; Wall, J. S.; Zuo, X.; Lian, T.; Salaita, R.; Ni, C.; Pochan, D.; Conticello, V. P. *J. Am. Chem. Soc.* **2014**, *136*, 4300-4308.

58. Hartgerink, J. D.; Beniash, E.; Stupp, S. I. *Science* **2001**, *294*, 1684-1688.

59. Smith, A. M.; Williams, R. J.; Tang, C.; Coppo, P.; Collins, R. F.; Turner, M. L.; Saiani, A.; Ulijn, R. V. *Adv. Mater*. **2008**, *20*, 37-41.

60. Dobson, C. M. *Nature* **2004**, *432,* 824-828.

61. Sessler, J. L.; Lawrence, C. M.; Jayawickramarajah, J. *Chem. Soc. Rev.* **2007**, *36*, 314-325.

62. Dean, N. M.; Bennett, C. F. *Oncogene* **2003**, *22,* 9087-9096.

63. (a) Egholm, M.; Buchardt, O.; Nielsen, P. E.; Berg, R. H. *J. Am. Chem. Soc*. **1992**, *114,* 1895-1897; (b) Lundin, K. E.; Good, L.; Strömberg, R.; Gräslund, A.; Smith, C.I. *Adv. Genet.* **2006**, *56,* 1-51.

64. Shakeel, S.; Karim, S.; Ali, A. *J. Chem. Technol. Biotechnol*. **2006**, *81*, 892-899.

65. Egholm, M.; Buchardt, O.; Nielsen, P. E.; Berg, R. H. *J. Am. Chem. Soc*. **1992**, *114*, 1895-1897.

66. Egholm, M.; Nielsen, P. E.; Buchardt, O.; Berg, R. H. *J. Am. Chem. Soc*. **1992**, *114*, 9677-9678.

67. Wang, J. *Nucleic Acids Research* **2000**, *28*, 16, 3011-3016.

68. Uhlmann, E.; Will, D. W.; Breipohl, G.; Langner, D.; Ryte, A. *Angew. Chem. Int. Ed. Engl.* **1996**, *35*, 2632-2635.

69. Nielsen, P. E.; Egholm, M.; Berg, R. H.; Buchardt, O. *Science* **1991**, *254*, 1497-1501.

70. Costa, M. D.; Kumar, V. A.; Ganesh, K. N. *J. Org. Chem*. **2003**, *68*, 4439-4445.

71. (a) Nielsen, P. E.; Egholm, M.; Berg, R. H.; Buchardt, O. *Science* **1991**, *254*, 1497-1501; (b) Nielsen, P. E.; Egholm, M.; Buchardt, O. *J. Mol. Recogn*. **1994**, *7*, 165-170.

72. Davis, J. T. *Angew. Chem. Int. Ed.* **2004**, *43*, 668-698.

73. Simonsson, T. *Biol. Chem.* **2001**, *382*, 621-628.

74. Egholm, M.; Buchardt, O.; Christensen, L.; Behrens, C.; Freier, S. M.; Driver, D. A.; Berg, R. H.; Kim, S. K.; Norden, B.; Nielsen, P. E. *Nature* **1993**, *265*, 566-568.

75. Ghosh, Y. K.; Stephens, E.; Balasubramanian, S. *J. Am. Chem. Soc.* **2004**, *126*, 5944-5945.

76. Datta, B.; Schmitt, C.; Armitage, B. A. *J. Am. Chem. Soc*. **2003**, *125*, 4111-4118; (b) Marin, V. L.; Armitage, B. A. *J. Am. Chem. Soc*. **2005**, *127*, 8032-8033.

77. Koppelhus, U.; Nielsen, P. E. *Adv. Drug Delivery Rev*. **2003**, *55*, 267-280.

78. Vernille, J. P.; Kove, L. C.; Schneider, J. W. *Bioconjugate Chem.* **2004**, *15*, 1314-1321.

79. Kumar, V. A.; Ganesh, K. N. *Acc. Chem. Res*. **2005**, *38*, 404-412.

80. Guler, M. O.; Pokorski, J. K.; Appella, D. H.; Stupp, S. I. *Bioconjugate Chem.* **2005**, *16*, 501-503.

81. Ellipilli, S.; Vasudeva M. R.; Ganesh, K. N. *Chem. Commun.* **2016**, *52*, 3, 521-524.

82. Lukeman, P. S.; Mittal, A. C.; Seeman, N. C. *Chem. Commun.* **2004**, *15*, 1694-1695.

83. Berger, O.; Abramovich, L. A.; Sakin, M. L.; Grunwald, A.; Peer, Y. L.; Bachar, M.; Buzhansky, L.; Mossou, E.; Forsyth, V. T.; Schwartz, T.; Ebenstein, Y.; Frolow, F.; Shimon, L. J. W.; Patolsky, F.; Gazit, E. *Nat. Nanotechnol*. **2015**, *10*, 353-360.

84. Datta, D.; Tiwari, O.; Ganesh, K. N. *Nanoscale* **2018**, *10*, 3212-3224.

85. Datta, D.; Tiwari, O.; Gupta, M. K. *ACS Omega* **2019**, *4*, 10715-10728.

# Chapter 2

# Self-assembly of Diphenylalanine (Phe-Phe)-Nucleoside Conjugates

## 2.1 Introduction

The hierarchical architectures induced by self-assembly of peptides have opened up a new avenue for novel applications in biological and material sciences. Nanostructures originating from the supramolecular assembly of peptides have wide range of applications in tissue engineering, drug delivery and nanoelectronics.[1] The unique mode of peptide self-assembly is amenable for effective bottom-up tuning of nanomaterial architecture.[2,3] Owing to their structural versatility, chemical stability and ease of modification, peptides are favored templates for biological mimics and supramolecular chemistry.[4,5] The discretely well-organized structures of a series of diphenylalanine analogues seen from single crystal X-ray diffraction[6] and their wide range of applications have propelled the scientific achievements in the field of biomaterial, bio-sensing and nanotechnology.[7-10] The pioneering work from Gazit *et*. *al*.,[11,12] on Phe-Phe motif (Figure 2.1) has demonstrated controlled growth of hollow tubular structures for free aromatic dipeptide,[11,13,14] and nanospheres with metal-like stiffness of 885 Nm$^{-1}$ for the *protected tert*-butyloxycabonyl diphenylalanine (Boc-Phe-Phe-OH)[15] validates the phase diagram of self-assembling process with formation of a homogeneous population of either spherical or tubular nanosturctures.[14c,16]
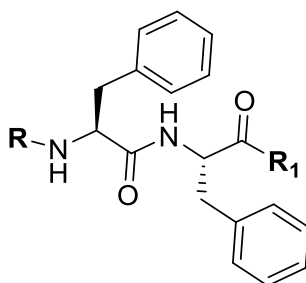


**Figure 2.1**: Structure of Phe-Phe dipeptide (where, R = Boc, H etc. and R$_1$ = OMe, OH etc.).

While the central role of Phe-Phe core is well established, the structural role of C/N-terminal groups is not systematically studied. Various N-terminal substituents of Phe-Phe including nucleobases lead to wide range of hydrogelation from self-assembled structures,[17] whereas those used at C-termini for hydrogel formation include thiol, pyridinium derivatives, alkyl groups, tertiary amines, and oligoethylene glycol (OEG) chain.[17] The structural origin of tunable microscopic architecture of C-terminus modified Boc-Phe-Phe scaffold is interesting since they generate a variety of self-sorted structures (Table 2.1) *viz*., nanorods, micelles, nanoribbons and

soft materials. It has been observed that formation of very large vesicles,[18] nanofibers[19] and generation of light emitting organo-gels[20,21] are attributed to conjugation with chromophores such as porphyrin and photosensitive moiety stilbene. Charge transferring (CT) Phe-Phe organo-gel was produced when the C-terminus was modified with long hydrocarbon tail and N-capped with monopyrrolotetrathiafulvalene (MPTTF)[22] while N- and C-terminus capped with benzoperylene

**Table 2.1**: Substituent based variations in the microscopic structures of Phe-Phe unit containing short peptides.

| Entry | Substituent at C-terminus (X) | Morphology | Reference |
|---|---|---|---|
| 1. Boc-Phe-Phe-X | OMe | Nano rods | 19 |
| | *p*-aminobenzyl porphyrin | Large vesicle | 18 |
| | Stilbene methyl ester | Organo gel | 20,21 |
| | Tyrosine methyl ester | Organo gel | 24 |
| | Phenylalanine carbroxylic acid | Hydro gel | 25 |
| 2. MPTTF-CH$_2$CO-Phe-Phe-NHC$_{12}$H$_{25}$ | Dodecyl amine | Organo gel | 22 |
| 3. Benzoperylenemonoimide (BPI) capped Phe-Phe-OMe | OMe | Nano particles | 23 |
| 4. Pro-Phe-Phe-Pro | Proline | Vesicles | 26 |
| 5. (Phe-Phe)$_2$EDA and (Phe-Phe)$_3$TREN | Ethylenediamino, Tris(2-aminoethyl) amino | Fibrous bundles and fibers with the spherical structures | 27 |

monoimide (BPI) and methyl ester respectively produced nanoparticles.[23] Attachment of tyrosine/phenylalanine as an additional aromatic amino acid residues at C-terminus of Boc-Phe-Phe motif resulted in CT-organogel[24] and hydrogel[25] respectively. Addition of proline at both termini of Phe-Phe motif[26] lead to vesicular morphology, whereas peptides with Phe-Phe as a part of symmetric molecules having ethylenediamino and tris (2-aminoethyl) amino C-termini, furnished fibrous aggregates and spherical structures respectively.[27]

Being central to Phe-Phe motif is the $\pi-\pi$ interaction of aromatic rings, the modulation of this by presence of nearby chromophores or ligands may lead to different morphologies. Herein, we examine the hitherto unknown effects of imparting additional stacking and H-bonding with C-terminal ligands such as purine and pyrimidine nucleosides adenosine, thymidine and uridine on the morphological features of the Phe-Phe dipeptide.

The relative hydrophobic effects in different structures were qualitatively estimated by contact angle measurements.[28] The morphologies of self-assembled peptides visualized through scanning electron microscopy (SEM), high resolution transmission electron microscopy (HRTEM) and atomic force microscopy (AFM) exhibited wide ranging nano-vesicular particles that undergo transition to molecular necklace.[29,30] The robustness of the assembled spherical particles were tested under various stimuli like temperature, pH and cationic peptides.

## 2.2 Rationale and objectives of present work

The present work attempts to examine the effect of structure and property (hydrophobic and H-bonding) modification, via functional C-terminus conjugated substituents on Boc-Phe-Phe on its self-assembly process. In this context, the C-terminus was modified by nucleosides since nucleobases can further modulate the self-assembly of Phe-Phe structure through hydrogen bonding and $\pi-\pi$ stacking interactions. A linker (triazole or amide) between Phe-Phe and nucleoside provides the functional flexibility to the molecule. The presence of Boc group on the N-terminus, helps study of the effects of hydrophobicity and hydrophilicity on self-assembly (Figure 2.2).

The consequent self-sorting due to H-bonding, Van der Waals force and $\pi-\pi$ interactions, generation of morphological nanostructures from these peptides may be characterized via their FESEM, HRTEM, AFM images and DLS experiments. The stability of these nanostructures towards different external stimuli such as pH and temperature, encapsulation of fluorescent probes inside the vesicles and their release by external trigger will be interesting. The results enable new directions in the study and applications of Phe-Phe motif to rationally engineer new functional nanoarchitectures.
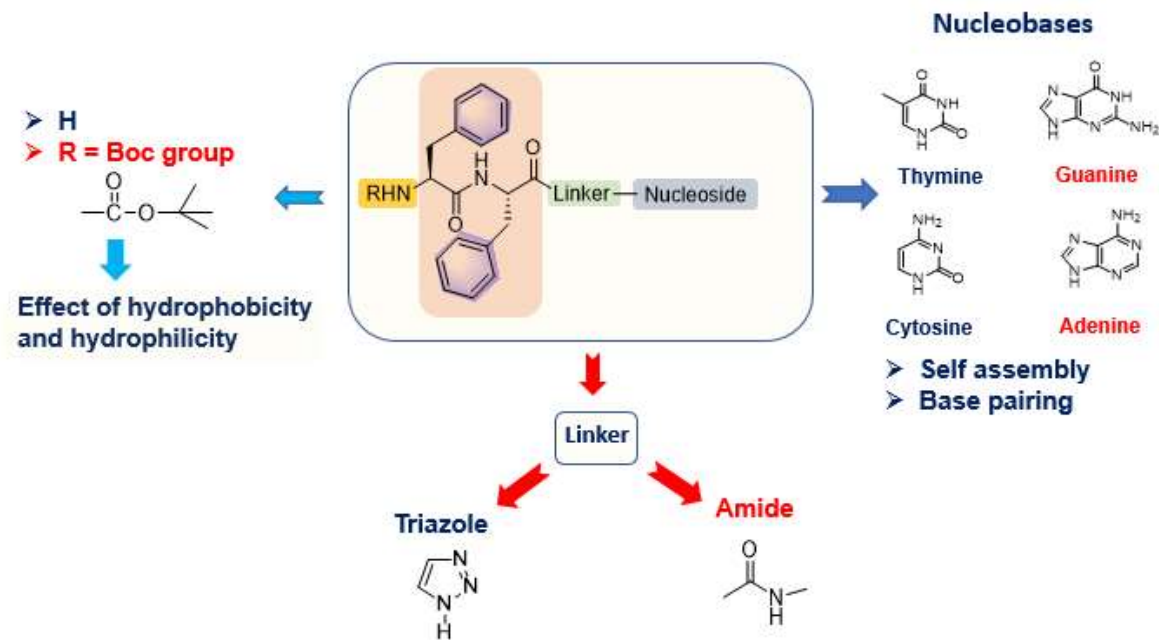
**Figure 2.2**: Effect of conjugation with other self-assembling ligands.

The specific objectives of this chapter are following:

➢ Synthesis of various C and N-terminus substituted Phe-Phe derivatives: (A) Boc-Phe-Phe-*tz*-A$^{N(Boc)_2}$ **(7)**, (B) Boc-Phe-Phe-*tz*-A$^{NH_2}$ **(8)**, (C) H-Phe-Phe-*tz*-A$^{NH_2}$ **(9)**, (D) Boc-Leu-Leu-*tz*-A$^{N(Boc)_2}$ **(10)**, (E) Boc-Phe-Phe-*am*-A$^{N(Boc)_2}$ **(12)**, (F) Fmoc-Phe-Phe-*tz*-A$^{N(Boc)_2}$ **(15)**, (G) Boc-Phe-Phe-*tz*-U **(18)** and (H) Boc-Phe-Phe-*tz*-T **(19)** (Figure 2.3).
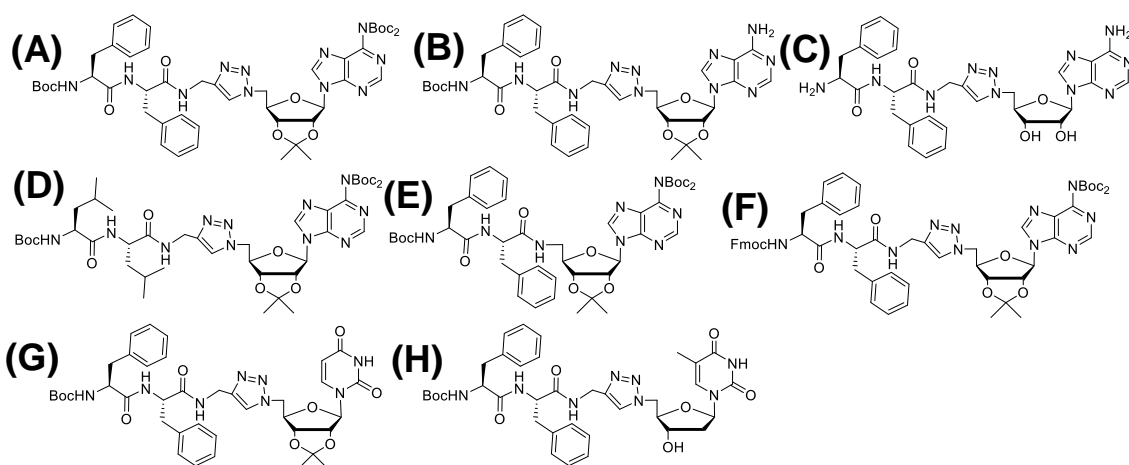


**Figure 2.3**: Structures of (A) Boc-Phe-Phe-*tz*-A$^{N(Boc)_2}$ **(7)**; (B) Boc-Phe-Phe-*tz*-A$^{NH_2}$ **(8)**; (C) H-Phe-Phe-*tz*-A$^{NH_2}$ **(9)**; (D) Boc-Leu-Leu-*tz*-A$^{N(Boc)_2}$ **(10)**; (E) Boc-Phe-Phe-*am*-A$^{N(Boc)_2}$ **(12)**; (F) Fmoc-Phe-Phe-*tz*-A$^{N(Boc)_2}$ **(15)**; (G) Boc-Phe-Phe-*tz*-U **(18)** and (H) Boc-Phe-Phe-*tz*-T **(19)**.

- ➢ Characterization of the peptides by HRMS, MALDI, IR, $^1$H, $^{13}$C NMR spectroscopy.

- ➢ Study of packing in the solid state by powder XRD (PXRD), thermal stability by thermo gravimetric analysis (TGA) and molecular hydrophobicity by contact angle (CA) measurements.

- ➢ Study of self-assembled morphological structures through field emission scanning electron microscopy (FESEM), high resolution transmission electron microscopy (HRTEM) and atomic force microscopy (AFM) to determine the role of conformation on dictating the resultant morphology.

- ➢ Investigation of the size distribution of nanospheres and rods in solution by DLS studies and encapsulated fluorescent probes by confocal microscopy and fluorescence spectroscopy.

## 2.3 Results and discussions

The synthesis of various peptides were followed by purification, structural characterization by spectroscopic techniques and study of self-assembly by various microscopic techniques.

### 2.3.1 Diphenyl (Phe-Phe)-nucleoside conjugates

**2.3.1a Synthesis of target peptides**: The dipeptide Boc-Phe-Phe-OMe[19] was hydrolyzed under basic conditions to afford the acid Boc-Phe-Phe-OH (**1**).[24] This was then coupled with propargylamine hydrochloride to afford the propargyl amide Boc-Phe-Phe-Propyne (**2**). The peptide without any aromatic moieties Boc-Leu-Leu-OH[22] (**3**) was transformed to the corresponding propargyl amide derivative Boc-Leu-Leu-Propyne (**4**) through coupling with propargylamine hydrochloride in high yield (Scheme 2.1). The alkyne group of **2** (Boc-Phe-Phe-Propyne) was subjected to click reaction with 5′-azido-N$^6$-Boc adenosine (**5**)[31] and 5′-azidoadenosine (**6**)[32] in presence of CuSO$_4$.5H$_2$O and sodium-*L*-(+)-ascorbate to afford the conjugated peptides **7** [Boc-Phe-Phe-*tz*-A$^{N(Boc)_2}$] and **8** (Boc-Phe-Phe-*tz*-A$^{NH_2}$) respectively in good yields.
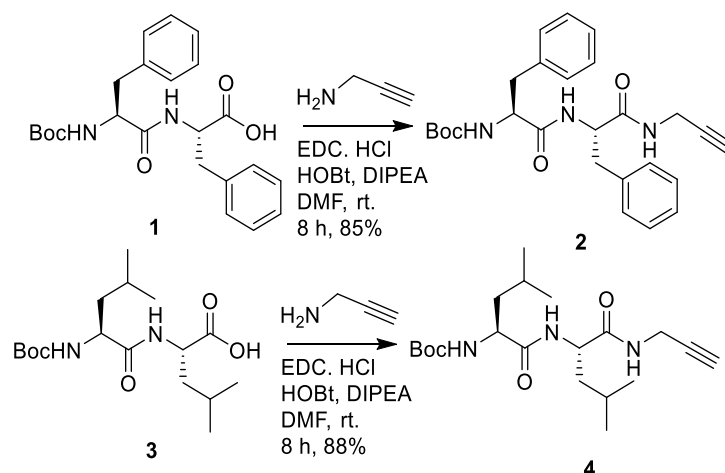
**Scheme 2.1**: Synthesis of intermediate dipeptide propynes **2** and **4**.

The deprotection of protected peptides **7** / **8** with TFA gave free peptide **9** (H-Phe-Phe-*tz*-A$^{NH_2}$). Conjugated peptides **7-9** allow a comparative study of the additional effects of H-bonding by adenosine moiety in free and N$^6$-Boc-protected forms on Phe-Phe self-association process. Similarly, the leucine peptide **10** [Boc-Leu-Leu-*tz*-A$^{N(Boc)_2}$] was obtained in good yield by "clicking" dipeptide **4** with 5′-azido-N$^6$-Boc adenosine **5** (Scheme 2.2) and (Scheme 2.3). The analogue **12** [Boc-Phe-Phe-*am*-A$^{N(Boc)_2}$] with amide in place of triazole moiety was obtained by coupling the acid Boc-Phe-Phe-OH **(1)** with the 5′-aminoadenosine[32] **(11)** (Scheme 2.4) to study the effect of linker in the self-assembly process.
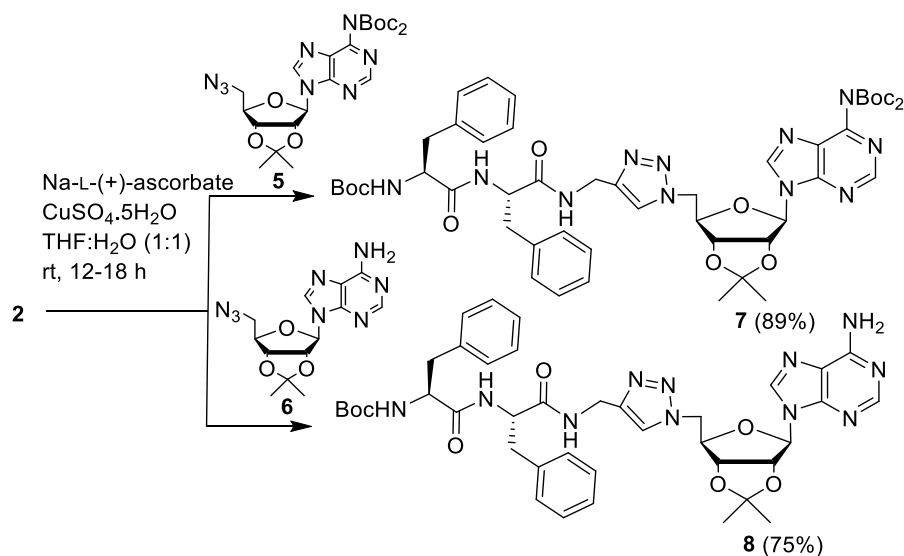


**Scheme 2.2**: Synthesis of peptides **7** and **8**.
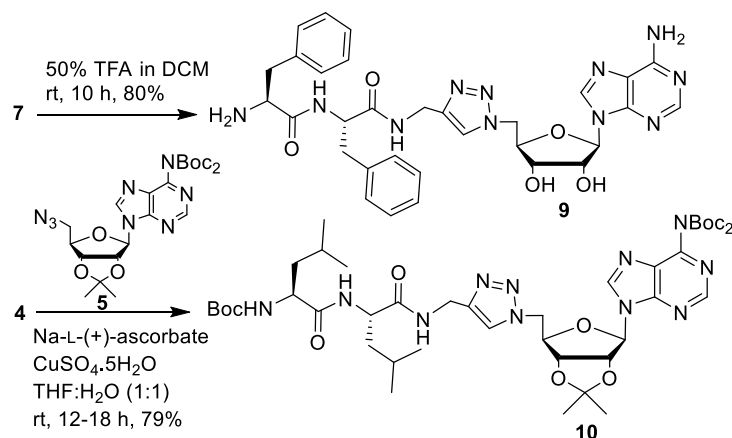
**Scheme 2.3**: Synthesis of peptides **9** and **10**.

Simultaneously, the Fmoc analogue of peptide **7** [Fmoc-Phe-Phe-*tz*-A$^{N(Boc)2}$] was synthesized (Scheme 2.5) to check the effect of a different amino acid protecting group at the N-terminus of Phe-Phe moiety.
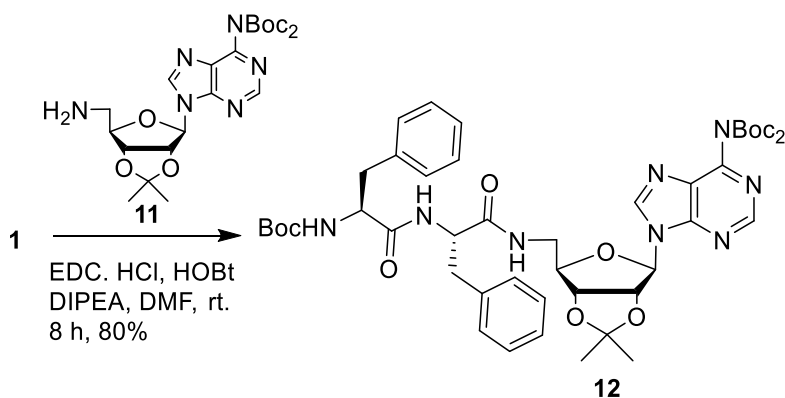


**Scheme 2.4**: Synthesis of peptide **12**.

Finally, to compare the self-assembling ability of purine nucleobase with the pyrimidine analogues, corresponding Phe-Phe conjugated with uridine and thymidine nucleosides were synthesized. The Boc-Phe-Phe-propyne **2** was clicked with 5′-azidouridine[33] (**16**) and 5′-azido thymidine[34] (**17**) to afford corresponding conjugates **18** (Boc-Phe-Phe-*tz*-U) and **19** (Boc-Phe-Phe-*tz*-T) respectively in good yields (Scheme 2.6).
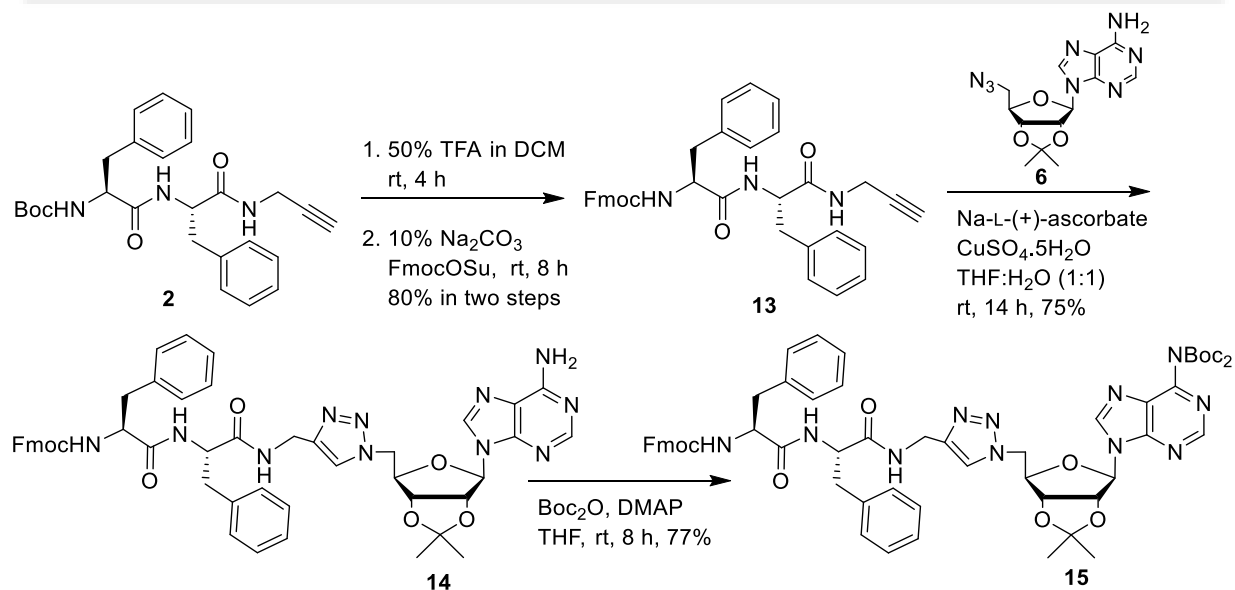
**Scheme 2.5**: Synthesis of Fmoc-Phe-Phe-*tz*-A$^{N(Boc)2}$ **(15)**.
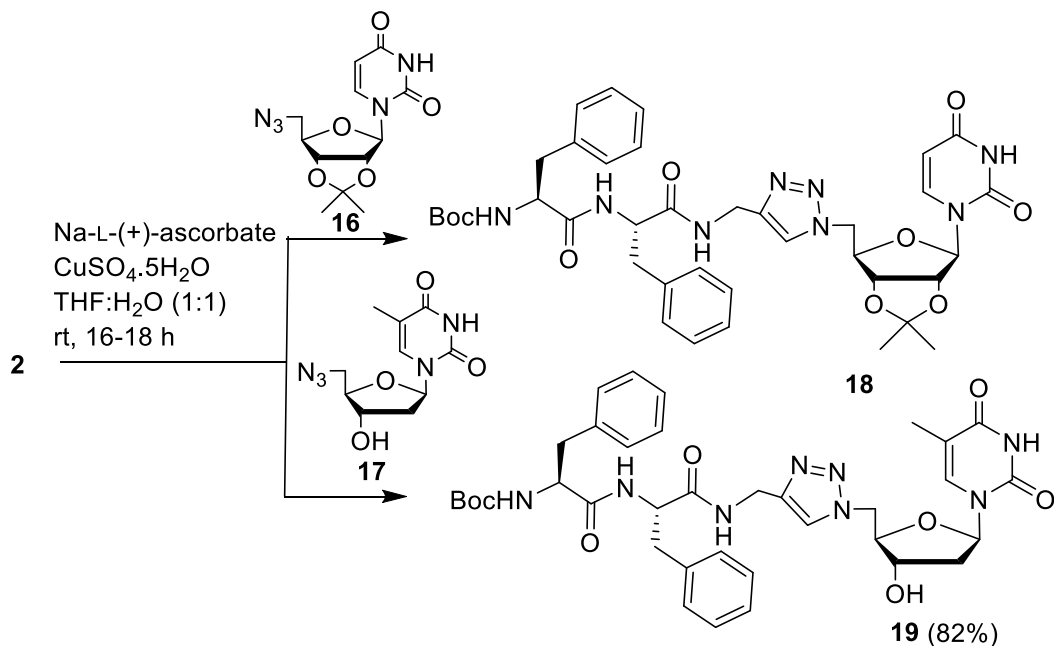


**Scheme 2.6**: Synthesis of peptides **18** and **19**.

**2.3.1b Characterization of peptides**: All peptides were purified by column chromatography over silica gel and structurally characterized by NMR and HRMS (see experimental section).

**2.3.1c Powder XRD of peptides**: The organized packing (self-assembly) in the solid state of the peptides, were examined by the powder XRD (PXRD). In the PXRD data, the broad peaks observed for all peptides **(7-10, 12, 18, and 19)** indicated their amorphous nature (Figure 2.4). Among the three intermediates, the dipeptide **4** (Boc-Leu-Leu-Propyne) (Figure 2.4B) and Boc-Phe-Phe-OMe (Figure 2.4J) exhibited crystallinity in PXRD. Unfortunately, their single crystal structure could not be obtained and its crystalline nature disappeared in the conjugate peptide **10** [Boc-Leu-Leu-*tz*-A$^{N(Boc)_2}$].
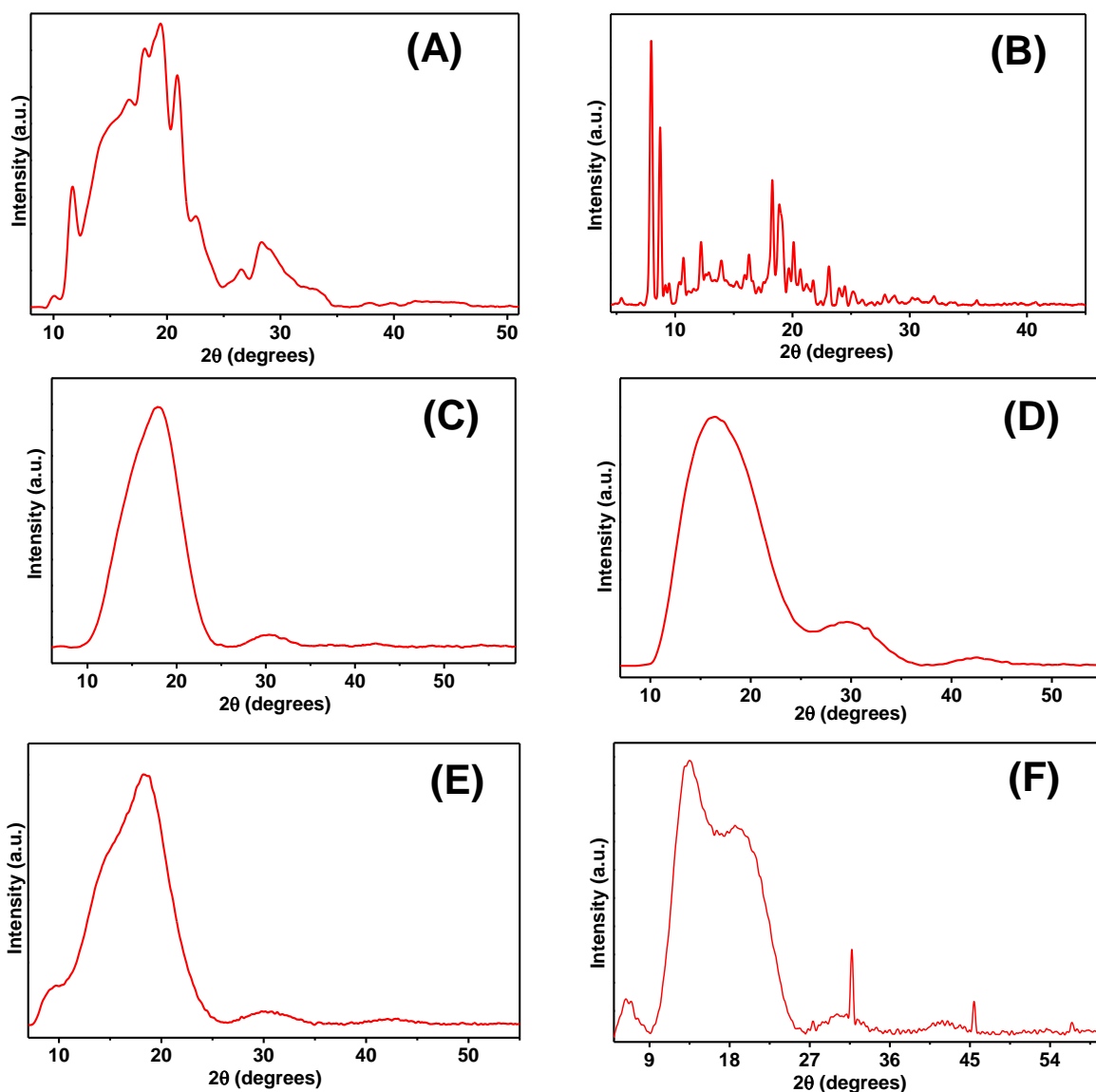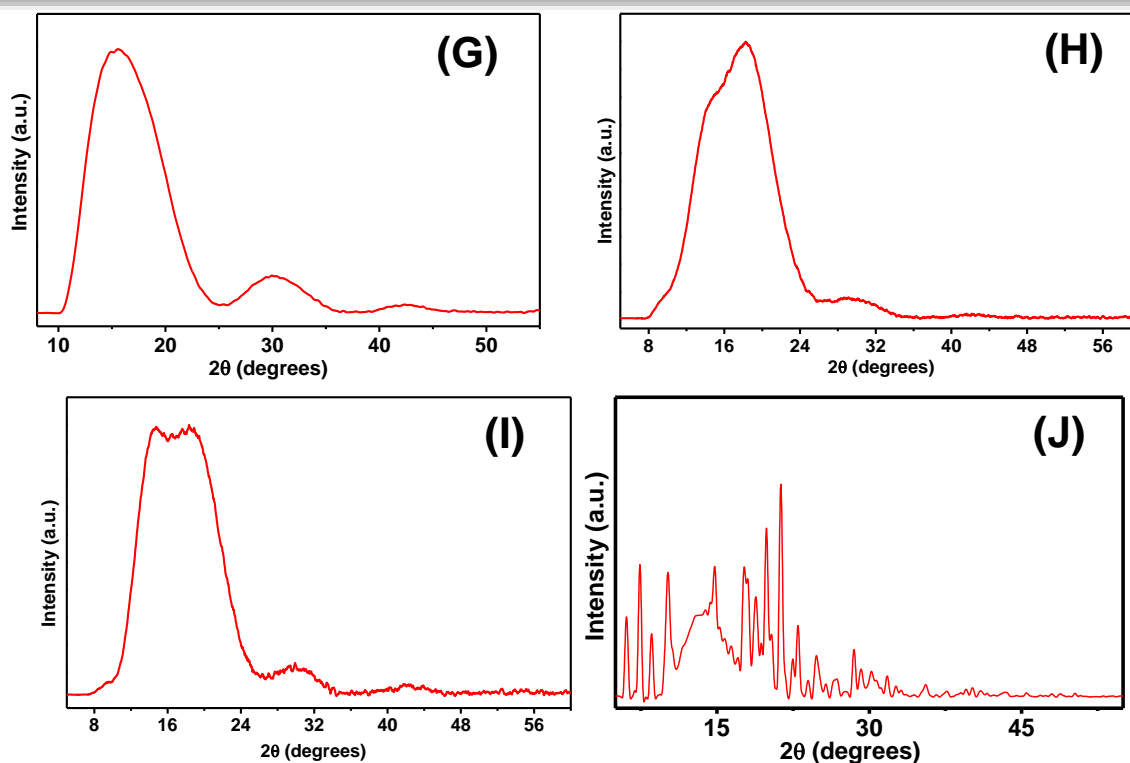
**Figure 2.4**: PXRD patterns of (A) peptide **2** (Boc-Phe-Phe-Propyne); (B) peptide **4** (Boc-Leu-Leu-Propyne); (C) peptide **7** [Boc-Phe-Phe-*tz*-A$^{N(Boc)2}$]; (D) peptide **8** (Boc-Phe-Phe-*tz*-A$^{NH2}$); (E) peptide **10** [Boc-Leu-Leu-*tz*-A$^{N(Boc)2}$]; (F) peptide **9** (H-Phe-Phe-*tz*-A$^{NH2}$); (G) peptide **12** [Boc-Phe-Phe-*am*-A$^{N(Boc)2}$]; (H) peptide **18** (Boc-Phe-Phe-*tz*-U); (I) peptide **19** (Boc-Phe-Phe-*tz*-T) and (J) Boc-Phe-Phe-OMe.

**2.3.1d Contact angle measurement**: The self-organization of peptides originates from weak forces such as H-bonding, π-π, ionic, and hydrophobic interactions. The extent of molecular hydrophobicity of peptides was determined through the contact angle (CA) measurements by addition of nanodroplets of water on a thin layer of peptides on glass surface (Figure 2.5). The CA values are referenced to CA measurement on bare glass surface and CA > 90° indicate high hydrophobicity.[28] The CA data revealed that protected and partially protected peptides **(7, 8, 10, 12, 18** and **19)** are moderately hydrophobic in nature with CA values above 80° with almost similar values for peptides **7**, **8** and **10**. The Boc-Phe-Phe-*tz*-A$^{NH2}$ peptide **8** lacking two hydrophobic Boc groups are almost as hydrophobic as peptide **7** [Boc-Phe-Phe-*tz*-A$^{N(Boc)2}$]. On the other hand, the adenine analogue of peptide **7**, Boc-Leu-Leu-*tz*-A$^{N(Boc)2}$ **(10)** showed similar contact angle (CA 84°) with almost equal hydrophobicity. A lower CA value for triazole peptide compared to amido peptide **12** (CA 93°) indicated trizole linker to be more hydrophilic nature than the amide bond. The fully deprotected peptide **9** (H-Phe-Phe-*tz*-A$^{NH2}$) had low CA value (32°), less than the CA of bare glass surface (60°).
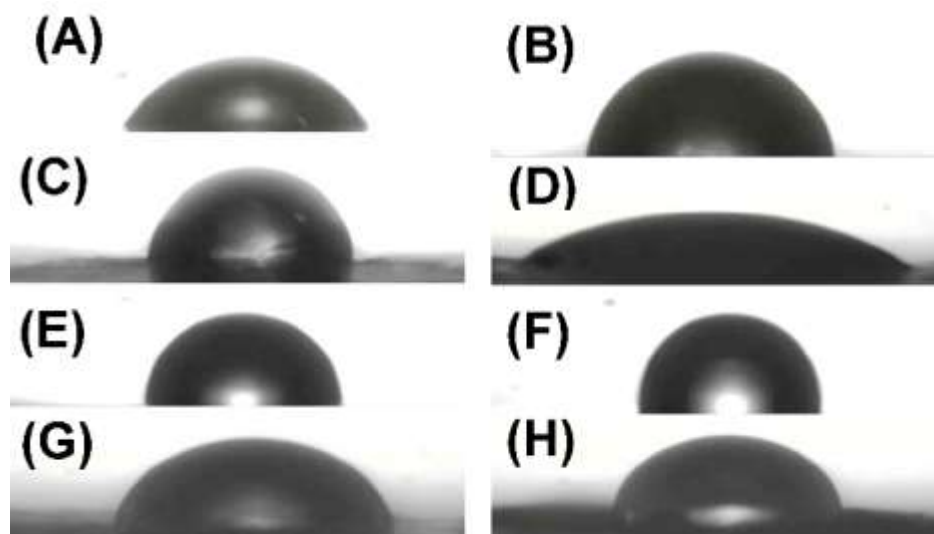
**Figure 2.5**: Water droplet images captured after 2 seconds on substances for measuring contact angles of (A) bare glass; (B) peptide **7** [Boc-Phe-Phe-*tz*-A$^{N(Boc)2}$]; (C) peptide **8** (Boc-Phe-Phe-*tz*-A$^{NH2}$); (D) peptide **9** (H-Phe-Phe-*tz*-A$^{NH2}$); (E) peptide **10** [Boc-Leu-Leu-*tz*-A$^{N(Boc)2}$]; (F) peptide **12** [Boc-Phe-Phe-*am*-A$^{N(Boc)2}$]; (G) peptide **18** (Boc-Phe-Phe-*tz*-U) and (H) peptide **19** (Boc-Phe-Phe-*tz*-T).

It was interesting to note that the pyrimidine nucleoside conjugated peptides (**18** and **19**) had appreciably low CA values (73° and 75° for U and T analogues respectively) than the corresponding purine conjugated derivatives **10** and **12** (83° and 93°) indicating higher hydrophobicity of purines. The data in (Table 2.2) and (Figure 2.5) show that the peptide Boc-Phe-Phe-*am*-A$^{N(Boc)2}$ (**12**) is least hydrophilic and wettable, whereas the peptide H-Phe-Phe-*tz*-A$^{NH2}$ (**9**) was the most hydrophilic in nature. This points strongly to the role of N- and C- terminal groups in dictating the hydrophobicity of peptides.

**Table 2.2**: Contact angle (CA) measured for peptides on glass surface.

| Sample/Surface | Contact angle (CA in degree)[a] | ΔCA (in degree) |
|---|---|---|
| Bare glass | 60 ± 2 | - |
| Peptide **7** Boc-Phe-Phe-*tz*-A$^{N(Boc)2}$ | 84 ± 2 | +24 |
| Peptide **8** Boc-Phe-Phe-*tz*-A$^{NH2}$ | 81 ± 1 | +21 |
| Peptide **9** H-Phe-Phe-*tz*-A$^{NH2}$ | 32 ± 2 | −28 |
| Peptide **10** Boc-Leu-Leu-*tz*-A$^{N(Boc)2}$ | 83 ± 2 | +23 |
| Peptide **12** Boc-Phe-Phe-*am*-A$^{N(Boc)2}$ | 93 ± 1 | +33 |
| Peptide **18** Boc-Phe-Phe-*tz*-U | 73 ± 2 | +13 |
| Peptide **19** Boc-Phe-Phe-*tz*-T | 75 ± 2 | +15 |

[a] Data are the mean ± SD (n=4)

**2.3.1e IR data of peptides**: To identify the role of H-bonding from amide bonds involved in peptide secondary structures, FTIR data (Figure 2.6) were recorded. The peptides **7** [Boc-Phe-Phe-*tz*-A$^{N(Boc)2}$], **8** (Boc-Phe-Phe-*tz*-A$^{NH_2}$), **10** [Boc-Leu-Leu-*tz*-A$^{N(Boc)2}$] and **12** [Boc-Phe-Phe-*am*-A$^{N(Boc)2}$] displayed broad NH stretching vibration ($v_{NH}$) at 2980 cm$^{-1}$ in FTIR. The amide I due to C=O stretching frequency for backbone conformation[35] was found at 1646 cm$^{-1}$ for peptides **7**, **8**, **10** and **12** and shifted to 1670 cm$^{-1}$ for peptide **9** (H-Phe-Phe-*tz*-A$^{NH_2}$). For pyrimidine nucleoside conjugated peptide **18** (Boc-Phe-Phe-*tz*-U) and **19** (Boc-Phe-Phe-*tz*-T) the amide I bands were observed at 1677 and 1660 cm$^{-1}$ respectively. This observation confirmed a β-sheet like conformation for the peptides.[35]
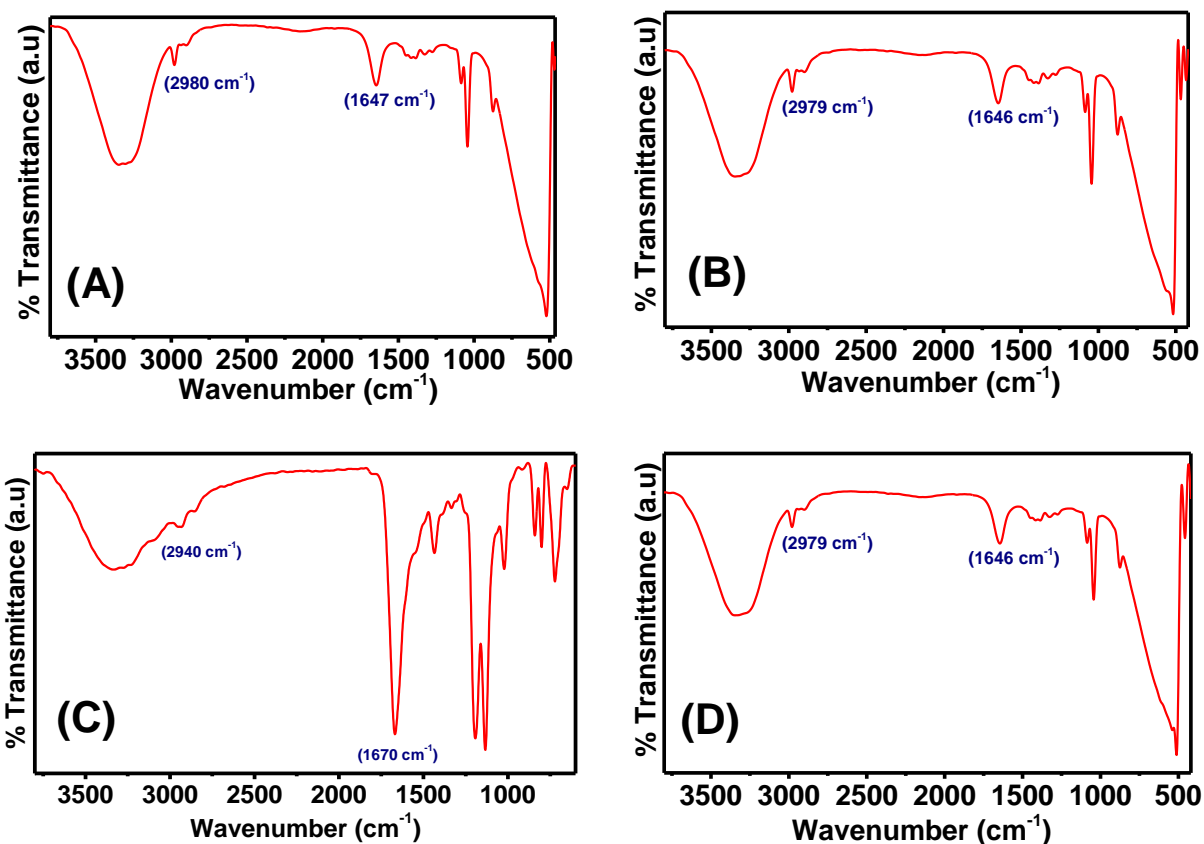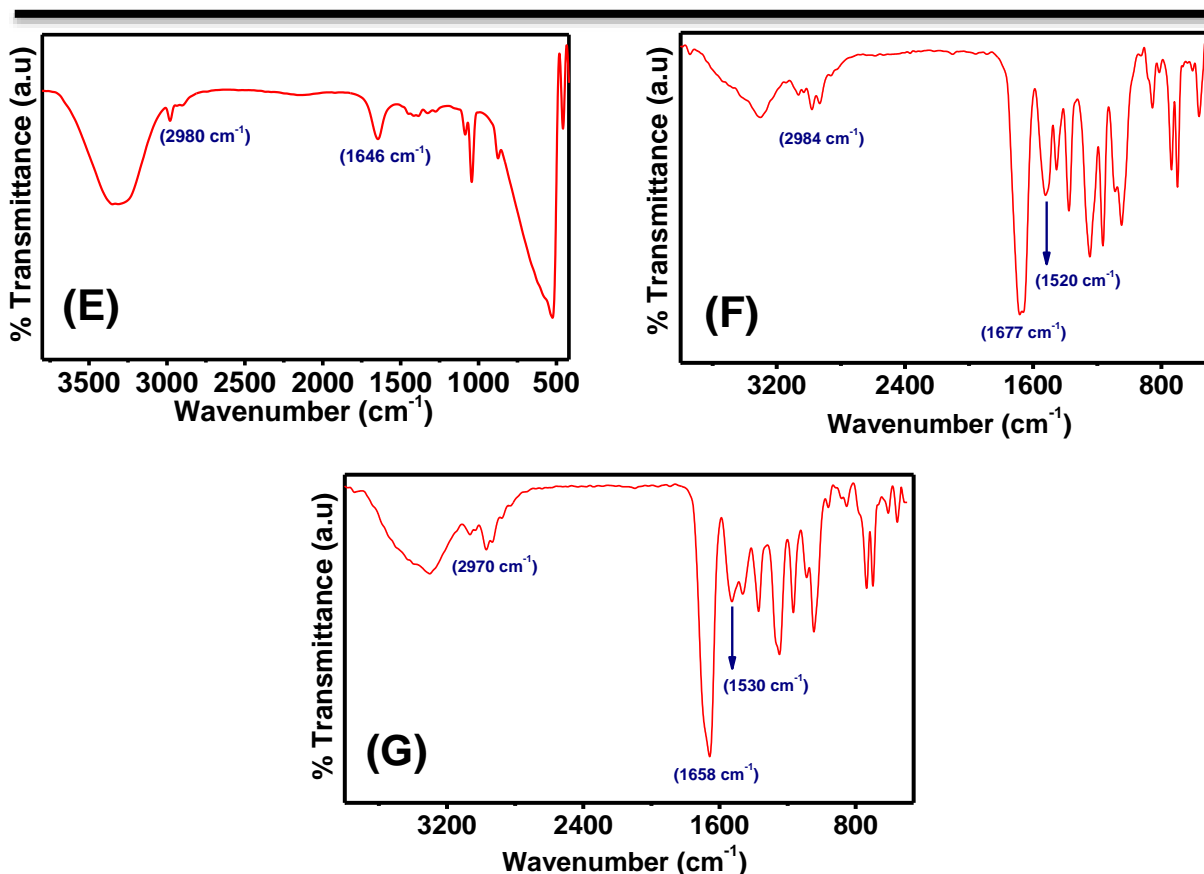
**Figure 2.6**: FTIR spectra of (A) peptide **7** [Boc-Phe-Phe-*tz*-A$^{N(Boc)2}$]; (B) peptide **8** (Boc-Phe-Phe-*tz*-A$^{NH2}$); (C) peptide **9** (H-Phe-Phe-*tz*-A$^{NH2}$); (D) peptide **10** [Boc-Leu-Leu-*tz*-A$^{N(Boc)2}$]; (E) peptide **12** [Boc-Phe-Phe-*am*-A$^{N(Boc)2}$]; (F) peptide **18** (Boc-Phe-Phe-*tz*-U) and (G) peptide **19** (Boc-Phe-Phe-*tz*-T).

### 2.3.2 Morphologies and microscopic architectures

The self-assembly of peptides are best manifested by formation of their nanostructures and morphology of such structures were visualised by FESEM, HRTEM and AFM images.

**2.3.2a Morphologies of the peptides**: The morphological features of the molecular self-assembles of the synthesized peptides were examined after preparation of the samples by standard protocols (see experimental section) and drop casted on silicon wafers / copper grid for recording SEM, AFM and HRTEM images. The peptide ester Boc-Phe-Phe-OMe exhibited thick fibrillar structures compared to discrete fibrillar rods reported earlier,[19] which is attributable to differences in sample preparation and incubation time (Figure 2.7A). In comparison, the propargylated dipeptide Boc-Phe-Phe-Propyne (**2**) displayed dense aggregated fibres (Figure 2.7B and 2.8A), while the

propargylated leucine analogue **4** (Boc-Leu-Leu-Propyne) showed short hollow nanotube structures (Figure 2.7C, 2.8B and C).
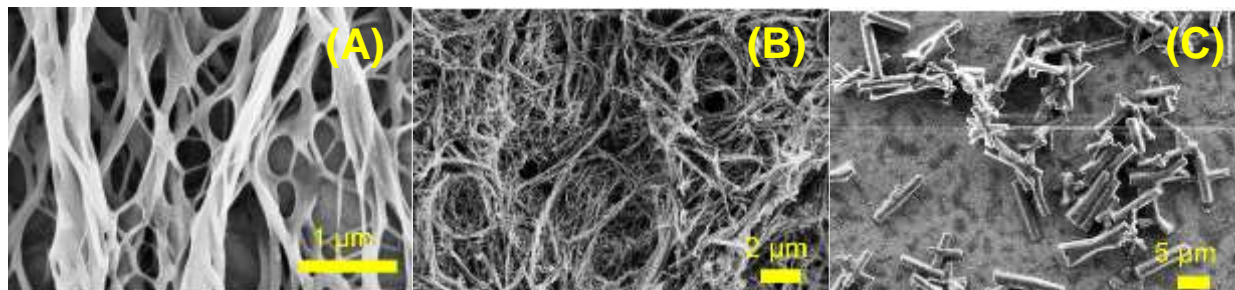


**Figure 2.7**: SEM images of (A) Boc-Phe-Phe-OMe; (B) dipeptide **2** (Boc-Phe-Phe-Propyne) and (C) dipeptide **4** (Boc-Leu-Leu-Propyne).
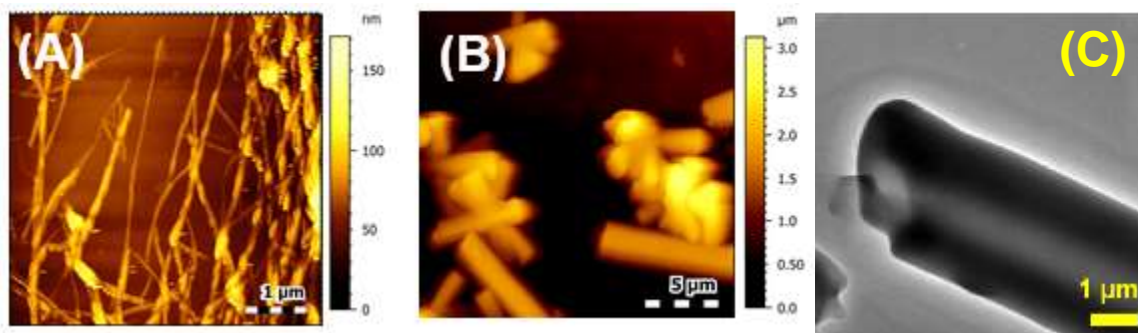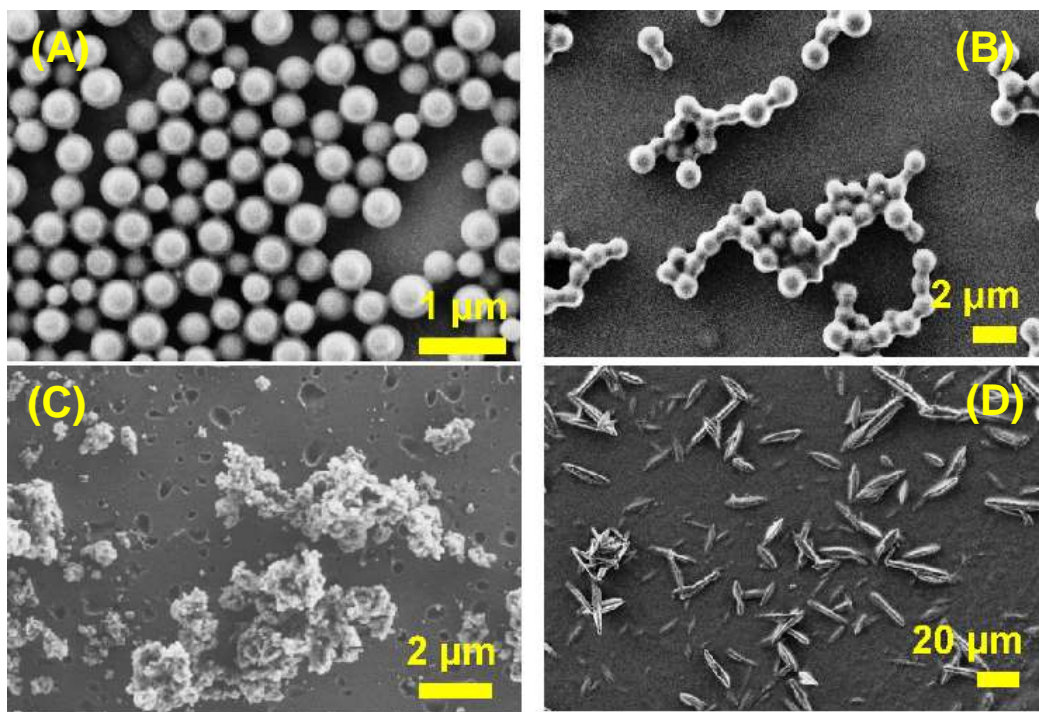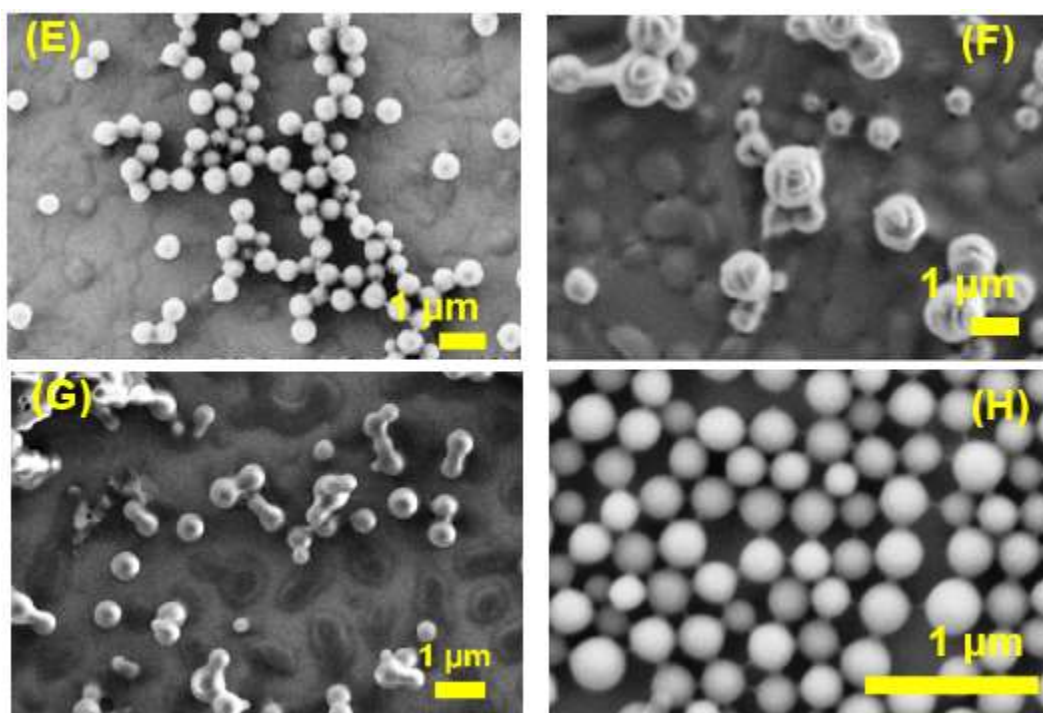


**Figure 2.8**: AFM images of (A) dipeptide **2** (Boc-Phe-Phe-Propyne); (B) dipeptide **4** (Boc-Leu-Leu-Propyne) and (C) HRTEM image of dipeptide **4** (Boc-Leu-Leu-Propyne).

After click-conjugation of adenosine with dipeptide **2**, well-distributed spherical nanoparticles was observed (Figure 2.9A) for peptide **7** [Boc-Phe-Phe-*tz*-A$^{N(Boc)_2}$] whereas, corresponding leucine analogue **10** [Boc-Leu-Leu-*tz*-A$^{N(Boc)_2}$] elicited spindle shaped morphology which might be derived from the crystalline nature of its precursor peptide Boc-Leu-Leu-Propyne (**4**) (Figure 2.9D). In contrast, absence of two Boc groups in peptide **8** (Boc-Phe-Phe-*tz*-A$^{NH_2}$) lead to interlinked spherical particles (Figure 2.9B) which was not observed for Boc containing peptide **7** [Boc-Phe-Phe-*tz*-A$^{N(Boc)_2}$]. This phenomenon occurred probably due to a better H-bonding ability of Boc-Phe-Phe-*tz*-A$^{NH_2}$ with solvent molecules or self-pairing and leading to molecular necklace formation. It was observed that the fully and partially protected peptides **7** and **8** exhibited self-assembled spherical particles, whereas the completely deprotected peptide **9** (H-Phe-Phe-*tz*-A$^{NH_2}$) was devoid of any morphology. It exhibited irregular aggregates of small particles (Figure 2.9C).

The comparative SEM images of peptides **7** (Figure 2.9A) and **12** [Boc-Phe-Phe-*am*-A$^{N(Boc)_2}$] (Figure 2.9E) indicate no change in self-assembled morphology confirming that replacement of the triazole linker by amide did not affect the shape of self-assembled nanostructure. It was also noted that, pyrimidine nucleosides uridine and thymidine conjugated diphenylalanine analogues **18** (Boc-Phe-Phe-*tz*-U) (Figure 2.9F) and **19** (Boc-Phe-Phe-*tz*-T) exhibited poor self-assembling abilities (Figure 2.9G) than their purine counterpart peptide **7** and peptide **8**. Here, the free form of nucleobases in peptide **18** and **19** (uracil and thymine respectively) could not lead to any special morphology like 'molecular necklace' observed for peptide **8**. The nanospheres formed after self-assembly of these two peptides were neither prominent and nor well organized in nature which may be attributed to the less π-π staking abilities of pyrimidine nucleosides than the purine analogue adenosine. On the other hand, the Fmoc analogue of peptide **7**, Fmoc-Phe-Phe-*tz*-A$^{N(Boc)_2}$ **(15)** exhibited perfectly spherical nanoparticles with an average diameter of 250 nm (Figure 2.9H).
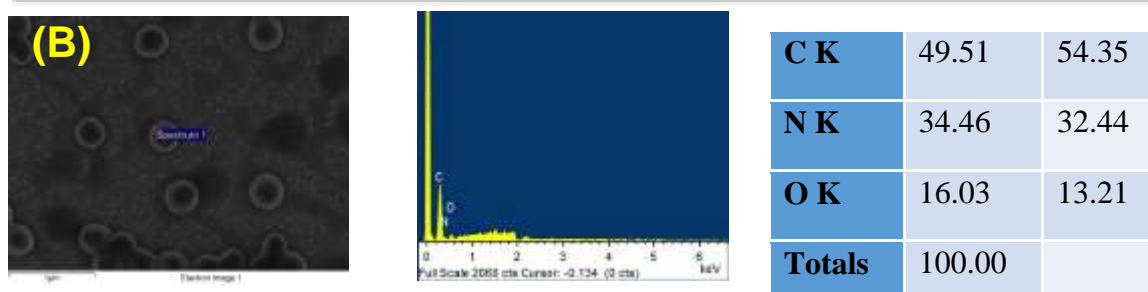
**Figure 2.9**: SEM images of (A) peptide **7** [Boc-Phe-Phe-*tz*-A$^{N(Boc)2}$]; (B) peptide **8** (Boc-Phe-Phe-*tz*-A$^{NH2}$); (C) peptide **9** (H-Phe-Phe-*tz*-A$^{NH2}$); (D) peptide **10** [Boc-Leu-Leu-*tz*-A$^{N(Boc)2}$]; (E) peptide **12** [Boc-Phe-Phe-*am*-A$^{N(Boc)2}$]; (F) peptide **18** (Boc-Phe-Phe-*tz*-U); (G) peptide **19** (Boc-Phe-Phe-*tz*-T) and (H) peptide **15** [Fmoc-Phe-Phe-*tz*-A$^{N(Boc)2}$].

Further, from EDX analysis it is clear that Boc-Phe-Phe-*tz*-A$^{N(Boc)2}$ and Boc-Phe-Phe-*am*-A$^{N(Boc)2}$ both contain carbon (C), nitrogen (N) and oxygen (O) elements proving the elemental composition of the compounds (Figure 2.10A and B).
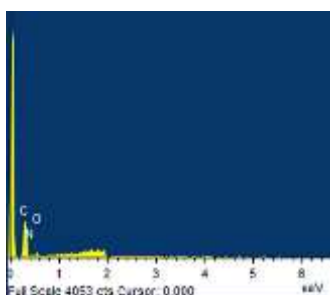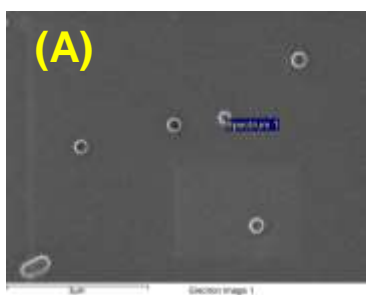


| | | |
|---|---|---|
| **C K** | 49.74 | 54.83 |
| **N K** | 30.51 | 28.83 |
| **O K** | 19.75 | 16.34 |
| **Totals** | 100.00 | |

| (B) | | |
|---|---|---|
| **C K** | 49.51 | 54.35 |
| **N K** | 34.46 | 32.44 |
| **O K** | 16.03 | 13.21 |
| **Totals** | 100.00 | |

**Figure 2.10**: EDX image of (A) peptide **7** [Boc-Phe-Phe-*tz*-A$^{N(Boc)2}$] and (B) peptide **12** [Boc-Phe-Phe-*am*-A$^{N(Boc)2}$].

For AFM studies the peptide solutions were drop-casted on silicon wafers to avoid influence of surface during self-assembly process observed in SEM. In AFM we observed perfect spherical morphology for peptides **7** [Boc-Phe-Phe-*tz*-A$^{N(Boc)2}$], necklace like interlinked spheres for **8** (Boc-Phe-Phe-*tz*-A$^{NH2}$), spindle like of peptide **10** [Boc-Leu-Leu-*tz*-A$^{N(Boc)2}$] and spherical particles of peptide **12** [Boc-Phe-Phe-*am*-A$^{N(Boc)2}$] (Table 2.3). Also the height profiles obtained from AFM data of [Boc-Phe-Phe-*tz*-A$^{N(Boc)2}$] and [Boc-Phe-Phe-*am*-A$^{N(Boc)2}$] (Figure 2.11A and B) supports the size obtained from the SEM. For peptide **18** (Boc-Phe-Phe-*tz*-U) and **19** (Boc-Phe-Phe-*tz*-T), nanospheres became less pronounced while fully deprotected peptide **9** (H-Phe-Phe-*tz*-A$^{NH2}$) showed only disordered structures. The results were in good agreement with the particle size and dimension obtained from SEM results (Table 2.3).

**Table 2.3**: Comparative self-assembled morphologies of Phe-Phe nucleoside conjugates.

| Peptide | SEM | AFM | HRTEM |
|---|---|---|---|
| **7** [Boc-Phe-Phe-*tz*-A$^{N(Boc)2}$] |  |  |  |
| **8** (Boc-Phe-Phe-*tz*-A$^{NH2}$) |  |  |  |

**9** (H-Phe-Phe-*tz*-A^NH2^)

**12** [Boc-Phe-Phe-*am*-A^N(Boc)2^]

**18** (Boc-Phe-Phe-*tz*-U)

**19** (Boc-Phe-Phe-*tz*-T)

**(A)**

**(B)**
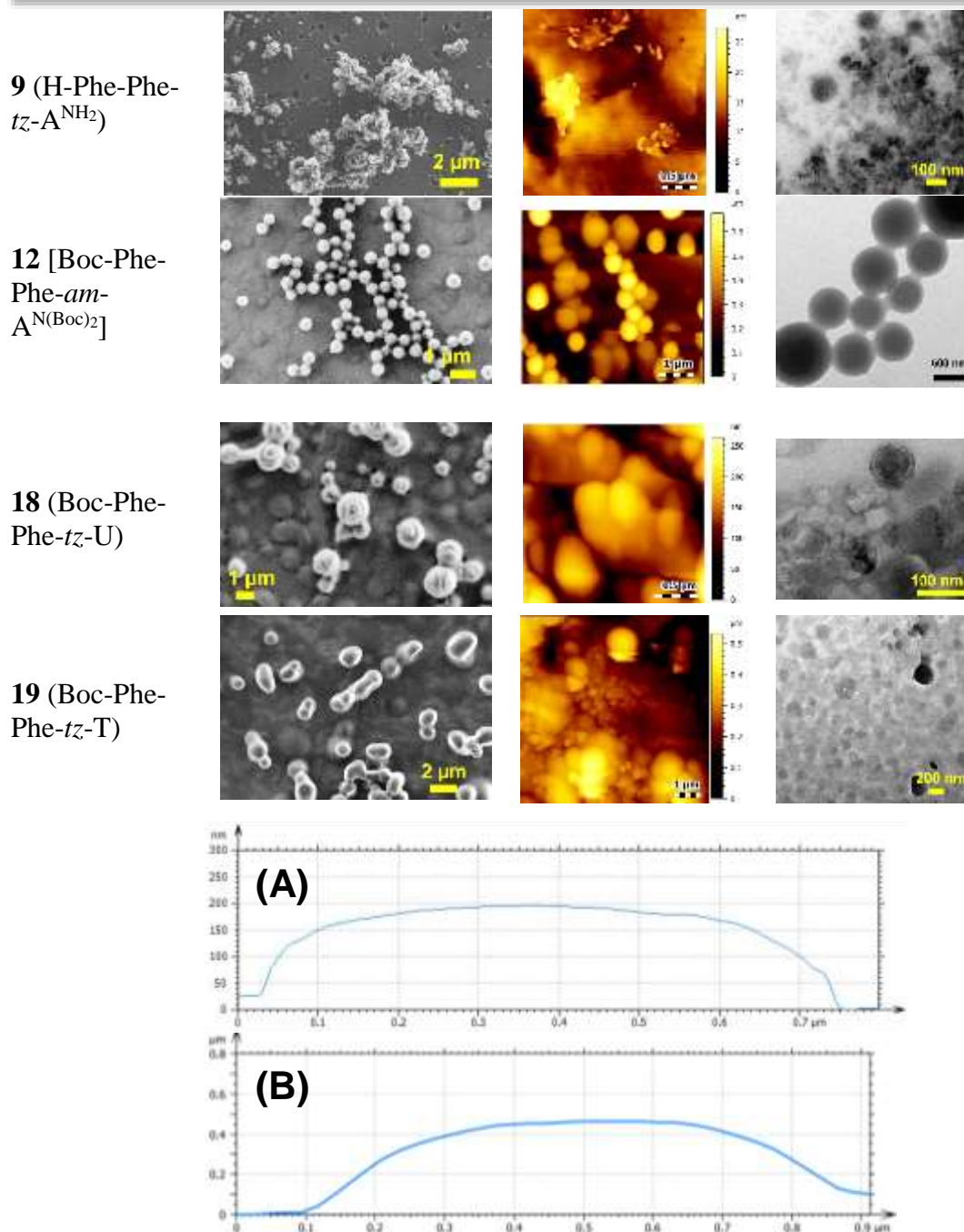
**Figure 2.11**: Height profile diagrams of perfect spheres of **(A)** peptide **7** [Boc-Phe-Phe-*tz*-A^N(Boc)2^] and **(B)** peptide **12** [Boc-Phe-Phe-*am*-A^N(Boc)2^] obtained from AFM.

HRTEM images corroborated well with the morphologies observed by SEM and AFM. The core-shell like spheres for peptide **7** [Boc-Phe-Phe-*tz*-A^N(Boc)2^] and peptide **12** [Boc-Phe-Phe-*am*-A^N(Boc)2^] were evident. Peptide **8** (Boc-Phe-Phe-*tz*-A^NH2^) exhibited rapid self-aggregation

tendency and interlinked solid spheres was observed. Better H-bonding abilities of peptide **8** than the fully protected analogue **7**, lead to interlinked necklace-like spherical particles.

In absence of any hydrophobic substituent, peptide **9** (H-Phe-Phe-*tz*-A$^{NH_2}$) elicited disordered structures. The pyrimidine-clicked peptides **18** (Boc-Phe-Phe-*tz*-U) and **19** (Boc-Phe-Phe-*tz*-T) furnished less defined spherical particles in HRTEM. The wide range of microscopic self-assembly of these peptides observed suggests that the hydrophobic substituent at N/C-termini and aromatic π-π interaction play an important role in dictating the final shape of nanoparticles from the nucleobase conjugated Phe-Phe peptides.

Considering the mono disperse nature and lower aggregation tendency of peptide **7** [Boc-Phe-Phe-*tz*-A$^{N(Boc)_2}$], we examined the effect of increasing peptide concentration from 1 mg/mL to 4 mg/mL on self-assembly (Figure 2.12). Here, the observed size of the spherical particle increased remarkably up to ~ 2 µm which happened most possibly due to the deposition of additional layers of peptide molecules on the initially formed spherical particles. Such growth of particles observed in SEM images and confirmed from AFM and HRTEM images (Figure 2.12A, B and C). Similarly, the effect of increased concentration of peptide **8** and peptide **9** was followed (Figure 2.13A and B) which indicated an increment of nanoparticle size and agglomeration respectively.
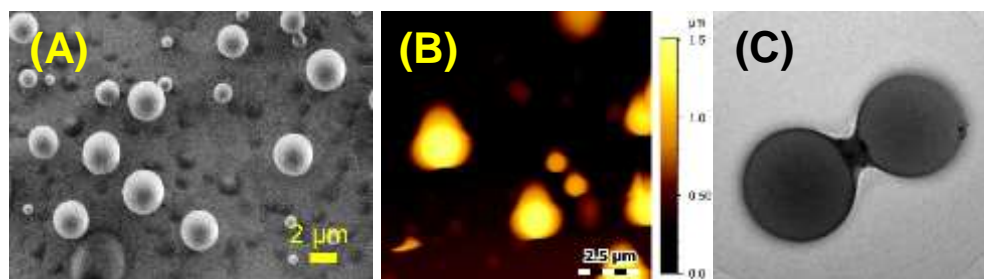


**Figure 2.12**: (A) SEM image; (B) AFM image and (C) HRTEM image of peptide **7** [Boc-Phe-Phe-*tz*-A$^{N(Boc)_2}$] with high concentration (4 mg /mL).
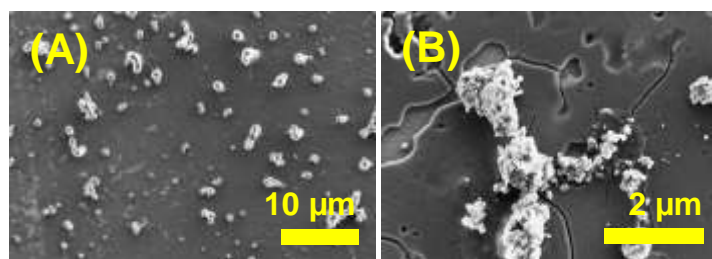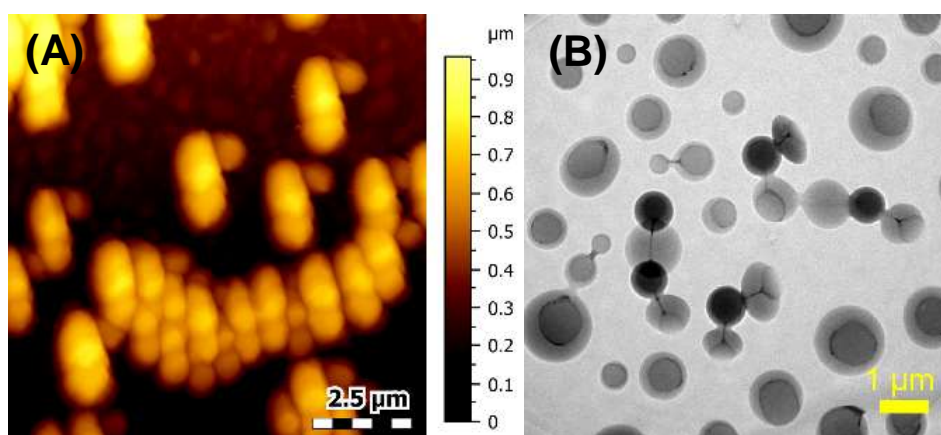


**Figure 2.13**: SEM images of (A) peptide **8** [Boc-Phe-Phe-*tz*-A$^{NH_2}$] and (B) peptide **9** [H-Phe-Phe-*tz*-A$^{NH_2}$] with higher concentration (4 mg / mL).

The size and shape of peptide **7** were monitored upon incubation in 50% ethanol and water for 15 days at room temperature. At different time intervals of 3, 6 and 10 days, the stable spherical particles were found (Figure 2.14A-C). Beyond 10 days of incubation, formation of 'molecular necklace' was observed which is a well-known phenomenon for Phe-Phe peptides[29,30] (Figure 2.15). The molecular necklace arises from head to tail linear linking of neighbouring nanospheres attached through microscopic elongated threads (Figure 2.15B). The lengths of the fused structures were found to be lesser than the summation of the equal number of individual particles in SEM and AFM which was further confirmed by the height profile obtained from AFM data (Figure 2.16).
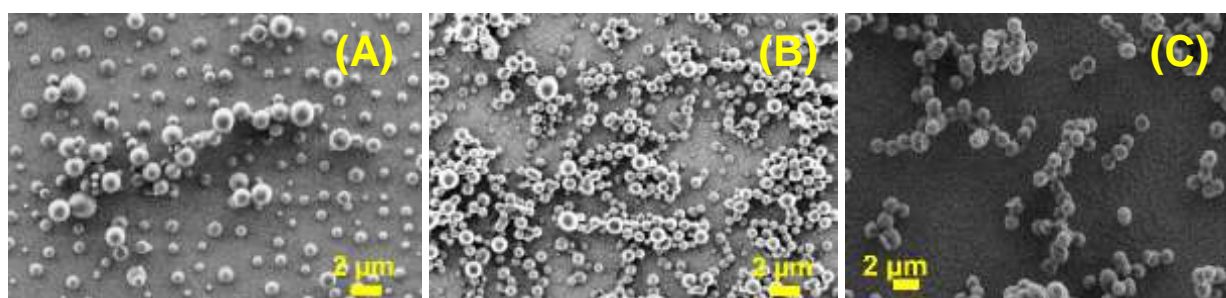


**Figure 2.14**: SEM images of peptide **7** [Boc-Phe-Phe-*tz*-A$^{N(Boc)2}$] after (A) 3 days; (B) 6 days and (C) 10 days of incubation (concentration = 1 mg / mL).



**Figure 2.15**: (A) AFM and (B) HRTEM images of peptide **7** [Boc-Phe-Phe-*tz*-A$^{N(Boc)2}$] after 10 days of incubation.
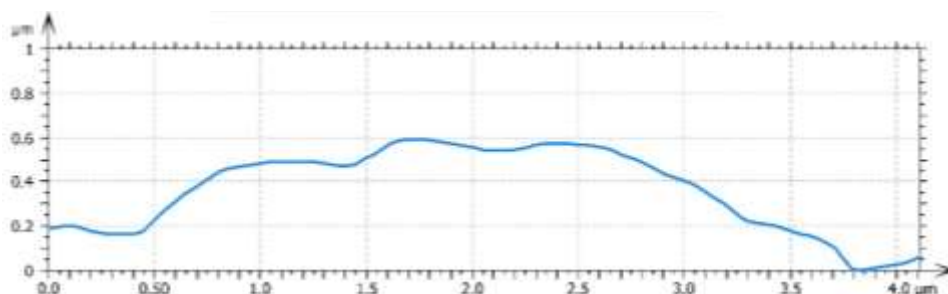
**Figure 2.16**: Height profile diagrams of aggregated peptide **7** [Boc-Phe-Phe-*tz*-A$^{N(Boc)2}$] after 10 days of incubation obtained from AFM.

**2.3.2b DLS studies for peptide 7 [Boc-Phe-Phe-*tz*-A$^{N(Boc)2}$]**: The size distribution of nanospheres in solution analysed from DLS studies (Figure 2.17) showed distribution of diameter in the range 580-1120 nm for peptide **7** [Boc-Phe-Phe-*tz*-A$^{N(Boc)2}$] depending on its concentration or incubation time. Irrespective of lyophilisation process in 1,1,1,3,3,3-hexafluoro-2-propanol (HFIP), the peptide **7** [Boc-Phe-Phe-*tz*-A$^{N(Boc)2}$] consistently produced nanoparticles ranging between 500-650 nm with a low polydispersive index (PDI) suggesting mono-dispersed nature of the spherical particles in solution (Figure 2.17A, B and E). Upon aging or increasing the concentration of peptide **7**, the average particle size enhanced up to 1200 nm (Figure 2.17C, D). The higher PDI value of the larger nanoparticles indicated loss of monodisperse nature of peptides in solution. The self-aggregation tendency of peptide **7** with time was observed in SEM, HRTEM and AFM images and quantitatively confirmed by DLS studies.
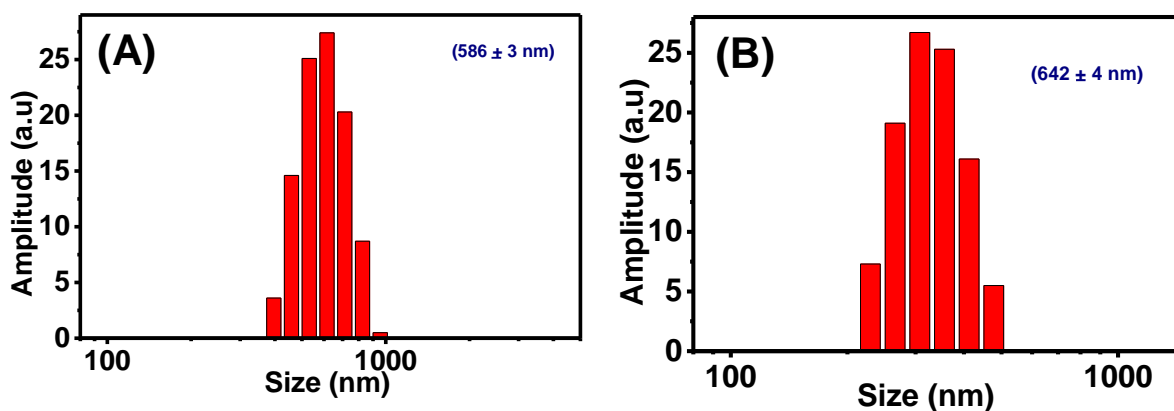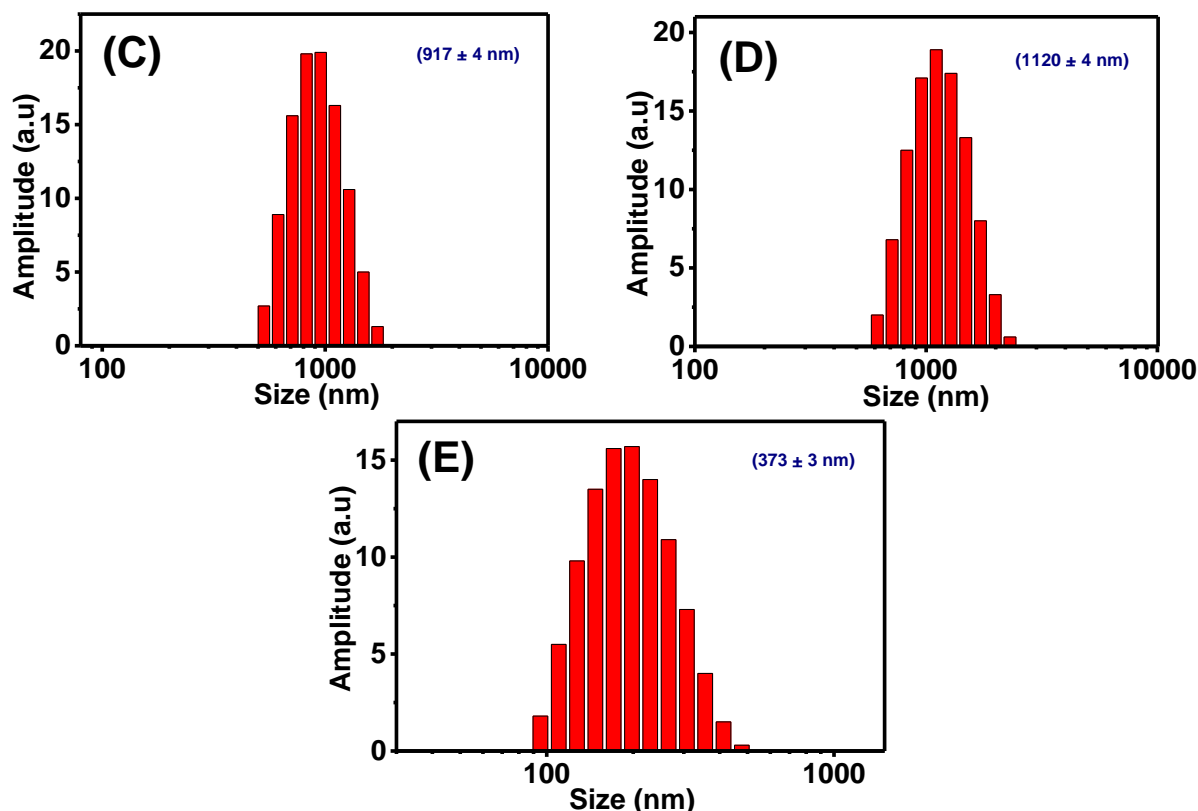
**Figure 2.17**: DLS spectra of (A) peptide **7** [Boc-Phe-Phe-*tz*-A$^{N(Boc)2}$] without lyophilization (PDI = 0.015); (B) peptide **7** after lyophilization (PDI = 0.012); (C) peptide **7** with higher concentration (4 mg/mL, PDI = 0.142); (D) peptide **7** after 10 days of incubation (PDI = 0.224) and (E) peptide **12** [Boc-Phe-Phe-*am*-A$^{N(Boc)2}$] (PDI = 0.168).

**2.3.2c Solvent dependent morphology of peptide 7 [Boc-Phe-Phe-*tz*-A$^{N(Boc)2}$]**: The morphological variations of peptide **7** [Boc-Phe-Phe-*tz*-A$^{N(Boc)2}$] was examined in different solvent combinations. The size and shape of the nanoparticles were independent of lyophilization in HFIP with a very low aggregation tendency. Peptide **7** (1 mg/mL) in neat solvents (toluene, HFIP, ethanol) and in solvent combinations (CH$_3$OH:H$_2$O, THF:H$_2$O and CH$_3$OH:CHCl$_3$) formed nanospheres (Figure 2.18); although, the distribution, size, and shape of particles were not as good as in 50% ethanol in water. In pure hydrophobic solvents like HFIP and toluene, the particle size reduced to ≤ 200 nm, suggesting that water molecules play a vital role for the self-assembly process of the peptide. In pure isopropanol, no spherical particle formation was observed but aggregated micro plates were obtained.
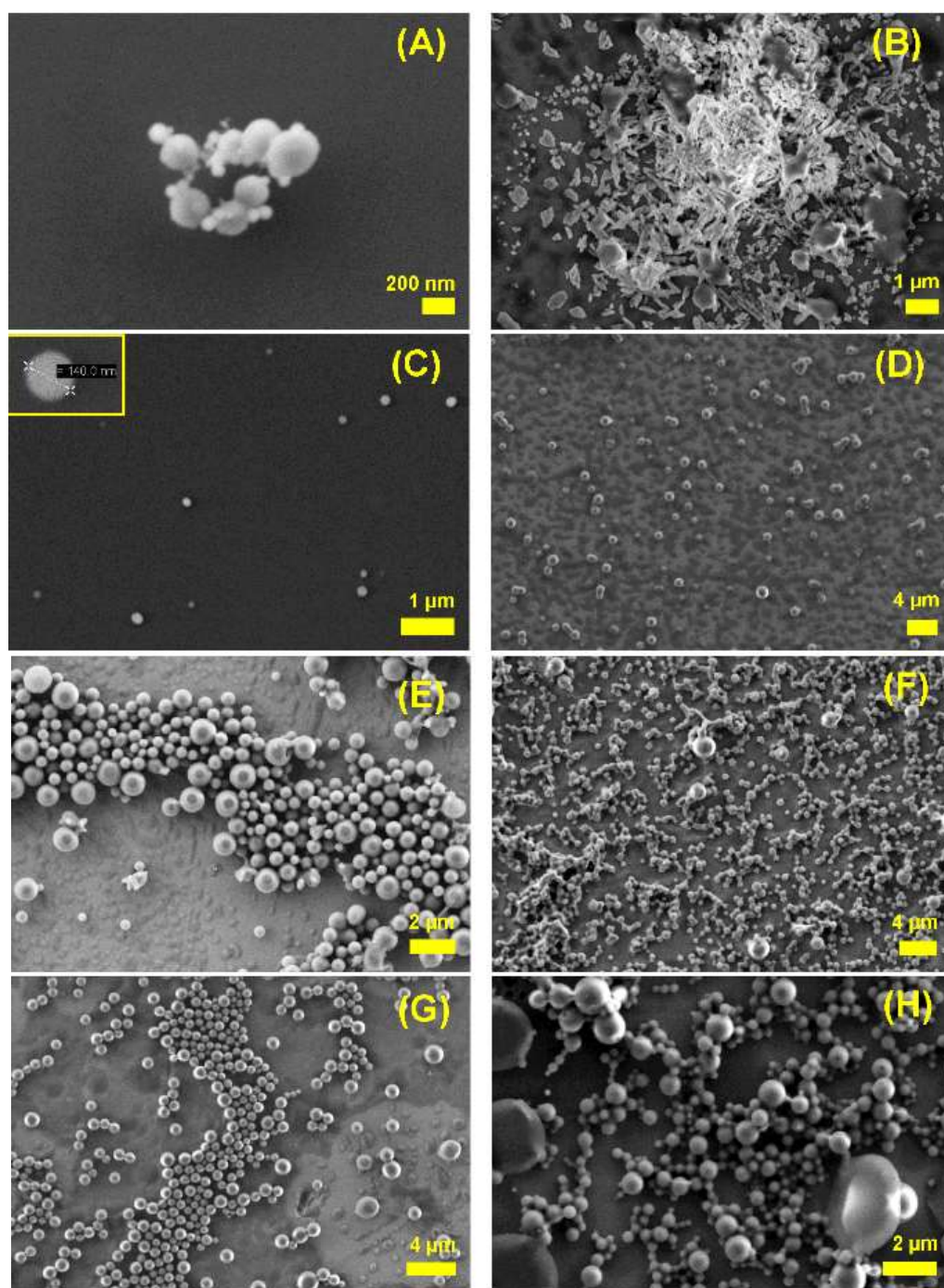
**Figure 2.18**: Solvent dependent morphology in SEM images of peptide **7** [Boc-Phe-Phe-*tz*-A$^{N(Boc)2}$] (A) in toluene; (B) in isopropyl alcohol; (C) in HFIP; (D) in ethanol; (E) in 7:1 MeOH and water; (F) in 1:1 MeOH and water; (G) in 1:1 CHCl$_3$ and MeOH and (H) in 1:1 THF and water.

**2.3.3 Effect of external stimuli on peptides**: The peptides **7** [Boc-Phe-Phe-*tz*-A$^{N(Boc)_2}$] and **12** [Boc-Phe-Phe-*am*-A$^{N(Boc)_2}$] showing spherical morphologies were examined for their stabilities under different conditions like temperature, acidity, basicity and external additives.

**2.3.3a Effects of variable pH and metal ions**: It was opined that the triazole ring in peptide **7** [Boc-Phe-Phe-*tz*-A$^{N(Boc)_2}$] can be protonated easily under mild acidic condition (pH 6) which might influence the self-assembled morphology. Thus, nanoparticles from triazole peptide **7** [Boc-Phe-Phe-*tz*-A$^{N(Boc)_2}$] and amide peptide **12** [Boc-Phe-Phe-*am*-A$^{N(Boc)_2}$] were incubated overnight at pH 6, pH 2 and pH 10 and drop-casted on silicon wafers for SEM studies. It was observed that the spherical morphology seen at pHs 6.0 and 10.0 for both peptides completely disappeared at acidic pH 2.0 (Figure 2.19A-C and Figure 2.20A-C). To check the thermal stability of the spherical particles, Peptides **7** and **12** were drop-casted on silicon wafers, dried at room temperature, and then kept at 200 °C for 2 hrs followed by cooling to room temperature for imaging by SEM. It was observed that the peptides retained the spherical morphology (Figure 2.19D,E and Figure 2.20D,E). Again, the effect of metal ions like Cu$^{2+}$ and Zn$^{2+}$ on peptide self-assembly was also examined. It was observed that these two metal ions did not change the morphology of nanoparticles despite the presence of metal ion co-ordinating triazole ring and adenine (Figure 2.21).

Thermal stability was further confirmed from the thermogravimetric analysis (TGA) of the self-assembled peptides **7** [Boc-Phe-Phe-*tz*-A$^{N(Boc)_2}$] and **12** [Boc-Phe-Phe-*am*-A$^{N(Boc)_2}$] which indicated that their stability is >150 °C (Figure 2.22A and B). In TGA, the initial 20% weight loss was attributed to entrapped solvent molecules[8] and significant destruction was observed above 220 °C. Thermal stability was further confirmed when the peptide **7** drop-casted silicon wafer after heat treatment was eluted with methanol and its MALDI-TOF data indicated the mass of parent molecule (Figure 2.23).
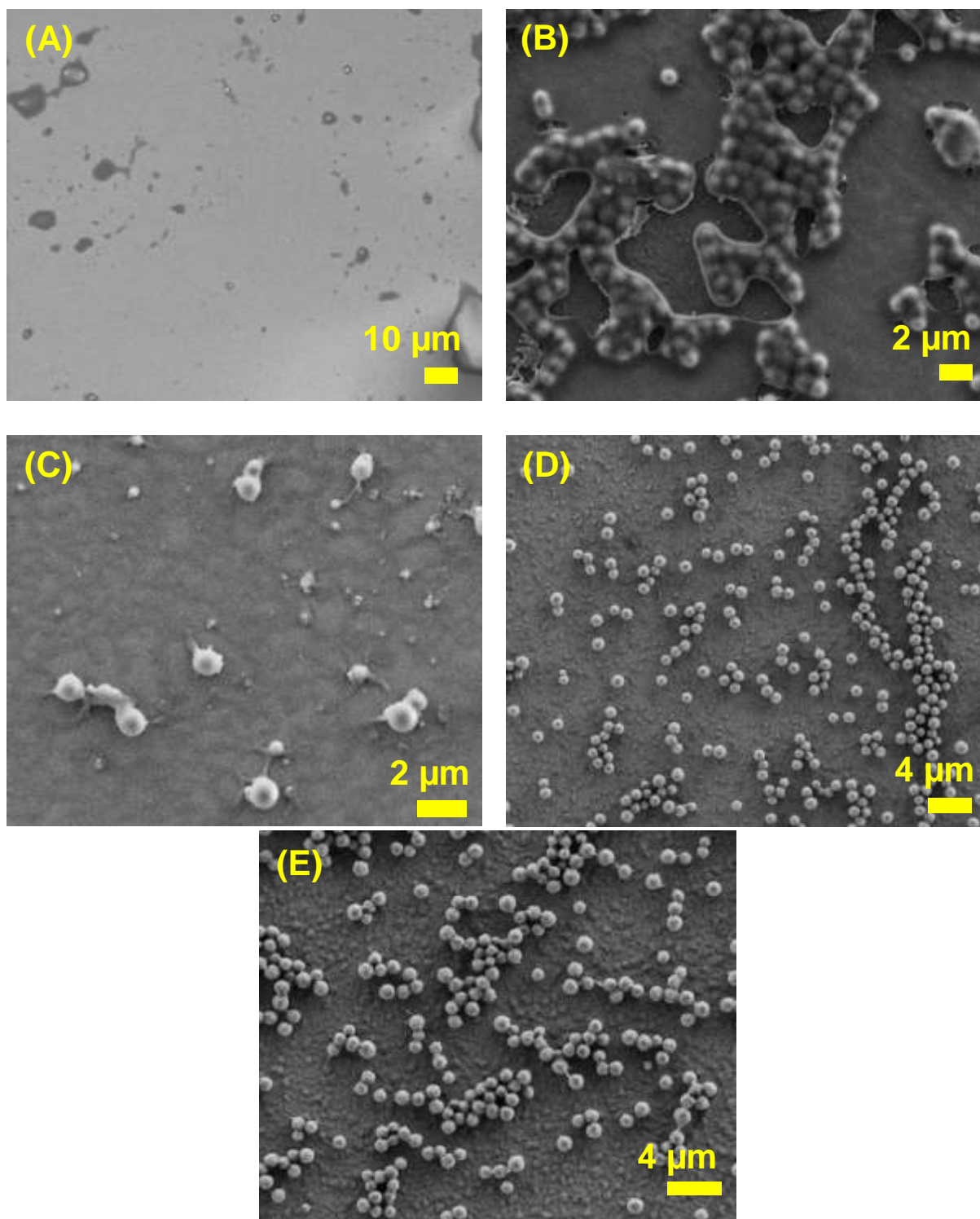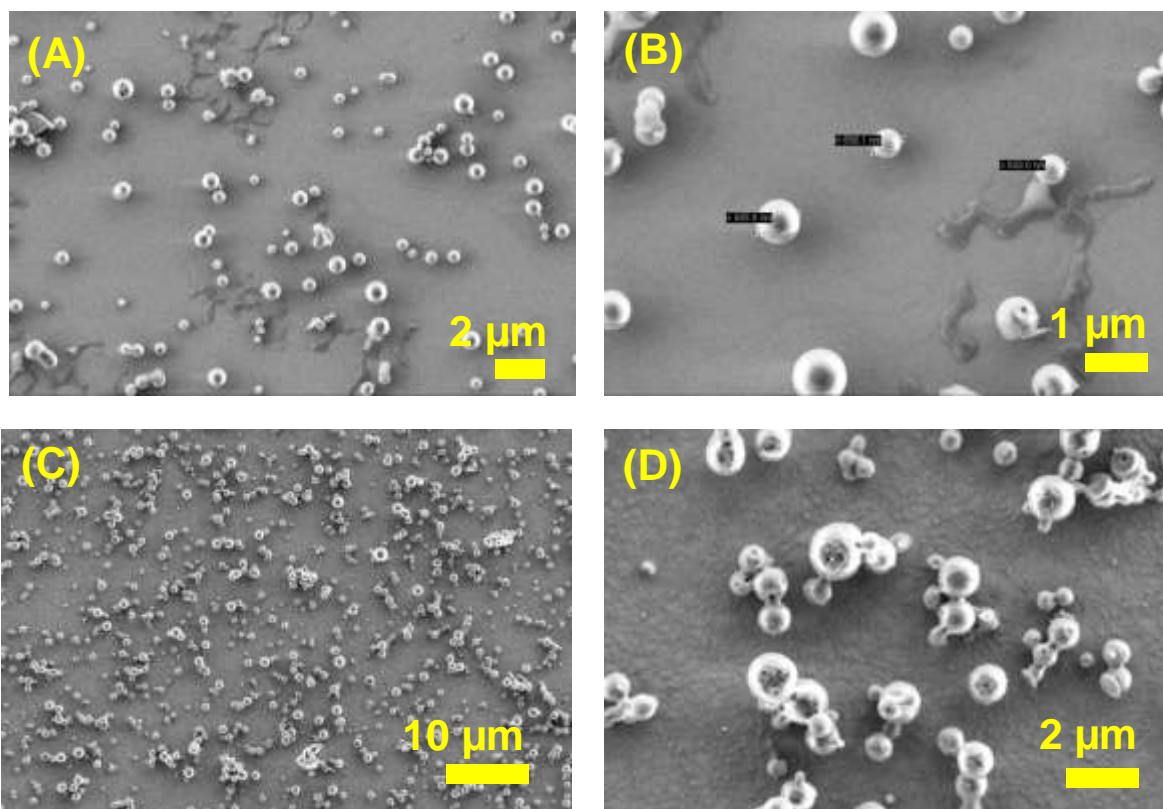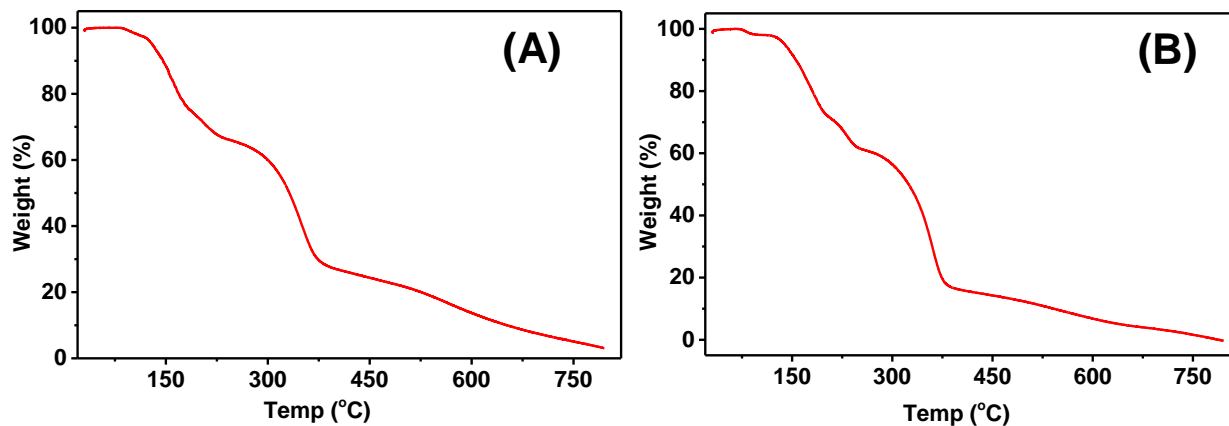
**Figure 2.19**: SEM images of peptide **7** [Boc-Phe-Phe-*tz*-A$^{N(Boc)2}$] (A) at pH 2; (B) at pH 6; (C) at pH 10; (D) after heating at 100 ºC and (E) after heating at 200 ºC.
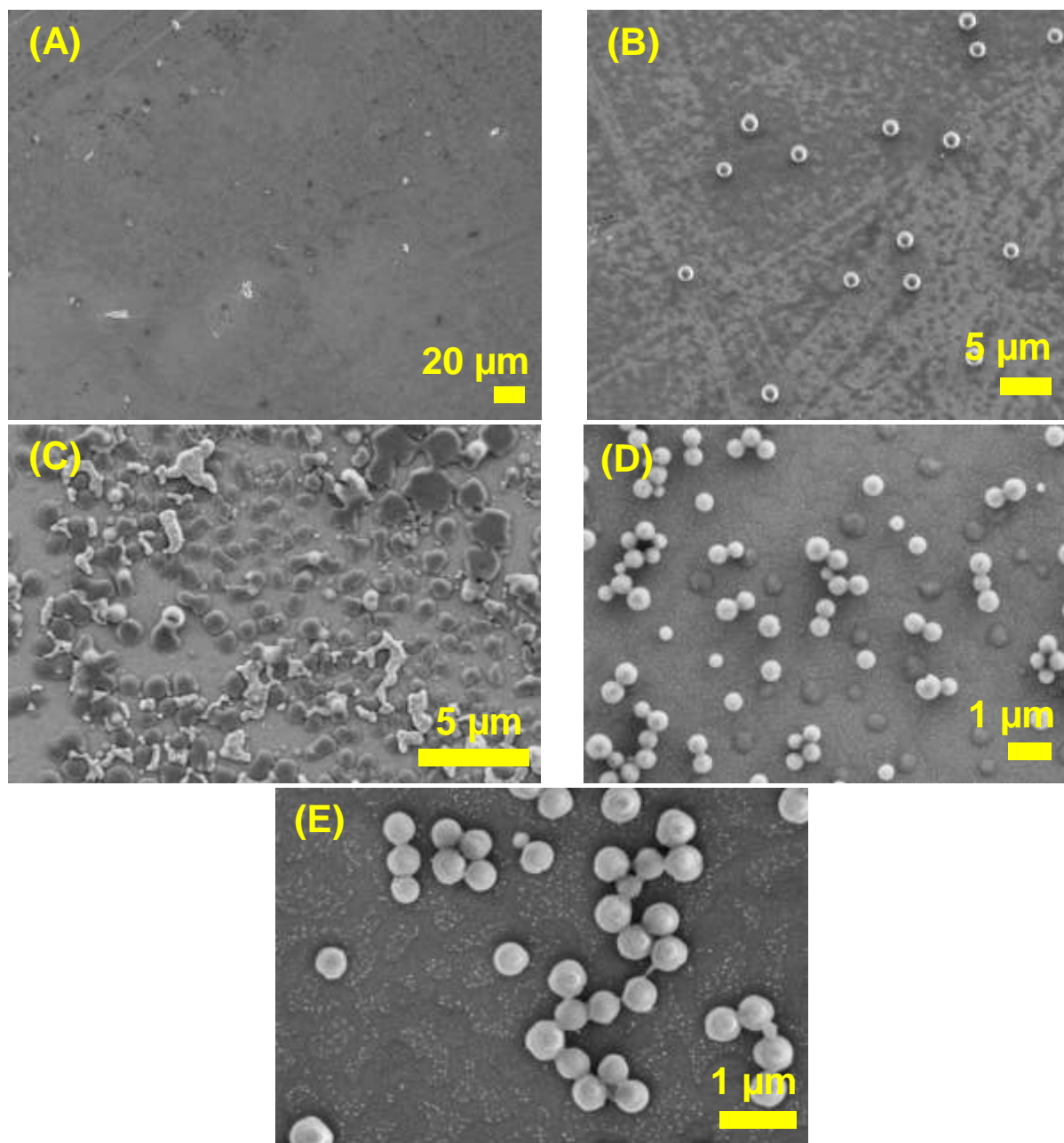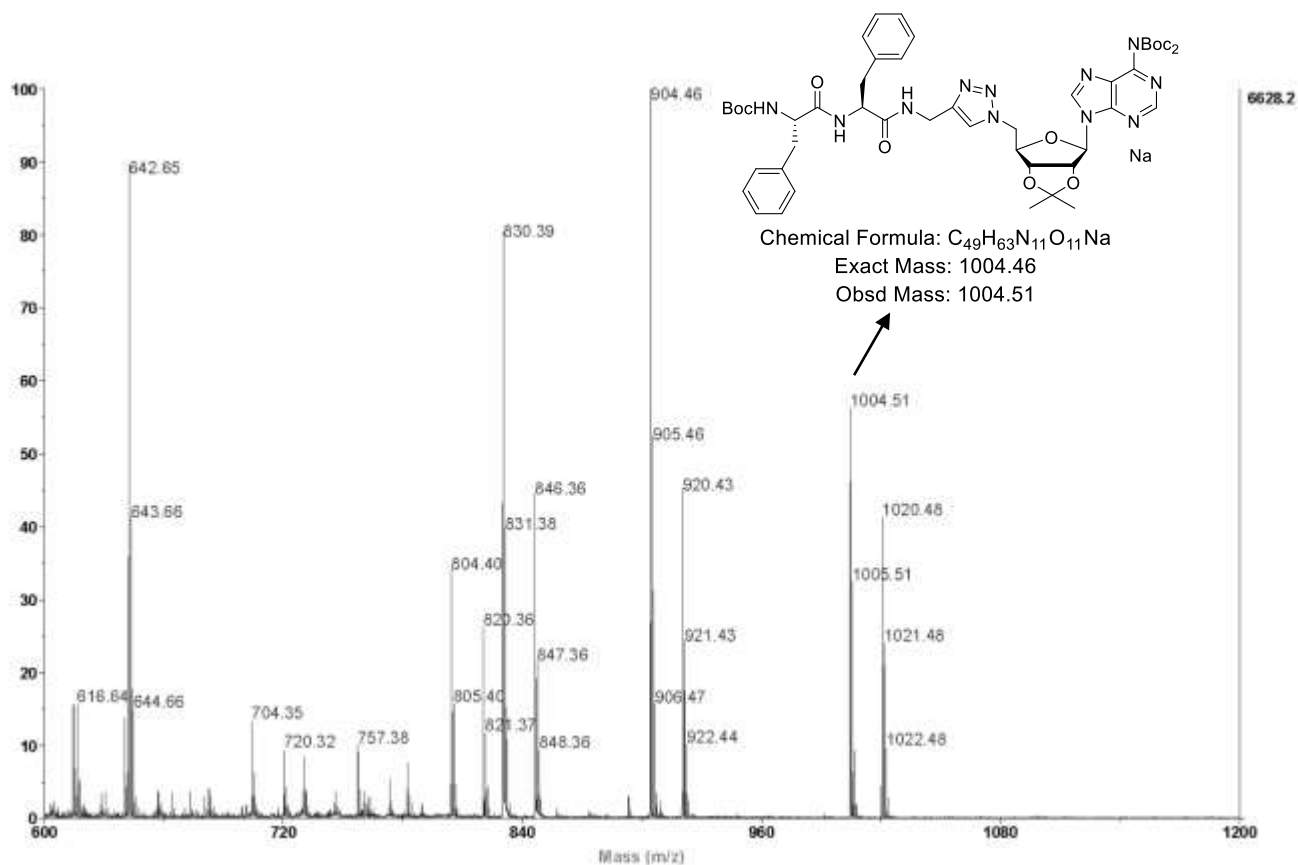
**Figure 2.20**: SEM images of peptide **12** [Boc-Phe-Phe-*am*-A$^{N(Boc)2}$] (A) at pH 2; (B) at pH 6; (C) at pH 10; (D) after heating at 100 ºC and (E) after heating at 200 ºC.

**Figure 2.21**: SEM images of peptide 7 [Boc-Phe-Phe-*tz*-A$^{N(Boc)2}$] (A); (B) after addition of 1.0 equiv. of Zn(NO$_3$)$_2$ and (C), (D) after addition of 1.0 equiv. of Cu(NO$_3$)$_2$.



**Figure 2.22**: TGA of (A) peptide **7** [Boc-Phe-Phe-*tz*-A$^{N(Boc)2}$] and (B) peptide **12** [Boc-Phe-Phe-*am*-A$^{N(Boc)2}$].

Chemical Formula: $C_{49}H_{63}N_{11}O_{11}Na$
Exact Mass: 1004.46
Obsd Mass: 1004.51

**Figure 2.23**: MALDI-TOF spectrum after thermal stability experiment of peptide **7** [Boc-Phe-Phe-*tz*-A^N(Boc)2].

## 2.3.4 Encapsulation of dye and stimuli triggered disruption of nanospheres

The addition of 0.1 mM carboxyfluorescein dye to a freshly prepared solution of **7** [Boc-Phe-Phe-*tz*-A^N(Boc)2] yielded spherical nanoparticles which exhibited green fluorescent emission in confocal microscopy (Figure 2.24). The confocal images of peptide **7** showing dark spots at the center of each particle indicated a "core-shell"-type structure consistent with that seen in HRTEM image (Table 2.3).

In order to trigger the release of the entrapped carboxyfluorescein,[36,37] the dicationic dipeptide Boc-Lys-Lys-OMe (for synthesis and characterization of Boc-Lys-Lys-OMe see experimental section, Scheme 2.7) and cationic amino acid *L*-arginine were used separately as external stimuli.

The strong cation-π interaction[38] for Phe-Lys and Phe-Arg in proteins / peptides lead to the disassembly of spherical structure. Here, it is assumed that cation-π interaction will overcome the weak π-π stacking forces. The controlled release of dye after external addition of dicationic dipeptide Boc-Lys-Lys-OMe to trigger the release of dye encapsulated nanoparticle peptide **7** [Boc-Phe-Phe-*tz*-A$^{N(Boc)2}$] in a dialysis bag was monitored by the rise of fluorescence in solution outside the dialysis bag as a function of time observed for 40 hrs (Figure 2.25). The amount of dye released in presence of dicationic dipeptide after 40 hrs was more than double of the dye released in the absence of the cationic peptide and the release was also faster. However, in the initial 5 hrs, the amount of dye released was more than 4 times in the presence of dicationic dipeptide.
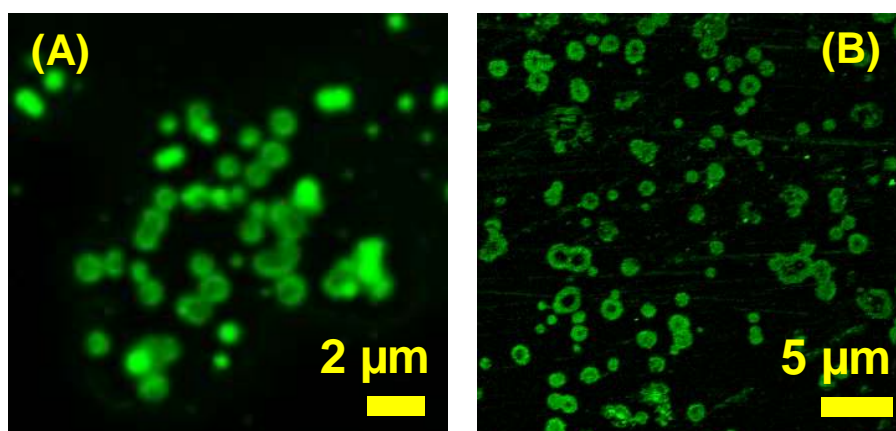


**Figure 2.24**: (A) and (B) are the confocal microscope images of fluorescent dye encapsulated of peptide **7** [Boc-Phe-Phe-*tz*-A$^{N(Boc)2}$].
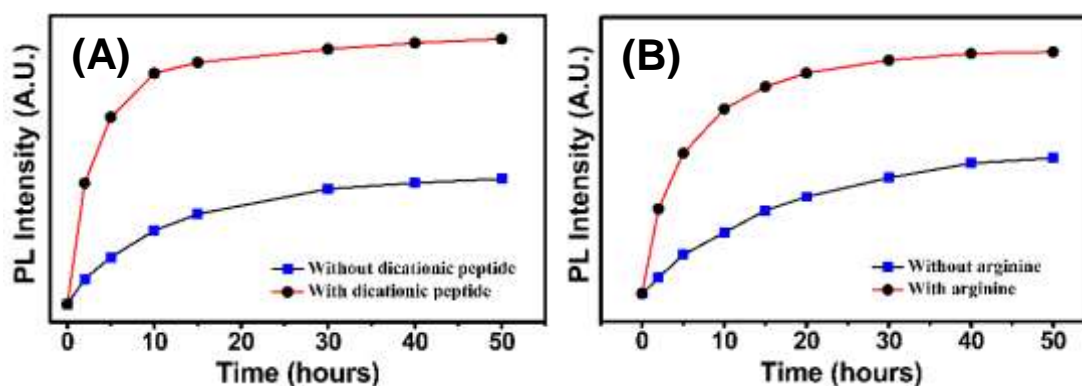


**Figure 2.25**: Fluorescence emission spectra of carboxyfluorescein (at 517 nm) showing increasing intensity after the addition of (A) dicationic dipeptide (Boc-Lys-Lys-OMe) and (B) *L*-arginine into dye encapsulated peptide **7** [Boc-Phe-Phe-*tz*-A$^{(Boc)2}$].

## 2.4 Summary

A series of short hybrid-peptides containing a Phe-Phe motif with C-terminus conjugated with A/T/U nucleosides via triazole or amide linker were studied to examine the effects of C-terminus substituents with hydrophobic or H-bonding groups on the self-assembly of Phe-Phe motif.

1. The nature of the linker (triazole/amide) *per se* did not have any significant effect on the self-assembled microscopic structures.

2. The chemical / structural nature of substituents at C/N-terminus imparted remarkable influences. Hydrophobic substituents (Boc groups) at C/N-terminus lead to well-defined microscopic morphologies such as nanoparticles or nanospheres resulting from aromatic stacking of Phe-Phe motifs; its absence as in Leu-Leu peptide generated spindles.

3. The microscopic structures formed by peptide **7** [Boc-Phe-Phe-*tz*-A$^{N(Boc)_2}$] is stable to external changes such as pH and solvent. Long term storage of spherical particles of peptide **7** (>72 hrs) lead to formation of molecular necklace perhaps through hydrogen bonded nanospheres since peptide **7** has lower tendency to aggregate.

4. The hydrophobic protecting groups on peptides induced larger contact angles measurement compared to the free peptide **9** (H-Phe-Phe-*tz*-A$^{NH_2}$), suggesting importance of hydrophobic induced self-assembly resulting in nanosphere morphology.

5. Nanospheres of peptide **7** is thermally stable up to 200 $^o$C and capable of encapsulating dye within the nanosphere which can be released by addition of cationic peptide and amino acids.

The results point to the ability to rationally change nanostructures, balancing hydrophobic / hydrophilic features. Introduction of other nucleobases (C/G/T) at either C- or N- terminus of the Phe-Phe moiety has potential to introduce base pairing of nanoparticles as another repertoire to further influence morphologies of resultant nanoparticles, through supramolecular engineering (Figure 2.26).
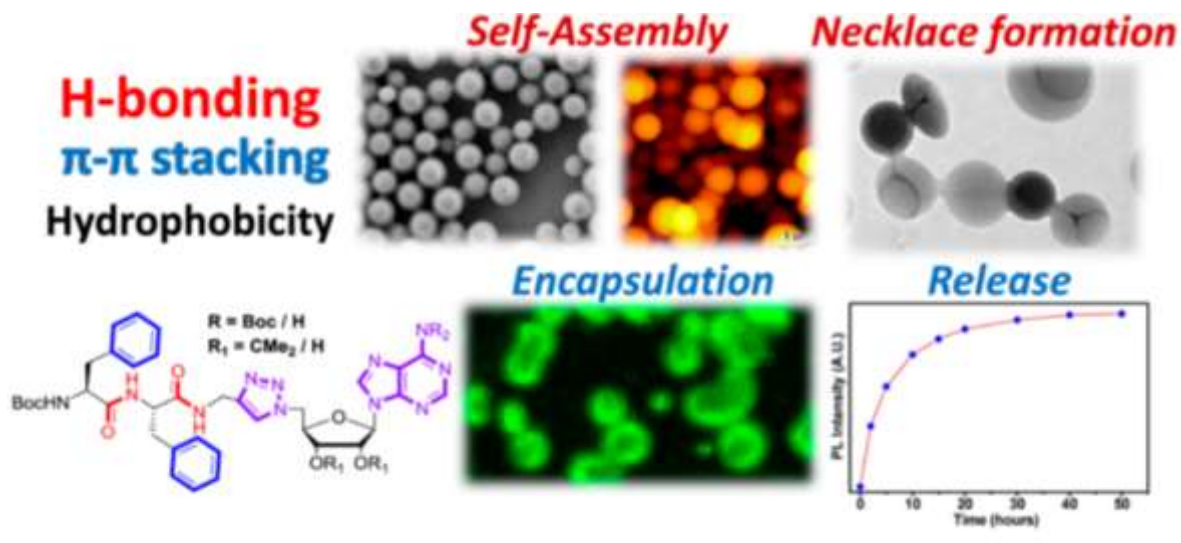
**Figure 2.26**: Hybrid-peptides containing diphenylalanine and nucleoside were studied to understand the effects of C-terminus substituents, hydrophobicity and H-bonding groups on the self-assembly. The results indicated the ability of this new class of peptides to change nanostructures rationally, balancing hydrophobic / hydrophilic nature.

## 2.5 Experimental section

**2.5.1 Materials and methods**: All reagents were commercially purchased from Sigma Aldrich. Column chromatographic separations were done using silica gel (230-400 mesh). Solvents were dried and distilled following standard procedures. TLC was carried out on pre-coated plates (Merck silica gel 60, $f_{254}$) and the spots were visualized with UV light or by charring the plates after dipping in 5% $H_2SO_4$ in MeOH or 5% vanillin in MeOH solutions. $^1$H-NMR (400 MHz) and $^{13}$C-NMR (100 MHz) spectra were recorded on Bruker NMR spectrometer. All $^1$H and $^{13}$C NMR were recorded in CDCl$_3$, DMSO-$d_6$ and ACN-$d_3$. Chemical shifts are reported in parts per million (ppm, $\delta$ scale). Mass spectroscopy data were obtained from Synapt G2QTof mass spectrometer in ESI$^+$ mode. Melting points were determined in open-end capillary tubes and are uncorrected. Powder X-ray diffraction (PXRD, Bruker), Fourier Transform Infrared Spectroscopy (ATR-FTIR, Bruker alpha-E), UV-Visible spectrophotometry (Perkin Elmer Lambda 45 double beam UV-Vis spectrophotometer), DLS (Nano ZS-90 Malvern Zetasizer), and contact angle (Holmarc, opto-mechatronics) measurements were used for characterization. Steady state emission and excitation spectra were recorded using Fluorolog-3 HORIBA JOBIN YVON fluorescence

spectrophotometer. TGA (thermogravimetric analysis) analysis was performed using Perkin Elmer STA 6000 simultaneous thermal analyser.

Self-assembly process of the peptides was monitored after dissolving 1 mg/mL in 1,1,1,3,3,3-hexafluoro-2-propanol (HFIP), lyophilized, and then diluted with 50% ethanol in water. After immediate deposition of these solution of peptides on silicon surface or copper grid, samples were dried at room temperature and SEM, AFM and HRTEM images were recorded unless stated otherwise.

### 2.5.2 Synthesis of Peptides

**Dipeptide 2 (Boc-Phe-Phe-Propyne)**: A mixture of compound **1**[24] (1.0 g, 2.4 mmol), EDC.HCl (0.5 g, 2.4 mmol) and HOBT (0.2 g, 1.2 mmol) was dissolved in dry DMF (10 mL) at 0 $^{\circ}$C. To the reaction mixture, DIPEA (0.9 mL, 4.0 mmol) was added. After 30 min, propargylamine hydrochloride, (0.2 g, 2.4 mmol) dissolved in dry DMF (3 mL), was added slowly into the reaction mixture and stirred at room temperature under $N_2$ atmosphere. After 8 hrs, aq. brine solution (50 mL) was added into it and the aq. layer was washed with ethyl acetate (EtOAc) (3 x 25 mL). Organic layer was washed with satd. $NaHCO_3$, 10% citric acid and brine solutions. The organic layer was separated, dried over anhyd. $Na_2SO_4$, filtered and the filtrate was concentrated under reduced pressure. The crude mass thus obtained, was purified by column chromatography [Eluent: 20-50% of EtOAc in pet ether] to afford compound **2** (0.9 g, 85% with respect to **1**). White solid; m.p. 130-135 °C; $^{1}$H NMR, 400 MHz (CDCl$_3$, 25 °C, TMS): $\delta$ = 7.23-6.91 (m, 11H), 6.87-6.85 (m, 1H), 6.82-6.73 (m, 1H), 5.38 (d, $J$ = 7.0 Hz, 0.34H), 5.11 (d, $J$ = 4.9 Hz, 0.5H), 4.68 (dt, $J$ = 13.2, 6.6 Hz, 1H), 4.32 (d, $J$ = 5.5 Hz, 0.5H), 4.18 (q, $J$ = 7.2 Hz, 0.4H), 3.94 – 3.69 (m, 2H), 3.12 – 2.65 (m, 4H), 2.12 – 2.02 (m, 1H), 1.28-1.26 ppm (s, 9H); $^{13}$C NMR, 100 MHz (CDCl$_3$, 25 °C, TMS): $\delta$ = 171.8, 171.4, 170.7, 170.5, 155.8, 136.6, 136.4, 136.3, 129.6, 129.50, 129.5, 129.4, 128.8, 128.7, 128.7, 127.2, 127.1, 127.1, 80.6, 80.4, 79.3, 71.6, 56.7, 56.1, 53.9, 53.8, 38.3, 38.1, 37.8, 29.2, 29.1, 28.4, 28.4 ppm. HRMS (ESI$^+$), m/z calculated for (M+Na)$^+$ $C_{26}H_{31}N_3O_4Na$: 472.2212, found: 472.2213.

**Dipeptide 4 (Boc-Leu-Leu-Propyne)**: Compound **3**[22] (1.0 g, 2.9 mmol) was coupled with propargylamine hydrochloride (0.3 g, 2.9 mmol) following the method described for compound **2** to afford compound **4** (1.0 g, 88% with respect to **3**) which was purified by column chromatography [Eluent: 10-30% of EtOAc in pet ether]. White solid; m.p. 120-124 °C; $^1$H NMR, 400 MHz (CDCl$_3$, 25 °C, TMS): $\delta$ = 7.25 (t, $J$ = 8.8 Hz, 1H), 6.99 (d, $J$ = 6.5 Hz, 1H), 5.25 (d, $J$ = 5.8 Hz, 1H), 4.59 – 4.44 (m, 1H), 4.20 – 4.07 (m, 1H), 4.05 – 3.92 (m, 2H), 2.17 (t, $J$ = 2.5 Hz, 1H), 1.72 – 1.46 (m, 6H), 1.41 (s, 9H), 0.92 – 0.85 ppm (m, 12H); $^{13}$C NMR, 100 MHz (CDCl$_3$, 25 °C, TMS): $\delta$ = 173.1, 172.0, 156.0, 80.3, 79.6, 71.5, 53.4, 51.6, 41.2, 40.8, 29.2, 28.5, 24.8, 23.1, 23.0, 22.2, 22.1 ppm. HRMS (ESI$^+$), m/z calculated for (M+Na)$^+$ C$_{20}$H$_{35}$N$_3$O$_4$Na: 404.2525, found: 404.2523.

**Peptide 7 [Boc-Phe-Phe-*tz*-A$^{N(Boc)_2}$]**: A mixture of **2** (0.3 g, 0.6 mmol), CuSO$_4$.5H$_2$O (7 mg, 0.03 mmol) and sodium ascorbate (0.1 g, 0.3 mmol) were stirred in tetrahydrofuran (THF) (6.0 mL). To the resulting suspension, azide **5**[31] (0.6 g, 1.1 mmol) dissolved in THF (6.0 mL) was added. Distilled water (10 mL) was added to the reaction mixture and stirred at room temperature. After 12 hrs, EtOAc (20 mL) was added into it and aq. layer was further washed with EtOAc (3 x 20 mL). Organic layer was separated, dried over anhyd. Na$_2$SO$_4$, filtered and the filtrate was concentrated under reduced pressure. The crude mass thus obtained, was purified by column chromatography [Eluent: 0-5% of MeOH in DCM] to afford compound **7** (0.5 g, 89% with respect to **2**). White solid; m.p. 96-100 °C; $^1$H NMR, 400 MHz (CD$_3$CN, 25 °C): $\delta$ = 8.89 (s, 1H), 8.39 (s, 1H), 7.52 (d, $J$ = 10.2 Hz, 1H), 7.38 – 7.12 (m, 12H), 7.02 (d, $J$ = 6.6 Hz, 1H), 6.32 (d, $J$ = 1.8 Hz, 1H), 5.62 (dd, $J$ = 16.9, 6.6 Hz, 1H), 5.54 – 5.47 (m, 1H), 5.25 (dd, $J$ = 6.1, 3.1 Hz, 1H), 4.79 – 4.62 (m, 3H), 4.56 (dd, $J$ = 13.7, 7.1 Hz, 1H), 4.33 (dd, $J$ = 23.5, 6.1 Hz, 2H), 4.27 – 4.15 (m, 1H), 3.19 – 2.89 (m, 3H), 2.86 – 2.72 (m, 1H), 1.63 (s, 3H), 1.48 (s, 18H), 1.41 – 1.29 ppm (m, 12H); $^{13}$C NMR, 100 MHz, (CD$_3$CN, 25 °C): $\delta$ = 171.5, 170.7, 152.6, 152.0, 150.6, 150.2, 145.2, 137.5, 137.3, 129.5, 129.4, 129.4, 129.1, 128.50, 128.47, 128.4, 126.7, 114.6, 90.40, 90.36, 85.6, 84.2, 83.97, 83.96, 81.89, 81.86, 79.5, 56.3, 54.5, 54.3, 51.5, 37.4, 34.7, 27.6, 27.1, 26.5, 24.7 ppm. HRMS (ESI$^+$), m/z calculated for (M+H)$^+$ C$_{49}$H$_{64}$N$_{11}$O$_{11}$: 982.4787, found: 982.4797.

**Peptide 8 (Boc-Phe-Phe-*tz*-A^NH₂)**: Alkyne **2** (0.3 g, 0.6 mmol) was clicked with azide **6**[32] (0.4 g, 1.1 mmol) following the method described for compound **7** to afford compound **8** (0.3 g, 75% with respect to **2**) which was purified by column chromatography [Eluent: 0-10% of MeOH in DCM]. Yellow solid; m.p. 89-94 °C; $^1$H NMR, 400 MHz (DMSO-$d_6$, 25 °C): $\delta$ = 8.45 (dd, $J$ = 9.8, 4.7 Hz, 1H), 8.30 (s, 1H), 8.21 (s, 1H), 7.96 (d, $J$ = 8.2 Hz, 1H), 7.60 (s, 1H), 7.38 (s, 2H), 7.29 – 7.04 (m, 11H), 6.89 (d, $J$ = 8.5 Hz, 0.6H), 6.73 (d, $J$ = 8.4 Hz, 0.2H), 6.24 (d, $J$ = 2.0 Hz, 1H), 5.46 (dd, $J$ = 6.3, 2.1 Hz, 1H), 5.15 (dd, $J$ = 6.2, 3.3 Hz, 1H), 4.79 – 4.71 (m, 1H), 4.69 – 4.58 (m, 1H), 4.56 – 4.48 (m, 2H), 4.32 – 4.06 (m, 3H), 3.02 – 2.91 (m, 1H), 2.86 – 2.72 (m, 2H), 2.70 – 2.57 (m, 1H), 1.52 (s, 3H), 1.31 (s, 3H), 1.26-1.28 ppm (s, 9H); $^{13}$C NMR, 100 MHz (DMSO-$d_6$, 25 °C): $\delta$ = 171.2, 170.6, 156.2, 155.1, 152.8, 144.6, 140.1, 138.0, 137.4, 129.3, 129.1, 128.0, 127.9, 126.2, 126.1, 123.1, 113.6, 89.0, 84.7, 83.4, 81.6, 78.1, 55.8, 53.6, 51.1, 37.9, 37.4, 34.1, 28.1, 26.9, 25.2 ppm. HRMS (ESI$^+$), m/z calculated for (M+H)$^+$ C$_{39}$H$_{48}$N$_{11}$O$_7$: 782.3738, found: 782.3732.

**Peptide 9 (H-Phe-Phe-*tz*-A^NH₂)**: Peptide **7** (0.3 g, 0.3 mmol) was stirred with TFA in DCM (20%, 15 mL) at room temperature. After 10 hrs, the volatile matters were evaporated to dryness under reduced pressure and residual liquid was co-evaporated with toluene (2 x 5 mL). The residue thus obtained was loaded onto silica gel column and purified to obtain peptide **9** (0.2 g, 80%) [Eluent: 0-10% MeOH in DCM]. White solid; m.p. 129-132 °C; $^1$H NMR, 400 MHz (DMSO-d₆, 25 °C): $\delta$ = 8.77 (d, $J$ = 8.0 Hz, 1H), 8.56 (t, $J$ = 5.5 Hz, 1H), 8.30 (s, 1H), 8.16 (s, 1H), 7.56 (s, 1H), 7.36 – 7.12 (m, 12H), 5.92 (d, $J$ = 5.2 Hz, 1H), 5.67 (d, $J$ = 5.1 Hz, 1H), 5.54 (d, $J$ = 4.9 Hz, 1H), 4.75-4.69 (m, 2H), 4.55 (dd, $J$ = 14.2, 8.1 Hz, 1H), 4.39 – 4.16 (m, 3H), 4.01 (dd, $J$ = 13.4, 8.9 Hz, 1H), 3.20 – 3.03 (m, 2H), 2.97-2.91 ppm (m, 3H); $^{13}$C NMR, 100 MHz (DMSO-d₆, 25 °C): $\delta$ = 170.2, 168.1, 158.4, 158.1, 156.2, 152.8, 149.3, 144.5, 140.1, 137.3, 134.9, 129.7, 129.3, 128.5, 128.4, 128.2, 127.1, 126.5, 123.4, 119.3, 118.8, 115.8, 88.0, 82.6, 72.8, 71.1, 65.0, 54.3, 53.3, 51.7, 37.9, 37.1, 34.2 ppm; HRMS (ESI$^+$), m/z calculated for (M+H)$^+$ C$_{31}$H$_{36}$N$_{11}$O$_5$: 642.2901, found: 642.2897.

**Peptide 10 [Boc-Leu-Leu-*tz*-A^N(Boc)₂]**: Alkyne **4** (0.4 g, 1.0 mmol) was clicked with azide **5** (1.0 g, 2.0 mmol) following the method described for compound **7** to afford compound **10** (0.5 g, 79% with respect to **4**) which was purified by column chromatography [Eluent: 0-4% of MeOH in DCM]. White solid; m.p. 95-99 °C; $^1$H NMR, 400 MHz (CDCl₃, 25 °C, TMS): $\delta$ = 8.92 – 8.79

(m, 1H), 8.13 (s, 1H), 7.44 (brs, 1H), 7.29 (s, 1H), 6.82 – 6.61 (m, 1H), 6.17 (d, $J$ = 2.1 Hz, 1H), 5.39-5.37 (m, 1H), 5.22-5.21 (m, 1H), 5.13 (brs, 1H), 4.80-4.75 (m, 1H), 4.60-4.59 (m, 2H), 4.49 – 4.38 (m, 3H), 4.14 – 3.85 (m, 1H), 1.60 (s, 9H), 1.55 – 1.44 (m, 18H), 1.40-1.37 (m, 12H), 0.96 – 0.74 ppm (m, 12H); $^{13}$C NMR, 100 MHz (CDCl$_3$, 25 °C, TMS): $\delta$ = 172.9, 172.3, 156.1, 152.4, 152.4, 150.9, 150.6, 145.1, 144.3, 129.5, 123.5, 115.3, 90.5, 90.4, 85.3, 84.2, 84.0, 81.8, 81.7, 80.4, 53.6, 51.8, 51.5, 40.9, 35.1, 28.4, 28.0, 27.3, 25.5, 24.8, 23.2, 23.1, 22.0, 21.8 ppm. HRMS (ESI$^+$), m/z calculated for (M+H)$^+$ C$_{43}$H$_{68}$N$_{11}$O$_{11}$: 914.5100, found: 914.5109.

**Peptide 12 [Boc-Phe-Phe-*am*-A$^{N(Boc)2}$]:** Compound **1** (0.5 g, 2.2 mmol) was coupled with compound **11**[32] (1.1 g, 2.2 mmol) following the method described for compound **2** to afford peptide **12** which was purified by column chromatography [Eluent: 0-4% of MeOH in DCM]. Peptide **12** (0.9 g, 80% with respect to **1**) was obtained as white solid; m.p. 77-80 °C; $^1$H NMR, 400 MHz (CDCl$_3$, 25 °C, TMS): $\delta$ = 9.09 (s, 1H), 8.11 (s, 1H), 7.52 (s, 1H), 7.22 – 6.99 (m, 10H), 6.50 (s, 1H), 5.80 (s, 1H), 4.98-4.96 (m, 1H), 4.73-4.70 (m, 1H), 4.50 (s, 1H), 4.38 – 4.19 (m, 3H), 3.86 – 3.73 (m, 1H), 3.17 (dt, $J$ = 14.2, 3.1 Hz, 1H), 3.14-2.85 (m, 4H), 1.52 (s, 3H), 1.40 (s, 18H), 1.33 – 1.22 ppm (m, 12H); $^{13}$C NMR, 100 MHz (CDCl$_3$, 25 °C, TMS): $\delta$ = 171.1, 155.7, 152.8, 152.3, 151.1, 150.5, 144.3, 136.5, 129.64, 129.56, 129.5, 129.4, 128.9, 128.8, 128.6, 127.2, 115.0, 91.6, 84.1, 83.5, 82.8, 81.4, 80.7, 56.1, 54.8, 41.0, 38.4, 29.8, 28.3, 28.0, 27.8, 25.8 ppm. HRMS (ESI$^+$), m/z calculated for (M+H)$^+$ C$_{46}$H$_{61}$N$_8$O$_{11}$: 901.4460, found: 901.4476.

**Dicationic peptide Boc-(*L*)-Lys-(*L*)-Lys-OMe:**
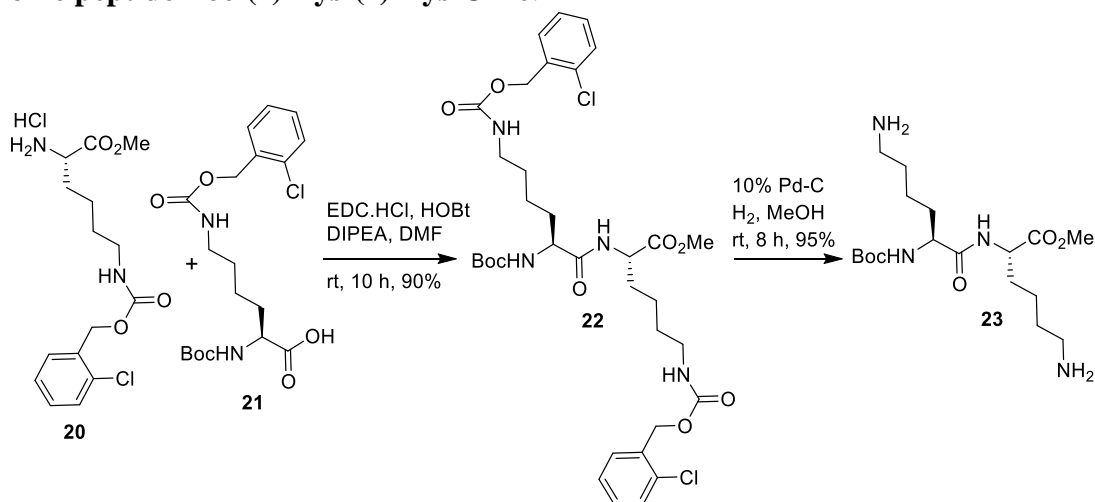


**Scheme 2.7**: Synthesis of dicationic peptide **23**.

Dicationic peptide **23** [Boc-(*L*)-Lys-(*L*)-Lys-OMe] was synthesized after minor modification of the known procedure.[39,40] Commercially available (*L*)-Lys(*O*-Cl-Cbz)-OMe.HCl (**20**; 0.4 g, 1.2 mmol) and Boc-(*L*)-Lys(*O*-Cl-Cbz)-OH (**21**; 0.5 g, 1.2 mmol) were dissolved in dry DMF (10 mL). Diisopropylethylamine (DIPEA) (0.4 mL, 3.0 mmol) was added to the mixture and cooled to 0 °C in an ice bath. HOBt (0.2 g, 1.2 mmol) and EDC.HCl (0.2 g, 1.2 mmol) were added in portions into the reaction mixture and the reaction mixture was stirred for 1 hr at 0 °C and kept at room temperature for overnight. EtOAc (100 mL) was added in to the reaction mixture. The organic layer was then washed successively with $H_2O$ (100 mL), 10% aqueous solution of $NaHCO_3$ (100 mL), 10% aqueous solution of citric acid (100 mL), and with brine (300 mL). The organic layer was dried over anhyd. $Na_2SO_4$ and then evaporated under reduced pressure to give **22** as a colorless viscous compound which was purified by flash column chromatography. The spectral data (NMR and HRMS) corresponded to the desired protected dipeptide **22** (0.8 g, 90% with respect to **21**). $^1$H NMR, 400 MHz (CDCl$_3$, 25 °C, TMS): $\delta$ = 7.42-7.36 (m, 4H), 7.26-7.24 (m, 4H), 6.74 (brs, 1H), 5.25-5.17 (m, 5H), 5.09 (brs, 1H), 4.58-4.53 (m, 1H), 4.11-4.09 (m, 1H), 3.70 (s, 3H), 3.22-3.11 (m, 4H), 1.85-1.80 (m, 2H), 1.70-1.66 (m, 2H), 1.64-1.60 (m, 4H), 1.54-1.35 ppm (m, 13H); $^{13}$C NMR, 100 MHz (CDCl$_3$, 25 °C, TMS) $\delta$ = 172.8, 172.4, 156.6, 156.0, 134.5, 134.4, 133.8, 133.7, 130.1, 130.0, 129.7, 129.5, 127.1, 80.3, 64.1, 54.4, 52.7, 52.0, 40.6, 32.0, 31.7, 29.5, 29.3, 28.5, 22.4 ppm. HRMS (ESI$^+$), m/z calculated for (M+H)$^+$ $C_{34}H_{47}Cl_2N_4O_9$: 725.2720, found: 725.2719.

To a mixture of **22** (0.5 g, 0.7 mmol) in MeOH (10 mL), Pd/C (10%) (50 mg) was added into a flask. The mixture was stirred under $H_2$ atmosphere for 8 hrs, filtered through Celite-545 and evaporated under reduced pressure. The residue was then co-evaporated with $CCl_4$ and dried under high vacuum to afford peptide **23** as a white solid (0.3 g, 95%); m.p. 226-228 °C (decomposes); $^1$H NMR 400 MHz (DMSO-$d_6$, 25 °C) $\delta$ = 8.31 (d, $J$ = 7.3 Hz, 1H), 8.06 (s, 4H), 6.85 (d, $J$ = 8.1 Hz, 1H), 4.23-4.14 (m, 1H), 4.02-3.86 (m, 1H), 3.61 (s, 3H), 2.79-2.66 (m, 4H), 1.68-1.43 (m, 8H), 1.37-1.28 ppm(m, 13H); $^{13}$C NMR, 100 MHz (DMSO-$d_6$, 25 °C): $\delta$ = 172.4, 155.3, 77.8, 53.8, 51.8, 51.7, 38.4, 38.3, 31.2, 30.1, 28.2, 26.5, 26.4, 23.2, 22.3, 22.1 ppm. HRMS (ESI$^+$), m/z calculated for (M+H)$^+$ $C_{18}H_{37}N_4O_5$: 389.2764, found: 389.2756.

**Fmoc-Phe-Phe-*tz*-A$^{NH_2}$ (14)**: Compound **2** (1.0 g, 2.2 mmol) was stirred with trifluoroacetic acid (TFA) in DCM (20%, 10 mL) at room temperature. After 4 hrs, the volatile matters were evaporated to dryness under reduced pressure and residual liquid was co-evaporated with toluene (2 x 5 mL). The residue, thus obtained was subjected for next reaction without further purification. HRMS (ESI$^+$), m/z calculated for (M+H)$^+$ $C_{21}H_{24}N_3O_2$: 350.1868, found: 350.1869.

To a mixture of 10% $Na_2CO_3$ solution (15 mL) and the crude residue, FmocOSu (0.8 g, 2.5 mmol) was added slowly in portions at 0 °C and then kept at room temperature for 8 hrs. The reaction mixture was then acidified with satd. $KHSO_4$ solution to adjust the pH between 4-5. The resulting aq. solution was washed with EtOAc (20 x 3 mL). The combined organic layer was then washed successively with $H_2O$ (50 x 2 mL) and with brine (30 x 3 mL). Organic layer was dried over anhyd. $Na_2SO_4$ and then evaporated under reduced pressure to give **22** as a white compound which was purified by column chromatography to obtain compound **13** (1.0 g, 80% with respect to **2**) [Eluent: 0-5% of MeOH in DCM] as hygroscopic solid; $^1$H NMR 400 MHz (DMSO-$d_6$, 25 °C) $\delta$ = 8.46 (t, $J$ = 5.4 Hz, 1H), 8.15 (d, $J$ = 8.2 Hz, 1H), 7.88 (d, $J$ = 7.6 Hz, 2H), 7.61 (t, $J$ = 8.3 Hz, 2H), 7.55 (d, $J$ = 8.8 Hz, 1H), 7.40 (td, $J$ = 7.4, 3.2 Hz, 2H), 7.33 – 7.26 (m, 2H), 7.24 – 7.22 (m, 8H), 7.19 – 7.13 (m, 2H), 4.51 (dd, $J$ = 13.6, 8.3 Hz, 1H), 4.28 – 4.19 (m, 1H), 4.16 (dd, $J$ = 14.4, 3.5 Hz, 1H), 4.13 – 4.07 (m, 2H), 3.93 – 3.80 (m, 2H), 3.15 (t, $J$ = 2.5 Hz, 1H), 3.01 – 2.88 (m, 2H), 2.83 (dd, $J$ = 13.7, 8.8 Hz, 1H), 2.70 ppm (dd, $J$ = 13.7, 10.7 Hz, 1H); $^{13}$C NMR, 100 MHz (DMSO-$d_6$, 25 °C): $\delta$ = 171.3, 170.6, 155.6, 143.8, 143.7, 140.64, 138.1, 137.4, 129.3, 129.2, 128.1, 128.0, 127.6, 127.1, 126.3, 126.2, 125.3, 125.2, 120.1, 80.8, 73.2, 65.6, 56.0, 53.8, 46.5, 39.5, 37.8, 37.4, 28.0 ppm. HRMS (ESI$^+$), m/z calculated for (M+H)$^+$ $C_{36}H_{34}N_3O_4$: 572.2549, found: 572.2549.

A mixture of **14** (0.6 g, 1.0 mmol), CuSO$_4$.5H$_2$O (15 mg, 0.05 mmol) and sodium ascorbate (0.1 g, 0.5 mmol) were stirred in THF (6.0 mL). To the resulting suspension, azide **6** (0.4 g, 1.1 mmol) dissolved in THF (6.0 mL) was added. 10 mL distilled water was added to the reaction mixture and stirred at room temperature. After 12 hrs, EtOAc (20 mL) was added into it and aq. layer was further washed with EtOAc (3 x 20 mL). Organic layer was separated, dried over anhyd. $Na_2SO_4$, filtered and the filtrate was concentrated under reduced pressure. The crude mass thus obtained, was purified by column chromatography [Eluent: 0-5% MeOH in DCM] to afford compound **14** as white solid (0.7 g, 77% with respect to **13**); m.p. 130-133 °C; $^1$H NMR 400 MHz

(DMSO-$d_6$, 25 °C) $\delta$ = 8.45 (t, $J$ = 5.4 Hz, 1H), 8.33 (s, 1H), 8.23 (s, 1H), 8.12 (d, $J$ = 8.1 Hz, 1H), 7.87 (d, $J$ = 7.5 Hz, 2H), 7.59 (dt, $J$ = 22.0, 8.4 Hz, 3H), 7.39 (t, $J$ = 7.0 Hz, 4H), 7.34 – 7.08 (m, 13H), 6.24 (d, $J$ = 1.8 Hz, 1H), 5.46 (dd, $J$ = 6.3, 2.0 Hz, 1H), 5.15 (dd, $J$ = 6.2, 3.3 Hz, 1H), 4.74 (dd, $J$ = 14.0, 5.1 Hz, 1H), 4.63 (dd, $J$ = 13.9, 7.8 Hz, 1H), 4.56 – 4.48 (m, 2H), 4.34 – 4.16 (m, 4H), 4.10 (dd, $J$ = 14.4, 7.5 Hz, 2H), 2.94 (td, $J$ = 14.3, 4.7 Hz, 2H), 2.82 (dd, $J$ = 13.7, 8.4 Hz, 1H), 2.75 – 2.66 (m, 1H), 1.52 (s, 3H), 1.31 ppm (s, 3H); $^{13}$C NMR, 100 MHz (DMSO-$d_6$, 25 °C): $\delta$ = 171.2, 170.5, 156.2, 155.6, 152.8, 143.7, 143.7, 140.6, 138.0, 137.4, 129.3, 129.2, 129.2, 127.9, 127.6, 127.0, 126.2, 125.3, 125.2, 123.1, 120.0, 113.6, 89.1, 84.7, 83.3, 81.6, 79.2, 65.6, 56.0, 53.8, 51.1, 46.5, 39.5, 37.8, 37.4, 34.2, 26.9, 25.1 ppm. HRMS (ESI$^+$), m/z calculated for (M+H)$^+$ $C_{49}H_{50}N_{11}O_7$: 904.3894, found: 904.3903.

**Fmoc-Phe-Phe-*tz*-A$^{N(Boc)2}$ (15)**: To a mixture of **14** (0.6 g, 0.7 mmol) in dry THF (50 mL), DMAP (10 mg, 0.1 mmol) was added. To the stirred suspension was added Boc$_2$O (0.4 g, 1.7 mmol) under an Ar atmosphere. The reaction mixture was stirred for 8 hrs at room temperature, at which point TLC analysis indicated completion of the reaction.

The excess amount of THF was evaporated under reduced pressure. The residue thus obtained was purified by column chromatography [Eluent: 20-70% EtOAc in hexane] to afford peptide **15** as white solid (0.6 g, 75%); m.p. 114-117 °C; $^1$H NMR, 400 MHz (CDCl$_3$, 25 °C) $\delta$ = 8.82 (s, 1H), 8.69 (t, $J$ = 8.1 Hz, 0.5H), 8.42 (s, 0.5H), 8.03 (s, 1H), 7.81 – 7.62 (m, 2H), 7.44 (t, $J$ = 7.8 Hz, 2H), 7.34 (d, $J$ = 7.5 Hz, 2H), 7.26 – 7.13 (m, 7H), 7.04 (dd, $J$ = 15.5, 8.3 Hz, 6H), 6.96 (d, $J$ = 6.4 Hz, 1H), 6.13 – 5.95 (m, 2H), 5.82 (d, $J$ = 7.2 Hz, 1H), 5.34 – 5.23 (m, 1H), 5.14 (dd, $J$ = 6.4, 3.6 Hz, 1H), 4.73 – 4.41 (m, 6H), 4.36 – 4.22 (m, 3H), 4.17 – 3.99 (m, 2H), 2.97 – 2.88 (m, 4H), 2.68 (s, 1H), 1.52 – 1.51 (m, 8H), 1.47 – 1.37 (m, 13H), 1.29 ppm (s, 3H); $^{13}$C NMR (100 MHz, CDCl$_3$) $\delta$ = 171.1, 170.7, 156.1, 153.1, 152.3, 152.2, 150.8, 150.6, 150.2, 149.9, 144.7, 144.2, 143.8, 143.7, 141.9, 141.2, 136.4, 136.4, 129.4, 129.3, 128.6, 128.4, 127.7, 127.1, 127.0, 126.8, 125.2, 125.1, 123.4, 122.3, 120.0, 115.2, 115.1, 90.3, 85.1, 84.2, 83.8, 83.8, 82.3, 81.6, 77.5, 77.2, 76.8, 67.1, 56.2, 54.3, 51.3, 47.00, 38.3, 38.1, 34.8, 28.1, 27.8, 27.8, 27.1, 25.3 ppm. . HRMS (ESI$^+$), m/z calculated for (M+H)$^+$ $C_{59}H_{66}N_{11}O_{11}$: 1104.4940, found: 1104.4924.

**Peptide 18 (Boc-Phe-Phe-*tz*-U)**: Alkyne **2** (0.3 g, 0.6 mmol) was clicked with 5′-azido-5′-deoxy-2′,3′-*O*-isopropylideneuridine **16** (0.4 g, 1.1 mmol) following method described for compound **7** to afford compound **18** (0.4 g, 90% with respect to **2**) which was purified by column chromatography [Eluent: 0-7% of MeOH in DCM]. Peptide **18** was obtained as white solid; m.p. 92-95 °C; $^1$H NMR, 400 MHz (CDCl$_3$, 25 °C, TMS): $\delta$ = 10.41 (d, $J$ = 32.6 Hz, 1H), 7.62 – 7.51 (m, 1H), 7.49 (s, 1H), 7.27 – 7.08 (m, 14H), 7.04 – 6.94 (m, 2H), 5.70 (d, $J$ = 8.0 Hz, 1H), 5.50 (d, $J$ = 14.0 Hz, 1H), 5.35 - 5.28 (m, 1H), 5.08 (d, $J$ = 7.3 Hz, 1H), 4.95 – 4.87 (m, 1H), 4.80 – 4.61 (m, 3H), 4.50 – 4.27 (m, 4H), 3.23 – 2.74 (m, 6H), 1.50 (s, 3H), 1.38 – 1.20 ppm (m, 12H); $^{13}$C NMR, 100 MHz (CDCl$_3$, 25 °C, TMS): $\delta$ = 171.9, 171.6, 171.3, 164.1, 155.8, 155.6, 150.4, 143.7, 136.3, 129.5, 128.7, 127.0, 124.1, 115.0, 114.9, 103.0, 96.4, 86.1, 85.6, 84.2, 84.0, 81.8, 81.4, 80.3, 77.5, 77.4, 77.2, 76.9, 56.3, 54.2, 51.8, 51.5, 38.5, 37.8, 35.1, 29.8, 28.4, 27.2, 25.4 ppm. HRMS (ESI$^+$), m/z calculated for (M+H)$^+$ C$_{38}$H$_{47}$N$_8$O$_9$: 759.3466, found: 759.3480.

**Peptide 19 (Boc-Phe-Phe-*tz*-T)**: Alkyne **2** (0.3 g, 0.6 mmol) was clicked with 5′-azido-5′-deoxythymidine **17** (0.3 g, 1.1 mmol) following the method described for compound **7** to afford compound **16** (0.3 g, 82% with respect to **2**) which was purified by column chromatography [Eluent: 0-10% of MeOH in DCM]. Peptide **19** was obtained as white solid; m.p. 148-151 °C; $^1$H NMR, 400 MHz (DMSO-d$_6$, 25 °C): $\delta$ = 11.31 (s, 1H), 8.58 – 8.41 (m, 1H), 8.31 (d, $J$ = 8.5 Hz, 0.5H), 7.98 (d, $J$ = 8.1 Hz, 0.5H), 7.79 (s, 0.5H), 7.70 (s, 0.5H), 7.45 – 7.34 (m, 1H), 7.27 – 7.06 (m, 10H), 6.89 (d, $J$ = 8.6 Hz, 0.5H), 6.75 (d, $J$ = 8.3 Hz, 0.5H), 6.18 (t, $J$ = 6.9 Hz, 1H), 5.59 – 5.43 (m, 1H), 4.69 (dt, $J$ = 14.1, 3.8 Hz, 1H), 4.62 – 4.49 (m, 2H), 4.39 – 4.22 (m, 3H), 4.20 – 4.05 (m, 2H), 3.19 – 2.59 (m, 4H), 2.25 – 2.04 (m, 2H), 1.80 (s, 3H), 1.35 – 1.21 ppm (m, 9H); $^{13}$C NMR, 100 MHz (DMSO-d$_6$, 25 °C): $\delta$ = 171.4, 171.3, 170.8, 170.6, 170.3, 163.6, 155.2, 155.1, 150.4, 144.6, 138.0, 137.7, 137.4, 136.1, 129.3, 129.2, 129.2, 129.1, 128.0, 127.9, 127.9, 126.3, 126.1, 126.0, 123.3, 109.9, 84.1, 84.0, 78.1, 78.0, 70.8, 59.7, 55.8, 55.5, 53.8, 53.7, 51.2, 39.5, 37.9, 37.5, 37.3, 34.2, 28.1, 27.7, 20.7, 14.1, 13.5, 12.1 ppm. HRMS (ESI$^+$), m/z calculated for (M+H)$^+$ C$_{36}$H$_{45}$N$_8$O$_8$: 717.3360, found: 717.3370.

**2.5.3 FT-IR spectroscopy**: All reported solid-state FTIR spectra were obtained with a Fourier-transform infrared (FT-IR, Bruker alpha-E) spectrophotometer.

**2.5.4 Powder X-ray diffraction study**: The crystallographic structure of the peptides were characterized by powder X-ray diffraction (PXRD) using a PXRD Bruker. The peptides were dried under vacuum for 4 days and then PXRD data were taken.

**2.5.5 Thermogravimetric Analysis**: Thermogravimetric analyses were carried out with a Perkin Elmer STA 6000 simultaneous thermal analyzer. To determine the exact parameters of the physical stability of the self-assembled peptide vesicles, we used TGA to monitor the weight as a function of increasing temperature. Analysis was conducted isothermally for 30 min at room temperature and afterward in a scan rate of 5 °C / min up to 250 °C, under dried, ultrahigh-purity argon atmosphere.

**2.5.6 Dynamic light scattering**: Dynamic light scattering was performed using a Nano ZS-90 apparatus utilizing 633 nm red laser beam (at 90° angle) from Malvern Instruments to find the size and dispersity of nanospheres of peptides. The average size values reported are based on an average of three consecutive measurements. Average diameter of the spherical peptides was measured in 50 % ethanol in water.

**2.5.7 Microscopy studies**: We performed microscopy experiments in order to characterize the size of the self-assembled architectures of the hybrid-peptides. Sample preparation was carried out carefully to minimize the effect of sample drying on aggregate formation. Then, 5 μL of peptide-solutions were drop casted on different substrates followed by drying under high vacuum (Formvar coated Cu grid for HRTEM, silicon wafers substrate for AFM and FESEM). FESEM images were recorded using Zeiss Ultra Plus scanning electron microscope and the samples were prepared by drop casting on silicon wafers and coated with gold.

AFM images were recorded for the peptide samples using Agilent instruments. The imaging was carried out in tapping mode using TAP-190AL-G50 probe from Budget sensors with a nominal spring constant of 48 N/m and the resonance frequency of 190. HRTEM images were taken with a 1024 x 1024 digital CCD camera using a Tecnai-G$^2$20-TWIN microscope instrument.

**2.5.8 FESEM, HRTEM, AFM study**: SEM samples were prepared by depositing peptide solution (5 μL, 1 mg / mL in 50:50 EtOH / H$_2$O after lyophilization in 1 mL HFIP) on silicon wafers, dried

at room temperature and imaged it. Similarly TEM samples were prepared by depositing peptide solution (5 µL, 1 mg / mL in 50:50 EtOH / $H_2O$) on copper grid, dried at room temperature and imaged it. For AFM, samples were drop casted on freshly cleaved $SiO_2$ / Si substrate, air dried at room temperature. Tapping-mode AFM imaging was used according to well-established procedures.

**2.5.9 Solvent dependent study of peptide 7 under SEM**: We studied the stability and morphology of peptide **7** under different solvent combinations. For this purpose, peptide solution was prepared with different solvents and incubated at room temperature for half an hour and kept for dry at room temperature. SEM analysis revealed chemical stability of the peptide **7** towards following solvents: toluene, ethanol, methanol, HFIP, THF and 2-propanol.

**2.5.10 Effect of external stimuli on the structure of vesicles under SEM**: To test pH sensitivity of the vesicles, we made two acidic solutions having pH 2 and 6 respectively. Similarly a basic solution was also prepared by 2 M NaOH and adjusted its pH to 10. Thereafter freshly prepared vesicles formed peptides **7** and **12** were added into aforementioned solutions. Similarly, to understand the effect of metal ions in self-assembly, copper and zinc nitrate solution was prepared and mixed separately with the peptide **7** solution in 1:1 molar ratio. The resulting solution was incubated overnight and drop-casted onto a $SiO_2$ / Si substrate to check the change in morphology through SEM. For thermal stability we drop casted peptide solution onto a $SiO_2$ / Si substrate and kept it in the oven at different temperatures and imaged. The resistance to enzymatic proteolysis of vesicles was investigated by treating them with proteinase K. Proteinase K solution was prepared by dissolving 0.1 mg enzyme in 1 mL water and added to the vesicle solutions. In order to maintain the proteolytic activity of proteinase K, the solution was incubated for 24 hrs at 37 °C.

**2.5.11 Carboxyfluorescein encapsulation study**: 1.3 mM carboxyfluorescein solution was added to the peptide vesicles solution of peptide **7** to make the final concentration 0.1 mM and then kept it overnight and dialyzed with 100-500 D cut-off dialysis tube (Float-A-Lyzer G2 Dialysis Device, Spectrum Labs). Carboxyfluorescein entrapped vesicles solution was drop casted on a glass slide, dried and then imaged using Carl Ziess LSM-710 laser scanning confocal microscopy. The SEM and DLS analysis showed that the uniform size and morphology of the dye encapsulated capsules.

In addition, experiments using laser scanning confocal microscope reveal the green fluorescence emission from the nanostructures suggesting the encapsulation of dye molecules in the nanospheres.

**2.5.12 Stimuli triggered release of encapsulated dye**

**2.5.12a TBAB mediated release**: After confirming encapsulation of the fluorescent dye, we subjected it for the controlled release experiment using a cationic dipeptide and TBAB as an external trigger. The controlled release of dye upon addition of the peptide trigger was monitored using increase in the fluorescence of the solution outside the dialysis tube. The control experiment was performed without addition of peptide stimuli. Peptide triggered controlled release of fluorescent dye was steadily continued for up to 40 hrs which was continued for 50 hrs to confirm the saturation in fluorescent intensity.

**2.5.12b Cationic peptide / amino acid mediated release**: Peptide vesicles (200 µL) loaded with carboxyfluorescein was sealed in dialysis membrane and then 200 µL of 5 mM solution of cationic dipeptide or amino acid *L*-arginine in water was added. This dialysis bag was suspended in agitating ethanol / water solution. Further, 300 µL aliquot of solution outside the dialysis bag was timely collected for the quantification of released carboxyfluorescein. Fluorescent measurement experiments were carried out using Fluorolog-3 HORIBA JOBIN YVON fluorescence fluorimeter, with 417 nm excitation and 437-750 nm emission range using 1/1 slit and 1 nm data interval.

**2.5.13 Contact angle measurement**: Contact angles on the peptide coated layers were measured by using a Contact Angle Meter (Model ID: HO-IAD-CAM-01; Holmarc Opto-Mechatronics Pvt. Ltd.), followed by LBADSA drop analysis (ImageJ software), which is based on the fitting of the Young-Laplace equation to the image data. To check out the hydrophobicity of the synthetic peptides, contact angle (CA) measurements were carried out. For these measurements, a $3 \times 3$ cm$^2$ uniform area of fabric was accurately cut, and gently stuck to a glass plate on which the peptides were coated in thin, uniform layers. The amount of water dispersion on the sample surface was around 4 µL per droplet. The CA measurements were recorded for six consecutive times from different areas of the sample at 1.0 s, following which the average CA value was calculated.

**2.5.14 MALDI-TOF characterization**: MALDI-TOF mass spectra were obtained on either Voyager-Elite instrument (Perspective Biosystems Inc., Farmingham, MA) equipped with delayed extraction or on Voyager-De-STR (Applied Biosystems) instrument. 2,5-Dihydroxy benzoic acid (DHB) and α-cyano-4- hydroxycinnamic acid (CHCA) both were used as matrix for peptides of which DHB was found to give satisfactory results. A saturated matrix solution was prepared with typical dilution solvent (50:50:0.1 Water: MeCN: TFA) and spotted on the metal plate along with the oligomers. The metal plate was loaded to the instrument and the analyte ions are then accelerated by an applied high voltage (15-25 kV) in reflector mode, separated in a field free flight tube and detected as an electrical signal at the end of the flight tube.

## 2.6 References

1. (a) Vauthey, S.; Santoso, S.; Gong, H.; Watson, N.; Zhang, S. *Proc. Natl. Acad. Sci. U. S. A.* **2002**, *99*, 5355-5360; (b) Zhang, S. *Nat. Biotechnol*. **2003**, *21*, 1171-1178; (c) Reches, M.; Gazit, E. *Nano Lett*. **2004**, *4*, 581-585; (d) Gazit, E. *Chem. Soc. Rev*. **2007**, *36*, 1263-1269; (e) Gazit, E. *Nat. Nanotechnol*. **2008**, *3*, 8-9; (f) Zelzer, M.; Ulijn, R. V. *Chem. Soc. Rev*. **2010**, *39*, 3351-3357; (g) Abramovich, L. A.; Gazit, E. *Chem. Soc. Rev*. **2014**, *43*, 6881-6893; (h) Levin, A.; Mason, T. O.; Abramovich, L. A.; Buell, A. K.; Meisl, G.; Galvagnion, C.; Bram, Y.; Stratford, S. A.; Dobson, C. M.; Knowles, T. P. J.; Gazit, E. *Nat. Commun*. **2014**, *5*, 5219; (i) Mondal, S.; Abramovich, L. A.; Lampel, A.; Bram, Y.; Lipstman, S.; Gazit, E. *Nat. Commun*. **2015**, *6*, 8615; (j) Mondal, S.; Gazit, E. *ChemNanoMat* **2016**, *2*, 323-332.

2. Webber, M. J.; Appel, E. A.; Meijer, E. W.; Langer, R. *Nat. Mater*. **2016**, *15*, 13-26.

3. Aida, T.; Meijer, E. W.; Stupp, S. I. *Science* **2012**, *335*, 813-817.

4. Yan, X.; Zhu, P.; Li, J. *Chem. Soc. Rev*. **2010**, *39*, 1877-1890.

5. Zhang, S. *Nat. Biotechnol*. **2004**, *22*, 151-152.

6. Gorbitz, C. H. *Chem. Eur. J*. **2001**, *7*, 5153-5159.

7. Reches, M.; Gazit, E. *Nat. Nano*. **2006**, *1*, 195-200.

8. Abramovich, L. A.; Reches, M.; Sedman, V. L.; Allen, S.; Tendler, S. J. B.; Gazit, E. *Langmuir* **2006**, *22*, 1313-1320.

9. Tamamis, P.; Abramovich, L. A.; Reches, M.; Marshall, K.; Sikorski, P.; Serpell, L.; Gazit, E.; G. Archontis, G. *Biophys. J*. **2009**, *96*, 5020-5029.

10. Azuri, I.; Abramovich, L. A.; Gazit, E.; Hod, O.; Kronik, L. *J. Am. Chem. Soc.* **2014**, *136*, 963-969.

11. Reches, M.; Gazit, E. *Science* **2003**, *300*, 625-627.

12. Gazit, E. *Nat. Chem.* **2015**, *7*, 14-15.

13. Arnon, Z. A.; Vitalis, A.; Levin, A.; Michaels, T. C. T.; Caflisch, A.; Knowles, T. P. J.; Abramovich, L. A.; Gazit, E. *Nat. Commun*. **2016**, *7*, 13190.

14. (a) Reches, M.; Gazit, E. *Science* **2003**, *300*, 625-627; (b) Reches, M.; Gazit, E. *Nano Lett.* **2004**, *4*, 581-585; (c) Reches, M.; Gazit, E. *Isr. J. Chem.* **2005**, *45*, 363-371; (d) Reches, M.; Gazit, E. *Phys. Biol.* **2006**, *3*, S10-S19.

15. Abramovich, L. A.; Kol, N.; Yanai, I.; Barlam, D.; Shneck, R. Z.; Gazit, E.; Rousso, I. *Angew. Chem. Int. Ed.* **2010**, *49*, 9939-9942.

16. Abramovich, L. A.; Gazit, E. *J. Pept. Sci.* **2008**, *14*, 217-223.

17. Fleming, S.; Ulijn, R. V. *Chem. Soc. Rev.* **2014**, *43*, 8150-8177.

18. Charalambidis, G.; Kasotakis, E.; Lazarides, T.; Mitraki, A.; Coutsolelos, A. G. *Chem. Eur. J.* **2011**, *17*, 7213-7219.

19. Bera, S.; Jana, P.; Maity, S. K.; Haldar, D. *Cryst. Growth Des.* **2014**, *14*, 1032-1038.

20. Maity, D. K.; Banerjee, A. *Chem. Asian. J.* **2013**, *8*, 113-120.

21. Maity, D. K.; Bhattacharjee, R.; Datta, A.; Banerjee, A. *J. Phys. Chem. C*. **2013**, *117*, 23178-23189.

22. Liu, Y.; Wang, Y.; Jin, L.; Chen, T.; Yin, B. *Soft Matter* **2016**, *12*, 934-945.

23. Manna, M. K.; Rasale, D. B.; Das, A. K. *RSC Adv*. **2015**, *5*, 90158-90167.

24. Jana, P.; Maity, S.; Maity, S. K.; Ghorai, P. K.; Haldar, D. *Soft Matter* **2012**, *8*, 5621-5628.

25. Basu, K.; Baral, A.; Basak, S.; Deshsorkhi, A.; Nanda, J.; Bhunia, D.; Ghosh, S.; Castelletto, V.; Hamley, I. W.; Banerjee, A. *Chem. Commun*. **2016**, *52*, 5045-5048.

26. Joshi, K. B.; Verma, S. *J. Pept. Sci*. **2008**, *14*, 118-126.

27. Ghosh, S.; Abramovich, L. A.; Gazit, E.; Verma, S. *Tetrahedron* **2013**, *69*, 2004-2009.

28. Zhu, C.; Gao, Y.; Li, H.; Meng, S.; Li, L.; Francisco, J. S.; Zeng, X. C. *Proc. Natl. Acad. Sci. U. S. A.* **2016**, *113*, 12946-12951.

29. (a) Yuran, S.; Razvag, Y.; Reches, M. *ACS Nano* **2012**, *11*, 9559-9566; (b) Levin, A.; Mason, T. O.; Abramovich, L. A.; Buell, A. K.; Meisl, G.; Galvagnion, C.; Bram, Y.; Stratford, S. A.; Dobson, C. M.; Knowles, T. P. J.; Gazit, E. *Nat. Commun*. **2014**, *5*, 5219.

30. Maity, S.; Jana, P.; Maity, S. K.; Haldar, D. *Langmuir* **2011**, *27*, 3835-3841.

31. Liu, F.; Austin, D. J. *Tetrahedron Lett.* **2001**, *42*, 3153-3154.

32. Ikeuchi, H.; Meyer, M. E.; Ding, Y.; Hiratake, J.; Richards, N. G. J. *Bioorg. Med. Chem*. **2009**, *17*, 6641-6650.

33. (a) Chi, X.; Pahari, P.; Nonaka, K.; Van Lanen, S. G. *J. Am. Chem. Soc*. **2011**, *133*, 15288-15291; (b) Zhang, W.; Ntai, I.; Bolla, M. L.; Malcolmson, S. J.; Kahne, D.; Kelleher, N. L.; Walsh, C. T. *J. Am. Chem. Soc*. **2011**, *133*, 5240-5243.

34. (a) Godeau, G.; Brun, C.; Arnion, H.; Staedel, C.; Barthelemy, P. *Tetrahedron Lett*. **2010**, *51*, 1012-1015; (b) Hiebl, J.; Zbiral, E.; Balzarini, J.; Clercq, E. D. *J. Med. Chem.* **1991**, *34*, 1426-1430.

35. (a) Mayans, E.; Casanovas, J.; Gil, A. M.; Jimenez, A. I.; Cativiela, C.; Puiggali, J.; Aleman, C. *Langmuir* **2017**, *33*, 4036-4048; (b) Khurana, R.; Fink, A. L. *Biophys. J.* **2000**, *78*, 994-1000; (c) Qian, W.; Bandekar, J.; Krimm, S. *Biopolymers* **1991**, *31*, 193-210; (d) Toniolo, C.; Palumbo, M. *Biopolymers* **1977**, *16*, 219-224.

36. Misra, R.; Reja, R. M.; Narendra, L. V.; George, G.; Raghothama, S.; Gopi, H. N. *Chem. Commun*. **2016**, *52*, 9597-9600.

37. Ingole, T. S.; Kale, S. S.; Babu, S. S.; Sanjayan, G. J. *Chem. Commun*. **2016**, *52*, 10771-10774.

38. Gallivan, J. P.; Dougherty, D. A.; *Proc. Natl. Acad. Sci. U. S. A.* **1999**, *96*, 9459-9464.

39. (a) Xu, H.; Rudkevich, D. M. *Chem. Eur. J.* **2004**, *10*, 5432-5442; (b) Rudkevich, D. M.; Woldemariam, G. A.; Xu, H. *Polym. Prepr.* **2005**, *6*, 1162-1163.

40. Stastny, V.; Anderson, A.; Rudkevich, D. M. *J. Org. Chem.* **2006**, *71*, 8696-8705.

## 2.7 Appendix I: Characterization data of synthesized compounds

| Entry | Table of contents | Page No. |
|---|---|---|
| 1 | $^{1}$H, $^{13}$C NMR and IR spectra of compounds | 74-96 |

**(A)**



**(B)**
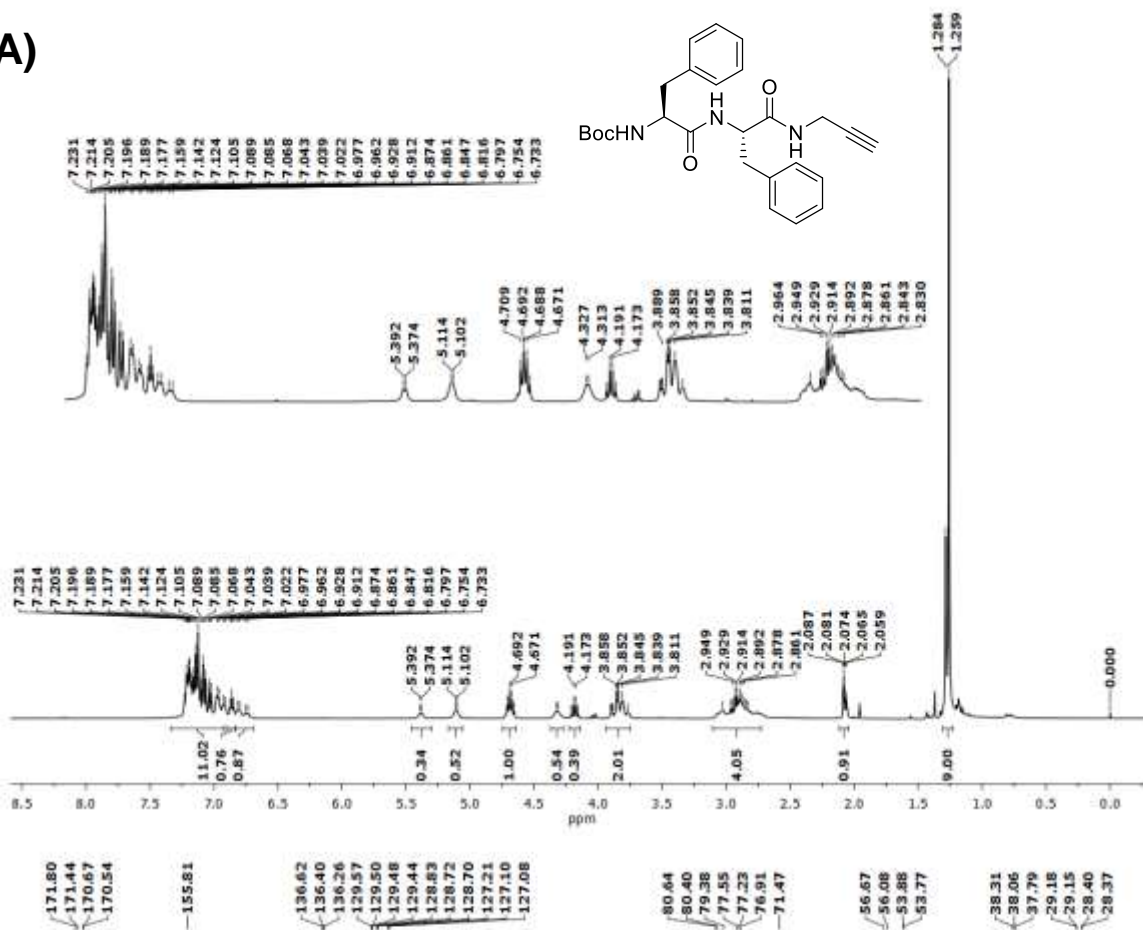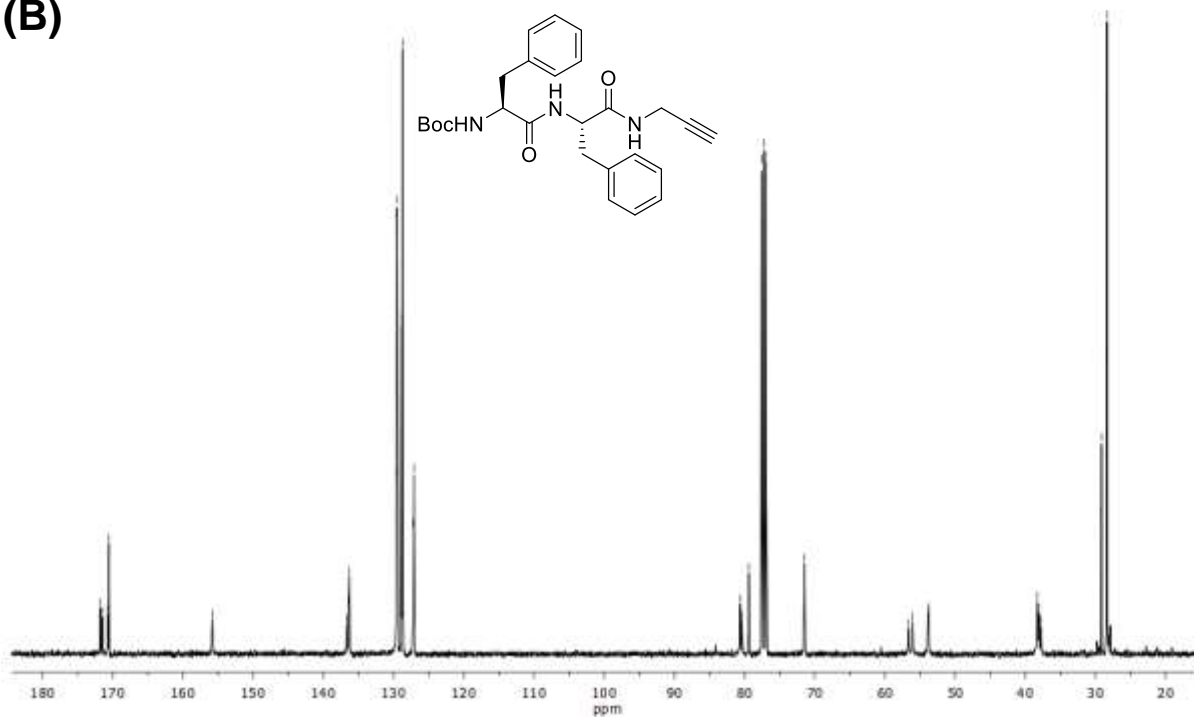


(A) $^1$H-NMR and (B) $^{13}$C-NMR spectra of peptide **2** (Boc-Phe-Phe-Propyne).

**(A)**



**(B)**
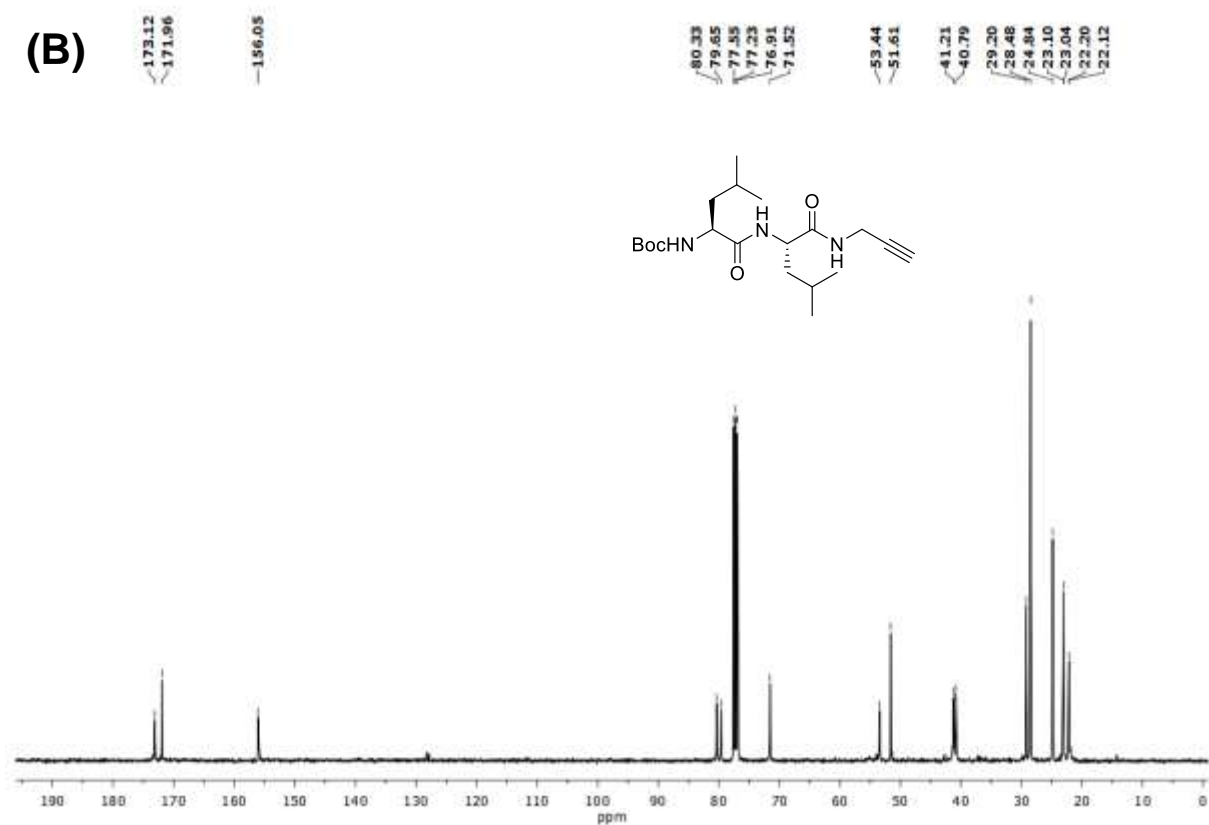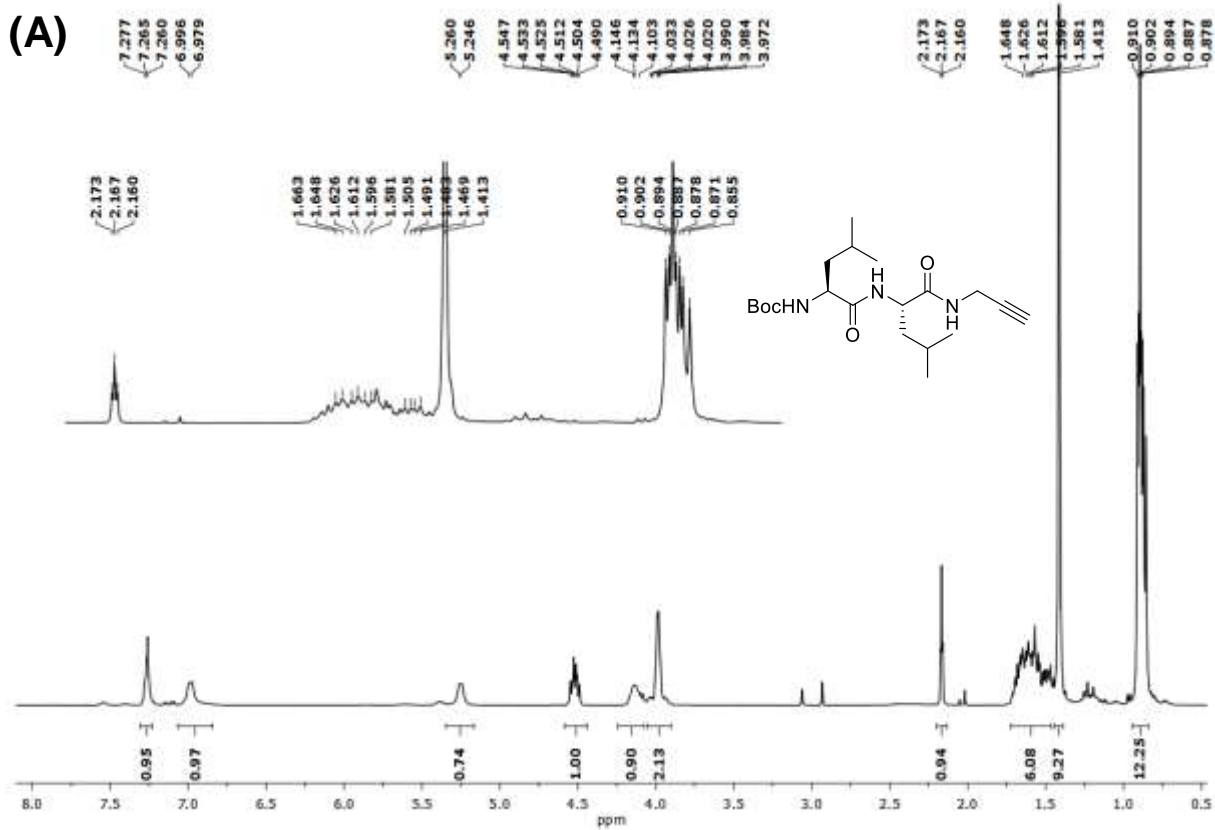


(A) $^1$H-NMR and (B) $^{13}$C-NMR spectra of peptide **4** (Boc-Leu-Leu-Propyne).
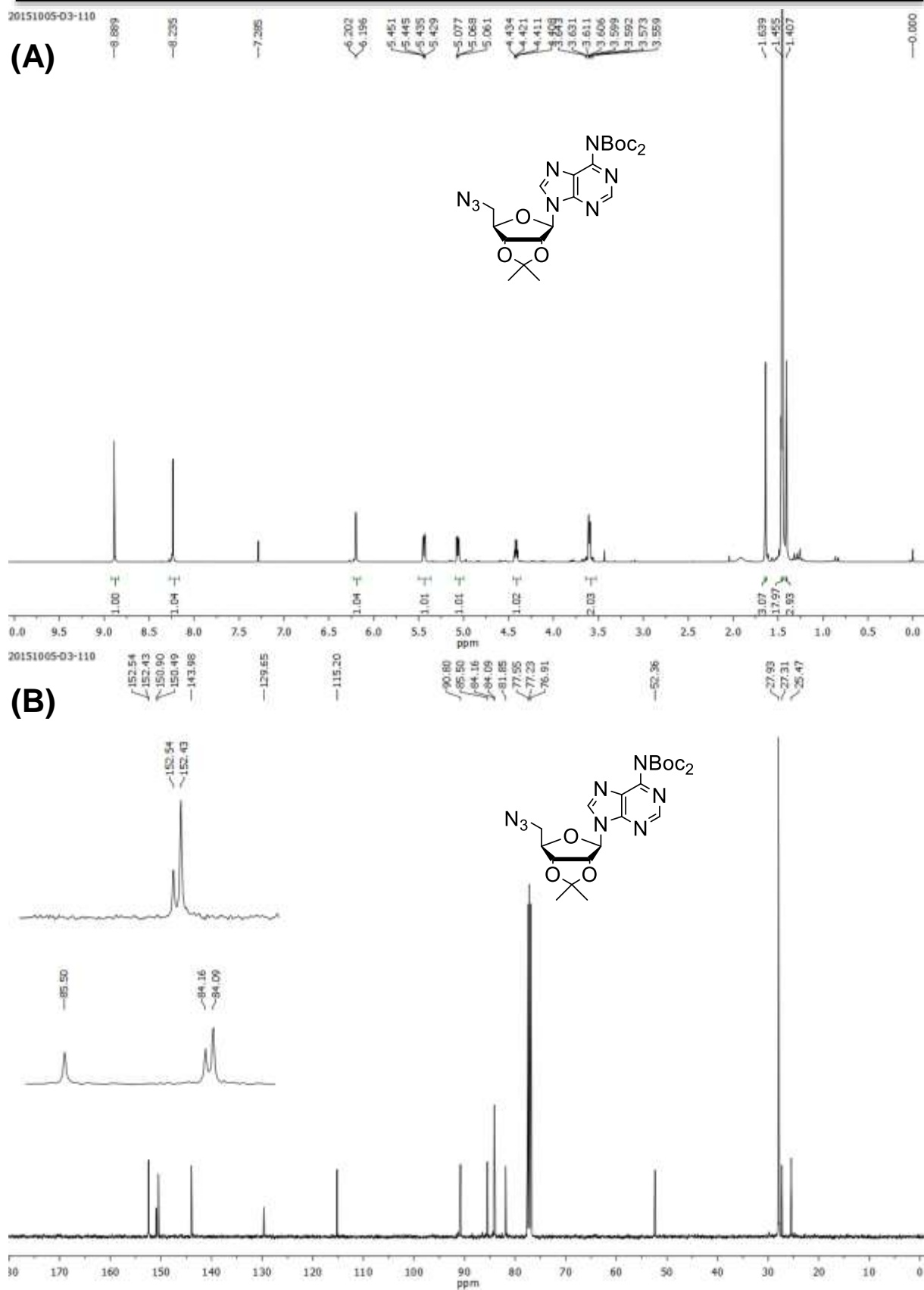
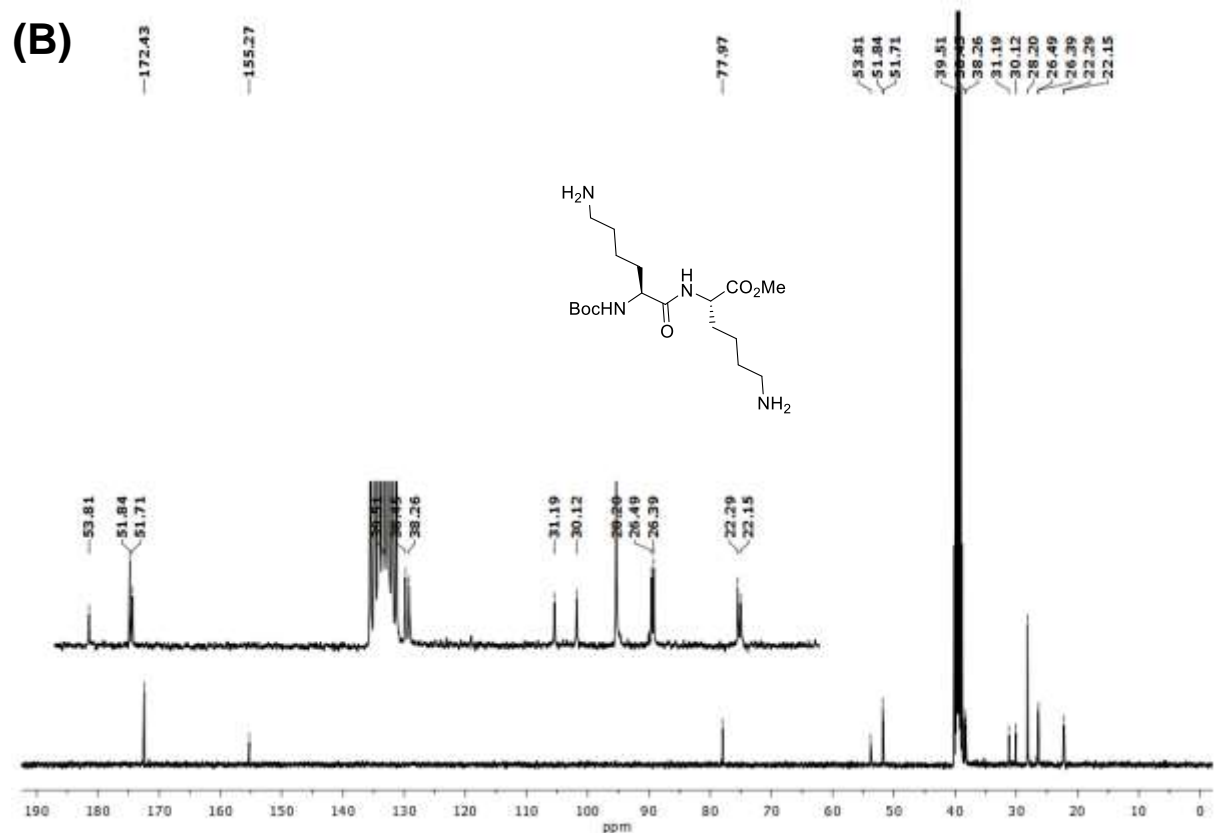(A) ¹H-NMR and (B) ¹³C-NMR spectra of **5**.
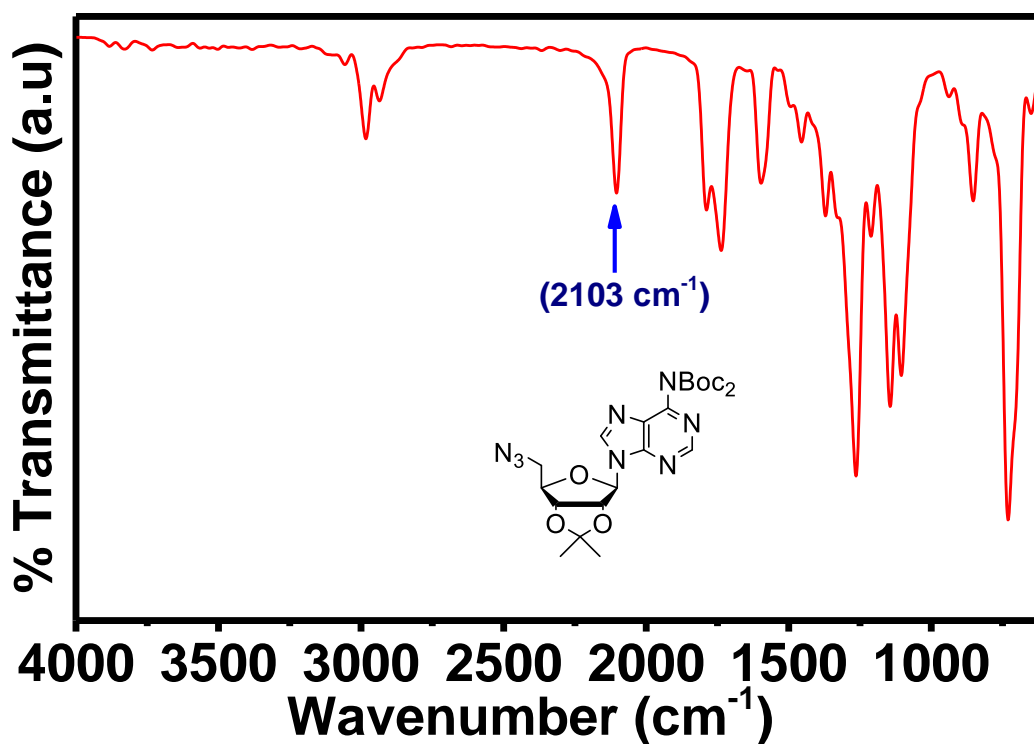
ATR-IR spectrum of azide **5**.
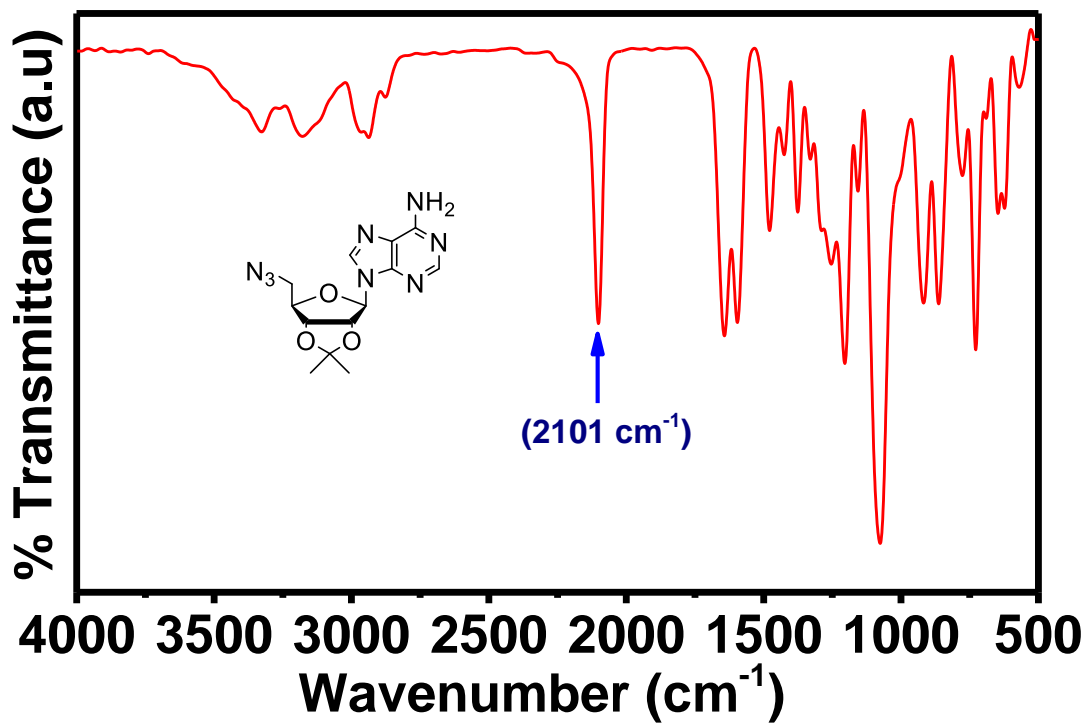


ATR-IR spectrum of azide **6**.

**(A)**



**(B)**
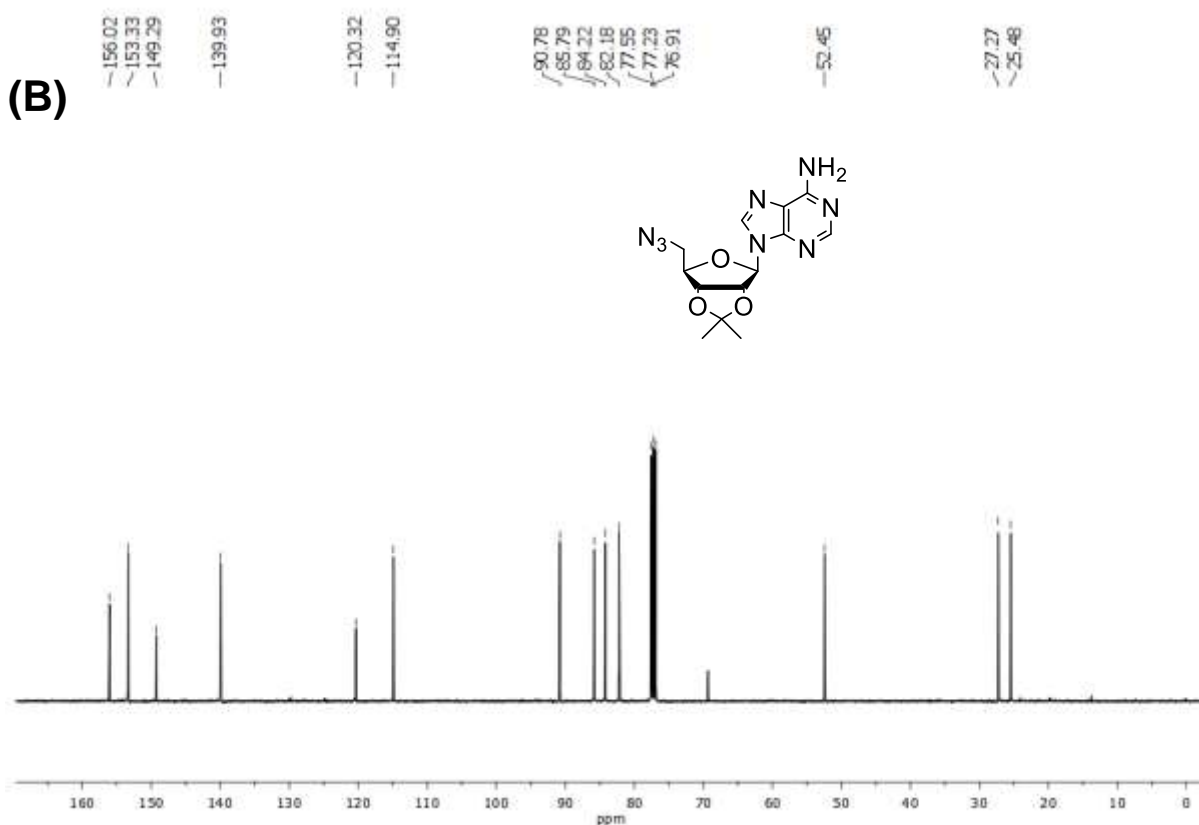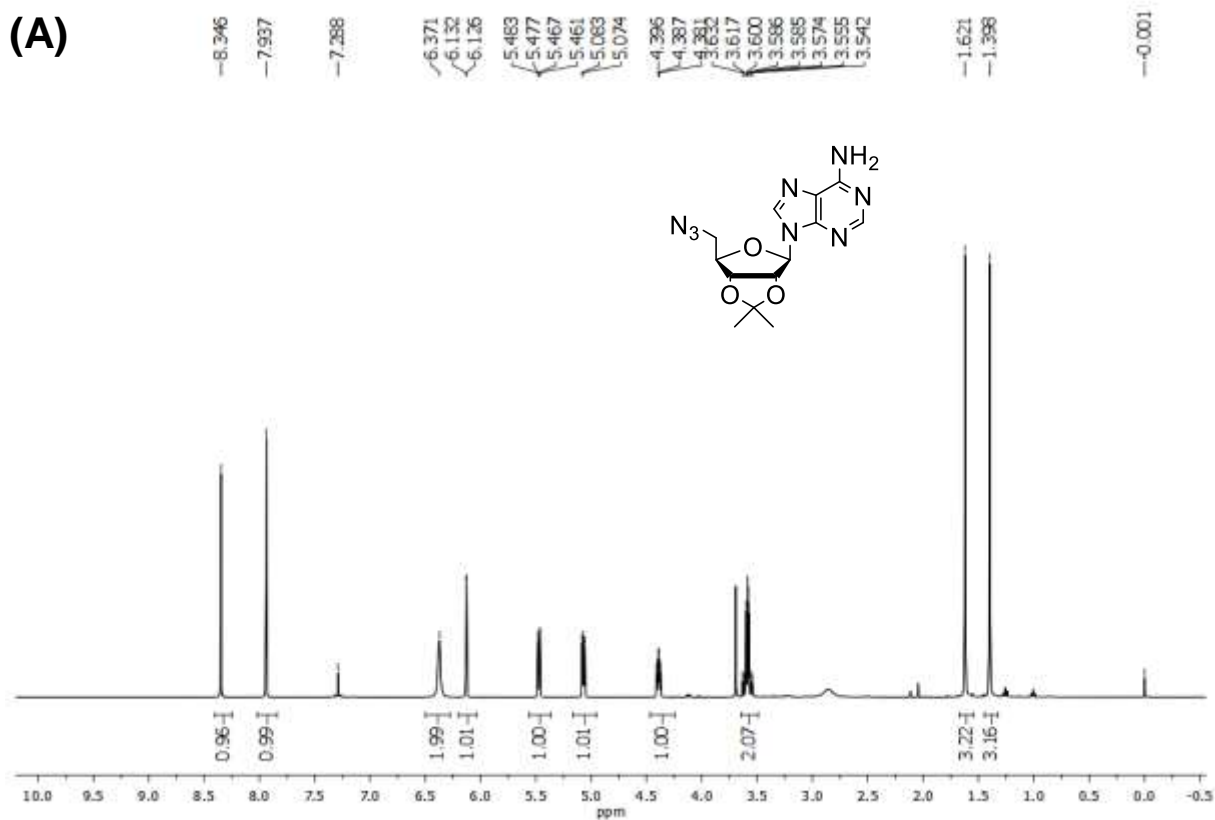


(A) ^{1}H-NMR and (B) ^{13}C-NMR of spectra of **6**.

**(A)**



**(B)**



(A) $^1$H-NMR and (B) $^{13}$C-NMR spectra of peptide **7** [Boc-Phe-Phe-*tz*-A$^{N(Boc)2}$].

**(A)**



**(B)**
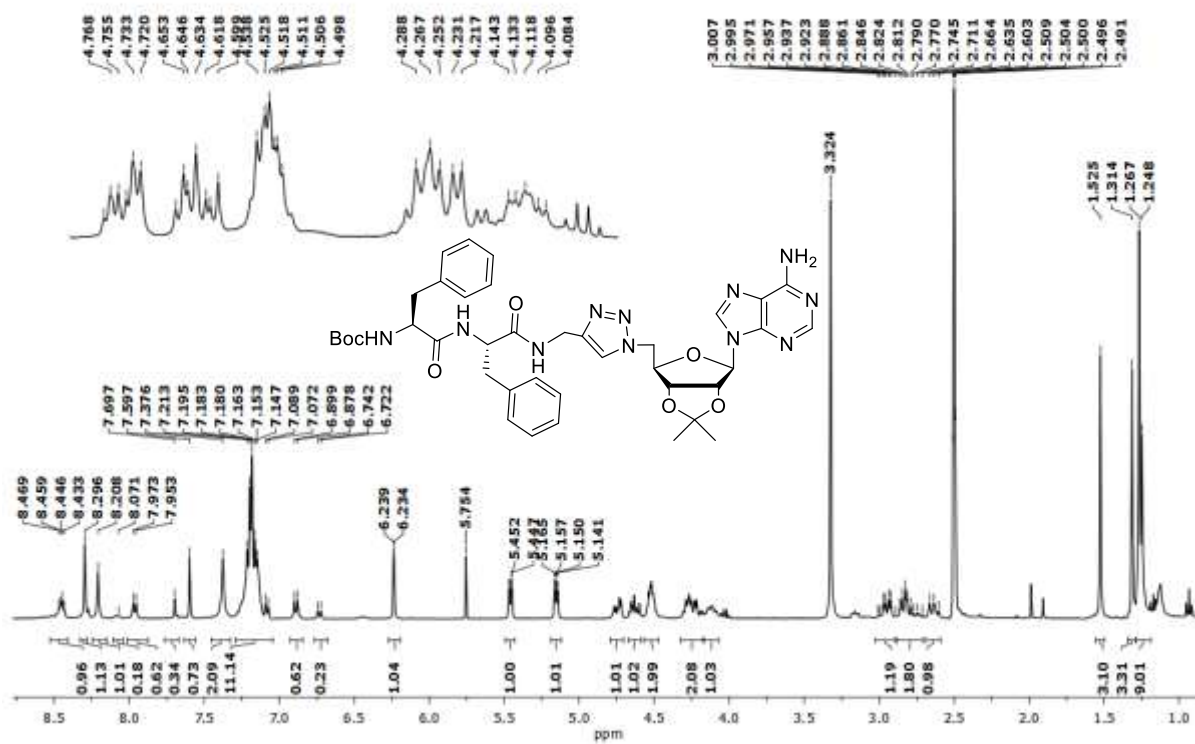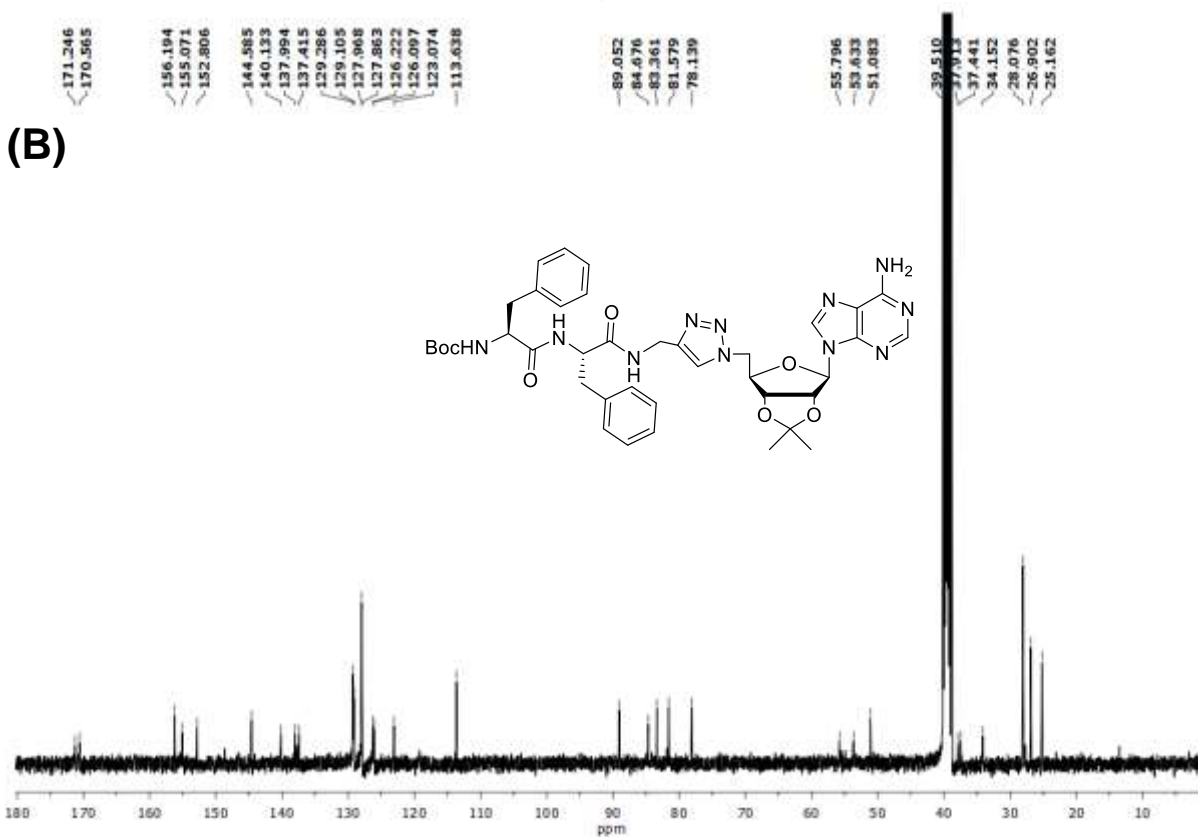


(A) $^1$H-NMR and (B) $^{13}$C-NMR spectra of peptide **8** (Boc-Phe-Phe-*tz*-A$^{NH2}$).

**(A)**



**(B)**
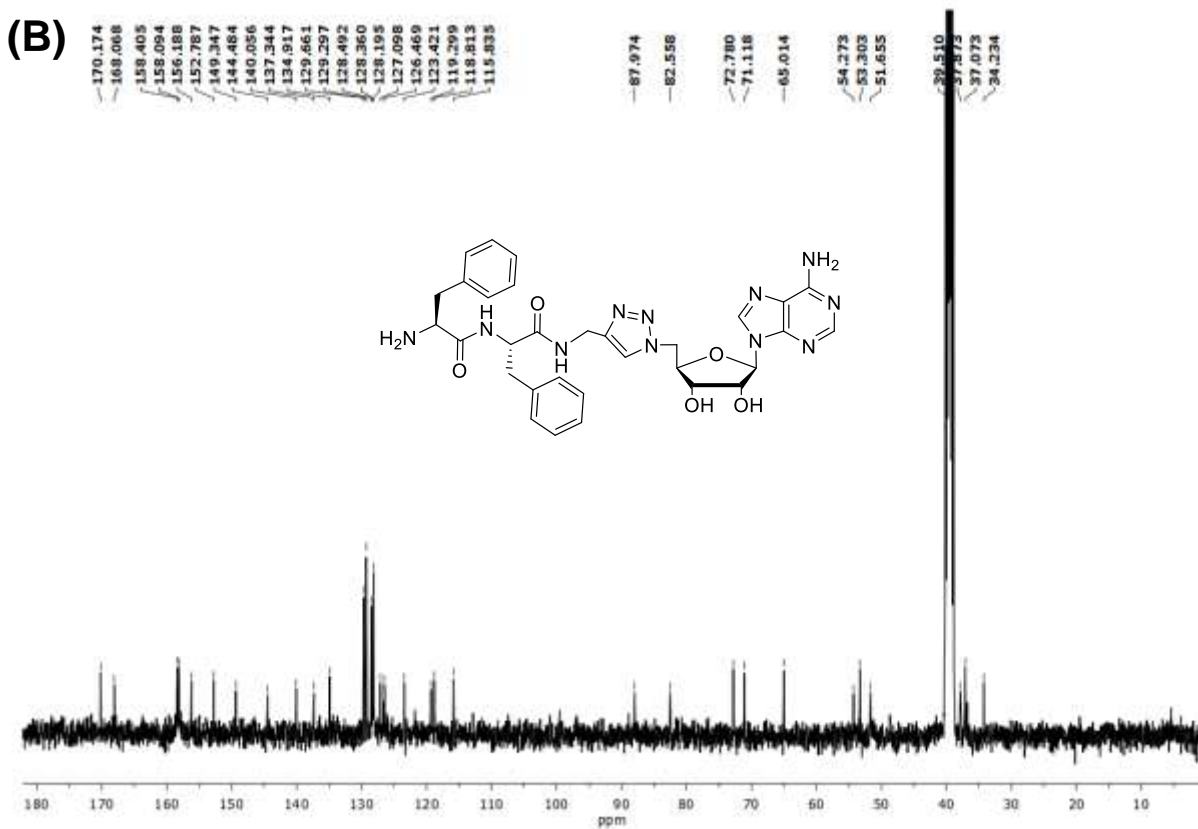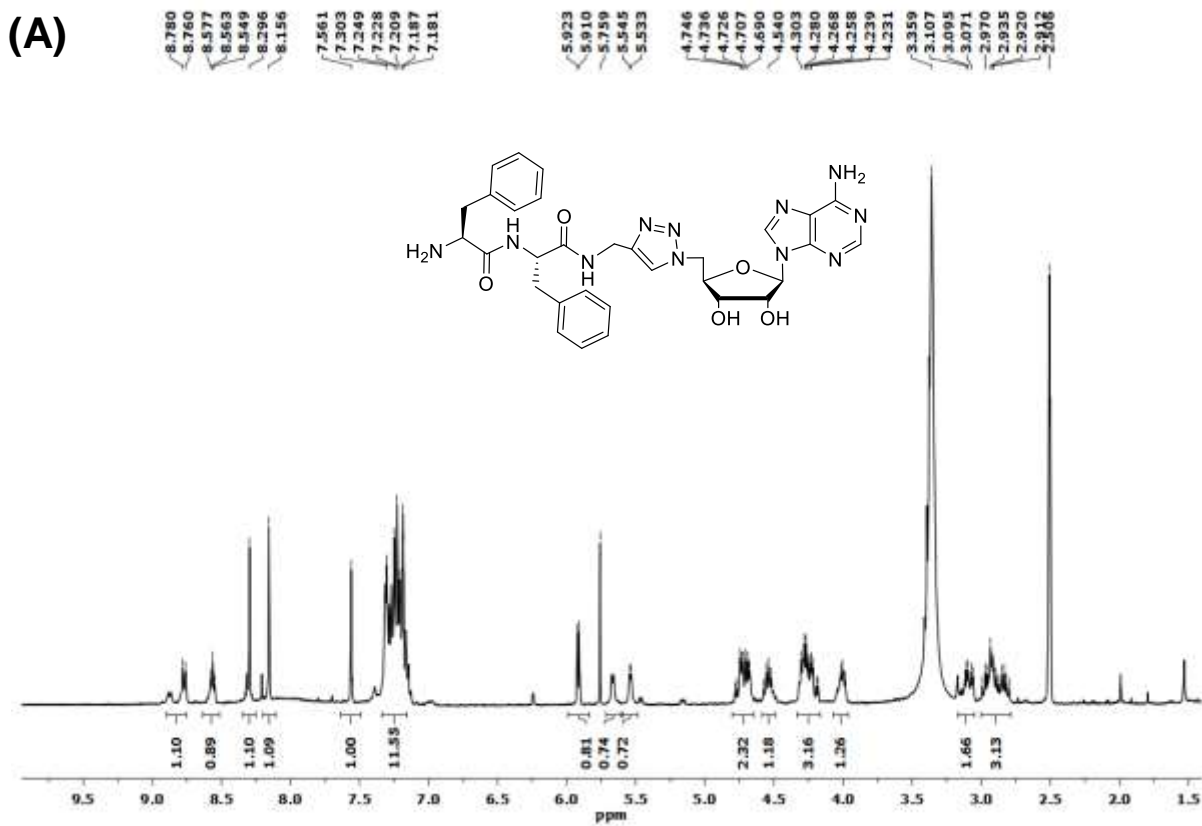


(A) $^1$H-NMR and (B) $^{13}$C-NMR spectra of peptide **9** (H-Phe-Phe-*tz*-A$^{NH2}$).

**(A)**



**(B)**



(A) ¹H-NMR and (B) ¹³C-NMR spectra of peptide **10** [Boc-Leu-Leu-*tz*-A^N(Boc)2].
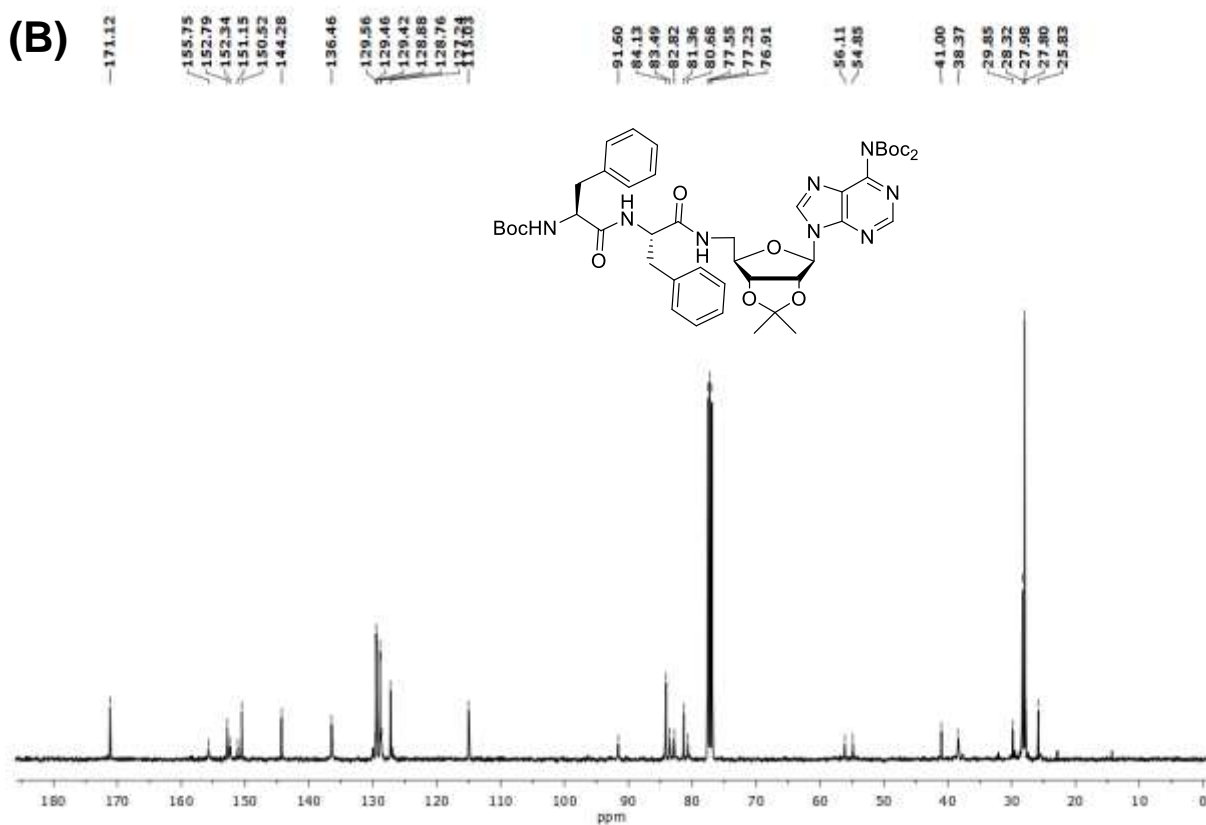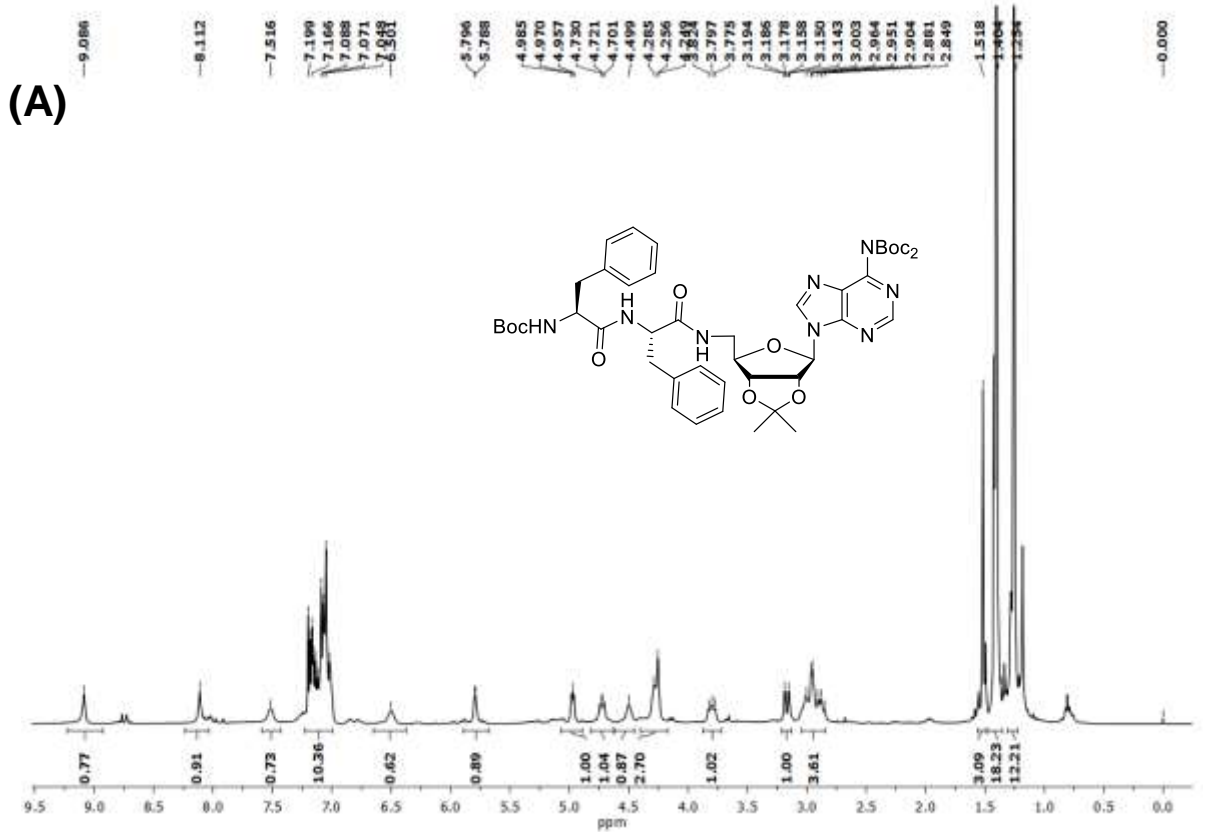
(A) $^1$H-NMR and (B) $^{13}$C-NMR spectra of peptide **12** [Boc-Phe-Phe-*am*-A$^{N(Boc)2}$].

**(A)**



**(B)**
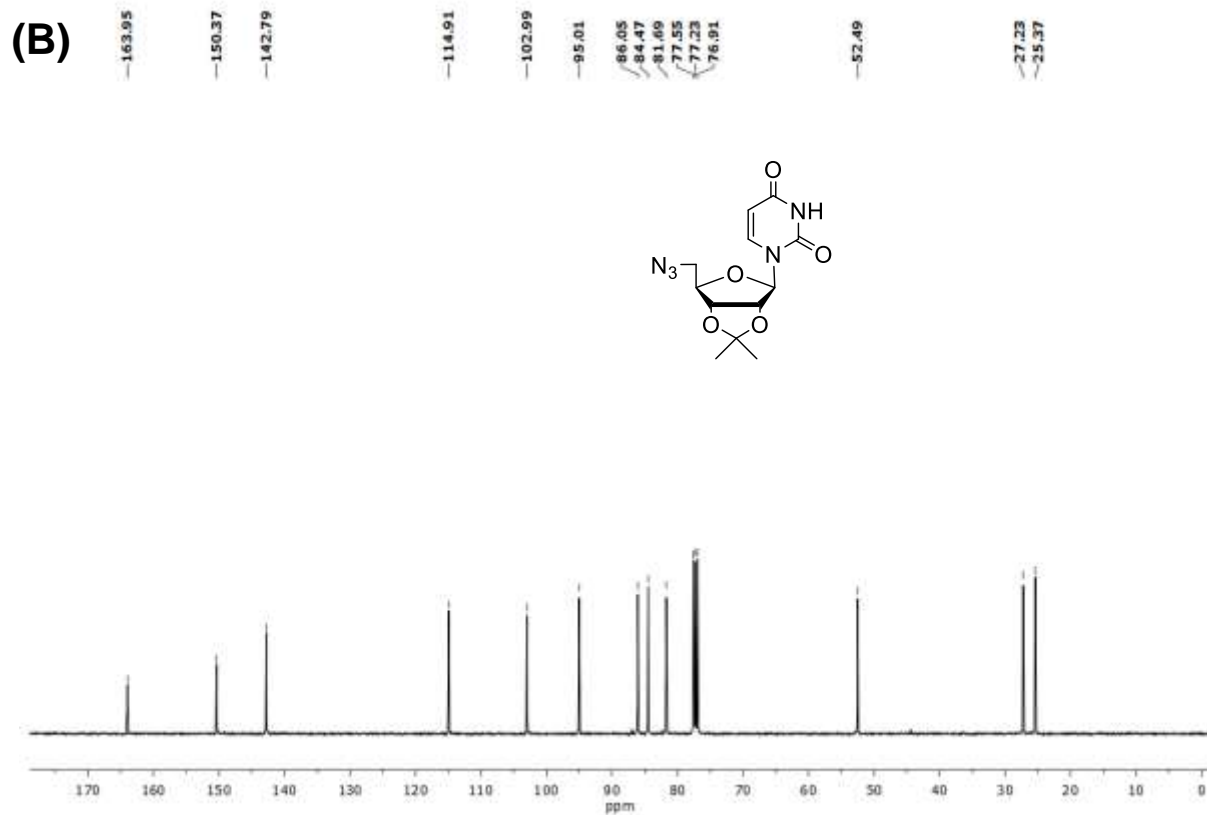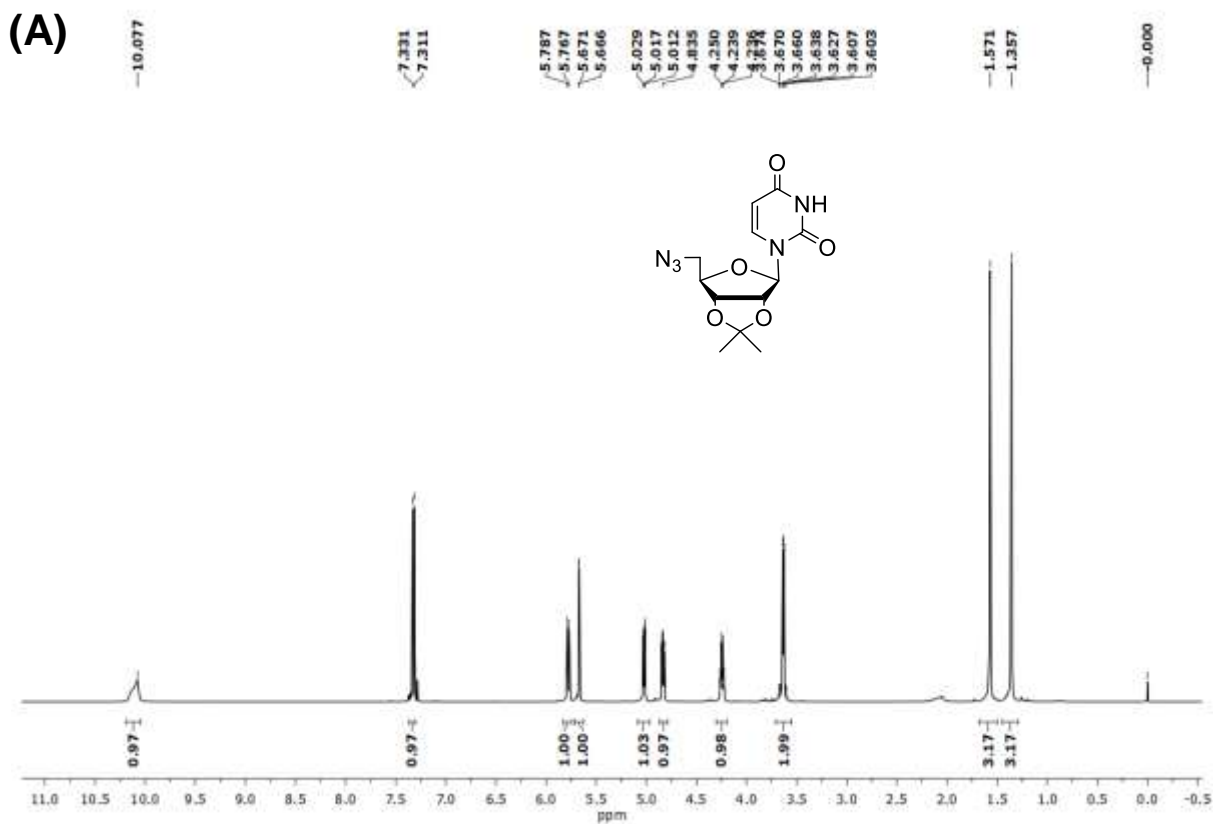


(A) $^1$H-NMR and (B) $^{13}$C-NMR spectra of azide **13**.
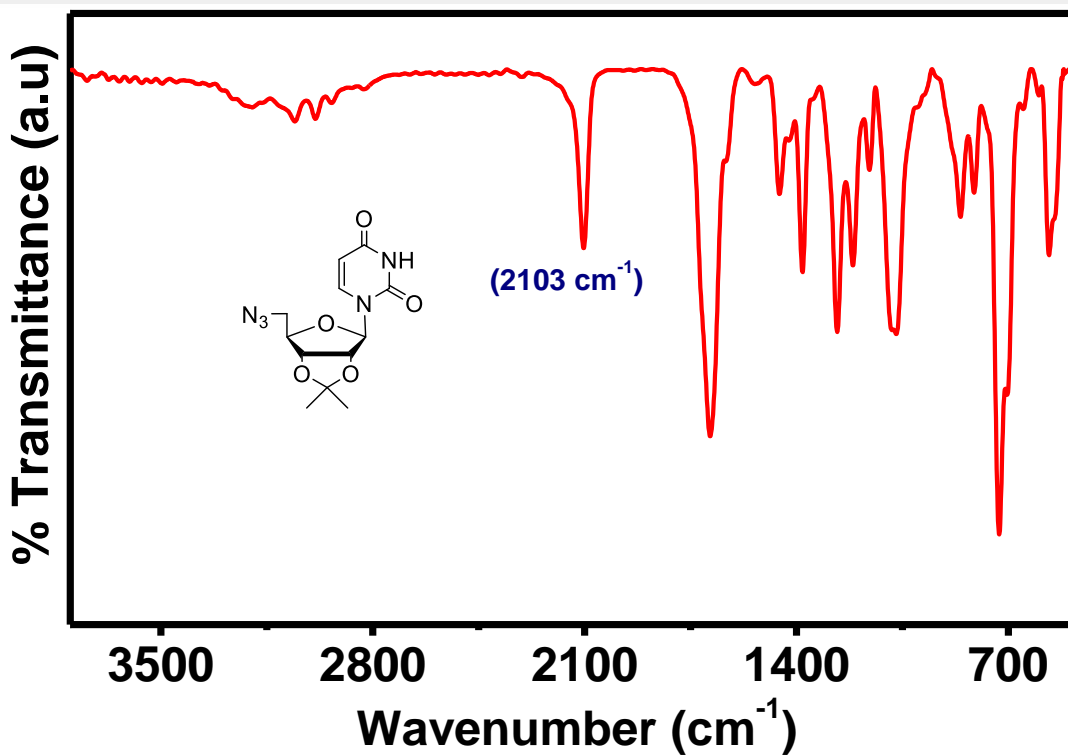
ATR-IR of azide **13**.



ATR-IR of azide **14**.

**(A)**



**(B)**
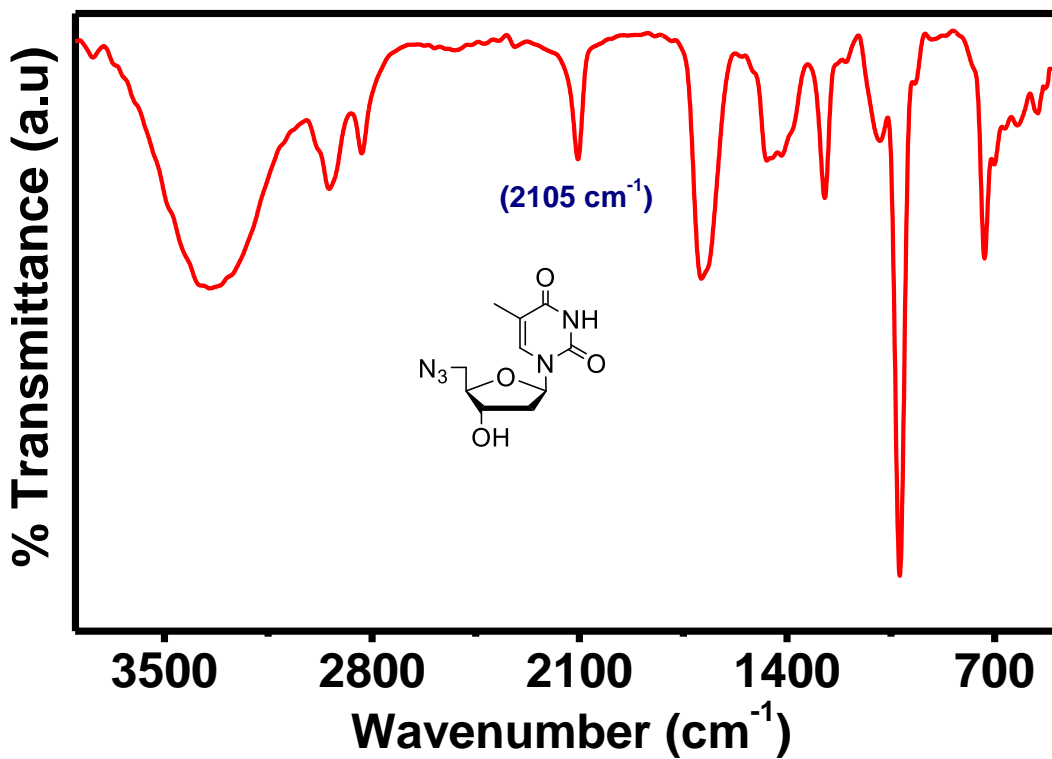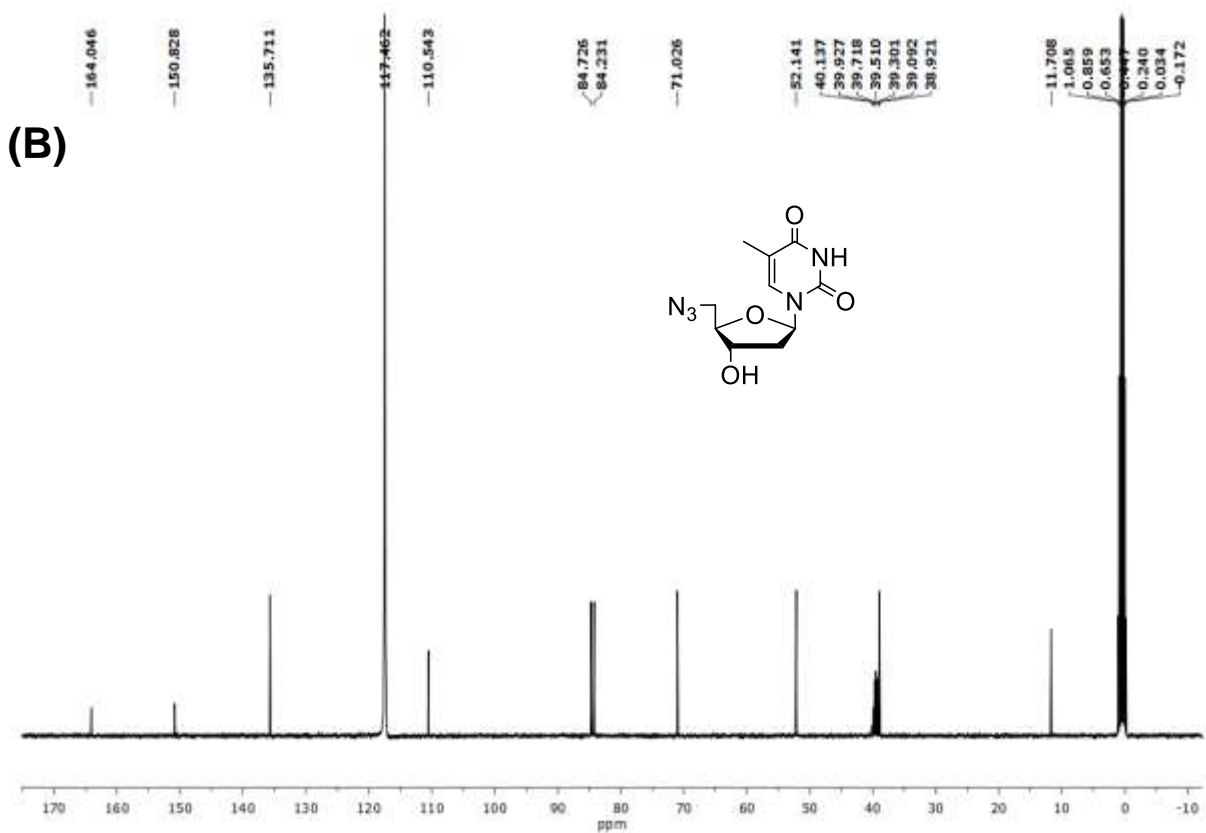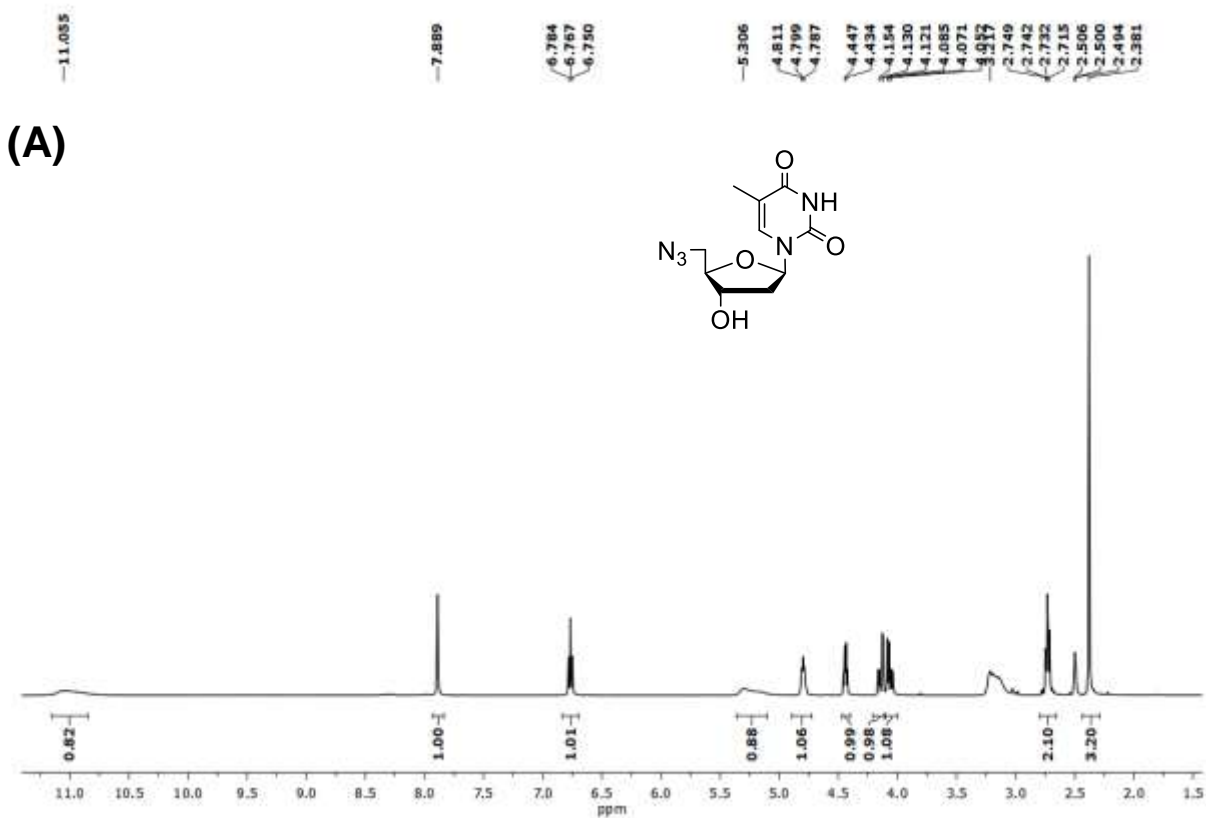


(A) $^1$H-NMR and (B) $^{13}$C-NMR spectra of azide **14** [in ACN-d$_3$ + DMSO-d$_6$ (5:1)].

**(A)**



**(B)**



(A) $^1$H-NMR and (B) $^{13}$C-NMR spectra of peptide **15** (Boc-Phe-Phe-*tz*-U).

**(A)**



**(B)**
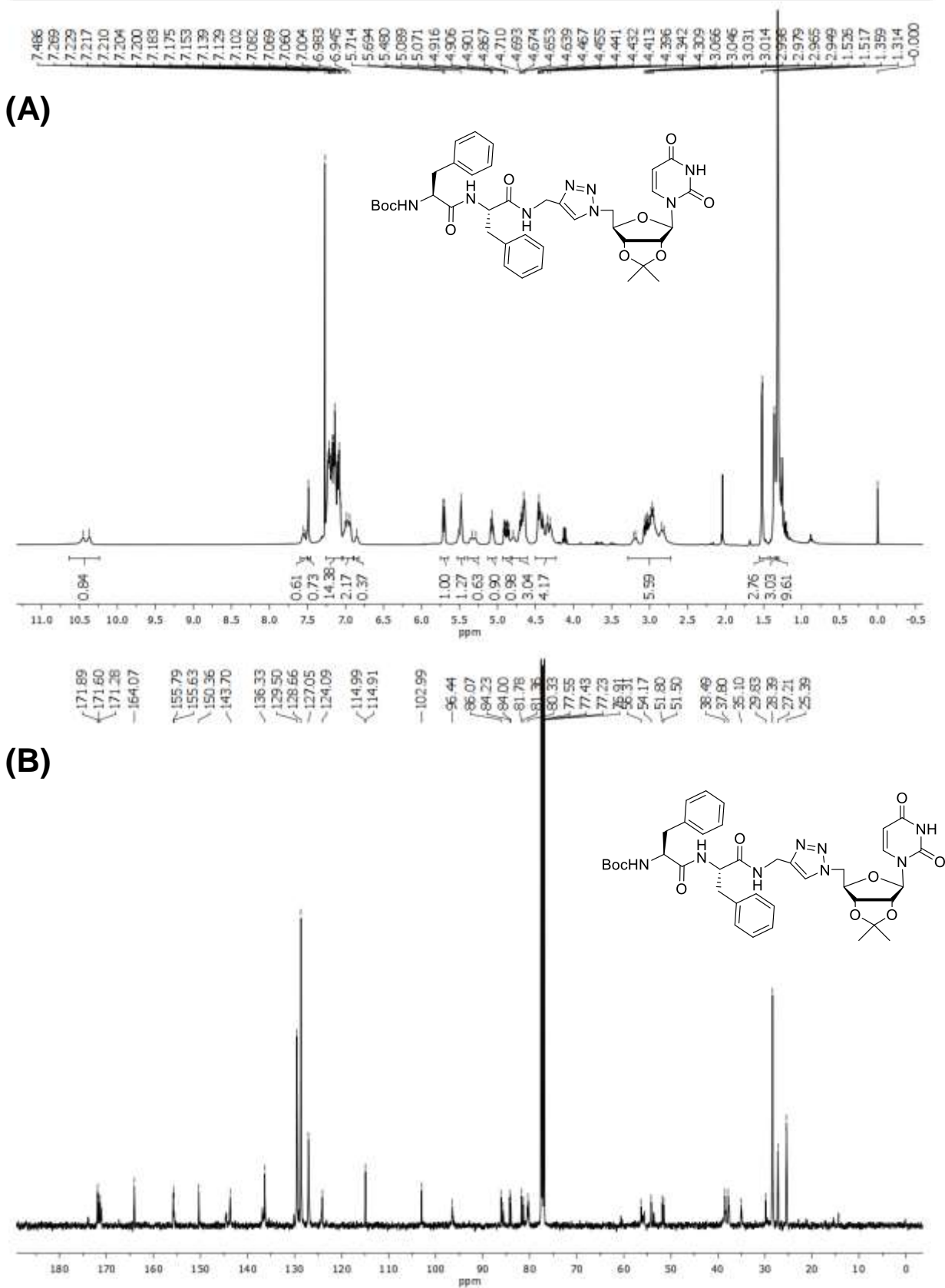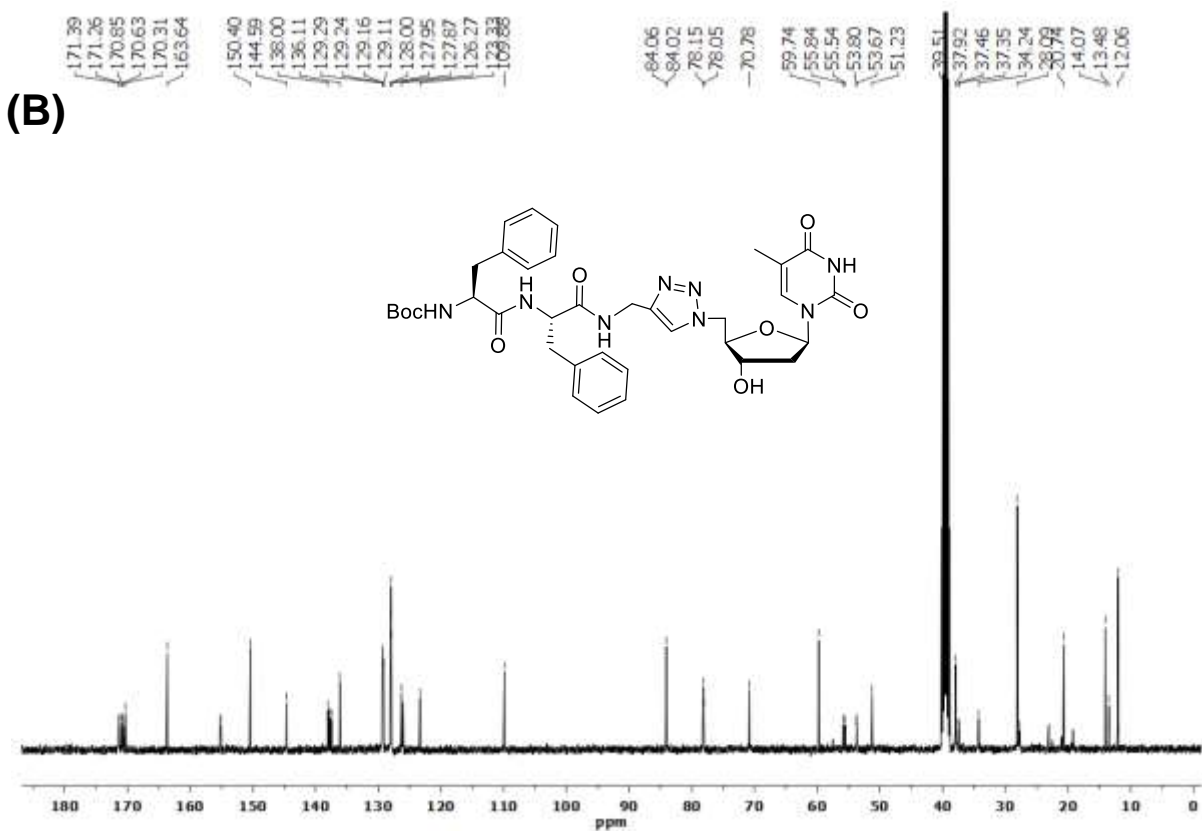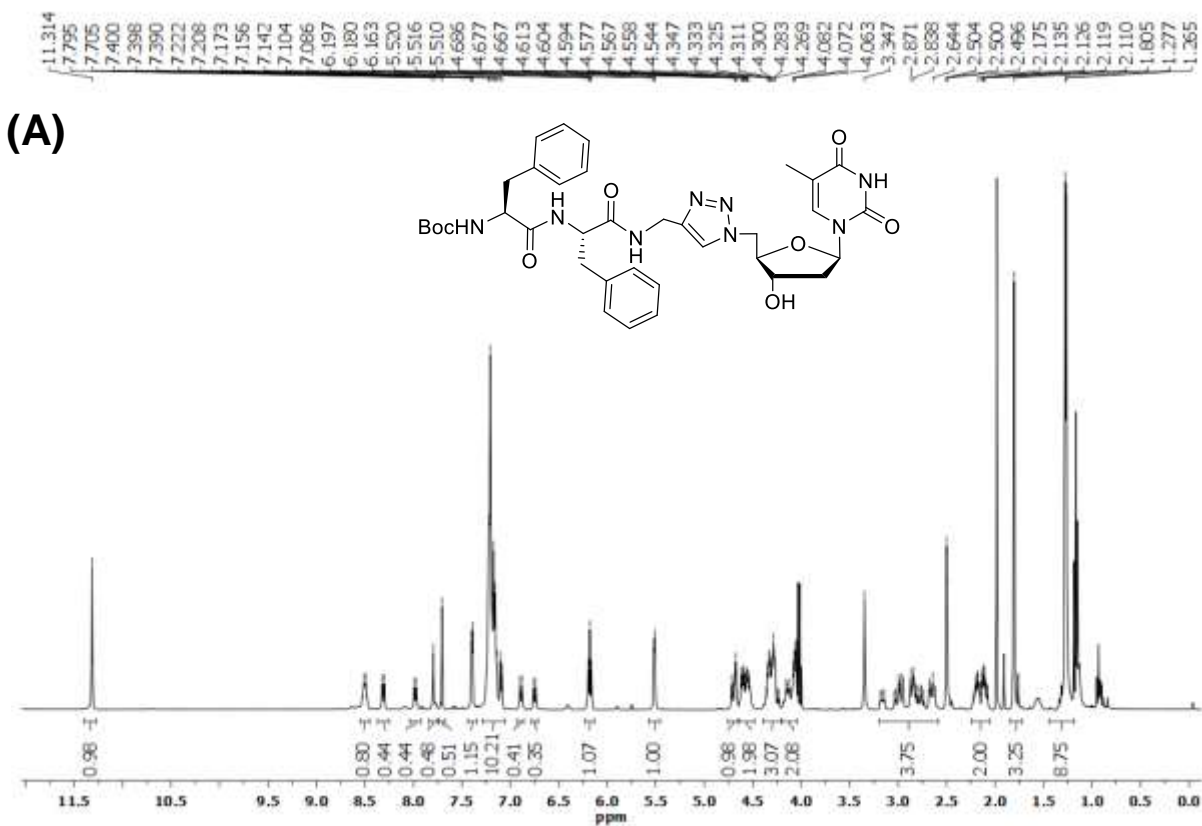


(A) ¹H-NMR and (B) ¹³C-NMR spectra of peptide **16** (Boc-Phe-Phe-*tz*-T).

**(A)**



**(B)**
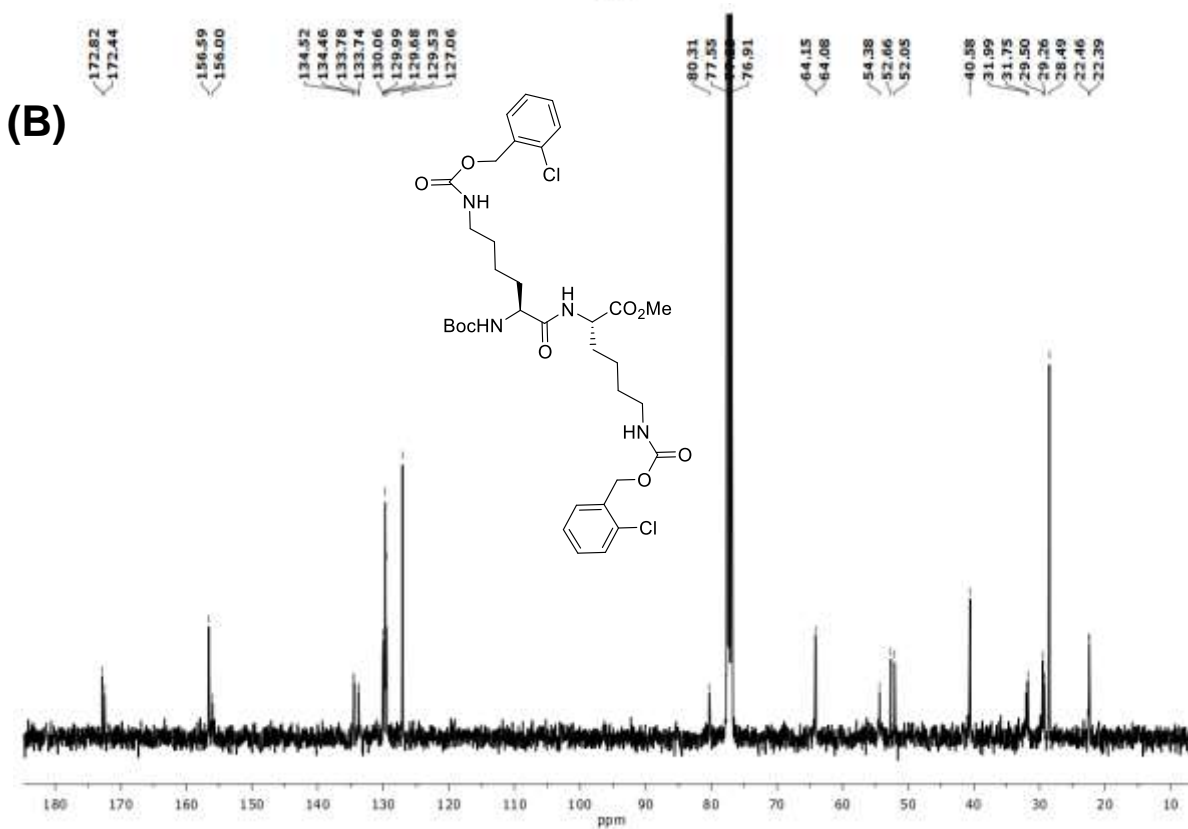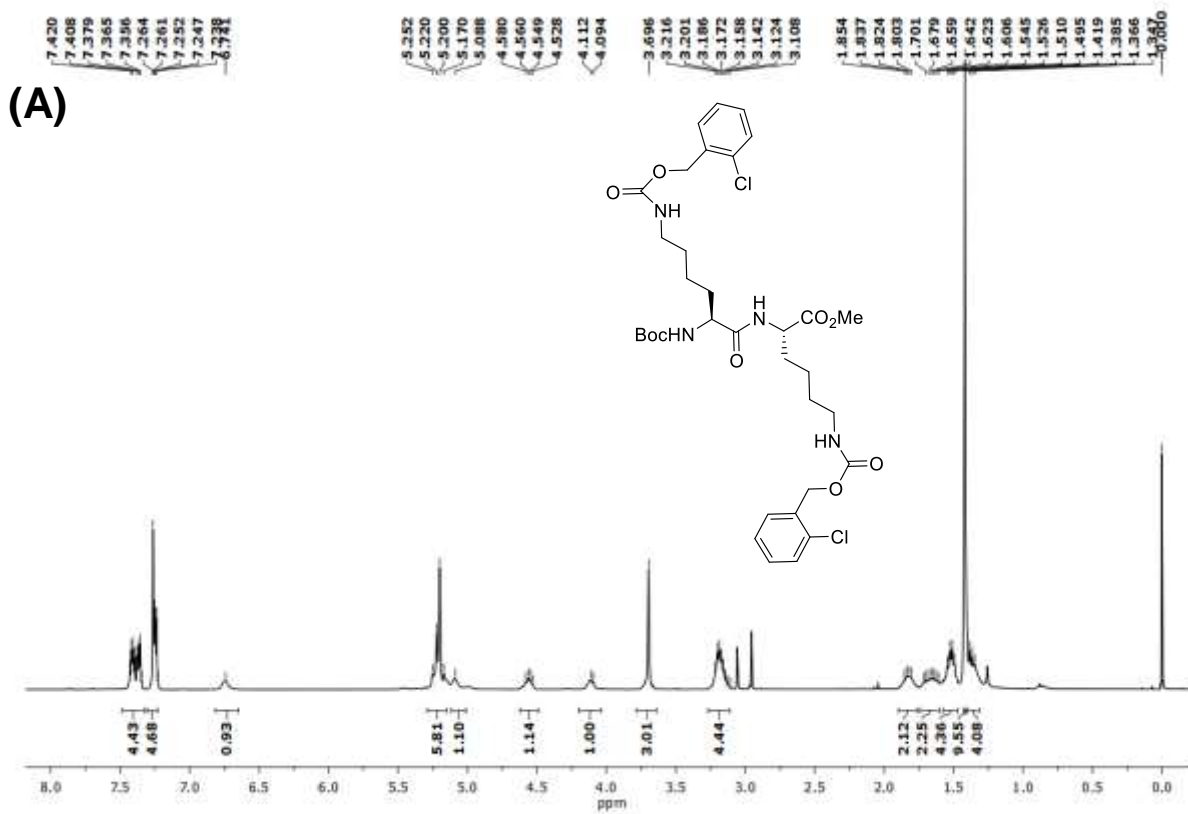


(A) $^1$H-NMR and (B) $^{13}$C-NMR spectra of Boc-Lys(Cl-Cbz)-Lys(Cl-Cbz)-OMe (**22**).

**(A)**



**(B)**
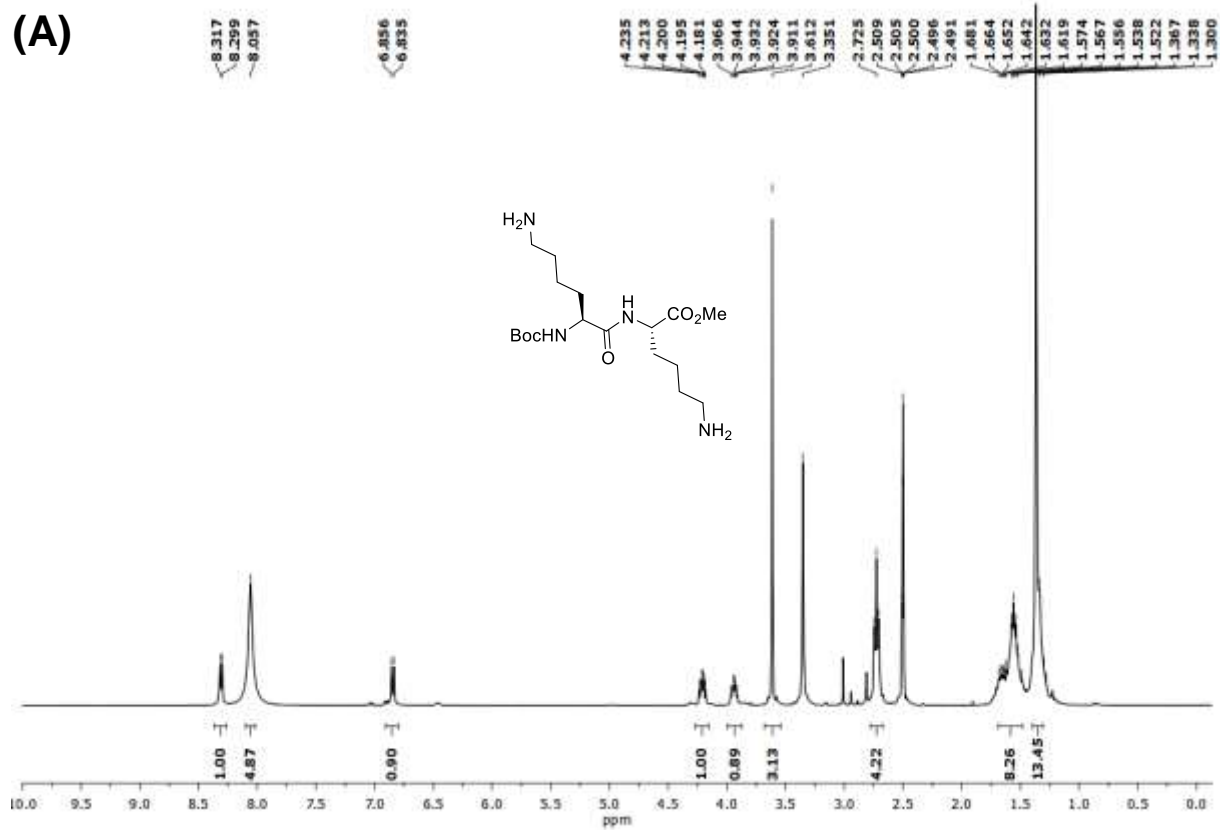


(A) ¹H-NMR and (B) ¹³C-NMR spectra of Boc-Lys-Lys-OMe (**23**).

**(A)**



**(B)**
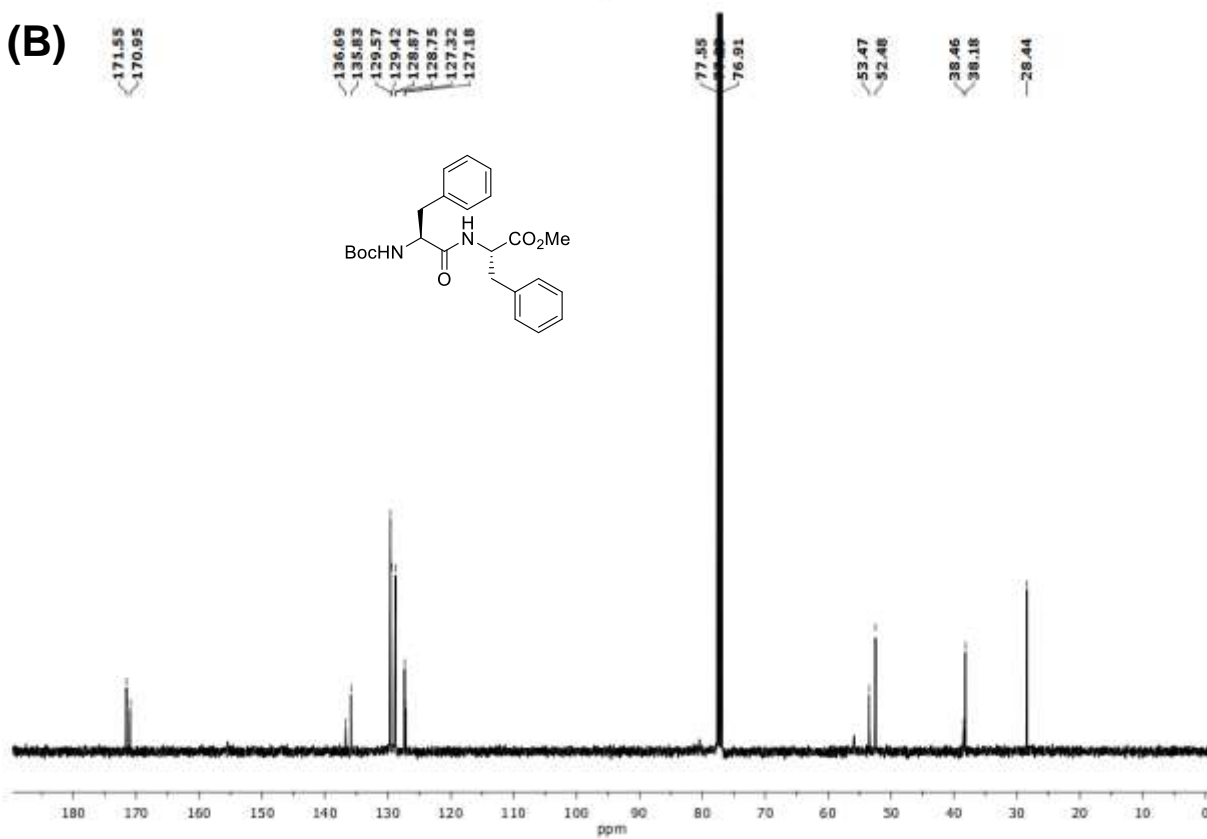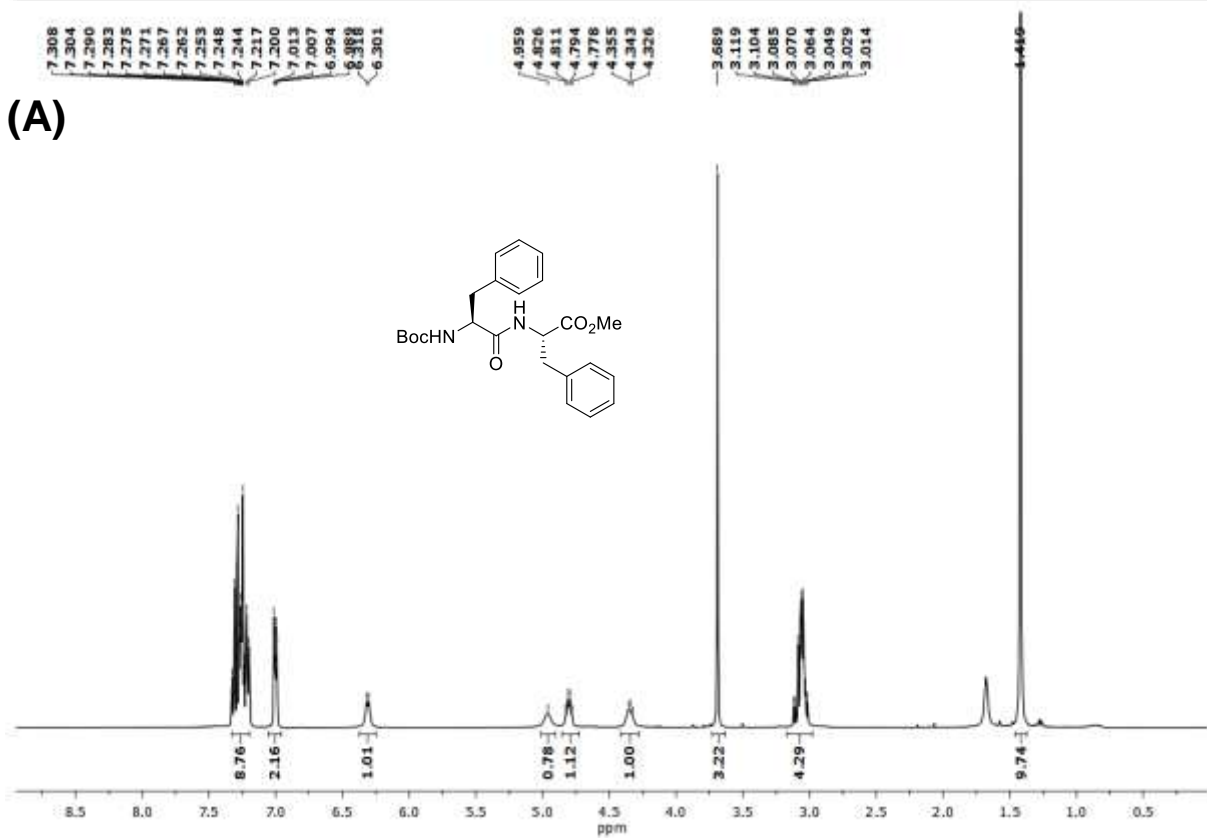


(A) $^{1}$H-NMR and (B) $^{13}$C-NMR spectra of Boc-Phe-Phe-OMe.

**(A)**



**(B)**



(A) $^1$H-NMR and (B) $^{13}$C-NMR spectra of Boc-Phe-Phe-OH (**1**).

**(A)**

8.795

7.260
7.024
7.004

5.354
5.332

4.643
4.631
4.621
4.519
4.510
4.217
4.200

1.694
1.680
1.670
1.645
1.629
1.606
1.587
1.559
1.413
0.917
0.904
0.883

0.92

0.78

0.77

1.00

0.80

6.08
9.39

12.41

10.0  9.5  9.0  8.5  8.0  7.5  7.0  6.5  6.0  5.5  5.0  4.5  4.0  3.5  3.0  2.5  2.0  1.5  1.0  0.5
ppm

175.99
173.13

156.28

80.66
77.55
77.23
76.91

53.13
50.78

41.52
40.92

28.43
24.89
24.79
23.13
22.83
22.46
21.89

**(B)**

190  180  170  160  150  140  130  120  110  100  90  80  70  60  50  40  30  20  10  0
ppm
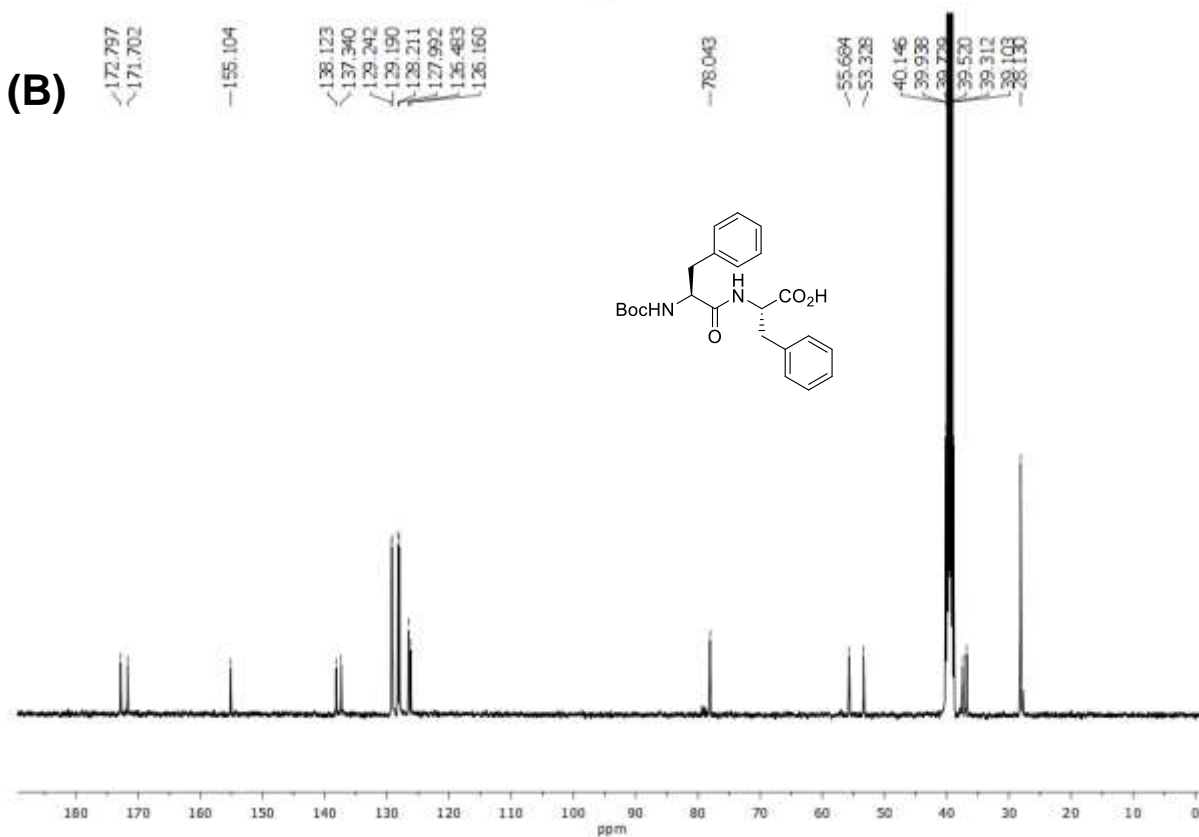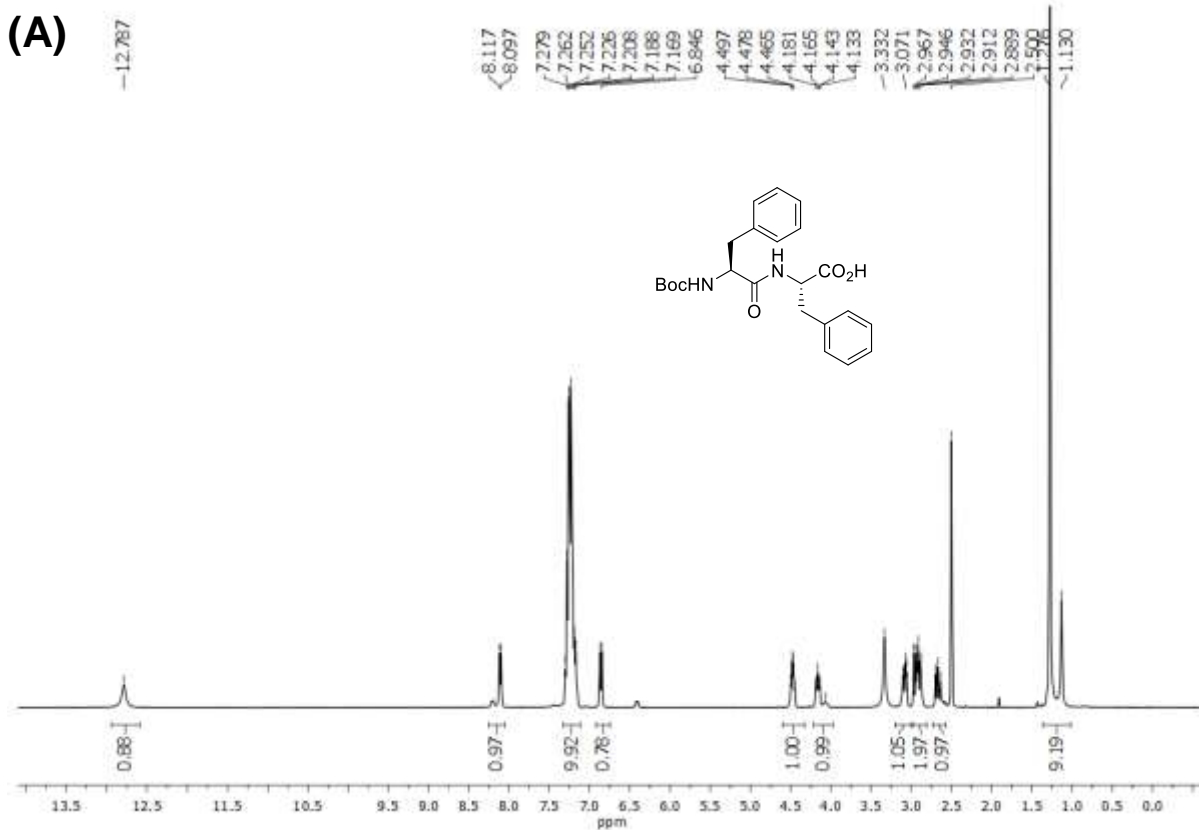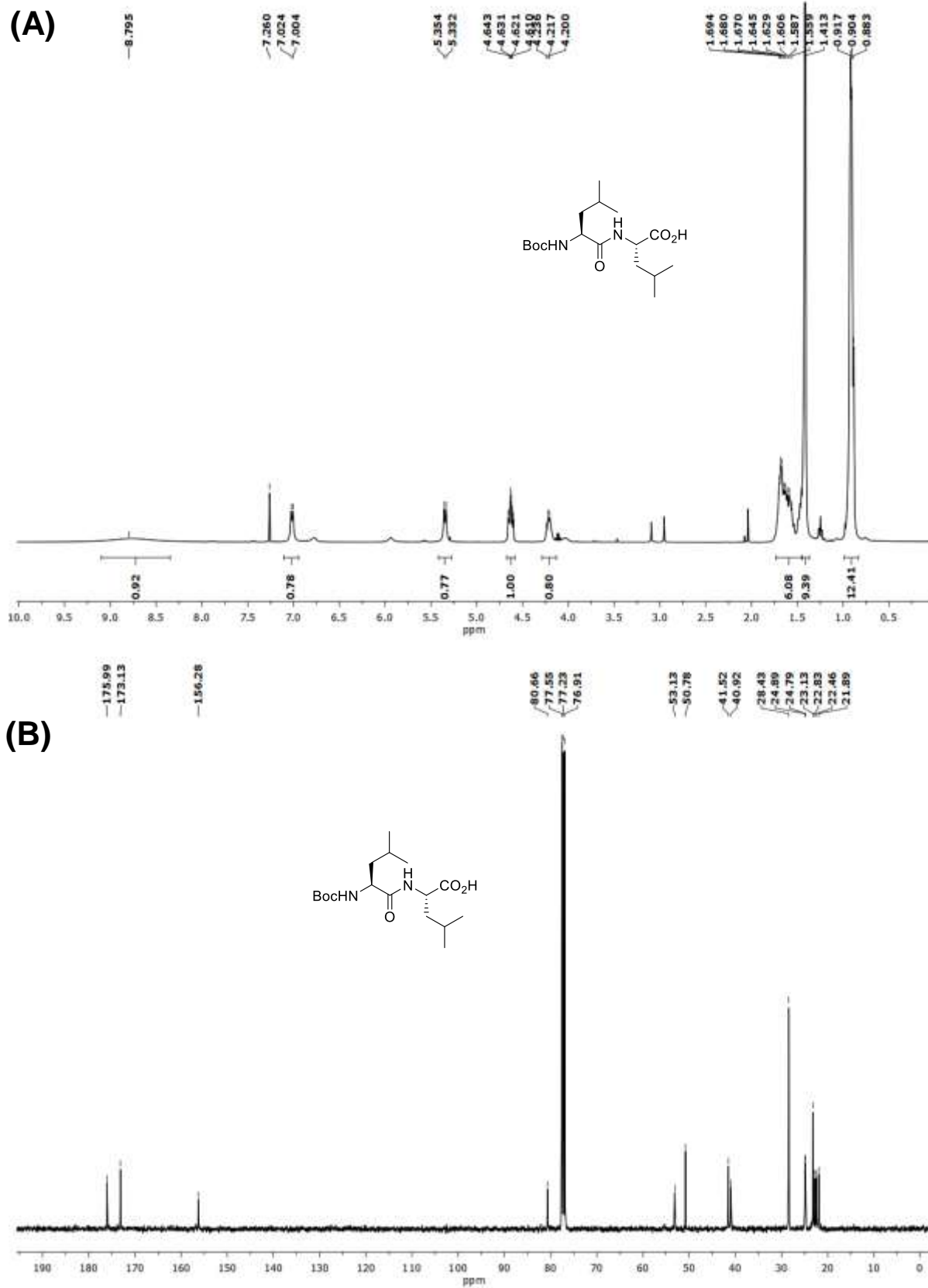
(A) $^1$H-NMR and (B) $^{13}$C-NMR spectra of Boc-Leu- Leu-OH (**2**).

**(A)**



**(B)**
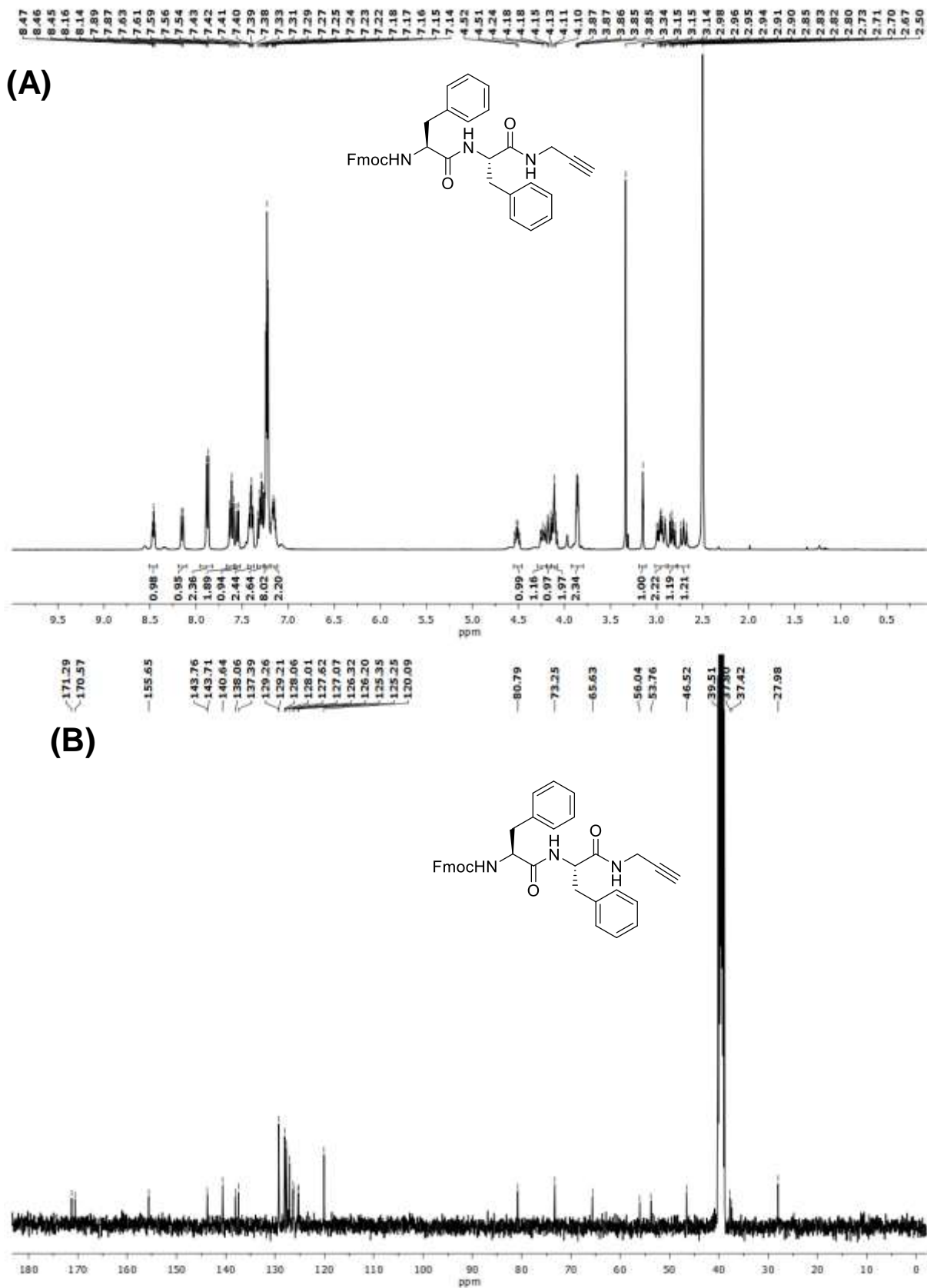


(A) $^{1}$H-NMR and (B) $^{13}$C-NMR spectra of Fmoc-Phe-Phe-Propyne (**17**).

**(A)**

8.452, 8.313, 8.226, 8.132, 8.112, 7.878, 7.859, 7.627, 7.607, 7.588, 7.568, 7.546, 7.412, 7.396, 7.377, 7.301, 7.285, 7.267, 7.249, 7.239, 7.225, 7.210, 7.190, 7.181, 7.166, 7.159, 7.133, 6.241, 6.237, 5.468, 5.463, 5.452, 5.447, 5.163, 5.155, 5.148, 5.140, 4.731, 4.718, 4.653, 4.633, 4.598, 4.531, 4.519, 4.280, 4.266, 4.239, 4.227, 4.183, 4.177, 4.149, 4.131, 4.109, 4.092, 3.348, 2.946, 2.932, 2.905, 2.846, 2.825, 2.500, 1.520, 1.309

0.90, 1.32, 0.98, 0.83, 2.01, 3.44, 4.07, 13.14, 1.02, 0.98, 1.00, 1.02, 1.16, 1.96, 3.80, 1.97, 2.08, 0.90, 0.98, 3.29, 3.14

**(B)**

171.18, 170.53, 156.18, 155.64, 152.76, 143.73, 143.67, 140.63, 138.01, 137.40, 129.22, 129.16, 127.95, 127.58, 127.03, 119.95, 119.83, 89.06, 84.67, 83.35, 81.57, 79.16, 65.63, 56.03, 53.79, 51.07, 46.51, 39.51, 37.83, 37.37, 34.17, 26.89, 25.15

(A) $^1$H-NMR and (B) $^{13}$C-NMR spectra of Fmoc-Phe-Phe-*tz*-A$^{NH2}$ (**18**).

**(A)**



**(B)**



(A) $^1$H-NMR and (B) $^{13}$C-NMR spectra of Fmoc-Phe-Phe-*tz*-A$^{N(Boc)2}$ **(19)**.

# Chapter 3

# Effect of Stereochemistry and Hydrophobicity on Self-assembly of Phe-Phe-Nucleoside Conjugates

## 3.1 Introduction

Molecular self-assembled structures of the diphenylalanine (Phe-Phe) dipeptide has been studied widely due to its crystal and amorphous solid state structures from microscopic to nano-metric levels.[1-5] The diphenylalanine (Phe-Phe) motif is a key element of the Alzheimer's *β*-amyloid peptide sequence.[6] Due to the stability, biocompatibility and water-solubility of Phe-Phe motifs it can be ideal for applications *in* bio-sensing and catalysis.[7-11] The beginning of life on earth though achiral, the building blocks of biopolymers acquired handedness at some point of evolution; the amino acids with *L* configuration and sugars (ex. the ribose of RNA) with *D* configuration.[12] It has been shown that small chiral preferences can be amplified into very highly dominant chirality of single enantiomer due to phenomena of autocatalysis, self-assembling processes and solubility characteristics of pure enantiomers over that of racemic mixtures (Figure 3.1).[12]
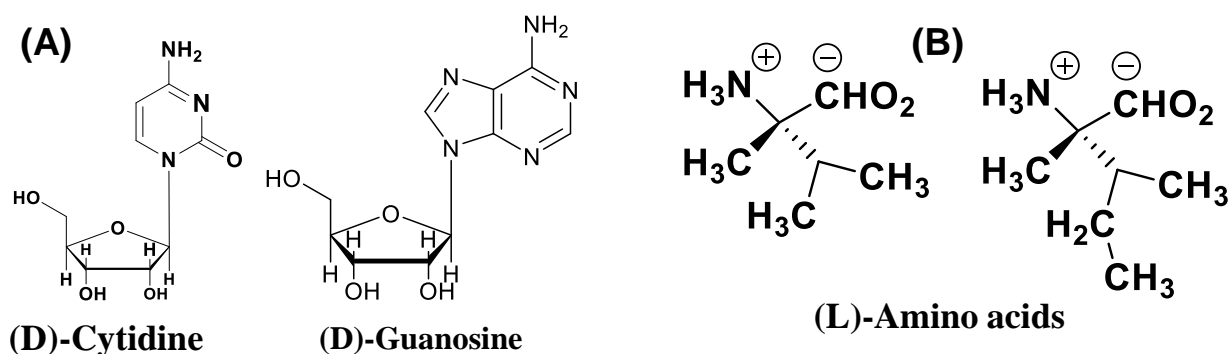


**Figure 3.1**: Structural representation of (A) RNA and (B) amino acids.[12]

There has been speculation about the origin of chirality as to why and how amino acids have the *L* configuration and the ribose and deoxyribose in nucleic acids have the *D* configuration.[13,14] During early prebiotic times homochirality was the natural consequence with equal amounts of *L* and *D* amino acids present in the primordial soup since chemical reactions for synthesis of amino acids and ribose would lead to equal mixture of *D-L* isomers.[13] However, as Rikken and Raupach[15] observed "clearly the question of the origin of the homochirality of life is far from answered." An important piece of experimental evidence on this question came in 1969, the Murchison meteorite that landed in Australia carried a number of α-methyl amino acids that

show small excesses of the *L* forms (Figure 3.1B) with methyl groups replacing the α protons of amino acids.[16,17] Gazit *et. al.*,[18] reported that homochiral dipeptides like *L*-Phe-*L*-Phe and *D*-Phe-*D*-Phe self-assembled the regular nanorod structures (Figure 3.2). But in case of mixture of stereomers (mixed chiral centers), the particles accumulated leading to sticky aggregates of particles (Figure 3.3)[19] indicating no self-assembled structures. Thus, understanding the role of stereochemistry in dictating self-assembly of peptides are important from fundamental understanding of the origin of chirality in biopolymers.
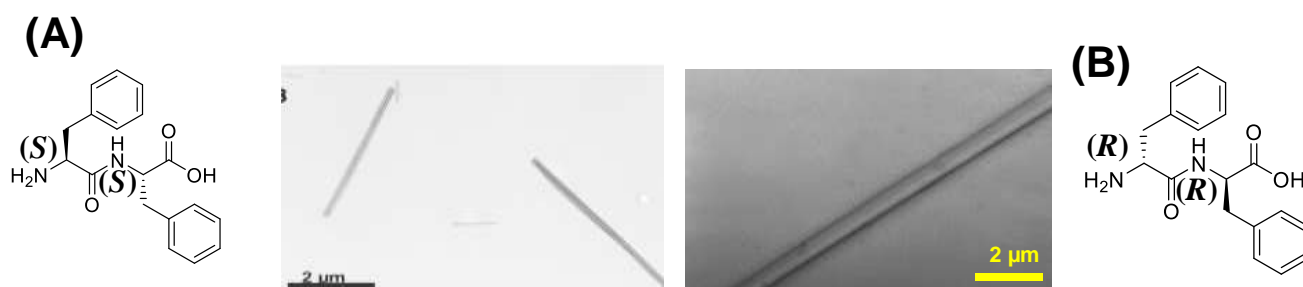


**Figure 3.2**: SEM images of (A) *L*-Phe-*L*-Phe and (B) *D*-Phe-*D*-Phe.[18]
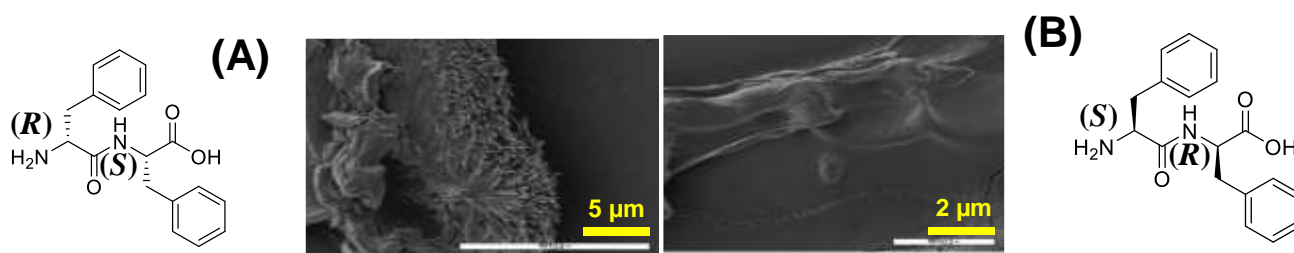


**Figure 3.3**: SEM images of (A) *D*-Phe-*L*-Phe and (B) *L*-Phe-*D*-Phe.[19]

It was seen from Chapter 2 that the nucleobase plays very important role to get the regular spherical nanostructures.[20-24] This chapter deals with stereochemical effects of conjugation of nucleoside with homo (*L*-Phe-*L*-Phe / *D*-Phe-*D*-Phe) as well as hetero (*L*-Phe-*D*-Phe and *D*-Phe-*L*-Phe) chiral peptides (Figure 3.4).
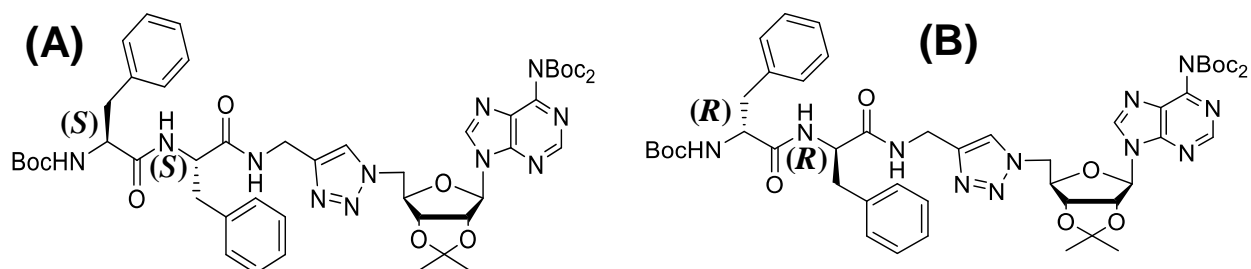
**Figure 3.4**: Structural representation of (A) Boc-(*L*)Phe-(*L*)Phe-*tz*-A[N(Boc)2] **(10)** and (B) Boc-(*D*)Phe-(*D*)Phe-*tz*-A[N(Boc)2] **(11)**.

## 3.2 Objectives of the present work

A series of nucleoside conjugated *L/D*-Phe-Phe peptides corresponding to all diastereomers were synthesized and their self-assembled morphologies were examined.

The specific objectives of this section are following:

➢ Synthesis of diastereomeric Boc-(*L*)Phe-(*L*)Phe-*tz*-A[N(Boc)2] **(10)**, Boc-(*D*)Phe-(*D*)Phe-*tz*-A[N(Boc)2] **(11)**, Boc-(*D*)Phe-(*L*)Phe-*tz*-A[N(Boc)2] **(12)** and Boc-(*L*)Phe-(*D*)Phe-*tz*-A[N(Boc)2] **(13)**.

➢ Characterization of peptides by the HRMS, ^{1}H NMR and ^{13}C NMR spectroscopy.

➢ Morphological characterization by FESEM imaging.

➢ Hydrophobicity monitored by the contact angle measurement of all chiral peptides.

➢ Conformational studies by the circular dichroism (CD) spectroscopy.

## 3.3 Results and the discussions

**3.3.1 Synthesis of target peptides**: The dipeptide Boc-(*L*)Phe-(*L*)Phe-OMe[25] was hydrolyzed under basic conditions to afford the acid Boc-(*L*)Phe-(*L*)Phe-OH **(1)**.[26] This was coupled with propargylamine hydrochloride to afford the propargyl amide Boc-(*L*)Phe-(*L*)Phe-Propyne **(2)** (Scheme 3.1). Starting from suitably protected Boc-(*D*)Phe-(*D*)Phe-OH **(3)**[26] (synthetic procedure followed as in Chapter 2) and using similar synthetic protocols as used for Boc-(*L*)Phe-(*L*)Phe-OH, the enantiomeric Boc-(*L*)Phe-(*L*)Phe-Propyne **(4)** was synthesized. The synthesis of *LL*, *DD*, *DL* and *LD* analogues of the final peptides, was achieved by coupling of following pairs of protected amino acids: *L*-Phe with *L*-Phe, *D*-Phe with *D*-Phe, *D*-Phe with *L*-Phe and *L*-Phe with

*D*-Phe by standard methods.[18-21] The synthesis of the diastereomeric dipeptides Boc-(*L*)Phe-(*D*)Phe-Propyne **(6)** and Boc-(*D*)Phe-(*L*)Phe-Propyne **(8)** was done starting from appropriate precursors and propargyl amine (Scheme 3.2). The click conjugation reaction of the dipeptide propargyl compounds (**2, 4, 6** and **8**) with base azide 2',3'-isoprylidene-5'-azido-$N^6$-Boc adenosine **(9)**[27] afforded the conjugated chiral target peptides Boc-(*L*)Phe-(*L*)Phe-*tz*-A$^{N(Boc)2}$ **(10)**, Boc-(*D*)Phe-(*D*)Phe-*tz*-A$^{N(Boc)2}$ **(11)** (Scheme 3.3) as well the hetero chiral target peptides Boc-(*D*)Phe-(*L*)Phe-*tz*-A$^{N(Boc)2}$ **(12)** and Boc-(*L*)Phe-(*D*)Phe-*tz*-A$^{N(Boc)2}$ **(13)** (Scheme 3.4).
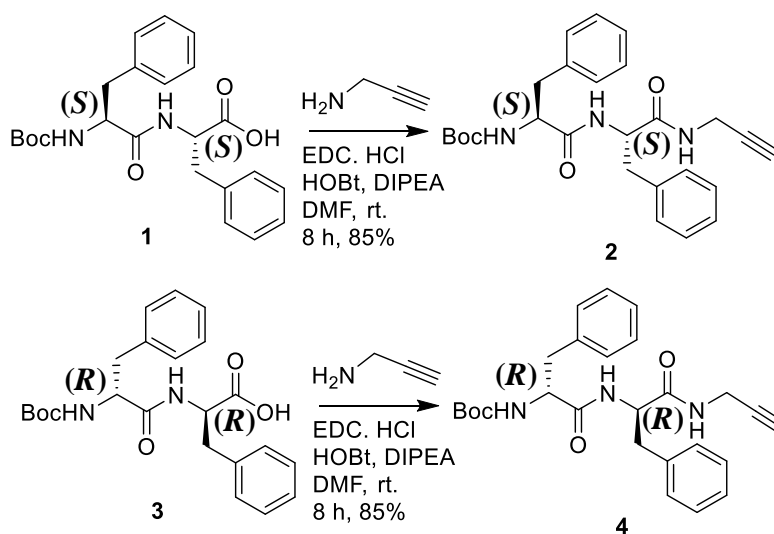


**Scheme 3.1**: Synthesis of homo chiral intermediate dipeptides Boc-(*L*)Phe-(*L*)Phe-Propyne **(2)** and Boc-(*D*)Phe-(*D*)Phe-Propyne **(4)**.
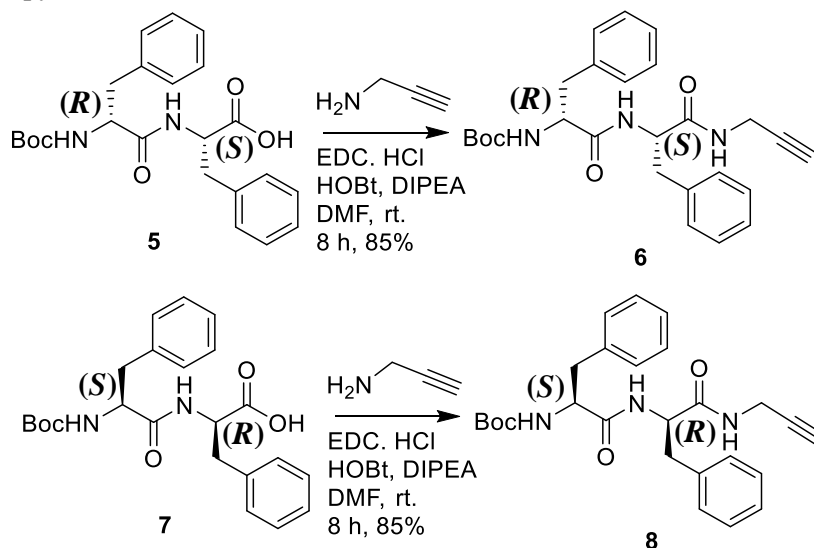


**Scheme 3.2**: Synthesis of hetero chiral intermediate dipeptides Boc-(*D*)Phe-(*L*)Phe-Propyne **(6)** and Boc-(*L*)Phe-(*D*)Phe-Propyne **(8)**.
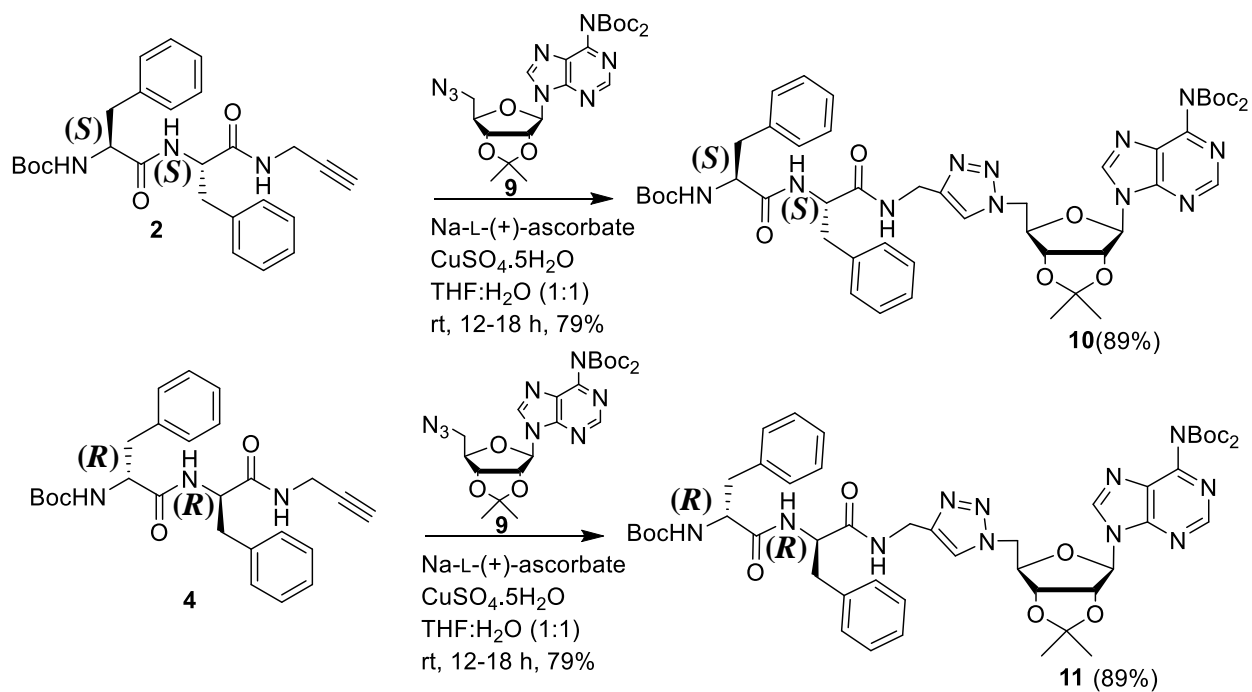
**Scheme 3.3**: Synthesis of homo chiral target peptides Boc-(*L*)Phe-(*L*)Phe-*tz*-A$^{N(Boc)2}$ **(10)** and Boc-(*D*)Phe-(*D*)Phe-*tz*-A$^{N(Boc)2}$ **(11)**.
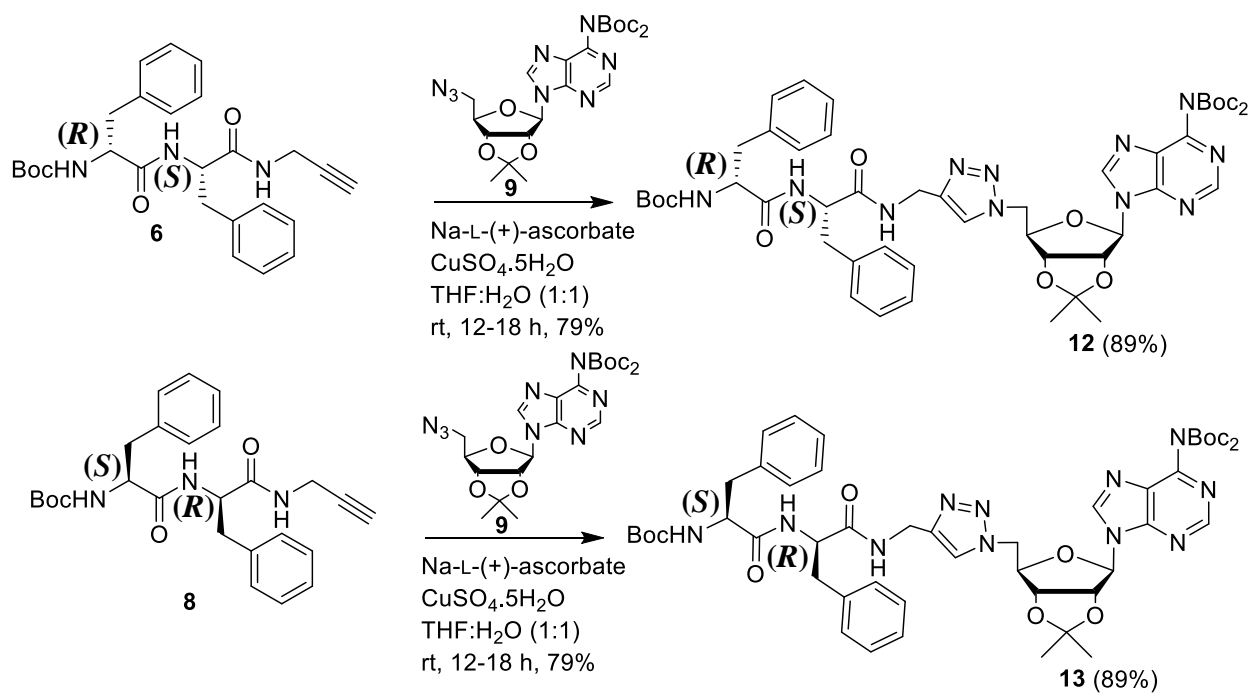


**Scheme 3.4**: Synthesis of hetero chiral target peptides Boc-(*D*)Phe-(*L*)Phe-*tz*-A$^{N(Boc)2}$ **(12)** and Boc-(*L*)Phe-(*D*)Phe-*tz*-A$^{N(Boc)2}$ **(13)**.

Further to study the effect of stereochemistry based hydrophobicity in homo chiral as well as hetero chiral peptides, the isopropylidene derivatives **10-13** were deprotected by the 50% TFA in DCM (Scheme 3.5) and (Scheme 3.6) to liberate the 2',3'-hydroxyls on the nucleoside conjugated with dipeptides through triazole linker to obtain peptides **14-17**. All peptides were purified by column chromatography over silica gel and structurally characterized by NMR and HRMS (see experimental section).
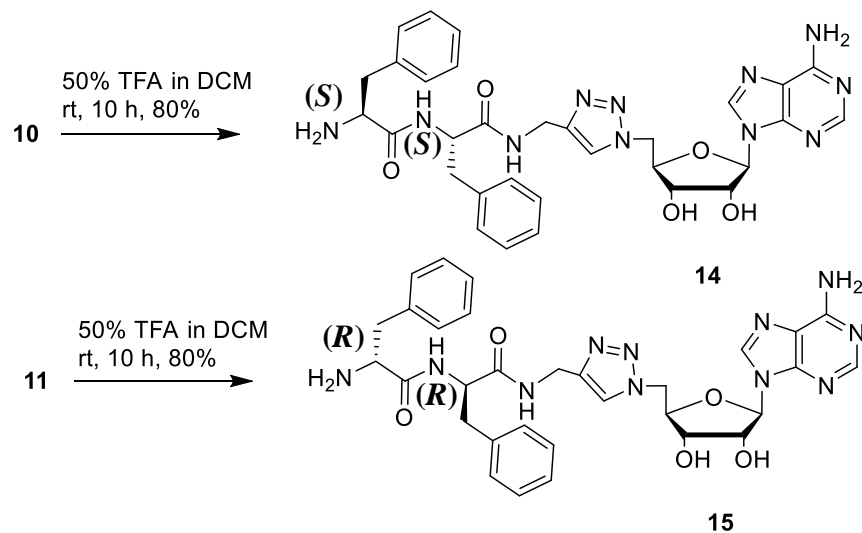


**Scheme 3.5**: Synthesis of homo chiral target peptides (*L*)Phe-(*L*)Phe-*tz*-A$^{NH2}$ (**14**) and (*D*)Phe-(*D*)Phe-*tz*-A$^{NH2}$ (**15**).
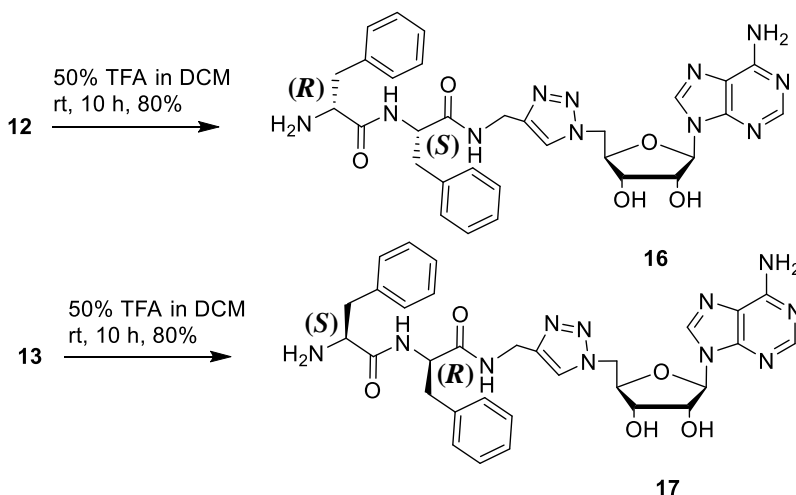


**Scheme 3.6**: Synthesis of hetero chiral target peptides (*D*)Phe-(*L*)Phe-*tz*-A$^{NH2}$ (**16**) and (*L*)Phe-(*D*)Phe-*tz*-A$^{NH2}$ (**17**).

**3.3.2 Morphologies and microscopic architectures**: The morphology arising from self-assembled structures of various chiral peptide conjugates was monitored by FESEM and AFM techniques. The images of the synthesized peptides were examined after preparing the samples by standard protocols (see experimental section) and drop casted on silicon wafers / copper grid for recording SEM and AFM images. These freshly prepared samples were used for microscopic analysis. All the fully protected chiral peptides either homo or hetero chiral peptides gave perfectly spherical particles which was confirmed by FESEM images (Figure 3.5) as well as AFM images (Figure 3.6). The height profile obtained from the AFM images confirm the height of the spherical particle to be in 150 nm to 700 nm range (Figure 3.7). It is known from literature that no regular structures are seen in case of the mixed chiral centres. In present work, conjugation of the nucleoside with the hetero chiral Phe-Phe dipeptides, exhibited regular spherical structures; the FESEM image of hetero chiral peptide Boc-(*L*)Phe-(*D*)Phe-*tz*-A$^{N(Boc)_2}$ (**11**) gives hollow spheres (Figure 3.5D and E). This was confirmed by dye encapsulation experiments (already discussed in Chapter 2) performed with the Boc-(*L*)Phe-(*D*)Phe-*tz*-A$^{N(Boc)_2}$ and as seen from confocal microscope images that the dye gets efficiently encapsulated inside the hollow spheres (Figure 3.8).
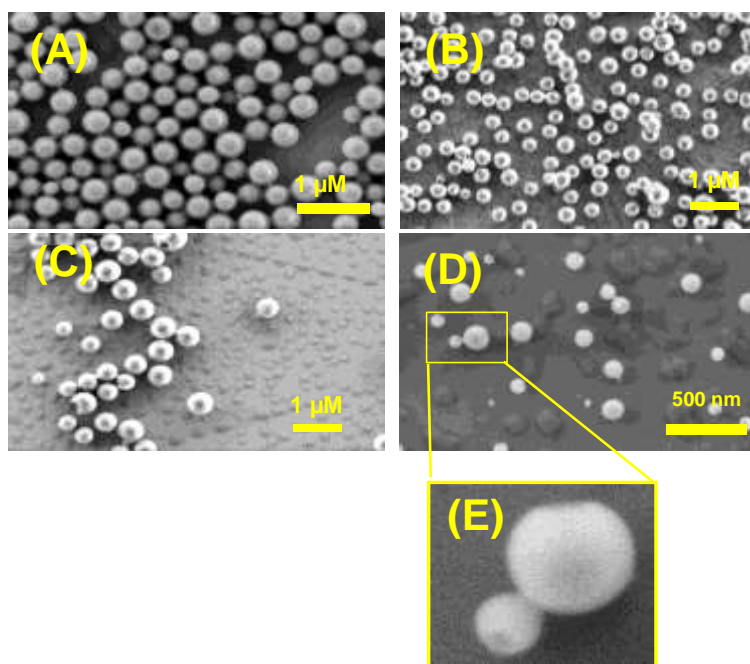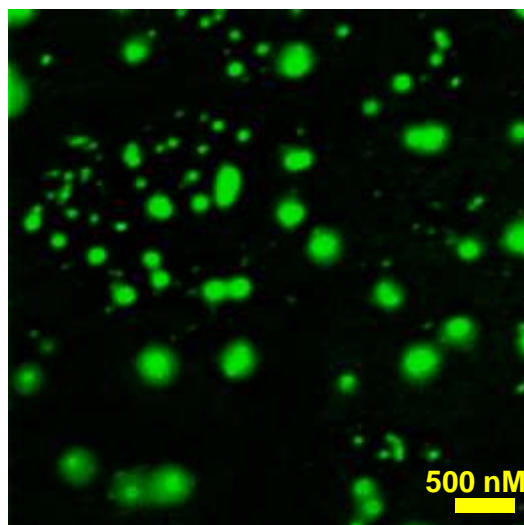


**Figure 3.5**: FESEM images of (A) Boc-(*L*)Phe-(*L*)Phe-*tz*-A$^{N(Boc)2}$ (**10**); (B) Boc-(*D*)Phe-(*D*)Phe-*tz*-A$^{N(Boc)2}$ (**11**); (C) Boc-(*D*)Phe-(*L*)Phe-*tz*-A$^{N(Boc)2}$ (**12**); (D) Boc-(*L*)Phe-(*D*)Phe-*tz*-A$^{N(Boc)2}$ (**13**) and (E) selected zoomed area of (D).
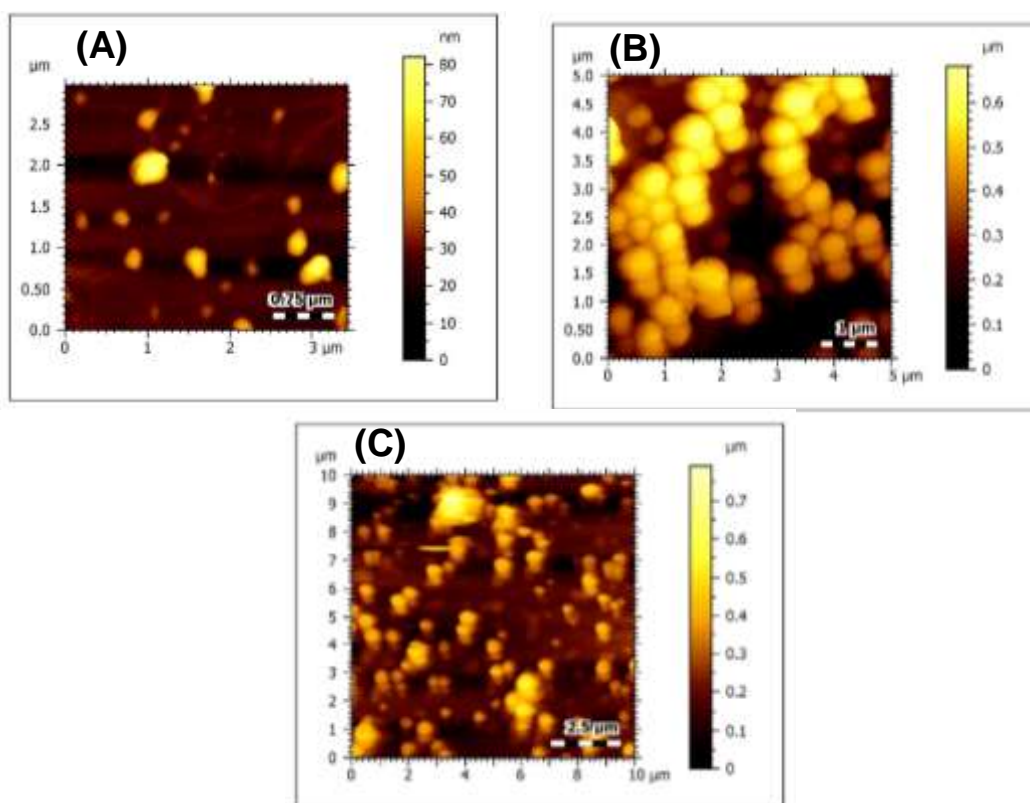
**Figure 3.6**: AFM images of (A) Boc-(*D*)Phe-(*D*)Phe-*tz*-A$^{N(Boc)2}$ **(11)**; (B) Boc-(*D*)Phe-(*L*)Phe-*tz*-A$^{N(Boc)2}$ **(12)** and (C) Boc-(*L*)Phe-(*D*)Phe-*tz*-A$^{N(Boc)2}$ **(13)**.
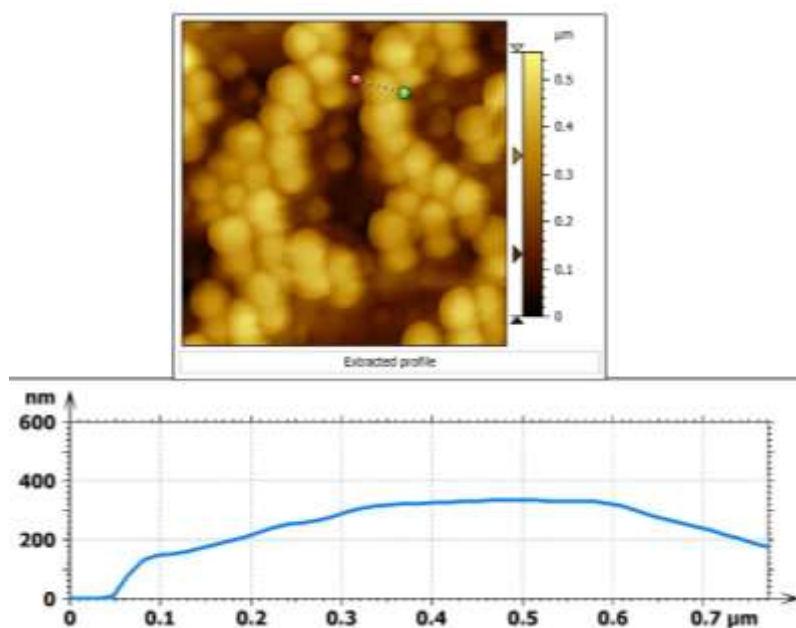


**Figure 3.7**: Height profile diagram of Boc-(*D*)Phe-(*L*)Phe-*tz*-A$^{N(Boc)2}$ **(12)** obtained from AFM.

**Figure 3.8**: Confocal microscope images of fluorescent dye encapsulated Boc-(*L*)Phe-(*D*)Phe-*tz*-A$^{N(Boc)2}$ (**13**).

The time course of nanoparticle formation was examined. It is known that the initially formed (kinetic control) nanospheres upon leaving for some time get closer to connect each other to form rods formation[28-31] (thermodynamically stable). The time dependent self-assembly of peptides **11**-**13** were followed through the FESEM images and even after 8 days no further growth into rods or any other features were seen, with structures remaining as spheres (Figure 3.9).
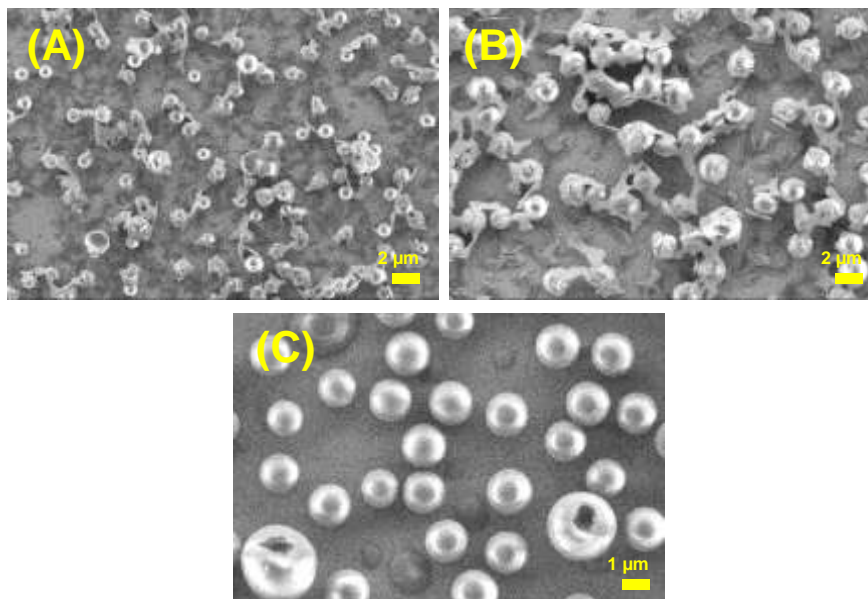


**Figure 3.9**: FESEM images of (A) Boc-(*D*)Phe-(*D*)Phe-*tz*-A$^{N(Boc)2}$ (**11**); (B) Boc-(*D*)Phe-(*L*)Phe-*tz*-A$^{N(Boc)2}$ (**12**) and (C) Boc-(*L*)Phe-(*D*)Phe-*tz*-A$^{N(Boc)2}$ (**13**) after 8 days.

The contact angle measurements (Figure 3.10) indicated that the homo chiral *D-D* dipeptide **(11)** had a higher contact angle 118° than the other chiral peptides (*L-L*, *L-D* and *D-L*, **12-13**) which suggested that homo chiral peptides are more hydrophobic than the hetero chiral peptides (Figure 3.10) and (Table 3.1).
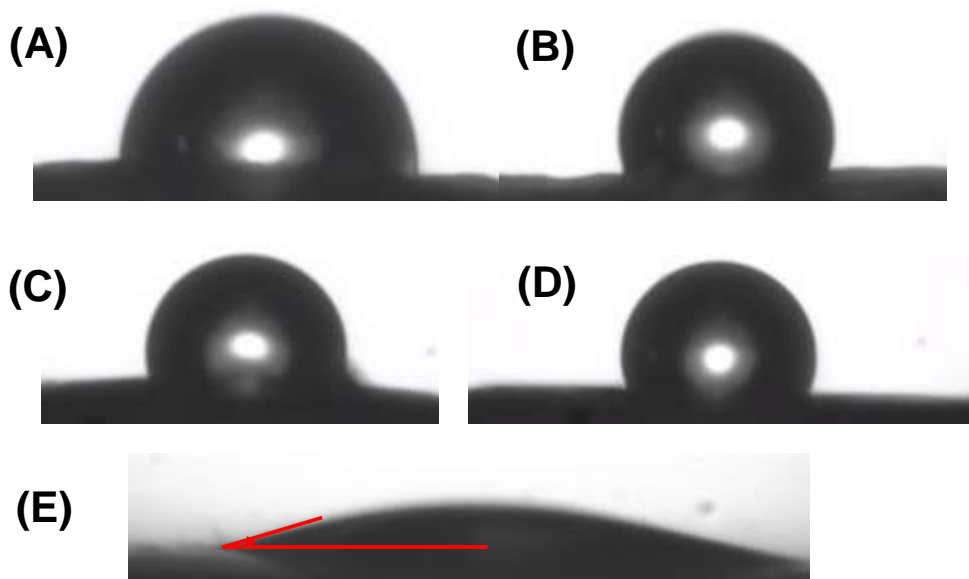


**Figure 3.10**: Contact angle of (A) Boc-(*L*)Phe-(*L*)Phe-*tz*-A$^{N(Boc)2}$ **(10)**; (B) Boc-(*D*)Phe-(*D*)Phe-*tz*-A$^{N(Boc)2}$ **(11)**; (C) Boc-(*D*)Phe-(*L*)Phe-*tz*-A$^{N(Boc)2}$ **(12)**; (D) Boc-(*L*)Phe-(*D*)Phe-*tz*-A$^{N(Boc)2}$ **(13)** and (E) Bare Mica surface.

**Table 3.1** Comparative contact angle on the mica surface.

| Sr. No. | Sample/Surface (Mica surface) | Contact angle (CA in degree) | ΔCA (in degree) |
|---|---|---|---|
| 1. | Bare Mica surface | 25 ± 2 | - |
| 2. | Boc-(*L*)Phe-(*L*)Phe-*tz*-A$^{N(Boc)2}$ **(10)** | 98 ± 2 | +73 |
| 3. | Boc-(*D*)Phe-(*D*)Phe-*tz*-A$^{N(Boc)2}$ **(11)** | 118 ± 1 | +93 |
| 4. | Boc-(*D*)Phe-(*L*)Phe-*tz*-A$^{N(Boc)2}$ **(12)** | 108 ± 2 | +83 |
| 5. | Boc-(*L*)Phe-(*D*)Phe-*tz*-A$^{N(Boc)2}$ **(13)** | 109 ± 2 | +84 |

In Chapter 2, it was observed that in case of completely deprotected peptides,[22] no regular spherical particles were seen. The solution of the homo chiral peptides **14-17** (*L-L* and *D-D*) were individually examined followed by mixing. After 12 hrs the samples were drop casted on silicon wafer, followed by drying and imaging (Figure 3.11) and no any regular structures were observed in case of both homo as well as hetero chiral peptides (Figure 3.12). This result was consistent with previous observation that the fully deprotected peptides did not exhibit good morphology. In case of completely deprotected chiral peptides which are very hydrophilic, self-assembly through the hydrogen bonding requires some bit of hydrophobicity and lack of it decreases the effectiveness of H-bonding to promote self-assembly.
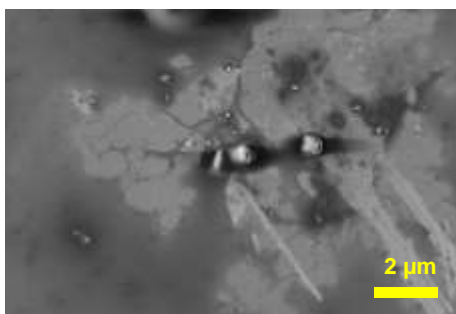


**Figure 3.11**: FESEM images of mixing (*L*)Phe-(*L*)Phe-*tz*-A$^{NH_2}$ (**14**) and (*D*)Phe-(*D*)Phe-*tz*-A$^{NH_2}$ (**15**) in solution and drop casted after 12 hrs.
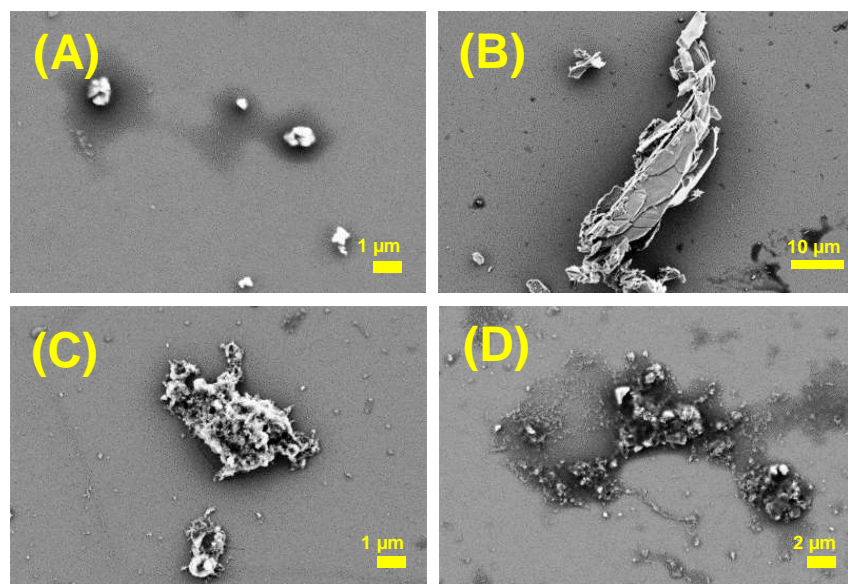


**Figure 3.12**: FESEM images of (A) (*L*)Phe-(*L*)Phe-*tz*-A$^{NH_2}$ (**14**); (B) (*D*)Phe-(*D*)Phe-*tz*-A$^{NH_2}$ (**15**); (C) (*D*)Phe-(*L*)Phe-*tz*-A$^{N(Boc)_2}$ (**16**) and (D) (*L*)Phe-(*D*)Phe-*tz*-A$^{NH_2}$ (**17**).

The completely deprotected chiral peptides were examined for their conformational preferences by Circular Dichroism (CD) spectra in water. The CD profiles did not show any recognisable conformational features for all the chiral peptides. (*L*)Phe-(*L*)Phe-*tz*-A$^{NH_2}$ gave one positive band at 218 nm which corresponds to the amide band of *L*-phenylalanine and one positive band at 265 nm which corresponds to the nucleobase linked to sugar residue. The diastereomeric (*D*)Phe-(*D*)Phe-*tz*-A$^{NH_2}$ gives one negative band at 218 nm corresponding to amide of the *D*-phenylalanine and one positive band at 265 nm for the base of nucleoside. Finally (*D*)Phe-(*L*)Phe-*tz*-A$^{NH_2}$ and (*L*)Phe-(*D*)Phe-*tz*-A$^{NH_2}$ did not give any peak around 218 nm perhaps due to the cancelation of bands of opposite signs for *L*-Phe with the *D*-Phe. The positive bands were seen at 250 nm and 260 nm for *LD* and *DL* diastereomers originating from the nucleoside (Figure 3.13). These suggested considerable conformational differences adapted by the diasteromeric peptide conjugates.
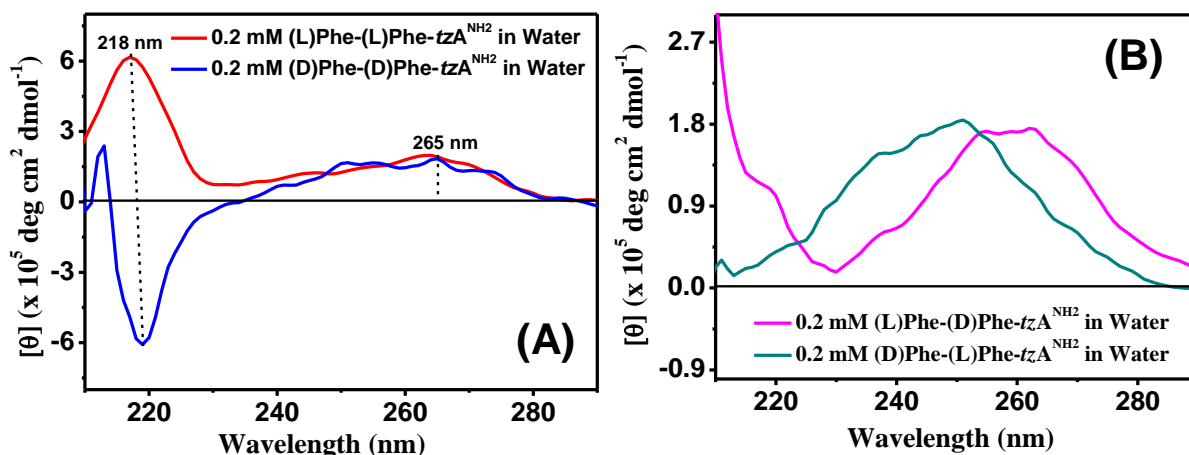


**Figure 3.13**: CD spectra of (A) homo (*L-L*, *D-D*) deprotected peptides and (B) hetero chiral (*L-D*, *D-L*) deprotected peptides.

## 3.4 Summary

A new series of homo chiral (*LL* and *DD*) and hetero chiral (*LD* and *DL*) Phe-Phe dipeptides conjugated with the nucleoside riboadenosine were synthesized, characterized and their self-assembled morphologies studied. As visualized from FESEM and AFM, regular nano structures were obtained only in the case of homo chiral dipeptides. Consistent with earlier literature reports no regular morphology were seen with hetero chiral peptides.

However upon conjugation with nucleoside A, the Phe-Phe dipeptides gave spherical particles in the cases either homo chiral (*L*)Phe-(*L*)Phe / (*D*)Phe-(*D*)Phe or hetero chiral (*L/D*)Phe-(*D/L*)Phe peptides. Also, it was found that hydrophobic dipeptide Boc-(*L*)Phe-(*D*)Phe-*tz*-A$^{N(Boc)_2}$ yielded hollow spherical particles as seen from the FESEM images. The fully deprotected chiral peptides resulted in sticky aggregates. The contact angle measurements indicated the homo chiral peptide (*D-D*) is more hydrophobic than the hetero chiral (*D-L/L-D*) peptides, showing more hydrophobic nature of homo chiral peptides. Finally, the circular dichroism study gave featureless spectra suggesting that the peptides are too short to assume any recognizable conformation. Thus the chirality and balanced hydrophobic / hydrophilic nature of peptides play a key role in self-assembly of the Phe-Phe dipeptide nucleoside conjugates.

## 3.5 Experimental procedures

**3.5.1 Materials and methods**: See the experimental section **(2.5.1)** of chapter **2**.

**3.5.2 Synthesis of peptides**: Peptides **2, 6, 8, 10, 12** and **13** were synthesized and characterized in the experimental section of Chapter **2**.

**3.5.2a Dipeptide Boc-(*D*)Phe-(*D*)Phe-Propyne (4)**: A mixture of compound **3**[26] (1.0 g, 2.4 mmol), EDC.HCl (0.5 g, 2.4 mmol) and HOBT (0.2 g, 1.2 mmol) was dissolved in dry DMF (10 mL) at 0 °C. To the reaction mixture, DIPEA (0.9 mL, 4.0 mmol) was added. After 30 min., propargylaminehydrochloride, (0.2 g, 2.4 mmol) dissolved in dry DMF (3 mL), was added slowly into the reaction mixture and stirred at room temperature under $N_2$ atmosphere. After 8 hrs brine solution (50 mL) was added into it and aq. layer was washed with ethyl acetate (EtOAc) (3 x 25 mL). Organic layer was washed with satd. NaHCO$_3$, 10% citric acid and brine solutions. The organic layer was separated, dried over anhyd. Na$_2$SO$_4$, filtered and the filtrate was concentrated under reduced pressure. The crude mass thus obtained, was purified by column chromatography [Eluent: 20-50% of EtOAc in pet ether] to afford compound **4** (0.9 g, 85% with respect to **3**). White solid; m.p. 109-113 °C; ^{1}H NMR, 400 MHz (CDCl$_3$, 25 °C, TMS): $\delta$ = 7.36 – 7.27 (m, 3H), 7.22 (dd, J = 9.3, 4.1 Hz, 3H), 7.19 – 7.14 (m, 2H), 7.03 (s, 2H), 6.68 (s, 1H), 6.45 (d, J = 6.0 Hz, 1H), 4.97 (d, J = 6.1 Hz, 1H), 4.70 (dd, J = 14.5, 6.3 Hz, 1H), 4.29 (dd, J = 12.5, 6.2 Hz, 1H), 3.99

(ddd, J = 17.6, 5.5, 2.4 Hz, 1H), 3.85 (dd, J = 17.5, 2.5 Hz, 1H), 3.20 (d, J = 8.8 Hz, 1H), 3.09 – 2.84 (m, 3H), 2.16 (t, J = 2.5 Hz, 1H), 1.33 (s, 9H); $^{13}$C NMR, 100 MHz (CDCl$_3$, 25 °C, TMS): $\delta$ = 171.18, 170.37, 155.87, 136.15, 136.09, 129.45, 129.35, 128.96, 128.79, 127.38, 127.18, 80.93, 79.29, 71.37, 56.25, 53.50, 37.88, 37.61, 29.17, 28.29 ppm. HRMS (ESI$^+$), m/z calculated for (M+H)$^+$ C$_{26}$H$_{32}$N$_3$O$_4$: 450.2393, found: 450.2397.

**3.5.2b Peptide Boc-(*D*)Phe-(*D*)Phe-*tz*-A$^{N(Boc)2}$ (11)**: A mixture of **4** (0.3 g, 0.6 mmol), CuSO$_4$.5H$_2$O (7 mg, 0.03 mmol) and sodium ascorbate (0.1 g, 0.3 mmol) were stirred in tetrahydrofuran (THF) (6.0 mL). To the resulting suspension, azide **5**[27] (0.6 g, 1.1 mmol) dissolved in THF (6.0 mL) was added. Distilled water (10 mL) was added to the reaction mixture and stirred at room temperature. After 12 hrs, EtOAc (20 mL) was added into it and aq. layer was further washed with EtOAc (3 x 20 mL). Organic layer was separated, dried over anhyd. Na$_2$SO$_4$, filtered and the filtrate was concentrated under reduced pressure. The crude mass thus obtained, was purified by column chromatography [Eluent: 0-5% of MeOH in DCM] to afford compound **11** (0.5 g, 89% with respect to **4**). White solid; m.p. 85-89 °C; $^1$H NMR, 400 MHz (CDCl$_3$, 25 °C): $\delta$ = $^1$H NMR (400 MHz, CDCl$_3$) $\delta$ 8.87 (s, 1H), 8.08 (s, 1H), 7.36 – 7.20 (m, 6H), 7.15 (dd, J = 15.6, 4.7 Hz, 6H), 6.96 (s, 2H), 6.52 (s, 1H), 6.15 (d, J = 2.2 Hz, 1H), 5.36 (dd, J = 6.3, 1.9 Hz, 1H), 5.24 (d, J = 3.1 Hz, 1H), 4.94 (s, 1H), 4.77 – 4.67 (m, 1H), 4.67 – 4.52 (m, 3H), 4.42 (d, J = 11.5 Hz, 1H), 4.31 – 4.19 (m, 2H), 3.02 (d, J = 36.6 Hz, 2H), 3.00 – 2.86 (m, 4H), 1.49 (s, 19H), 1.30 (s, 10H) ppm. HRMS (ESI$^+$), m/z calculated for (M+H)$^+$ C$_{49}$H$_{64}$N$_{11}$O$_{11}$: 982.4787, found: 982.4779.

**3.5.3 Spectroscopic data**

**Compound Boc-(*D*)Phe-(*D*)Phe-OMe**: HRMS (ESI$^+$), m/z calculated for (M+H)$^+$ C$_{24}$H$_{31}$N$_2$O$_5$: 427.2233, found: 427.2233.

**Compound Boc-(*D*)Phe-(*D*)Phe-OH**: HRMS (ESI$^+$), m/z calculated for (M+H)$^+$ C$_{23}$H$_{29}$N$_2$O$_5$: 413.2076, found: 413.2076.

**3.5.4 Microscopy (FESEM and AFM) studies**. Sample preparation was done carefully to minimize the effect of sample drying on aggregate formation. The peptide (5 µL) solutions were drop casted on different substrates followed by drying under high vacuum (silicon wafers substrate

for FESEM). FESEM images were recorded using Zeiss Ultra Plus scanning electron microscope and the samples were prepared by drop casting on silicon wafers and coated with gold. SEM samples were prepared by depositing peptide solution (5 μL, 1 mg / mL in 50:50 EtOH / $H_2O$ after lyophilization in 1 mL HFIP) on silicon wafers, dried at room temperature and imaged it. For AFM, samples were drop casted on freshly cleaved $SiO_2$ / Si substrate, air dried at room temperature. Tapping mode AFM imaging was used according to well established procedures.

**3.5.5 Carboxyfluorescein encapsulation study**: See the experimental section **(2.5.11)** of chapter **2**.

**3.5.6 Contact angle measurement**: See the experimental section **(2.5.13)** of chapter **2**.

**3.5.7 Circular dichroism (CD) Spectroscopy**: CD spectrometric study was carried out on JASCO J-815 spectropolarimeter using cylindrical, jacketed quartz cell (10 mm path length), which was connected to Julabo-UC25 water circulator. For reproducible data, each set of spectra were measured using at least three individually prepared solutions. CD spectra were recorded using a spectral bandwidth of 1.0 nm at 25 °C with a time constant of 1 s and a step resolution of 1 nm. All the spectra were recorded in the water solvent and are typically averaged over 3-5 scans. A quartz cell with a path length of 1 mm was used with solutions containing approximately 0.25 mL (0.2 mM). All peptides had same peptide concentration (0.2 mM) for CD measurements done in Milli Q water (pH 7.0). The data processing and curve fitting were performed using Origin 8.0 software. All spectra were collected at 25 ºC with a 1 nm resolution and a scan rate of 50 nm/min. Spectra are the averages of 5 scans.
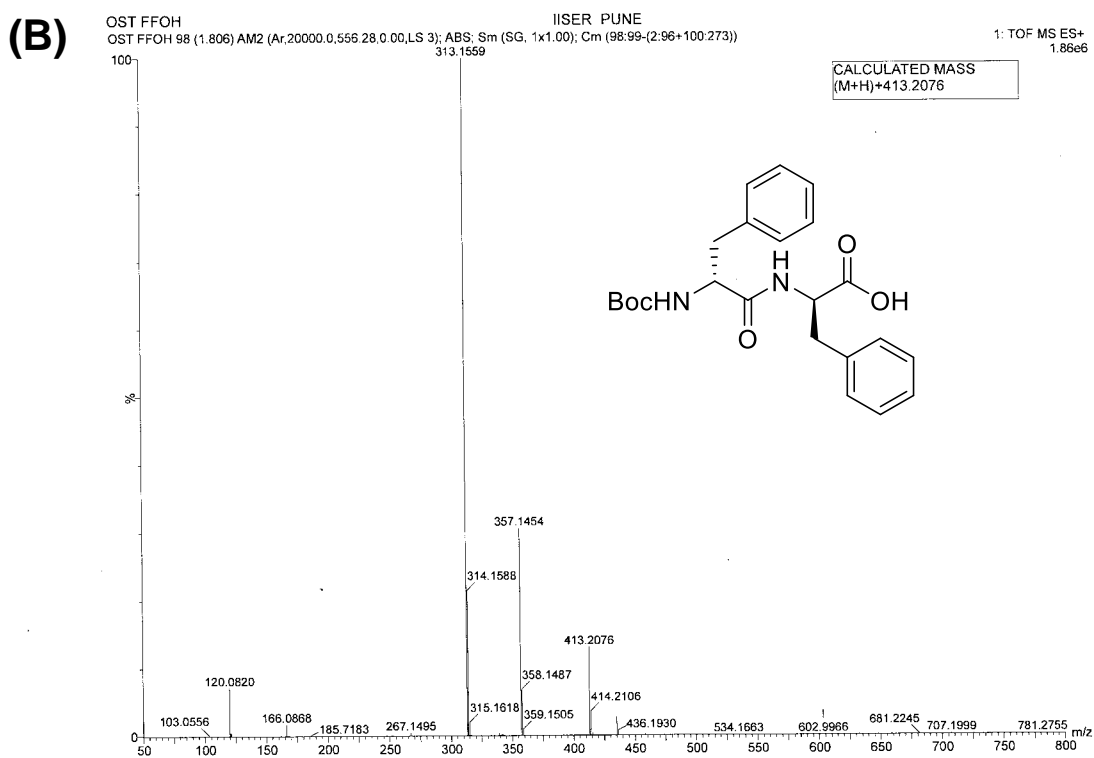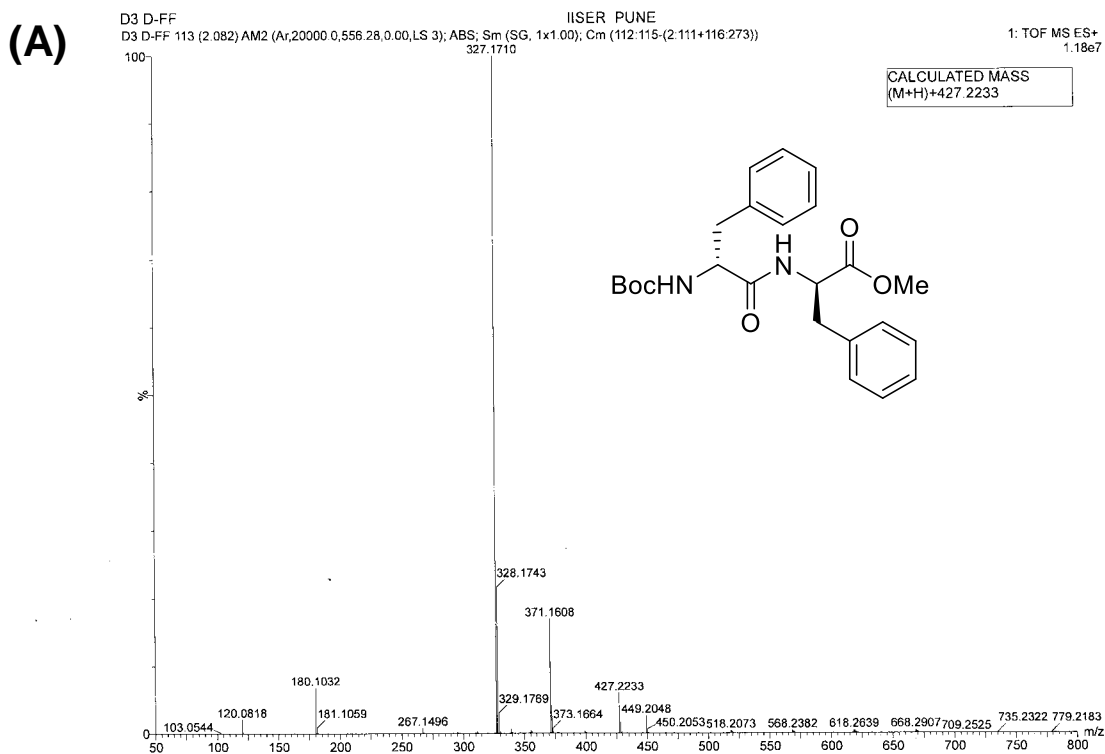
## 3.6 References

1. Gorbitz, C. H. *Chem. Eur. J.* **2001**, *7*, 5153-5159.
2. Hartgerink, J. D.; Beniash, E.; Stupp, S. I. *Science* **2001**, *294*, 1684-1688.
3. Aggeli, A.; Fytas, G.; Vlassopoulos, D.; McLeish, T. C. B.; Mawer, P. J.; Boden, N. *Biomacromolecules* **2001**, *2*, 378-388.
4. Lee, S. W.; Mao, C.; Flynn, C. E.; Belcher, A. M. *Science* **2002**, *296*, 892-895.
5. Zhang, S. *Nature Biotechnol*. **2003**, *21*, 1171-1178.

6. Reches, M.; Gazit, E. *Science* **2003**, *300*, 625-627.

7. Reches, M.; Gazit, E. *Nano Lett.* **2004**, *4*, 581-585.

8. Reches, M.; Gazit, E. *Nat. Nanotechnol.* **2006**, *1*, 195-200.

9. Abramovich, L. A.; Reches, M.; Sedman, V. L.; Allen, S.; Tendler, S. J. B.; Gazit, E. *Langmuir* **2006**, *22*, 1313-1320.

10. Tamamis, P.; Abramovich, L. A.; Reches, M.; Marshall, K.; Sikorski, P.; Serpell, L.; Gazit E.; Archontis, G. *Biophys. J.* **2009**, *96*, 5020-5029.

11. Azuri, I.; Abramovich, L. A.; Gazit, E.; Hod, O.; Kronik, L. *J. Am. Chem. Soc.* **2014**, *136*, 963-969.

12. Breslow. R.; Cheng, Z. L. *PNAS* **2009**, *106*, 9144-9146.

13. Bonner, W. A. *Orig. Life Evol. Biosphere* **1991**, *21*, 59-111.

14. Bonner, W. A.; Greenberg, J. M.; Rubenstein, E. *Orig. Life Evol. Biosphere* **1999**, *29*, 215-219.

15. Rikken, G. L. J. A.; Raupach, E. *Nature* **2000**, *405*, 932-935.

16. Cronin, J. R.; Pizzarello, S. *Science* **1997**, *275*, 951-955.

17. Pizzarello, S. *Acc. Chem. Res.* **2006**, *39*, 231-237.

18. Gazit, E.; Reches, M. *Science* **2003**, *300*, 625-627.

19. Gazit, E.; Carny, O. *Orig. Life Evol. Biosph.* **2011**, *41,* 121-132.

20. Ghadiri, M. R.; Granja, J. R.; Milligan, R. A.; McRee, D. E.; Khazanovich, N. *Nature* **1993**, *366*, 324-327.

21. Hartgerink, J. D.; Granja, J. R.; Milligan, R. A.; Ghadiri, M. R. *J. Am. Chem. Soc.* **1996**, *118*, 43.

22. Datta, D.; Tiwari, O.; Ganesh, K. N. *Nanoscale* **2018**, *10*, 3212-3224.

23. Deng, M.; Zhang, L.; Jiang, Y.; Liu, M. *Angew. Chem. Int. Ed.* **2016**, *55*, 15062-15066.

24. Hale, R. M.; Reilly, R. K. O. *Macromolecules* **2012**, *45*, 7665-7675.

25. Bera, S.; Jana, P.; Maity, S. K.; Haldar, D. *Cryst. Growth Des.* **2014**, *14*, 1032-1038.

26. Jana, P.; Maity, S.; Maity, S. K.; Ghorai, P. K.; Haldar, D. *Soft Matter* **2012**, *8*, 5621-5628.

27. Liu, F.; Austin, D. J. *Tetrahedron Lett.* **2001**, *42*, 3153-3154.

28. Yan, X. H.; He, Q.; Wang, K. W.; Duan, L.; Cui, Y.; Li, J. B. *Angew. Chem. Int. Ed.* **2007**, *46*, 2431-2434.
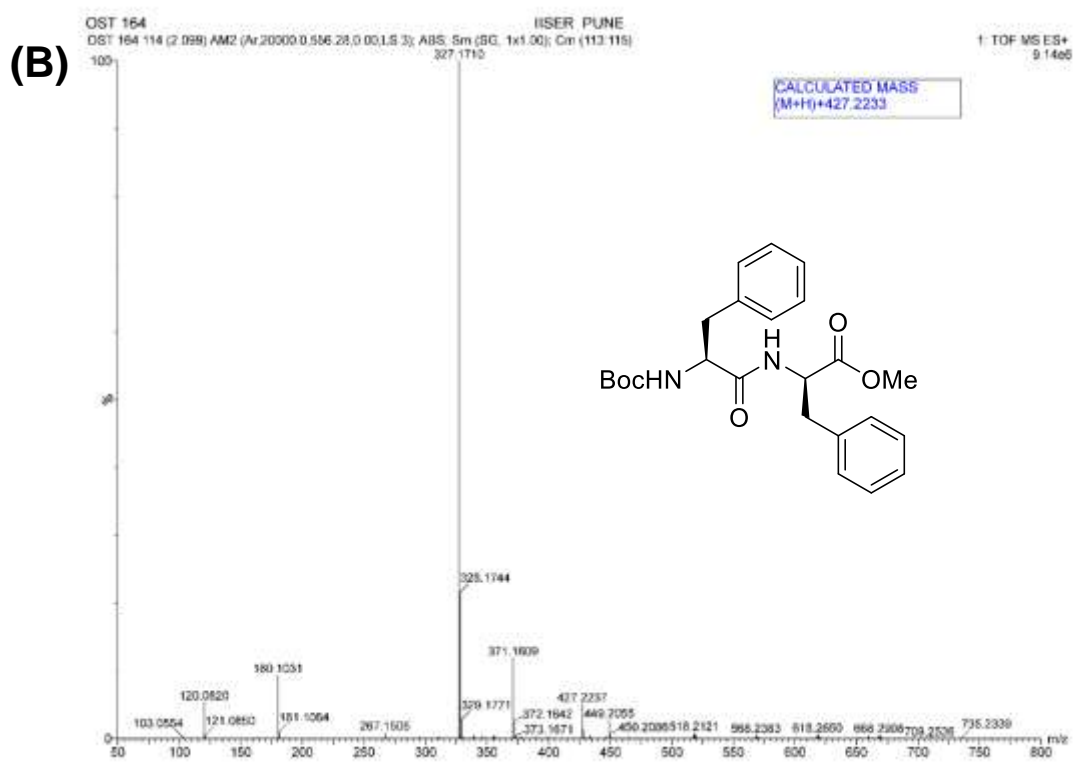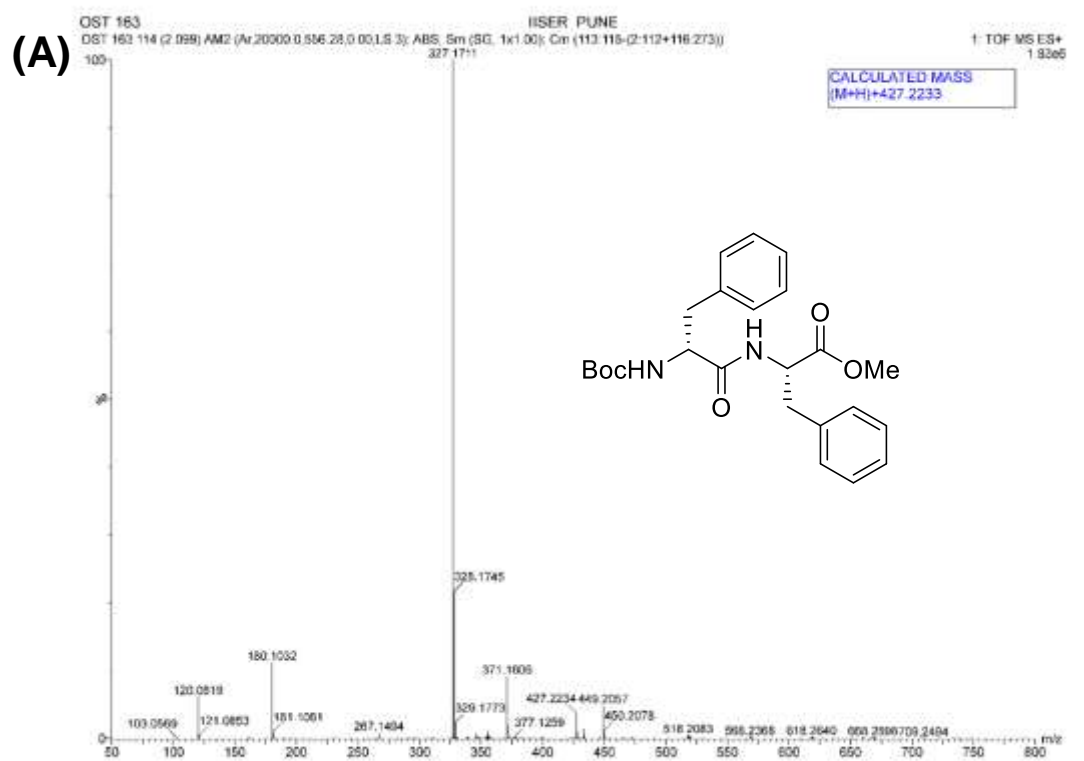
29. Yan, X. H.; Cui, Y.; He, Q.; Wang, K. W.; Li, J. B.; Mu, W. H.; Wang, B. L.; Yang, Z. C. O. *Chem. Eur. J.* **2008**, *14*, 5974-5980.

30. Zhang, Q.; Liu, S. J.; Yu, S. H. *J. Mater. Chem.* **2009**, *19*, 191-207.

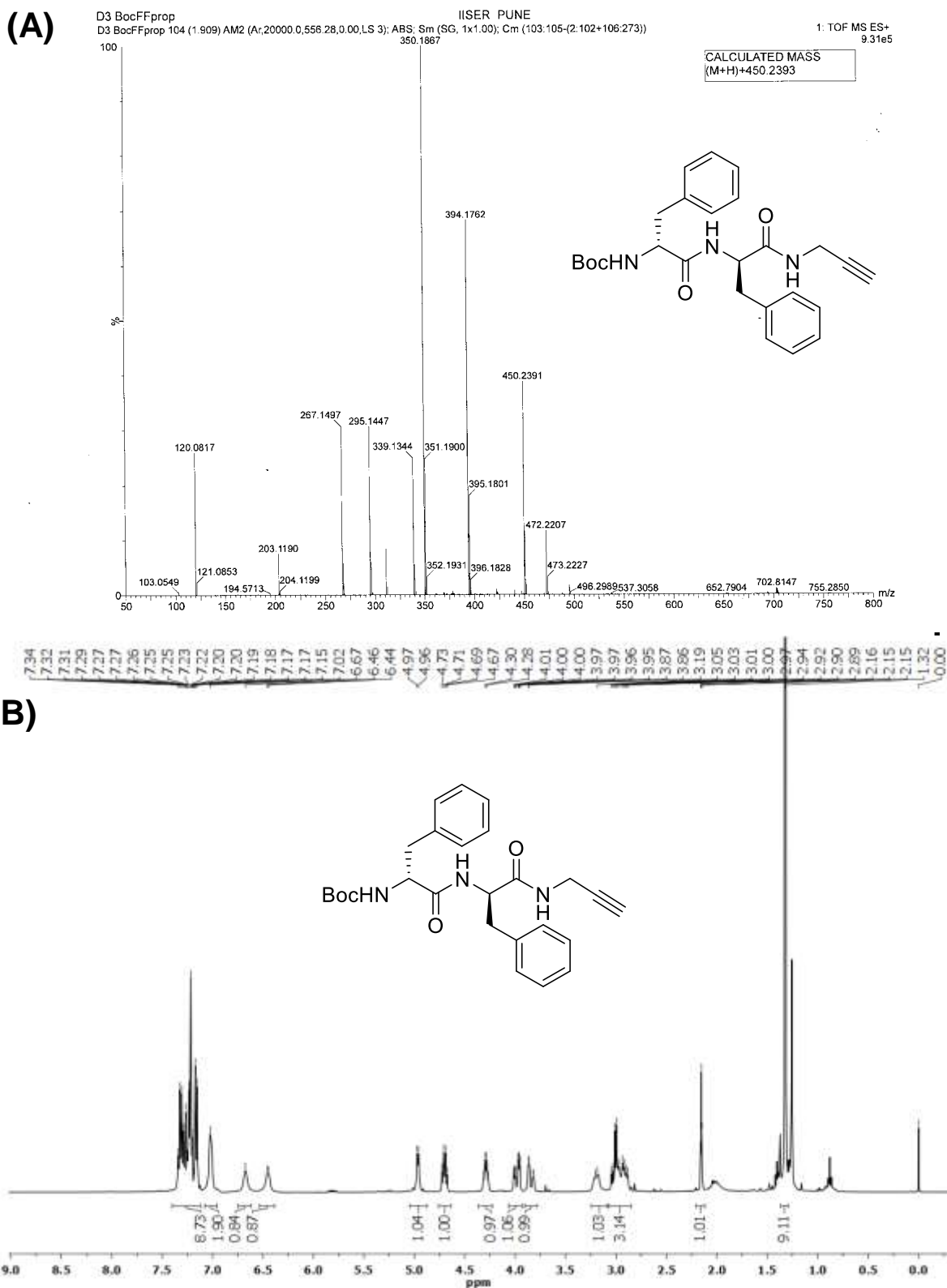31. Burda, C.; Chen, X.; Narayanan, R.; El-Sayed, M. A. *Chem. Rev*. **2005**, *105*, 1025-1102.

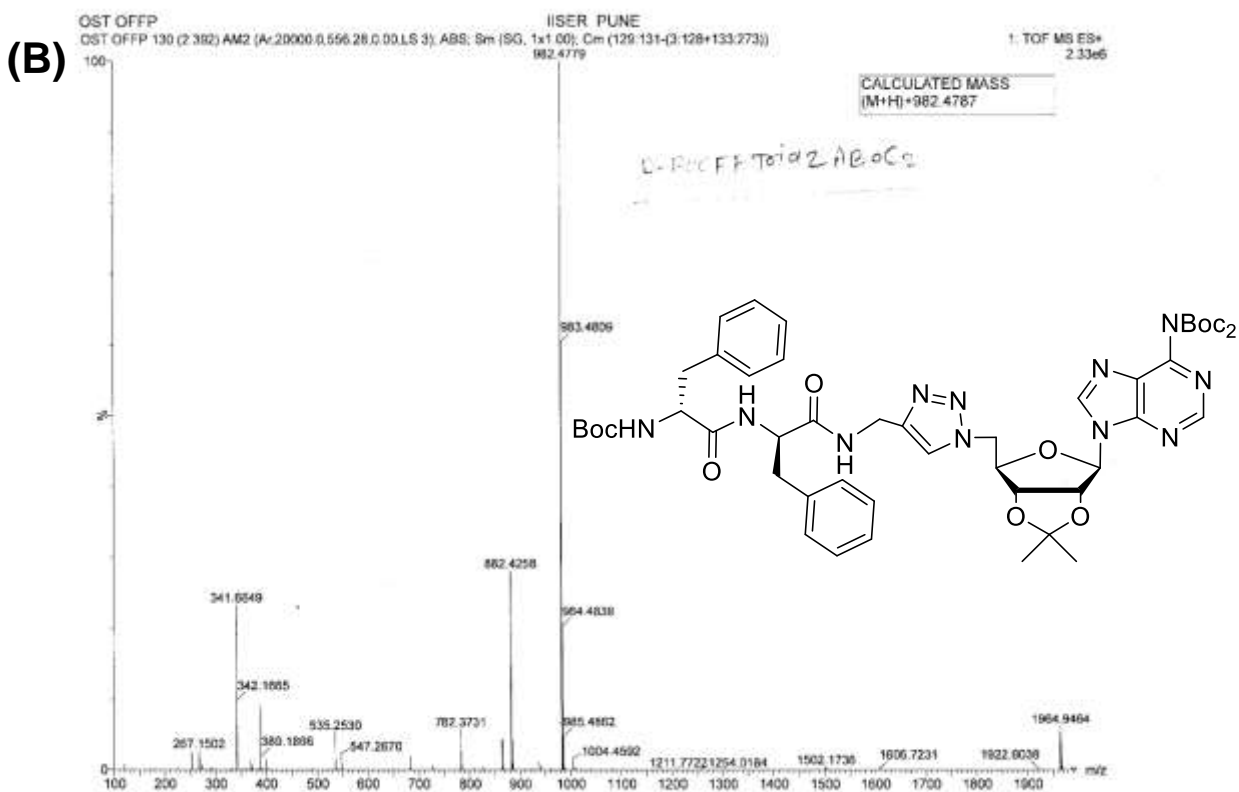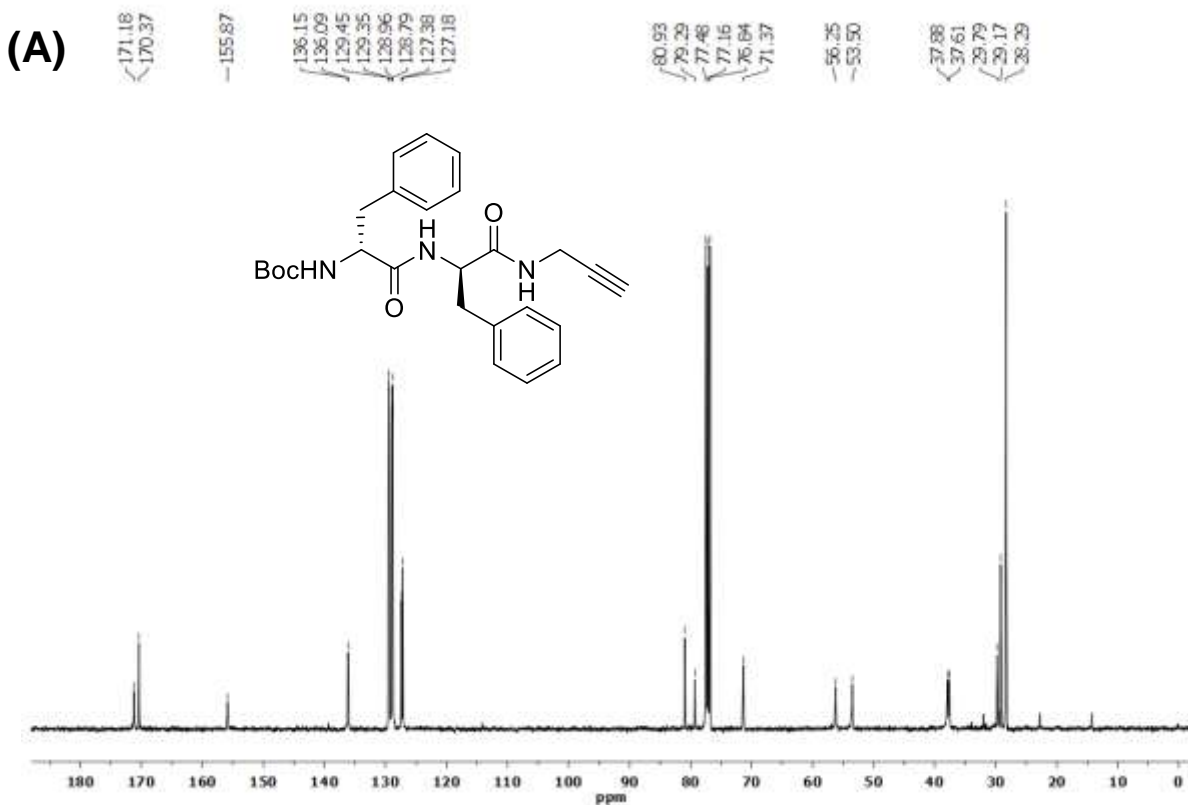## 3.7 Appendix II: Characterization data of synthesized compounds

| Entry | Table of contents | Page No. |
|---|---|---|
| 1 | HRMS, $^1$H NMR and $^{13}$C NMR spectra of compounds | 115-119 |

**(A)**

CALCULATED MASS
(M+H)+427.2233



327.1710
328.1743
371.1608
180.1032
329.1769
427.2233
103.0544 120.0818 181.1059 267.1496 373.1664 449.2048 450.2053 518.2073 568.2382 618.2639 668.2907 709.2525 735.2322 779.2183 m/z

**(B)**

CALCULATED MASS
(M+H)+413.2076



313.1559
357.1454
314.1588
413.2076
358.1487
120.0820
315.1618 359.1505 414.2106
103.0556 166.0868 185.7183 267.1495 436.1930 534.1663 602.9966 681.2245 707.1999 781.2755 m/z

HRMS of (A) Boc-(*D*)Phe-(*D*)Phe-OMe and (B) Boc-(*D*)Phe-(*D*)Phe-OH.

HRMS of (A) Boc-(*D*)Phe-(*L*)Phe-OMe and Boc-(*L*)Phe-(*D*)Phe-OMe.

**(A)**

D3 BocFFprop
D3 BocFFprop 104 (1.909) AM2 (Ar,20000.0,556.28,0.00,LS 3); ABS; Sm (SG, 1x1.00); Cm (103:105-(2:102+106:273))

IISER PUNE

1: TOF MS ES+
9.31e5

CALCULATED MASS
(M+H)+450.2393



**(B)**



(A) HRMS and (B) $^1$H-NMR spectra of Boc-(*D*)Phe-(*D*)Phe-Propyne **(4)**.

**(A)**



**(B)**

OST OFFP

OST OFFP 130 (2.392) AM2 (Ar,20000,0,556.28,0.00,LS 3); ABS; Sm (SG, 1x1.00); Cm (129:131-(3:128+133:273))

IISER PUNE

1: TOF MS ES+
2.33e6

CALCULATED MASS
(M+H)+982.4787



(A) ^{13}C-NMR spectra of Boc-(*D*)Phe-(*D*)Phe-Propyne (**4**) and (B) HRMS of Boc-(*D*)Phe-(*D*)Phe-*tz*-A[N(Boc)2] (**11**).
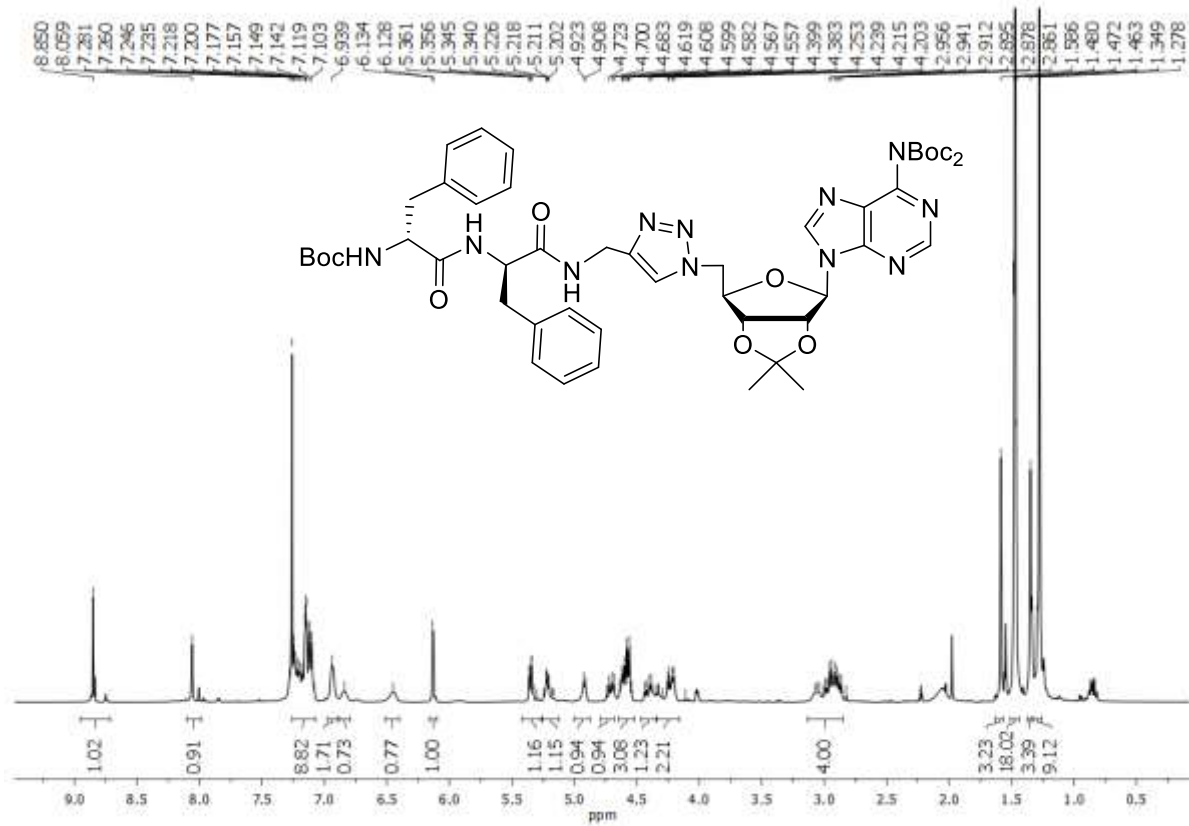
$^1$H-NMR spectra of Boc-(*D*)Phe-(*D*)Phe-*tz*-A$^{N(Boc)2}$ (**11**).

# Chapter 4

# Self-assembly of Diphenylalanine (Phe-Phe)-Peptide Nucleic Acid (PNA) Conjugates
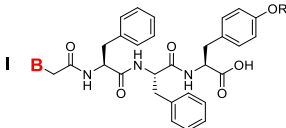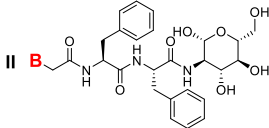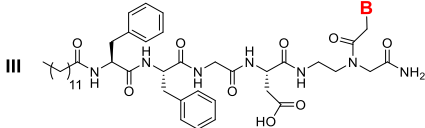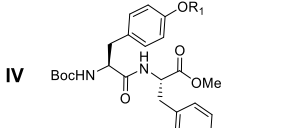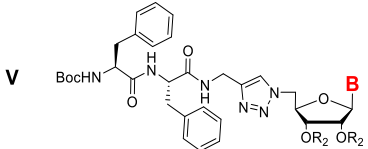
## 4.1 Introduction

Self-assembly of the dipeptide diphenylalanine (Phe-Phe) has been widely studied for its self assembling properties through its crystal and amorphous solid-state structures from mesoscopic to nano-metric levels.[1-5] As Phe-Phe is a key peptide element of the Alzheimer's *β*-amyloid peptide sequence,[6] formation of discrete and ordered peptide nanostructures by Phe-Phe derived motifs assumed importance. The stability, biocompatibility and water-solubility of Phe-Phe motifs also makes them ideal for applications *in* bio-sensing and catalysis.[7-11] It would be interesting to combine Phe-Phe motifs with other self assembling structures such as nucleosides as described in previous chapter and to modulate its self assembling properties. Watson-Crick specific base pairing in nucleosides are well known and unambiguous self-assembling systems.[12] In this context, Peptide nucleic acid (PNA) are good structural composites with peptide (polyamides) like backbone attached to nucleobases via tertiary amide link. Gazit *et. al.*,[13] demonstrated that among the sixteen possible PNA dimer combinations, three guanine (G)-containing analogues *viz*., CG, GC and GG exhibit luminescence in the visible region and unusual properties like voltage-dependent electroluminescence. Since G itself is not fluorescent, it is interesting to observe such luminescent properties in its base paired systems that perhaps arise from both stacking of bases and Watson-Crick base pairing as seen from the single crystal structure of GC pair.[13] The Fmoc protected GC PNA dimer also forms highly fluorescent aggregates[14] exhibiting aggregation induced emission (AIE) that promise new materials for organic light-emitting diodes. Self-assembly of PNA N-capped G-monomer *N*-(*N*-Fmoc-2-aminoethyl)-*N*-[(*N*-6-Bhoc-9-guanyl)acetyl]-glycine [Fmoc-G$^{NHBhoc}$-*aeg*-OH] is shown to result in nanospheres with unique optical[15] and 'structural color'[16] properties, with formation of photonic crystals useful for optoelectronics.

The interesting parallel developments in self-assemblies of dipeptide Phe-Phe and PNA G- monomer/dimers prompted us to explore the nucleopeptide conjugates of Phe-Phe with PNA monomers to examine their combined influence on mutual self-assembling properties. Previous reports depicted attachment of purine and pyrimidine nucleobases at the N-terminus of Phe-Phe motif through an amide linker to design nucleopeptides (**I**)[17,18] and (**II**)[19] which behave as hydrogelators that facilitate the delivery of oligonucleotides into human cells.[19] Self-assembly of an amphiphilic Phe-Phe (**III**)[20] consisting of hydrophobic alkyl tail at N-terminus and a nucleobase

at C-terminus elicited supramolecular nanohelices (Table 4.1) which were used to generate plasmonic nanomaterials with / without incorporation of AuNPs. Nucleobase peptide amphiphiles on dityrosine backbone (**IV**), formed helical or curved rod-like micelles leading to gelation and interaction with DNA.[21] Recently, self-assembly of a series of nucleopeptides consisting of purine / pyrimidine nucleoside conjugated diphenylalanine (**V**)[22] were shown to form stable spherical nanoparticles in 'molecular necklace' fashion.

**Table 4.1**: Self-assembled morophology of Phe-Phe motif containing nucleopeptides.

| Structure | Self-assembled nature | Reference |
|---|---|---|
|  **I** | Nanofibre and hydrogel | 18 |
|  **II** | Hydrogel | 19 |
|  **III** | Supramolecular nanohelices | 20 |
|  **IV** | Lamellae and ribbons | 21 |
|  **V** | Spherical nanoparticles | 22 |

**B** = Adenine (**A**) / Cytosine (**C**) / Guanine (**G**) / Thymine (**T**); R = H, $H_2PO_3$; $R_1$ = Hexyl, PEG; $R_2$ = C(Me)$_2$

## 4.2 Rationale for the present study

Nucleobases on a flexible PNA backbone form facile base pairing just as those on rather conformationally constrained ribose / deoxyribose backbones. In light of interesting aggregation properties of Phe-Phe petide motifs and PNA-G dimers as described in previous section, the work in this chapter is aimed to examine the structure and self-assembly properties of Boc-Phe-Phe linked to PNA monomers and oligomers. The C-terminus of Phe-Phe was conjugated to Peptide

Nucleic Acid (PNA) monomers through triazole or amide linker. The NH-protecting groups such as Boc, Cbz, $^i$Bu at the N-terminus or on nucleobase provide a handle to study the effect of hydrophobicity while the PNA strcutures offer to examine the effects of H-bonding and base stacking interactions. The morphologies of these conjugated nucleopeptides were monitored through microscopic techniques (SEM, HRTEM, and AFM) and stability of these nucleopeptides were tested with proteolytic enzymes.
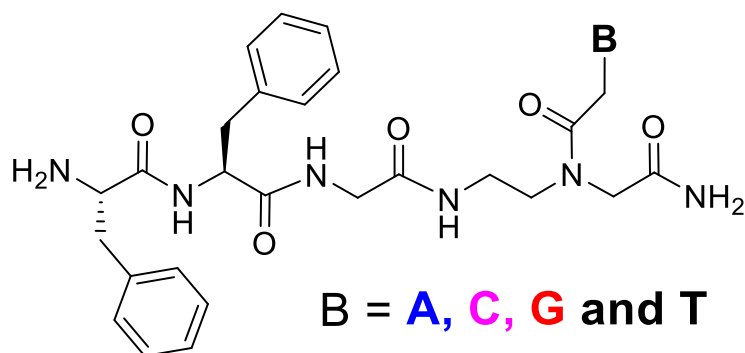


Structure of Phe-Phe-PNA conjugates

## 4.3 Objectives of the present work

The specific objectives of this chapter are following:

➢ Synthesis of Boc-Phe-Phe-*am-aeg*(A$^{NHCbz}$)-OEt **(3a)**, Boc-Phe-Phe-*am-aeg*(6-Cl-G$^{NHiBu}$)-OEt **(3b)**, Boc-Phe-Phe-*am-aeg*(G$^{NHiBu}$)-OEt **(3c)** and Boc-Phe-Phe-*tz-aeg*(G$^{NHiBu}$)-OEt **(6c)**.

➢ Synthesis of  deprotected peptide conjugates H-Phe-Phe-Gly-*aeg*(A/C/G/T)-NH$_2$ **(NP1-NP4)**.

➢ Characterization of the peptides by HRMS, MALDI, IR, $^1$H, $^{13}$C NMR spectroscopy.

➢ Contact angle (CA) measurements to evaluate molecular hydrophobicity.

➢ Study of self-assembly using FESEM, HRTEM and AFM.

➢ Size distribution of nanoparticles by DLS and thermal stability by TGA.

## 4.4 Results and discussions

The following section describes the synthesis of various Phe-Phe-PNA conjugates **(NP1-NP4)** followed by their characterization and morphological studies. The PNA monomer is conjugated through glycine spacer, with amide or triazole as linker.

**4.4.1 Synthesis of diphenylalanine-PNA conjugated peptides**: The nucleopeptides **(NP1-NP4)** were synthesized using Boc-strategy followed by cleavage and deprotection to afford nucleopeptides (Figure 4.1A). For peptide synthesis, the commercially available Boc-Gly-OH and Boc-PNA monomers 2(a-d) with suitable nucleobase protecting groups were used, while Boc-Phe-Phe-OH **(1)** was synthesized following literature procedure.[22] The peptide Phe-Phe **(1)** was tethered to PNA units *via* a glycyl linker. Unlike previous reports[20,23] the N-termini of these peptides **(NP1-NP4)** are uncapped and discriminated structurally by attached purine and pyrimidine nucleobases (A/C/G/T). Subsitituted 1,4-triazole ring is a known bioisoster of the *trans*-amide bond of peptides[24] and devoid of H-bond donor amide (CONH) group. Hence analogous peptides conjugated with triazole ring as a linker instead of amide bond were were also made to examine its effect in the self-assembly process.
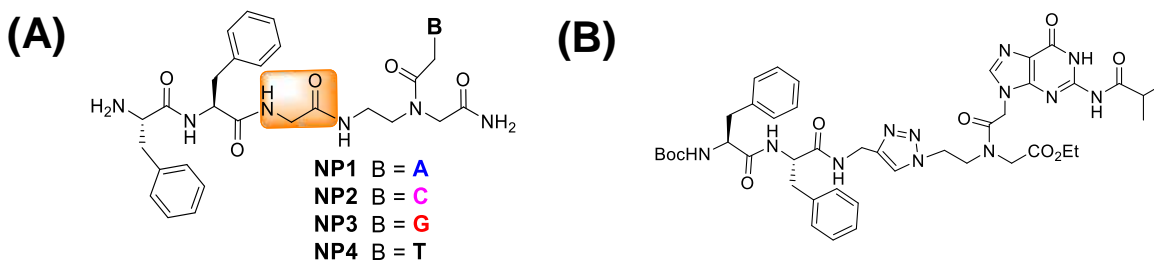


**(A)**
**NP1** B = A
**NP2** B = C
**NP3** B = G
**NP4** B = T

**(B)**

**Figure 4.1**: Strcutures of (A) nucleopeptides **NP1**-**NP4** with amide linker and (B) nucleopeptides **6c** with triazole linker.

The various protected PNA monomers required for conjugates with amide linker were synthesized by standard procedures reported in literature[25,26] (Scheme 4.1) and characterized by standard ^{1}H NMR and mass spectra. These were coupled with Boc-Phe-Phe-OH **(1)** with PNA monomers **2(a-d)** that have different bases (A/G/T) in presence of EDC.HCl and
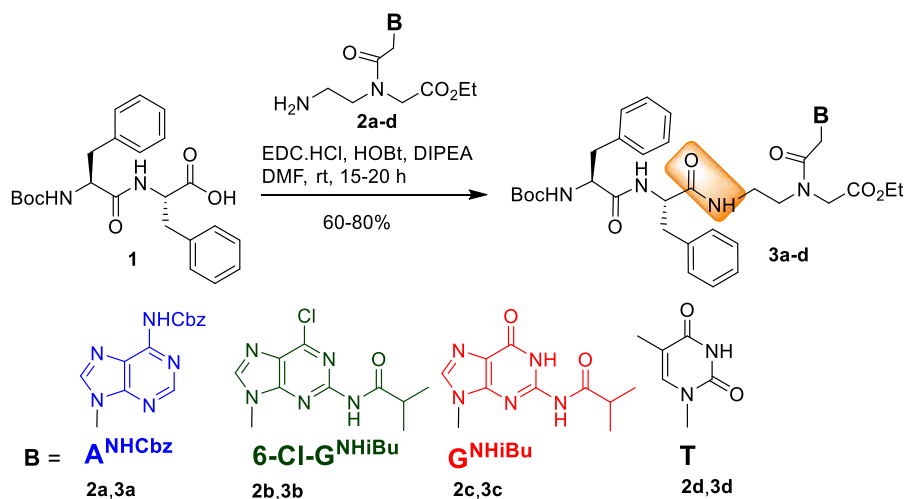
*N*-hydroxybenzotriazole (HOBt) (Scheme 4.2) to afford the conjugated peptides **3(a-d)** in moderate to good yields.
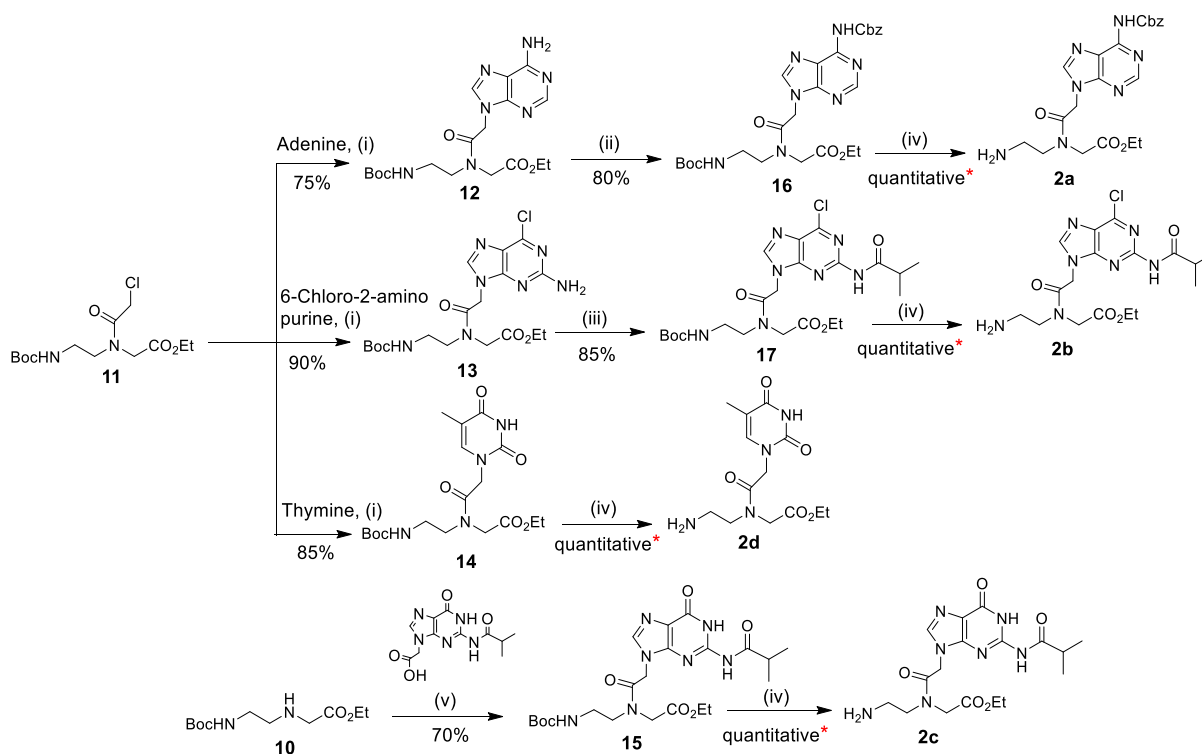


*According to converstion observed in TLC

Reagents and conditions: (i) K₂CO₃, DMF, 75°C, 3 h; (ii) Cbz-Cl, NaHCO₃, rt, 8 h; (iii) Isobutyrylchloride, dry Py, 12.5 h; (iv) 50% TFA in DCM, 0 °C-rt, 4-6 h; (v) EDC.HCl, HOBt, DIPEA, dry DMF, 0°C-rt, 36 h

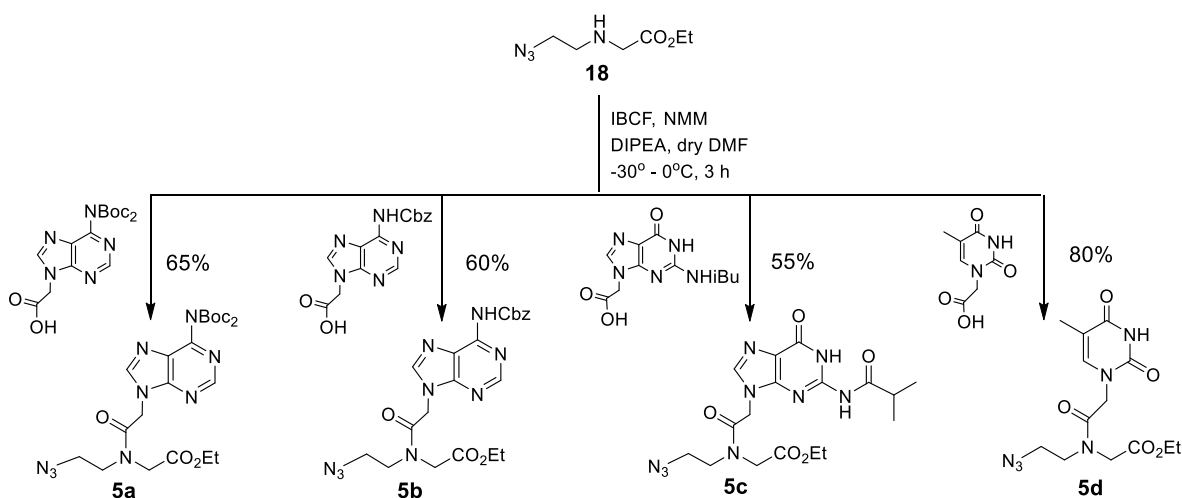**Scheme 4.1**: Synthesis of PNA monomers for amide coupling.



**Scheme 4.2**: Synthesis of fully protected amide linked nucleopeptide **3(a-d)**.

The Phe-Phe-PNA conjugates with triazole linker was **6(a-d)** were synthesized by conjugation of Boc-Phe-Phe-Propyne **(4)**[22] with PNA-azides **5(a-d)** (Scheme 4.3), using CuAAC based click chemistry.[27,28] The PNA azide monomers **5(a-d)** required for click conjugation (Scheme 4.4) were synthesized according to route shown in (Scheme 4.5). All intermediate and final compounds were characterized by NMR and mass spectral data.
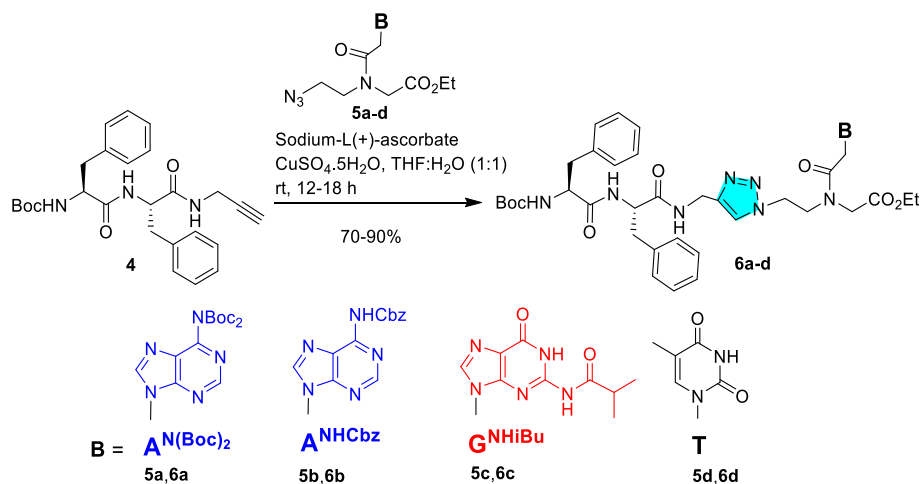


**Scheme 4.3**: Synthesis of fully protected triazole linked nucleopeptide **6(a-d)**.



**Scheme 4.4**: Synthesis of PNA monomers for 'Click' conjugation.

The partially deprotected nucleoppetides were aso synthesized for examining their potential for self assembly. The N-Boc group of fully substituted nucleopeptides **6(c-d)** was deprotected with TFA to afford N-deprotected ester peptides **7(c-d)**.

Alkaline hydrolysis of esters **6(c-d)** under basic conditions gave nucleopeptide acids **8(c-d)** that carry N-protection. To specifically see the role of nucleobases in self assembly process, peptide lacking only nucleobase Boc-Phe-Phe-*tz-aeg*-OEt **(9)** was made from click reaction of Boc-Phe-Phe-Propyne **(4)** with the azide ethyl(2-azidoethyl)glycinate (Scheme 4.6).
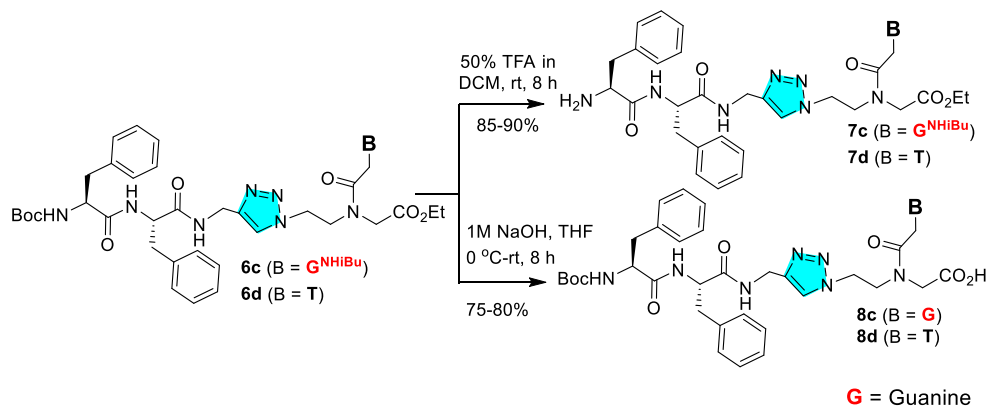


**Scheme 4.5**: Synthesis of partially protected nucleopeptides **7c**, **7d**, **8c** and **8d** peptide.
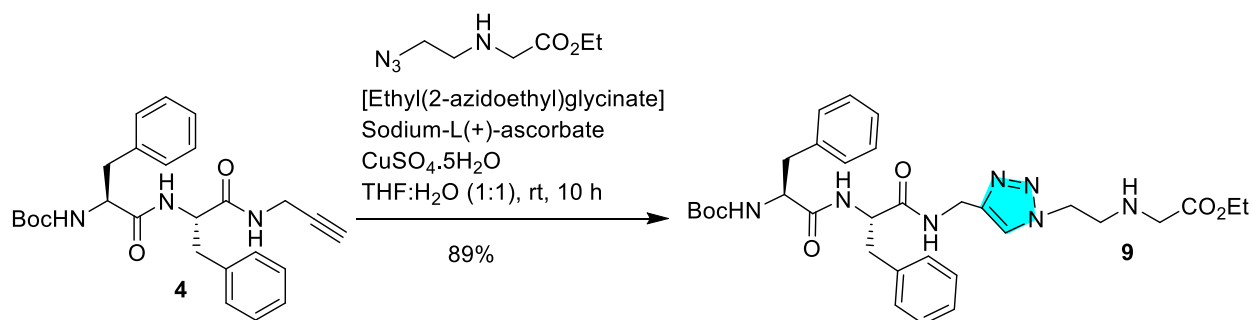


**Scheme 4.6**: Synthesis of protected peptide **9**.

The synthesised protected peptides **3(a-d)**, **6(a-d)**, **7c**, **7d**, **8c**, **8d**, and **9** were purified by column chromatography over silica gel and structurally characterized by NMR and HRMS. The deprotected glycine linked peptides **NP1-NP4** were purified by reverse-phase HPLC (see experimental section) and characterized by MALDI spectral data.

The characteristic amide I bands observed between 1688-1643 cm^{-1} for all nucleopeptides **6(a-d)** indicated the probability of both parallel and anti-parallel orientation of peptide chains in a mini β-strand type structure.[28a] For nucleopeptides **3(b-d)**, single IR stretching frequency seen around 1650 cm^{-1} in amide I region indicating β-strand secondary structures may self-assemble in several ways.[28] Nucleopeptides **3a** [Boc-Phe-Phe-*am-aeg*(A^NHCbz)-OEt], **3b** [Boc-Phe-Phe-*am-*

*aeg*(6-Cl-G$^{NHiBu}$)-OEt], **6c** [Boc-Phe-Phe-*tz*-*aeg*(G$^{NHiBu}$)-OEt], and **6d** [Boc-Phe-Phe-*tz*-*aeg*(T)-OEt] exhibited strong amide II bands around 1500 cm$^{-1}$ (see experimental section).

**4.4.2 Morphologies and microscopic architectures**: The morphology arising from self-assembled structures of various nucleopeptide conjugates was monitored by SEM, HRTEM, and AFM techniques. Peptide samples were prepared as mentioned in reported experimental procedures.[6] Nucleopeptides were dissolved in 1,1,1,3,3,3-hexafluoro-2-propanol (HFIP) (1 mg / mL) and lyophilized to obtain solid residues which were dissolved further in 1:1 EtOH / H$_2$O (1 mL). These freshly prepared samples were used for microscopic analysis. Self-assembly of completely deprotected NPs were observed first followed by partially and fully protected analogues.

The completely deprotected nucleopeptides **NP1-NP4** without any hydrophobic protecting groups exhibited different morphologies depending on the nature of attached nucleobases. The adenine A-peptide **NP1** [H-Phe-Phe-Gly-*aeg*(A)-NH$_2$] and cytosine C-peptide **NP2** [H-Phe-Phe-Gly-*aeg*(C)-NH$_2$] aggregated to form ill-defined clusters (Figure 4.2A and B). The thymine T-peptide **NP4** [H-Phe-Phe-Gly-*aeg*(T)-NH$_2$] showed sticky nanoparticles with average diameter of 200 nm (Figure 4.2D). In comparison, the guanine G-peptide **NP3** [H-Phe-Phe-Gly-*aeg*(G)-NH$_2$] self-assembled into small homogeneous spherical nanoparticles (Figure 4.2C) with average diameter of 15 nm. To examine if base pairing of complementary nucleobases can lead to better assembly than individual bases, 1:1 mixtures of the complementary A-peptide (**NP1**):T-peptide (**NP4)** and G-peptide (**NP3**):C-peptide (**NP4)** were mixed and images of their co-assembled structures are shown in (Figures 4.2E and F). The 1:1 assembly of A- and T-peptides (**NP1**+**NP4**) resulted in better defined nanoparticles, but still aggregated (Figure 4.2E) while mixture of C- and G-peptides (**NP2**+**NP3**) produced nice nanowires made of linear arrays of uniformly sized spherical nanoparticles (Figure 4.2F). Thus base paired nanoparticles show improved dependent on base-dependent morphological structures.
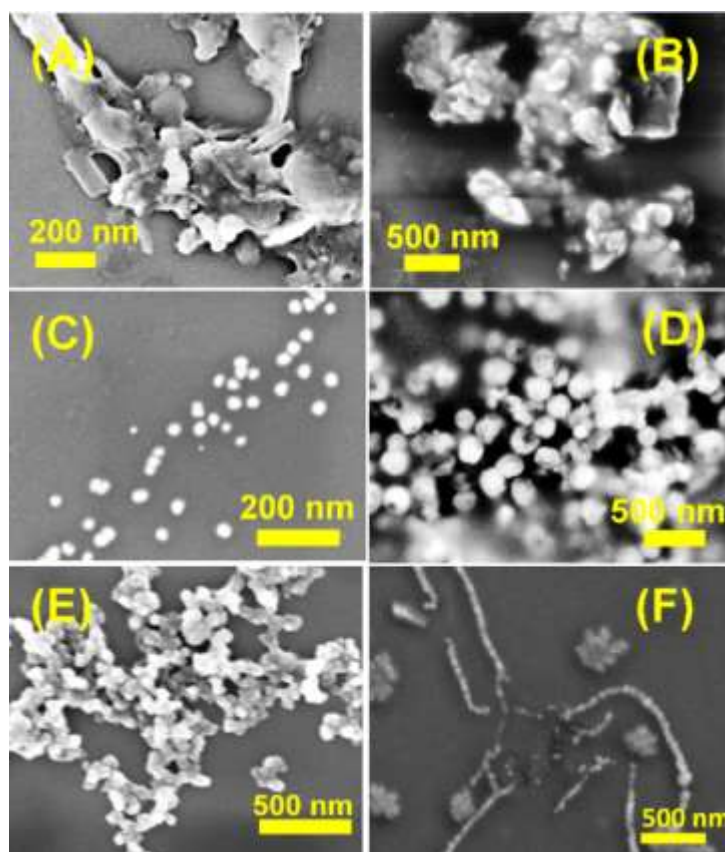
**Figure 4.2**: SEM images of nucleopeptide (A) **NP1** [H-Phe-Phe-Gly-*aeg*(A)-NH$_2$]; (B) **NP2** [H-Phe-Phe-Gly-*aeg*(C)-NH$_2$]; (C) **NP3** [H-Phe-Phe-Gly-*aeg*(G)-NH$_2$]; (D) **NP4** [H-Phe-Phe-Gly-*aeg*(T)-NH$_2$]; (E) 1:1 mixture of **NP1** and **NP4** and (F) 1:1 mixture of **NP2** and **NP3**.

Base pairing of peptides conjugated with complementary bases were examined by the electrospray ionization (ESI$^+$) mass spectroscopy. The mass spectra of individual A-peptide and T-peptide showed expected masses with addition of K (perhaps leached from ion sources) (Figures 4.3 and 4.4), while injection of 1:1 mixture of two peptides showed higher masses corresponding to combined masses of the two peptides (Figure 4.5 and 4.6), giving evidence of base pair formation under gaseous ionizing conditions of mass spectra. Further, the mass spectra of individual C-peptide and G-peptide showed expected masses with addition of K (perhaps leached from ion sources) (Figures 4.7 and 4.8), while injection of 1:1 mixture of two peptides showed higher masses corresponding to combined masses of the two peptides (Figure 4.9 and 4.10).

This is also giving evidence of base pair formation under gaseous ionizing conditions of mass spectra. The base paired mass spectra were observed only under ESI conditions (Figure 4.6 and Figure 4.10) and not under MALDI-TOF conditions (Figure 4.5 and 4.9).
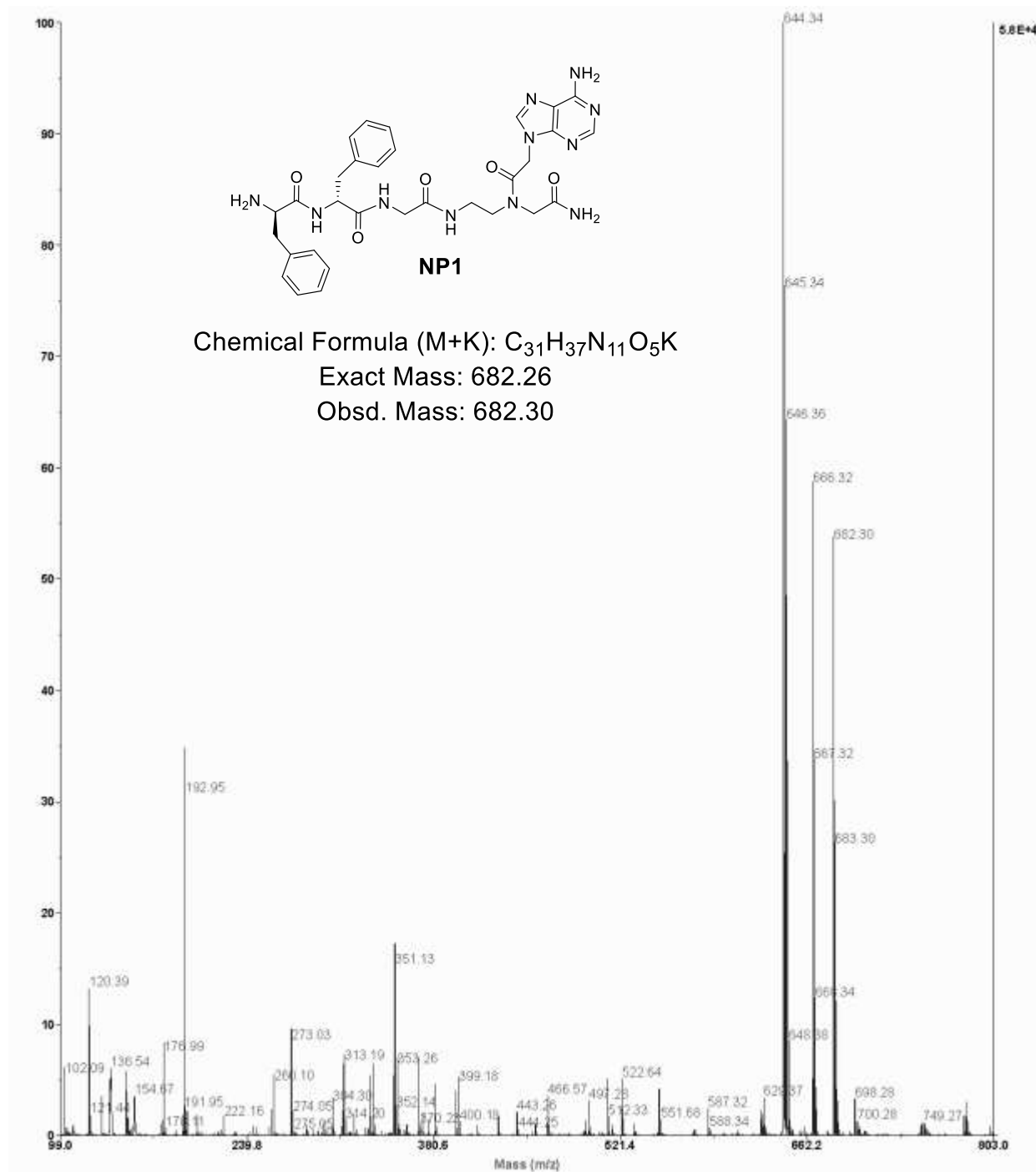


**Figure 4.3**: MALDI-TOF spectrum of **NP1**.
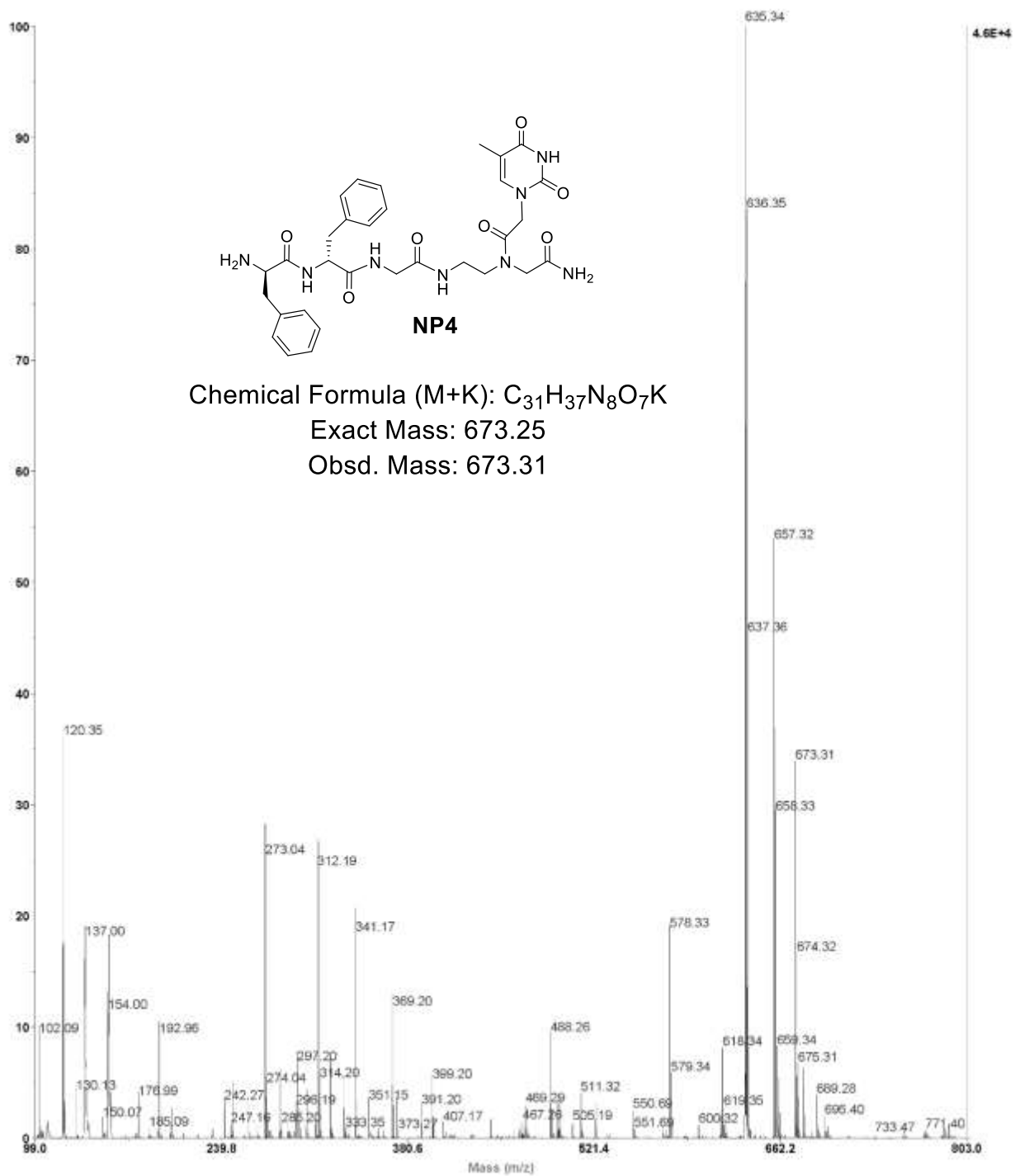
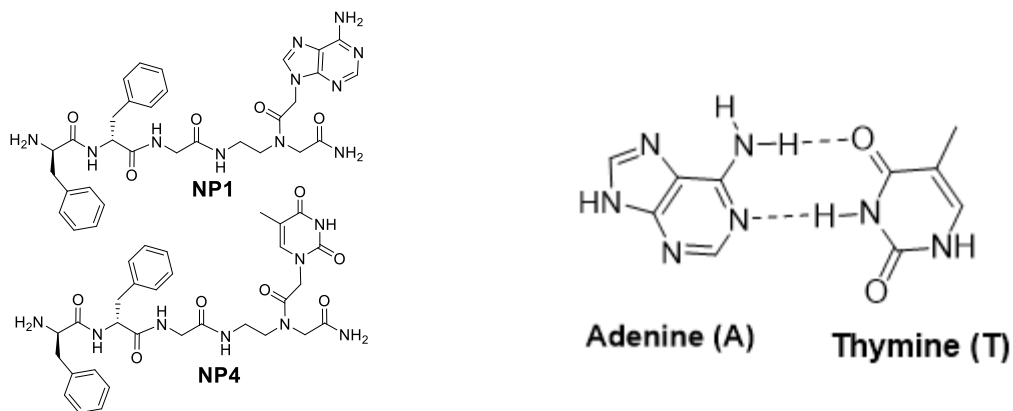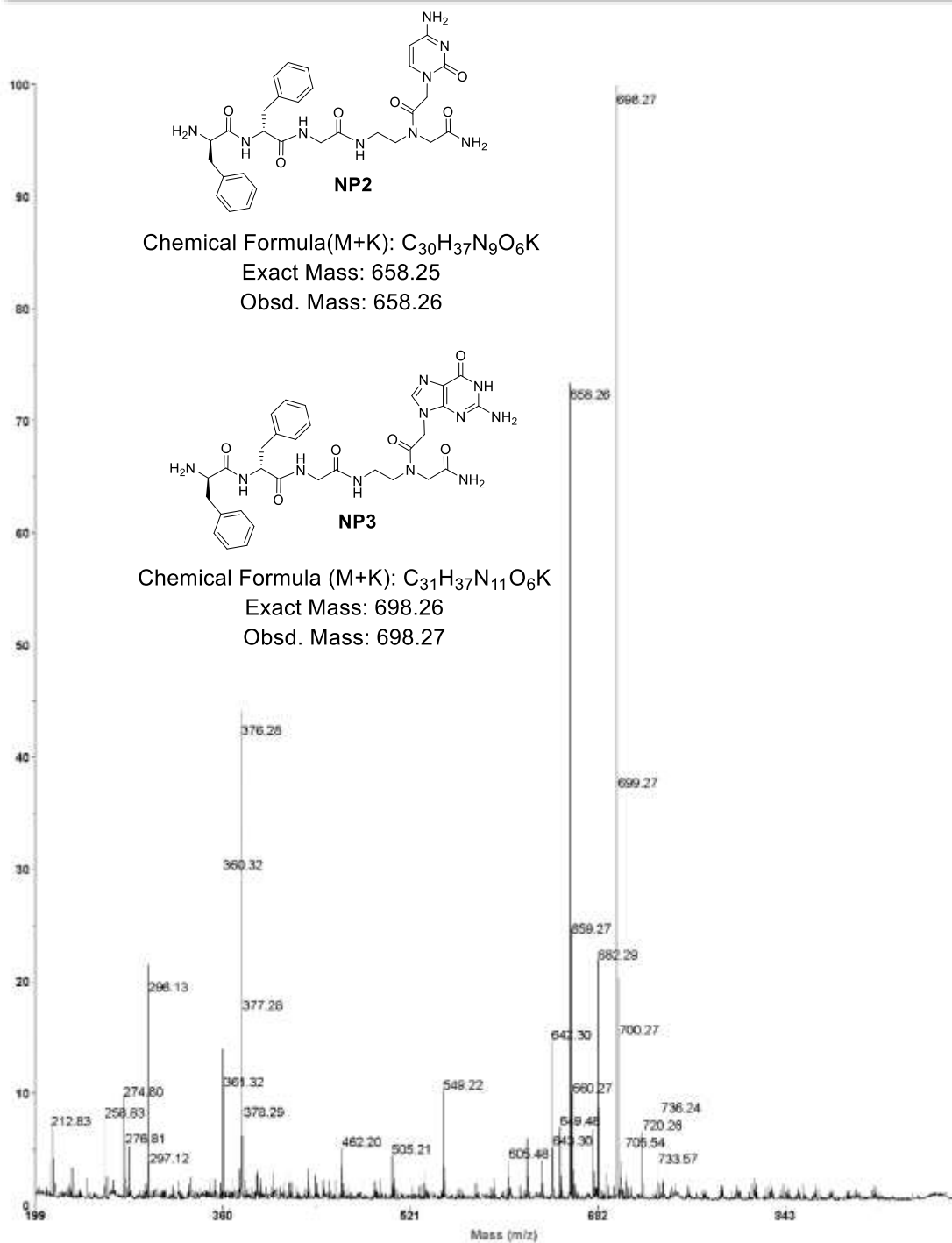**Figure 4.4**: MALDI-TOF spectrum of **NP4**.

**NP1**

Chemical Formula (M+K): $C_{31}H_{37}N_{11}O_5K$
Exact Mass: 682.26
Obsd. Mass: 682.28

**NP4**

Chemical Formula (M+K): $C_{31}H_{37}N_8O_7K$
Exact Mass: 673.25
Obsd. Mass: 673.27
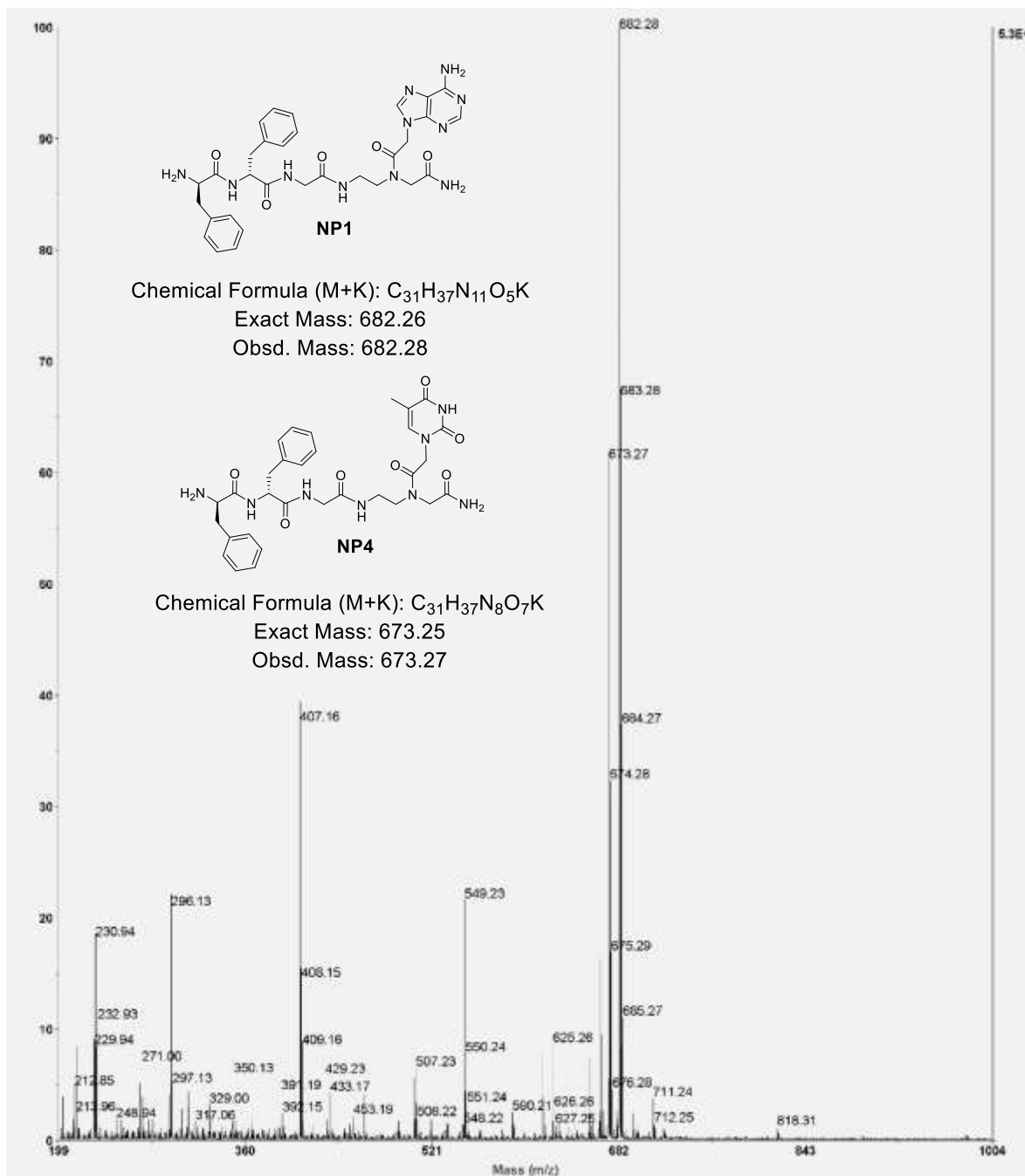
**Figure 4.5**: MALDI-TOF spectrum of **NP1** + **NP4** duplex.

**Chemical Formula of Duplex (M+H): $C_{62}H_{76}N_{19}O_{12}$**
**Calcd. Duplex Mass: 1278.5921**
**Obsd. Mass: 1278.5879**
**Error: -3.3 ppm**
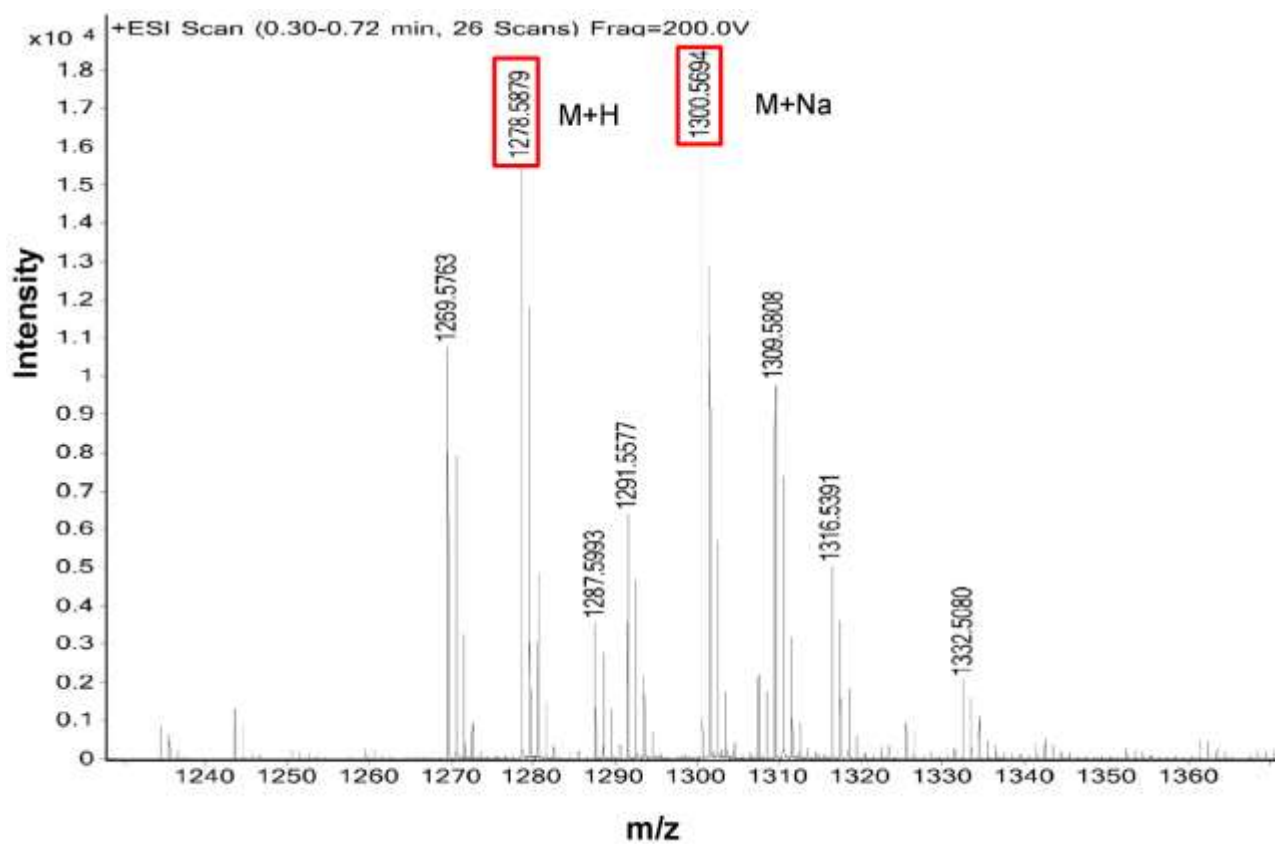


**Figure 4.6**: ESI mass spectrum of **NP1** + **NP4** duplex.
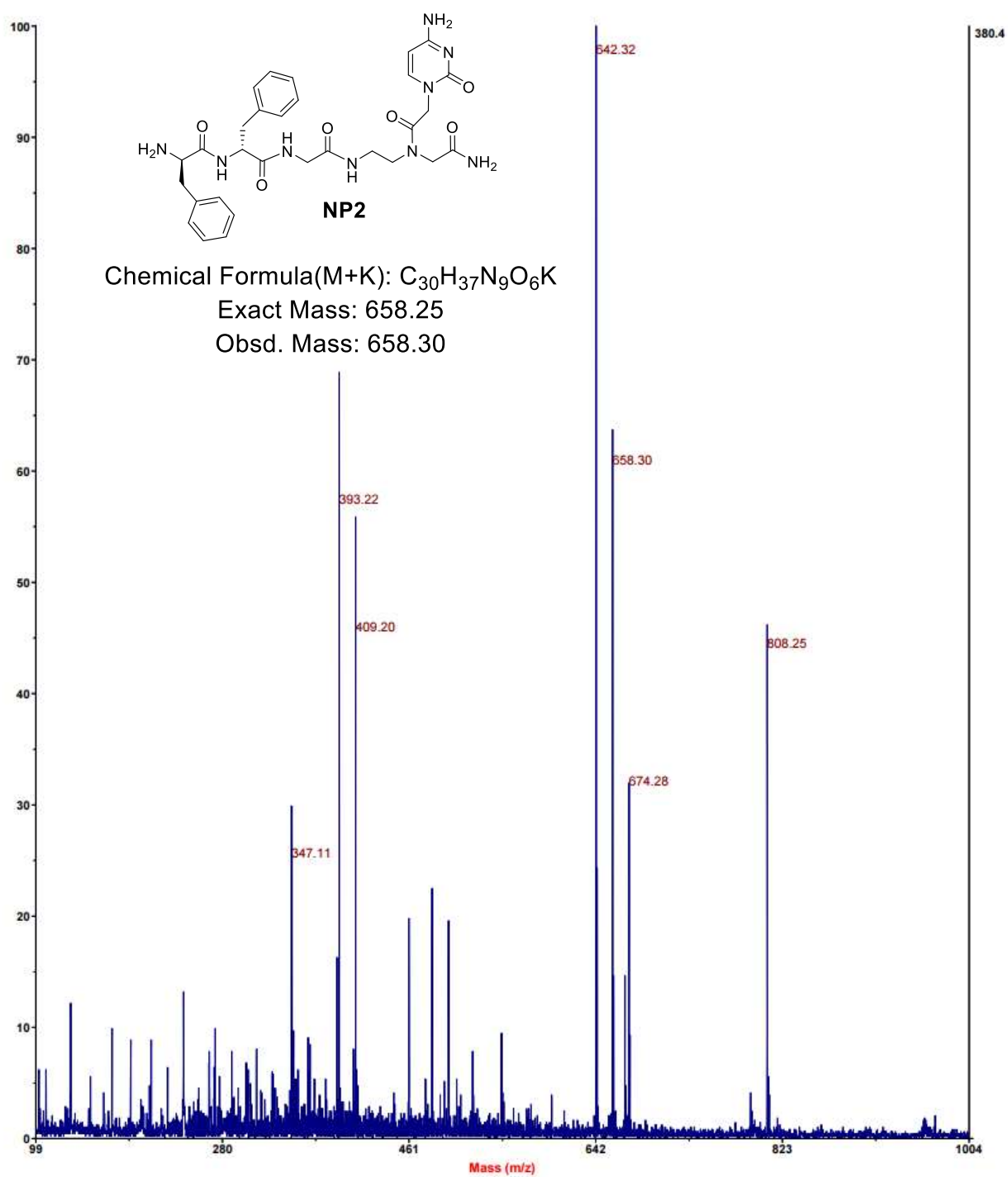
**Figure 4.7**: MALDI-TOF spectrum of **NP2**.
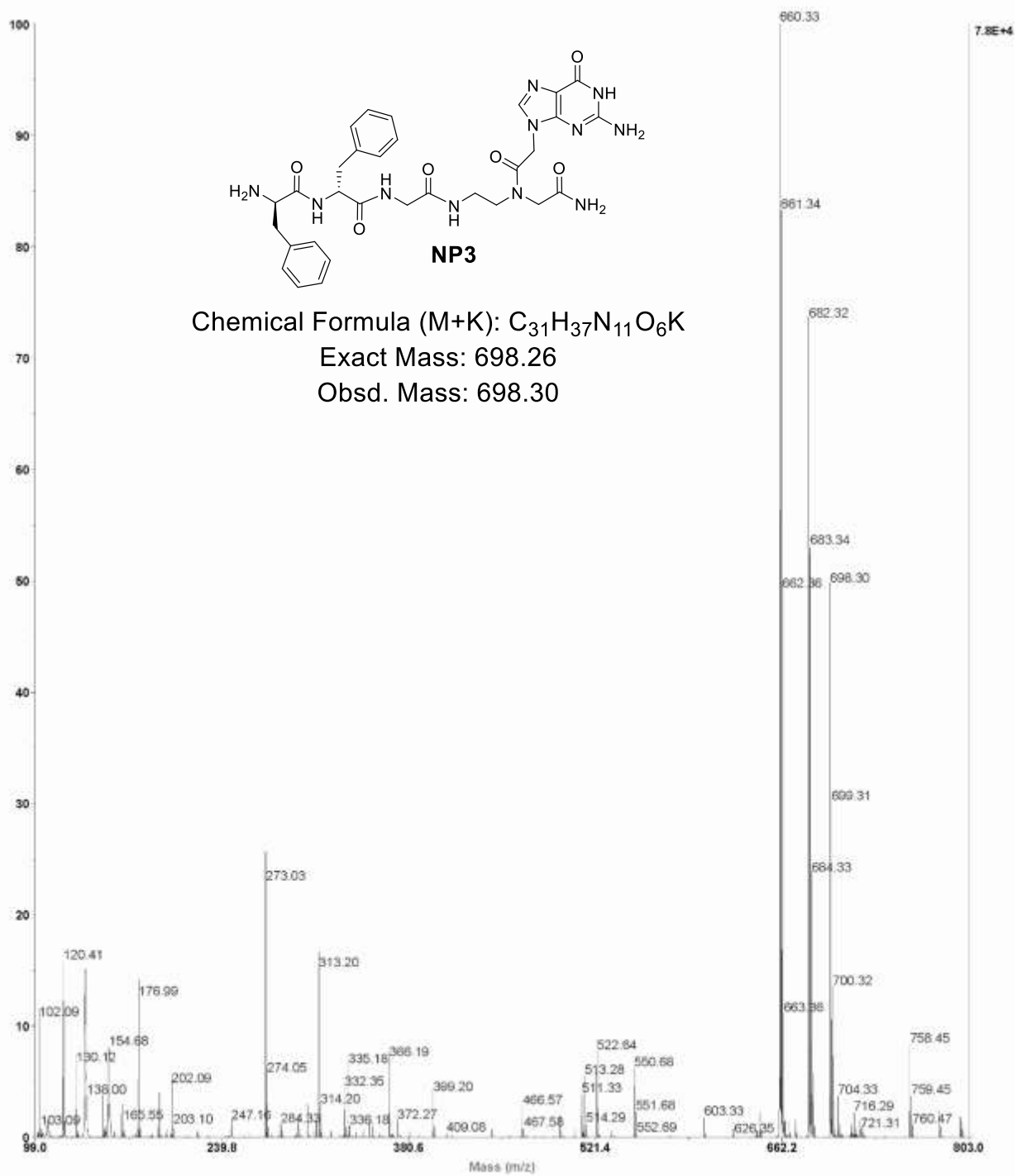
**Figure 4.8**: MALDI-TOF spectrum of **NP3**.

Chemical Formula(M+K): $C_{30}H_{37}N_9O_6K$
Exact Mass: 658.25
Obsd. Mass: 658.26

Chemical Formula (M+K): $C_{31}H_{37}N_{11}O_6K$
Exact Mass: 698.26
Obsd. Mass: 698.27

**Figure 4.9**: MALDI-TOF spectrum of **NP2** + **NP3** duplex.
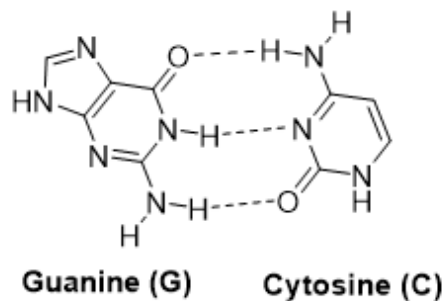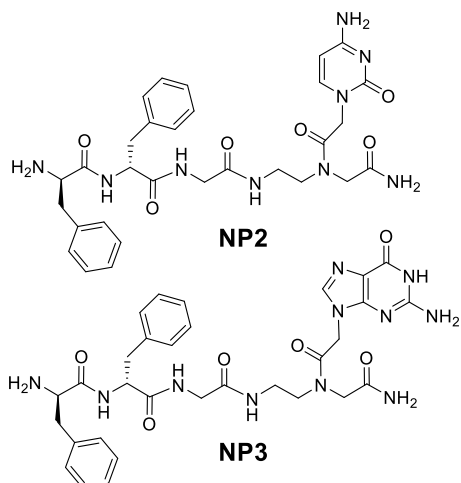
**Chemical Formula of Duplex (M+H): $C_{61}H_{75}N_{20}O_{12}$**
**Calcd. Duplex Mass: 1279.5873**
**Obsd. Mass: 1279.5886**
**Error: -1.3 ppm**
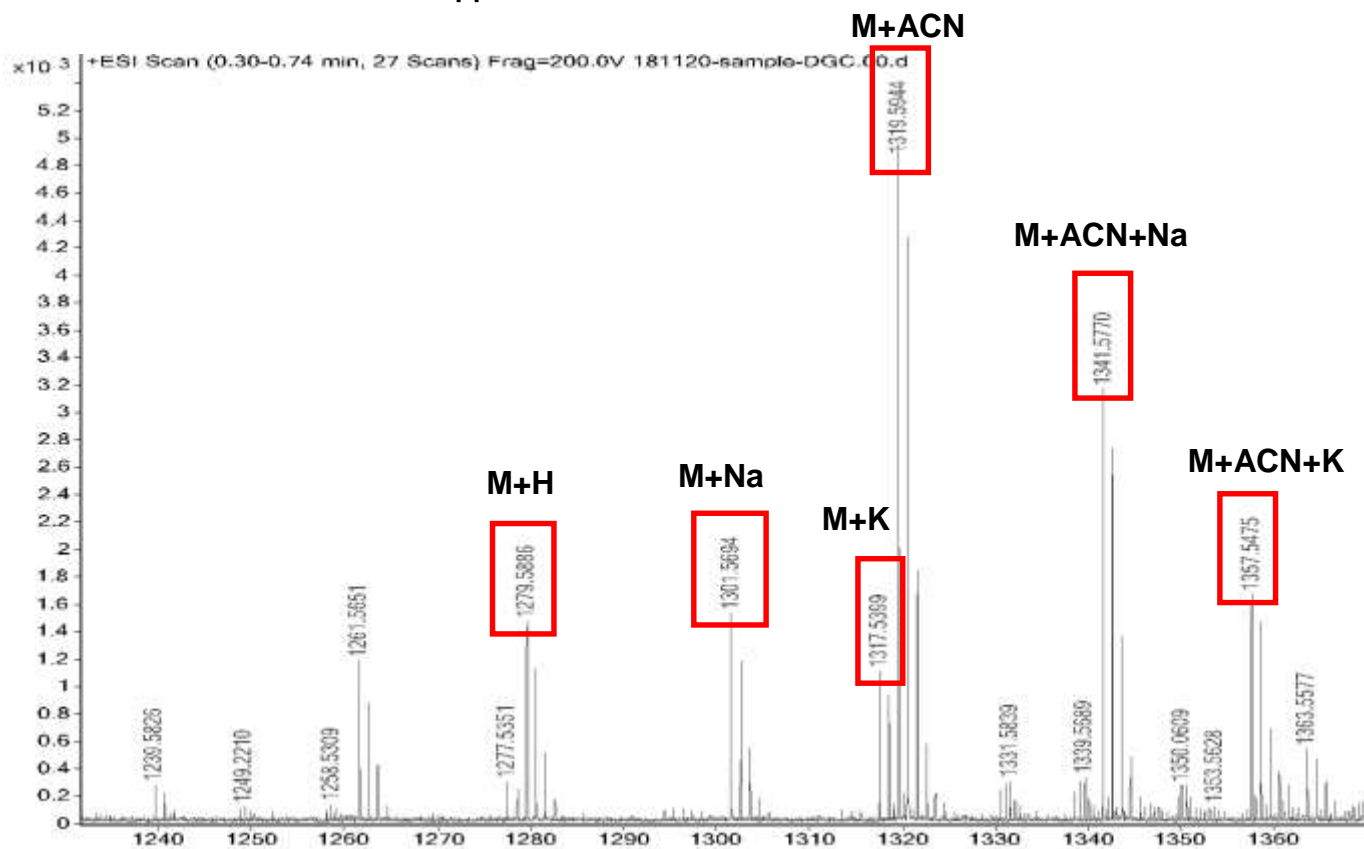


**Figure 4.10**: ESI mass spectrum of **NP2** + **NP3** duplex.

**4.4.3 Morphology of ester peptides**: The partially deprotected nucleopeptides (**7c,d**, and **8c,d**) carrying terminal free amine or carboxylic groups gave variable self-assembled morphologies (Figure 4.11). The peptide conjugate **7c** [H-Phe-Phe-*tz-aeg*(G$^{NHiBu}$)-OEt] and **7d** [H-Phe-Phe-*tz-aeg*(T)-OEt] with free –NH$_2$ groups at N-terminus produced small rod-like structures (Figure 4.11A and 4.11B) whereas nucleopeptides with the free –CO$_2$H group **8c** [Boc-Phe-Phe-*tz-aeg*(G)-OH] and **8d** [Boc-Phe-Phe-*tz-aeg*(T)-OH] resulted were simply agglomerate masses (Figure 4.11C and 4.11D).
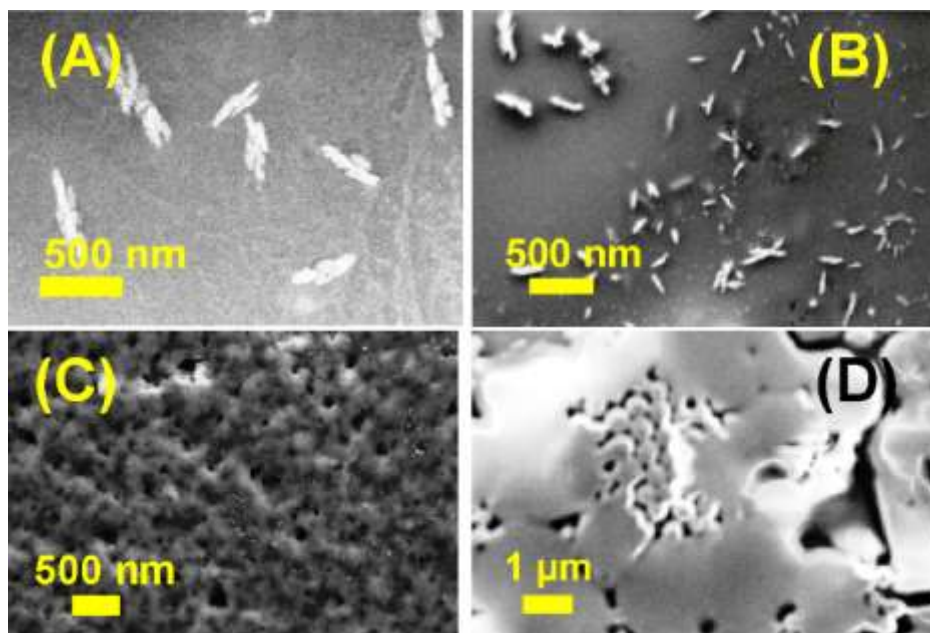


**Figure 4.11**: SEM images of nucleopeptide (A) **7c** [H-Phe-Phe-*tz-aeg*(G$^{NHiBu}$)-OEt]; (B) **7d** [H-Phe-Phe-*tz-aeg*(T)-OEt]; (C) **8c** [Boc-Phe-Phe-*tz-aeg*(G)-OH] and (D) **8d** [Boc-Phe-Phe-*tz-aeg*(T)-OH].

Since nucleopeptides **7c** and **7d** are present as salts with trifluoroacetate as counterion, to examine the role of conuterions influencing the self assembling properties, the Boc peptides **6c** and **6d** were deprotected 1 M aq. HCl to yield peptides **7c** and **7d** as HCl salts with Cl⁻ as counter anion. However the peptides did not produce ordered self-assembled morphologies indicating the possible effects of counterion in self assembly process (Figure 4.12).
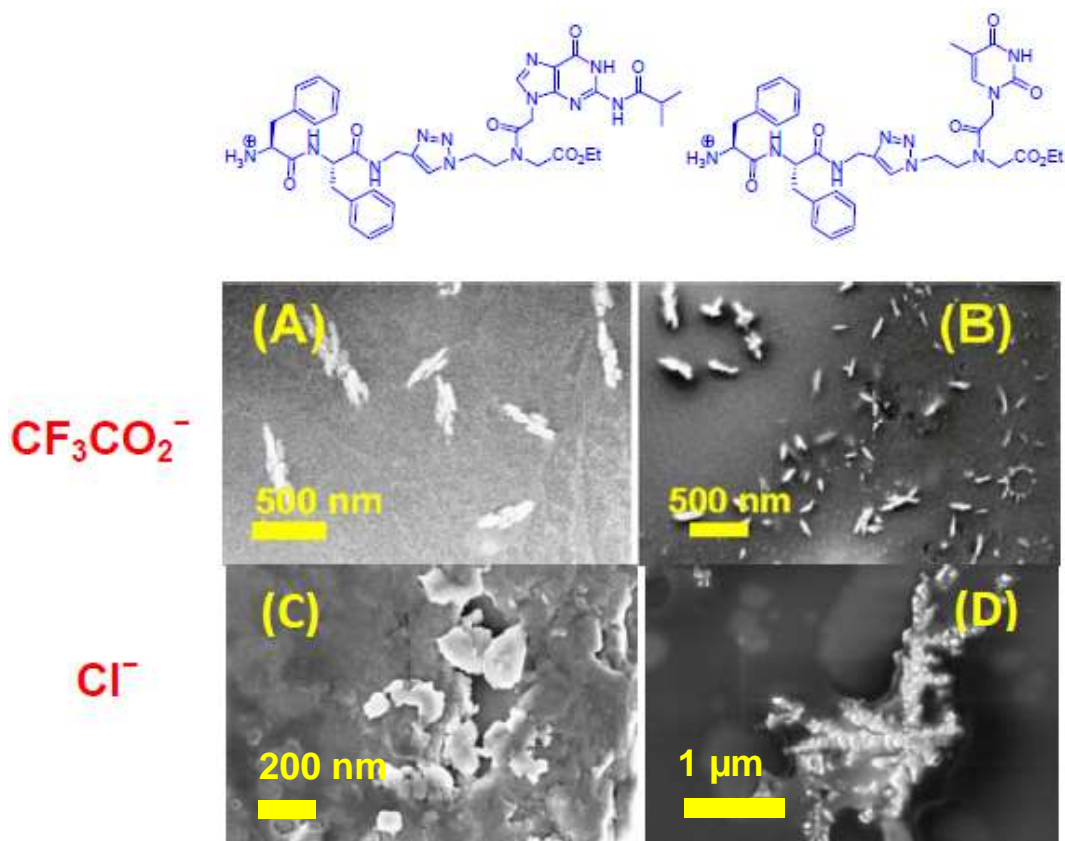
**Figure 4.12**: Effect of counter anion on self-assembled morphologies for nucleopeptide **7c** and **7d** in the presence of trifluoroacetate (A, B) and chloride (C, D) respectively through SEM images.

**4.4.4 Morphology of fully protected peptides**: To examine the role of hydrophobic groups in self assembly, the SEM images of fully protected nucleopeptides **3(a-d)** with amide linker were recorded (Figure 4.13). These depicted spherical nanoparticles with subtle distinctions. The amide linked peptide conjugate **3a** with adenine (A) [Boc-Phe-Phe-*am-aeg*(A$^{NHCbz}$)-OEt] exhibited solid nanosphere of fairly uniform size (200-600 nm diameter), while nucleopeptides **3b** [Boc-Phe-Phe-*am-aeg*(6-Cl-G$^{NHiBu}$)-OEt], **3c** [Boc-Phe-Phe-*am-aeg*(G$^{NHiBu}$)-OEt], and **3d** [Boc-Phe-Phe-*am-aeg*(T)-OEt] exhibited solid spheres (Figure 4.13) with average diameters ranging from (500-1000 nm), but with doughnut like hollow cavity in center. Thus the hydrophobic protecting groups in amide linked peptide conjugates have a distinct role in dictating the self assembly process, giving rise to well defined nanospheres having hollow cavity. Evidently, nucleobases have less effect on the self-assembled morphologies for the amide linked nucleopeptides.
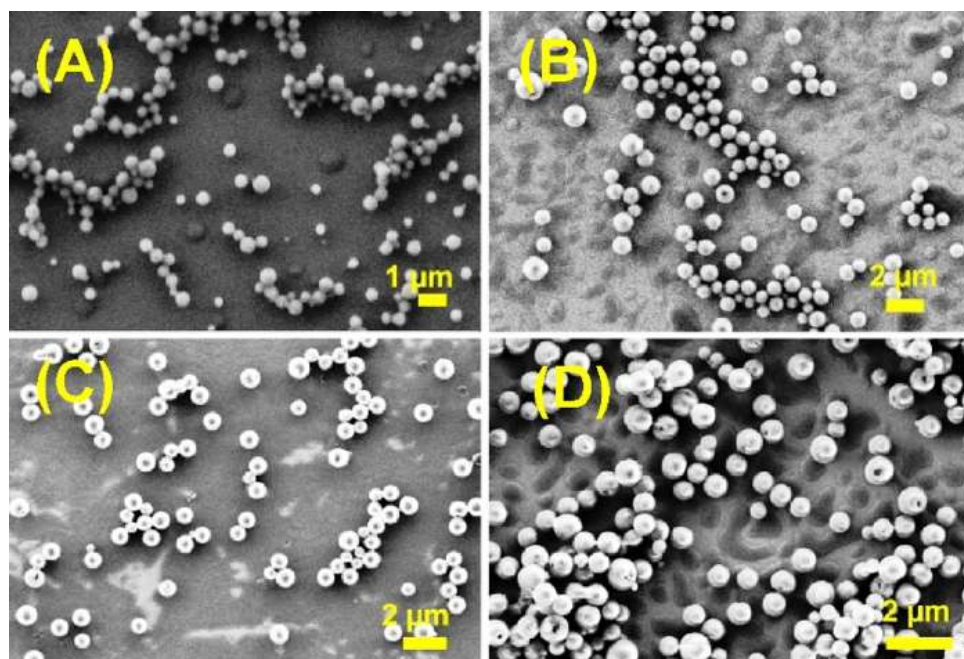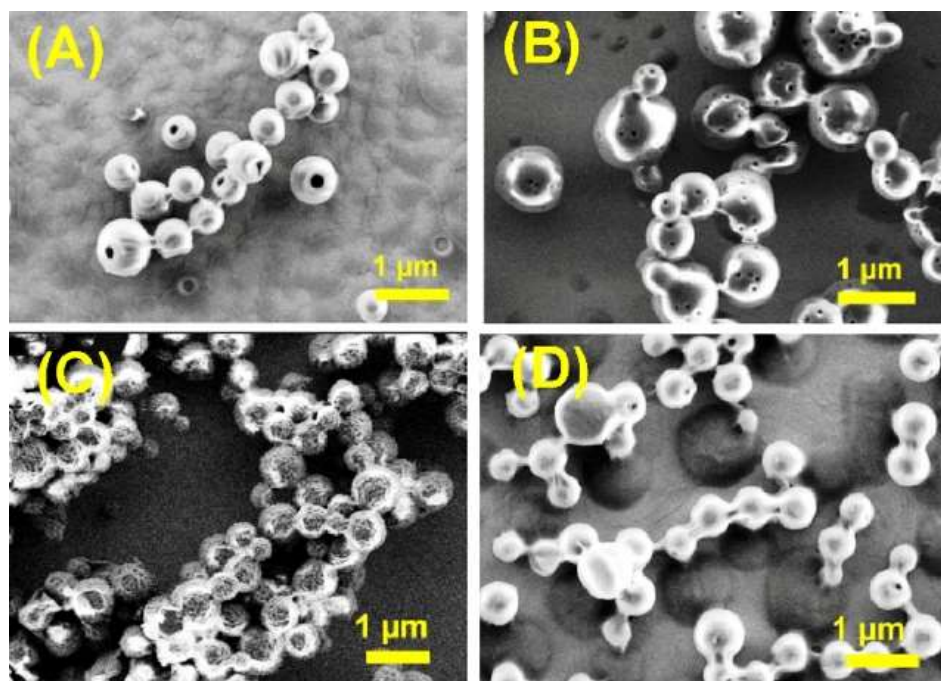
**Figure 4.13**: SEM images of nucleopeptide (A) **3a** [Boc-Phe-Phe-*am-aeg*(A^NHCbz)-OEt]; (B) **3b** [Boc-Phe-Phe-*am-aeg*(6-Cl-G^NHiBu)-OEt]; (C) **3c** [Boc-Phe-Phe-*am-aeg*(G^NHiBu)-OEt] and (D) **3d** [Boc-Phe-Phe-*am-aeg*(T)-OEt].

In comparison, the triazole (*tz*) linked analogues **6(a-c)** exhibited slightly larger spheres (Figure 4.14) with average diameter for nanoparticles ranging from 450-900 nm, but these spheres had a much wider and open hollow spaces in sphere. The T-nucleopeptide **6d** [Boc-Phe-Phe-*tz-aeg*(T)-OEt] was less porous and exhibited spheres that are linearly interlinked. The variability in size and base dependent subtle differences in shape among the nanoparticles of the protected peptides suggests that relative hydrophobicity is a critical factor in determining the self assembly process. Further the nature of the linker (amide vs. triazole) also seems to make a difference.

The hollowness of spherical nanoparticles of triazole peptides observed in SEM images were further confirmed by HRTEM and AFM analysis. Nucleopeptide **6a** [Boc-Phe-Phe-*tz-aeg*{A^N(Boc)2}-OEt] showed pronounced aperture on nanoparticle surface in HRTEM (Figure 4.15A) whereas the two other triazolyl nucleopeptides, **6b** [Boc-Phe-Phe-*tz-aeg*(A^NHCbz)-OEt] and **6d** [Boc-Phe-Phe-*tz-aeg*(T)-OEt] showed hollowness similar to **6a** on spherical self-assembly (Figure 4.15B and D). The guanine containing nucleopeptide **6c** [Boc-Phe-Phe-*tz-aeg*(G^NHiBu)-OEt] showed nanospheres with uneven surface (Figure 4.15C).

**Figure 4.14**: SEM images of nucleopeptide (A) **6a** [Boc-Phe-Phe-*tz-aeg*{A^N(Boc)2}-OEt]; (B) **6b** [Boc-Phe-Phe-*tz-aeg*(A^NHCbz)-OEt]; (C) **6c** [Boc-Phe-Phe-*tz-aeg*(G^NHiBu)-OEt] and (D) **6d** [Boc-Phe-Phe-*tz-aeg*(T)-OEt].

When PNA moieties were attached to Phe-Phe through amide bonds *viz.*, **3a** [Boc-Phe-Phe-*am-aeg*(A^NHCbz)-OEt], **3b** [Boc-Phe-Phe-*am-aeg*(6-Cl-G^NHiBu)-OEt], **3c** [Boc-Phe-Phe-*am-aeg*(G^NHiBu)-OEt] and **3d** [Boc-Phe-Phe-*am-aeg*(T)-OEt], solid spheres without perforation were seen in HRTEM (Figure 4.15E-H). The hollow spherical self-assembly observed for triazole peptides was clearly visible from their height profiles recorded through AFM. AFM images of the nanoparticles from **6a** [Boc-Phe-Phe-*tz-aeg*{A^N(Boc)2}-OEt] and **6b** [Boc-Phe-Phe-*tz-aeg*(A^NHCbz)-OEt] did clearly show the hollow nature with the depth found to be 20-60 nm (Figure 4.15I and J). The rough surfaced and aggregated nanoparticles were observed for nucleopeptides **6c** and **6d** respectively (Figure 4.15K and L). The origin of pore formation on such spherical particles are attributed by Feringa *et. al.*, to processes involving both solvent and non-solvents (Here, water is the non-solvent in which the protected nucleopeptides are poorly soluble).[29,30] Height profile of the particles were further confirmed by AFM images (Figure 4.16).
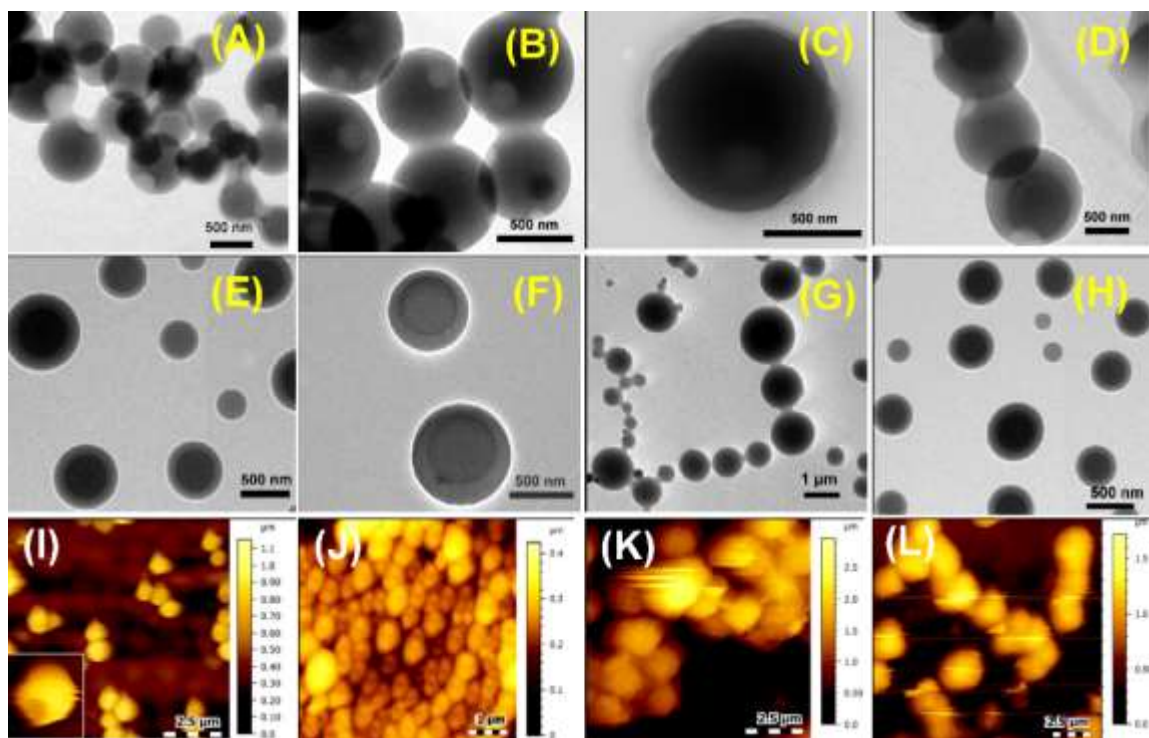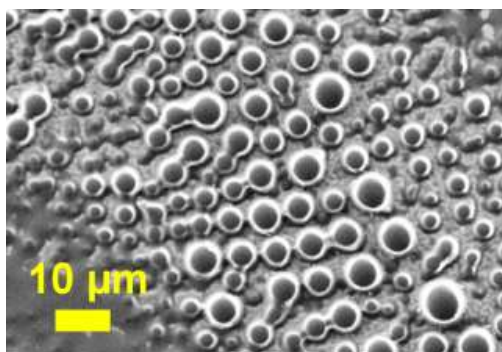
**Figure 4.15**: HRTEM images showing morphology for **6(a-d)** (A-D) and **3(a-d)** (E-H); AFM images showing surface topology for **6(a-d)** (I-L) nanoparticles.
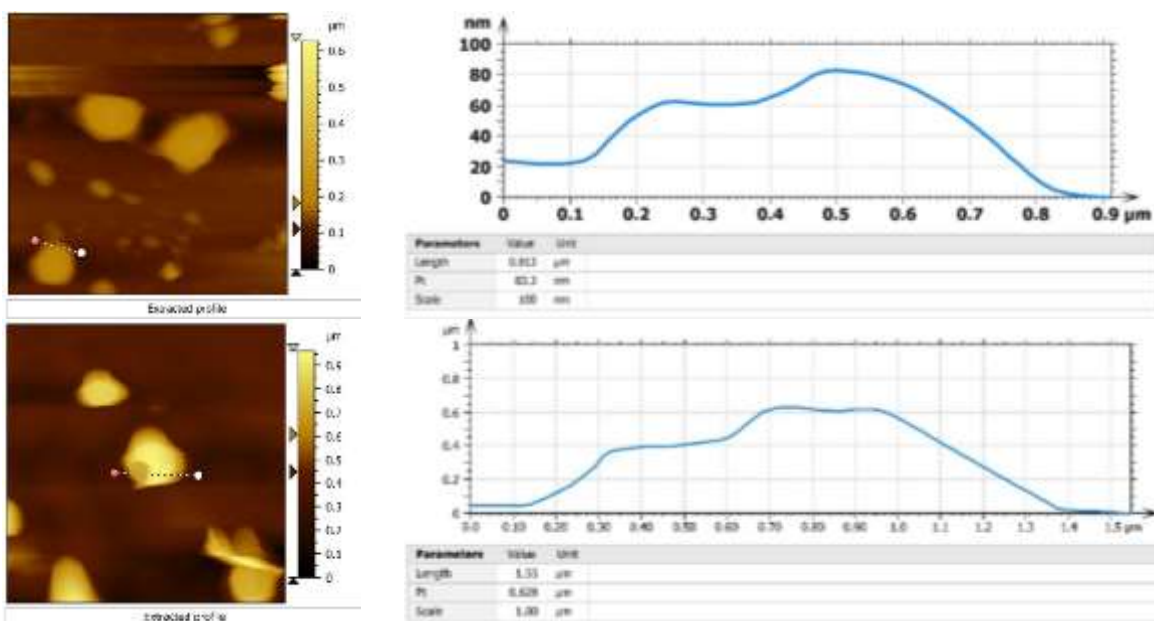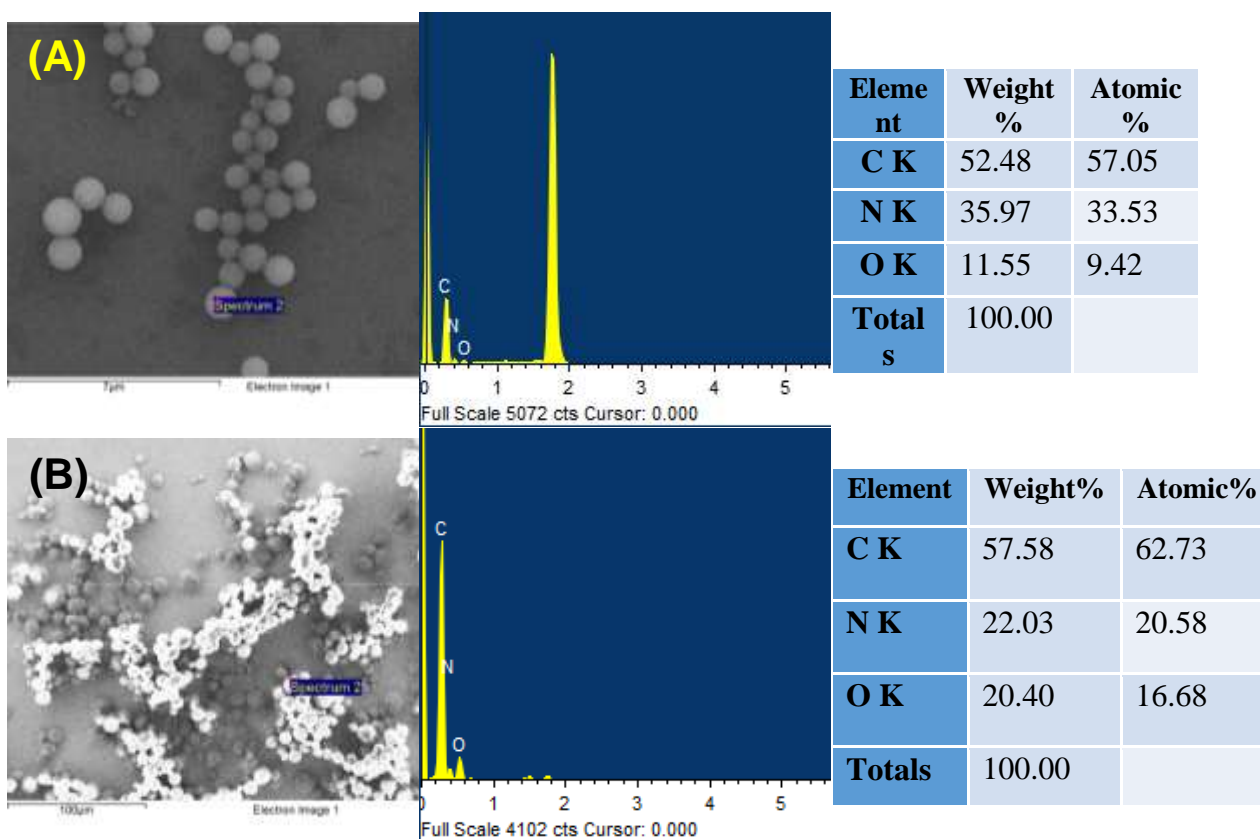


**Figure 4.16**: Height profiles diagrams of peptide **6a** [Boc-Phe-Phe-*tz-aeg*{$A^{N(Boc)2}$}-OEt] at different places of nanoparticles obtained from AFM.

The peptide **9** (Boc-Phe-Phe-*tz-aeg*-OEt) devoid of purine and pyrimidine nucleobase, self-organized to form large disk like particles (Figure 4.17) which was apparently different form morphology generated from rest of the protected and unprotected NP analogues. The elemental composition of the carbon (C), nitrogen (N) and oxygen (O) was further confirmed from the EDX spectroscopy (Figure 4.18).



**Figure 4.17**: SEM image of peptide **9** (Boc-Phe-Phe-*tz-aeg*-OEt).



| Element | Weight % | Atomic % |
|---|---|---|
| C K | 52.48 | 57.05 |
| N K | 35.97 | 33.53 |
| O K | 11.55 | 9.42 |
| Totals | 100.00 | |

| Element | Weight% | Atomic% |
|---|---|---|
| C K | 57.58 | 62.73 |
| N K | 22.03 | 20.58 |
| O K | 20.40 | 16.68 |
| Totals | 100.00 | |

**Figure 4.18**: EDX images of (A) peptide **6b** [Boc-Phe-Phe-*tz-aeg*(A$^{NHCbz}$)-OEt] and (B) peptide **6c** [Boc-Phe-Phe-*tz-aeg*(G$^{NHiBu}$)-OEt].

**4.4.5 Contact angle measurements**. The previous section clearly established that the hydrophobic substituents play a crucial role in forming an array of self-assembled structures. The extent of hydrophobicity of these nucleopeptides was qualitatively ascertained through contact angle (CA) measurements of water droplets on thin layers of peptides on silicon-wafers (Figure 4.19) and (Table 4.2). The measured CA values ranged from 70°-95° indicating their moderate to high hydrophobicity.[22,31] It was observed that G-containing nucleopeptides (**3c** and **6c**) had CA values above 90° indicating high hydrophobicity while T (**3d**, **6d**) and A-Cbz nucleopeptides (**3a**, **6b**), had CA values less than 80°, being less hydrophobic than G-analogues. The bis Boc-A nucleopeptide **6a** (CA = 88°) and 6-chloro-G nucleopeptide **3b** (CA = 84°) were moderately hydrophobic. As expected, peptide with free amine **7d** [H-Phe-Phe-*tz-aeg*(T)-OEt] was less hydrophobic with lower CA value (70°). However, in presence of free carboxylic group **8d** [Boc-Phe-Phe-*tz-aeg*(T)-OH] exhibited moderate hydrophobic nature (CA = 81°). The control peptide **9** (Boc-Phe-Phe-*tz-aeg*-OEt) for this study without nucleobase showed lower hydrophobicity with CA value of 71°. Corroboration between SEM images and contact angle measurements clearly indicates the role of hydrophobic substituents to produce ordered spherical nanoparticles.
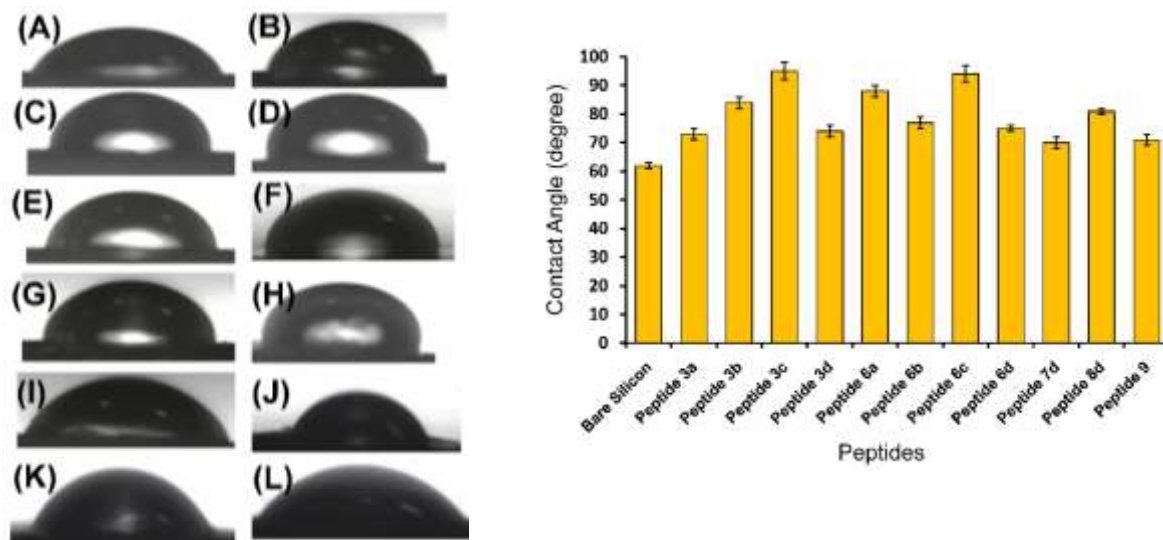


**Figure 4.19**: Images captured at 0.5 second for contact angle measurement of (A) bare silicon-wafer; silicon-wafer coated with nucleopeptide (B) **3a** [Boc-Phe-Phe-*am-aeg*(A$^{NHCbz}$)-OEt]; (C) **3b** [Boc-Phe-Phe-*am-aeg*(6-Cl-G$^{NHiBu}$)-OEt]; (D) **3c** [Boc-Phe-Phe-*am-aeg*(G$^{NHiBu}$)-OEt]; (E) **3d** [Boc-Phe-Phe-*am-aeg*(T)-OEt]; (F) **6a** [Boc-Phe-Phe-*tz-aeg*{A$^{N(Boc)2}$}-OEt]; (G) **6b** [Boc-Phe-Phe-*tz-aeg*(A$^{NHCbz}$)-OEt]; (H) **6c** [Boc-Phe-Phe-*tz-aeg*(G$^{NHiBu}$)-OEt]; (I) **6d** [Boc-Phe-Phe-*tz-aeg*(T)-OEt]; (J) **7d** [H- Phe-Phe-*tz-aeg*(T)-OEt]; (K) **8d** [Boc-Phe-Phe-*tz-aeg*(T)-OH] and (L) peptide **9** (Boc-Phe-Phe-*tz-aeg*-OEt).

**Table 4.2**: Contact angle (CA) measured for peptides on glass surface.

| Sample/Surface | CA (in degree) | ΔCA (in degree) |
|---|---|---|
| Bare silicon-wafer | 62 ± 1 | - |
| Peptide **3a** [Boc-Phe-Phe-*am-aeg*(A$^{NHCbz}$)-OEt] | 73 ± 2 | +11 |
| Peptide **3b** [Boc-Phe-Phe-*am-aeg*(6-Cl-G$^{NHiBu}$)-OEt] | 84 ± 2 | +22 |
| Peptide **3c** [Boc-Phe-Phe-*am-aeg*(G$^{NHiBu}$)-OEt] | 95 ± 3 | +33 |
| Peptide **3d** [Boc-Phe-Phe-*am-aeg*(T)-OEt] | 74 ± 2 | +12 |
| Peptide **6a** [Boc-Phe-Phe-*tz-aeg*{A$^{N(Boc)_2}$}-OEt] | 88 ± 2 | +16 |
| Peptide **6b** [Boc-Phe-Phe-*tz- aeg*(A$^{NHCbz}$)-OEt] | 77 ± 2 | +15 |
| Peptide **6c** [Boc-Phe-Phe-*tz-aeg*(G$^{NHiBu}$)-OEt] | 94 ± 3 | +32 |
| Peptide **6d** [Boc-Phe-Phe-*tz-aeg*(T)-OEt] | 75 ± 1 | +13 |
| Peptide **7d** [H-Phe-Phe-*tz-aeg*(T)-OEt] | 70 ± 2 | +8 |
| Peptide **8d** [Boc-Phe-Phe-*tz-aeg*(T)-OH] | 81 ± 1 | +19 |
| Peptide **9** (Boc-Phe-Phe-*tz-aeg*-OEt) | 71 ± 2 | +9 |

[a]Data are the mean ± SD (n=4)

**4.4.6 Effect of external stimuli on nucleopeptides**: Representative nucleopeptides with prominent and large self-assembled nanoparticles in this series were examined for their thermal stability and influence of external triggers like different pHs, and enzyme (proteinase K). The nanoparticles from triazole peptides **6a** [Boc-Phe-Phe-*tz-aeg*-{A$^{N(Boc)_2}$}-OEt] and **6b** [Boc-Phe-Phe-*tz-aeg*(A$^{NHCbz}$)-OEt] sustained their morphology beyond 100 °C. Thermal stability of peptides **3b**, **6b** and **6d** was confirmed by thermogravimetric analysis (TGA) which confirmed their stabilities up to 220 °C (Figure 4.20). However, under pH 2 and pH 10, the spherical assembly of **6a** was completely disrupted, perhaps due to deprotection of acid and base labile hydrophobic protecting groups. Both amide and triazole bridged nucleopeptides were proteolytically stable after incubation with proteinase K as monitored by HPLC trace, MALDI-TOF analysis (see experimental section) and SEM images (Figure 4.21). Thus, the nucleopeptides were found to be more stable than unmodified diphenylalanine (Phe-Phe) under similar proteolytic conditions.[6]
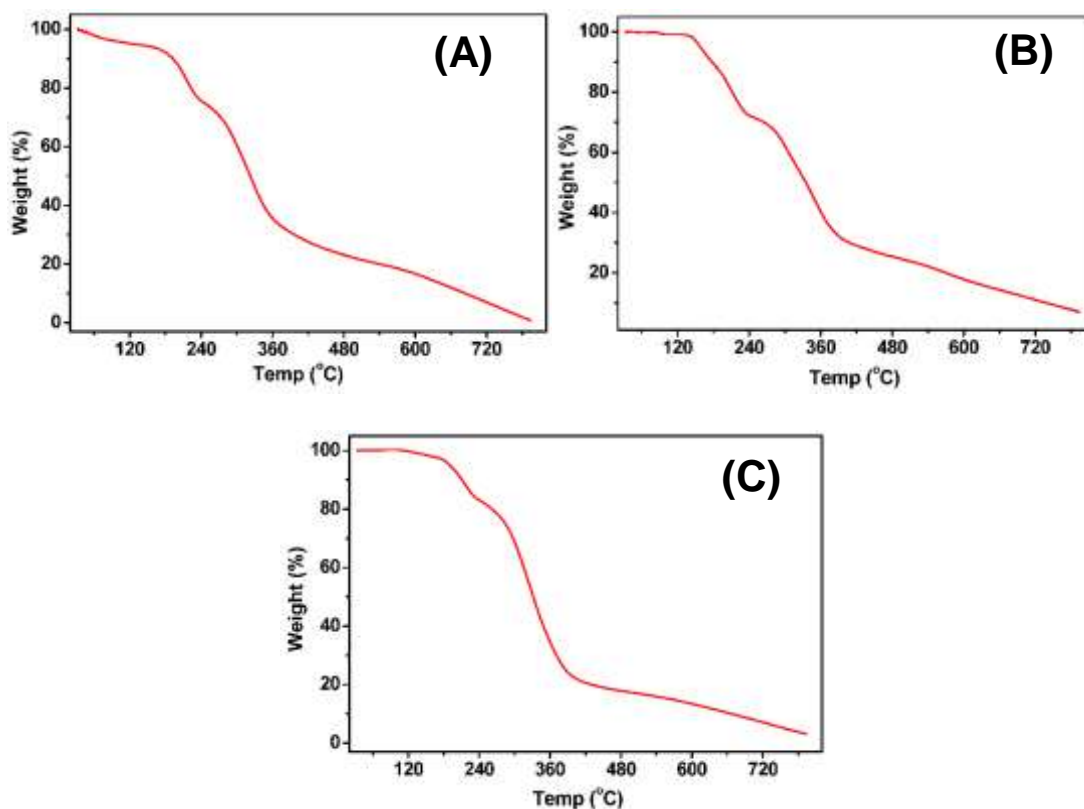
**Figure 4.20**: TGA of (A) peptide **3b** [Boc-Phe-Phe-*am-aeg*(6-Cl-G$^{NHiBu}$)-OEt]; (B) peptide **6b** [Boc-Phe-Phe-*tz-aeg*(A$^{NHCbz}$)-OEt] and (C) peptide **6d** [Boc-Phe-Phe-*tz-aeg*(T)-OEt].
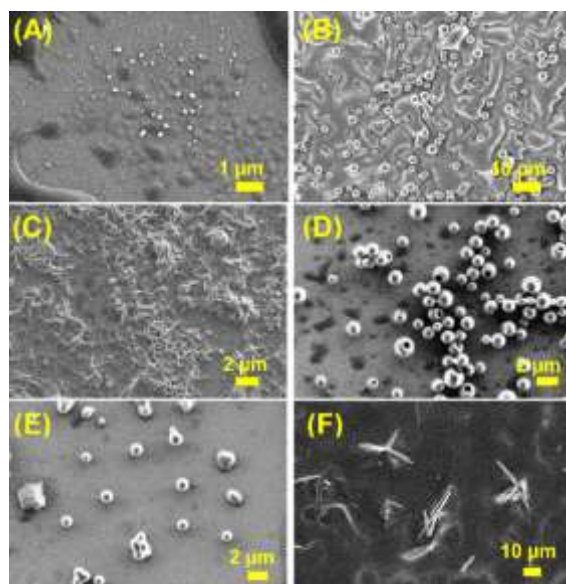


**Figure 4.21**: SEM images of **6a** [Boc-Phe-Phe-*tz-aeg*{A$^{N(Boc)2}$}-OEt] (A) at pH 2; (B) at pH 7; (C) at pH 10; (D) after heating at 100 ℃ for 4 hrs; (E) after incubation with proteinase K and (F) SEM image of proteinase K.

**4.4.7 Solvent dependent morphology of [Boc-Phe-Phe-*tz-aeg*{A$^{N(Boc)_2}$}-OEt] (6a)**: As of nucleopeptide morphology was found to depend on their hydrophobicity, their self assembly in different solvent conditions were investigated. The peptide **6a** [Boc-Phe-Phe-*tz-aeg*{A$^{N(Boc)_2}$}-OEt] was chosen owing to its discrete porous spherical nature seen microscopic technique FESEM images and its self-assembly was examined in pure THF, MeOH, CHCl₃, DCM and binary solvents *viz.*, HFIP:water, MeOH:water, CHCl₃:MeOH and THF:water in 1:1 ratio. It was noted that except for MeOH (Figure 4.22B), other pure solvents failed to produce spherical morphology (Figure 4.22A, C, D). However, in binary solvent combinations nucleopeptide **6a** assembled either into spherical particles (Figure 4.22E, F, H) or aggregated large bubble (Figure 4.22G). Notably, such solvent effect was observed for both the highest and lowest hydrophobic peptide **3c** [Boc-Phe-Phe-*am-aeg*(G$^{NHiBu}$)-OEt] and **7d** [H-Phe-Phe-*tz-aeg*(T)-OEt] respectively in this series. These observations suggested the crucial role of water as a non-solvent for the self-assembly process of nucleopeptide.
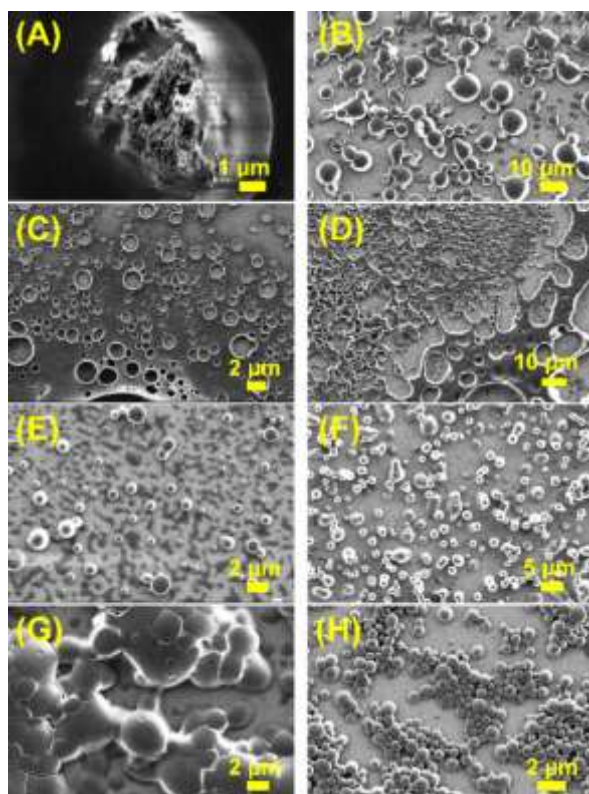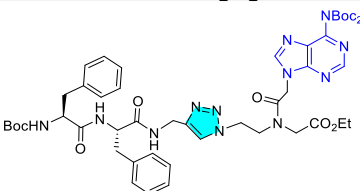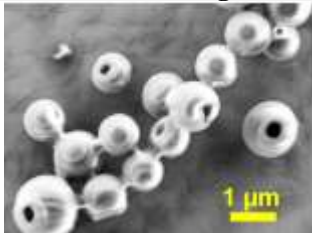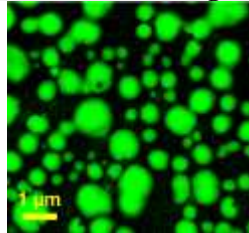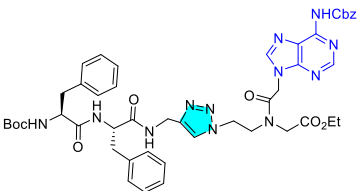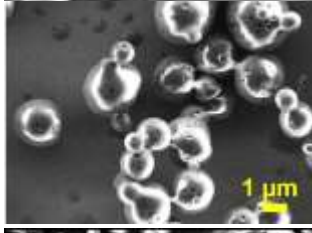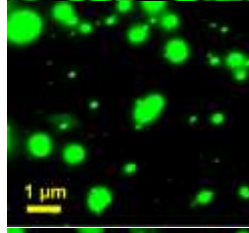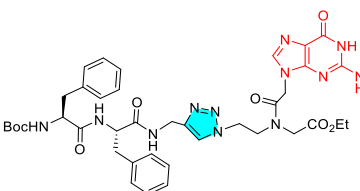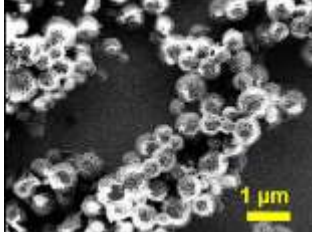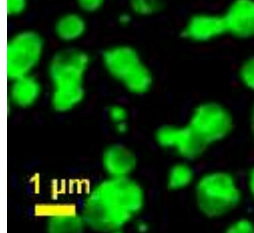


**Figure 4.22**: Solvent dependent morphology in SEM images of nucleopeptide **6a** [Boc-Phe-Phe-*tz-aeg*{A$^{N(Boc)_2}$}-OEt] in (A) THF; (B) MeOH; (C) CHCl₃; (D) DCM; (E) 1:1 HFIP and water; (F) 1:1 MeOH and water; (G) 1:1 CHCl₃ and MeOH; and (H) 1:1 THF and water.

**4.4.8. Encapsulation and release of dye and stimuli triggered disruption of nanospheres**: Triggered release[32] of dye and drugs encapsulated in biomaterial carriers under various stimulus are one of the potent requirements in pharmaceutical field. The hollow spheres of peptide nanoparticles of **6a** [Boc-Phe-Phe-*tz-aeg*{A$^{N(Boc)_2}$}-OEt] allows encapsulation of carboxyfluorescein (CF).[22,33,34] The confocal images for **6a** incubated with dye CF show that fluorescent molecules enter the cavity of spherical peptide nanoparticles (Figure 4.23A) and (Table 4.3). The slow release of encapsulated CF upon addition of dicationic dipeptide (Boc-Lys-Lys-OMe)[22] (Figure 4.23B) clearly indicated that the fluorescent small molecules were encapsulated inside the hollow nanoparticles and not simply adhered on the outer layer. The amount of CF release reached saturation after 30 hrs which was relatively sluggish compared to that seen with core-shell like nanoparticles.[22]

**Table 4.3**: Comparative microscopic morphology of trizolylated nucleopeptide nanoparticles.

| Nucleopeptide | SEM Image | Confocal Image |
|---|---|---|
|  **6a** [Boc-Phe-Phe-*tz-aeg*{A$^{N(Boc)2}$}-OEt] |  |  |
|  **6b** [Boc-Phe-Phe-*tz-aeg*(A$^{NHCbz}$)-OEt] |  |  |
|  **6c** [Boc-Phe-Phe-*tz-aeg*(G$^{NHiBu}$)-OEt] |  |  |

**6d** [Boc-Phe-Phe-*tz-aeg*(T)-OEt]
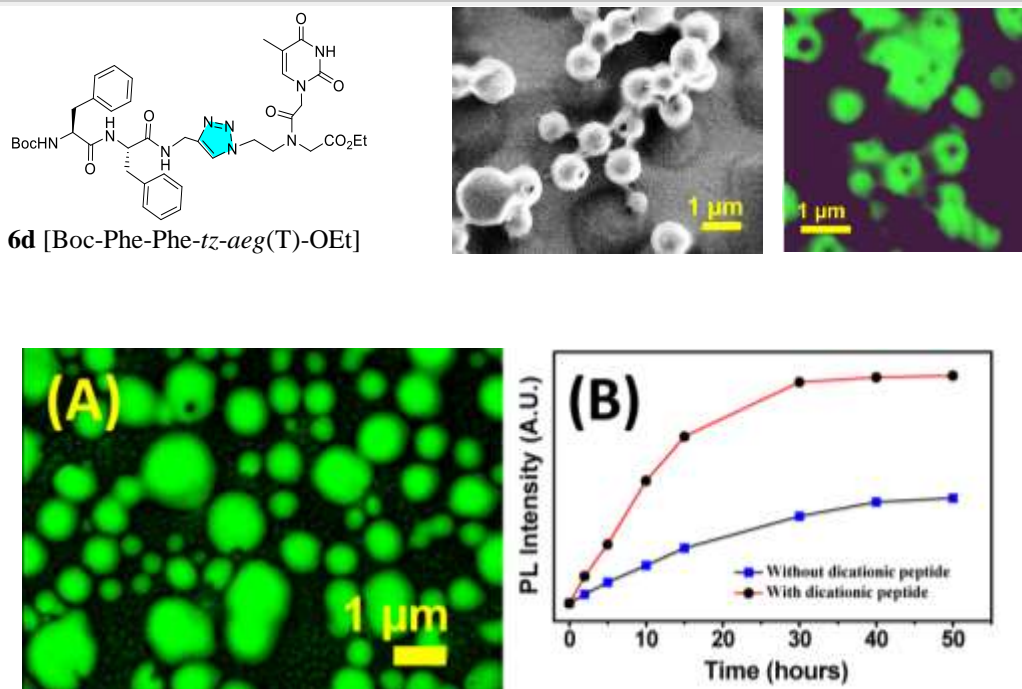


**Figure 4.23**: (A) Confocal microscope images of fluorescent dye encapsulated **6a** [Boc-Phe-Phe-*tz-aeg*{A$^{N(Boc)2}$}-OEt] and (B) Release of encapsulated CF with and without addition of dicationic peptide from peptide nanoparticles.

**4.4.9 Turbidity assay**: To study the aggregation of hydrophobic peptides in aqueous solvents, the turbidity assay[35] was performed following their absorbance at 405 nm (Figure 4.24). The results showed that A-peptides **3a** [Boc-Phe-Phe-*am-aeg*(A$^{NHCbz}$)-OEt], **6a** [Boc-Phe-Phe-*tz-aeg*{A$^{N(Boc)2}$}-OEt] and **6b** [Boc-Phe-Phe-*tz-aeg*(A$^{NHCbz}$)-OEt] have greater tendency to aggregate than other nucleopeptides with high absorbance values. Guanine-peptides (**3c**, **6c**) also showed aggregation while T-peptides **3d**, **6d** and 6-Cl-G$^{NHiBu}$ peptide **(3b)** were least prone towards aggregation. This is attributed to better H-bonding and π-π stacking abilities of purine nucleobases A and G than pyrimidine analogue T. The turbidity measured at 570 nm[35b] wavelength showed identical pattern of absorbance reflecting aggregation properties of Phe-Phe containing nucleopeptides. In addition, the high aggregation tendency of **6a** [Boc-Phe-Phe-*tz-aeg*{A$^{N(Boc)2}$}-OEt] and **6b** [Boc-Phe-Phe-*tz-aeg*(A$^{NHCbz}$)-OEt] was confirmed in DLS experiments from their increased polydispersive index (PDI) (from 0.03 to 0.34 and 0.07 to 0.57 for nucleopeptide **6a** and **6b** respectively) and visualized in AFM, SEM images recorded after 10 days of incubation of peptide solutions (Figure 4.25 and 4.26). Increment of average particle size for **6a** (0.45 to 1.8 µm) and **6b** (0.32 to 0.77 µm) was noticed after incubation.
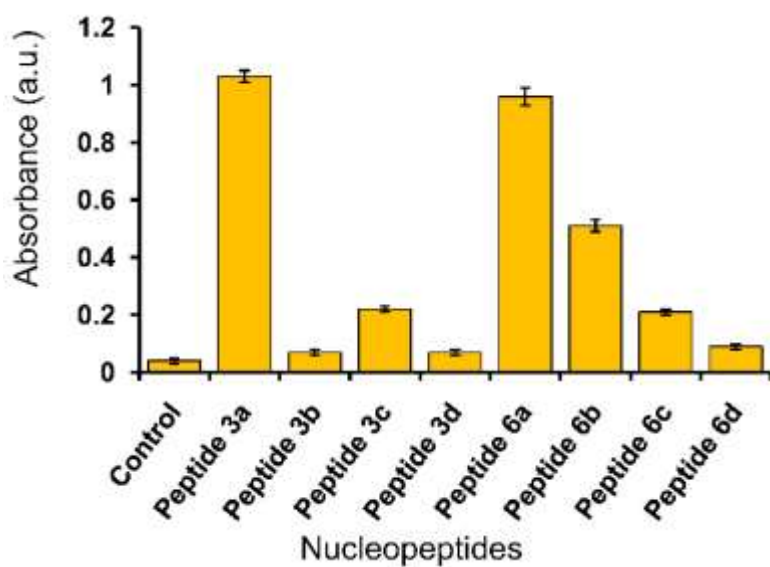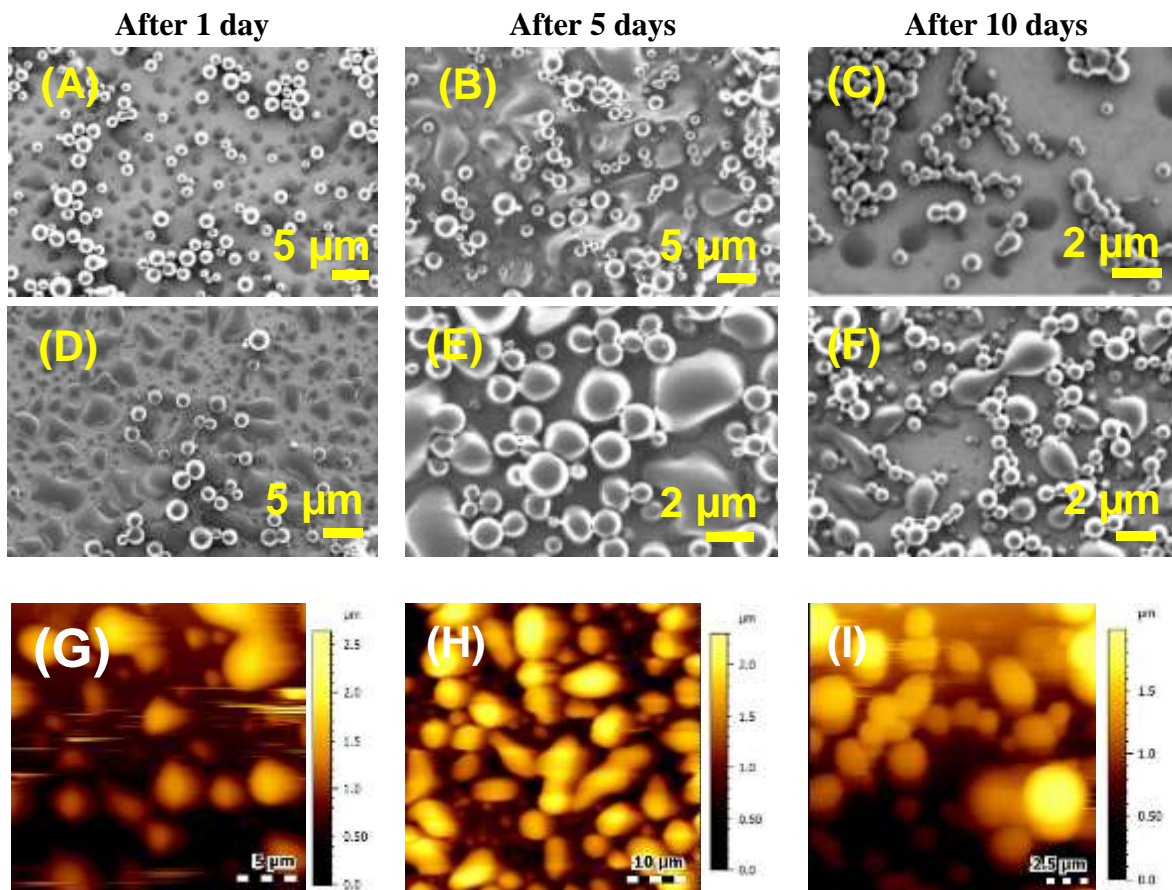
**Figure 4.24**: Absorbance values measured from turbidity assay of nucleopeptides at 405 nm.

| After 1 day | After 5 days | After 10 days |
|:---:|:---:|:---:|
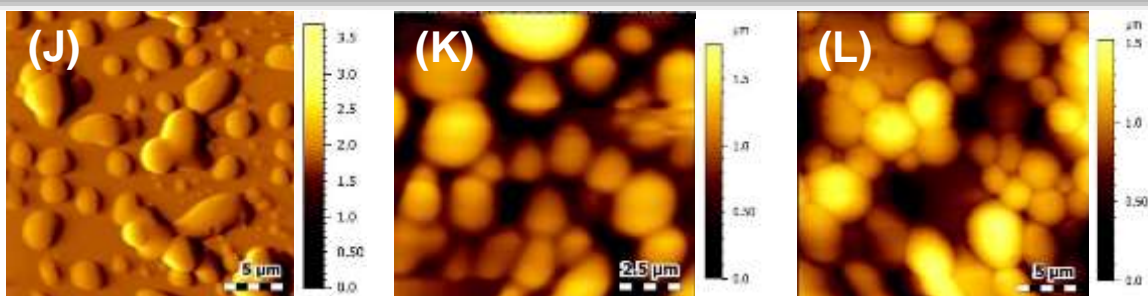
**Figure 4.25**: Time dependent morphologies observed through SEM for nucleopeptide **6a** [Boc-Phe-Phe-*tz-aeg*{A$^{N(Boc)2}$}-OEt] (Figures A-C); **6b** [Boc-Phe-Phe-*tz-aeg*(A$^{NHCbz}$)-OEt] (Figures D-F) and AFM for nucleopeptide.
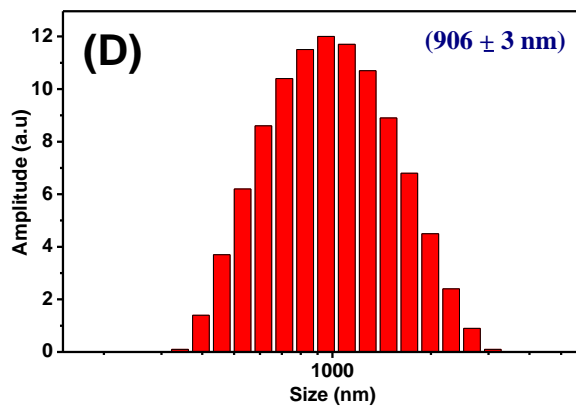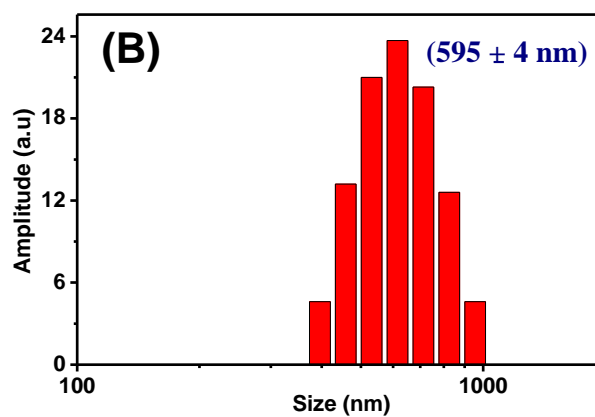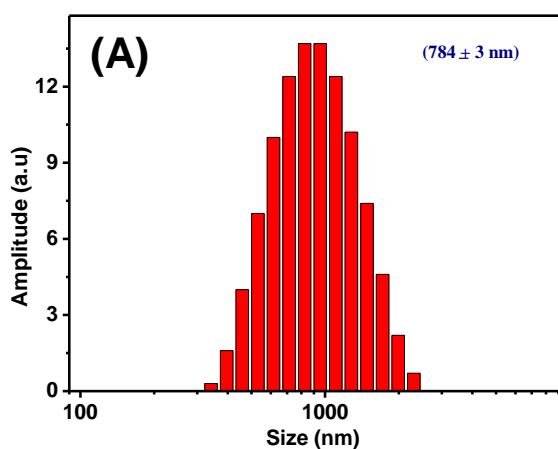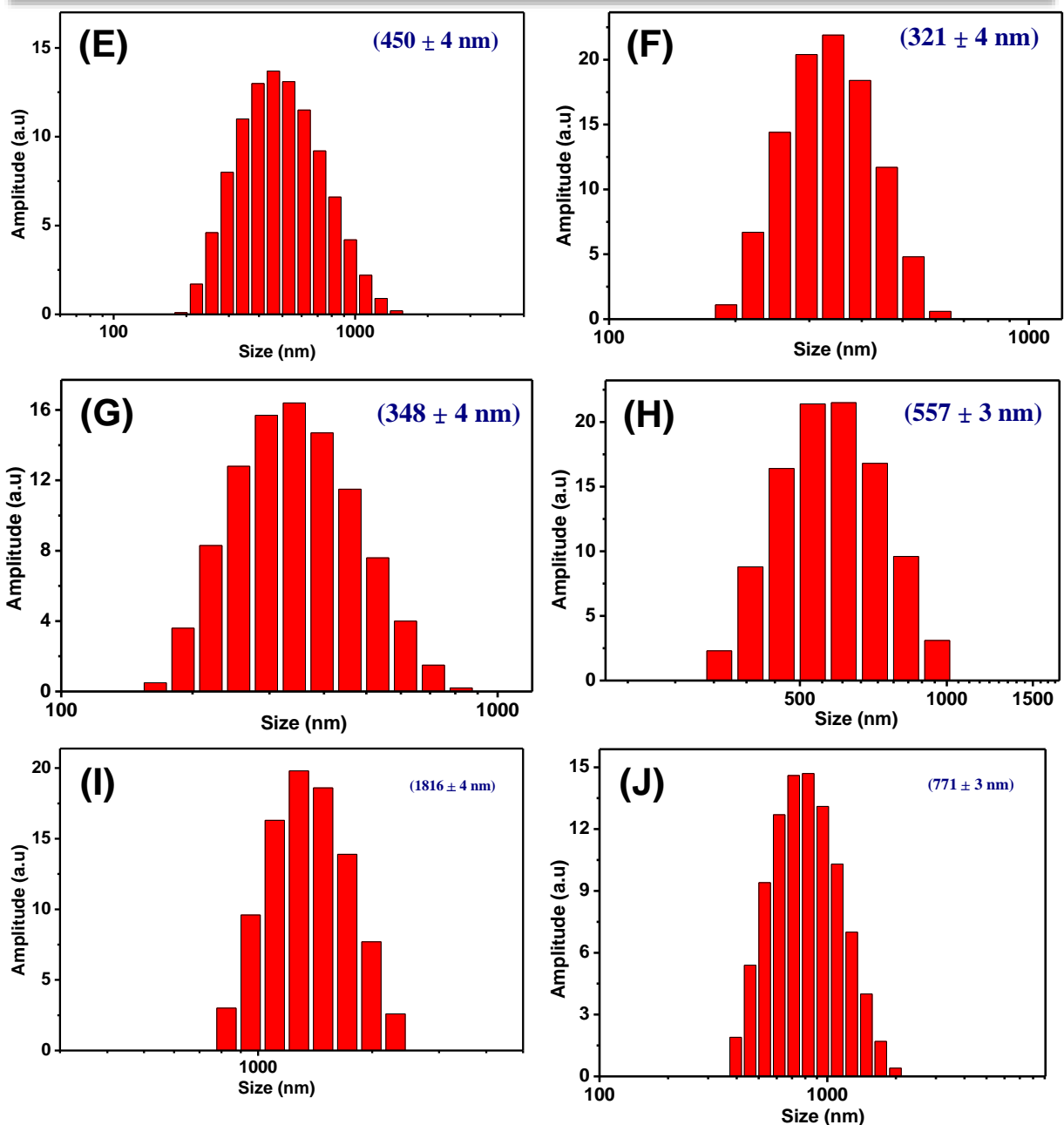
**Figure 4.26**: DLS spectra of fresh peptide solution of (A) **3a** [Boc-Phe-Phe-*am-aeg*(A^NHCbz)-OEt]; (B) **3b** [Boc-Phe-Phe-*am-aeg*(6-Cl-G^NHiBu)-OEt]; (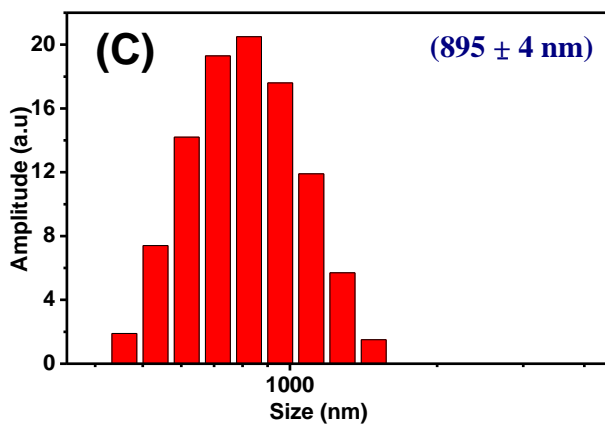C) **3c** [Boc-Phe-Phe-*am-aeg*(G^NHiBu)-OEt]; (D) **3d** [Boc-Phe-Phe-*am-aeg*(T)-OEt]; (E) **6a** [Boc-Phe-Phe-*tz-aeg*{A^N(Boc)2}-OEt] (PDI = 0.03); (F) **6b** [Boc-Phe-Phe-*tz-aeg*(A^NHCbz)-OEt] (PDI = 0.07); (G) **6c** [Boc-Phe-Phe-*tz-aeg*(G^NHiBu)-OEt]; (H) **6d** [Boc-Phe-Phe-*tz-aeg*(T)-OEt] and after 10 days incubation of (I) **6a** (PDI = 0.34), (J) **6b** (PDI = 0.57).

## 4.5 Summary

A new series of nucleopeptides (NPs) containing the dipeptide Phe-Phe conjugated to PNA unit corresponding to A/C/G/T via amide or triazole linker and possessing protected groups or deprotected were synthesized and their self-assembled morphologies were systematically studied by variety of techniques. Self-assembly of these conjugates are influenced by both Phe-Phe and PNA components. The favourable self assembly of completely N/C-protected Phe-Phe-PNA conjugates resulted in well defined solid and porous nanospheres. The completely deprotected nucleopeptides without C-/N-termini capping and free nucleobases which are less hydrophobic did not show good self-assembled morphologies. Partial removal of capping groups also lead to poorly organized agglomerated structures. These results established the importance of hydrophobic substituents on nucleobases and C-/ N-termini of nucleopeptide for self-assembled structures and the necessicity of a good hydrophobic/hydrophilic balance for efficient self assembly of peptides. The extent of hydrophobicity was assessed qualitatively by contact angle measurement. An equal mixture of nucleopeptides with complementary base pairs elicited better nanoarchitectures among completely deprotected analouges. Effects of linkers (triazole/amide) in protected nucleopeptides were evident from self-assembled morphologies albeit the reason is not clearly understood. Effect of mixed solvents incorporating hydrophobic components was also crucial for observing regular morphologies from these peptides. Adenine containing nucleopeptides were more prone for self-aggregation as indicated by the turbidity and DLS measurements. The hydrophobic nucleopeptides **6a** was found stable under wide range of pH, high temperature and proteolytic enzymes which showed ability of these NPs to behave as stable biocompatible templates. Noncovalent encapsulation of CF inside the porous nanospheres was evident from the confocal images. Slow release of dye from peptide nanoparticle upon treatment of dicationic dipeptide as an external stimulus (Figure 4.27).
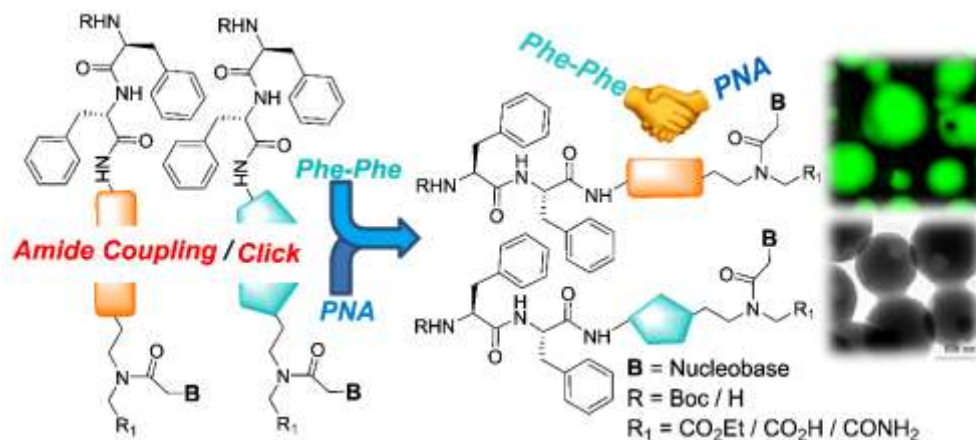
**Figure 4.27**: Hybrid-peptides containing diphenylalanine and nucleobase were studied to understand the effects of C-terminus substituents, hydrophobicity and H-bonding groups on the self-assembly. The results indicated the ability of this new class of peptides to change nanostructures rationally, balancing hydrophobic / hydrophilic nature.

## 4.6 Experimental section

**4.6.1 Materials and methods**: See the experimental section **(2.5.1)** of chapter **2**.

**4.6.2 Synthesis of Nucleopeptides on Solid Phase**: Boc-PNA monomers, Boc-Gly-OH and Boc-Phe-Phe-OH were incorporated into peptide sequence by solid phase synthesis on MBHA resin having 0.7 mmol/g loading value. After swelling of resin beads in DCM for overnight these were washed with 15% DIPEA in DCM (3 x 10 min) to generate free amines from the commercially available salt form. Free amine groups were then coupled with carboxylic acid of PNA monomers first in dry DMF (0.5 mL) using HOBt (3 equiv.), HBTU (3 equiv.), and DIPEA (3 equiv.). The reagents were removed by filtration and washed with DMF (3 x 10 mL) and DCM (3 x 10 mL). Deprotection of Boc group from the N-terminus of the resin bound PNA monomers with 50% TFA in DCM (3 x 15 min) was followed by washing with DCM and DMF (3 x 10 mL) to give a TFA salt of amine which was neutralized using 10% DIPEA in DCM (3 x 10 min) to generate free amine. After washing with DCM and DMF (3 x 10 mL), the free amine was coupled with carboxylic acid of incoming monomers (Boc-Gly-OH and Boc-Phe-Phe-OH) in dry DMF (0.5 mL) under aforementioned amide coupling condition. Protocol for washing and regeneration of free amine was repeated to afford the desired peptides. The resin bound peptides were cleaved from solid support by TFA and trifluoromethanesulfonic acid (TFMSA).

**4.6.3 Purification of Nucleopeptides by Reverse-Phase HPLC**: For the purification of nucleopeptides, a semi-preparative BEH130 $C_{18}$ (10 x 250 mm) column was used. Purification of PNA oligomers was performed with the gradient elution method: A to 100 % B in 33 min; A = 0.1% TFA in $CH_3CN$ / $H_2O$ (5:95); B = 0.1 % TFA in $CH_3CN$ / $H_2O$ (1:1) with a flow rate of 2 mL / min. Oligomers were monitored at 220 and 260 nm wavelengths during purification.

**4.6.4 Synthesis of Nucleopeptides in Solution Phase**

**[Boc-Phe-Phe-*am-aeg*($A^{NHCbz}$)-OEt] (3a)**: To a mixture of compound **1** (1.0 g, 2.4 mmol) in dry DMF (10 mL), EDC.HCl (0.5 g, 2.4 mmol) and HOBT (0.2 g, 1.2 mmol) were added at 0 $^o$C. To the reaction mixture, DIPEA (0.9 mL, 4.9 mmol) was added. After 0.3 hr, TFA salt of **2a** (1.4 g, 2.4 mmol) dissolved in dry DMF (5 mL), was added slowly into the reaction mixture and stirred at room temperature (rt) under inert atmosphere. After 12 hrs brine solution (40 mL) was added into it and aq. layer was washed with ethyl acetate (EtOAc) (3 x 25 mL). Organic layer was washed with satd. $NaHCO_3$, 10% citric acid and brine solutions (2 x 50 mL). The organic layer was separated, dried over anhyd $Na_2SO_4$, filtered and the filtrate was concentrated under reduced pressure. The crude mass thus obtained, was purified by column chromatography [Eluent: 50-80% of EtOAc in pet ether] to afford peptide **3a** (1.4 g, 70% with respect to **1**). White hygroscopic solid; $^1$H NMR (400 MHz, $CDCl_3$, 25 °C, TMS): $\delta$ = 8.94 (s, 1H), 8.22 (d, $J$ = 10.7 Hz, 1H), 7.41 – 7.08 (m, 20H), 7.06 – 6.84 (m, 3H), 6.66 – 6.23 (m, 2H), 5.09 (ddd, $J$ = 26.8, 11.3, 5.8 Hz, 4H), 4.99 – 4.86 (m, 1H), 4.63 – 4.52 (m, 1H), 4.37 – 3.87 (m, 7H), 3.56 – 3.20 (m, 4H), 3.13 – 2.73 (m, 5H), 1.31 – 1.19 ppm (m, 12H); $^{13}$C NMR (100 MHz, $CDCl_3$, 25 °C, TMS): $\delta$ = 171.6, 171.3, 171.1, 170.8, 170.1, 169.4, 169.1, 160.0, 159.5, 156.0, 155.6, 154.6, 154.4, 153.6, 151.2, 136.0, 135.5, 129.3, 129.3, 129.2, 128.8, 128.6, 128.6, 128.5, 128.5, 128.4, 128.0, 127.1, 114.1, 80.9, 80.7, 67.9, 67.5, 62.1, 61.7, 60.5, 56.3, 55.8, 54.2, 49.7, 48.7, 47.8, 47.5, 42.7, 37.4, 37.3, 37.2, 37.1, 37.1, 33.9, 32.0, 29.7, 28.2, 28.1, 14.2, 14.1 ppm. HRMS (ESI$^+$), m/z calculated for (M+H)$^+$ $C_{44}H_{52}N_9O_9$: 850.3888, found: 850.3899.

**[Boc-Phe-Phe-*am-aeg*(6-Cl-$G^{NHiBu}$)-OEt] (3b)**: Compound **1** (0.5 g, 1.2 mmol) was coupled with the TFA salt of **2b** (0.6 g, 1.2 mmol) following the method described for peptide **3a** to afford peptide **3b** (0.7 g, 70% with respect to **1**) which was purified by column chromatography [Eluent: 60-80% of EtOAc in pet ether]. Yellowish white solid; m.p. 110-113 °C; $^1$H NMR

(400 MHz, CDCl$_3$, 25 °C, TMS): $\delta$ = 12.36 (s, 1H), 10.64 (s, *J* = 23.8 Hz, 1H), 7.94 (s, 1H), 7.65 (s, *J* = 8.5 Hz, 1H), 7.55 (s, 1H), 7.28 – 7.03 (m, 10H), 5.95 (s, 1H), 5.04 – 4.81 (m, 2H), 4.30 – 4.17 (m, 2H), 4.16 – 4.08 (m, 2H), 4.00 (d, *J* = 17.4 Hz, 1H), 3.82 (d, *J* = 7.6 Hz, 1H), 3.53 – 3.42 (m, 1H), 3.21 (dd, *J* = 13.8, 4.5 Hz, 1H), 3.12 – 2.84 (m, 3H), 2.69 – 2.52 (m, 1H), 2.19 (d, *J* = 29.8 Hz, 2H), 1.26 – 1.15 ppm (m, 18H); $^{13}$C NMR (100 MHz, CDCl$_3$, 25 °C, TMS): $\delta$ = 180.2, 172.6, 172.2, 169.4, 166.8, 156.3, 156.2, 149.4, 148.5, 140.4, 137.0, 136.7, 129.5, 129.3, 128.8, 128.7, 128.5, 127.1, 126.9, 120.2, 114.19, 80.3, 61.7, 56.9, 54.4, 47.8, 47.3, 44.2, 37.9, 37.5, 37.1, 35.9, 33.9, 32.0, 29.8, 29.8, 29.7, 22.8, 19.4, 19.0, 14.3, 14.2 ppm. HRMS (ESI$^+$), m/z calculated for (M+H)$^+$ C$_{40}$H$_{51}$ClN$_9$O$_8$: 820.3549, found: 820.3539.

**[Boc-Phe-Phe-*am-aeg*(G$^{NHiBu}$)-OEt] (3c)**: Compound **1** (0.4 g, 1.0 mmol) was coupled with the TFA salt of **2c** (0.5 g, 1.0 mmol) following the method described for peptide **3a** to obtain peptide **3c** (0.5 g, 60% with respect to **1**) which was purified by column chromatography [Eluent: 0-3% of MeOH in DCM]. White solid; m.p. 105-108 °C; $^1$H NMR (400 MHz, DMSO-d$_6$, 25 °C): $\delta$ = 12.07 (s, 1H), 11.57 (s, 1H), 8.17 (t, *J* = 12.7 Hz, 1H), 7.89 (s, 0.6H), 7.85 (s, 0.4H), 7.32 – 7.02 (m, 12H), 6.89 (d, *J* = 8.5 Hz, 1H), 5.18 – 4.89 (m, 2H), 4.64 – 4.51 (m, 1H), 4.40 (s, 1H), 4.22 (q, *J* = 7.0 Hz, 1H), 4.10 (dt, *J* = 14.1, 6.1 Hz, 2H), 3.45 (dd, *J* = 24.8, 18.2 Hz, 2H), 3.26 – 3.13 (m, 1H), 3.06 – 2.62 (m, 6H), 1.30 – 1.20 (m, 9H), 1.19 – 1.13 (m, 3H), 1.11 ppm (dd, *J* = 6.8, 3.6 Hz, 6H); $^{13}$C NMR (100 MHz, DMSO-d$_6$, 25 °C): $\delta$ = 180.1, 171.7, 169.1, 167.0, 166.6, 154.9, 149.1, 147.9, 140.8, 138.0, 137.5, 129.2, 129.1, 128.1, 127.9, 126.3, 126.1, 119.5, 78.2, 61.3, 60.6, 55.8, 54.1, 47.7, 46.7, 44.0, 37.6, 37.5, 37.2, 34.7, 33.2, 31.5, 29.4, 29.0, 28.1, 27.7, 18.9, 14.0 ppm. HRMS (ESI$^+$), m/z calculated for (M+H)$^+$ C$_{40}$H$_{52}$N$_9$O$_9$: 802.3888, found: 802.3889.

**[Boc-Phe-Phe-*am-aeg*(T)-OEt] (3d)**: Compound **1** (0.2 g, 0.5 mmol) was coupled with TFA salt of **2d** (0.2 g, 0.5 mmol) following the procedure described for peptide **3a** to afford peptide **3b** (0.3 g, 80% with respect to **1**) which was purified by column chromatography [Eluent: 3-6% of MeOH in DCM]. White solid; m.p. 92-95 °C; $^1$H NMR (400 MHz, CDCl$_3$, 25 °C, TMS): $\delta$ = 10.03 (s, 1H), 7.77 (d, *J* = 9.2 Hz, 1H), 7.34 – 6.97 (m, 11H), 6.49 (s, 1H), 5.42 – 5.14 (m, 1H), 4.86 – 4.61 (m, 2H), 4.36 – 4.18 (m, 1H), 4.16 – 3.91 (m, 4H), 3.77 (t, *J* = 21.3 Hz, 1H), 3.69 – 3.41 (m, 1H), 3.37 – 3.13 (m, 2H), 3.09 – 2.99 (m, 1H), 2.93 – 2.73 (m, 3H), 1.90 (d, *J* = 12.0 Hz, 3H), 1.44 – 1.26 (m, 9H), 1.23 – 1.13 (m, 3H); $^{13}$C NMR (100 MHz, CDCl$_3$, 25 °C, TMS): $\delta$ = 172.4, 172.0,

171.0, 169.3, 167.1, 164.3, 155.6, 151.2, 140.9, 137.1, 136.6, 130.0, 129.7, 129.5, 129.3, 128.6, 128.3, 128.2, 126.4, 126.2, 110.9, 80.6, 61.7, 55.3, 53.5, 48.6, 48.3, 47.3, 38.2, 36.9, 36.6, 28.3, 14.0, 12.4 ppm. HRMS (ESI$^+$), m/z calculated for (M+H)$^+$ C$_{36}$H$_{47}$N$_6$O$_9$: 707.3404, found: 707.3395.

**[Boc-Phe-Phe-*tz-aeg*{A$^{N(Boc)2}$}-OEt] (6a)**: To a mixture of peptide **4** (0.3 g, 0.6 mmol) in tetrahydrofuran (THF) (5.0 mL) and 10 mL distilled water, CuSO$_4$.5H$_2$O (7 mg, 0.03 mmol) and sodium-*L*-(+)-ascorbate (0.1 g, 0.3 mmol) were added and stirred. To the resulting suspension, azide **5a** (0.3 g, 0.6 mmol) dissolved in THF (5.0 mL) was added and stirred at room temperature. After 12 hrs, EtOAc (20 mL) was added into it and aq. layer was further washed with EtOAc (3 x 20 mL). Organic layer was separated, dried over anhyd. Na$_2$SO$_4$, filtered and the filtrate was concentrated under reduced pressure. The crude mass thus obtained, was purified by column chromatography [Eluent: 0-3% of MeOH in DCM] to afford peptide **6a** (0.4 g, 80% with respect to **4**). White hygroscopic solid; $^1$H NMR (400 MHz, CDCl$_3$, 25 °C, TMS): $\delta$ = 8.80 (t, $J$ = 5.5 Hz, 1H), 8.28 (d, $J$ = 2.3 Hz, 1H), 7.90 – 7.77 (m, 1H), 7.49 (d, $J$ = 14.2 Hz, 1H), 7.36 – 7.03 (m, 10H), 6.96 (d, $J$ = 21.6 Hz, 2H), 6.40 (d, $J$ = 24.3 Hz, 1H), 5.31 – 4.88 (m, 2H), 4.68 (d, $J$ = 25.0 Hz, 3H), 4.54 – 4.41 (m, 2H), 4.27 – 4.16 (m, 3H), 4.08 (dd, $J$ = 14.9, 11.7 Hz, 2H), 3.96 – 3.74 (m, 2H), 3.16 (s, 1H), 3.05 – 2.74 (m, 3H), 1.42 (dd, $J$ = 13.0, 1.9 Hz, 18H), 1.33 – 1.23 ppm (m, 12H); $^{13}$C NMR (100 MHz, CDCl$_3$, 25 °C, TMS): $\delta$ = 171.9, 171.6, 171.1, 170.9, 169.0, 168.8, 167.2, 156.1, 153.7, 152.2, 150.5, 146.2, 136.0, 129.3, 129.2, 129.0, 128.9, 128.9, 128.4, 127.3, 123.8, 83.9, 83.9, 83.9, 81.3, 80.9, 62.4, 61.9, 56.7, 54.0, 50.6, 49.7, 47.9, 47.8, 44.2, 37.6, 37.1, 35.5, 35.4, 28.2, 28.0, 14.2 ppm. HRMS (ESI$^+$), m/z calculated for (M+H)$^+$ C$_{49}$H$_{65}$N$_{12}$O$_{11}$: 997.4896, found: 997.4894.

**[Boc-Phe-Phe-*tz- aeg*(A$^{NHCbz}$)-OEt] (6b)**: Boc-Phe-Phe-Propyne **4** (0.3 g, 0.6 mmol) was clicked with azide **5b** (0.3 g, 0.6 mmol) following the procedure described for peptide **6a** to afford peptide **6b** (0.4 g, 75% with respect to **4**) which was purified by column chromatography [Eluent: 0-3% of MeOH in DCM]. White hygroscopic solid; $^1$H NMR (400 MHz, CDCl$_3$, 25 °C, TMS): $\delta$ = 8.83 – 8.61 (m, 2H), 8.09 (d, $J$ = 5.3 Hz, 0.7H), 7.83 (s, 0.3H), 7.52 – 7.31 (m, 5H), 7.27 – 7.05 (m, 8H), 7.03 – 6.88 (m, 2H), 6.60 (dd, $J$ = 23.7, 6.9 Hz, 1H), 5.37 – 5.20 (m, 2H), 5.05 (dt, $J$ = 32.8, 16.5 Hz, 2H), 4.73 – 4.60 (m, 2H), 4.58 – 4.32 (m, 3H), 4.26 – 4.11 (m, 3H), 4.03 (d, $J$ = 23.8 Hz,

2H), 3.94 – 3.70 (m, 2H), 3.16 – 2.76 (m, 4H), 1.34 – 1.19 ppm (m, 12H); $^{13}$C NMR (100 MHz, CDCl$_3$, 25 °C, TMS): $\delta$ = 172.0, 171.7, 171.1, 170.9, 169.0, 168.8, 167.3, 156.0, 152.9, 151.7, 151.2, 149.5, 145.7, 144.2, 138.0, 136.2, 135.6, 129.2, 129.2, 129.1, 128.9, 128.8, 128.8, 128.7, 128.7, 128.6, 128.3, 127.2, 127.2, 125.4, 124.3, 123.7, 121.4, 81.1, 80.9, 80.7, 67.8, 62.4, 61.9, 56.5, 54.1, 50.5, 49.4, 48.4, 47.7, 44.1, 43.1, 37.7, 37.2, 35.3, 28.2, 14.2 ppm. HRMS (ESI$^+$), m/z calculated for (M+H)$^+$ C$_{47}$H$_{55}$N$_{12}$O$_9$: 931.4215, found: 931.4214.

**[Boc-Phe-Phe-*tz-aeg*(G$^{NHiBu}$)-OEt] (6c)**: Alkyne **4** (0.3 g, 0.6 mmol) was reacted with azide **5c** (0.3 g, 0.6 mmol) following the procedure described for peptide **6a** to afford peptide **6c** (0.4 g, 70% with respect to **4**) which was purified by column chromatography [Eluent: 0-10% of MeOH in CHCl$_3$]. White solid; m.p. 100-103 °C; $^1$H NMR (400 MHz, DMSO-d$_6$, 25 °C): $\delta$ = 12.09 (d, *J* = 10.9 Hz, 1H), 11.64 (d, *J* = 14.1 Hz, 1H), 8.62 – 8.47 (m, 1H), 8.38 – 8.33 (m, 0.3H), 8.04 – 7.98 (m, 0.7H), 7.96 (s, 0.5H), 7.83 (s, 0.5H), 7.74 (d, *J* = 10.1 Hz, 1H), 7.30 – 7.05 (m, 11H), 6.93 – 6.87 (m, 0.7H), 6.71 (t, *J* = 9.2 Hz, 0.3H), 5.00 (s, 1H), 4.94 (s, 1H), 4.70 (s, 1H), 4.60 – 4.50 (m, 1H), 4.48 – 4.26 (m, 4H), 4.18 (dt, *J* = 16.3, 8.1 Hz, 1H), 4.13 – 4.02 (m, 3H), 3.97 (s, 1H), 3.73 (t, *J* = 6.1 Hz, 1H), 2.99 (d, *J* = 13.8 Hz, 1H), 2.89 – 2.72 (m, 3H), 2.62 (d, *J* = 11.8 Hz, 1H), 1.26 (t, *J* = 4.4 Hz, 9H), 1.16 (t, *J* = 7.1 Hz, 3H), 1.11 ppm (d, *J* = 6.8 Hz, 6H); $^{13}$C NMR (100 MHz, DMSO-d$_6$, 25 °C): $\delta$ = 180.2, 180.1, 171.4, 170.9, 170.8, 169.4, 168.9, 167.4, 166.8, 155.1, 154.9, 149.3, 149.2, 147.9, 145.0, 144.6, 140.5, 140.4, 138.0, 137.7, 137.5, 129.3, 129.2, 129.1, 128.0, 128.0, 127.9, 126.3, 126.1, 123.7, 123.2, 119.6, 79.2, 78.2, 61.4, 60.7, 55.9, 53.7, 49.1, 47.9, 47.6, 47.4, 46.6, 44.1, 43.7, 37.8, 37.5, 34.7, 34.3, 28.1, 18.9, 14.0 ppm. HRMS (ESI$^+$), m/z calculated for (M+Na)$^+$ C$_{43}$H$_{54}$N$_{12}$O$_9$Na: 905.4034, found: 905.4028.

**[Boc-Phe-Phe-*tz-aeg*(T)-OEt] (6d)**: Alkyne **4** (0.3 g, 0.6 mmol) was clicked with azide **5d**[36] (0.2 g, 0.6 mmol) following the procedure described for peptide **6a** to afford peptide **6d** (0.4 g, 90% with respect to **4**) which was purified by column chromatography [Eluent: 0-6% of MeOH in CHCl$_3$]. White solid; m.p. 132-135 °C; $^1$H NMR (400 MHz, CDCl$_3$ + DMSO-d$_6$, 2:1, 25 °C, TMS): $\delta$ = 10.82 (s, 0.5H), 10.72 (s, 0.5H), 7.85 (s, 1H), 7.66 (d, *J* = 8.4 Hz, 1H), 7.63 (dd, *J* = 20.9, 8.1 Hz, 0.5H), 7.61 (d, *J* = 7.7 Hz, 0.5H), 7.28 – 7.10 (m, 10H), 7.06 (d, *J* = 1.2 Hz, 0.5H), 6.94 (d, *J* = 1.2 Hz, 0.5H), 6.00 (d, *J* = 7.3 Hz, 0.4H), 5.85 (d, *J* = 7.8 Hz, 0.6H), 4.77 – 4.68 (m, 1H), 4.62 (d, *J* = 5.2 Hz, 1H), 4.55 – 4.42 (m, 1H), 4.40 – 4.24 (m, 3H), 4.23 – 4.15 (m, 2H), 4.10 (s, 1H),

3.92 (d, $J$ = 20.2 Hz, 3H), 3.62 (d, $J$ = 19.0 Hz, 1H), 3.17 – 3.07 (m, 1H), 3.04 – 2.96 (m, 3H), 1.91 (d, $J$ = 0.7 Hz, 1.5H), 1.86 (d, $J$ = 0.7 Hz, 1.5H), 1.34 (d, $J$ = 11.7 Hz, 9H), 1.26 ppm (dt, $J$ = 14.0, 5.7 Hz, 3H); $^{13}$C NMR (100 MHz, CDCl$_3$ + DMSO-d$_6$, 2:1, 25 °C, TMS): $\delta$ = 171.6, 171.3, 170.8, 170.6, 168.7, 168.4, 167.6, 167.1, 164.3, 164.2, 155.3, 155.2, 151.2, 150.9, 140.6, 140.4, 136.8, 136.6, 128.9, 128.8, 127.9, 126.2, 124.0, 123.0, 110.2, 79.5, 61.6, 61.1, 55.8, 55.4, 53.6, 49.6, 48.9, 48.8, 48.3, 47.9, 47.7, 46.8, 39.6, 37.7, 37.6, 37.0, 36.8, 35.0, 34.7, 27.9, 13.7, 11.9 ppm. HRMS (ESI$^+$), m/z calculated for (M+H)$^+$ C$_{39}$H$_{50}$N$_9$O$_7$: 788.3731, found: 788.3722.

**[H-Phe-Phe-*tz-aeg*(G$^{\text{NHiBu}}$)-OEt] (7c)**: To a of ice-cold mixture of peptide **6c** (0.2 g, 0.2 mmol) in DCM (2 mL), TFA (2 mL) was added slowly and stirred for 4 hrs at rt. Completion of reaction was monitored by TLC. The volatile portion of the reaction mixture was completely removed by co-evaporation with toluene and carbontetrachloride. The residue was washed with CHCl$_3$ first and then triturated well with chilled Et$_2$O to obtain peptide **7c** (0.2 g, 85%) as a yellowish white hygroscopic solid. $^1$H NMR (400 MHz, DMSO-d$_6$, 25 °C): $\delta$ = 12.18 – 11.99 (m, 1H), 11.71 – 11.54 (m, 1H), 8.94 – 8.79 (m, 1H), 8.78 – 8.59 (m, 1H), 8.02 (d, $J$ = 6.7 Hz, 2H), 7.96 (s, 2H), 7.85 – 7.78 (m, 1H), 7.69 (d, $J$ = 3.5 Hz, 1H), 7.34 – 7.12 (m, 11H), 6.98 (d, $J$ = 3.4 Hz, 1H), 6.51 (s, 1H), 5.00 (s, 1H), 4.85 (dd, $J$ = 15.4, 7.8 Hz, 1H), 4.63 (dd, $J$ = 36.2, 9.1 Hz, 3H), 4.44 (t, $J$ = 12.4 Hz, 2H), 4.33 (dd, $J$ = 18.4, 8.0 Hz, 2H), 4.20 (dt, $J$ = 7.2, 5.8 Hz, 2H), 4.11 – 3.93 (m, 5H), 3.73 (s, 1H), 3.00 (ddd, $J$ = 31.9, 23.2, 11.5 Hz, 2H), 2.86 – 2.58 (m, 3H), 1.26 (td, $J$ = 7.1, 1.3 Hz, 1.5H), 1.19 – 1.13 (m, 1.5H), 1.11 ppm (d, $J$ = 6.8 Hz, 6H); $^{13}$C NMR (100 MHz, DMSO-d$_6$, 25 °C): $\delta$ = 170.7, 170.5, 170.4, 169.4, 168.9, 167.9, 167.8, 167.4, 166.7, 166.7, 154.9, 154.8, 149.3, 149.2, 148.0, 144.8, 144.4, 144.3, 140.4, 137.3, 134.7, 129.6, 129.5, 129.3, 129.2, 128.5, 128.5, 128.2, 127.1, 126.5, 123.9, 123.2, 119.5, 61.4, 60.7, 54.2, 54.0, 53.3, 53.2, 47.4, 46.6, 44.1, 43.7, 38.2, 37.8, 36.9, 36.8, 34.7, 34.2, 18.9, 14.0 ppm. HRMS (ESI$^+$), m/z calculated for (M+H)$^+$ C$_{38}$H$_{47}$N$_{12}$O$_7$: 783.3691, found: 783.3686.

**[H-Phe-Phe-*tz-aeg*(T)-OEt] (7d)**: Peptide **6d** (0.5 g, 0.6 mmol) was hydrolyzed with TFA in DCM as described for **7c** to afford peptide **7d** (0.4 g, 90%) as a white solid; m.p. 98-100 °C; $^1$H NMR (400 MHz, DMSO-d$_6$, 25 °C): $\delta$ = 11.36 – 11.19 (m, 1H), 8.92 (dd, $J$ = 8.6, 2.6 Hz, 0.5H), 8.82 (d, $J$ = 8.1 Hz, 0.5H), 8.74 (dt, $J$ = 10.9, 5.4 Hz, 0.5H), 8.66 – 8.59 (m, 0.5H), 8.08 (s, 1H), 8.01 (s, 1H), 7.97 (s, 0.5H), 7.89 (s, 0.5H), 7.82 (s, 0.5H), 7.70 (s, 0.5H), 7.31 – 7.16 (m, 11H),

6.97 (dd, *J* = 6.4, 2.8 Hz, 1H), 4.75 – 4.55 (m, 3H), 4.52 – 4.23 (m, 6H), 4.19 – 4.03 (m, 5H), 3.87 (d, *J* = 3.5 Hz, 1H), 3.81 – 3.65 (m, 1H), 3.16 – 3.07 (m, 1H), 3.04 – 2.53 (m, 4H), 1.74 (ddd, *J* = 6.6, 4.9, 1.2 Hz, 3H), 1.23 (td, *J* = 7.1, 1.2 Hz, 1.5H), 1.19 – 1.15 ppm (m, 1.5H); $^{13}$C NMR (100 MHz, DMSO-$d_6$, 25 °C): $\delta$ = 170.8, 170.5, 170.5, 170.2, 170.2, 170.2, 169.2, 168.9, 168.1, 167.9, 167.7, 167.5, 164.4, 158.3, 158.0, 151.5, 151.0, 150.9, 150.9, 144.7, 144.7, 144.4, 144.3, 142.0, 141.9, 137.7, 137.4, 137.3, 134.7, 134.6, 129.6, 129.5, 129.3, 129.2, 129.2, 129.1, 128.5, 128.4, 128.2, 128.1, 128.0, 127.1, 126.5, 126.4, 123.7, 123.2, 108.3, 107.7, 61.3, 60.6, 60.0, 54.2, 54.0, 53.3, 53.1, 49.0, 48.0, 47.9, 47.8, 47.5, 47.4, 47.3, 46.6, 38.2, 37.8, 37.0, 36.9, 34.2, 34.2, 22.5, 14.0, 14.0, 11.9, 11.8 ppm. HRMS (ESI$^+$), m/z calculated for (M+H)$^+$ $C_{34}H_{42}N_9O_7$: 688.3207, found: 688.3210.

**[Boc-Phe-Phe-*tz-aeg*(G)-OH] (8c)**: To solution of peptide **6c** (0.1 g, 0.1 mmol) in THF (4 mL), 1 M NaOH solution (3 mL) was added at 0 °C and the resulting mixture was stirred for 8 hrs. The volatile part of the mixture was evaporated under reduced pressure. The residue was neutralized with cold 1 M HCl solution and resulting aq layer was extracted with EtOAc (20 x 3 mL). The combined organic layer was separated, dried over anhyd. $Na_2SO_4$, filtered and the filtrate was concentrated under reduced pressure. The crude mass thus obtained, was purified by column chromatography [Eluent: 5-50% of MeOH in CHCl$_3$] to afford peptide **8c** (0.1 g, 75%) as white hygroscopic solid. $^1$H NMR (400 MHz, DMSO-$d_6$, 25 °C): $\delta$ = 11.04 (s, 1H), 8.76 (s, 0.5H), 8.48 (d, *J* = 21.1 Hz, 1.5H), 7.83 (s, 0.5H), 7.94 (s, 0.5H)7.51 (d, *J* = 3.3 Hz, 1H), 7.30 – 6.92 (m, 12H), 6.76 (d, *J* = 23.2 Hz, 2H), 4.82 (s, *J* = 50.2 Hz, 2H), 4.48 (dd, *J* = 16.5, 10.4 Hz, 3H), 4.32 (dd, *J* = 33.5, 7.4 Hz, 2H), 4.12 (dd, *J* = 26.3, 22.1 Hz, 1H), 3.75 – 3.56 (m, 3H), 3.07 – 2.96 (m, 1H), 2.90 – 2.78 (m, 2H), 2.74 – 2.60 (m, 9H), 2.13 (t, *J* = 6.9 Hz, 1H), 1.24 ppm (d, *J* = 4.8 Hz, 9H); $^{13}$C NMR (150 MHz, DMSO-$d_6$, 25 °C): $\delta$ = 171.7, 171.5, 170.9, 170.7, 170.5, 167.6, 166.2, 157.1, 155.3, 155.1, 153.8, 151.8, 144.3, 138.3, 138.1, 137.9, 137.7, 129.3, 128.0, 127.9, 126.3, 126.0, 123.6, 123.5, 115.9, 79.2, 78.0, 56.1, 55.8, 54.2, 53.9, 53.1, 48.6, 48.4, 47.3, 47.1, 43.6, 34.5, 28.1, 27.7 ppm. HRMS (ESI$^+$), m/z calculated for (M+H)$^+$ $C_{37}H_{45}N_{12}O_8$: 785.3483, found: 785.3474.

**[Boc-Phe-Phe-*tz-aeg*(T)-OH] (8d)**: Peptide **6d** (0.3 g, 0.3 mmol) was ester hydrolyzed under basic condition as described for peptide **8c** to afford peptide **8d** (0.2 g, 80%) as a white solid; m.p. 120-123 °C; $^1$H NMR (400 MHz, DMSO-$d_6$, 25 °C): $\delta$ = 11.28 (d, *J* = 2.5 Hz, 1H), 8.51 (t, *J* = 9.5 Hz,

1H), 8.32 (s, 1H), 8.04 – 7.95 (m, 0.7H), 7.89 (s, 0.5H), 7.81 (s, 0.3H), 7.73 (s, 0.5H), 7.32 – 7.05 (m, 11H), 6.90 (d, $J$ = 6.8 Hz, 0.75H), 6.75 (d, $J$ = 7.1 Hz, 0.25H), 4.63 (s, 1H), 4.50 (dd, $J$ = 24.6, 13.8 Hz, 3H), 4.39 – 4.23 (m, 4H), 4.20 – 4.05 (m, 2H), 3.96 (s, 1H), 3.84 (s, 1H), 3.70 (s, 1H), 3.06 – 2.94 (m, 1H), 2.90 – 2.60 (m, 3H), 1.74 (d, $J$ = 3.9 Hz, 2H), 1.27 (d, $J$ = 3.7 Hz, 9H) ppm; $^{13}$C NMR (100 MHz, DMSO-d$_6$, 25 °C): $\delta$ = 171.4, 171.0, 170.8, 170.7, 170.4, 168.0, 167.4, 164.5, 164.4, 155.3, 155.2, 151.1, 151.0, 144.9, 144.6, 142.1, 142.0, 138.1, 137.8, 137.6, 129.4, 129.2, 129.2, 128.1, 128.0, 127.9, 126.3, 126.2, 123.8, 123.3, 108.3, 79.3, 78.2, 78.1, 55.9, 55.6, 53.8, 49.0, 47.9, 47.7, 47.5, 46.8, 37.9, 37.5, 34.4, 28.2, 27.8, 12.0 ppm. HRMS (ESI$^+$), m/z calculated for (M+H)$^+$ C$_{37}$H$_{46}$N$_9$O$_9$: 760.3418, found: 760.3417.

**Boc-Phe-Phe-*tz-aeg*-OEt (9)**: Alkyne **4** (0.2 g, 0.4 mmol) was reacted with ethyl(2-azidoethyl)glycinate[22] (0.1 g, 0.5 mmol) following the method described for peptide **6a** to afford peptide **9** (0.3 g, 89% with respect to **4**) which was purified by column chromatography [Eluent: 0-5% of MeOH in DCM]. Hygroscopic solid; $^1$H NMR (400 MHz, CDCl$_3$, 25 °C, TMS): $\delta$ = 7.43 (d, $J$ = 8.9 Hz, 1H), 7.26 – 6.86 (m, 11H), 6.60 (s, 1H), 5.29 (s, 0.5H), 4.99 (s, 0.5H), 4.63 (dt, $J$ = 14.1, 6.9 Hz, 1H), 4.47 – 4.19 (m, 5H), 4.09 (tt, $J$ = 11.7, 5.7 Hz, 2H), 3.63 (s, 2H), 3.41 (s, 1H), 3.31 (s, 2H), 3.15 (t, $J$ = 6.3 Hz, 1H), 3.08 – 2.75 (m, 5H), 1.23 (s, $J$ = 5.5 Hz, 9H), 1.21 – 1.15 ppm (m, 3H); $^{13}$C NMR (100 MHz, CDCl$_3$, 25 °C, TMS): $\delta$ = 172.6, 171.6, 171.3, 171.2, 171.2, 170.8, 170.7, 155.8, 136.6, 136.3, 129.4, 129.4, 129.3, 128.8, 128.7, 128.6, 127.2, 127.0, 123.1, 80.6, 80.4, 61.0, 60.9, 56.6, 56.5, 56.1, 56.1, 55.9, 55.8, 55.0, 54.9, 54.4, 54.0, 53.9, 53.9, 52.0, 50.4, 49.3, 48.7, 38.2, 38.0, 37.7, 37.5, 35.2, 35.0, 28.3, 28.2, 14.3 ppm. HRMS (ESI$^+$), m/z calculated for (M+H)$^+$ C$_{32}$H$_{44}$N$_7$O$_6$: 622.3353, found: 622.3354.

### 4.6.5 Synthesis of PNA monomer for amide / click conjugation with Phe-Phe moiety

Boc protected aminoethylglycyl (*aeg*) backbones **10** and **11** were synthesized first for free NH$_2$ containing PNA motifs following known literature procedure.[37] Compound **11** was treated with nucleobase adenine, 2-amino-6-chloropurine and thymine under heating condition in presence of K$_2$CO$_3$ to afford intermediates **12**, **13** and **14** in good yields. Again, **10** was coupled with $N^2$-(Isobutyryl)-9-(carboxymethyl)guanine to afford compound **15** in moderate yield. The spectroscopic data matched perfectly with the literature values.[37] The exo-cyclic amine groups at

N$^6$ and N$^2$ of **12** and **13** was therefore protected by Cbz and isobutyl groups respectively to obtain **16** and **17** in good yields. Finally, acid labile Boc groups were removed from **16**, **17**, **14**, and **15** in presence of TFA in DCM to obtain **2(a-d)**. After removal of volatile materials from the respective reaction mixtures and without further purification these PNA backbones were subjected for amide coupling with Boc-Phe-Phe-OH. Formation of compounds **2(a-d)** was confirmed by high resolution mass spectroscopy, supported by the NMR data of **2c**.

To conjugate PNA motifs with Boc-Phe-Phe-Propyne (**4**), azidoethylglycyl backbone **18**[38] was synthesized following the literature procedure. Secondary amine of **18** was coupled with $N^6$-Bis(*tert*butyloxycarbonyl)-9-(carboxymethyl)adenine, $N^6$-(Benzyloxycarbonyl)-9 (carboxymethyl) adenine, $N^2$-(Isobutyryl)-9-(carboxymethyl)guanine and, thymine-1-ylacetic acid in presence of isobutyl chloroformate (IBCF) and N-methylmorpholine (NMM) to afford **5(a-d)** respectively.

### 4.6.6 Spectroscopic data

Compound **10**: Compound **10** was prepared following the known literature procedure.[37] $^1$H NMR, (400 MHz, CDCl$_3$, 25 °C, TMS) $\delta$ = 5.10 (s, 1H), 4.19 (q, $J$ = 7.1 Hz, 2H), 3.40 (s, 2H), 3.22 (d, $J$ = 5.2 Hz, 2H), 2.74 (t, $J$ = 5.6 Hz, 2H), 1.44 (s, 9H), 1.28 ppm (td, $J$ = 7.1, 1.2 Hz, 3H); $^{13}$C NMR (100 MHz, CDCl$_3$) $\delta$ = 172.7, 156.3, 79.4, 61.0, 50.6, 48.9, 40.3, 28.6, 14.4 ppm. HRMS (ESI$^+$), m/z calculated for (M+H)$^+$ C$_{11}$H$_{23}$N$_2$O$_4$: 247.1658, found: 247.1666.

Compound **11**: Compound **11** was synthesized following the known literature procedure[37]. $^1$H NMR, (400 MHz, CDCl$_3$, 25 °C, TMS) $\delta$ = 5.60 (s, 1H), 4.28 – 4.17 (m, 4H), 4.05 (s, 2H), 3.54 (t, $J$ = 5.8 Hz, 2H), 3.29 (dd, $J$ = 11.7, 5.9 Hz, 2H), 1.50 – 1.38 (m, 9H), 1.35 – 1.21 ppm (m, 3H); $^{13}$C NMR (100 MHz, CDCl$_3$) $\delta$ = 169.6, 169.1, 167.7, 167.6, 156.2, 156.1, 79.7, 79.3, 62.1, 61.6, 50.5, 49.5, 49.0, 48.2, 41.2, 40.8, 38.6, 38.3, 28.3, 14.1 ppm. HRMS (ESI$^+$), m/z calculated for (M+Na)$^+$ C$_{13}$H$_{23}$ClN$_2$O$_5$Na: 345.1192, found: 345.1198.

Compound **12**: Compound **12** was synthesized following the known procedure.[37] $^1$H NMR, (400 MHz, CDCl$_3$, 25 °C, TMS) $\delta$ = 8.28 (d, $J$ = 5.2 Hz, 1H), 7.92 (d, $J$ = 16.5 Hz, 1H), 6.22 (d, $J$ = 17.1 Hz, 2H), 5.84 (s, 0.75H), 5.23 (s, 0.25H), 5.07 (d, $J$ = 8.1 Hz, 1.5H), 4.93 (s, 0.5H), 4.27 (s, 0.5H), 4.23 (dd, $J$ = 14.3, 7.2 Hz, 0.5H), 4.16 (q, $J$ = 7.2 Hz, 1.5H), 4.03 (s, 1.5H), 3.60 (t, $J$ = 5.4

Hz, 1.5H), 3.52 (d, $J$ = 5.5 Hz, 0.5H), 3.36 (d, $J$ = 5.4 Hz, 1.5H), 3.25 (d, $J$ = 5.8 Hz, 0.5H), 1.39 (s, 9H), 1.29 (t, $J$ = 7.1 Hz, 1H), 1.23 ppm (t, $J$ = 7.1 Hz, 2H); ^{13}C NMR (100 MHz, CDCl$_3$) δ = 169.6, 169.2, 167.4, 167.0, 156.2, 155.7, 153.1, 150.3, 141.6, 119.0, 80.1, 79.6, 62.4, 61.8, 50.6, 49.2, 48.8, 43.9, 43.6, 38.8, 38.5, 28.5, 14.2, 14.2 ppm. HRMS (ESI[+]), m/z calculated for (M+H)[+] C$_{18}$H$_{28}$N$_7$O$_5$: 422.2152, found: 422.2148.

Compound **13**: Compound **13** was synthesized following the known literature procedure.[37] ^{1}H NMR, (400 MHz, CDCl$_3$, 25 °C, TMS) δ = 7.82 (s, 1H), 5.75 (s, 1H), 5.41 (dd, $J$ = 38.2, 19.2 Hz, 2H), 4.96 (s, 1.5H), 4.80 (s, 0.5H), 4.27 – 4.12 (m, 2H), 4.03 (s, 2H), 3.55 (dt, $J$ = 28.7, 5.8 Hz, 2H), 3.39 – 3.19 (m, 2H), 1.38 (s, 9H), 1.22 ppm (td, $J$ = 7.2, 1.8 Hz, 3H); ^{13}C NMR (100 MHz, CDCl$_3$) δ = 171.3, 169.6, 167.1, 166.7, 159.3, 156.2, 154.1, 151.2, 143.3, 124.5, 80.2, 62.5, 61.9, 60.5, 49.2, 49.1, 48.8, 43.6, 38.8, 28.5, 21.1, 14.2, 14.2, 14.1 ppm. HRMS (ESI[+]), m/z calculated for (M+H)[+] C$_{18}$H$_{27}$ClN$_7$O$_5$: 456.1762, found: 456.1762.

Compound **14**: ^{1}H NMR, (400 MHz, CDCl$_3$, 25 °C, TMS) δ = 8.88 (s, 1H), 7.02 (s, 0.35H), 6.96 (s, 0.65H), 5.61 (s, 1H), 4.56 (s, 1.5H), 4.41 (s, 0.5H), 4.29 – 4.14 (m, 4H), 4.03 (d, $J$ = 3.5 Hz, 2H), 3.51 (dt, $J$ = 12.2, 6.3 Hz, 2H), 3.31 (ddd, $J$ = 18.3, 12.7, 6.7 Hz, 2H), 1.93 – 1.90 (m, 3H), 1.46 – 1.39 (m, 9H), 1.31 – 1.23 ppm (m, 3H); ^{13}C NMR (100 MHz, CDCl$_3$) δ = 169.8, 169.5, 168.0, 167.6, 164.6, 156.2, 151.4, 141.1, 110.8, 79.9, 79.5, 62.3, 61.7, 50.5, 49.1, 48.8, 47.9, 47.8, 38.8, 28.5, 14.2, 12.4 ppm. HRMS (ESI[+]), m/z calculated for (M+Na)[+] C$_{18}$H$_{28}$N$_4$O$_7$Na: 435.1856, found: 435.1860.

Compound **15**: Compound **15** was synthesized following the known literature procedure.[38,39] ^{1}H NMR, (400 MHz, DMSO-d$_6$, 25 °C) δ = 12.08 (d, $J$ = 5.5 Hz, 1H), 11.65 (d, $J$ = 7.6 Hz, 1H), 7.83 (s, 0.7H), 7.82 (s, 0.3H), 7.03 (t, $J$ = 5.5 Hz, 0.7H), 6.76 (s, 0.3H), 5.13 (s, 1.4H), 4.97 (s, 0.6H), 4.42 (s, 0.6H), 4.22 (q, $J$ = 7.1 Hz, 0.6H), 4.08 (q, $J$ = 7.0 Hz, 2.8H), 3.50 (t, $J$ = 6.5 Hz, 1.4H), 3.32 (d, $J$ = 11.9 Hz, 0.6H), 3.24 (d, $J$ = 6.1 Hz, 1.4H), 3.02 (d, $J$ = 6.1 Hz, 0.6H), 2.84 – 2.71 (m, 1H), 1.37 (d, $J$ = 6.5 Hz, 9H), 1.27 (t, $J$ = 7.1 Hz, 1H), 1.17 (t, $J$ = 7.1 Hz, 2H), 1.11 ppm (d, $J$ = 6.7 Hz, 6H); ^{13}C NMR (100 MHz, DMSO-d$_6$, 25 °C) δ = 180.2, 180.1, 169.5, 169.0, 167.0, 166.6, 155.8, 155.6, 154.9, 149.1, 149.2, 147.9, 147.9, 140.5, 140.4, 119.6, 78.2, 77.8, 61.3, 60.6, 49.1,

47.8, 46.9, 44.1, 43.9, 38.3, 37.7, 34.7, 34.7, 28.2, 18.9, 14.0 ppm. HRMS (ESI⁺), m/z calculated for (M+H)⁺ C$_{22}$H$_{34}$N$_7$O$_7$: 508.2520, found: 508.2535.

Compound **16**: To a suspension of **12** (0.4g, 1.00 mmol) in satd. NaHCO$_3$ solution (30 mL) at 0 °C was added Cbz-Cl (0.2 g, 1.2 mmol). The resulting mixture was stirred at room temperature for 8 hrs. EtOAc (20 mL) was added to the reaction mixture and the organic layer was separated. Aqueous layer was further extracted with EtOAc (25 x 2 mL). The combined organic layer was dried over anhyd. Na$_2$SO$_4$, filtered and the filtrate was evaporated to dryness in vacuo. The crude residue was purified by column chromatography [Eluent: 20-90% EtOAc in hexane] to afford compound **16** (0.4 g, 80%) as hygroscopic solid. ¹H NMR, (400 MHz, CDCl$_3$, 25 °C, TMS) $\delta =$ 8.97 (s, 1H), 8.16 (s, 1H), 7.36 – 7.18 (m, 8H), 6.36 (d, *J* = 11.2 Hz, 1H), 5.61 – 5.25 (m, 0.6H), 5.10 (s, 2H), 5.07 (d, *J* = 4.8 Hz, 2H), 4.93 (d, *J* = 5.4 Hz, 0.3H), 4.27 – 4.09 (m, 4H), 4.08 – 3.94 (m, 2H), 3.45 (dd, *J* = 24.5, 5.4 Hz, 2H), 3.29 – 3.16 (m, 2H), 1.38 – 1.29 (m, 9H), 1.25 – 1.16 ppm (m, 3H); ¹³C NMR (100 MHz, CDCl$_3$) δ = 169.9, 169.6, 169.5, 169.0, 159.8, 156.1, 155.6, 154.4, 153.9, 151.0, 136.1, 136.1, 135.5, 128.7, 128.6, 128.6, 128.6, 128.4, 128.3, 128.2, 128.1, 105.9, 80.0, 79.6, 68.1, 67.7, 67.6, 62.2, 61.8, 49.7, 48.9, 48.8, 48.3, 42.9, 38.7, 28.5, 14.2 ppm. HRMS (ESI⁺), m/z calculated for (M+H)⁺ C$_{26}$H$_{34}$N$_7$O$_7$: 556.2520, found: 556.2511.

Compound **17**: Compound **13** was converted to **17** following the procedure described in the *Eur. Pat. Appl.* **2001**, EP 1085020 A1 20010321. To a solution of **13** (0.5 g, 1.00 mmol) in dry pyridine (10 mL) at 0 °C was added isobutyrylchloride (0.1 g, 1.2 mmol). The resulting mixture was stirred at 0°C for 30 min, followed by 12 hrs at room temperature. Satd. NaHCO$_3$ solution (20 mL) was added to the reaction mixture and extracted with EtOAc (25 x 3 mL). The combined organic layer was dried over anhyd. Na$_2$SO$_4$, filtered and the filtrate was evaporated to dryness in vacuo. The crude residue was purified by flash column chromatography [Eluent: 20-70% EtOAc in hexane] to afford compound **15** (0.4 g, 85%) as hygroscopic solid. ¹H NMR, (400 MHz, CDCl$_3$, 25 °C, TMS) $\delta =$ 8.31 (s, 1H), 8.21 (s, 0.7H), 8.13 (s, 0.3H), 6.29 (s, 0.75H), 5.30 (d, *J* = 16.6 Hz, 0.25H), 5.14 (s, 1.7H), 4.98 (d, *J* = 12.4 Hz, 0.3H), 4.36 (s, 0.3H), 4.27 (q, *J* = 7.1 Hz, 0.3H), 4.17 (q, *J* = 7.1 Hz, 1.7H), 4.14 – 4.08 (m, 1.7H), 3.67 (t, *J* = 5.8 Hz, 1.7H), 3.55 (t, *J* = 5.8 Hz, 0.3H), 3.43 (dd, *J* = 11.9, 5.9 Hz, 1.7H), 3.29 – 3.21 (m, 0.3H), 2.77 - 2.71 (m, 1H), 1.40 (s, 2H), 1.32 (dd, *J* = 13.7, 6.6 Hz, 1H), 1.27 (d, *J* = 3.5 Hz, 4H), 1.25 (d, *J* = 1.0 Hz, 5H), 1.22 ppm (s, 6H); ¹³C NMR

(100 MHz, CDCl$_3$) δ = 175.4, 169.4, 166.5, 156.6, 152.9, 151.9, 151.1, 146.0, 127.8, 79.5, 62.5, 61.7, 60.5, 50.9, 49.1, 48.8, 44.3, 43.6, 38.5, 36.7, 28.5, 28.4, 19.4, 14.3, 14.2 ppm. HRMS (ESI$^+$), m/z calculated for (M+H)$^+$ C$_{22}$H$_{33}$ClN$_7$O$_6$: 526.2181, found: 526.2173.

**4.6.7 General procedure of Boc deprotection**: To an ice-cold mixture of compound (0.5 mmol in 5 mL), 2 mL TFA was added slowly and stirred for 4-6 hrs at rt. Completion of reaction was monitored by TLC. The volatile part of the reaction mixture was completely removed by co-evaporation with toluene and carbontetrachloride to afford TFA salts of compound **2(a-d)** as brown oil which were used for amide coupling reaction without further purification.

Compound **2a**: HRMS (ESI$^+$), m/z calculated for (M+H)$^+$ C$_{21}$H$_{26}$N$_7$O$_5$: 456.1995, found: 456.1985.

Compound **2b**: HRMS (ESI$^+$), m/z calculated for (M+H)$^+$ C$_{17}$H$_{25}$ClN$_7$O$_4$: 426.1656, found: 426.1642.

Compound **2c**: White solid; m.p. 97-100 °C; $^1$H NMR, (400 MHz, DMSO-d$_6$, 25 °C): δ = 12.09 (d, $J$ = 5.1 Hz, 1H), 11.63 (d, $J$ = 6.1 Hz, 1H), 8.04 (s, 1H), 7.87 (s, 0.5H), 7.82 (s, 0.5H), 7.78 (s, 1H), 5.17 (s, 1H), 4.98 (s, 1H), 4.46 (s, 1H), 4.22 (q, $J$ = 7.1 Hz, 1H), 4.10 (dd, $J$ = 12.2, 4.9 Hz, 2H), 3.70 (t, $J$ = 6.7 Hz, 1H), 3.52 (t, $J$ = 6.3 Hz, 1H), 3.17 (d, $J$ = 5.4 Hz, 1H), 2.97 (dd, $J$ = 10.9, 5.1 Hz, 1H), 2.86 – 2.68 (m, 1H), 1.27 (t, $J$ = 7.1 Hz, 1.5H), 1.18 (t, $J$ = 7.1 Hz, 1.5H), 1.11 ppm (d, $J$ = 6.8 Hz, 6H); $^{13}$C NMR (100 MHz, DMSO-d$_6$, 25 °C): δ = 180.2, 180.1, 169.5, 169.3, 168.0, 166.8, 158.9, 158.6, 158.3, 154.9, 149.3, 148.0, 147.9, 140.6, 119.4, 61.4, 60.9, 48.6, 47.7, 44.9, 44.8, 44.2, 44.1, 36.9, 36.7, 34.7, 34.7, 18.9, 18.9, 14.0, 14.0 ppm; HRMS (ESI$^+$), m/z calculated for (M+H)$^+$ C$_{17}$H$_{26}$N$_7$O$_5$: 408.1995, found: 408.1992.

Compound **2d**: HRMS (ESI$^+$), m/z calculated for (M+H)$^+$ C$_{13}$H$_{21}$N$_4$O$_5$: 313.1512, found: 313.1514.

Compound **18**: Compound **18** was synthesized following previously mentioned literature[36]. $^1$H NMR, (400 MHz, CDCl$_3$, 25 °C, TMS) δ = 4.20 (q, $J$ = 7.2 Hz, 2H), 3.46 – 3.39 (m, 4H), 2.88 – 2.79 (m, 2H), 2.00 (s, 1H), 1.32 – 1.24 ppm (m, 3H); $^{13}$C NMR (100 MHz, CDCl$_3$) δ = 172.2,

60.9, 51.5, 50.6, 48.2, 14.3 ppm; IR: $v_{N_3}$ = 2101 cm$^{-1}$; HRMS (ESI$^+$), m/z calculated for (M+H)$^+$ $C_6H_{13}N_4O_2$: 173.1038, found: 173.1044.

<u>Compound 4</u>: Compound **4** was synthesized following the reported procedure.[22] $^1$H NMR, (400 MHz, CDCl$_3$, 25 °C, TMS) $\delta$ = 7.24 (dt, $J$ = 6.4, 4.1 Hz, 3H), 7.18 – 7.02 (m, 6H), 6.91 (t, $J$ = 18.1 Hz, 2H), 6.54 (s, 1H), 6.28 (s, 1H), 4.84 (d, $J$ = 5.9 Hz, 1H), 4.72 – 4.54 (m, 1H), 4.20 (d, $J$ = 6.0 Hz, 1H), 3.92 (ddd, $J$ = 21.0, 11.9, 9.0 Hz, 1H), 3.77 (dd, $J$ = 17.5, 2.4 Hz, 1H), 3.14 (s, 1H), 2.99 – 2.76 (m, 3H), 2.08 (t, $J$ = 2.5 Hz, 1H), 1.25 ppm (s, 9H); $^{13}$C NMR (100 MHz, CDCl$_3$) $\delta$ = 171.0, 170.3, 155.9, 136.0, 129.4, 129.3, 129.0, 128.8, 81.02, 79.2, 71.3, 56.3, 53.4, 37.8, 37.5, 29.2, 28.3, 28.2 ppm. HRMS (ESI$^+$), m/z calculated for (M+Na)$^+$ $C_{26}H_{31}N_3O_4Na$: 472.2212, found: 472.2213.

**4.6.8 General procedure of coupling azide backbone with nucleobase acetic acid**

1.  To a mixture of nucleobase acetic acid (0.5 mmol) in dry DMF (5mL), NMM (0.5 mmol) and IBCF (0.5 mmol) were added slowly and cooled to −50 °C. To the white semisolid mass obtained after 0.5 hr, compound **18** (0.4 mmol) dissolved in dry DMF (1.5 mL) and disopropylethylamine (DIPEA) (2.0 mmol) were slowly added at 0 °C. Reaction mixture was maintained at 0 °C for 0.5 hr and then kept at rt for 6 hrs. Brine solution was added and extracted with EtOAc (3 x 50 mL). Combined organic layer was dried over anhyd. Na$_2$SO$_4$ and evaporated to dryness. Crude mass thus obtained was purified by column chromatography.

2.  $N^2$-(Isobutyryl)-9-(carboxymethyl)guanine was coupled with the azide backbone **18** following the procedure mentioned for compound **3(a-d)** to afford **5c** in good yield (75%).

<u>Compound 5a</u>: $^1$H NMR, (400 MHz, CDCl$_3$, 25 °C, TMS) $\delta$ = 8.83 (d, $J$ = 3.0 Hz, 1H), 8.24 (s, 1H), 5.32 (s, 1H), 5.09 (s, 1H), 4.37 (s, 1H), 4.32 (q, $J$ = 7.2 Hz, 1H), 4.20 (q, $J$ = 7.1 Hz, 1H), 4.14 (s, 1H), 3.74 – 3.70 (m, 1H), 3.67 (d, $J$ = 4.8 Hz, 1H), 3.60 – 3.52 (m, 2H), 1.43 (d, $J$ = 2.7 Hz, 18H), 1.36 (t, $J$ = 7.1 Hz, 1.5H), 1.26 ppm (t, $J$ = 7.1 Hz, 1.5H); $^{13}$C NMR (100 MHz, CDCl$_3$) $\delta$ = 169.0, 168.7, 166.8, 166.6, 153.6, 153.6, 152.1, 150.5, 150.4, 150.4, 146.1, 146.0, 128.4, 83.9, 83.8, 62.6, 61.8, 51.2, 50.1, 50.0, 48.8, 48.4, 48.2, 44.1, 44.0, 27.9, 14.3, 14.2 ppm; IR: $v_{N_3}$ = 2103 cm$^{-1}$; HRMS (ESI$^+$), m/z calculated for (M+H)$^+$ $C_{23}H_{34}N_9O_7$: 548.2581, found: 548.2587.

Compound **5b**: $^1$H NMR, (400 MHz, CD$_3$OD + DMSO-d$_6$, 2:1, 25 °C) $\delta$ = 8.22 (t, *J* = 12.7 Hz, 1H), 7.39 (d, *J* = 7.4 Hz, 1H), 7.31 (ddd, *J* = 22.2, 21.7, 7.0 Hz, 5H), 5.36 (s, 1H), 5.19 (s, 1H), 5.12 (d, *J* = 17.3 Hz, 1H), 4.20 (dd, *J* = 14.3, 7.1 Hz, 1H), 4.12 – 3.93 (m, 3H), 3.66 (d, *J* = 11.7 Hz, 3H), 3.53 – 3.42 (m, 1H), 3.38 (dd, *J* = 13.7, 8.0 Hz, 1H), 1.25 (dd, *J* = 14.3, 7.2 Hz, 1H), 1.13 ppm (t, *J* = 7.1 Hz, 2H); $^{13}$C NMR (100 MHz, CD$_3$OD + DMSO-d$_6$, 2:1) $\delta$ = 170.1, 168.8, 168.4, 153.2, 153.1, 152.8, 150.4, 146.2, 137.3, 129.4, 129.1, 129.0, 67.8, 62.7, 61.9, 61.0, 50.7, 50.6, 49.9, 49.4, 45.1, 45.1, 14.4 ppm; IR: $\nu_{N3}$ = 2102 cm$^{-1}$; HRMS (ESI$^+$), m/z calculated for (M+H)$^+$ C$_{21}$H$_{24}$N$_9$O$_5$: 482.1900, found: 482.1897.

Compound **5c**: $^1$H NMR (400 MHz, DMSO-d$_6$, 25 °C) $\delta$ = 12.08 (s, 1H), 11.65 (s, 0.3H), 11.62 (s, 0.7H), 7.88 (s, 0.6H), 7.83 (s, 0.4H), 5.20 (s, 1.3H), 4.99 (s, 0.7H), 4.48 (s, 0.7H), 4.22 (q, *J* = 7.1 Hz, 0.7H), 4.13 – 4.05 (m, 2.6H), 3.73 – 3.62 (m, 2.5H), 3.50 – 3.41 (m, 1.5H), 2.82 – 2.71 (m, 1H), 1.27 (t, *J* = 7.2 Hz, 1H), 1.17 (t, *J* = 7.1 Hz, 2H), 1.12 (s, 3H), 1.10 ppm (s, 3H); $^{13}$C NMR (400 MHz, DMSO-d$_6$, 25 °C) $\delta$ = 180.1, 169.5, 168.9, 167.3, 166.9, 154.9, 149.3, 147.9, 140.7, 140.5, 119.6, 61.3, 60.6, 49.0, 48.3, 48.0, 46.8, 46.4, 44.2, 34.6, 18.9, 14.0 ppm; IR: $\nu_{N3}$ = 2105 cm$^{-1}$; HRMS (ESI$^+$), m/z calculated for (M+H)$^+$ C$_{17}$H$_{24}$N$_9$O$_5$: 434.1900, found: 434.1903.

Compound **5d**: $^1$H NMR, (400 MHz, DMSO-d$_6$, 25 °C): $\delta$ = 11.29 (s, 1H), 7.36 (d, *J* = 1.2 Hz, 0.7H), 7.29 (d, *J* = 1.2 Hz, 0.3H), 4.71 (s, 1.3H), 4.50 (s, 0.7H), 4.37 (s, 0.7H), 4.18 (q, *J* = 7.1 Hz, 0.8H), 4.13 – 4.03 (m, 2.5H), 3.63 (t, *J* = 5.4 Hz, 1.3H), 3.56 (t, *J* = 5.5 Hz, 1.3H), 3.50 – 3.46 (m, 0.7H), 3.43 (t, *J* = 5.3 Hz, 0.7H), 1.75 (d, *J* = 1.1 Hz, 3H), 1.25 (t, *J* = 7.1 Hz, 1H), 1.18 ppm (t, *J* = 7.1 Hz, 2H); $^{13}$C NMR (100 MHz, DMSO-d$_6$, 25 °C): $\delta$ = 169.3, 168.9, 168.0, 167.6, 164.4, 164.4, 151.0, 142.2, 142.0, 108.2, 108.1, 61.2, 60.6, 49.1, 48.3, 48.1, 47.9, 46.8, 46.3, 14.0, 14.0, 11.9 ppm; IR: $\nu_{N3}$ = 2103 cm$^{-1}$; HRMS (ESI$^+$), m/z calculated for (M+H)$^+$ C$_{13}$H$_{17}$N$_6$O$_5$: 339.1417, found: 339.1420.

**4.6.9 FTIR spectroscopy**: See the experimental section (**2.5.3**) of chapter **2**.

**4.6.10 Thermogravimetric Analysis (TGA)**: See the experimental section (**2.5.5**) of chapter **2**.

**4.6.11 Dynamic light scattering**: See the experimental section (**2.5.6**) of chapter **2**.

**4.6.12 Microscopy studies**: See the experimental section (**2.5.7**) of chapter **2**.

**4.6.13 Carboxyfluorescein encapsulation study**: See the experimental section **(2.5.11)** of chapter **2**.

**4.6.14 Dicationic dipeptide mediated release**: See the experimental section **(2.5.12b)** of chapter **2**.

**4.6.15 Contact angle measurement**: See the experimental section **(2.5.13)** of chapter **2**.

**4.6.16 MALDI-TOF characterization**:  See the experimental section **(2.5.14)** of chapter **2**.

**4.6.17 Turbidity assay experiment**: Turbidity assay experiment was done in the 96 well micro test plate flat bottom wells (Tarsons, CAT No. 941196) by using VARIOSKAN FLASH (Thermo scientific). Samples were prepared by putting peptide solution (400 µL, 1 mg / 400 µL in 50:50 EtOH / $H_2O$ after lyophilization in 1 mL HFIP) in 96 well micro test plate flat bottom wells (Tarsons, CAT No. 941196).

**4.6.18 Purifications and characterization of the peptides**: The peptides were purified using the routine reverse phase HPLC using a semi preparative C18 column. A linear gradient system between water and acetonitrile was used similar to the ones used for linear peptides. The purity of the peptides was finally checked using C18 analytical column. The integrity of the purified peptides was confirmed by MALDI-TOF spectrometry using DHB and CHCA as matrix.

## 4.7 References

1. Gorbitz, C. H. *Chem. Eur. J.* **2001**, *7*, 5153-5159.
2. Hartgerink, J. D.; Beniash, E.; Stupp, S. I. *Science* **2001**, *294*, 1684-1688.
3. Aggeli, A.; Fytas, G.; Vlassopoulos, D.; McLeish, T. C. B.; Mawer, P. J.; Boden, N. *Biomacromolecules* **2001**, *2*, 378-388.
4. Lee, S. W.; Mao, C.; Flynn, C. E.; Belcher, A. M. *Science* **2002**, *296*, 892-895.
5. Zhang, S. *Nature Biotechnol.* **2003**, *21*, 1171-1178.
6. Reches, M.; Gazit, E. *Science* **2003**, *300*, 625-627.
7. Reches, M.; Gazit, E. *Nano Lett.* **2004**, *4*, 581-585.
8. Reches, M.; Gazit, E. *Nat. Nanotechnol.* **2006**, *1*, 195-200.
9. Abramovich, L. A.; Reches, M.; Sedman, V. L.; Allen, S.; Tendler, S. J. B.; Gazit, E. *Langmuir* **2006**, *22*, 1313-1320.

10. Tamamis, P.; Abramovich, L. A.; Reches, M.; Marshall, K.; Sikorski, P.; Serpell, L.; Gazit E.; Archontis, G. *Biophys. J.* **2009**, *96*, 5020-5029.

11. Azuri, I.; Abramovich, L. A.; Gazit, E.; Hod O.; Kronik, L. *J. Am. Chem. Soc.* **2014**, *136*, 963-969.

12. Berger, O.; Gazit, E. *Peptide Science* **2017**, *108*, e22930.

13. Berger, O.; Abramovich, L. A.; Sakin, M. L.; Grunwald, A.; Peer, Y. L.; Bachar, M.; Buzhansky, L.; Mossou, E.; Forsyth, V. T.; Schwartz, T.; Ebenstein, Y.; Frolow, F.; Shimon, L. J. W.; Patolsky, F.; Gazit, E. *Nat. Nanotechnol*. **2015**, *10*, 353-360.

14. Avitabile, C.; Diaferia, C.; Ventura, B. D.; Mercurio, F. A.; Leone, M.; Roviello, V.; Saviano, M.; Velotta, R.; Morelli, G.; Accardo, A.; Romanelli, A. *Chem. Eur. J.* **2018**, *24*, 4729-4735.

15. Berger, O.; Yoskovitz, E.; Abramovich, L. A.; Gazit, E. *Adv. Mater.* **2016**, *28*, 2195-2200.

16. (a) Kinoshita, S.; Yoshioka, S. *ChemPhysChem* **2005**, *6*, 1442-1459; (b) Tadepalli, S.; Slocik, J. M.; Gupta, M. K.; Naik, R. R.; Singamaneni, S. *Chem. Rev.* **2017**, *117*, 12705-12763.

17. Nikoloudakis, E.; Karikis, K.; Han, J.; Kokotidou, C.; Charisiadis, A.; Folias, F.; Douvas, A. M.; Mitraki, A.; Charalambidis, G.; Yan, X.; Coutsolelos, A. G. *Nanoscale* **2018**, *11*, 3557-3566.

18. Li, X.; Kuang, Y.; Lin, H. C.; Gao, Y.; Shi, J.; Xu, B. *Angew. Chem. Int. Ed.* **2011**, *50*, 9365-9369.

19. Li, X.; Kuang, Y.; Shi, J.; Gao, Y.; Lin, H. C.; Xu, B. *J. Am. Chem. Soc*. **2011**, *133*, 17513-17518.

20. Lin, Y.; Pashuck, E. T.; Thomas, M. R.; Amdursky, N.; Wang, S. T.; Chow, L. W.; Stevens, M. M. *Angew. Chem. Int. Ed*. **2017**, *56*, 2361-2365.

21. Serpell, C. J.; Barlog, M.; Basu, K.; Fakhoury, J. F.; Bazzi, H. S.; Sleiman, H. F. *Mater. Horiz.* **2014**, *1*, 348-354.

22. Datta, D.; Tiwari, O.; Ganesh, K. N. *Nanoscale* **2018**, *10*, 3212-3224.

23. Zhu, X.; Zou, R.; Sun, P.; Wang, Q.; Wu, J. *Polym. Chem.* **2018**, *9*, 69-76.

24. (a) Angell, Y. L.; Burgess, K. *Chem. Soc. Rev.* **2007**, *36*, 1674-1689; (b) Pedersen, D. S.; Abell, A. *Eur. J. Org. Chem.* **2011**, 2399-2411; (c) Tiwari, V. K.; Mishra, B. B.; Mishra, K. B.; Mishra, N.; Singh, A. S.; Chen, X. *Chem. Rev*. **2016**, *116*, 3086-3240.

25. Kramer, R. A.; Bleicher, K. H.; Wennemers, H. *Helvetica Chimica Acta* **2012**, *95*, 2621-2634.

26. Porcheddu, A.; Giacomelli, G.; Piredda, I.; Carta, M.; Nieddu, G. *Eur. J. Org. Chem.* **2008**, 5786-5797.

27. Tornøe, C. W.; Christensen, C.; Meldal, M. *J. Org. Chem.* **2002**, *67*, 3057-3064.

28. Kolb, H. C.; Finn, M.; Sharpless, K. B. *Angew. Chem. Int. Ed.* **2001**, *40*, 2004-2021.

29. (a) Mayans, E.; Casanovas, J.; Gil, A. M.; Jimenez, A. I.; Cativiela, C.; Puiggali, J.; Aleman, C. *Langmuir* **2017**, *33*, 4036-4048; (b) Brown, N.; Lei, J.; Zhan, C.; Shimon, L. J. W.; Abramovich, L. A.; Wei, G.; Gazit, E. *ACS Nano* **2018**, *12*, 3253-3262; (c) Kong, J.; Yu, S. *Acta Biochim. Biophys. Sin.* **2007**, *39*, 549-559; (d) Khurana, R.; Fink, A. L. *Biophys. J.* **2000**, *78*, 994-1000; (e) Haris, P. I.; Chapman, D. *Biopolymers* **1995**, *37*, 251-263; (f) Qian, W.; Bandekar, J.; Krimm, S. *Biopolymers* **1991**, *31*, 193-210; (g) Toniolo, C.; Palumbo, M. *Biopolymers* **1977**, *16*, 219-224.

30. Franken, L. E.; Wei, Y.; Chen, J.; Boekema, E. J.; Zhao, D.; Stuart, M. C. A.; Feringa, B. L. *J. Am. Chem. Soc.* **2018**, *140*, 7860-7868.

31. Zhu, C.; Gao, Y.; Li, H.; Meng, S.; Li, L.; Francisco J. S.; Zeng, X. C. *Proc. Natl. Acad. Sci. U. S. A.* **2016**, *113*, 12946-12951.

32. (a) Baral, A.; Roy, S.; Dehsorkhi, A.; Hamley, I. W.; Mohapatra, S.; Ghosh, S.; Banerjee, A. *Langmuir* **2014**, *30*, 929-936; (b) Basu, K.; Baral, A.; Basak, S.; Dehsorkhi, A.; Nanda, J.; Bhunia, D.; Ghosh, S.; Castelletto, V.; Hamley, I. W.; Banerjee, A. *Chem. Commun.* **2016**, *52*, 5045-5048.

33. Misra, R.; Reja, R. M.; Narendra, L. V.; George, G.; Raghothama, S.; Gopi, H. N. *Chem. Commun.* **2016**, *52*, 9597-9600.

34. Ingole, T. S.; Kale, S. S.; Santhosh Babu, S.; Sanjayan, G. J. *Chem. Commun.* **2016**, *52*, 10771-10774.

35. (a) Wang, Steven S. S.; Chen, Y. T.; Chou, S. W. *Biochim. Biophys. Acta* **2005**, *1741*, 307-313; (b) Carny O.; Gazit, E. *Orig. Life Evol. Biosph.* **2011**, *41*, 121-132; (c) Zhao, R.; So, M.; Maat, H.; Ray, N. J.; Arisaka, F.; Goto, Y.; Carver, J. A.; Hall, D. *Biophys. Rev.* **2016**, *8*, 445-471.

36. Efthymiou, T. C.; Desaulniers, J. P. *J. Heterocyclic Chem.* **2011**, *48*, 533-539.

37. Meltzer, P.C.; Y. Liang, A. Y.; Matsudaira, P. *J. Org. Chem.* **1995**, *60*, 4305-4308.

38. Englund, E. A.; Xu, Q.; Witschi, M. A.; Appella, D. H. *J. Am. Chem. Soc*. **2006**, *128*, 16456-16457.

39. Datta, D.; Tiwari, O.; Gupta, M. K. *ACS Omega* **2019**, *4*, 10715-10728.

(https://pubs.acs.org/doi/abs/10.1021/acsomega.9b00047)

## 4.8 Appendix III: Characterization data of synthesized compounds

| Entry | Table of contents | Page No. |
|-------|-------------------|----------|
| 1 | $^1$H, $^{13}$C NMR, IR spectra, UV-Vis spectra and HPLC Trace of compounds | 172-213 |

**(A)**



**(B)**
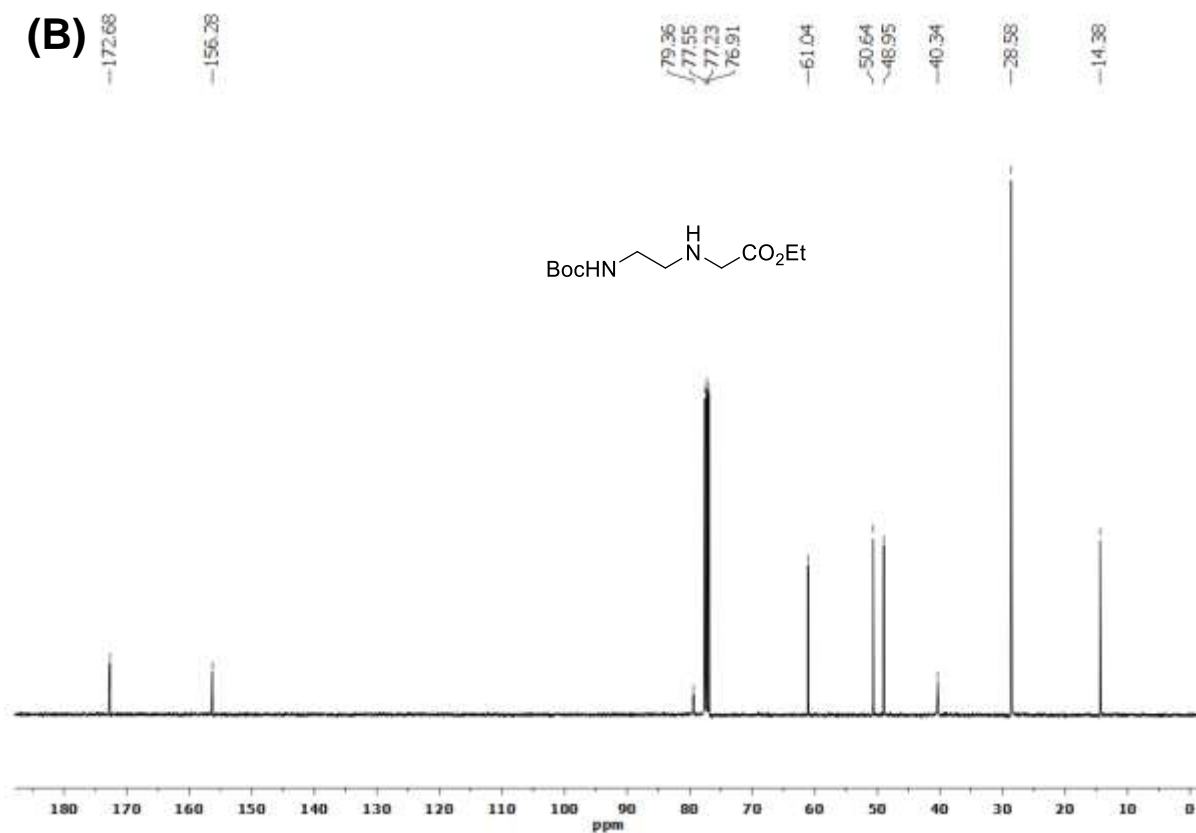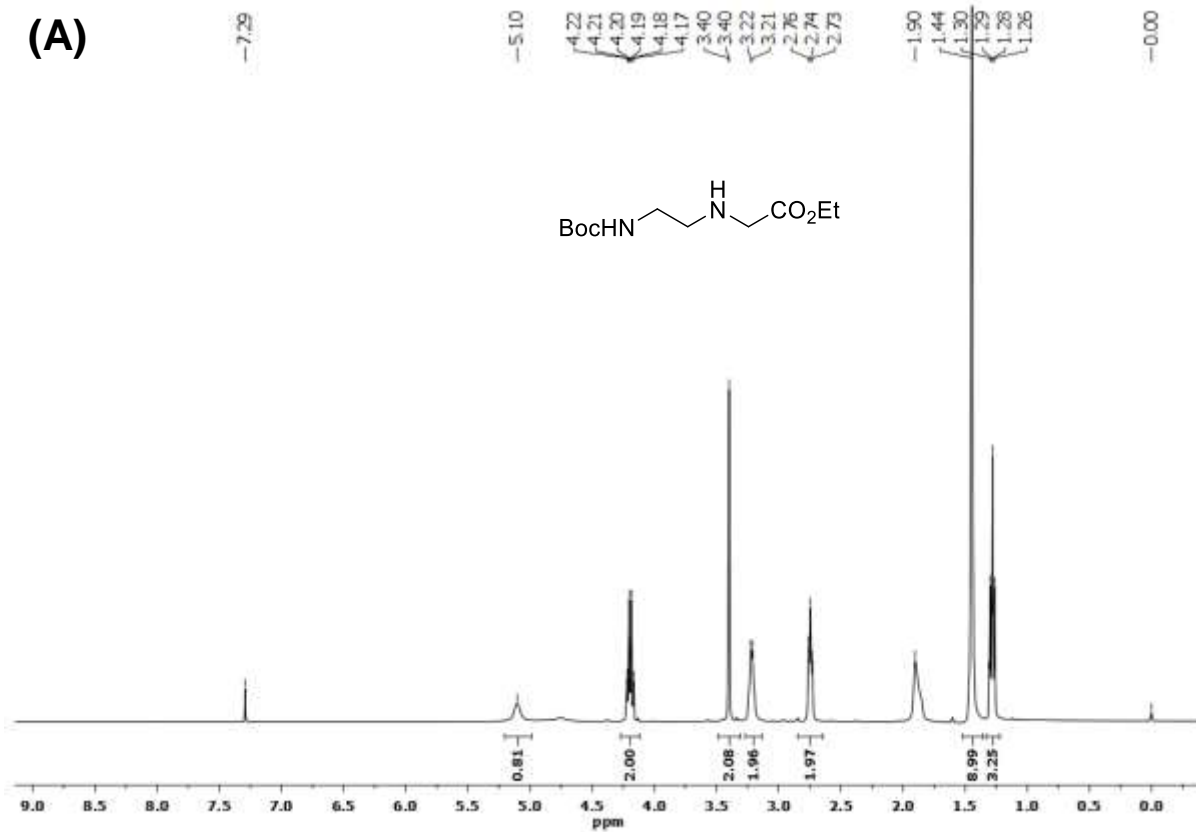


(A) $^1$H-NMR and (B) $^{13}$C-NMR spectra of **10**.
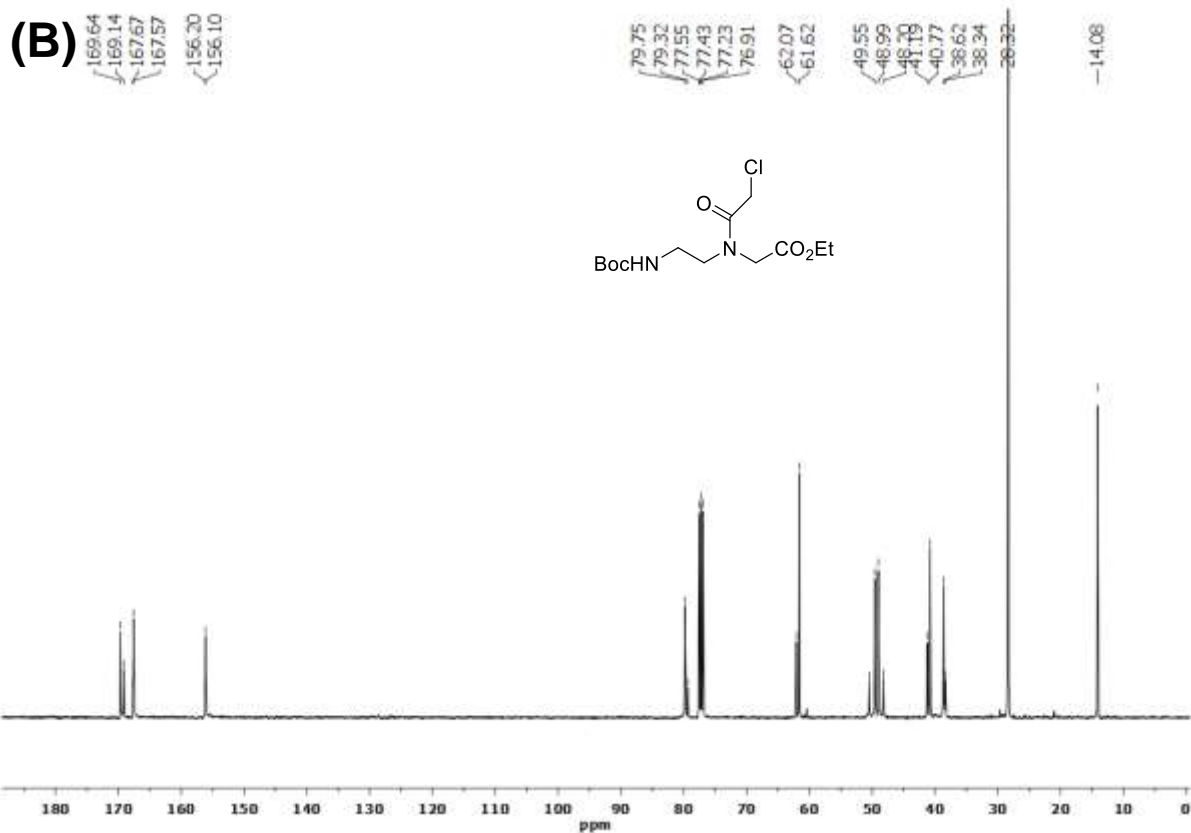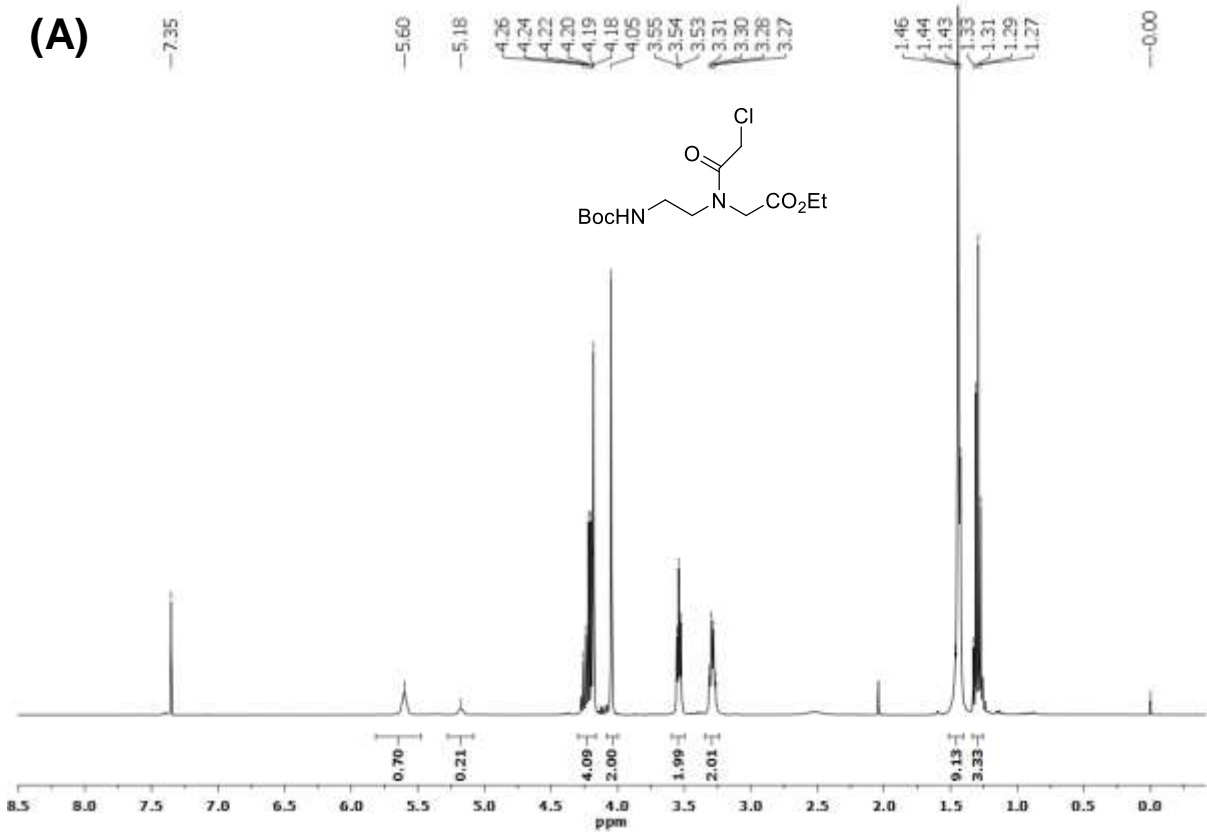
(A) $^1$H-NMR and (B) $^{13}$C-NMR spectra of **11**.

**(A)**



**(B)**
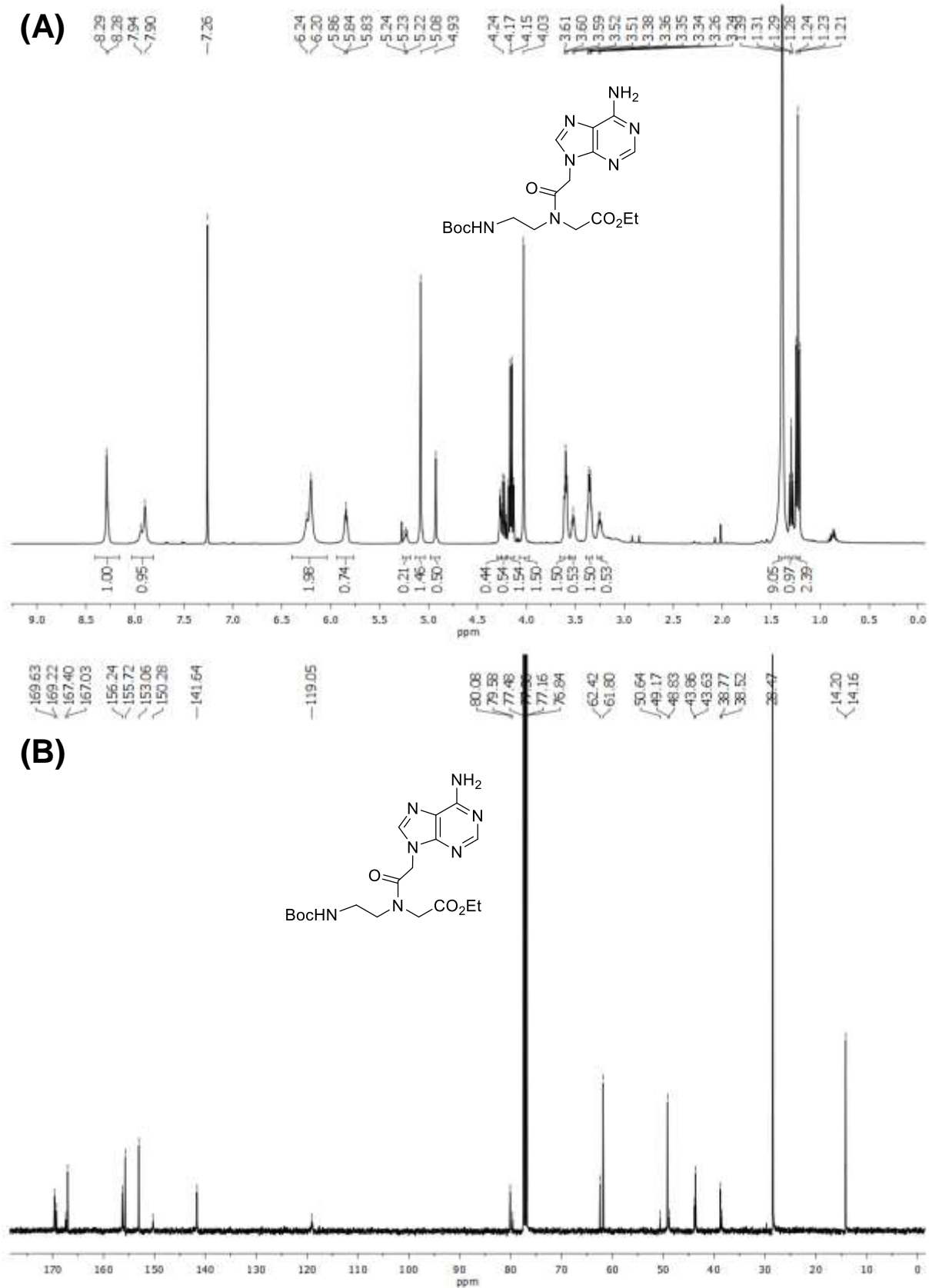


(A) $^1$H-NMR and (B) $^{13}$C-NMR spectra of **12**.

**(A)**



**(B)**
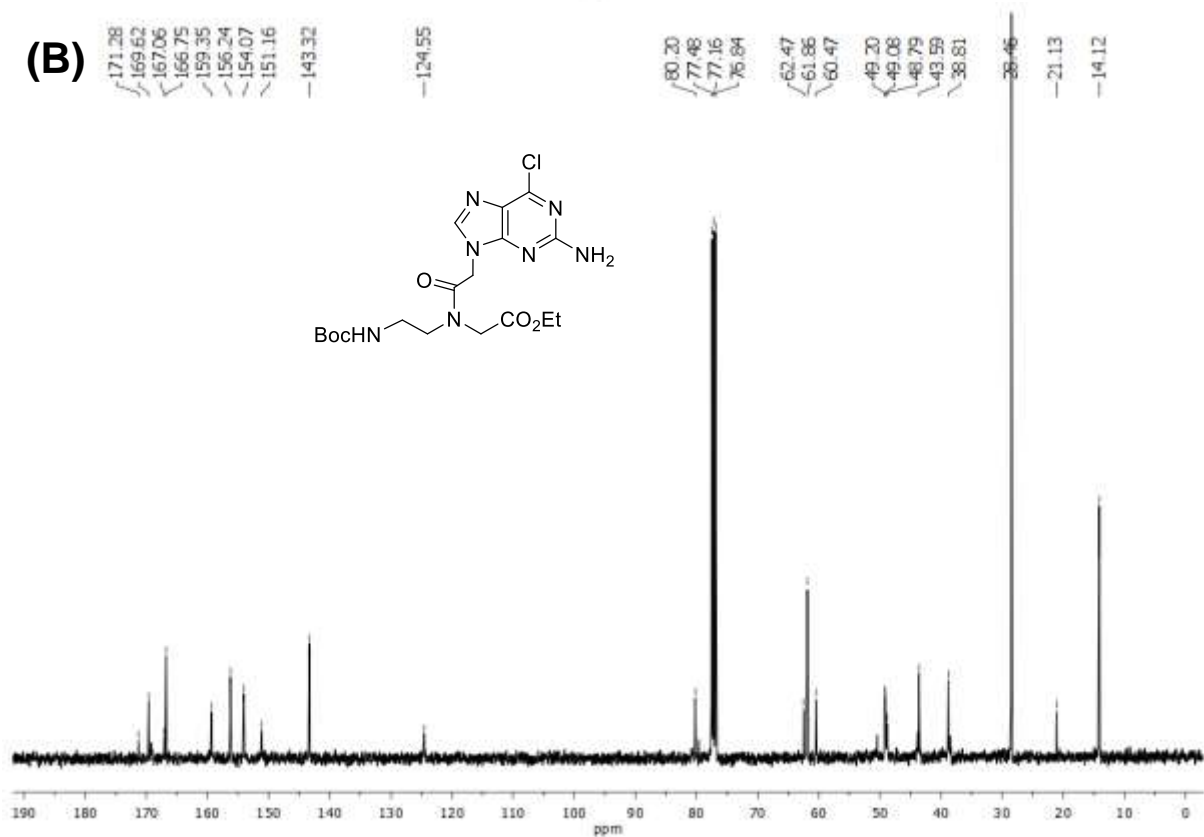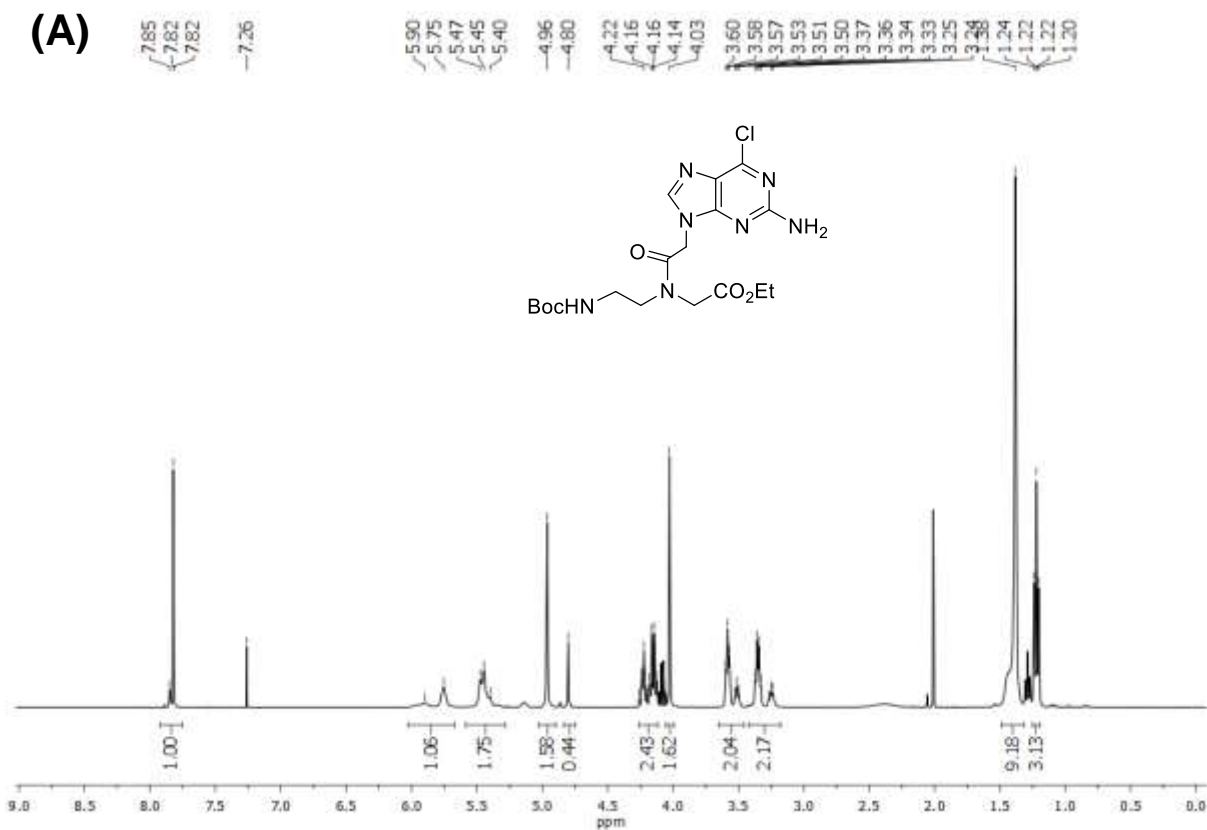


(A) ¹H-NMR and (B) ¹³C-NMR spectra of **13**.

**(A)**



**(B)**
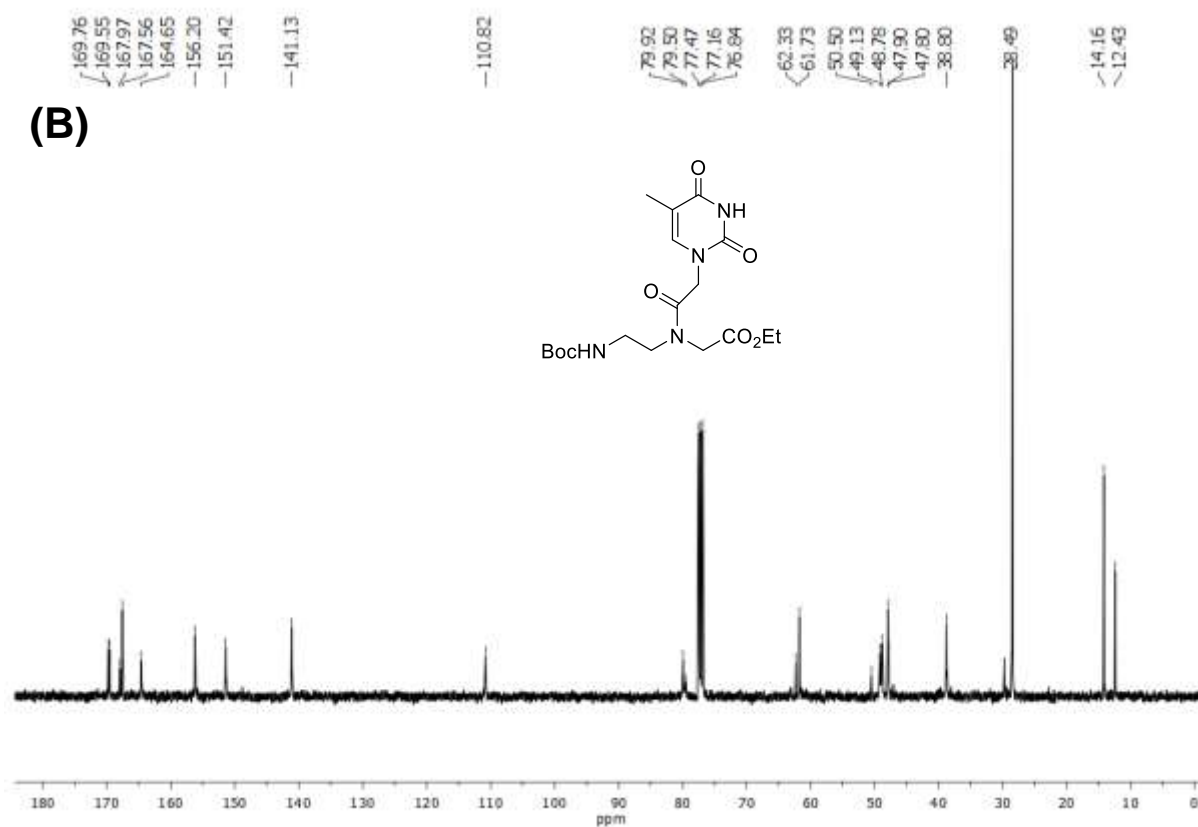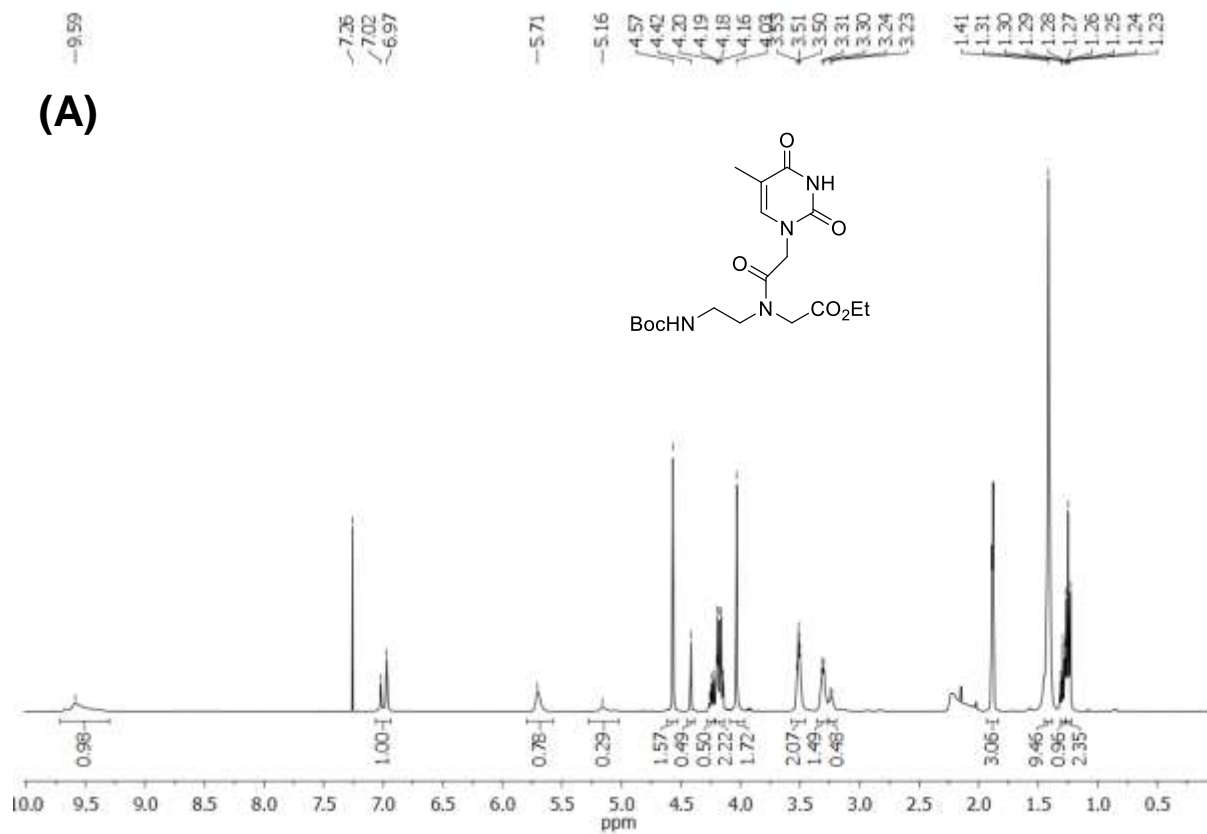


(A) $^1$H-NMR and (B) $^{13}$C-NMR spectra of **14**.

**(A)**

**(B)**
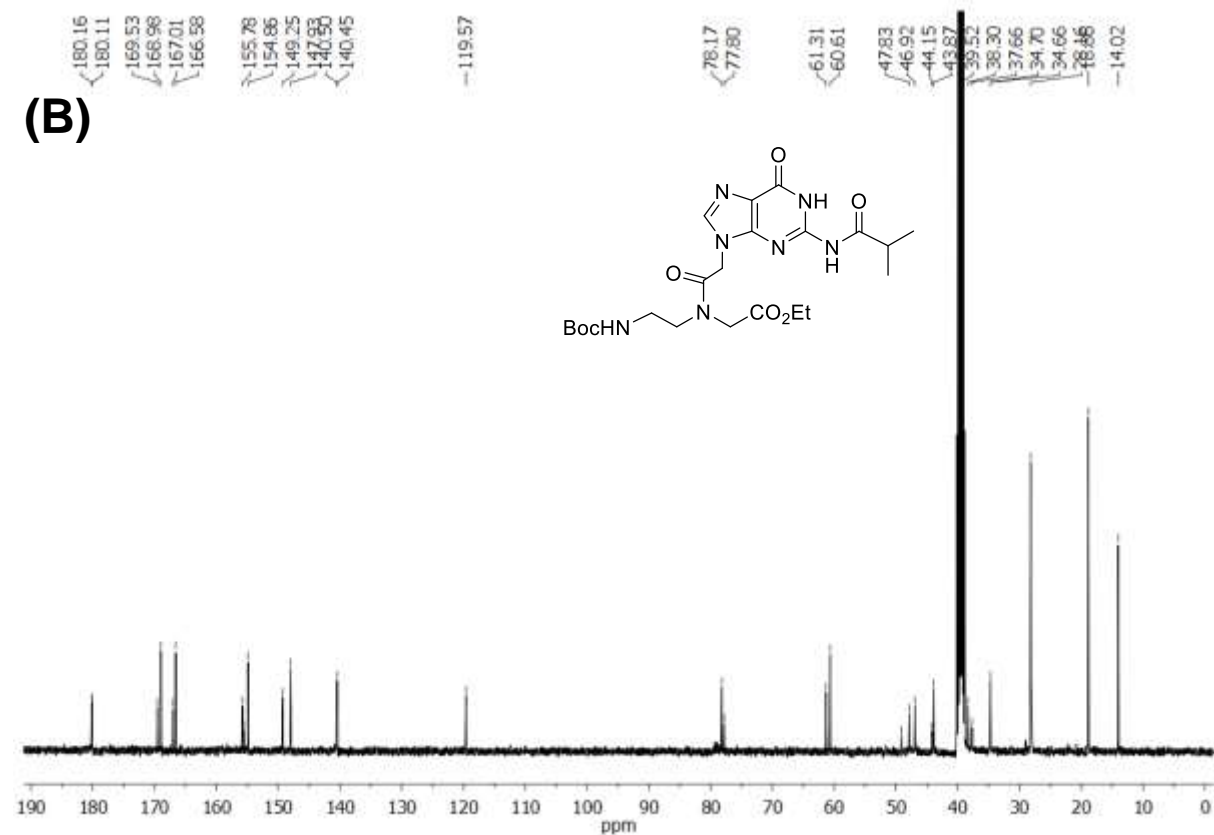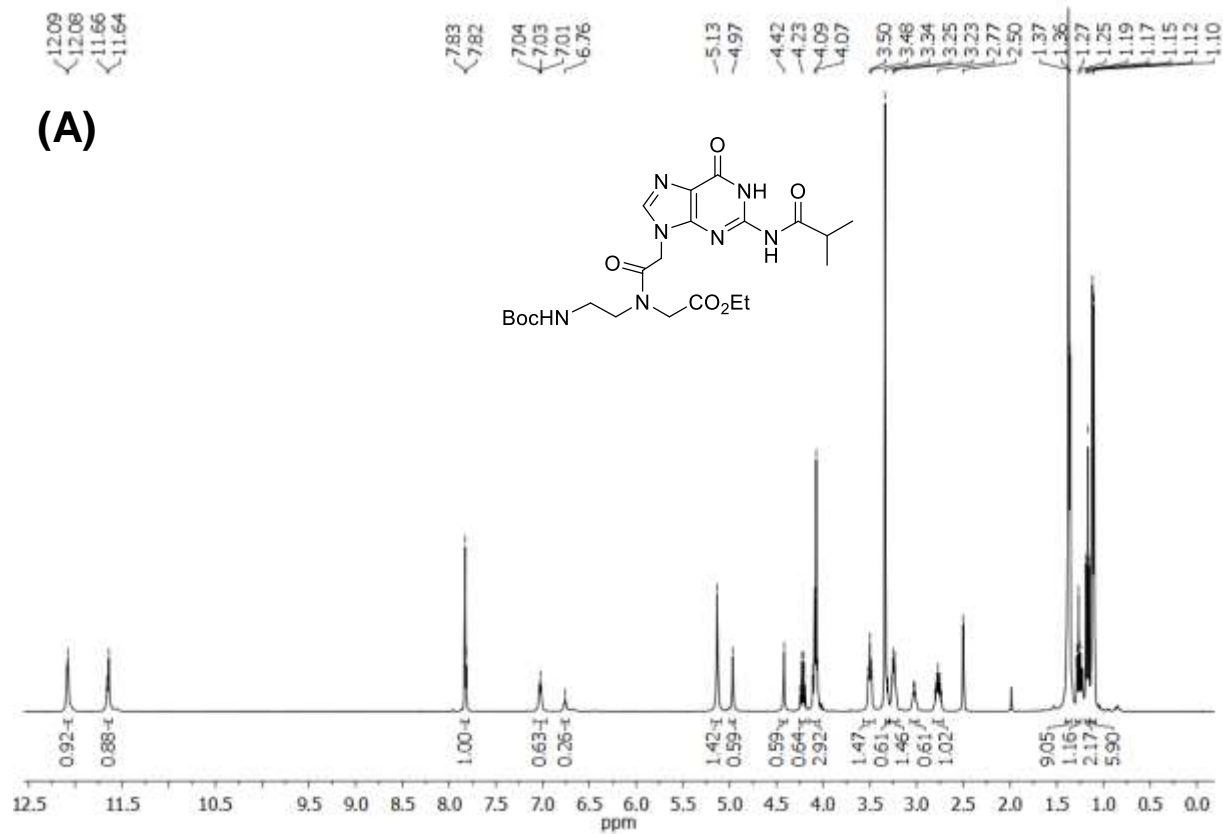
(A) $^1$H-NMR and (B) $^{13}$C-NMR spectra of **15**.

**(A)**



**(B)**
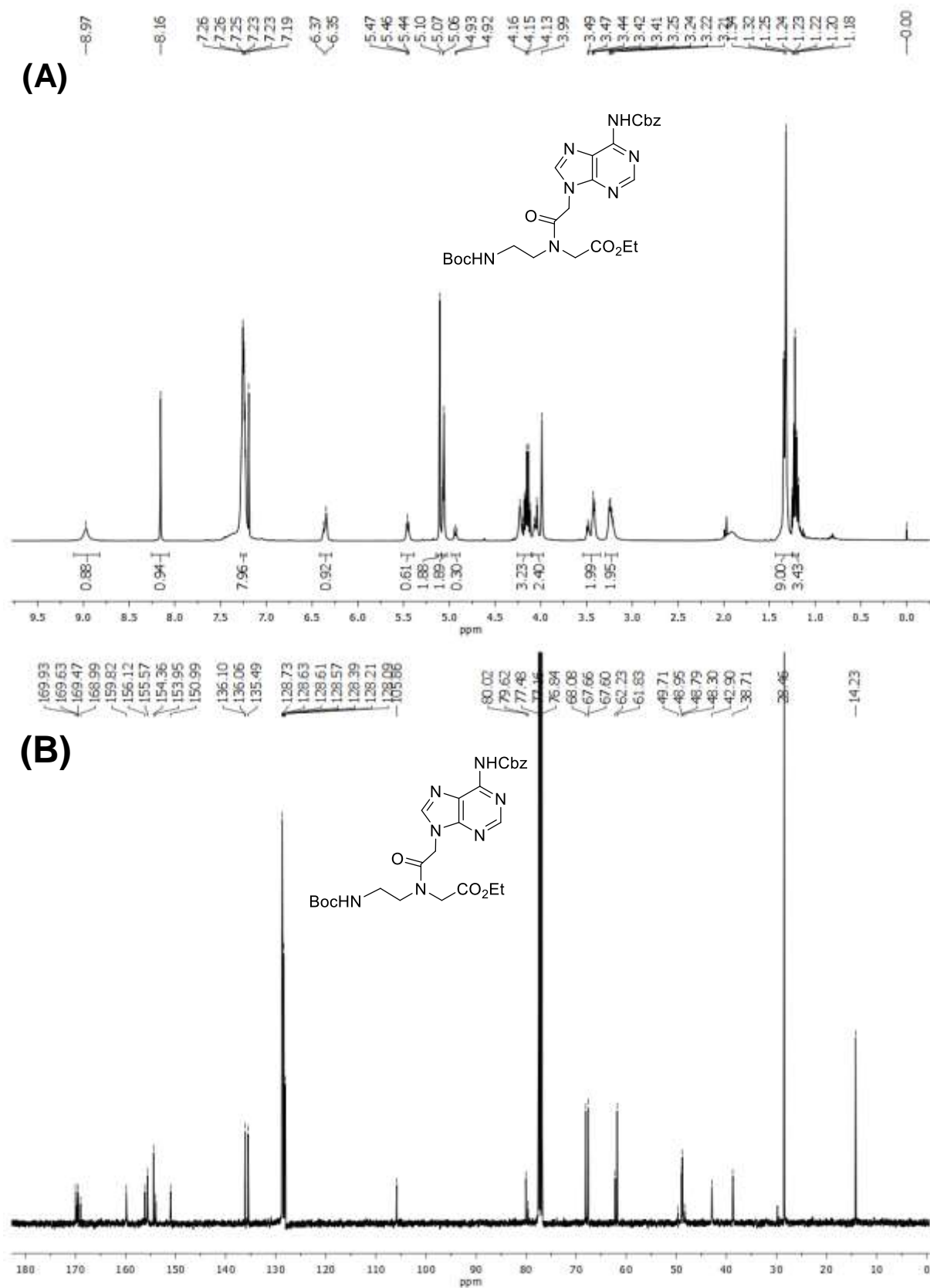


(A) $^1$H-NMR and (B) $^{13}$C-NMR spectra of **16**.

**(A)**



**(B)**
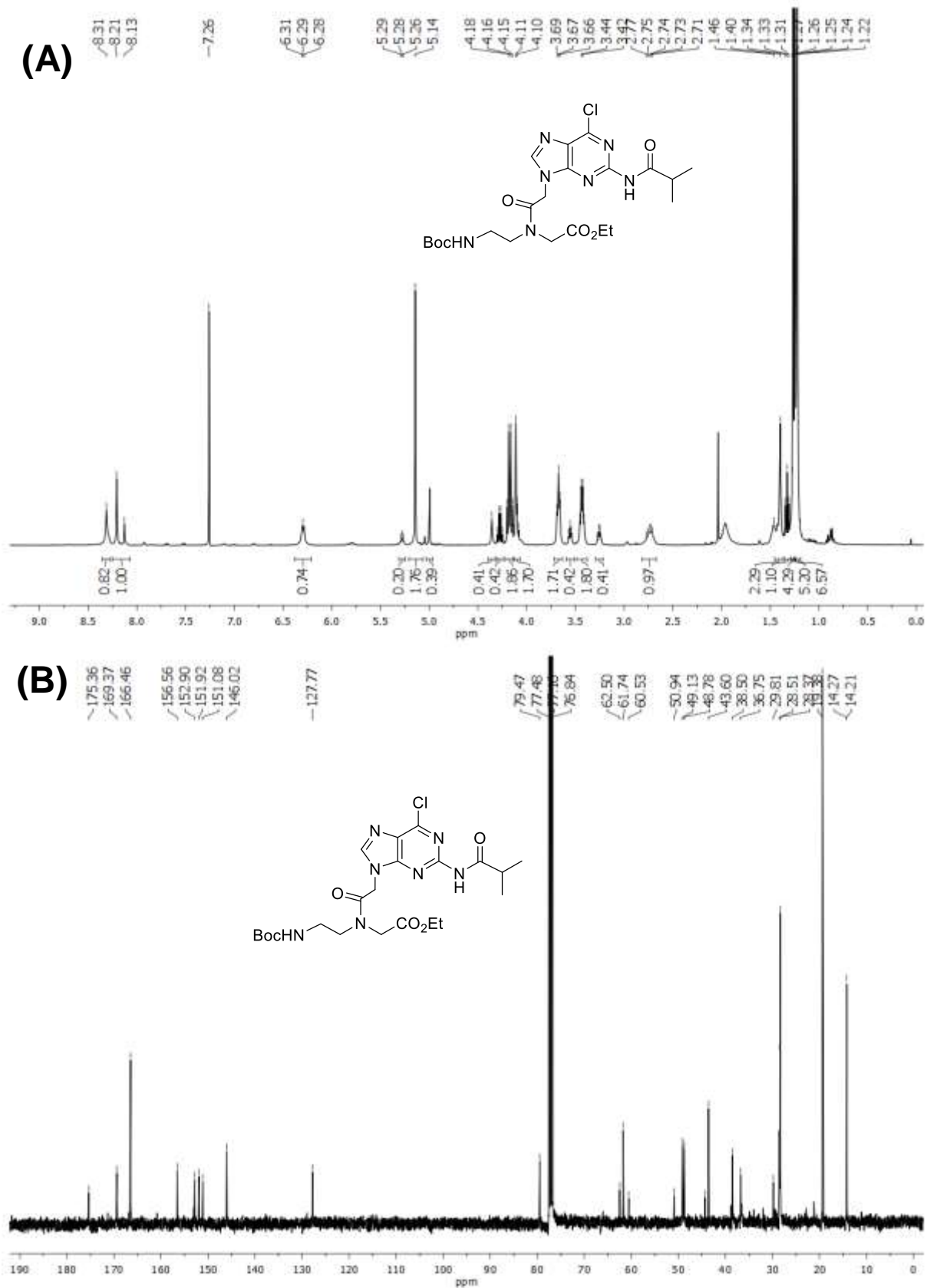


(A) $^1$H-NMR and (B) $^{13}$C-NMR spectra of **17**.
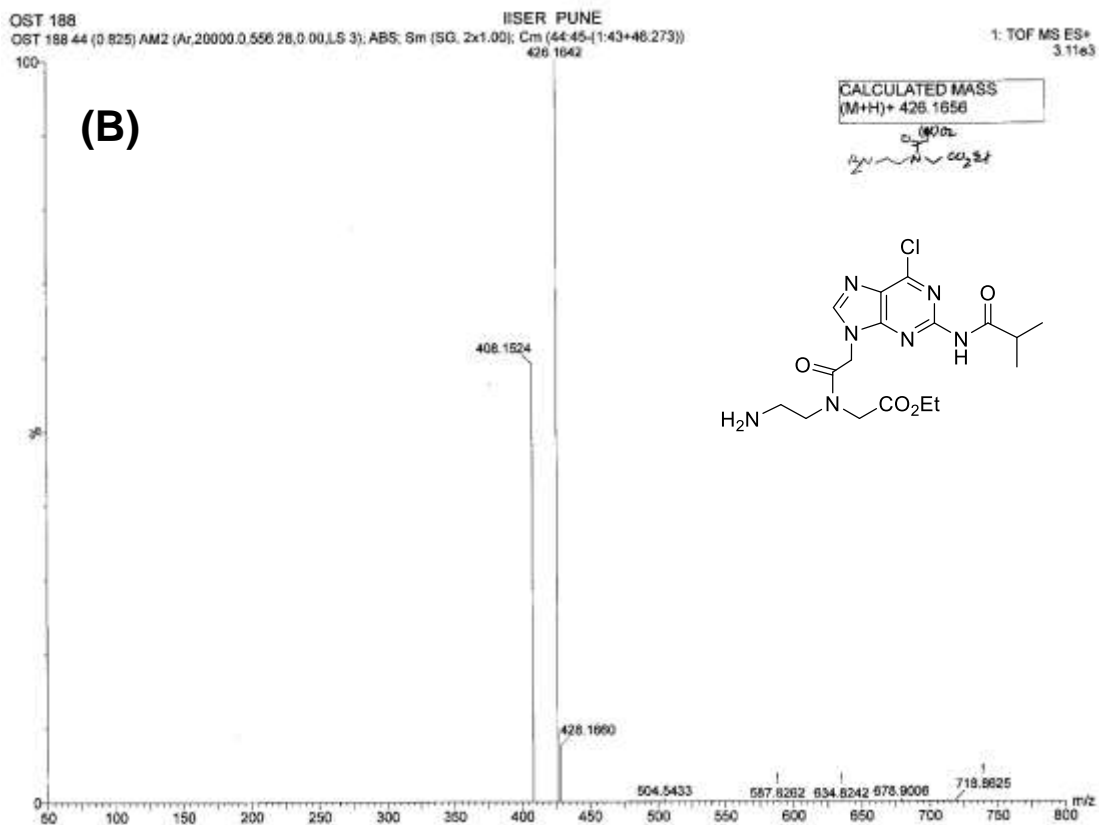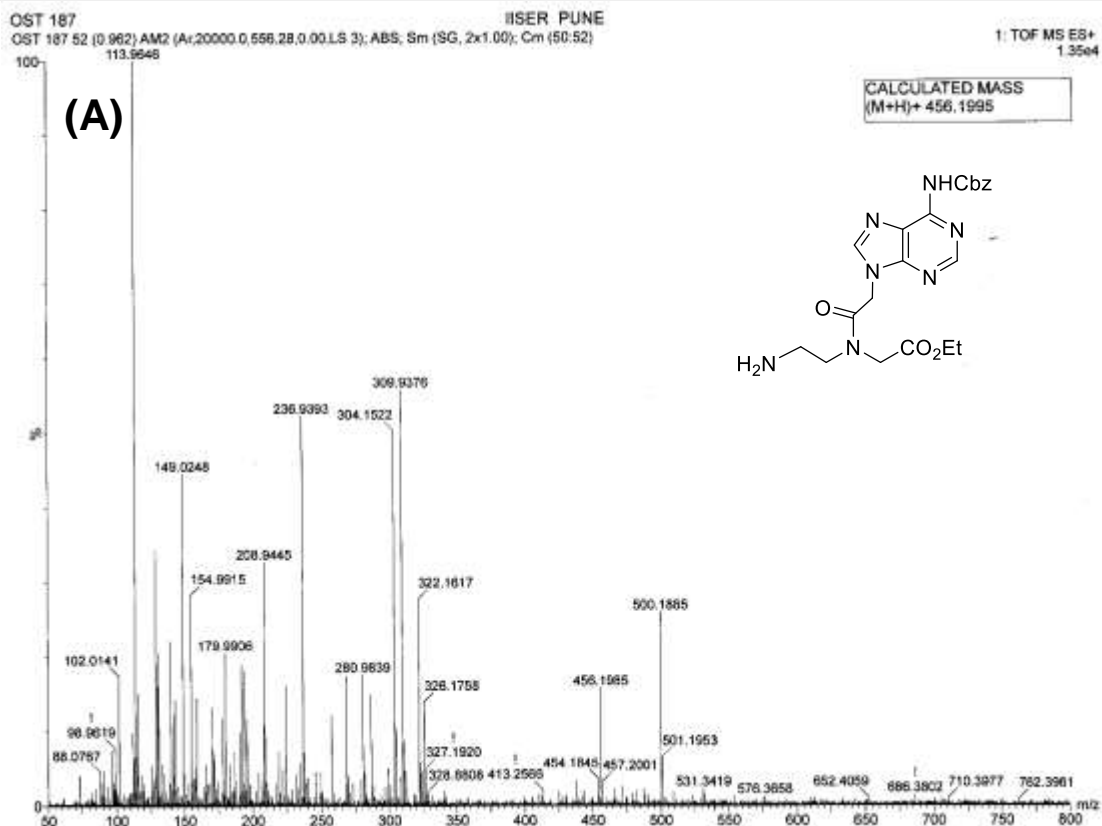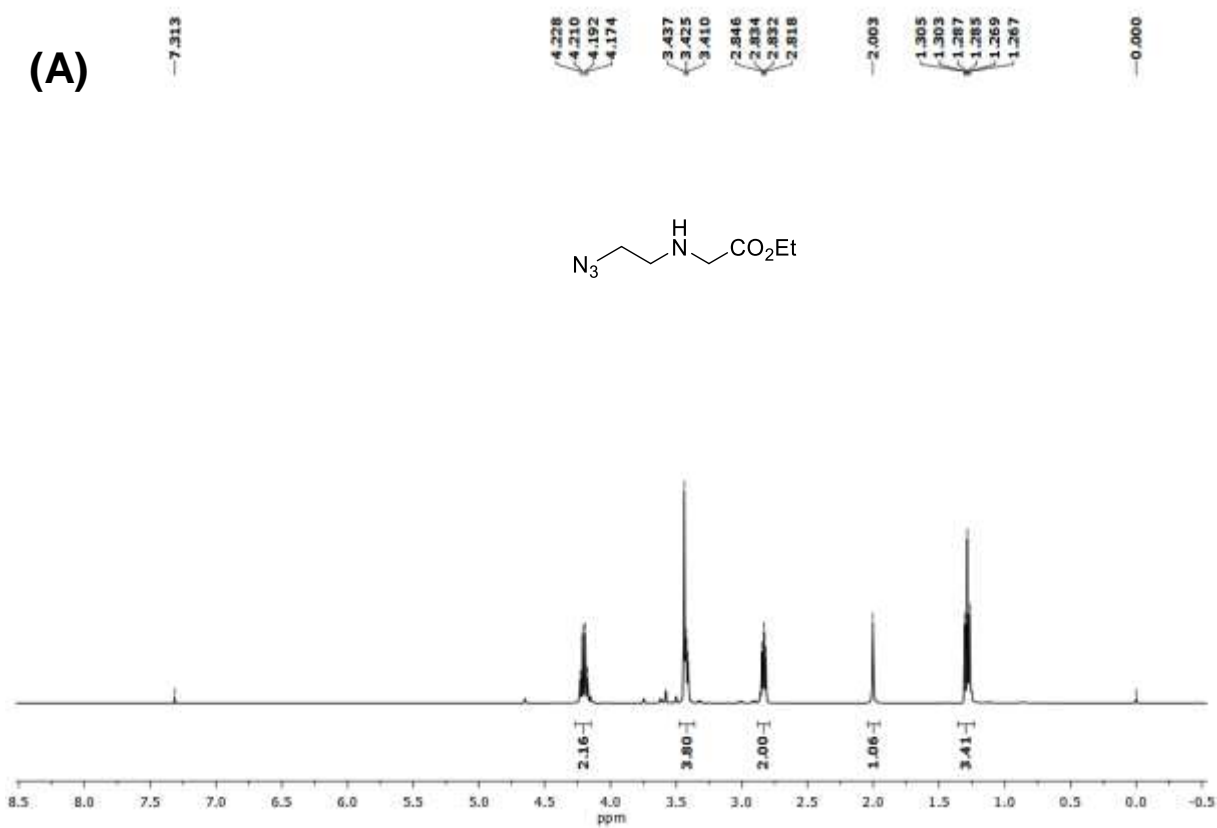
HRMS of crude intermediates (A) **2a** and (B) **2b**.

**(A)**



**(B)**



(A) $^1$H-NMR and (B) $^{13}$C-NMR spectra of **2c**.

**(A)**



**(B)**
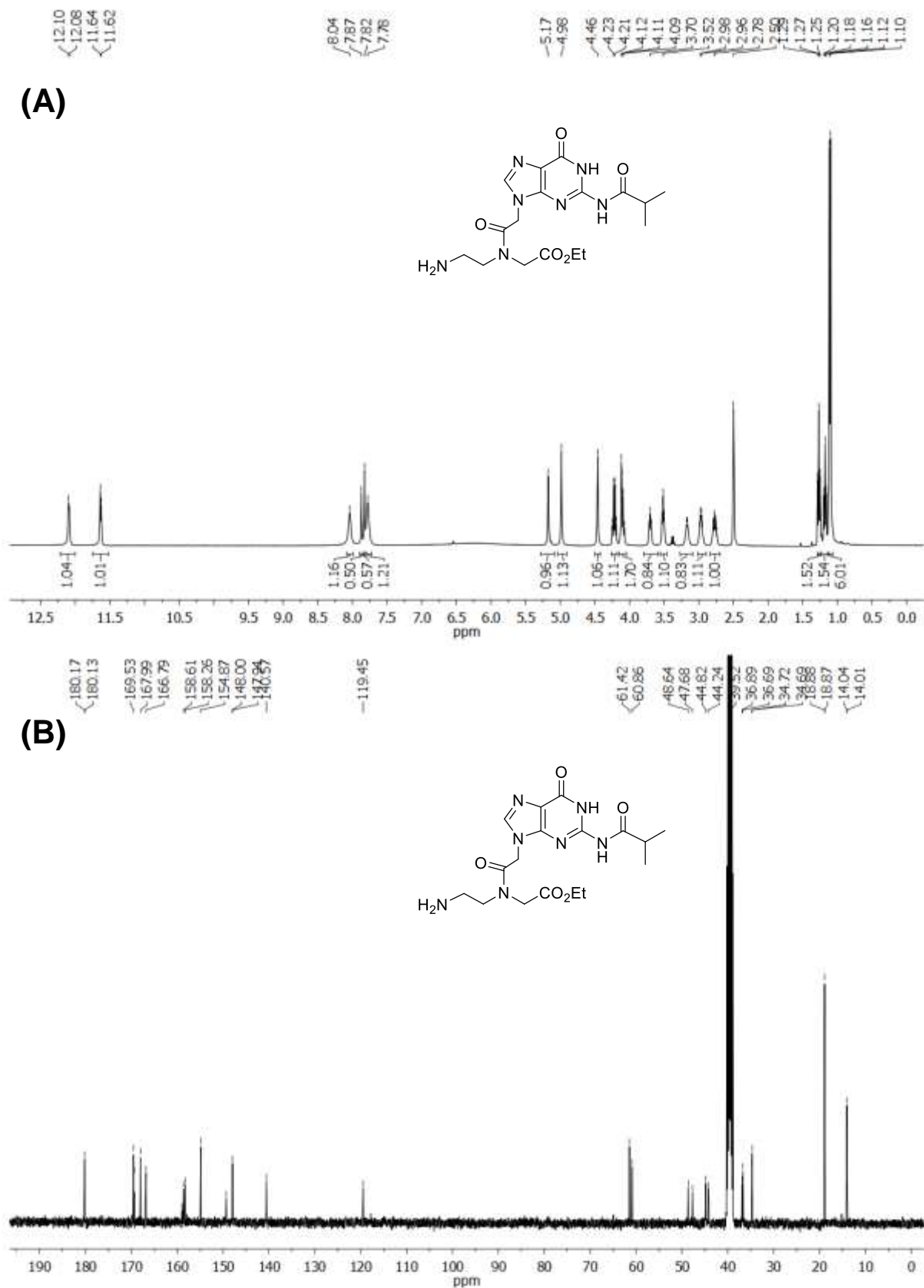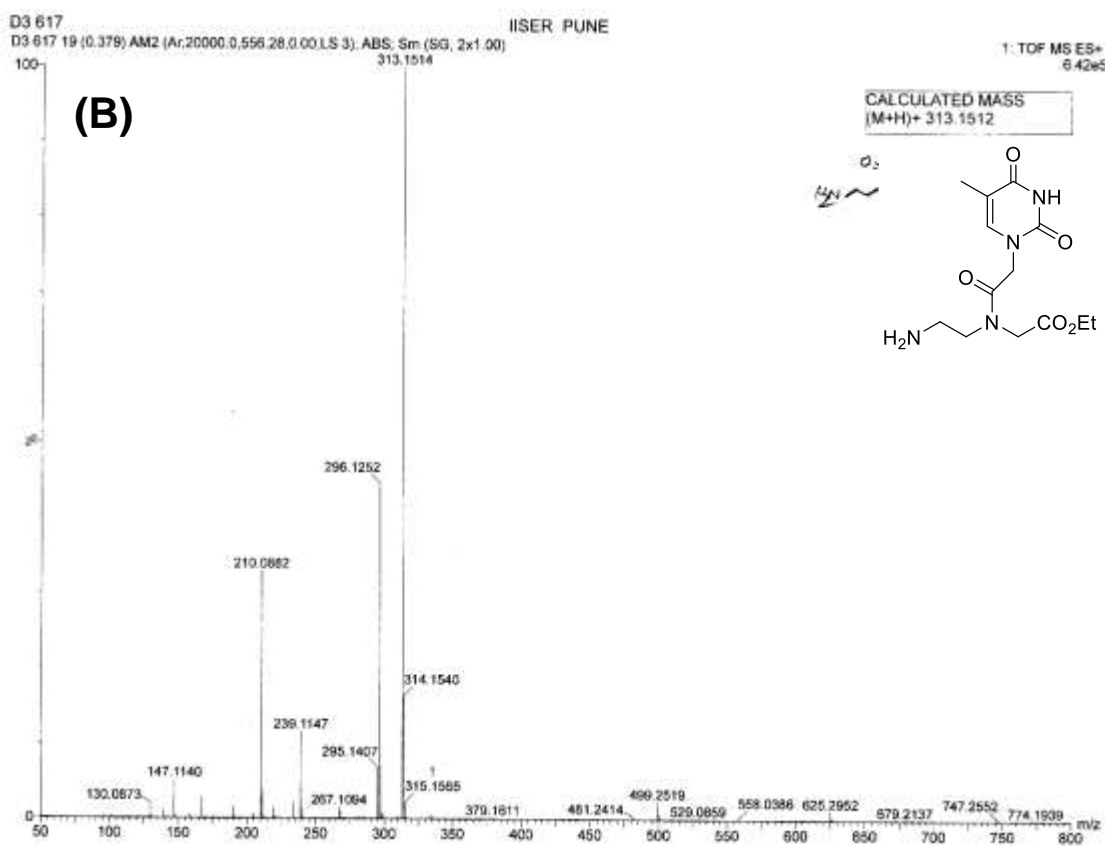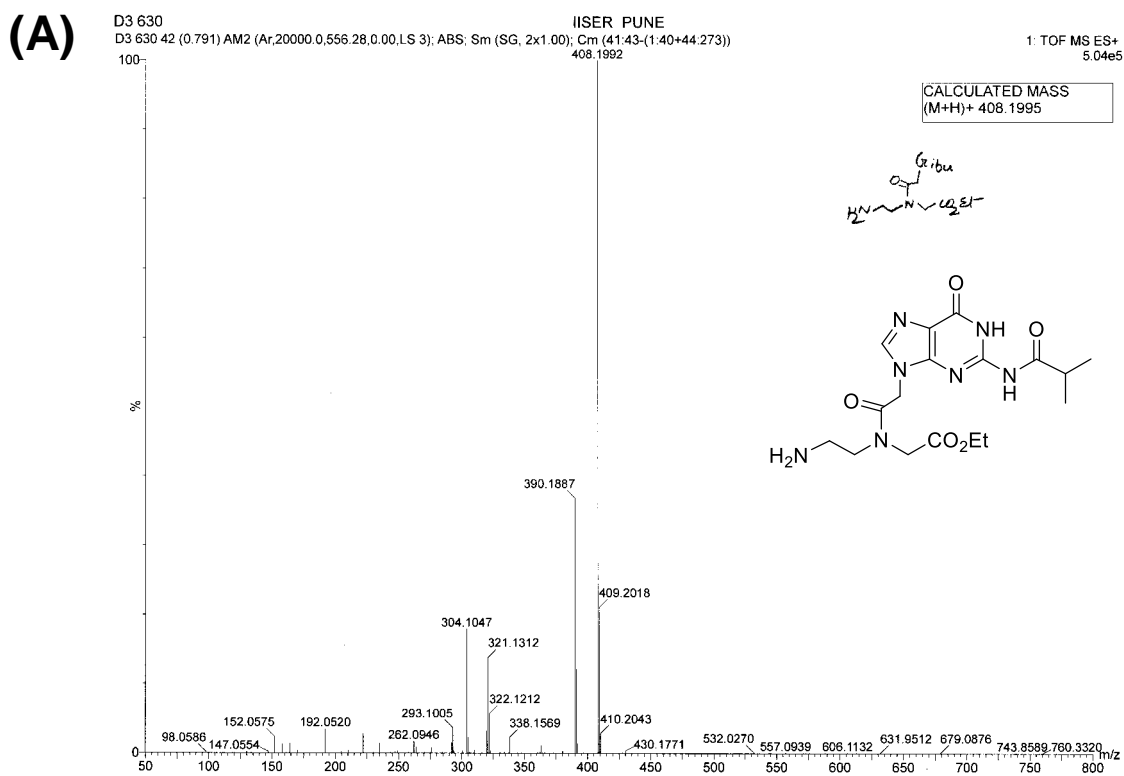


HRMS of intermediates (A) **2c** and (B) crude **2d**.

**(A)**



**(B)**
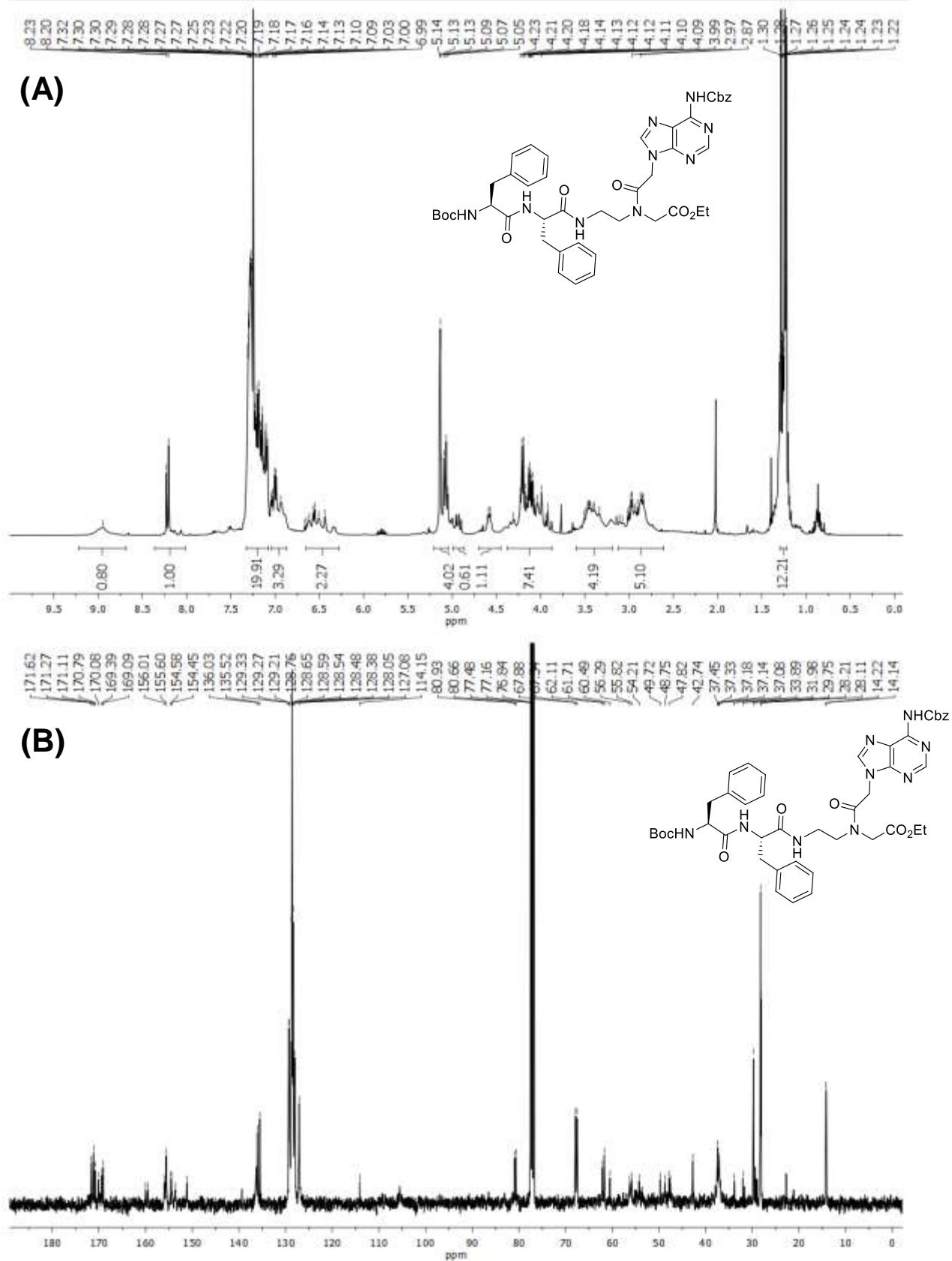


(A) ¹H-NMR and (B) ¹³C-NMR spectra of peptide **3a**.

(A) $^1$H-NMR and (B) $^{13}$C-NMR spectra of peptide **3b**.
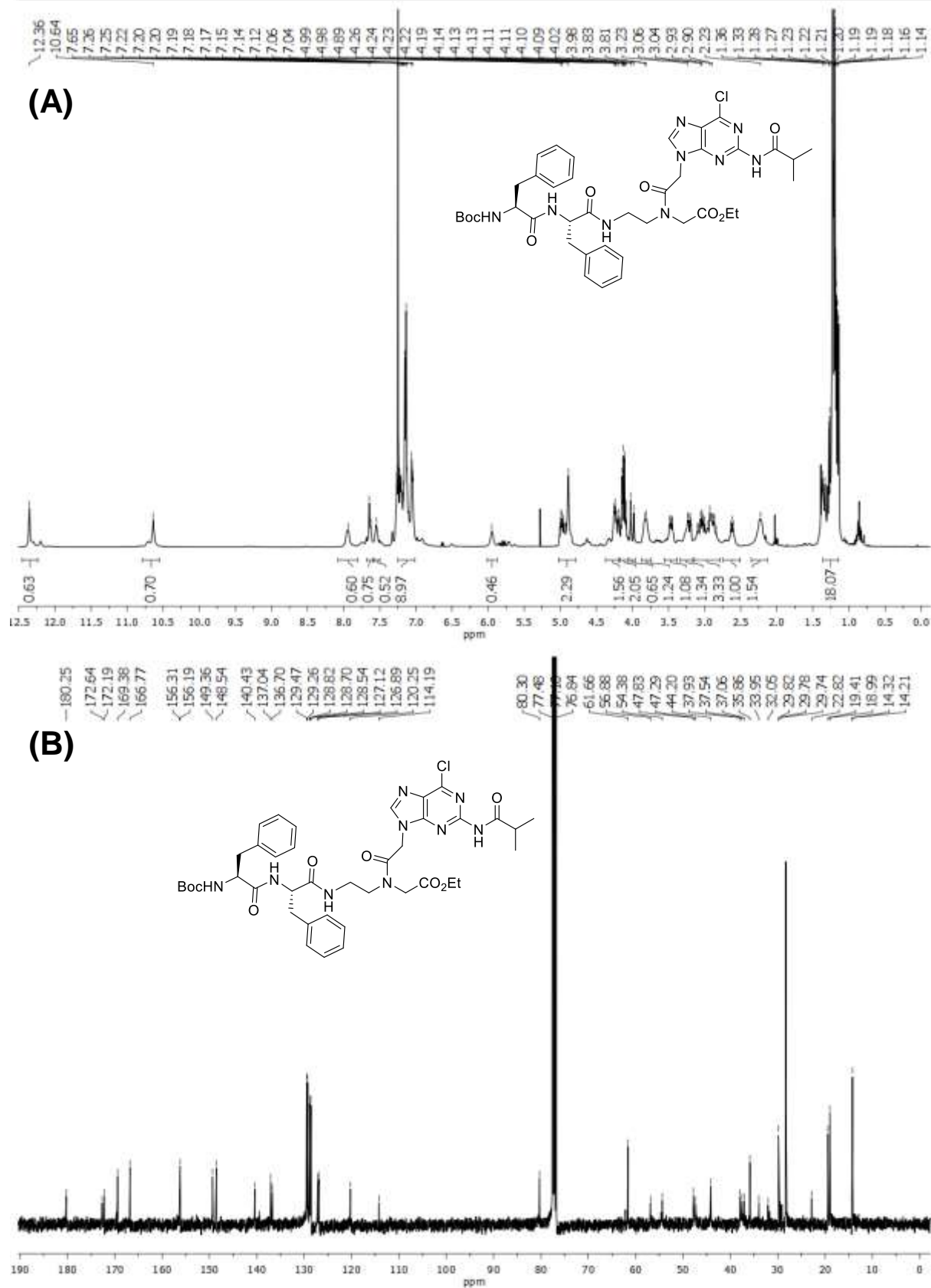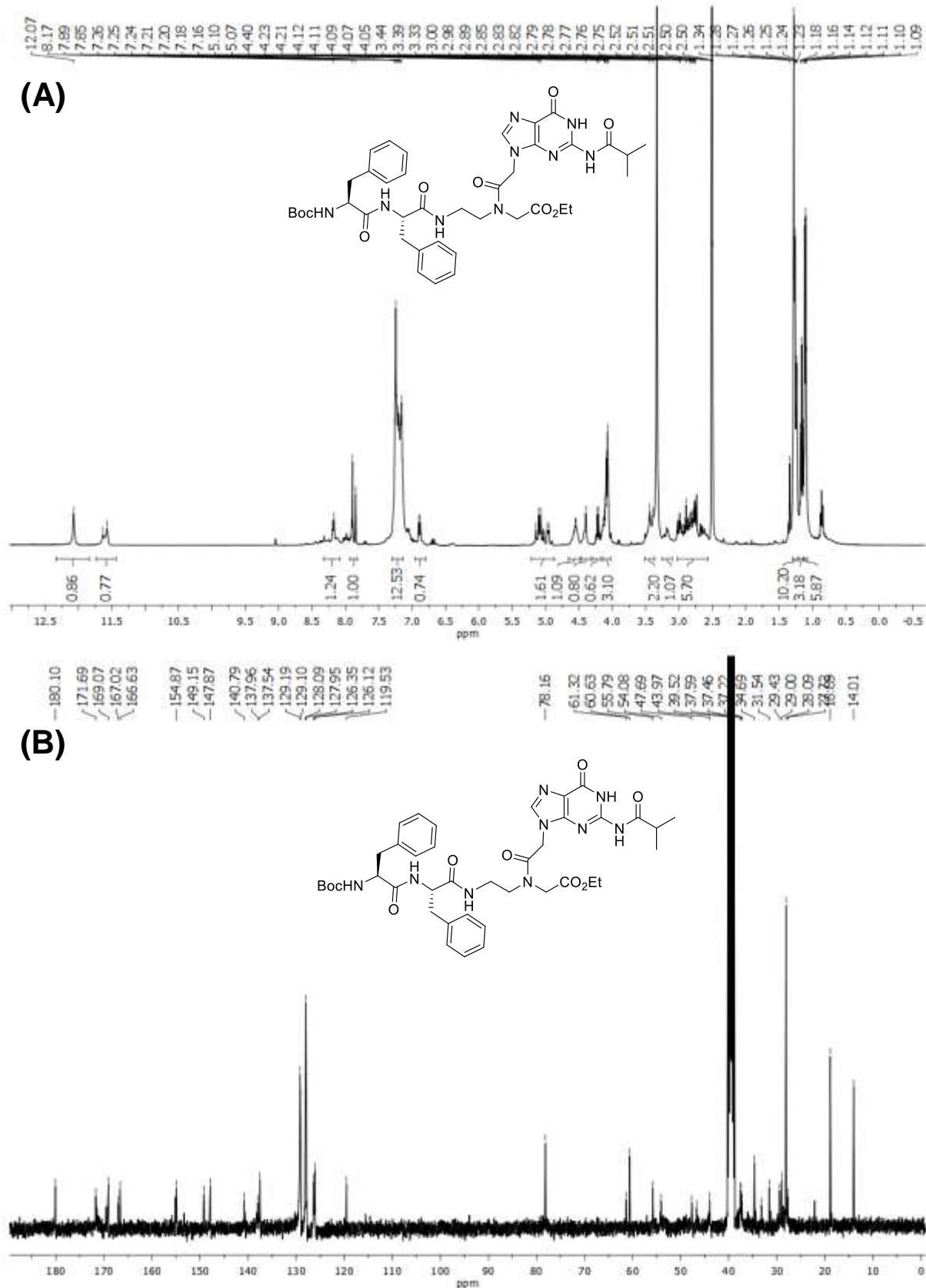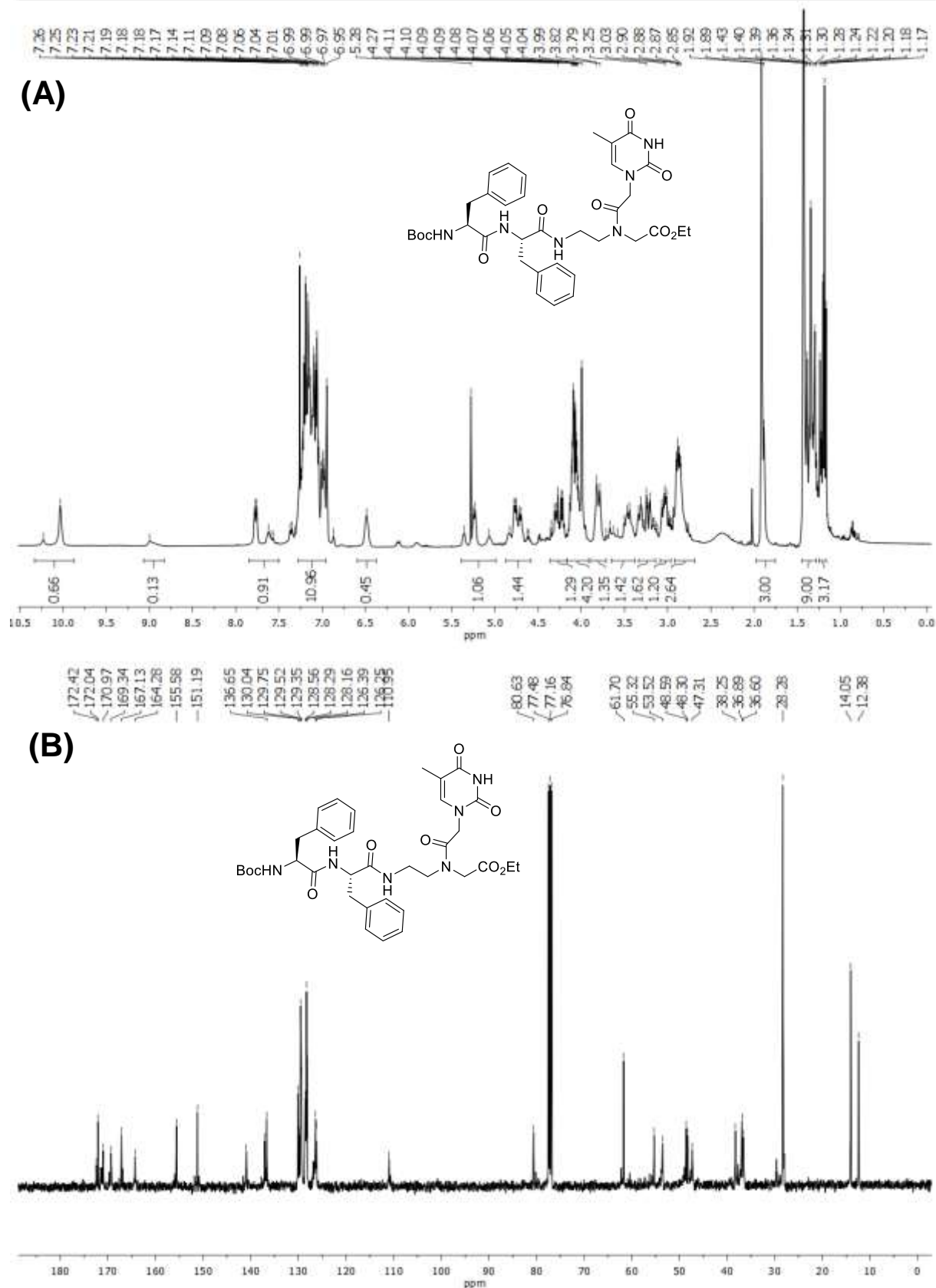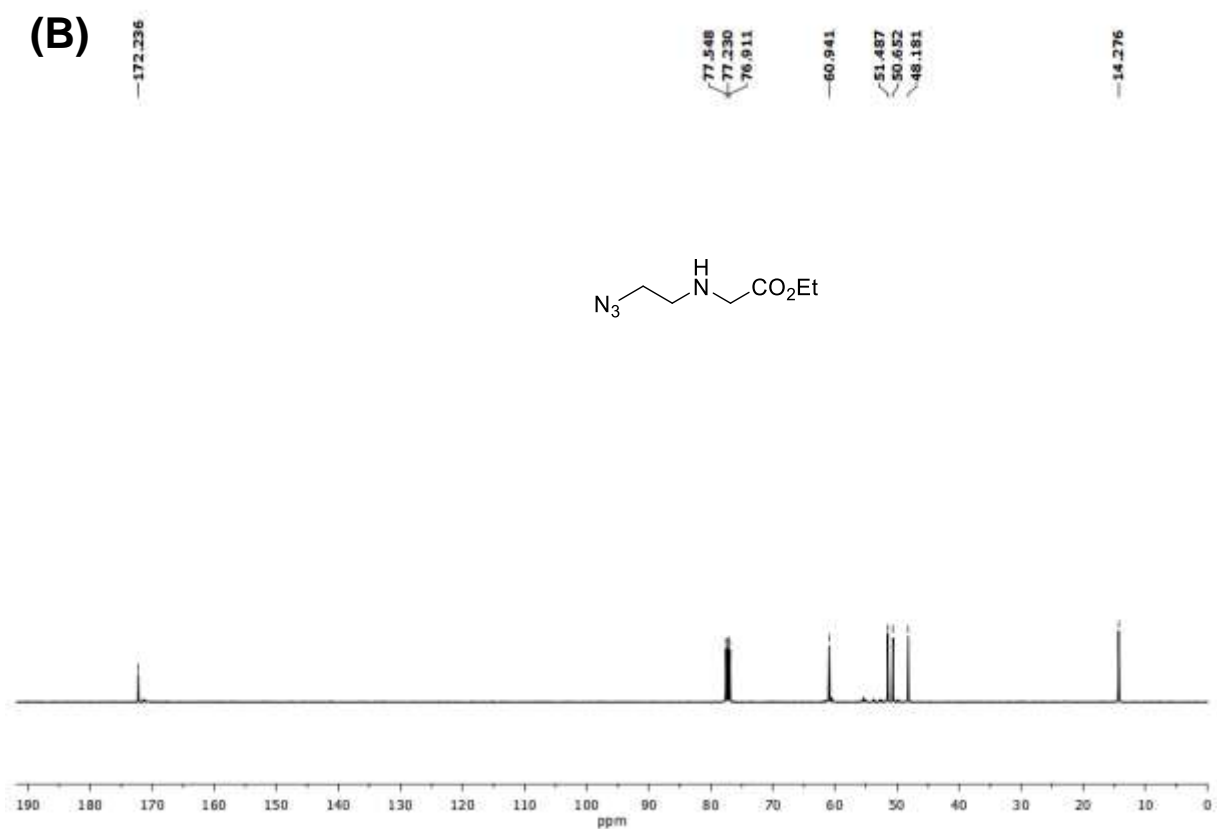
(A) ¹H-NMR and (B) ¹³C-NMR spectra of peptide **3c**.
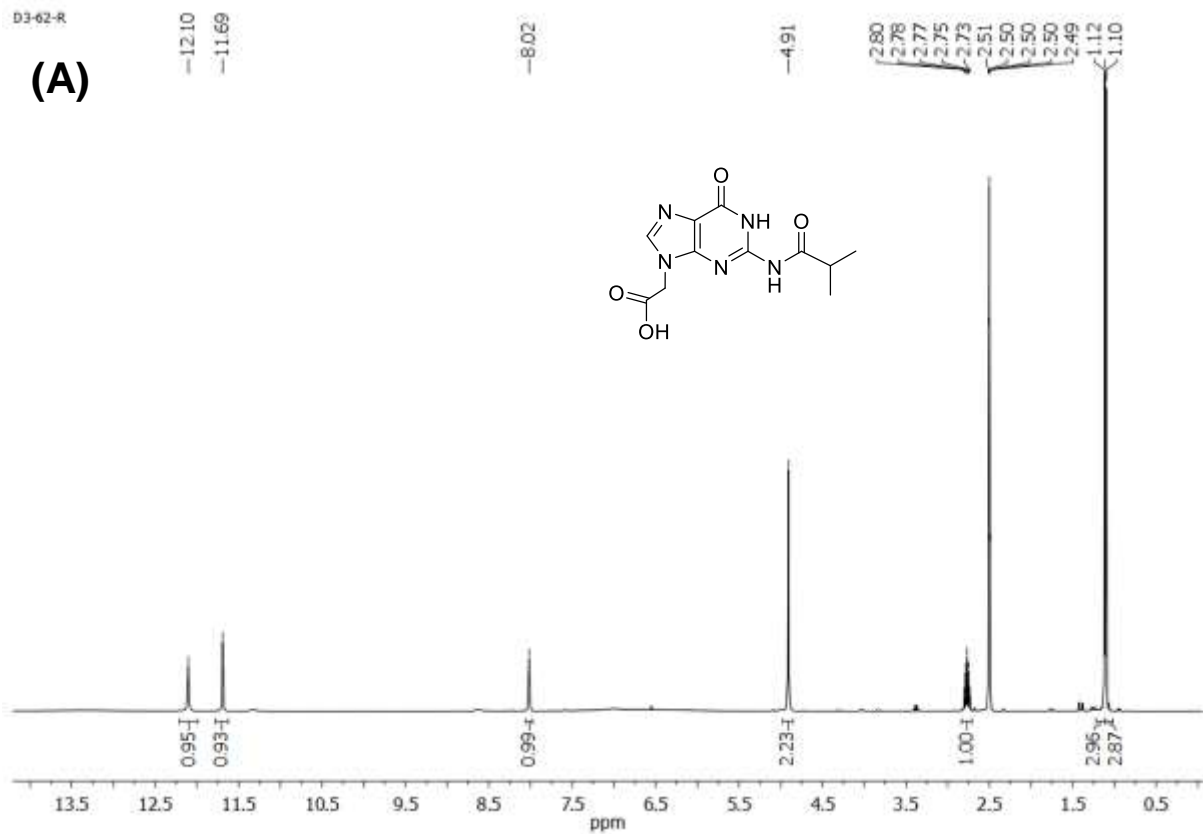
**(A)**



**(B)**



(A) ^{1}H-NMR and (B) ^{13}C-NMR spectra of peptide **3d**.

**(A)**



**(B)**



(A) $^1$H-NMR and (B) $^{13}$C-NMR spectra of **18**.

**(A)**



**(B)**



(A) $^1$H-NMR and (B) $^{13}$C-NMR spectra of peptide **4**.

**(A)**



**(B)**



(A) $^1$H-NMR and (B) $^{13}$C-NMR spectra of $\mathbf{A^{N(Boc)2}}$-$\mathbf{\textit{N}^9}$-**acetic acid**.

**(A)**

D3-62-R

−12.10
−11.69
−8.02
−4.91
2.80
2.78
2.77
2.75
2.73
2.51
2.50
2.50
2.50
2.49
1.12
1.10

0.95
0.93
0.99
2.23
1.00
2.96
2.87

13.5  12.5  11.5  10.5  9.5  8.5  7.5  6.5  5.5  4.5  3.5  2.5  1.5  0.5
ppm

**(B)**

D3-621

−180.18
−168.98
−154.68
148.94
148.17
−140.31
−119.34
44.49
34.70
−18.96

190  180  170  160  150  140  130  120  110  100  90  80  70  60  50  40  30  20  10  0
ppm
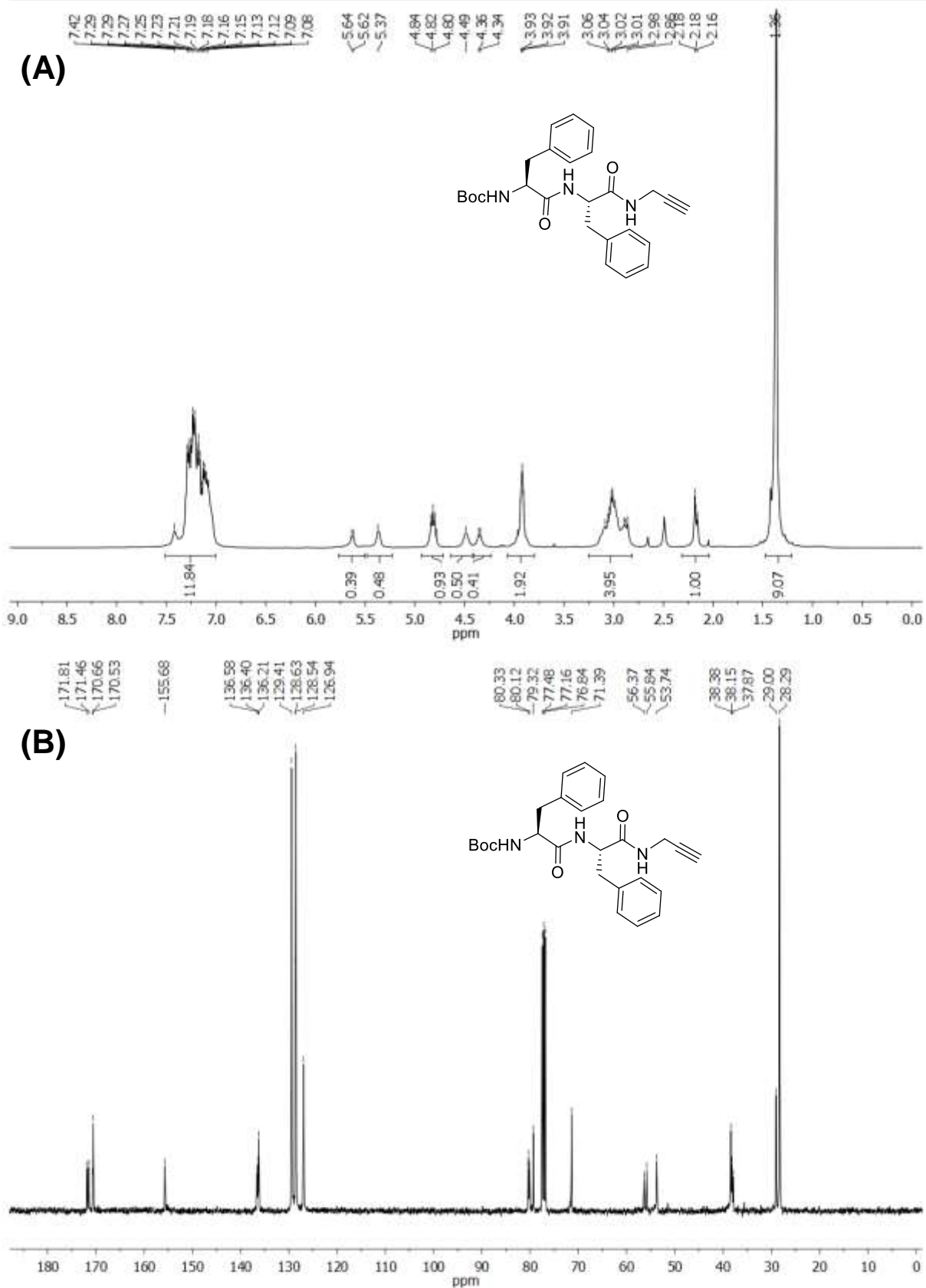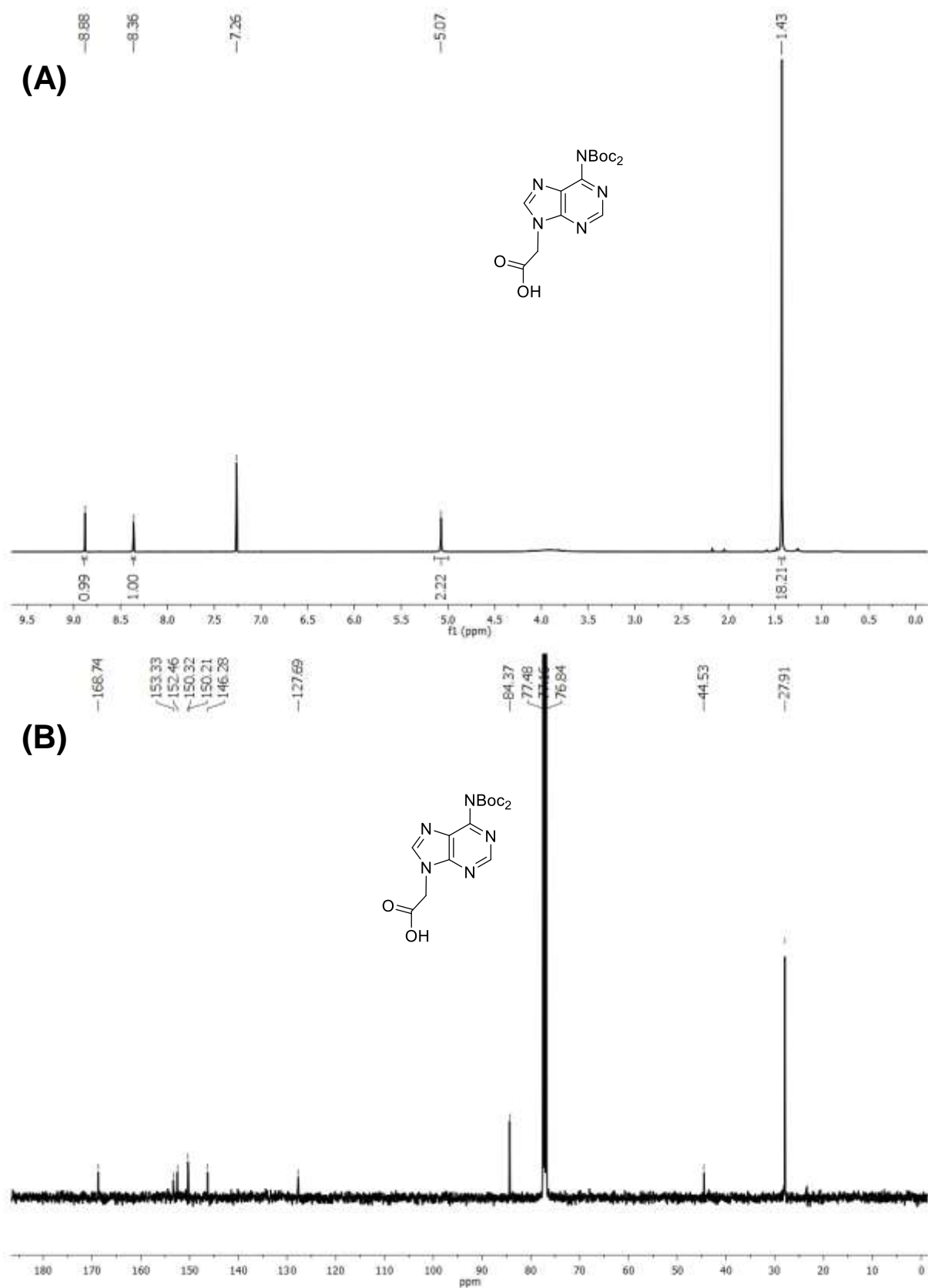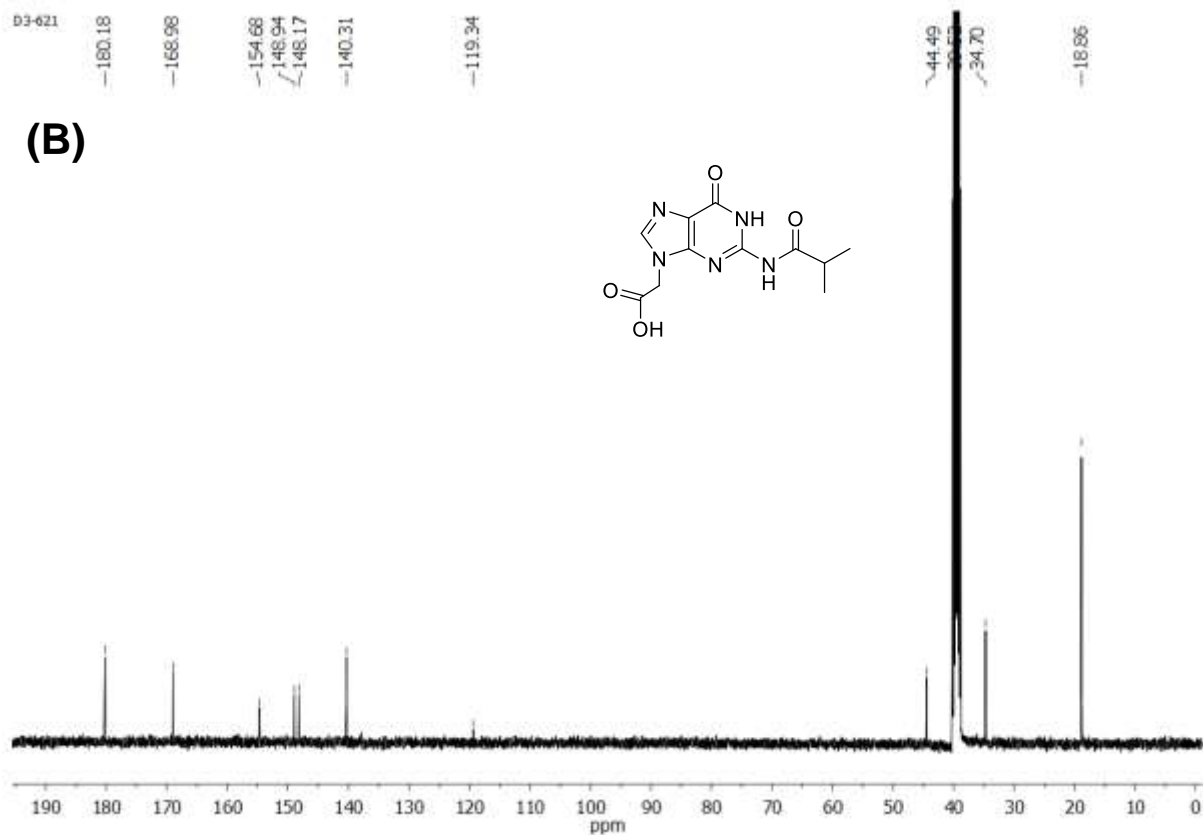
(A) $^1$H-NMR and (B) $^{13}$C-NMR spectra of **G$^{ibu}$-$N^9$-acetic acid**.

**(A)**



**(B)**
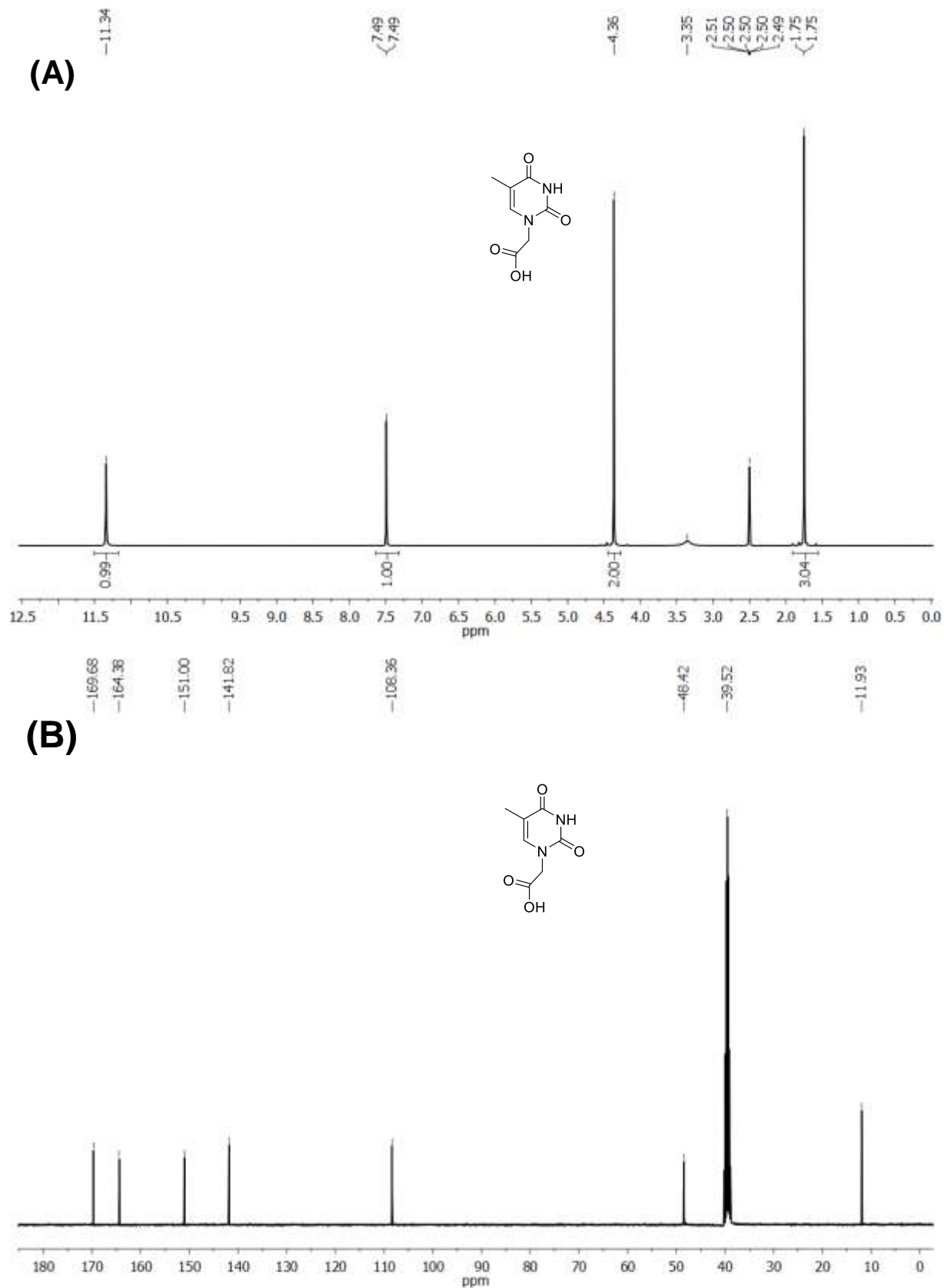


(A) ^{1}H-NMR and (B) ^{13}C-NMR spectra of **Thymine-1-acetic acid**.

**(A)**



**(B)**
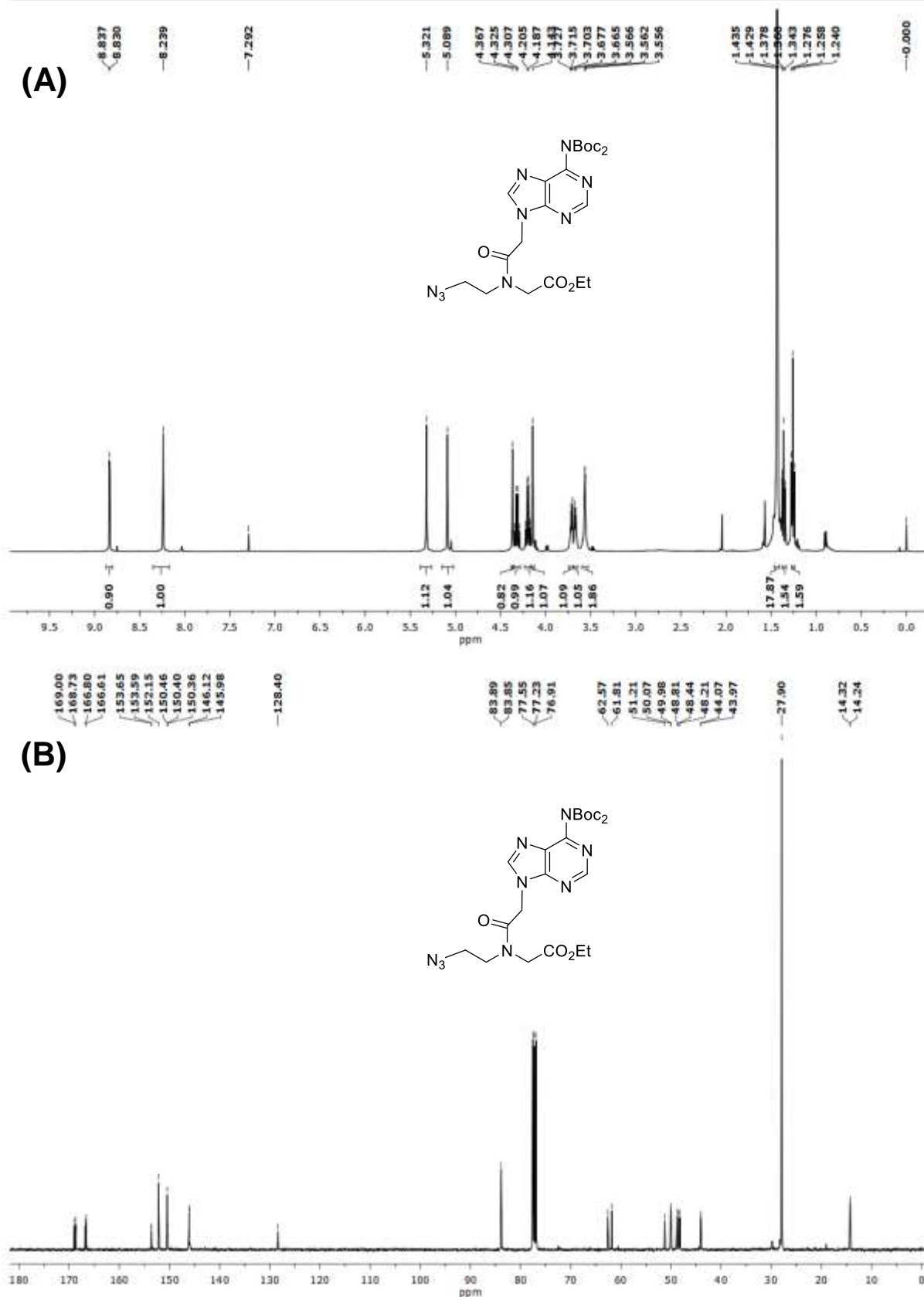


(A) $^1$H-NMR and (B) $^{13}$C-NMR spectra of **5a**.
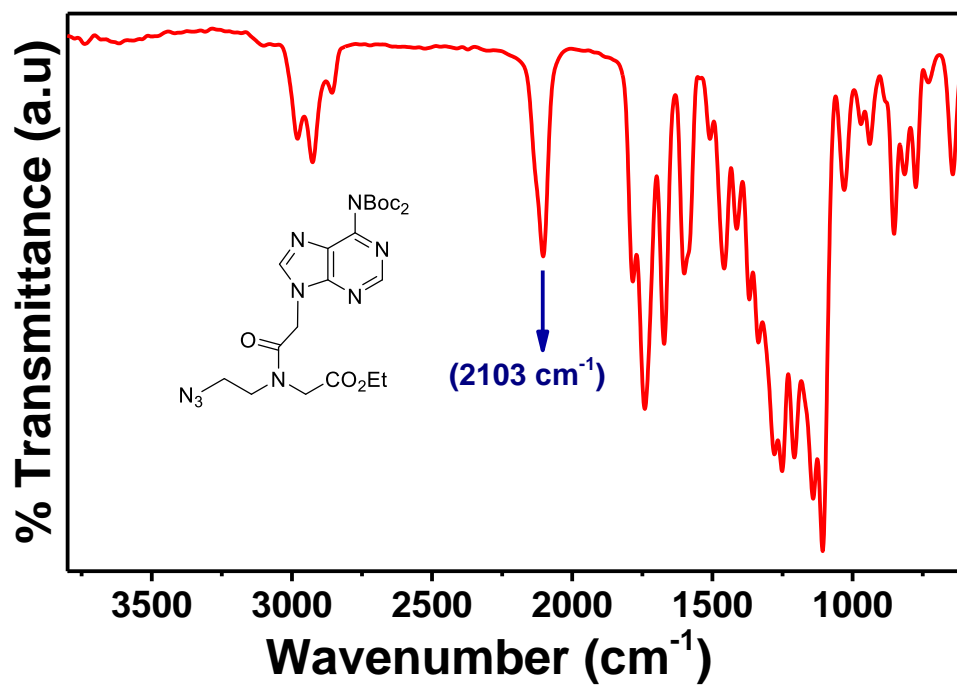
FTIR spectrum of **5a**.
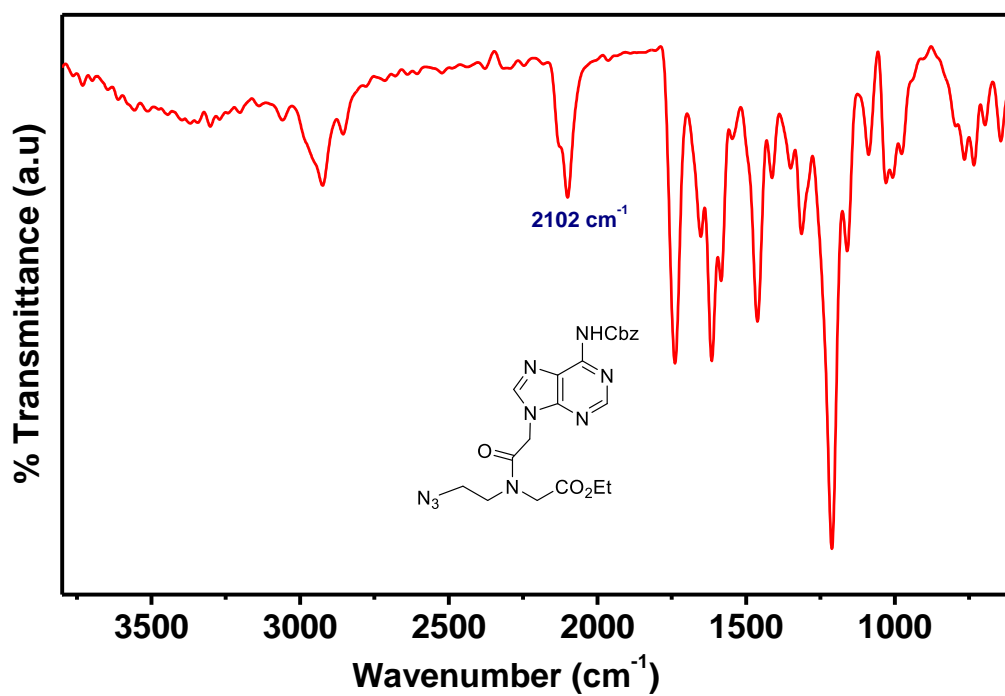


FTIR spectrum of **5b**.
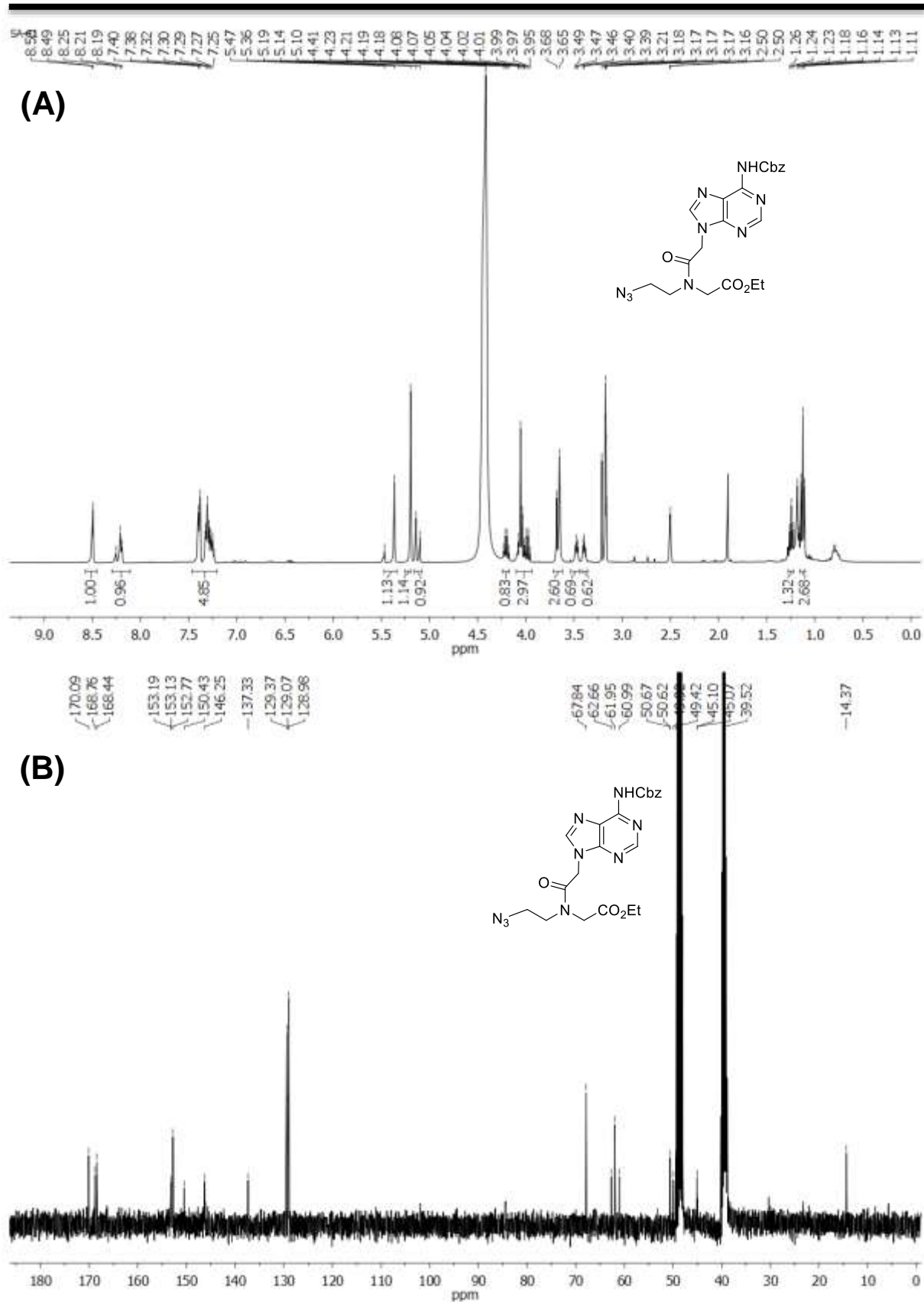
(A) $^1$H-NMR and (B) $^{13}$C-NMR spectra of **5b**.

**(A)**



**(B)**
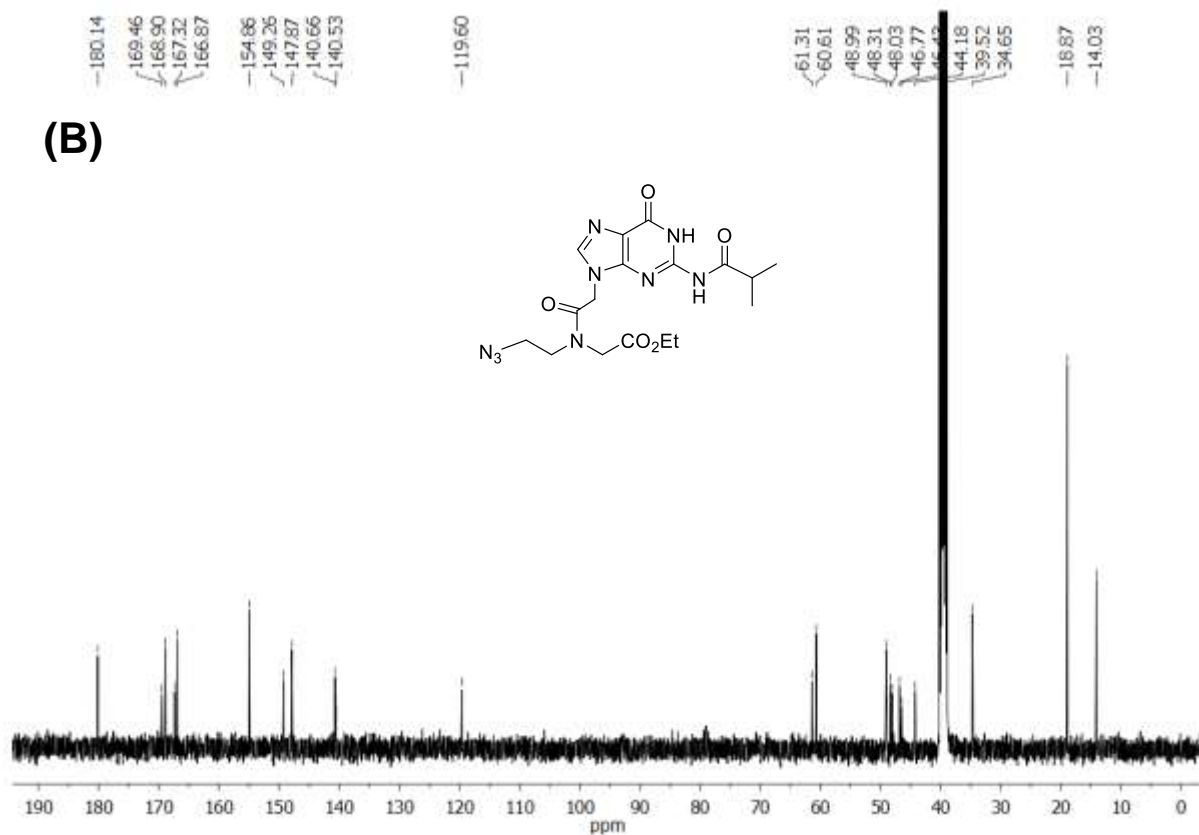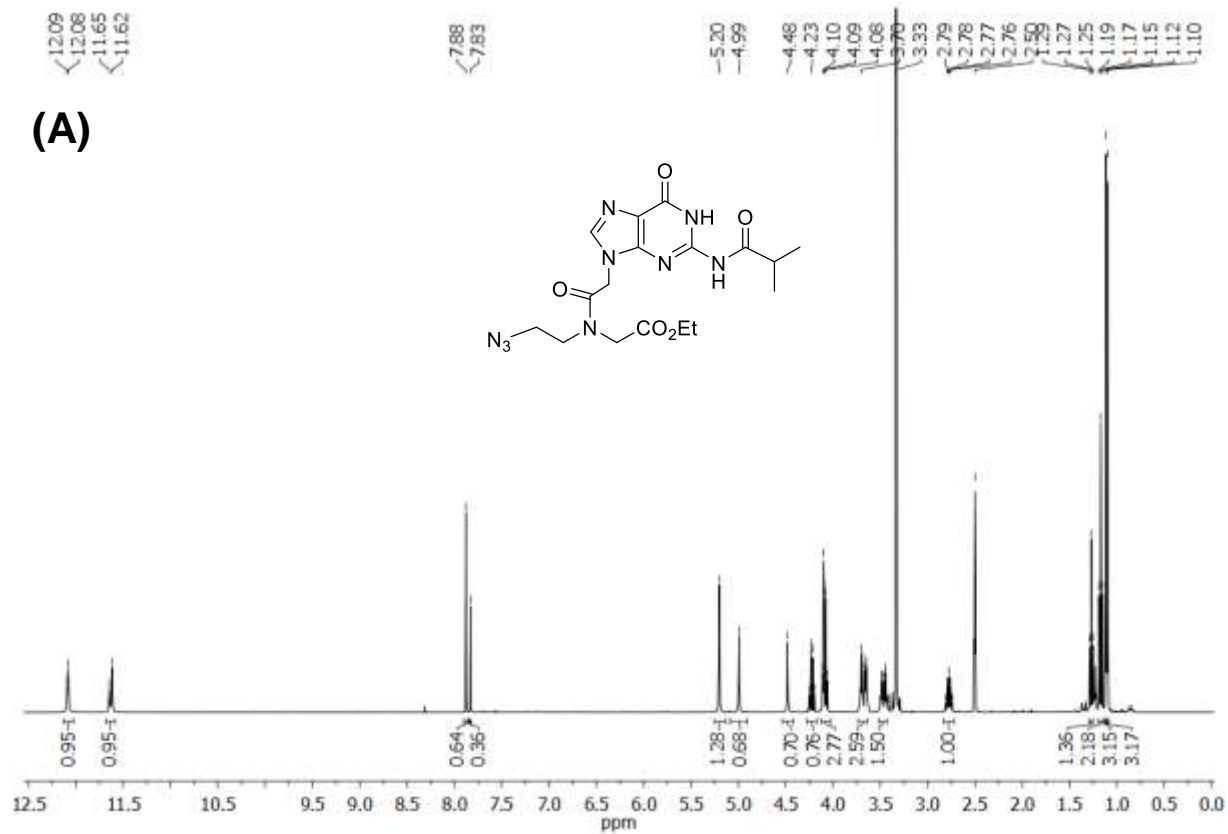


(A) $^1$H-NMR and (B) $^{13}$C-NMR spectra of **5c**.
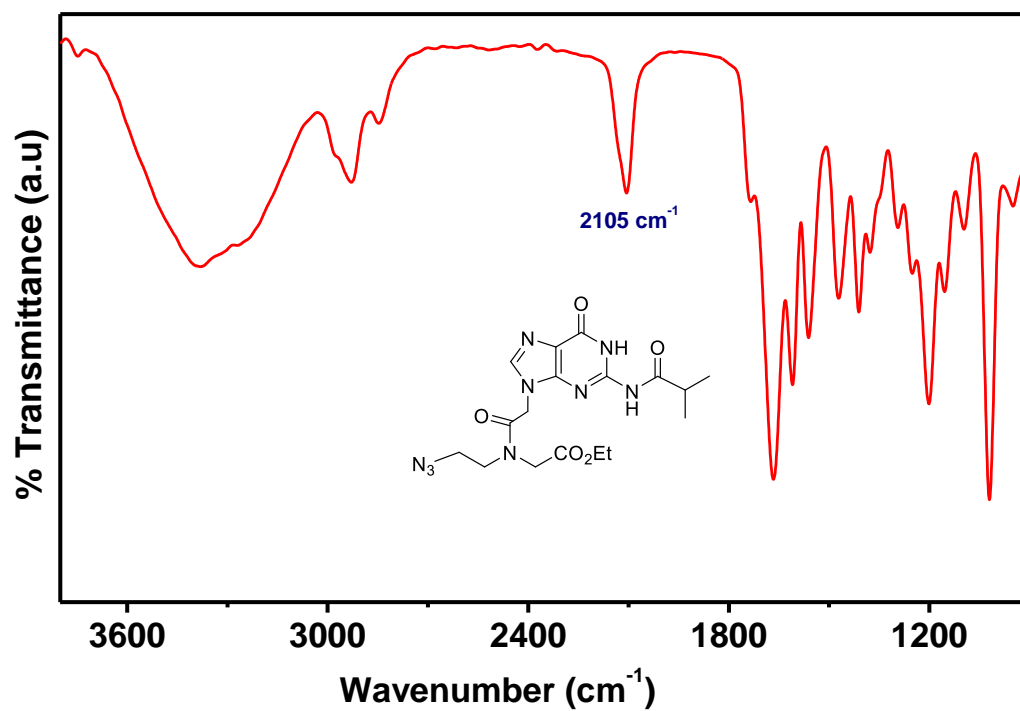
FTIR spectrum of **5c**.
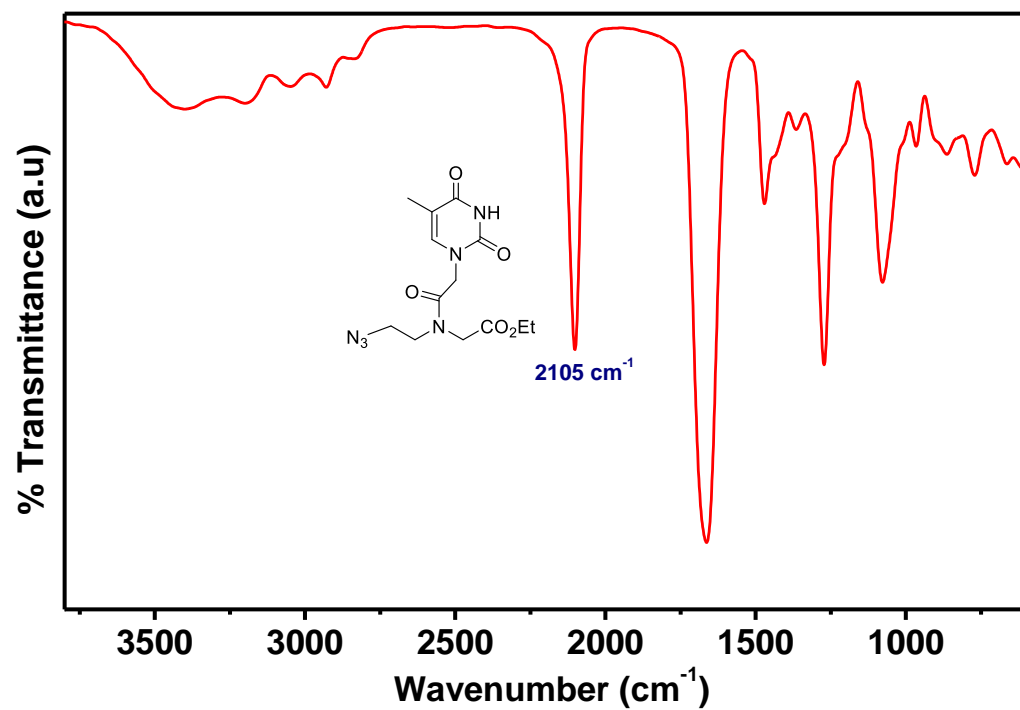


FTIR spectrum of **5d**.

**(A)**



**(B)**
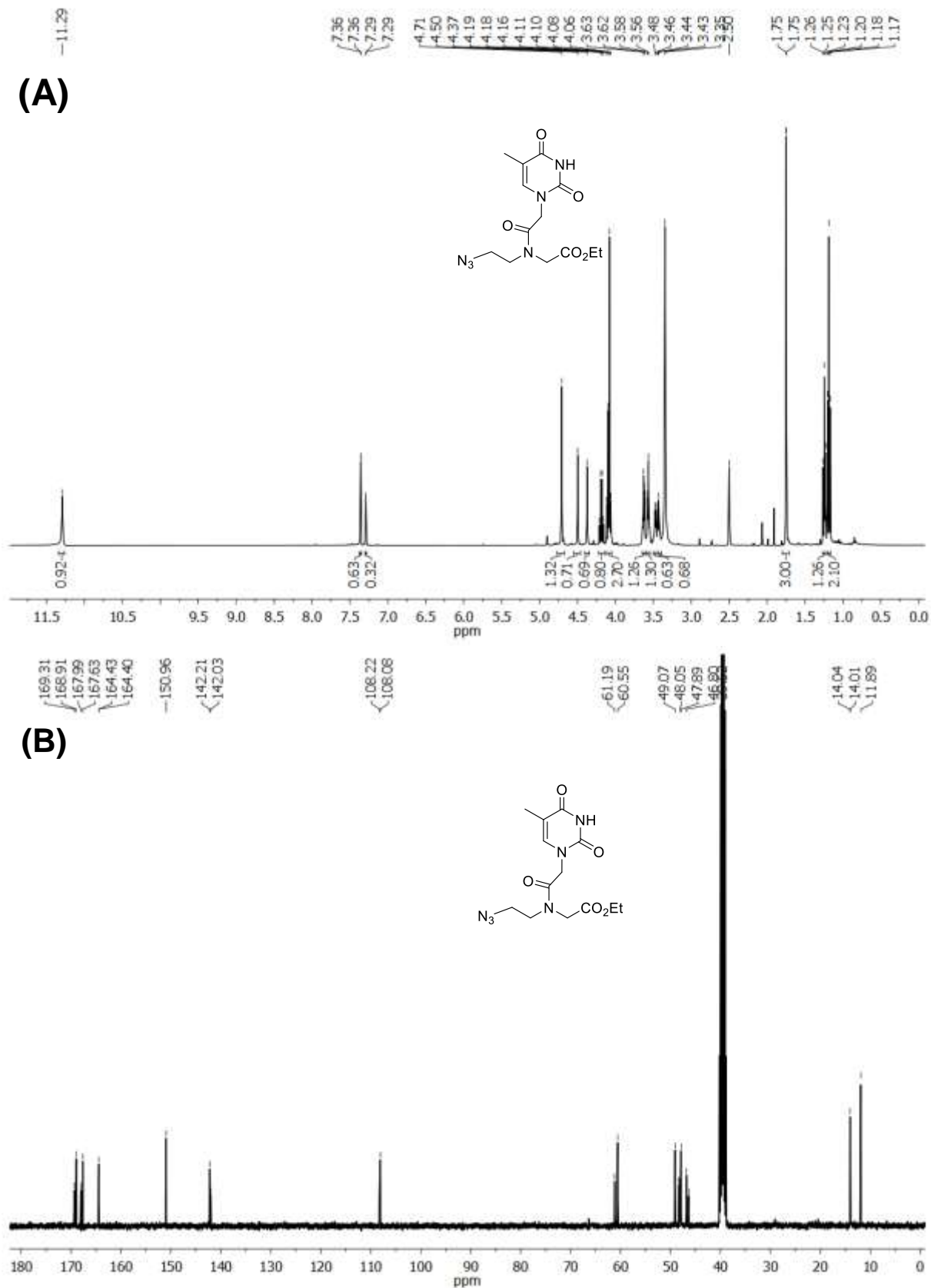


(A) $^1$H-NMR and (B) $^{13}$C-NMR spectra of **5d**.

**(A)**



**(B)**



(A) $^1$H-NMR and (B) $^{13}$C-NMR spectra of peptide **6a**.

**(A)**



**(B)**
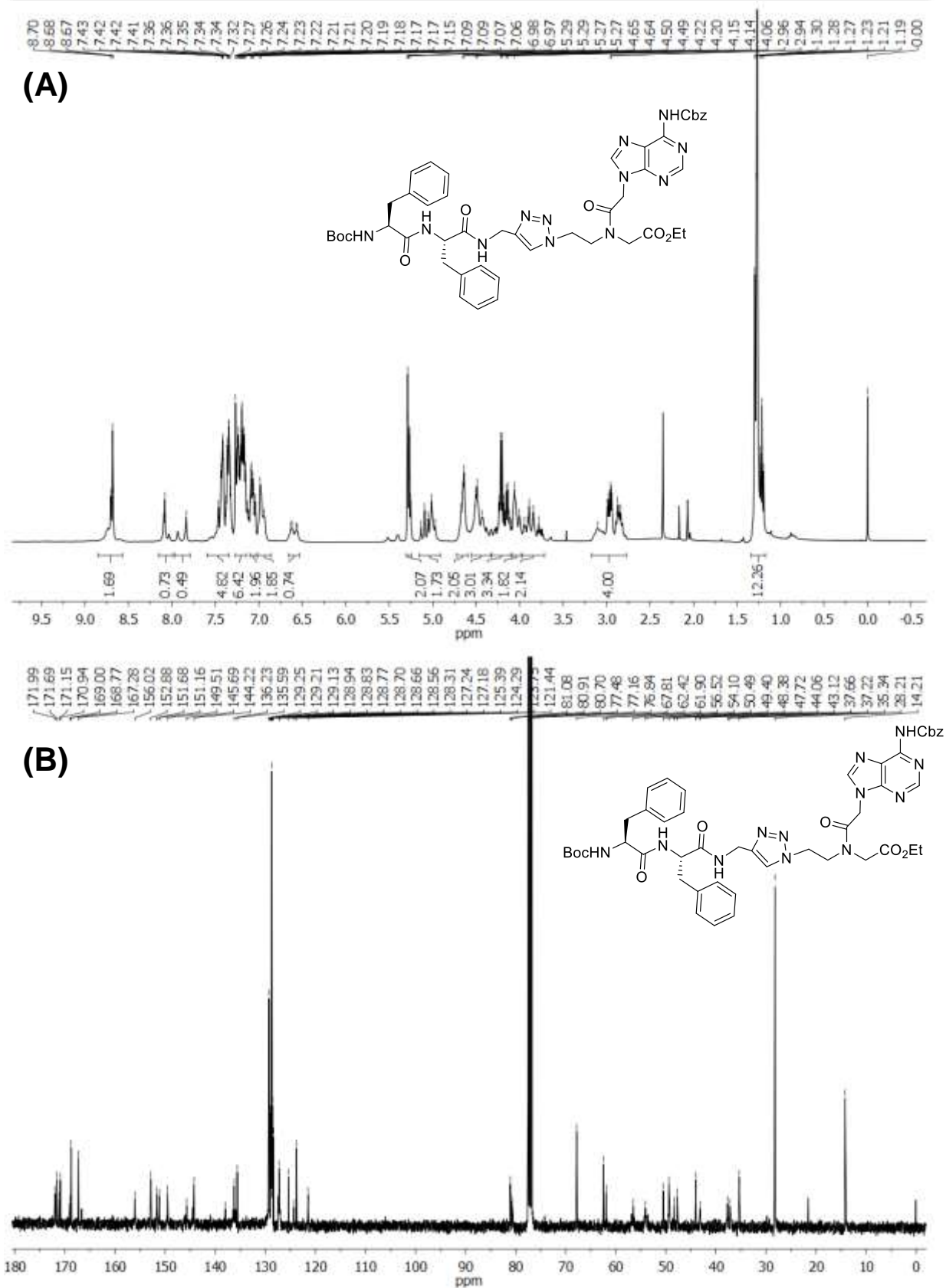


(A) [^1]H-NMR and (B) [^13]C-NMR spectra of peptide **6b**.

**(A)**

CHCl<sub>3</sub>



**(B)**
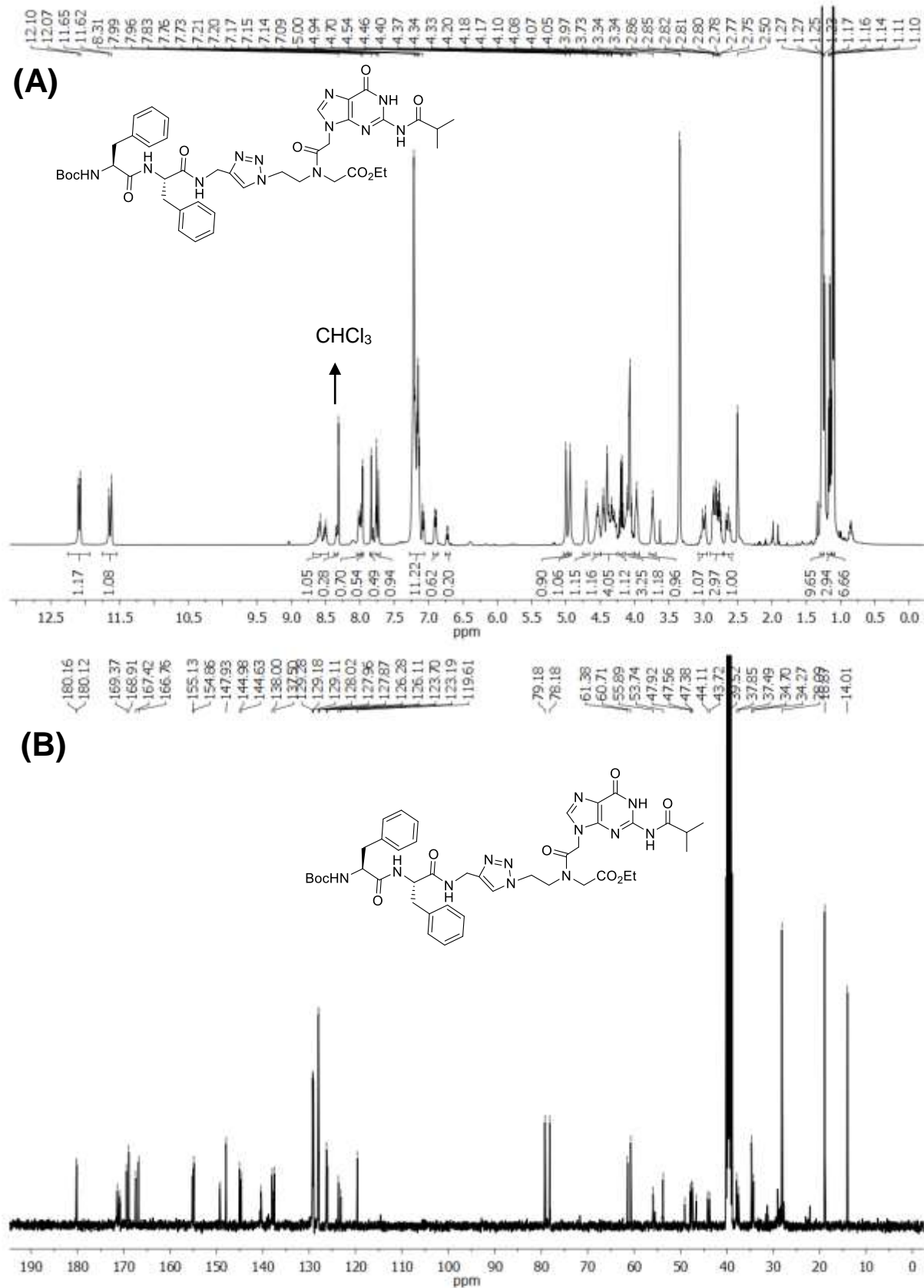


(A) $^1$H-NMR and (B) $^{13}$C-NMR spectra of peptide **6c**.

**(A)**



**(B)**



(A) $^1$H-NMR and (B) $^{13}$C-NMR spectra of peptide **6d**.

**(A)**



**(B)**



(A) $^{1}$H-NMR and (B) $^{13}$C-NMR spectra of peptide **7c**.

**(A)**



**(B)**
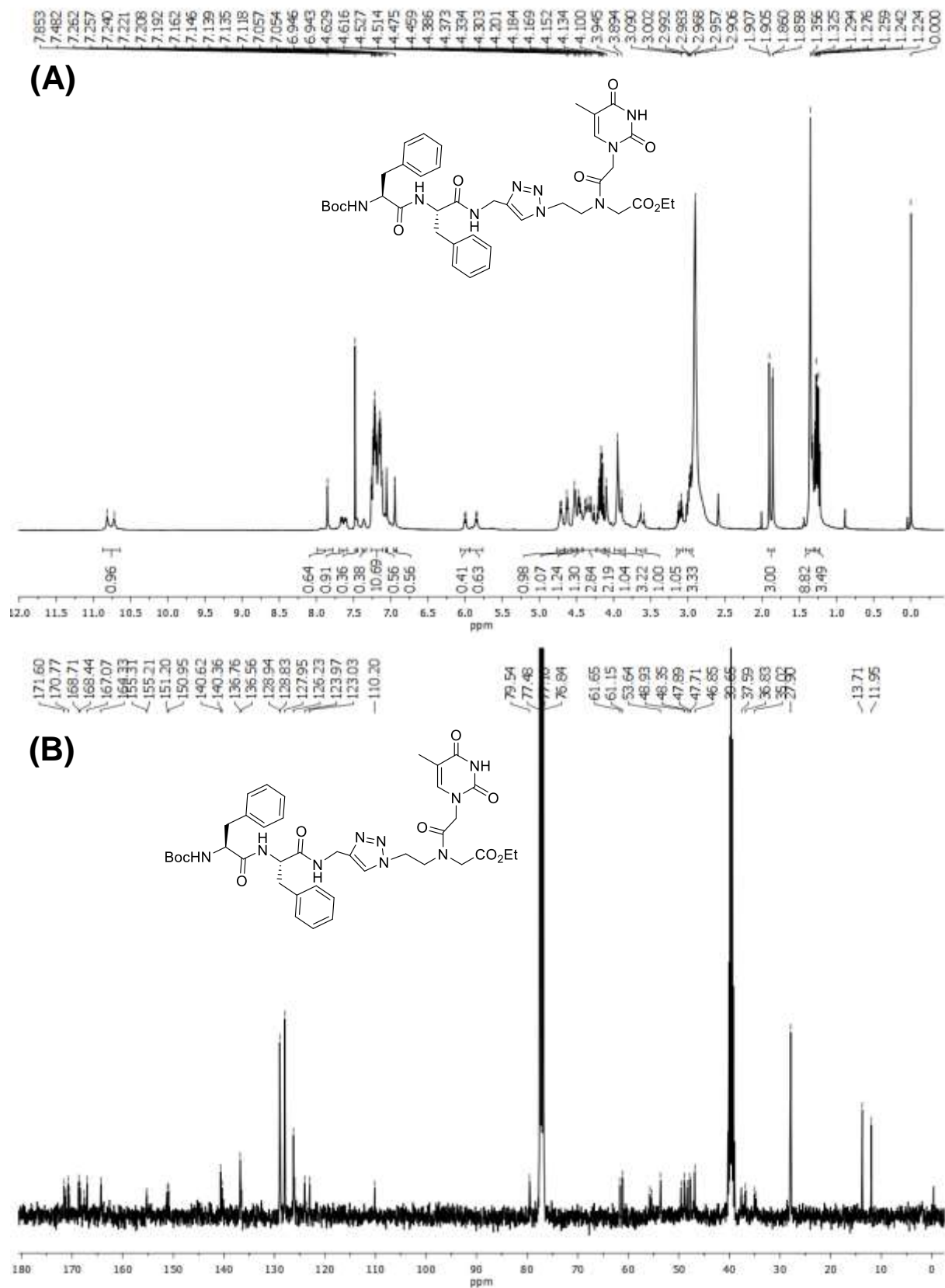


(A) ¹H-NMR and (B) ¹³C-NMR spectra of nucleopeptide **7d**.

(A) $^1$H-NMR and (B) $^{13}$C-NMR spectra of nucleopeptide **8c**.

**(A)**



**(B)**
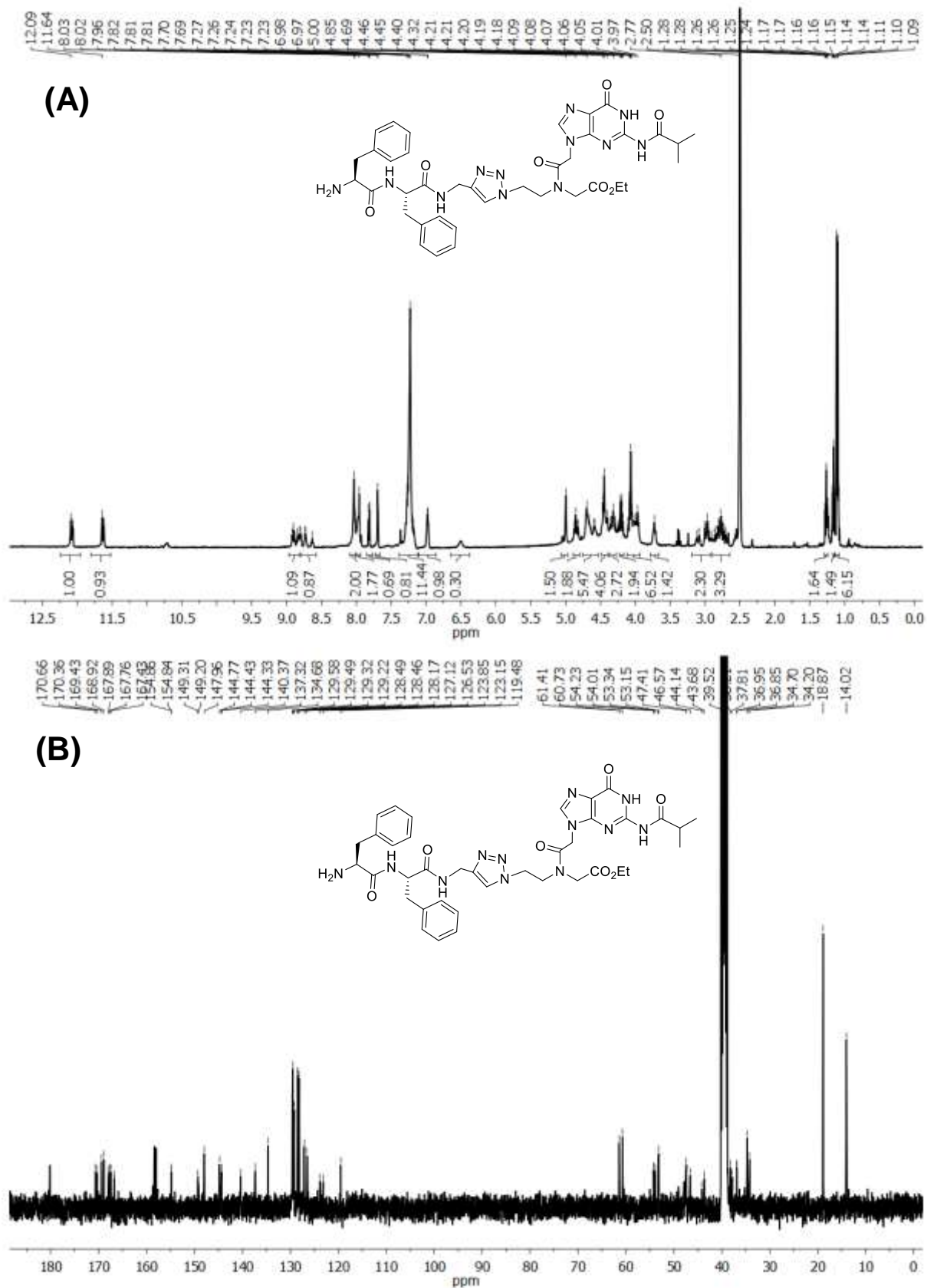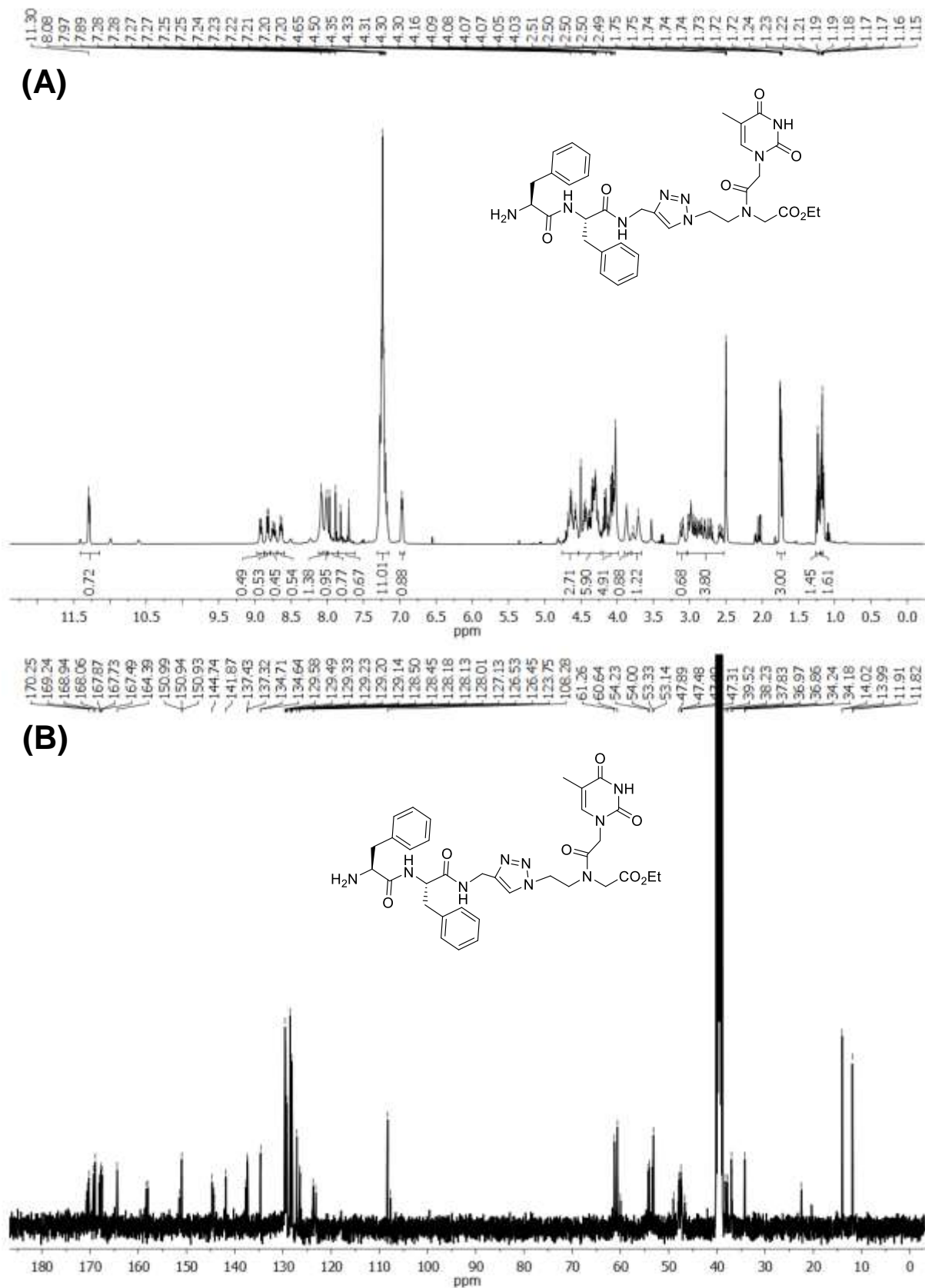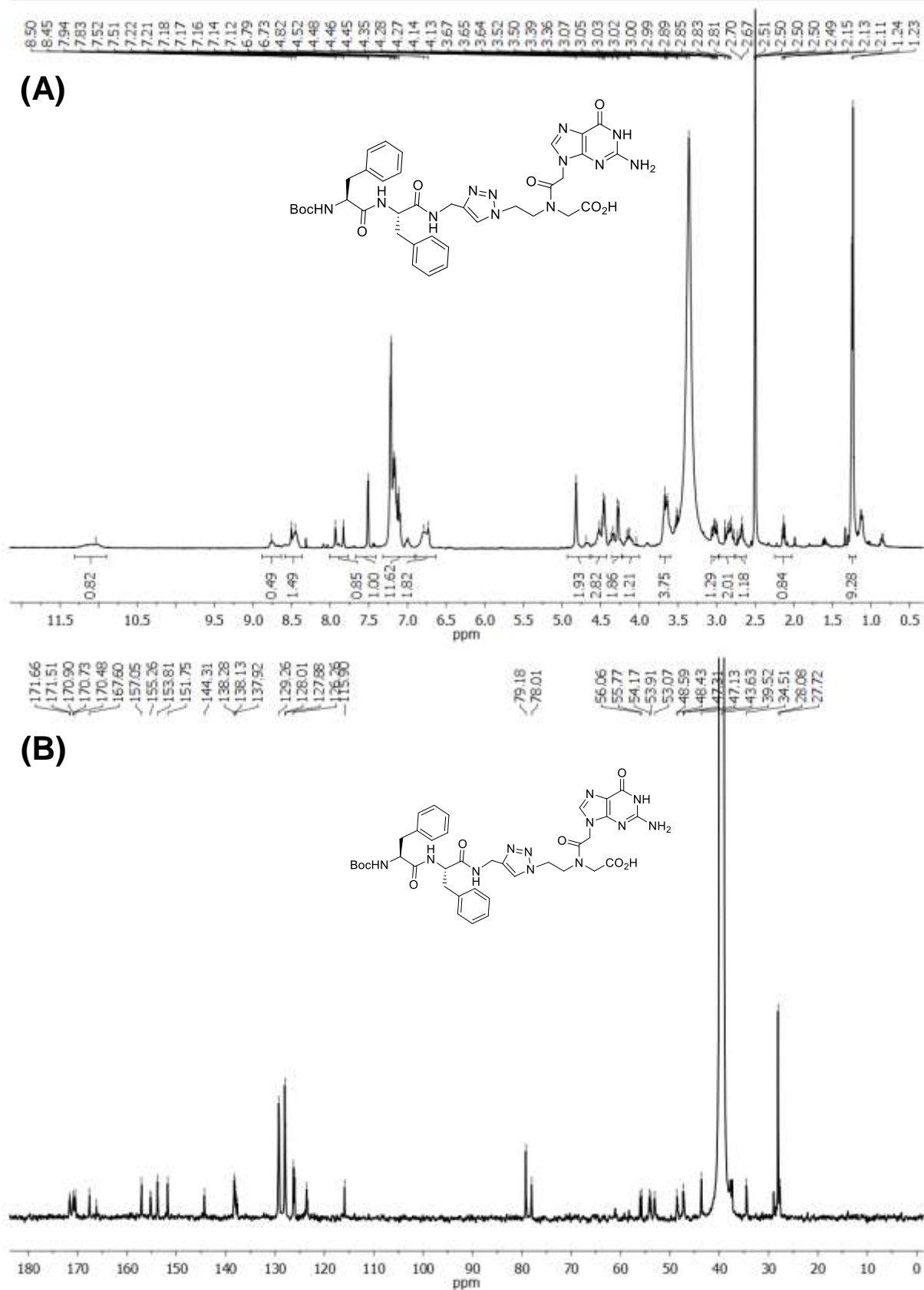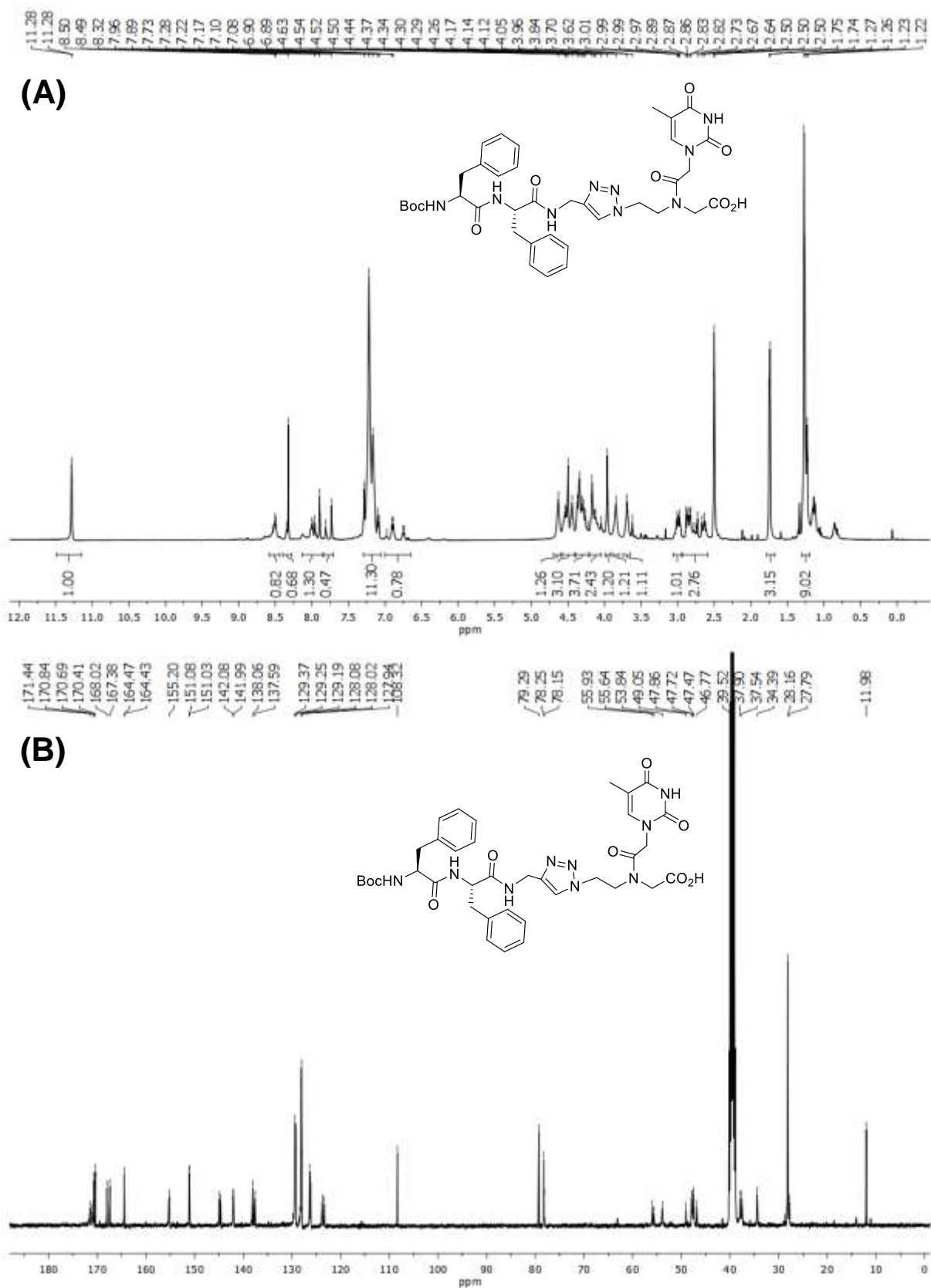


(A) ¹H-NMR and (B) ¹³C-NMR spectra of peptide **8d**.
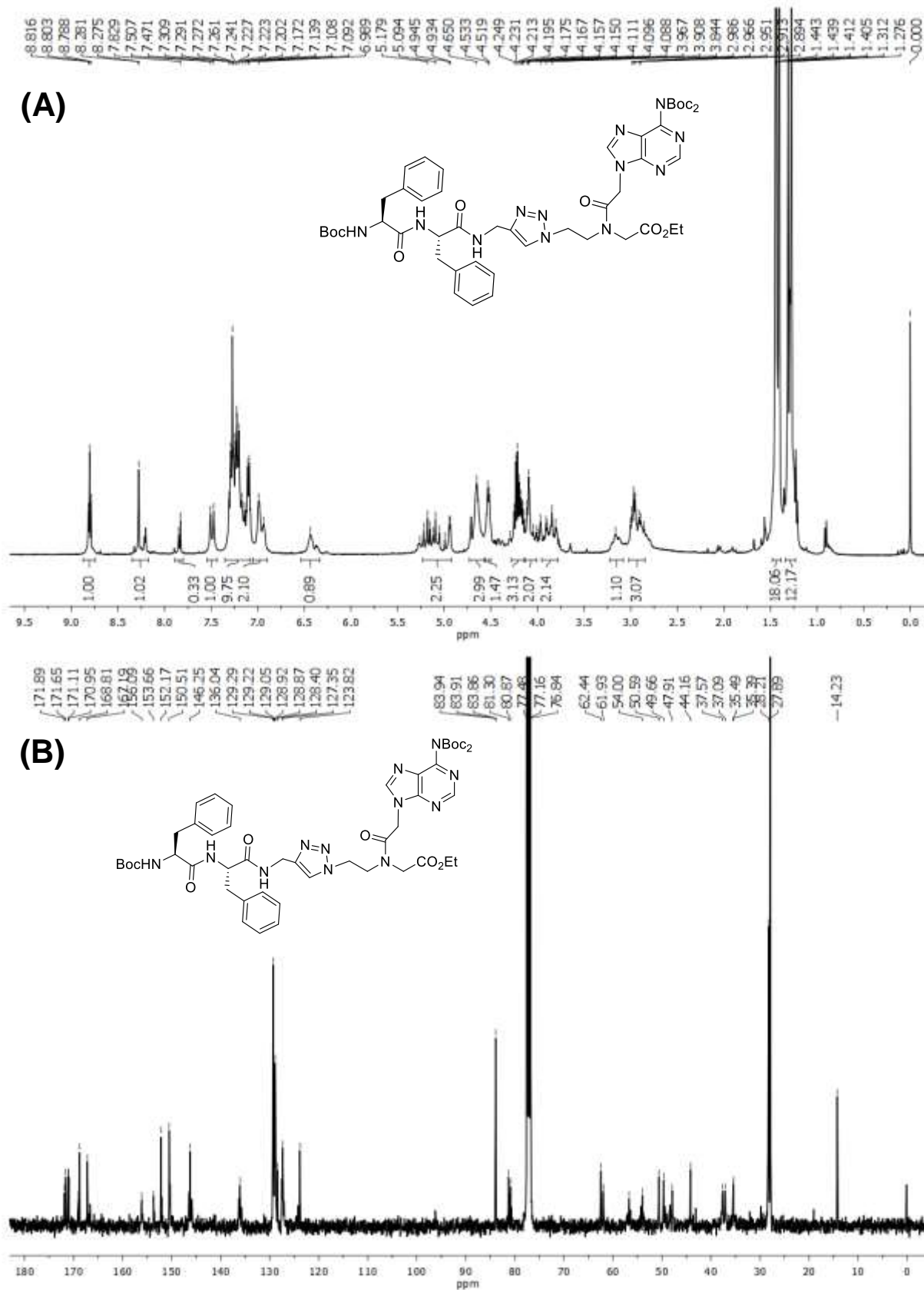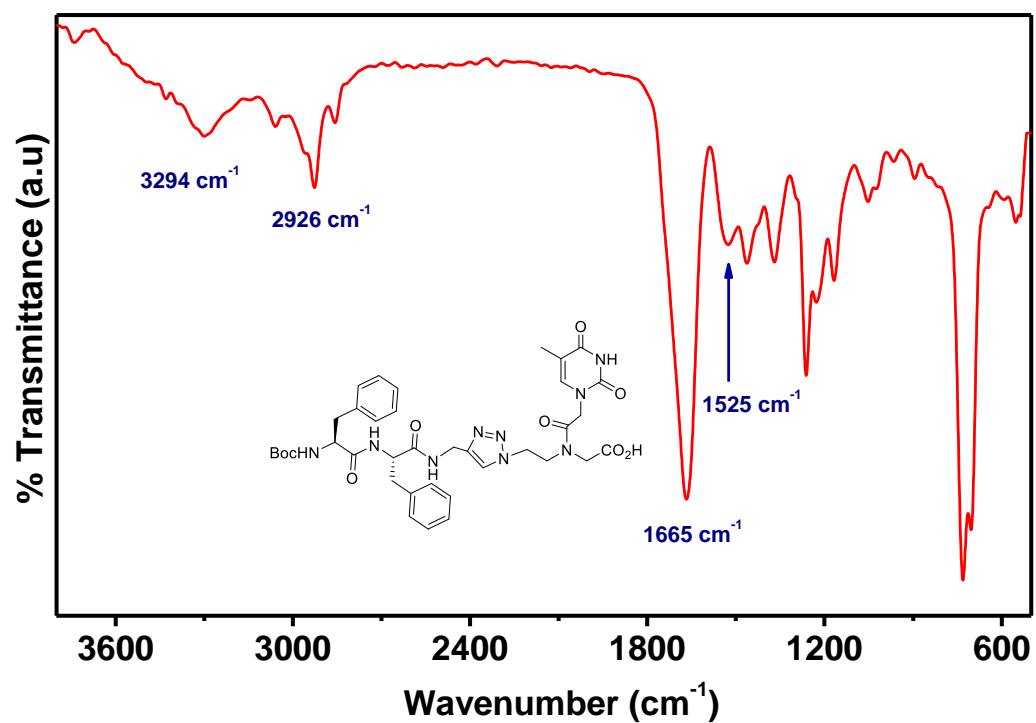
FTIR spectrum of **8d**.



FTIR spectrum of **9**.

**(A)**



**(B)**



(A) ¹H-NMR and (B) ¹³C-NMR spectra of **9**.

**(A)**

8.32 8.13 8.11   7.28 7.26 7.25 7.23 7.17 6.89 6.87   4.47 4.46 4.16 3.34 3.09 3.07 2.97 2.94 2.93 2.91 2.89 2.73 2.69 2.66 2.63 2.50   1.27

CHCl₃

0.89   10.03 0.86   1.00 1.01   1.03 1.91 1.07   9.38

9.5  9.0  8.5  8.0  7.5  7.0  6.5  6.0  5.5  5.0  4.5  4.0  3.5  3.0  2.5  2.0  1.5  1.0  0.5  0.0
ppm

**(B)**

172.81 171.69   155.11   138.13 137.37 129.25 129.19 128.21 128.00 126.47 126.16   78.04   55.70 53.36   39.52 37.44 36.79   28.13

190  180  170  160  150  140  130  120  110  100  90  80  70  60  50  40  30  20  10  0
ppm
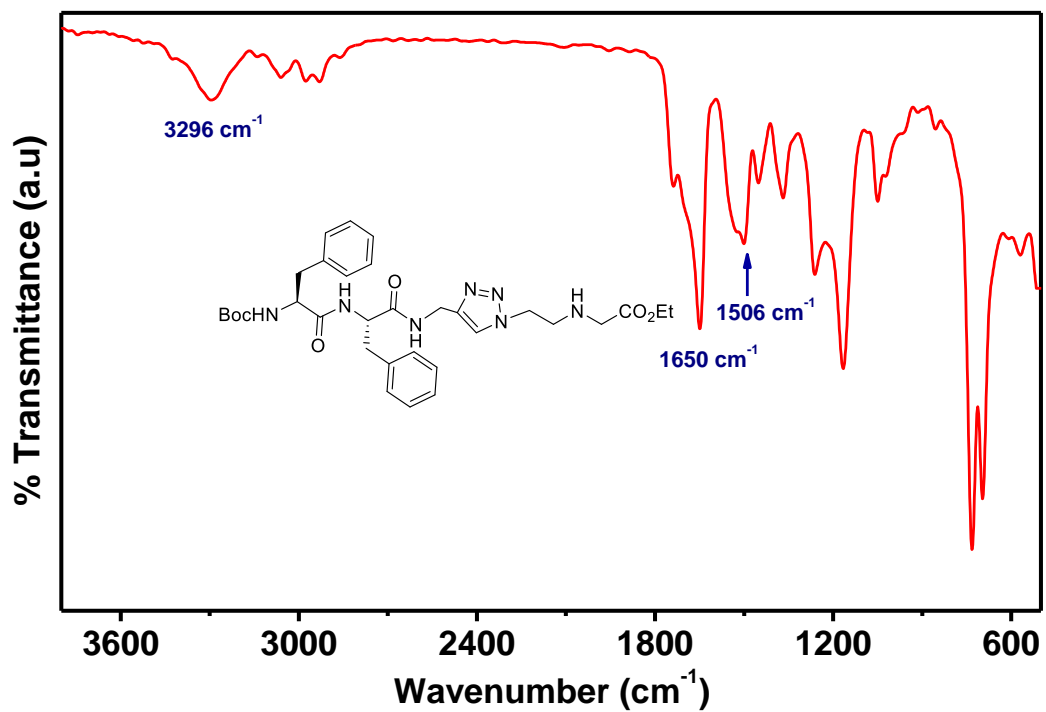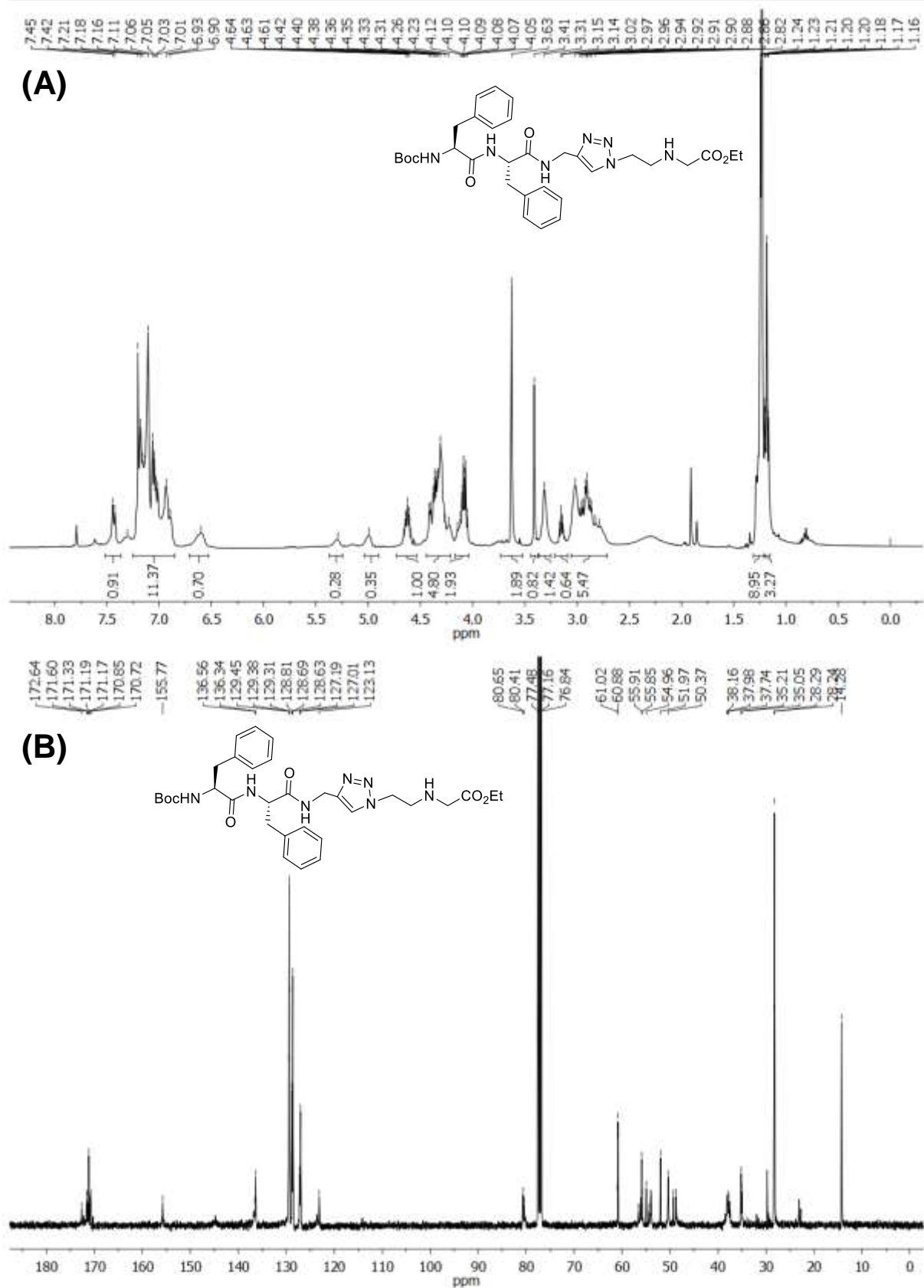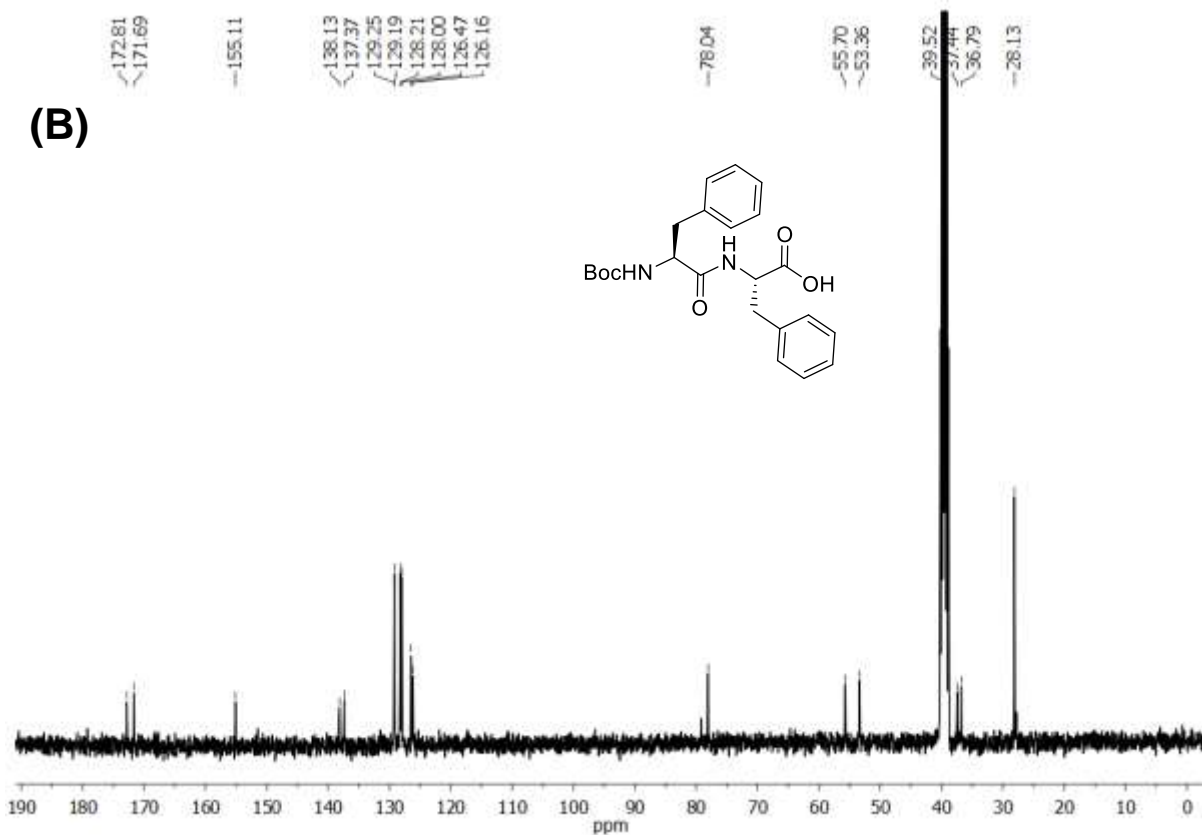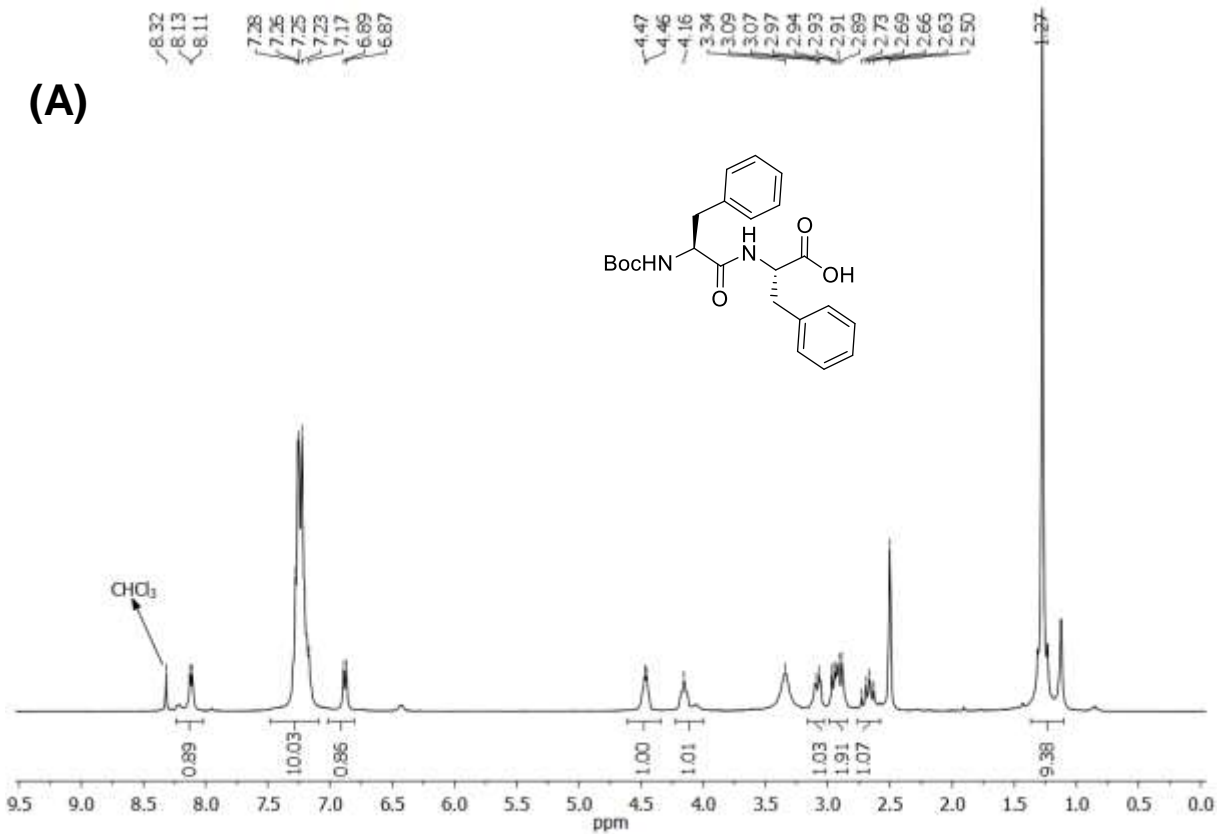
(A) ¹H-NMR and (B) ¹³C NMR of Boc-Phe-Phe-OH (in DMSO-d₆).

208
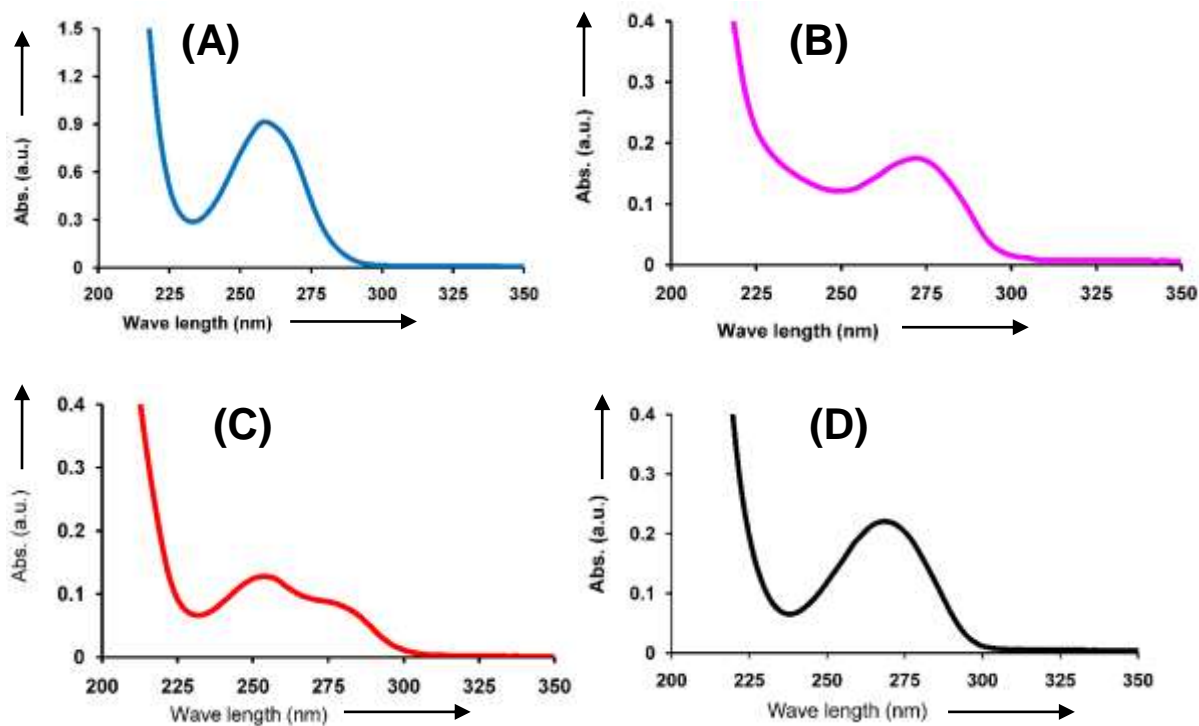
UV-Vis spectrum (concentration = 1.34 mM) after purification of (A) **NP1**; (B) **NP2**; (C) **NP3** and (D) **NP4**.
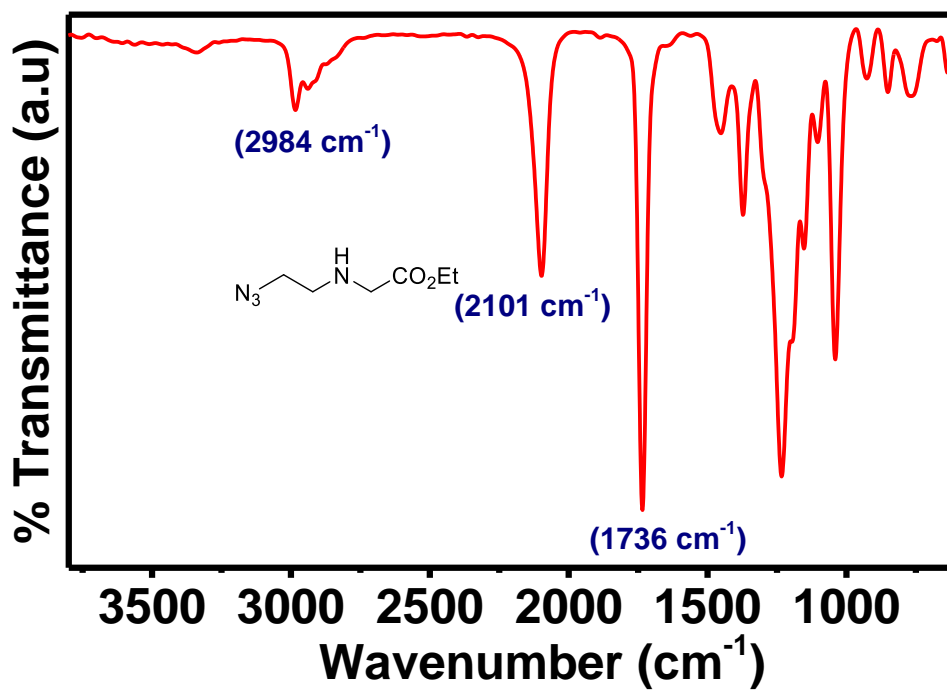


FTIR spectrum of **18**.
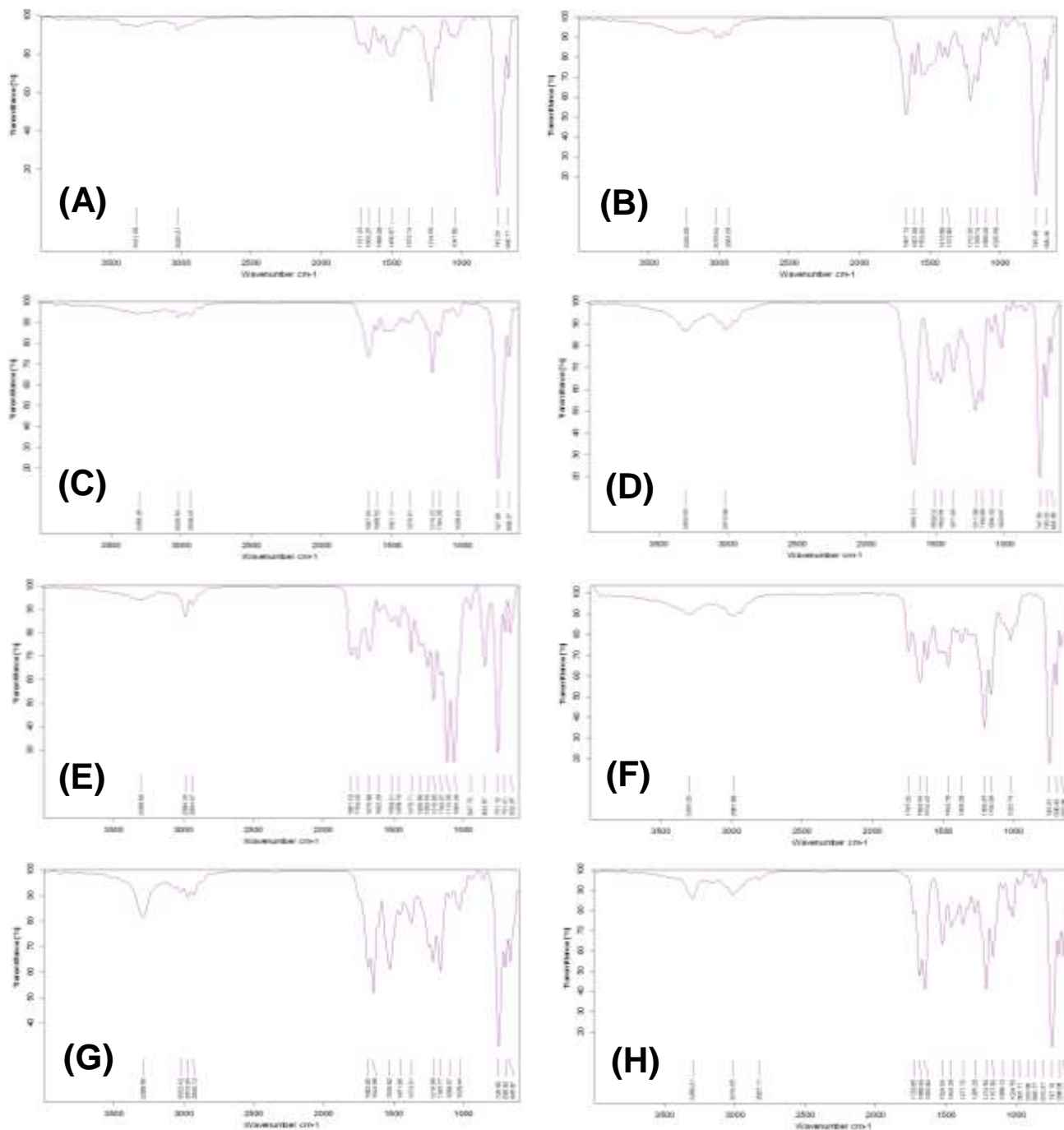
FTIR spectra of peptide (A) **3a** [Boc-Phe-Phe-*am-aeg*(A^NHCbz)-OEt]; (B) **3b** [Boc-Phe-Phe-*am-aeg*(6-Cl-G^NHiBu)-OEt]; (C) **3c** [Boc-Phe-Phe-*am-aeg*(G^NHiBu)-OEt]; (D) **3d** [Boc-Phe-Phe-*am-aeg*(T)-OEt]; (E) **6a** [Boc-Phe-Phe-*tz-aeg*{A^N(Boc)2}-OEt]; (F) **6b** [Boc-Phe-Phe-*tz-aeg*(A^NHCbz)-OEt]; (G) **6c** [Boc-Phe-Phe-*tz-aeg*(G^NHiBu)-OEt] and (H) **6d** [Boc-Phe-Phe-*tz-aeg*(T)-OEt).
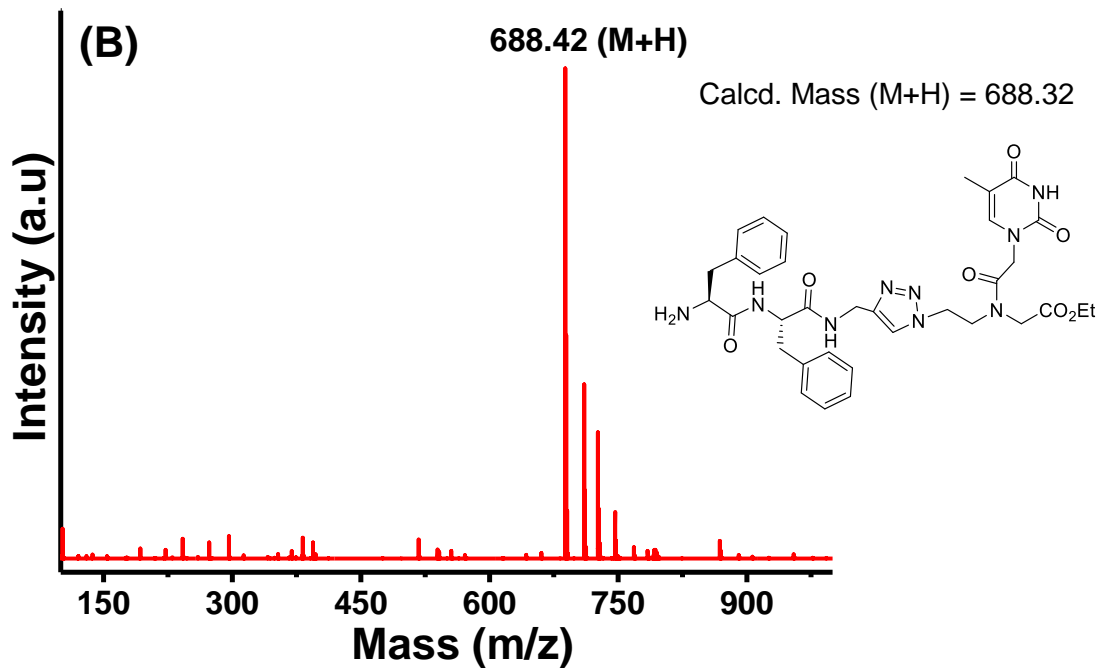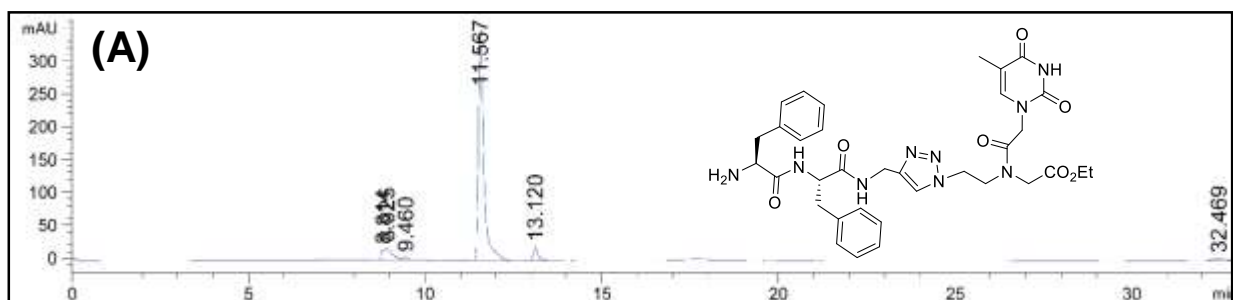
(A) HPLC Trace and (B) MALDI Mass for peptide.
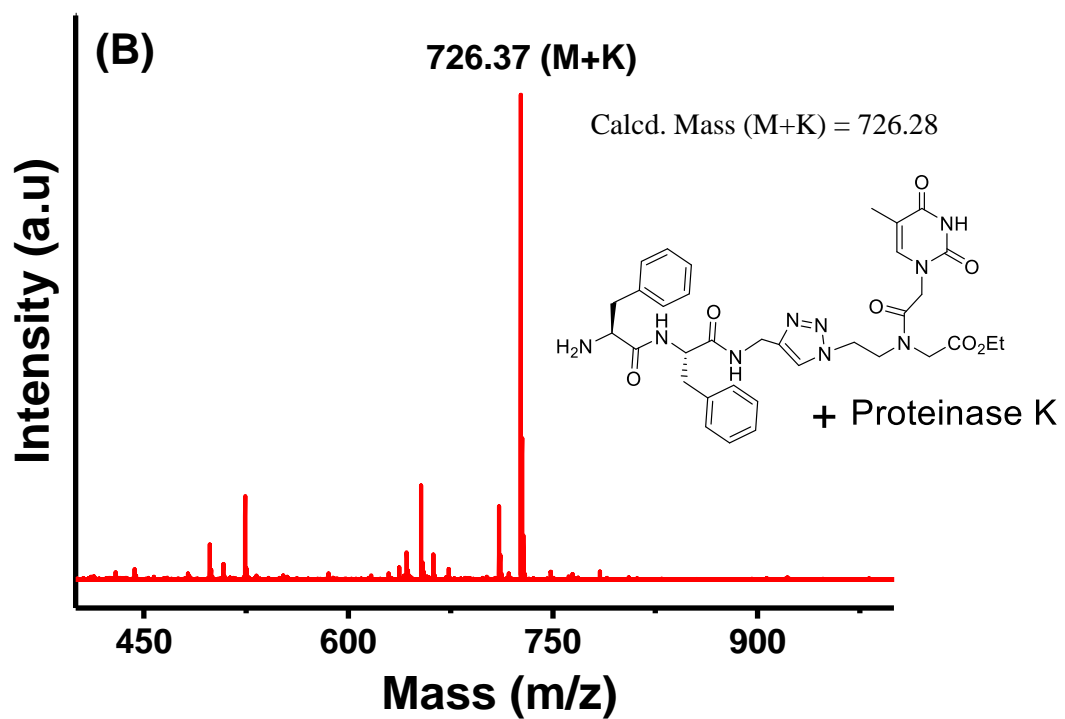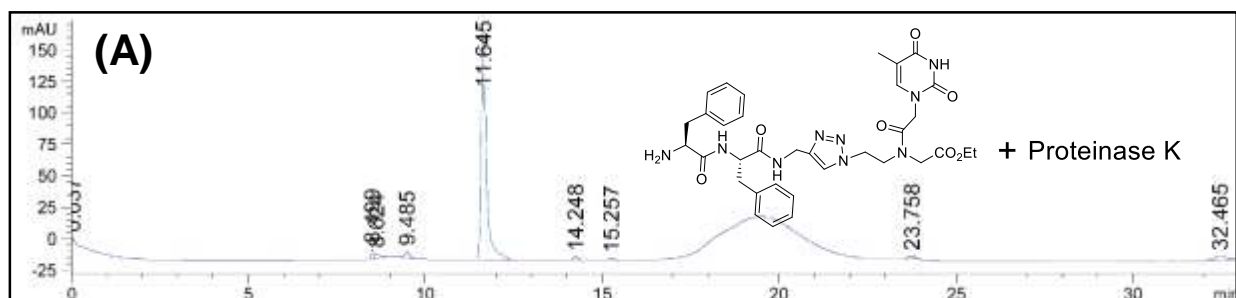
(A) HPLC Trace and (B) MALDI Mass for proteinase K incubated peptide.
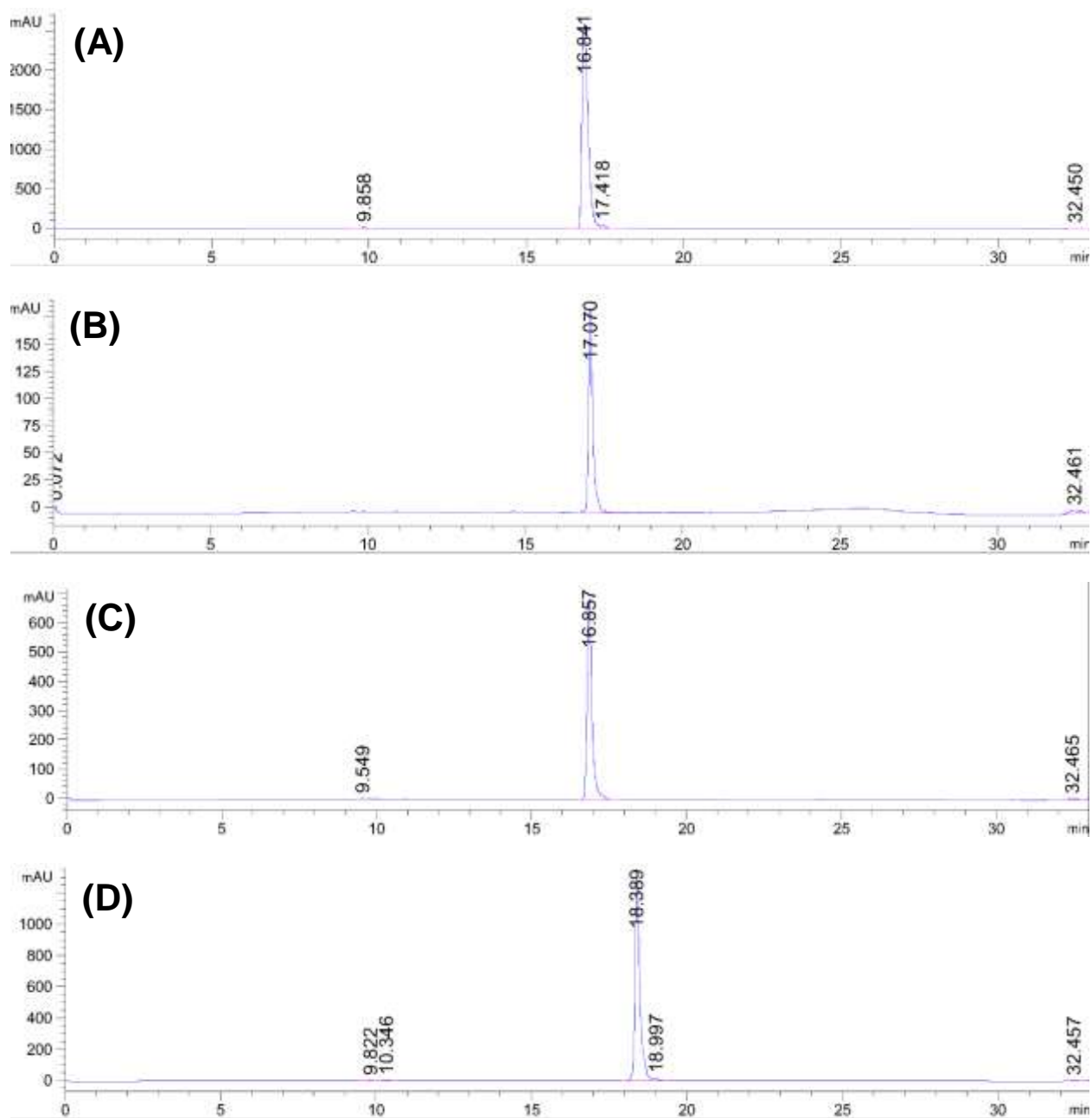
HPLC Trace of (A) **NP1**; (B) **NP2**; (C) **NP3** and (D) **NP4**.

# Chapter 5

# Self-assembly and Biophysical Studies of Diphenylalanine (Phe-Phe)-Peptide Nucleic Acid-$G_n$ Conjugates (Tetraplex Studies)

## 5.1 Introduction

DNA is a carrier of genetic information and consists of a right-handed double helical structure. It is comprised of Watson-Crick base pairing: adenine (A):thymine (T) and cytosine (C): guanine (G), under ordinary physiological conditions.[1] Several non-canonical (non-Watson-Crick) base pairing have been observed in DNA structures, chiefly Hoogsteen base pairing and some self-base pairing (ex. C-C, G-G) which are present in repetitive DNA sequences.[2] While Hoogsteen base pairing is a feature observed in triplexes (polypurine:polypyrimidine stretches), self-base pairing of C leads to *i*-motif from interdigitated $CH^+$-C base pairing[3] and that by G results in $G_4$-tetraplex formation. G-quadruplexes $(G_4)$[4] (Figure 5.1) are present *in-vivo* and has biological significance in triggering telomerase activity during cell division. Apart from its importance in biology, $G_4$ tetraplexes arising in designed and programmable sequences have emerged as interesting supramolecular structures and are assuming importance in material chemistry as components of several nanodevices. These are being purposed for versatile electronics, biosensors, biomimetic applications and DNA nanotechnology.[5-10]
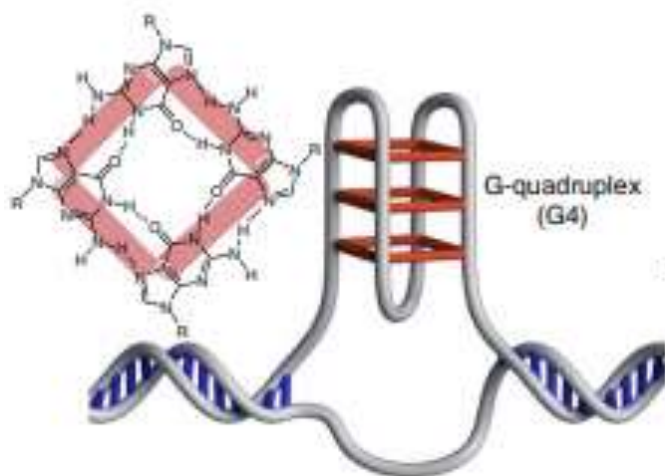


**Figure 5.1**: Schematic representation of the G-tetraplex.[6]

### 5.1.1 Importance of G₄-DNA Quadruplex

It is known that many promoter regions in the genes contain repeating sequences that are capable of forming structures other than double helix. Contiguous guanine repeats have been shown to have the potential to form G-quadruplex.[4] In 1962, formation of G-quartet tetrad, which is a building block of G quadruplex structure, was first identified to be as the basis of the

aggregation of 5' monophosphate guanosines to form guanosine gel.[11] The stacking of two or more G-tetrads on top of each other, leads to a G-quadruplex structure (Figure 5.2A). This structure is stabilized by monovalent metal cation, such as $K^+$ or $Na^+$, through coordination with $O^{12}$ carbonyl of guanines.[12] G-quadruplex structures can arise from wrapping of one continuous stretch of $G_n$ or two hairpins of $G_4$ in parallel, antiparallel side by side or diagonal orientations or four independent $G_n$ strands form tetraplexes.[13]

Upon folding into a G-quadruplex structure, the nucleotides between two tandem G-rich repeats form loops. Formation of hairpin structures requires a sequence with four G-rich stretches separated by at least one nucleotide. Based on the strand orientations, a G-quadruplex can be parallel (the same polarity for all strands) or antiparallel (each strand has opposite polarity with respect to the two adjacent strands). Figure 5.2B highlights general types of G-quadruplexes based on strand orientation. To date, several G-quadruplex formations have been reported in the human genome. G-quadruplex structures are polymorphic, with a specific conformation depending on the DNA sequence, strand orientation, loop size, and other factors such as cation species and molecular crowding conditions.[14-16] DNA and RNA oligomers with multiple stretches of consecutive guanine (G) nucleotides fold into stable G-quadruplex[17-20] that are implied in regulation of gene expression.[21]
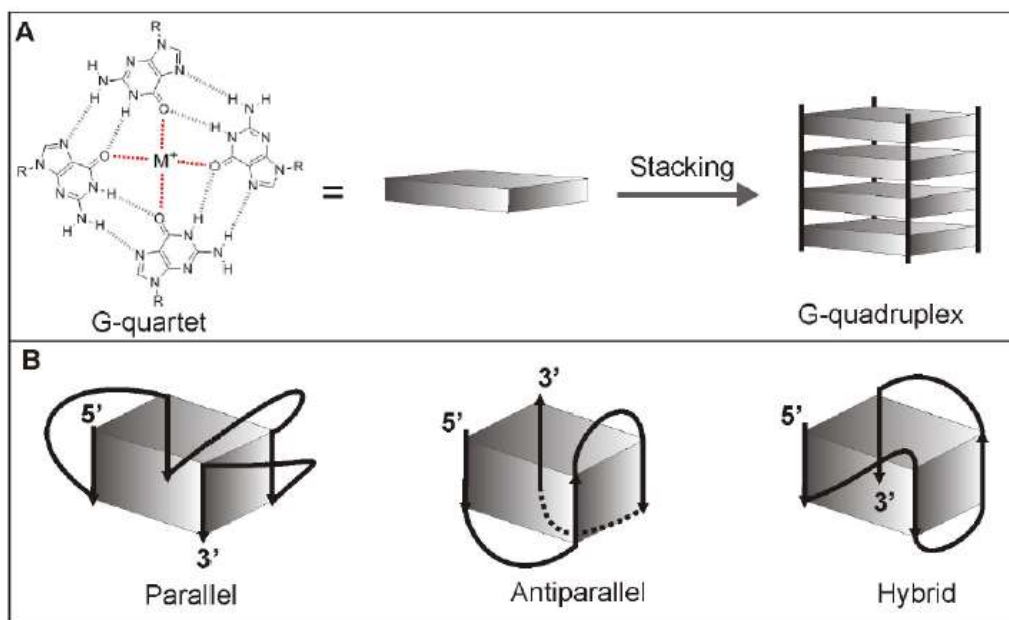


**Figure 5.2**: (A) Formation of G-quadruplex by stacking of G-quartets and (B) three general types of G-quadruplexes based on DNA strand orientation.[13,14]

Several DNA analogues exhibit $G_4$ tetraplex structures. Peptide nucleic acid (PNA)[15] with aminoethylglycine (*aeg*) backbone also forms G-quadruplex structure that is found to be more stable than that of DNA.[16] Balasubramanian *et. al.*,[22] have shown the formation of quadruplex composed entirely of PNA (Q-PNA) (Figure 5.3B). A homologous PNA (i.e. a PNA having the same sequence as the target) forms a stable $PNA_2:DNA_2/RNA_2$ hybrid quadruplex by disrupting a bimolecular DNA/RNA G-quadruplex (Figure 5.3A).[23]
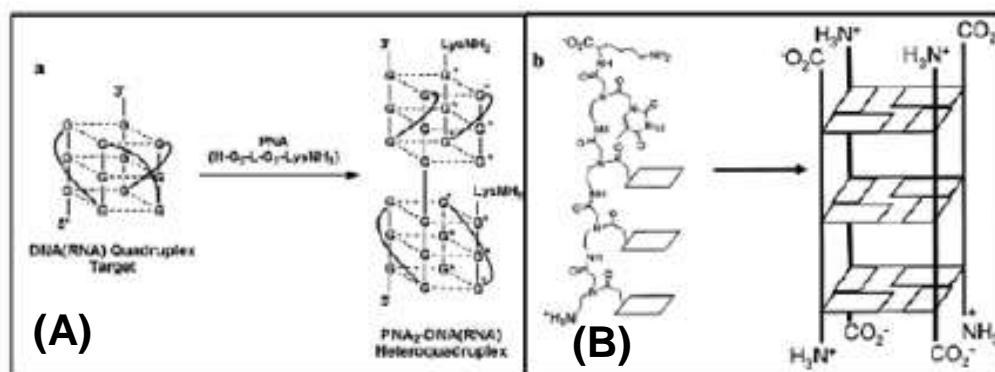


**Figure 5.3** (A) Schematic diagram for PNA:DNA/RNA homologous quadruplex[22] and (A) schematic representation for PNA-Q4 quadruplex.[23]

**5.1.2 Biophysical techniques used to study G-tetraplexes**: Formation of $G_4$-tetraplexes can be studied by a number of biophysical techniques such as temperature dependent UV absorbance at 290 nm, characteristic CD bands and MALDI-TOF mass spectroscopy. Thermal denaturation (UV-$T_m$) studies of $G_4$-tetraplexes and duplexes were performed on Cary 300 Bio UV-Visible Spectrophotometer. The samples were heated at 90 °C for 1 min and cooled slowly to ambient temperature. The solution was moved to cold room and kept in freeze at (4 °C) for 24 hrs. The variation of absorbance at 290 nm for G-quadruplex study and 260 nm for the duplex study were measured as a function of temperature from 20 °C-90 °C, with absorbance recordings at every 1 °C increment. Each melting experiment was repeated at least three times and $T_m$ values were determined from first derivative curves of normalized UV-temperature plots. The concentrations of oligonucleotides were calculated on the basis of absorbance at 260 nm, using molar extinction coefficients of the corresponding nucleobases: $G = 11.7 \text{ cm}^2/\mu\text{mol}$ and for $Phe = 0.2 \text{ cm}^2/\mu\text{mol}$.[24,25] The samples were prepared in 10 mM Potassium Phosphate buffer at pH 7.24, salt is KCl (100 mM) and peptide concentration was 50 μM.

CD spectrometric study was carried out on JASCO J-815 spectropolarimeter using cylindrical, jacketed quartz cell (10 mm path length), which was connected to Julabo-UC25 water circulator. For reproducible data, each set of spectra were measured using at least three individually prepared solutions. CD spectra were recorded using a spectral bandwidth of 1.0 nm at 25 °C with a time constant of 1 second and a step resolution of 1 nm. All the spectra were corrected for respective buffer conditions and are typically averaged over 3-5 scans. A quartz cell with a path length of 1 mm was used with solutions containing approximately 0.25 mL (50 μM). All peptides had same concentration (50 μM) for CD measurements done in 20 mM sodium cacodylate at pH 7.4, salt is NaCl (100 mM). The data processing and curve fitting were performed using Origin 8.0 software. All spectra were collected at 25 °C with a 1 nm resolution and a scan rate of 50 nm/min. Spectra are the averages of 3-5 scans.

## 5.2 Rationale and objectives of the present work

In view of the importance of $G_4$-tetraplexes which are self-assembled structures as detailed above and the interesting results on modulation of self-assembly of dipeptide Phe-Phe through conjugation with nucleosides/PNA, linker, stereochemistry and hydrophobicity, it was thought to the study the self-assembly of Phe-Phe peptides that are conjugated with the PNA $G_n$-tetraplex oligomers. A series of such nucleopeptides (NPs) with Phe-Phe conjugation to PNA $G_n$ oligomers with variable length and linkers were synthesized and their self-assembled morphologies were tested systematically using different biophysical spectroscopic and microscopic techniques.

The specific objectives of this section are:

➢ Synthesis and the characterization of the PNA-$G_n$ oligomers [PNA-G **(P1)**; PNA-$G_2$ **(P2)**; PNA-$G_3$ **(P3)** and PNA-$G_4$ **(P4)**] and their conjugated derivatives with Phe-Phe [Phe-Phe-*gly*-PNA-G **(P5)**; Phe-Phe-*gly*-PNA-$G_2$ **(P6)**; Phe-Phe-*gly*-PNA-$G_3$ **(P7)** and Phe-Phe-*gly*-PNA-$G_4$ **(P8)**].

➢ Purification by HPLC, characterization by the MALDI-TOF mass spectroscopy and stability studies with the temperature dependent UV spectroscopy.

➢ Morphological characterization was performed through the FESEM technique.

## 5.3 Results and the discussions

**5.3.1 Synthesis and characterization**: As we have seen in Chapter 4 among various Phe-Phe conjugates, only Phe-Phe-*gly*-PNA-G **(P5)** exhibited good self-assembly defined morphology of derived nanoparticles. Hence it would be interesting to study the effect of increasing number of conjugated PNA-G **(P1)** units into $G_2$-$G_4$ oligomeric level to examine the superposition of $G_4$-tetraplex formation on that of Phe-Phe motif (Figure 5.4). A total of eight peptides (four with Phe-Phe and four without Phe-Phe) were synthesized through solid phase peptide synthesis (SPPS) using Boc-strategy to afford unprotected nucleopeptides (Figure 5.4) and (Scheme 5.1). For peptide synthesis, the commercially available Boc-Gly-OH and Boc-PNA monomers with suitable nucleobase protecting groups were used and Boc-Phe-Phe-OH **(9)** was synthesized following literature procedure. The dipeptide Phe-Phe was tethered to PNA-$G_n$ *via* a glycyl linker. Unlike previous reports[26,27] N-termini of these peptides **(P5-P8)** are uncapped. These nucleopeptides therefore can self-assemble with dominant Phe-Phe motif, PNA-$G_n$ motif or a combination of both components. After synthesis all peptides were purified by HPLC and characterized by the MALDI-TOF mass spectroscopy (Table 5.1).
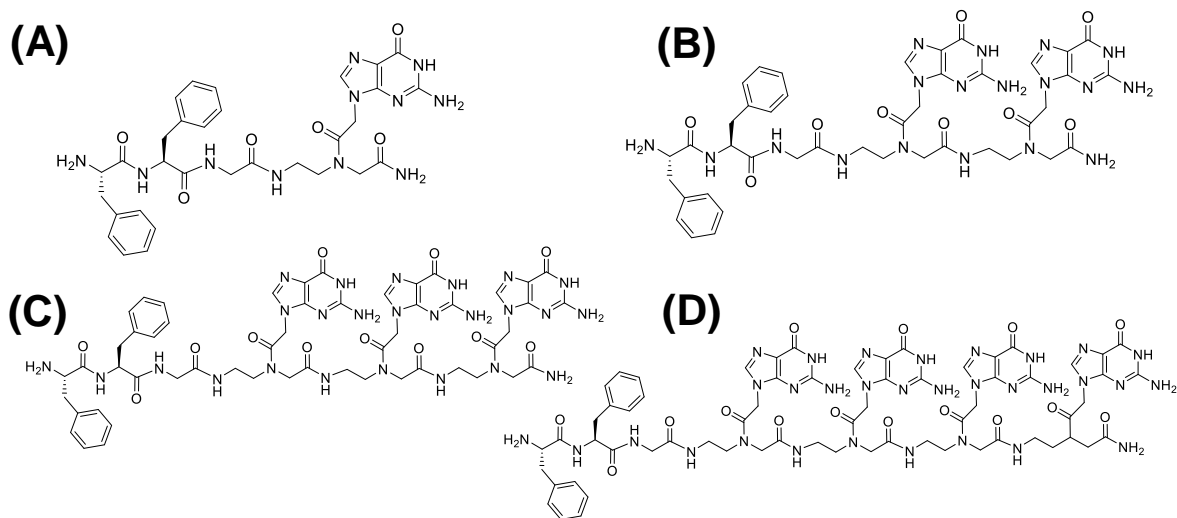


**Figure 5.4**: Structures of (A) Phe-Phe-*gly*-PNA-G **(P5)**; (B) Phe-Phe-*gly*-PNA-$G_2$ **(P6)**; (C) Phe-Phe-*gly*-PNA-$G_3$ **(P7)** and (D) Phe-Phe-*gly*-PNA-$G_4$ **(P8)**.
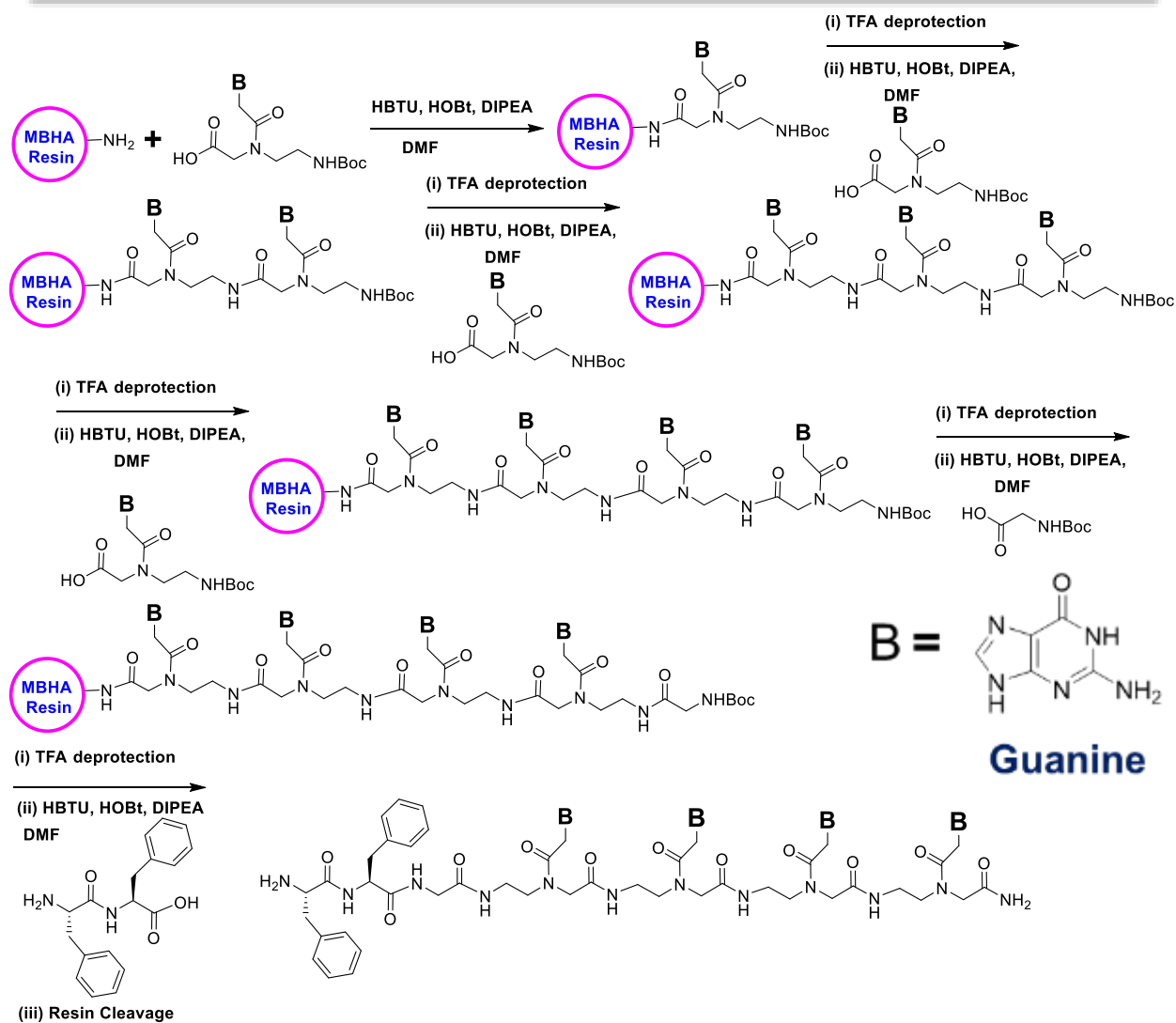
**Scheme 5.1**: Synthesis of the PNA-G$_n$ oligomers with and without Ph-Phe.

**Table 5.1**: MALDI-TOF analysis of peptides.

| Sr. No. | Peptide | Molecular Formula | Calcd. Mass (M) | Obsd. Mass |
|---------|---------|-------------------|-----------------|------------|
| 1 | PNA-G **(P1)** | $C_{11}H_{16}N_8O_3$ | 309.14 $[M+H]^+$ | 309.25 $[M+H]^+$ |
| 2 | PNA-G$_2$ **(P2)** | $C_{22}H_{29}N_{15}O_6$ | 600.25 $[M+H]^+$ | 600.28 $[M+H]^+$ |
| 3 | PNA-G$_3$ **(P3)** | $C_{33}H_{42}N_{22}O_9$ | 891.36 $[M+H]^+$ | 891.45 $[M+H]^+$ |
| 4 | PNA-G$_4$ **(P4)** | $C_{44}H_{55}N_{29}O_{12}$ | 1182.47 $[M+H]^+$ | 1182.25 $[M+H]^+$ |
| 5 | Phe-Phe-*gly*-PNA-G **(P5)** | $C_{31}H_{37}N_{11}O_6$ | 660.30 $[M+H]^+$ | 660.33 $[M+H]^+$ |
| 6 | Phe-Phe-*gly*-PNA-G$_2$ **(P6)** | $C_{42}H_{50}N_{18}O_9$ | 973.39 $[M+Na]^+$ | 973.36 $[M+Na]^+$ |

| 7 | Phe-Phe-*gly*-PNA-G$_3$ **(P7)** | C$_{50}$H$_{63}$N$_{19}$O$_{12}$ | 1242.52 [M+H]$^+$ | 1242.52 [M+H]$^+$ |
|---|---|---|---|---|
| 8 | Phe-Phe-*gly*-PNA-G$_4$ **(P8)** | C$_{64}$H$_{76}$N$_{32}$O$_{15}$ | 1555.61 [M+Na]$^+$ | 1555.57 [M+Na]$^+$ |
| 9 | H-Phe-Phe-OH **(9)** | C$_{18}$H$_{20}$N$_2$O$_3$ | 351.11 [M+K]$^+$ | 351.10 [M+K]$^+$ |

**5.3.2 G-Quadruplex study by UV-$T_m$ plot at 290 nm**: The formation of G-tetraplexes in DNA is characterized by appearance of UV-band at 290 nm and melting of G-tetraplexes are characterized by a decrease in absorbance of this band.[22] Since, all the PNA-G$_n$ oligomers contain the nucleobase guanine (G), band at 260 nm band is also observed in the UV-Vis spectra (Figure 5.5), overlapping with that of Phe-Phe.
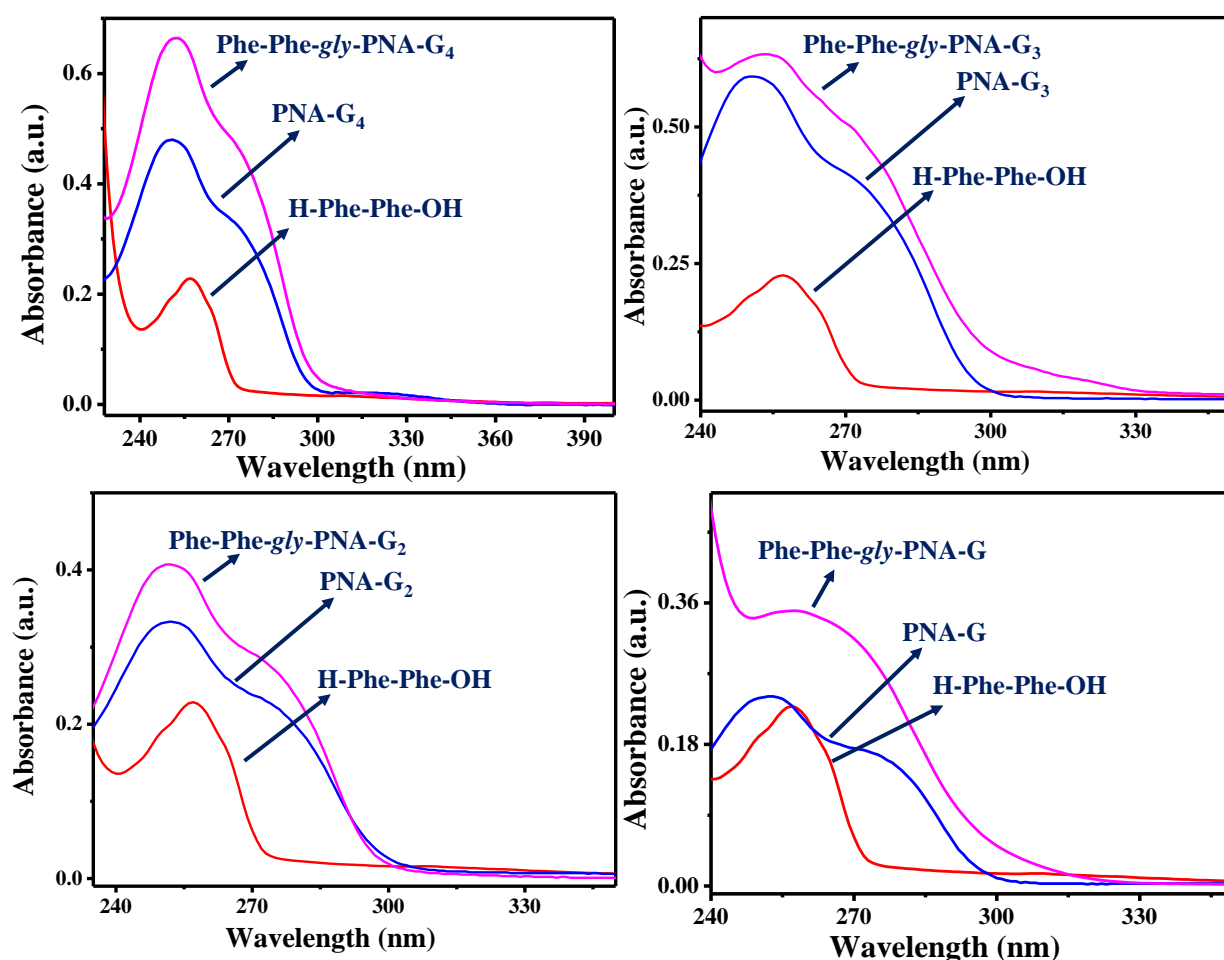


**Figure 5.5**: Comparison of the UV-Vis spectra of Phe-Phe-PNA-G$_n$ conjugates.

To study G-tetraplex formation in PNA-G$_n$ oligomers, UV thermal melting experiments were followed by change in absorbance at 290 nm with increase in temperature from the 20 $^oC$ to 90 $^oC$. It is known that absorbance at 260 nm increases for DNA duplex in a sigmoidal manner and $T_m$ for duplex melting is obtained from midpoint of sigmoidal transition maximum in first derivative plot. Formation of tetraplex in PNA requires at least there contiguous guanines (G).[22] It was observed that among all PNA-G oligomers synthesized, only PNA-G$_3$ **(P3)** (with $T_m$ 40.7 $^oC$) (Figures 5.6A and B) and PNA-G$_4$ **(P4)** (with $T_m$ 46.6 $^oC$) show decrease in UV absorbance at 290 nm formation of G-quadruplex structure as they show the inverse sigmoidal curve of absorbance at 290 nm in the UV-$T_m$ plot (Figures 5.6C and D).
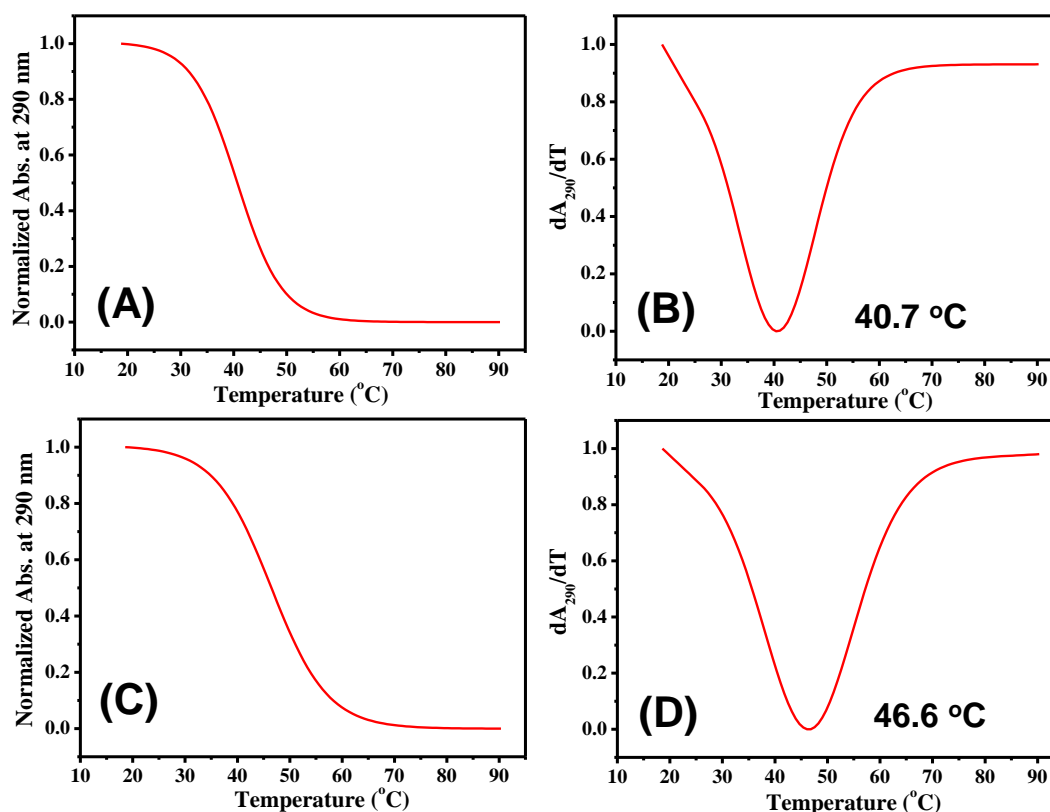


**Figure 5.6**: (A) UV-$T_m$ plot of PNA-G$_3$ **(P3)** and (B) its derivative curve; (C) UV-$T_m$ plot of PNA-G$_4$ **(P4)** and (D) its derivative curve at 290 nm in potassium phosphate buffer 10 mM, (pH 7.24), KCl (100 mM), 50 μM concentration 1 $^oC$/min temperature.

The corresponding PNA-G$_3$ **(P3)** and PNA-G$_4$ **(P4)** oligomers conjugated with the Phe-Phe [Phe-Phe-*gly*-PNA-G$_3$ **(P7)**] and PNA-G$_4$ [Phe-Phe-*gly*-PNA-G$_4$ **(P8)**] did not show any

G-quadruplex formation as observed by absence of inverse sigmoidal transitions (Figures 5.7A and B) in UV-$T_m$ plots at 290 nm. Further, PNA-$G_1$ **(P1)** and PNA-$G_2$ **(P2)** also did not show any G-quadruplex formation as observed by absence of inverse sigmoidal transitions (Figures 5.8A and B) which is due to only one guanine in PNA-$G_1$ **(P1)** and two guanine in the PNA-$G_2$ **(P2)**.
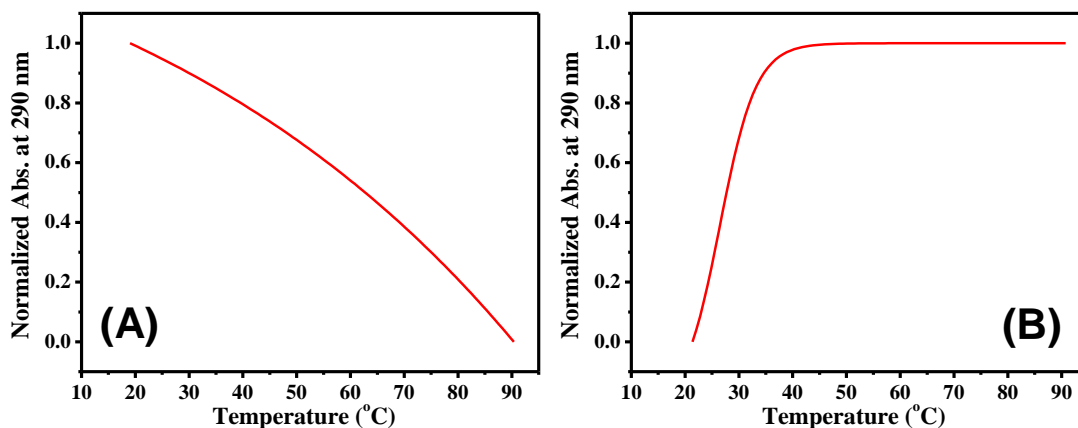


**Figure 5.7**: UV-$T_m$ plots of (A) Phe-Phe-*gly*-PNA-$G_3$ **(P7)** and (B) Phe-Phe-*gly*-PNA-$G_4$ **(P8)** at 290 nm wavelength in potassium phosphate buffer 10 mM, (pH 7.24), KCl (100 mM), 50 µM concentration 1 ºC/min temperature.
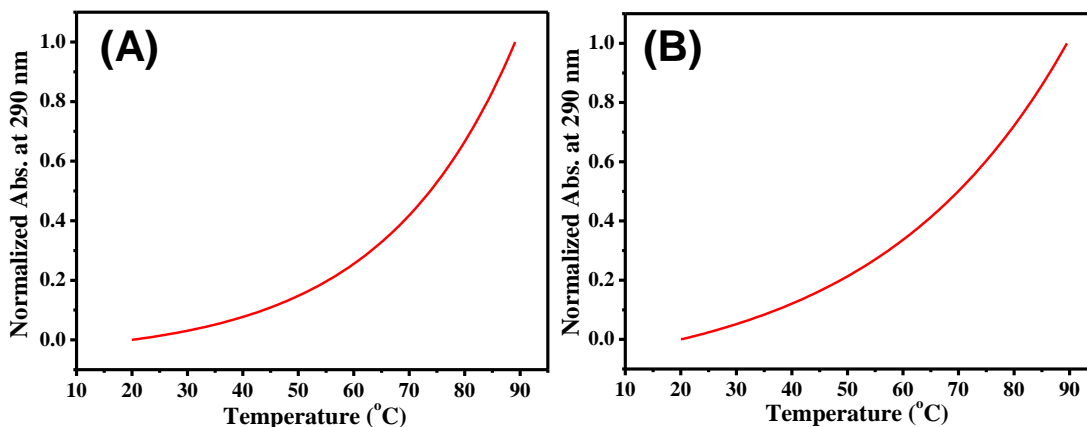


**Figure 5.8**: UV-$T_m$ plots of (A) PNA-G **(P1)** and (B) PNA-$G_2$ **(P2)** at 290 nm wavelength in potassium phosphate buffer 10 mM, (pH 7.24), KCl (100 mM), 50 µM concentration 1 ºC/min temperature.

This suggested that Phe-Phe conjugation to PNA-$G_n$ oligomers impairs the formation of PNA G-quadruplex structures. This may be because of either steric or electronic reasons or both. Even shorter peptides [PNA-G **(P1)**; PNA-$G_2$ **(P2)**; Phe-Phe-*gly*-PNA-G **(P5)**; Phe-Phe-*gly*-PNA-

223

G$_2$ **(P6)**; Phe-Phe-*gly*-PNA-G$_3$ **(P7)** and Phe-Phe-*gly*-PNA-G$_4$ **(P8)**] did not show the any G-quadruplex formation at 290 nm wavelength (Figure 5.8 and 5.9).
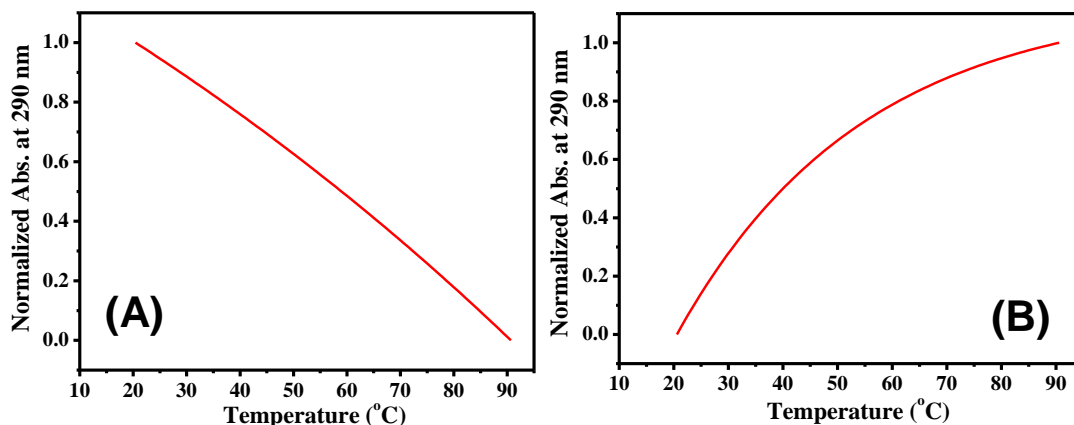


**Figure 5.9**: UV-$T_m$ plots of (A) Phe-Phe-*gly*-PNA-G **(P5)** and (B) Phe-Phe-*gly*-PNA-G$_2$ **(P6)** at 290 nm wavelength in potassium phosphate buffer 10 mM, (pH 7.24), KCl (100 mM), 50 µM concentration 1 °C/min temperature.

**5.3.3 Duplex study by UV-$T_m$ plot at 260 nm**: In order to see if these form any other secondary structures, the temperature dependent UV-$T_m$ plot of PNA-G$_2$ **(P2)** and PNA G$_3$ **(P3)** was followed at 260 nm, as normally done for studying duplex formation (Figure 5.10). Interestingly, an increase in UV absorbance was observed in temperature range 20 °C-90 °C, with characteristic sigmoidal transition for duplex formation. The $T_m$ obtained for PNA-G$_2$ **(P2)** and PNA-G$_3$ **(P3)** were 53.7 °C and 49.3 °C respectively. In comparison, $T_m$ for Phe-Phe-*gly*-PNA-G **(P5)** was 42.3 °C and so the nucleopeptide conjugates are also able to form duplexes via self-pairing through hydrogen bonding.
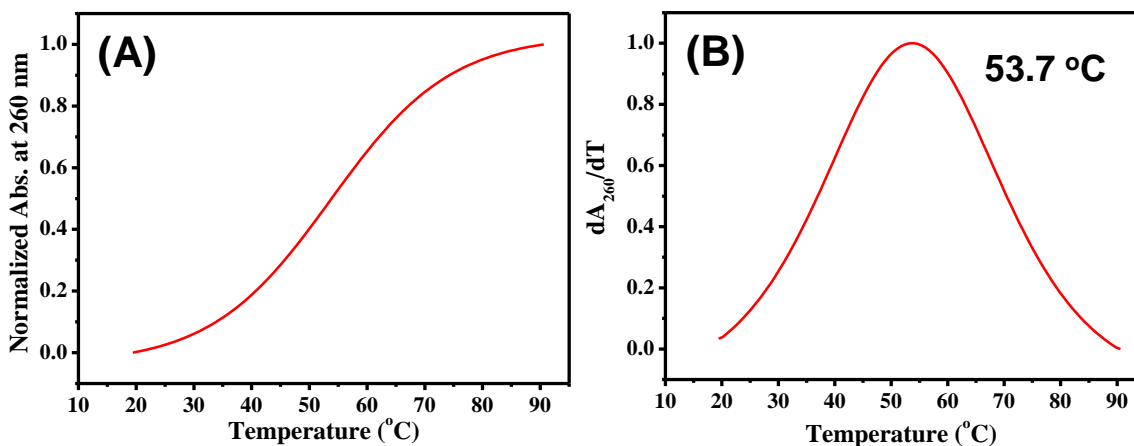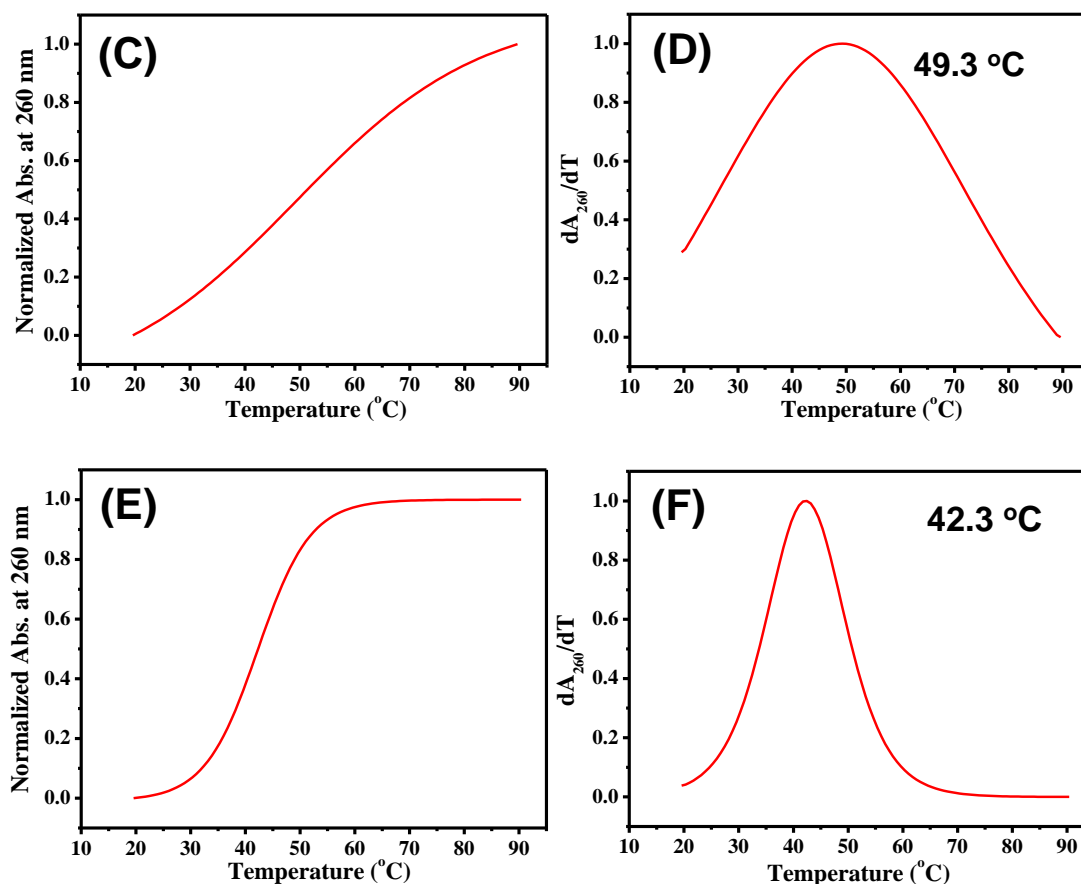
**Figure 5.10**: UV-$T_m$ plot of (A) PNA-G$_2$ **(P2)** and (B) its derivative curve; (C) UV-$T_m$ plot of PNA-G$_3$ **(P3)** and (D) its derivative curve; (E) UV-$T_m$ plot of Phe-Phe-*gly*-PNA-G **(P5)** and (F) its derivative curve at 260 nm in potassium phosphate buffer 10 mM, (pH 7.24), KCl (100 mM), 50 μM concentration 1 °C/min temperature.

Further, PNA-G **(P1)** and PNA-G$_4$ **(P4)** did not show any duplex formation as observed by absence of sigmoidal transitions (Figures 5.11A and B). After conjugation of Phe-Phe with PNA-G$_2$ (Phe-Phe-*gly*-PNA-G$_2$) **(P6)**, PNA-G$_3$ (Phe-Phe-*gly*-PNA-G$_3$) **(P7)** and PNA-G$_4$ (Phe-Phe-*gly*-PNA-G$_4$) **(P8)**, the oligomers did not show duplex structure (absence of sigmoidal transition at 260 nm) (Figure 5.11C-E) confirming that the Phe-Phe component disrupts the duplex structures.
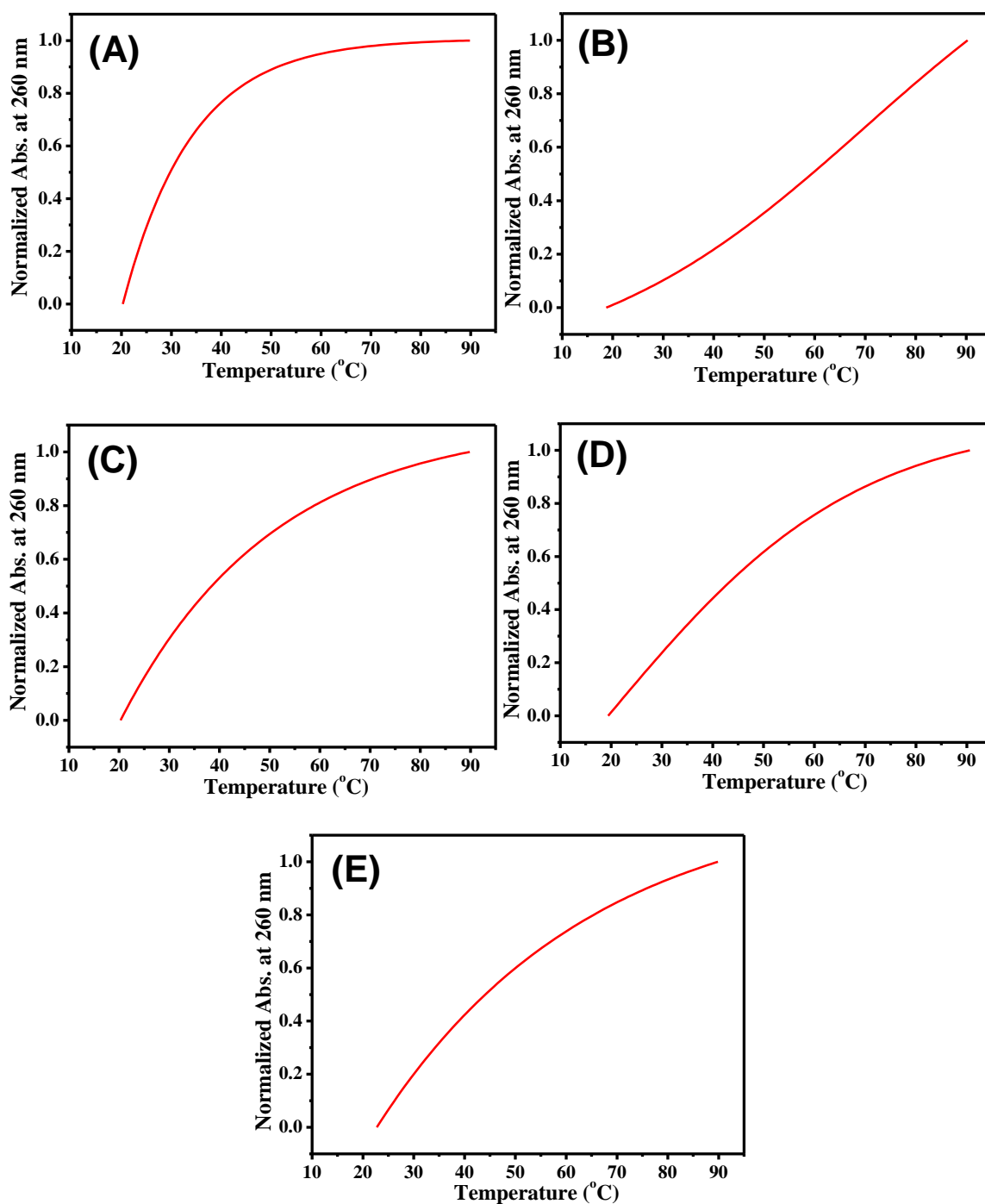
**Figure 5.11**: UV-$T_m$ plots of (A) PNA-G **(P1)**; (B) PNA-G$_4$ **(P4)**; (C) Phe-Phe-*gly*-PNA-G$_2$ **(P6)**; (D) Phe-Phe-*gly*-PNA-G$_3$ **(P7)** and (E) Phe-Phe-*gly*-PNA-G$_4$ **(P8)** at 260 nm wavelength in potassium phosphate buffer 10 mM, (pH 7.24), KCl (100 mM), 50 µM concentration 1 ºC/min temperature.

Thus Phe-Phe conjugation with the PNA-$G_n$ oligomers does not help in the formation of G-tetraplex. On the other hand, in case of Phe-Phe-*gly*-PNA-G **(P5)** it allows the formation of duplexes under conditions similar to that with PNA-$G_2$ **(P2)**, PNA-$G_3$ **(P3)** that show duplexes, but not tetraplexes. This may be due to either steric or electronic factors disfavoring duplex / tetraplex formation. There is no any signature of the quadruplex structures (positive band at 290 nm in CD) and duplex structures (positive band at 260 nm in CD) even at higher concentration also. This may be due to absence of the chiral center in the PNA-Gn oligomers (see experimental section)

**Table 5.2**: Thermal melting (UV-$T_m$) study of duplex and G-quadruplex.

| Sr. No. | Peptides | $T_m$ (°C) at 260 nm | $T_m$ (°C) at 290 nm |
|---------|----------|----------------------|----------------------|
| 1. | PNA-G **(P1)** | N. T. | N. T. |
| 2. | PNA-$G_2$ **(P2)** | 53.7 | N. T. |
| 3. | PNA-$G_3$ **(P3)** | 49.3 | 40.7 |
| 4. | PNA-$G_4$ **(P4)** | N. T. | 46.6 |
| 5. | Phe-Phe-*gly*-PNA-G **(P5)** | 42.3 | N. T. |
| 6. | Phe-Phe-*gly*-PNA-$G_2$ **(P6)** | N. T. | N. T. |
| 7. | Phe-Phe-*gly*-PNA-$G_3$ **(P7)** | N. T. | N. T. |
| 8. | Phe-Phe-*gly*-PNA-$G_4$ **(P8)** | N. T. | N. T. |

**5.3.4 Morphologies from microscopic images**: The morphology arising from self-assembled structures of various nucleopeptide conjugates was studied by FESEM techniques. The various peptide samples were prepared as mentioned in experimental procedures.[28-31] Self-assembly of completely deprotected nucleopeptides, partially protected and fully protected analogues were studied.

Nucleopeptides **P5-P8** without hydrophobic substituents exhibited a wide range of morphologies depending on the attached nucleobases. All the control peptides without Phe-Phe [like PNA-G **(P1)**, PNA-$G_2$ **(P2)**, PNA-$G_3$ **(P3)** and PNA-$G_4$ **(P4)**] gave only sticky aggregate particles (Figures 5.12A-D). The G-containing nucleopeptides Phe-Phe-*gly*-PNA-G **(P5)** and Phe-Phe-*gly*-PNA-$G_2$ **(P6)** self-assembled into small spherical nanoparticles with size range from 50 nm to 200 nm (Figures 5.12E, F), while higher nucleopeptides Phe-Phe-*gly*-PNA-$G_3$ **(P7)** and Phe-Phe-*gly*-PNA-$G_4$ **(P8)** gave sticky particles (Figures 5.12G, H).
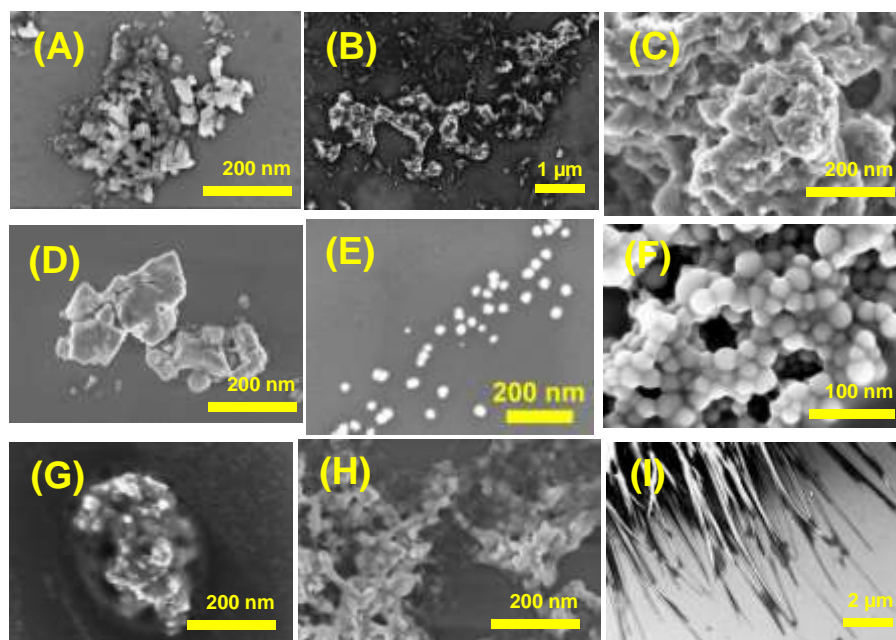
**Figure 5.12**: FESEM images of (A) PNA-G **(P1)**; (B) PNA-G$_2$ **(P2)**; (C) PNA-G$_3$ **(P3)**; (D) PNA-G$_4$ **(P4)**; (E) Phe-Phe-*gly*-PNA-G **(P5)**; (F) Phe-Phe-*gly*-PNA-G$_2$ **(P6)**; (G) Phe-Phe-*gly*-PNA-G$_3$ **(P7)**; (H) Phe-Phe-*gly*-PNA-G$_4$ **(P8)** and (I) H-Phe-Phe-OH (control) **(9)** in water solvent.

The morphological images of peptides in the various solvents in neat solvents (methanol, 1,4-dioxane, acetonitrile) and in mixed solvents (MeOH:H$_2$O; EtOH:H$_2$O and THF:H$_2$O, all 1:1 v/v) were recorded using FESEM. However, none of them exhibited any regular structures. And lead to only aggregate particles in all solvent (Figure 5.13). This indicated poor self-assembly of these peptides in aqueous and hydrophobic environments.
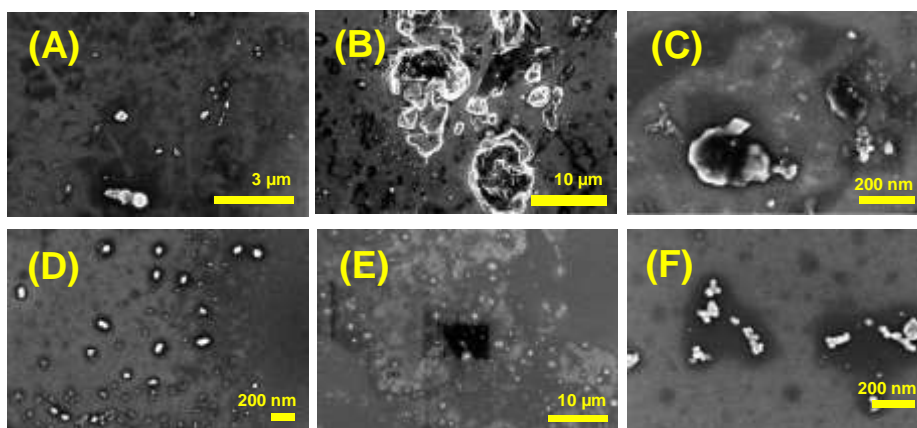


**Figure 5.13**: FESEM images of PNA-G$_2$ **(P2)** in (A) methanol; (B) 1,4-dioxane; (C) acetonitrile; (D) MeOH:H$_2$O (50:50); (E) EtOH:H$_2$O (50:50) and (F) THF:H$_2$O (50:50).

## 5.4 Summary

A series of nucleopeptides containing PNA-$G_n$ oligomers conjugated to Phe-Phe were synthesized, characterized and their ability to self-assemble were studied. Nucleopeptides without C-/N-termini capping and unprotected nucleobases that are mainly hydrophilic in character exhibited poor self-assembly properties. The C/N-protected nucleopeptides that are predominantly hydrophobic showed spherical nanoparticles and these were restricted to lower oligomeric conjugates Phe-Phe-*gly*-PNA-G **(P5)** and Phe-Phe-*gly*-PNA-$G_2$ **(P6)**. Temperature dependent UV thermal melting of conjugated and free PNA $G_n$-oligomers studied at 290 nm for tetraplex formation suggested that only PNA-$G_3$ **(P3)** and PNA-$G_4$ **(P4)** formed tetraplexes like PNA-$G_n$ oligomers suggesting that Phe-Phe dipeptide sterically or electronically interfere with G-quadruplex formation. However, PNA-$G_2$ **(P2)**, PNA-$G_3$ **(P3)** and Phe-Phe-gly-PNA-G **(P5)** that did not form tetraplexes formed duplex structures as seen from temperature dependent UV thermal melting followed at 260 nm.

The Phe-Phe conjugated PNA-$G_{2/3/4}$ oligomers did not show even formation of duplex structures. The overall summary of work presented in this Chapter shows that Phe-Phe disrupt the secondary structure formation by PNA-$G_n$ oligomers perhaps due to either steric or electronic reasons.

## 5.5 Experimental section

**5.5.1 Synthesis of peptides**: Peptides were synthesized manually using a Boc strategy solid phase synthesis. Analytical grade DMF was purchased from (Merck, India) and stored over 4 Å molecular sieves for 2 days before using for peptide synthesis. Similarly, DCM was distilled over $CaH_2$ and stored over 4 Å molecular sieves. Coupling reactions were carried out using *in situ* active ester method, by HBTU as coupling reagent, HOBt as racemization suppresser and DIPEA as catalyst.

The Phe-Phe conjugates with PNA-$G_n$ oligomers were synthesized by solid phase synthesis. Commercially available MBHA (4-methyl benzhydrylamine) resin (Novabiochem, 100-200 mesh) the hydrochloride salt was neutralized performed prior to amino acid coupling and the following steps were done for synthesis (100 mg scale). The resin was washed and swollen in dry DCM for at least 1 hr. The DCM was drained and 50% solution of DIPEA in DCM was added

(3 x 3 mL; 10 min each) followed by thorough washing with DCM. Further washing and swelling with dry DMF for 1 hr. Boc-strategy was used for synthesis on MBHA resin for acid labile protecting groups.

- ➢ DCM wash (4 x 5 mL)
- ➢ 50% TFA in DCM (2 x 5 mL; 10 min each) for deprotection of t-Boc group
- ➢ 5% DIPEA in DCM (3 x 5 mL; 5 min each) for neutralization of TFA salt
- ➢ DCM, MeOH wash (3 x 3 mL each)
- ➢ Kaiser's test
- ➢ DCM, DMF wash (3 x 3 mL each)
- ➢ Coupling reaction (3 eq. each of amino acid, DIPEA, HOBt and HBTU in 10 eq. volume of DMF)
- ➢ Kaiser's test

These cycles ware repeated for every amino acid. The coupling and deprotection reactions were monitored by a combination of Kaiser's (ninhydrin) test. In case of negative test after coupling the re-coupling was performed with same amino acid followed by capping of the unreacted amino groups using $Ac_2O$, DIPEA & DMF (1:1:1), in case coupling does not go to completion even after re-coupling. PNA-$G_n$ oligomers with and without Phe-Phe were synthesized by using Boc-strategy.

**5.5.2 Kaiser's test**: Kaiser's test was used to monitor the Boc and coupling reactions in the solid phase peptide synthesis using three solutions. Solution A: Ninhydrin (5.0 g) dissolved in ethanol (100 ml).

- ➢ Few beads of resin to be tested were taken in a test tube and washed 3 times with ethanol.
- ➢ 3-4 drops of each of the three solutions described above were added to it.
- ➢ The test tube was heated to 120 °C for 4-6 min.
- ➢ The successful deprotection was indicated by blue resin beads while colorless beads indicate the completion of coupling step.

**5.5.3 Peptide cleavage from resin**: Finally after the last coupling the resin was washed with DMF (5 x 5 mL), DCM (5 x 5 mL), then with toluene (5 x 5 mL) and methanol (5 x 5 mL) then flushed with $N_2$-gas for 3 min.

The resin along with the sintered flask was dried in vacuum desiccator over KOH and $P_2O_5$ for 6 hrs. The resin MBHA (10 mg) with peptides attached to it was stirred with TFA (200 µL) and deionized water (10 µL) in an ice bath for 10 min. TFMSA (16 µL) was added slowly with vigorous shaking to dissipate the heat generated. The reaction mixture was stirred for 1.5 hrs at room temperature. The resin was removed by filtration under reduced pressure and washed with TFA (3 x 1 mL). The combined filtrate was concentrated, the product was precipitated with cold dry ether and the peptide was isolated by centrifugation (5 times at 5000 rpm) as white powder.

**5.5.4 High Performance liquid chromatography**: Peptides were purified by reverse phase-HPLC on Agilent Technologies 1260 Infinity equipped with Photodiode array detector (PDA). Semi-preparative RP-C18 columns (250 x 10 mm, 10 µm) of was used for peptides. The solvent system comprised of MeCN:Water (5:95) with 0.1% TFA for solution A and for solution B MeCN: Water (50:50), 0.1% TFA. A gradient of 0-100% at a flow rate of 2 mL/min was used to elute the peptide and the eluent was monitored at 260 nm. The peak corresponding to the peptide was collected and the fractions were freezed. Subsequently these peptides were concentrated by using speed vacuum. The purity of the final peptides was further analyzed on the Phenomenex Analytical RP-C18 (250 x 4 mm, 5 µm) column by using a gradient flow of 0 to 100% B in 30 min at a flow rate of 1 mL/min. The absorbance of the eluent was monitored at its corresponding wavelength and the purity was obtained from the integrator output. The purities of the hence purified peptides were found to be more than 95%.

**5.5.5 MALDI-TOF characterization**: See the experimental section **(2.5.14)** of chapter **2**.

**5.5.6 UV-Vis spectra**: The UV absorbance of various PNA-$G_n$ oligomers with and without Phe-Phe in pure Milli Q water were recorded using Shimadzu UV-2100 spectrophotometer at 25 °C. The points obtained were fitted (Boltzmann) using Origin 8.5 software, and by I[st] derivative of the fitted curve obtained.

**5.5.7 Microscopy studies**: Microscopy experiments were performed in order to characterize the size of the self-assembled morphologies of the nucleopeptides. Sample preparation was done carefully to minimize the effect of sample drying on aggregate formation. Then, 5 µL of peptide-solutions were drop casted on different substrates followed by drying under high vacuum (silicon wafers substrate for FESEM). FESEM images were recorded using Zeiss Ultra Plus scanning electron microscope and the samples were prepared by drop casting on silicon wafers and coated with gold. SEM samples were prepared by depositing nucleopeptide and control peptide solutions in water on silicon wafers, dried at room temperature and imaged it.

## 5.6 References

1. Watson, J. D.; Crick, F. H. C. *Nature* **1953**, *171*, 737-738.

2. (a) Bacolla, A.; Wells, R. D. *Mol. Carcinog.* **2009**, *48*, 273-285; (b) Wang, G.; Vasquez, K. M. *Mutat. Res.* **2006**, *598*, 103-119.

3. Sharma, N. K.; Ganesh K. N. *Chem. Commun*. **2005**, 4330-4332.

4. Dhakal, S.; Yu, Z.; Konik, Cui, R. Y.; Koirala, D.; Mao, H. *Biophys. J.* **2012**, *102*, 2575-2584.

5. Laisne, A.; Pompon, D.; Leroy, J. L. *Nucleic Acids Res.* **2010**, *38*, 3817-3826.

6. Zeraati, M.; Langley, D. B.; Schofield, P.; Moye, A. L.; Rouet, R.; Hughes, W. E.; Bryan, T. M.; Dinger, M. E.; Christ, D. *Nat. Chem*. **2018**, *10*, 631-637.

7. Ye, D.; Zuo, X.; Fan, C. *Annu. Rev. Anal. Chem*. **2018**, *11*, 171-195.

8. Grinsven, B. V.; Eersels, K.; Peeters, M.; Perez, P. L.; Vandenryt, T.; Cleij, T. J.; Wagner, P. *ACS Appl. Mater. Interfaces* **2014**, *6*, 13309-13318.

9. Dong, Y.; Yang, Z.; Liu, D. *Acc. Chem. Res*. **2014**, *47*, 1853-1860.

10. Lin, C.; Liu, Y.; Yan, H. *Biochemistry* **2009**, *48*, 8, 1663-1674.

11. Gellert, M.; Lipsett, M. N.; Davies, D. R. *Proc. Natl. Acad. Sci. U. S. A.* **1962**, *48*, 2013-2018.

12. Pinnavaia, T. J.; Marshall, C. L.; Mettler, C. M.; Fisk, C. L.; Miles, H. T.; Becker, E. D. *J. Am. Chem. Soc.* **1978**, *100*, 3625-3627.

13. *Fundamentals of Quadruplex Structres* (Eds.: Neidle, S.; Balasubramanian S.), The Royal Society of Chemistry, **2006**, pp. 1-30.

14. (a) Smargiasso, N.; Rosu, F.; Hsia, W.; Colson, P.; Baker, E. S.; Bowers, M. T.; De Pauw, Gabelica, E. V. *J. Am. Chem. Soc.* **2008**, *130*, 10208-10216; (b) Huppert, J. L. *The FEBS Journal* **2010**, *277*, 3452-3458; (c) Risitano, A.; Fox, K. R. *Nucleic Acids Res.* **2004**, *32*, 2598-2606; (d) Hazel, P.; Huppert, J.; Balasubramanian, S.; Neidle, S. *J. Am. Chem. Soc.* **2004**, *126*, 16405-16415; (e) Miller, M. C.; Buscaglia, R.; Chaires, J. B.; Lane, A. N.; Trent, J. O. *J. Am. Chem. Soc.* **2010**, *132*, 17105-17107; (f) B. Heddi, A. T. Phan, *J. Am. Chem. Soc.* **2011**, *133*, 9824-9833; (g) Hansel, R.; Lohr, F.; Trantirkova, S. F.; Bamberg, E.; Trantirek, L.; Dotsch, V. *Nucleic Acids Res.* **2011**, *39*, 5768-5775; (h) Guedin, A.; Gros, J.; Alberti, P.; Mergny, J. L. *Nucleic acids Res.* **2010**, *38*, 7858-7868.

15. Vernille, J. P.; Kovell, L. C.; Schneider, J. W. *Bioconj. Chem.* **2004**, *15*, 1314-1321.

16. Sharma, N. K.; Ganesh, K. N. *Org. Biomol. Chem.* **2011**, *9*, 725-729.

17. Davis, J. T. *Angew. Chem. Int. Ed.* **2004**, *43*, 668-698.

18. Simonsson, T. *Biol. Chem.* **2001**, *382*, 621-628.

19. Phan, A. T.; Kuryavyi, V.; Ma, J. B.; Faure, A.; Andreola, M. L.; Patel, D. J. *PNAS* **2005**, *102*, 3, 634-639.

20. Zhang, D. H.; Fujimoto, T.; Saxena, S.; Yu, H. Q.; Miyoshi, D.; Sugimoto, N. *Biochemistry* **2010**, *49*, 21, 4554-4563.

21. Egholm, M.; Buchardt, O.; Christensen, L.; Behrens, C.; Freier, S. M.; Driver, D. A.; Berg, R. H.; Kim, S. K.; Norden, B.; Nielsen, P. E. *Nature* **1993**, *265*, 566-568.

22. Datta, B.; Schmitt, C.; Armitage, B. A. *J. Am. Chem. Soc.* **2003**, *125*, 4111-4118; (b) Marin, V. L.; Armitage, B. A. *J. Am. Chem. Soc.* **2005**, *127*, 8032-8033.

23. Ghosh, Y. K.; Stephens, E.; Balasubramanian, S. *J. Am. Chem. Soc.* **2004**, *126*, 5944-5945.

24. Jain, D. R.; Ganesh, K. N. *J. Org. Chem.* **2014**, *79*, 6708-6714.

25. Kuipers, B. J. H.; Gruppen, H. *J. Agric. Food Chem.* **2007**, *55*, 5445-5451.

26. Lin, Y.; Pashuck, E. T.; Thomas, M. R.; Amdursky, N.; Wang, S. T.; Chow, L. W.; Stevens, M. M. *Angew. Chem. Int. Ed.* **2017**, *56*, 2361-2365.

27. Serpell, C. J.; Barlog, M.; Basu, K.; Fakhoury, J. F.; Bazzi, H. S.; Sleiman, H. F. *Mater. Horiz.* **2014**, *1*, 348-354.

28. Reches, M.; Gazit, E. *Science* **2003**, *300*, 625-627.

29. Datta, D.; Tiwari, O.; Ganesh, K. N. *Nanoscale* **2018**, *10*, 3212-3224.

30. Datta, D.; Tiwari, O.; Gupta, M. K. *ACS Omega* **2019**, *4*, 10715-10728.

31. Reches, M.; Gazit, E. *Nano Lett*. **2004**, *4*, 581-585.

## 5.7 Appendix IV: **Characterization data of synthesized compounds**

| Entry | Table of contents | Page No. |
|-------|-------------------|----------|
| 1 | HPLC trace, MALDI-TOF, HRMS and CD spectra of compounds | 235-239 |
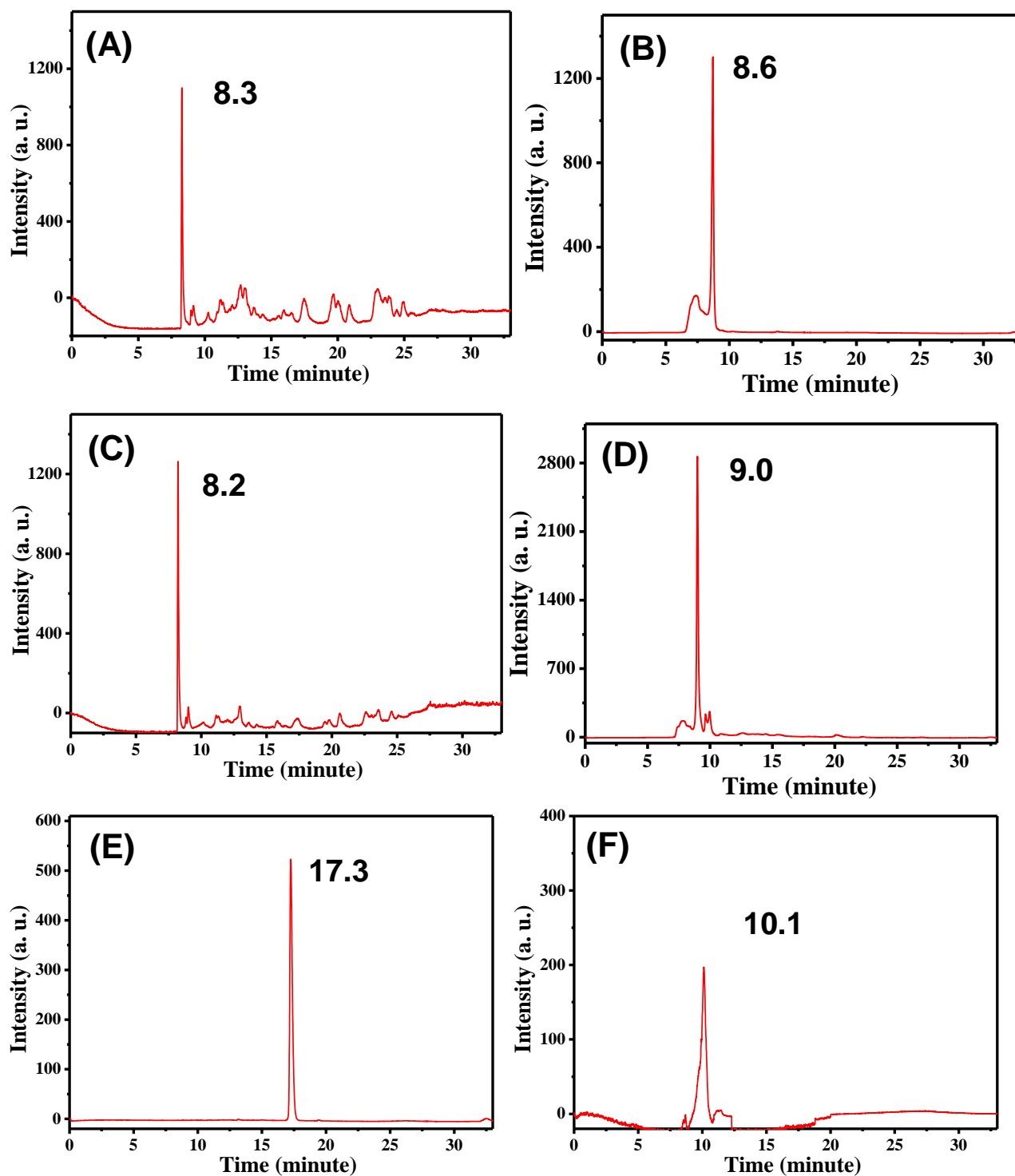
HPLC chromatograms of (A) Phe-Phe-*gly*-PNA-G$_4$ **(P8)**; (B) PNA-G$_4$ **(P4)**; (C) Phe-Phe-*gly*-PNA-G$_3$ **(P7)**; (D) PNA-G$_3$ **(P3)**; (E) Phe-Phe-*gly*-PNA-G$_2$ **(P6)** and (F) PNA-G$_2$ **(P2)**.
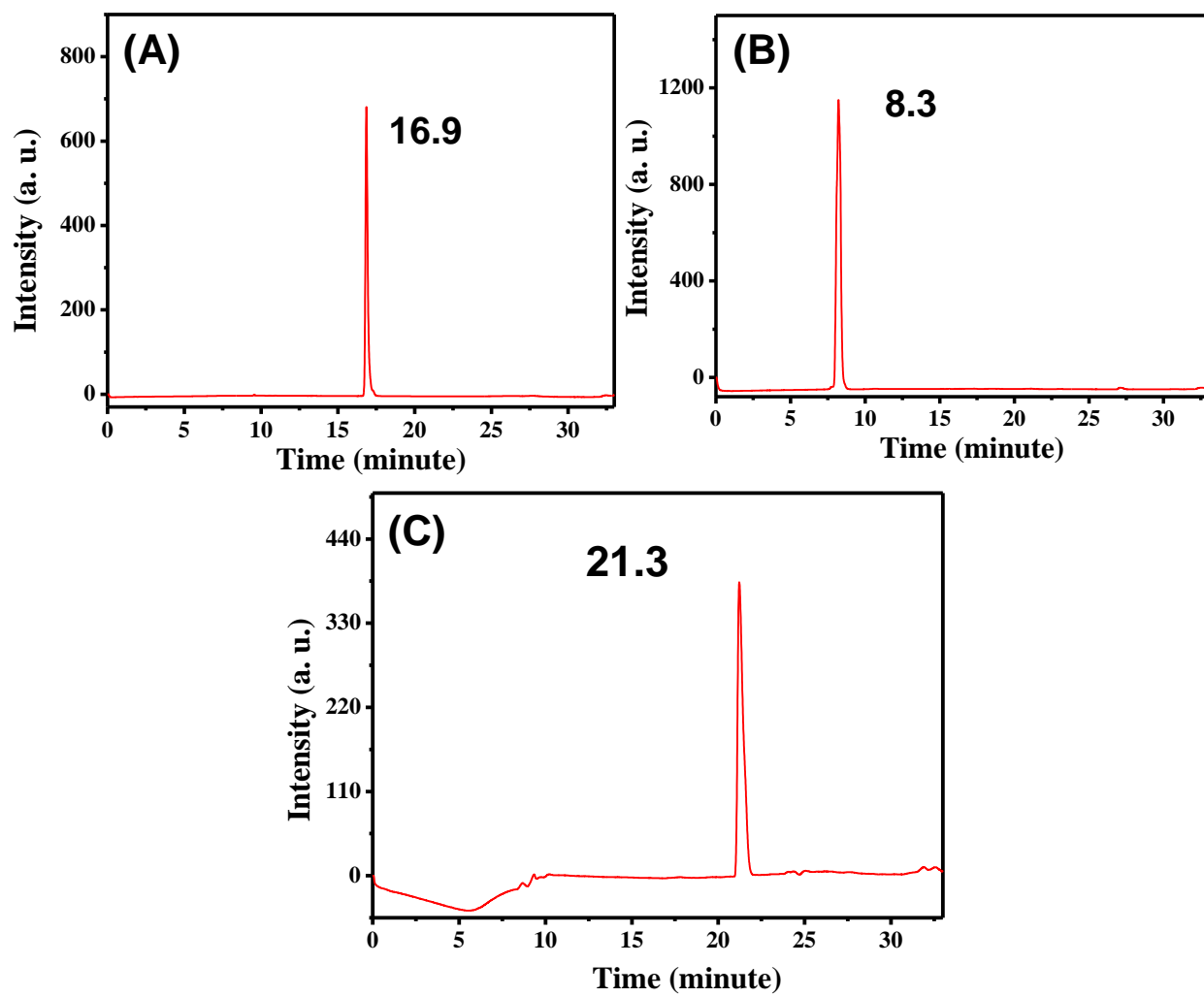
HPLC chromatograms of (A) Phe-Phe-*gly*-PNA-G **(P5)**; (B) PNA-G **(P1)** and (C) H-Phe-Phe-OH **(9)**.
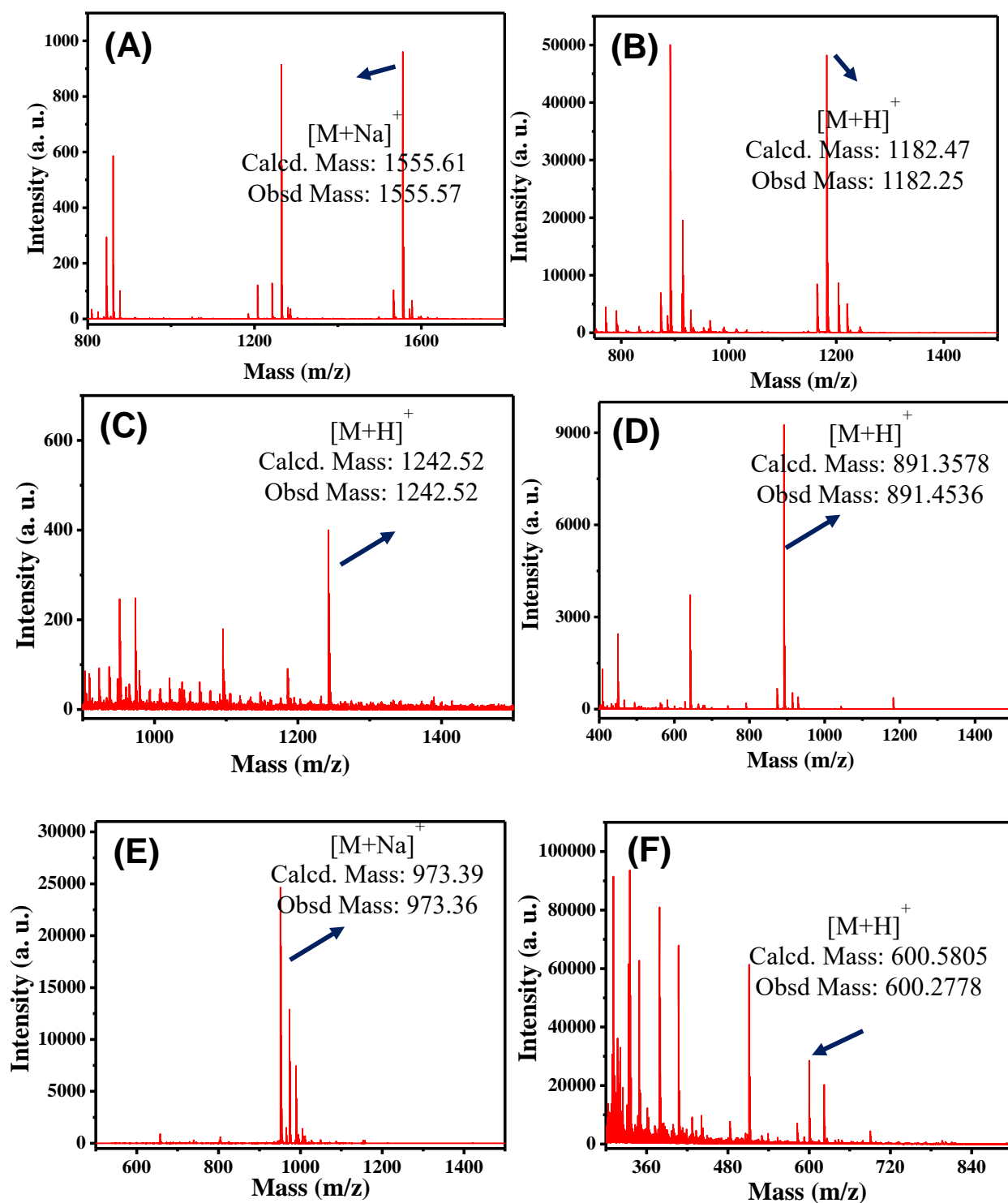
MALDI-TOF Spectrum of (A) Phe-Phe-*gly*-PNA-G$_4$ **(P8)**; (B) PNA-G$_4$ **(P4)**; (C) Phe-Phe-*gly*-PNA-G$_3$ **(P7)**; (D) PNA-G$_3$ **(P3)**; (E) Phe-Phe-*gly*-PNA-G$_2$ **(P6)** and (F) PNA-G$_2$ **(P2)**.
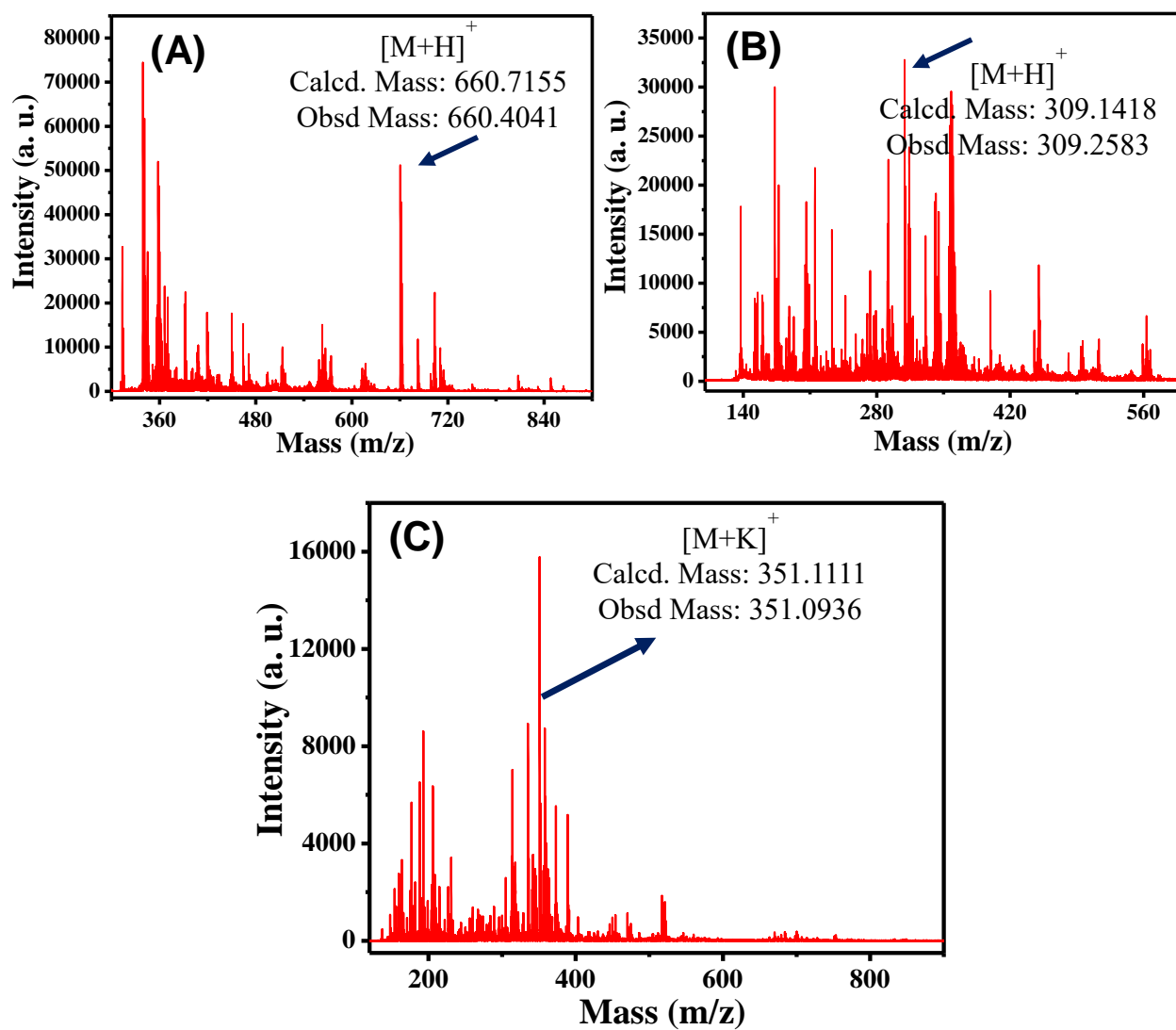
MALDI-TOF Spectrum of (A) Phe-Phe-*gly*-PNA-G **(P5)**; (B) PNA-G **(P1)** and (C) H-Phe-Phe-OH **(9)**.
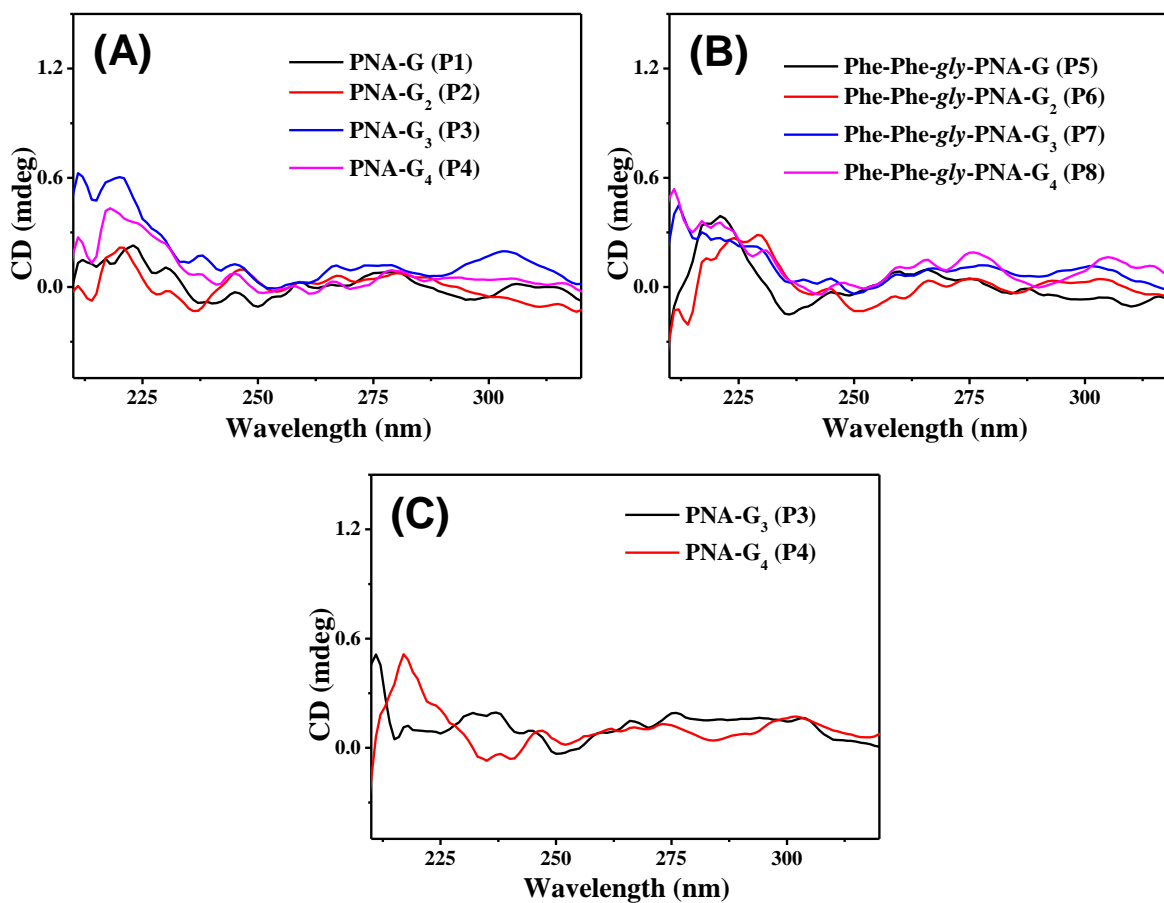
CD spectra of (A) PNA-$G_n$ oligomers without Phe-Phe (20 µm); (B) PNA-$G_n$ oligomers with Phe-Phe (20 µm) and (C) PNA-$G_n$ oligomers without Phe-Phe (50 µm) in sodium cacodylate buffer 20 mM, (pH 7.45), NaCl (100 mM), 25 °C temperature.
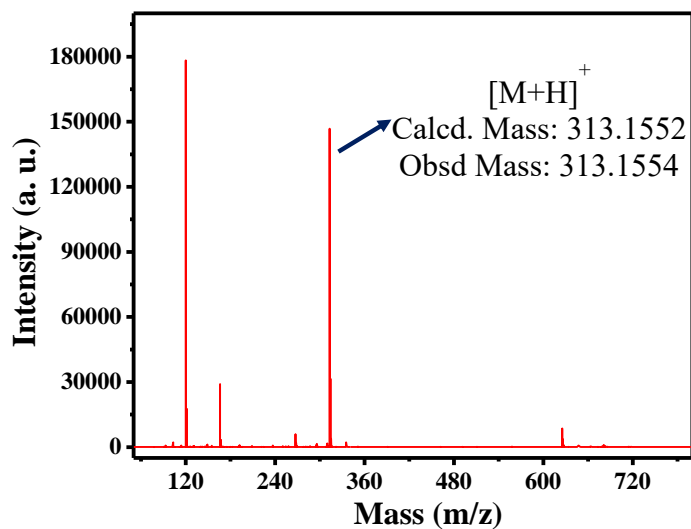


HRMS of H-Phe-Phe-OH (**9**).

# Chapter 6

# Capacitance and Redox Properties of Self-assembled Phe-Phe with PNA and Ferrocene Conjugates

## 6.1 Introduction

Identification of small peptide building blocks for self-assembly is necessary to understand the hierarchical processes through a bottom-up approach.[1] For example, aromatic and aliphatic *L*-amino acids *viz*., phenylalanine (Phe), tyrosine (Tyr), tryptophan (Trp), phenylglycine (Phg), leucine (Leu), isoleucine (Ile), valine (Val) etc. produce a plethora of peptides and proteins as self-assembled biomaterials[2-4] to showcase unique structural features. These architectures are frequently applied in nanophotonics[5], optoelectronics[6], biosensing[7,8] and in electrochemical devices like supercapacitors.[9-11] However, due to readily available starting materials, stability and synthetic ease, short peptides from natural amino acids are considered to be advantageous.[12,13] Self-assembled features of Phe-Phe, a key fragment for Amyloid peptide Aβ-42 in Alzheimer's disease[14,15] are more attractive than any other dipeptides, as they form robust nanotubular morphology[16] emerging as highly ordered biomaterial,[17] and a key element for various fields of biotechnology[18] and nanomedicine[19].

The increasing demand for environment friendly organic semiconductors that can be easily fabricated and tuned has inspired scientists to design self-assembling peptide nanostructures with enhanced semiconducting characteristics. Recently designed bioinspired peptide semiconductors display various supramolecular morphologies with diverse optical and electrical properties, including intrinsic fluorescence, which facilitates real time detection and quantitative assessment of the self-association process without the need for external conjugation. These assemblies have also been studied for their potential use in ferroelectric related devices and ultrasensitive electrochemical sensors. In addition to their low cost fabrication and structural diversity, bioinspired self-assembling peptide semiconductors may serve as candidates for advanced functional nanostructures. Promotion of the design principles of peptide based supramolecular materials are thus of great interest for both scientific and engineering development.

Short peptides, specifically those containing aromatic amino acids, can self-assemble into a wide variety of supramolecular structures that are kinetically or thermodynamically stable; the representative models are diphenylalanine and phenylalanine-tryptophan. Different assembly strategies can be used to generate specific functional organizations and nano-structural arrays, resulting in finely tunable morphologies with controllable semiconducting characteristics. Such strategies include molecular modification, microfluidics, co-assembly, physical or chemical vapor

deposition, and introduction of an external electromagnetic field. Density functional theory simulations have revealed that extensive, directional aromatic interactions and hydrogen-bonding networks lead to the formation of quantum confined domains within the nanostructures, underlying the molecular origin of their intrinsic conductivity. These computational studies provide a conceptual framework for the tenability of the conductivity of a peptide assembly, and also demonstrate the feasibility of theoretical probing of the mechanisms leading to band gap formation and the subsequent design of building blocks with desired electronic properties. Recent studies have further elucidated some remarkable physicochemical features of the bio-inspired supramolecular semiconductors, including absorption spectral characteristic of one-dimensional quantum dots or two-dimensional quantum wells, photoluminescence emission in the visible spectrum, optical wave guiding, temperature-dependent electrical conductivity, ferroelectric (piezoelectric, pyroelectric) and electrochemical properties useful in ultrasensitive detectors and ultra-capacitors. Semi conductive materials are at the foundation of the modern electronics and optics industries. Self-assembling peptide nanomaterials may serve as an alternative source for the semiconductor industry because they are eco-friendly, morphologically and functionally flexible, and easy to prepare, modify and dope. Moreover, the diverse bottom-up methodologies of peptide self-assembly facilitate easy and cost-effective device fabrication, with the ability to integrate external functional moieties. For example, the co-assembly of peptides and electron donors or acceptors can be used to construct n-p junctions, and vapor deposition technology can be applied to manufacture custom-designed electronics and chips on various substrates. The inherent bio-inspired nature of self-assembling peptide nanostructures allows them to bridge the gap between the semiconductor world and biological systems, thus making them useful for applications in fundamental biology and health care research. Short peptide self-assemblies may shed light on the roles of protein conductivity in physiology and pathology. For example, research into the relationship between the semiconducting properties of misfolded polypeptides characteristic of various neurodegenerative diseases and the resulting symptoms may offer opportunities to investigate the mechanisms controlling such ailments and to develop therapeutic solutions. Finally, self-assembling short peptide semiconductors could be used to develop autonomous bio-machines operating within biological systems. This would allow, for example, direct, label free, real time

monitoring of a variety of metabolic activities, and perhaps even interference with biological systems.

Semiconductors are central to the modern electronic industries. However, many conventional semiconducting materials have inherent limitations, especially while interfacing with biological systems and devices using bottom up fabrication. Some of these limitations can be alleviated when the family of self-assembled nanostructures comprising short peptides are used. This is mainly because the highly ordered and directional intermolecular π-π interactions and hydrogen-bonding network do allow the formation of quantum confined structures within the peptide self-assemblies, thus decreasing the band gap of the superstructures from insulating to semiconducting level regions. As a result of the diverse architectures and ease of modification of peptide self-assemblies, their conductivity can be readily tuned either by doping or functionalization or even both. Therefore, this family of electroactive supramolecular materials may bridge the gap between the inorganic semiconductors and biological systems.[20]

Since, the formation of discrete and well-ordered peptide nanotubes by Phe-Phe derived motifs, represents the key element of the Alzheimer's *β*-amyloid peptide[21] combined with their stability, biocompatibility and water-solubility attributes make them ideal for applications *in* bio-sensing and catalysis.[22-26] For example, by employing peptide nucleic acid (PNA) dimers, Gazit *et. al*., recently demonstrated that three guanine (G)-containing analogues *viz*., CG, GC and GG among the sixteen possible dimer combinations exhibit a wide-range of excitation-dependent fluorescence in the visible region along with unusual properties like voltage-dependent electroluminescence. These arise from a combination of both stacking interactions and Watson-Crick base pairing as evident from the single crystal structure of GC pair.[27] The Fmoc protected GC PNA dimer also forms highly fluorescent aggregates[28] exhibiting aggregation induced emission (AIE) that promise new materials for organic light emitting diodes. In comparison, self-assembly of PNA N-capped G-monomer *N*-(*N*-Fmoc-2-aminoethyl)-*N*-[(*N*-6-Bhoc-9-guanyl)acetyl]-glycine [Fmoc-G$^{NHBhoc}$-*aeg*-OH] leads to nanospheres with unique optical[29] and 'structure color'[30] properties, with the formation of photonic crystals useful for optoelectronics. Also, Porphyrin and BODIPY conjugates of PNA monomers have recently been reported as promising candidates for photocatalytic applications.[31]

These parallel developments in self-assembly of dipeptide Phe-Phe and PNA G- monomer prompted us to explore the nucleopeptide conjugates of Phe-Phe with monomeric PNA motifs to examine their combined influence on mutual self-assembling properties.

Nucleobases on a flexible PNA backbone form facile base pairing just as those on rather conformationally constrained ribose / deoxyribose backbones. Hence, PNA monomers were conjugated to C-terminus of Phe-Phe motif through different linkers [amide (*am*) and triazole (*tz*)] and effects of hydrophobic substituents (Boc, Cbz, $^i$Bu etc.) and nucleobases (A/G/C/T) were investigated on self-assembly of Phe-Phe nucleopeptides. The morphological changes of these conjugated nucleopeptides were monitored through microscopic techniques (SEM, and AFM) to reveal interesting hollow and solid nanospheres. Finally, the triazole modified nucleopeptides which showed porosity and excellent stability, prompted us to examine their possible electrochemical behavior using the cyclic voltammetry (CV). Subtle changes in the redox properties like the number of electrons transferred in the rate determining step as well as the relative charge storage ability were investigated by comparing the voltammograms under similar conditions by applying a suitable voltage sweep.[32]

## 6.2 Objectives of the present work

The specific objectives of this chapter are following:

➢ Investigation of the electrochemical properties like charge-storage (capacitance) and electron-transfer properties through cyclic voltammetry.

➢ Synthesis of Ferrocene (Fc) conjugated peptides: Fc-Phe-Phe-Propyne **(4)**, Fc-Phe-Phe-*tz*-A$^{N(Boc)2}$ **(6)**, Fc-Phe-Phe-*tz*-*aeg*{A$^{(Boc)2}$}-OEt **(8)**, Boc-Phe-Phe-*tz*-Fc **(10)** and Fc-Phe-Phe-*tz*-Fc **(11)**.

➢ Characterization of these peptides by HRMS, $^1$H, $^{13}$C NMR spectroscopy.

➢ Study of self-assembly by field emission scanning electron microscopy (FESEM) and atomic force microscopy (AFM) along with the analysis of the size distribution of nanospheres and rods in solution by Dynamic Light Scattering (DLS) studies.

## 6.3 Results and discussions

Porosity in materials plays an important role in regulating the interfacial surface area which can indirectly control several electrochemical properties like charge storage ability (capacitance) and redox behavior. In the previous chapter it was seen that the triazole modified peptides (Figure 6.1) form hollow/porous nanostructures while Boc-Phe-Phe-propyne (**1**) reveals fibrous morphology. This chapter, in comparison, explores the effect of conjugation of Phe-Phe with nucleosides as well as PNA on their electrochemical properties.
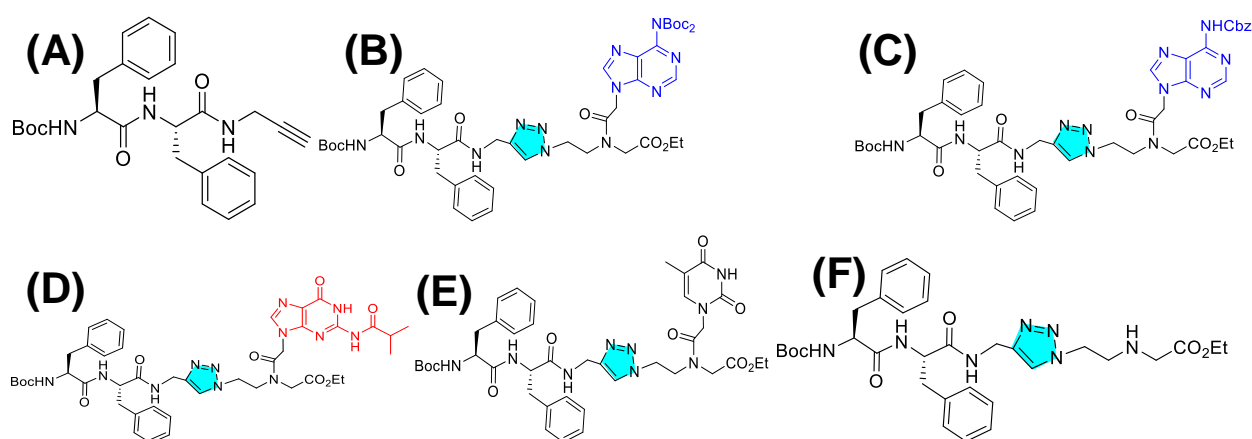


**Figure 6.1**: Structures of (A) Boc-Phe-Phe-Propyne (**1**); (B) Boc-Phe-Phe-*tz-aeg*{A$^{N(Boc)2}$}-OEt (**P2**); (C) Boc-Phe-Phe-*tz-aeg*(A$^{NHCbz}$)-OEt (**P3**); (D) Boc-Phe-Phe-*tz-aeg*(G$^{NHiBu}$)-OEt (**P4**); (E) Boc-Phe-Phe-*tz-aeg*(T)-OEt (**P5**) and (F) Boc-Phe-Phe-*tz-aeg*-OEt (**P6**).

**6.3.1 Cyclic voltammetry of modified electrodes**: The porous nature of the peptide films often modify the electrode properties by increasing the effective surface area in order to allow better interaction of the ions in the electrolyte at the interface. Further, the poor wettability of many semiconducting materials like graphite and carbon nanotubes also could be solved by facilitating interfacial bonding and consequently, many porous, self-assembled nucleopeptides exhibit semiconducting properties.[20] For example, by employing vapor deposition technique to generate vertically aligned diphenylalanine-peptide nanotubes on modified electrodes, Gazit *et. al.*,[33] observed that such modifications lead to better efficiency of hydrophobic graphite electrodes, which also enables longevity even after several cycles.[34]

Expecting such enhanced stability from porous Boc-Phe-Phe-*tz*-PNA, electrochemical studies were performed by cyclic voltammetry (CV) using Torey carbon electrodes coated with peptides as working electrodes. The CV profiles for all tested electrodes displayed a rectangular (Figure 6.2) and symmetric shape, consistent even after 500 cycles, which is a clear evidence of a charge-discharge storage using double layer capacitance with no obvious Faradaic effects.[35] The value of capacitance (Table 6.1) suggests that these peptides could be used as efficient supercapacitors. The capacitance of the unmodified Torey carbon electrode in comparison, was only 72.0 µF/cm$^2$ at a typical scan rate of 50 mV/s scan rate. Interestingly, after modification with the G-peptide [Boc-Phe-Phe-*tz*-*aeg*(G$^{NHiBu}$)-OEt **(P4)**], it exhibited a higher capacitance of 495 µF/cm$^2$ under similar conditions, almost 7 times more than that for the uncoated carbon electrode.
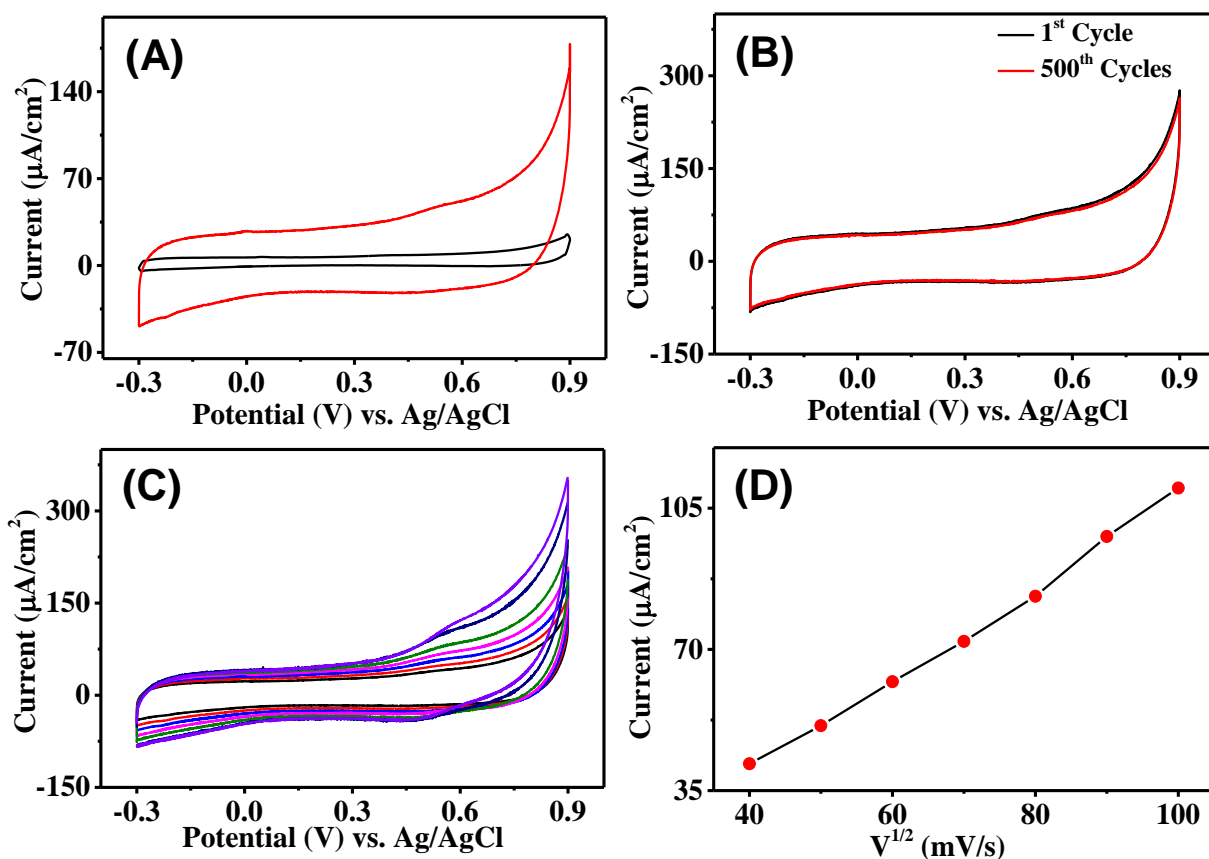


**Figure 6.2**: Cyclic voltammograms of Boc-Phe-Phe-*tz*-*aeg*(G$^{NHiBu}$)-OEt **(P4)** supported on Toray Carbon electrode in 0.1 M potassium phosphate buffer electrolytes at pH = 7.4 and 0.1 M KCl (A) at a scan rate of 50 mV/s; (B) at a scan rate of 100 mV/s of 1$^{st}$ and 500$^{th}$ cycles; (C) and (D) variation with different scan rates from 40 mV/s to 100 mV/s.

Electrodes coated with adenine and thymine modified peptides (**P2**, **P3** and **P5** respectively) however, displayed lower capacitance (Figure 6.3-6.5) values than that of G-analogue. Given the differences in their morphology, this could probably be attributed to the nature of self-assembly. As a control for nucleopeptides, peptide Boc-Phe-Phe-*tz-aeg*-OEt **(P6)** revealed a capacitance value of 142 µF/cm$^2$ under similar conditions although for peptide **P6,** a perturbed rectangular shape was observed unlike the symmetric nature for nucleopeptides (Figure 6.6) indicating the involvement of a Faradaic process.
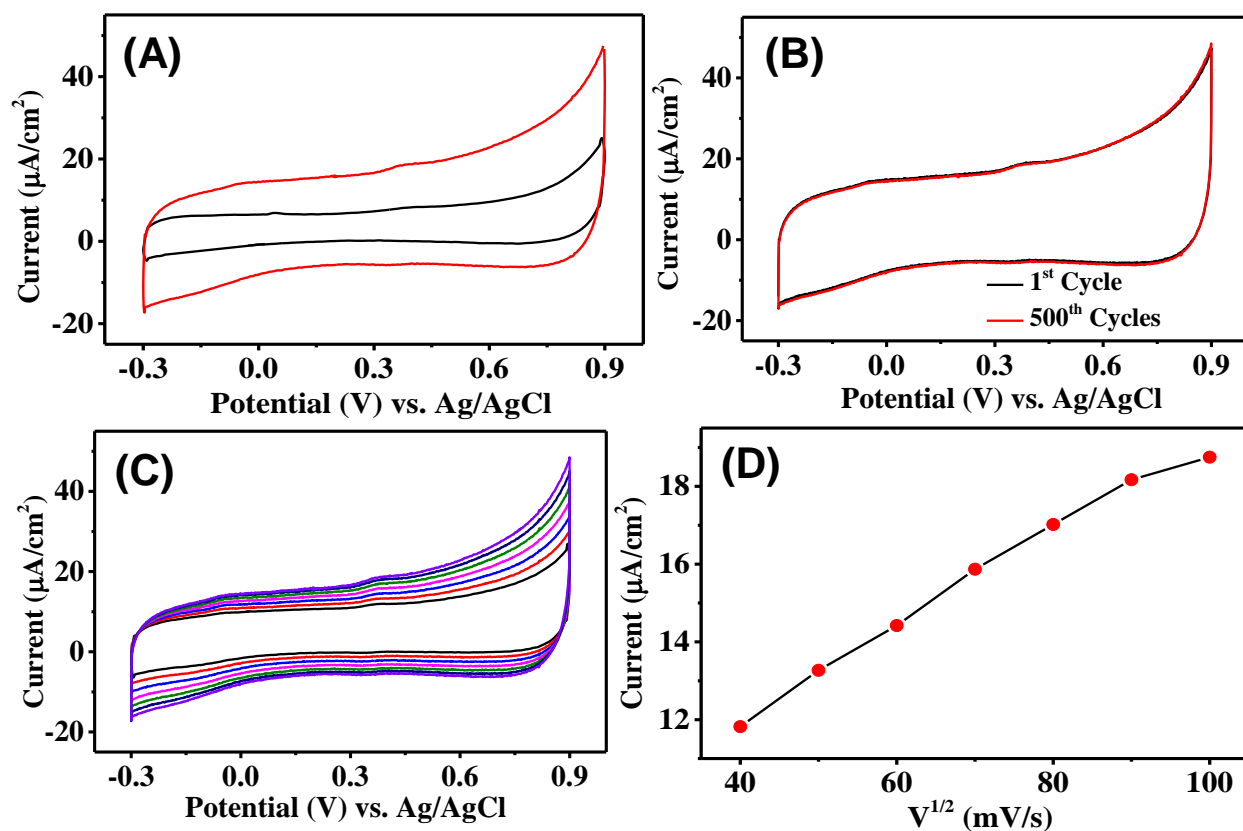


**Figure 6.3**: Cyclic voltammograms of Boc-Phe-Phe-*tz-aeg*{A$^{N(Boc)2}$}-OEt **(P2)** supported on Toray Carbon electrode in 0.1 M potassium phosphate buffer electrolytes at pH = 7.4 and 0.1 M KCl (A) at a scan rate of 50 mV/s; (B) at a scan rate of 50 mV/s of 1$^{st}$ and 500$^{th}$ cycles; (C) and (D) variation of current with different scan rates from 40 mV/s to 100 mV/s.

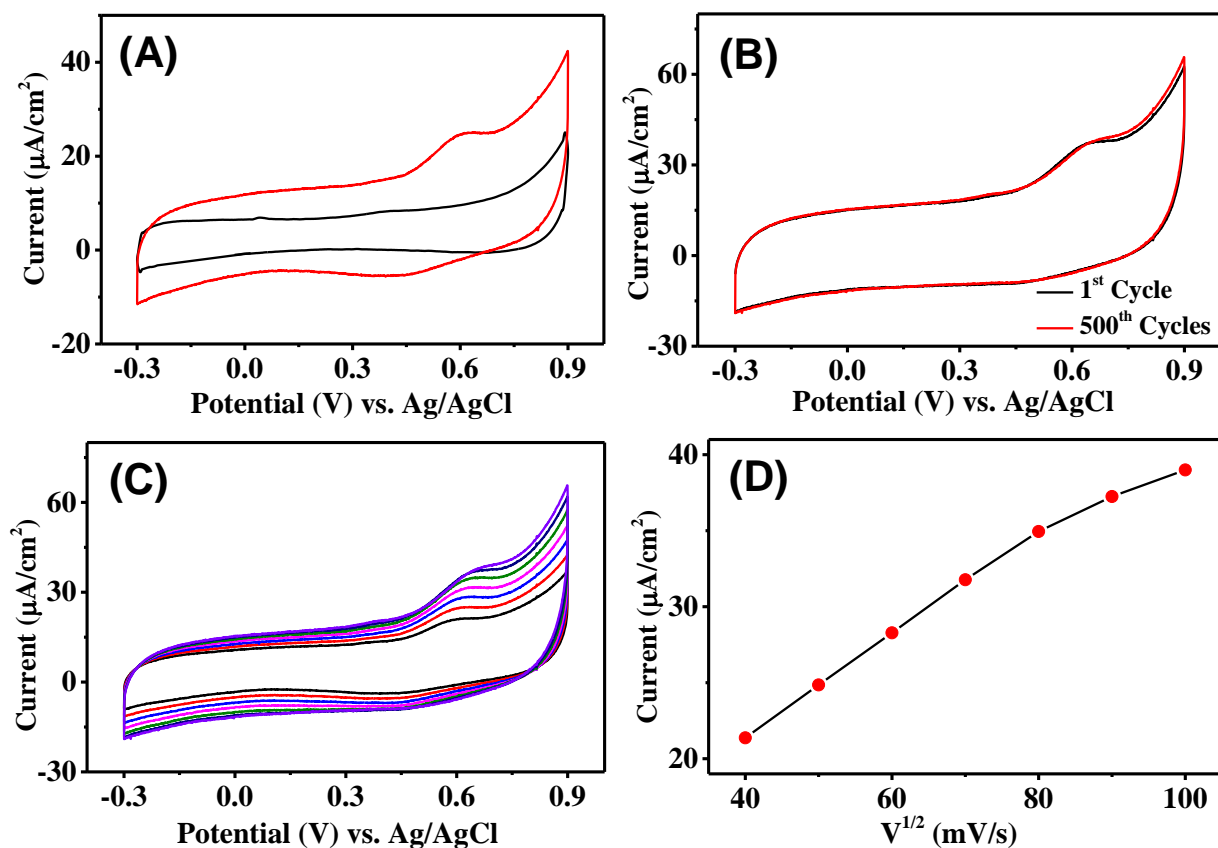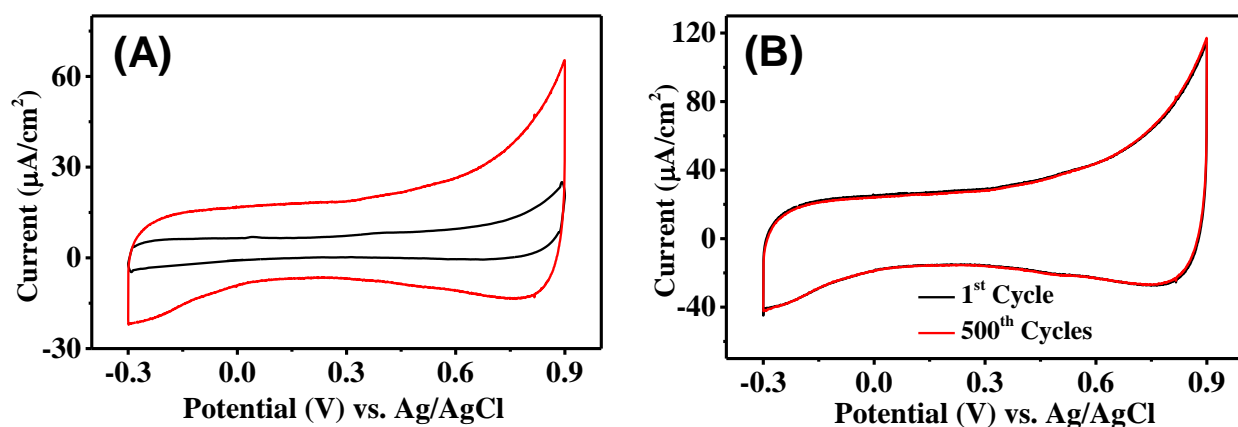**Figure 6.4**: Cyclic voltammograms of Boc-Phe-Phe-*tz-aeg*(A^NHCbz)-OEt **(P3)** supported on Toray Carbon electrode in 0.1 M potassium phosphate buffer electrolytes at pH = 7.4 and 0.1 M KCl (A) at a scan rate of 50 mV/s; (B) at a scan rate of 100 mV/s of 1st and 500th cycles; (C) and (D) variation with different scan rates from 40 mV/s to 100 mV/s.
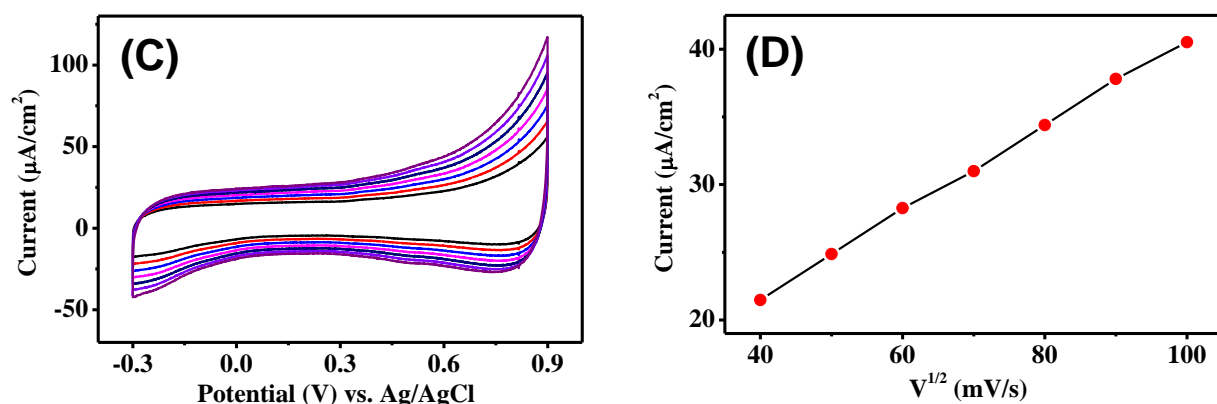
**Figure 6.5**: Cyclic voltammograms of Boc-Phe-Phe-*tz-aeg*(T)-OEt **(P5)** supported on Toray Carbon electrode in 0.1 M potassium phosphate buffer electrolytes at pH = 7.4 and 0.1 M KCl (A) at a scan rate of 50 mV/s; (B) at a scan rate of 100 mV/s of 1$^{st}$ and 500$^{th}$ cycles; (C) and (D) scan rate effect at different scan rate from 40 mV/s to 100 mV/s.
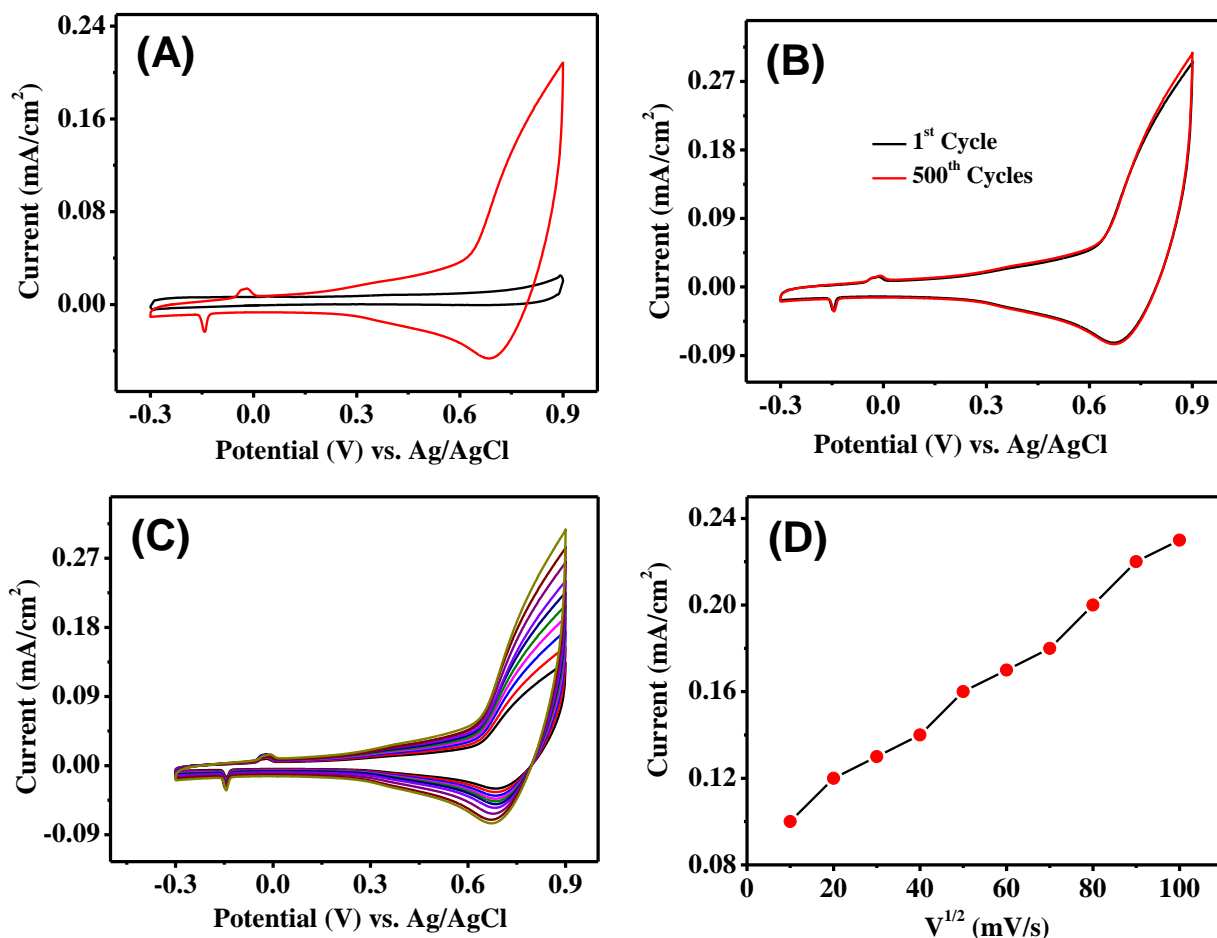


**Figure 6.6**: Cyclic voltammograms of Boc-Phe-Phe-*tz-aeg*-OEt **(P6)** supported on Toray Carbon electrode in 0.1 M potassium phosphate buffer electrolytes at pH = 7.4 and 0.1 M KCl (A) at a scan rate of 50 mV/s; (B) at a scan rate of 100 mV/s of 1$^{st}$ and 500$^{th}$ cycles; (C) and (D) scan rate effect at different scan rate from 10 mV/s to 100 mV/s.

**Table 6.1**: Capacitance values of peptide modified Torey carbon electrodes at scan rate (SR) of 50 mV/s.

| Peptide used for electrode modification | Capacitance ($\mu F/cm^2$) at 50 mV potential vs. Ag/AgCl |
|---|---|
| Boc-Phe-Phe-*tz-aeg*{A$^{N(Boc)_2}$}-OEt **(P2)** | 217.0 |
| Boc-Phe-Phe-*tz-aeg*(A$^{NHCbz}$)-OEt **(P3)** | 171.0 |
| Boc-Phe-Phe-*tz-aeg*(G$^{NHiBu}$)-OEt **(P4)** | 495.0 |
| Boc-Phe-Phe-*tz-aeg*(T)-OEt **(P5)** | 249.0 |
| Boc-Phe-Phe-*tz-aeg*-OEt **(P6)** | 142.0 |
| None (unmodified electrode) | 72.0 |

Based on these results, it is proposed that the porous nature of *tz*-linked NPs enhances the electrode-electrolyte contact, leading to improved electrical conductivity. Therefore, it is expected that these self-assembled NPs with perforated morphology follow a similar mechanism as reported by Gazit *et. al.*,[34-36] in enhancing the capacitance of modified electrodes. Thus, without sophisticated vapor deposition method, a simple coating of these peptides resulted (see experimental section) in attaining good charge storage efficacy. Self-assembled peptide nanoparticles can potentially create well-defined porous membranes which could efficiently interact with the electrolyte ions compared to bare and hydrophobic Torey carbon electrodes.

For a control study in the absence of the conjugation of the nucleoside and PNA, Boc-Phe-Phe-Propyne **(1)** was used. The cyclic voltammetry performed under similar conditions showed a clear reduction as well as oxidation peak (Figure 6.7). From the cyclic voltammogram (Figure 6.7) the peak current density is 135.0 $\mu A/cm^2$ at 100 mV/s with a half-wave potential of ($E_{redox}$) 199 mV. The morphology of nanorod seen before was retained even after drop casting on the electrode (Toray carbon) surface. This was confirmed with the help of the SEM and EDX images (Figure 6.8). The nanorods on the Toray carbon electrode surface was very much stable during the electrochemical measurement as confirmed through FESEM images (Figure 6.9).
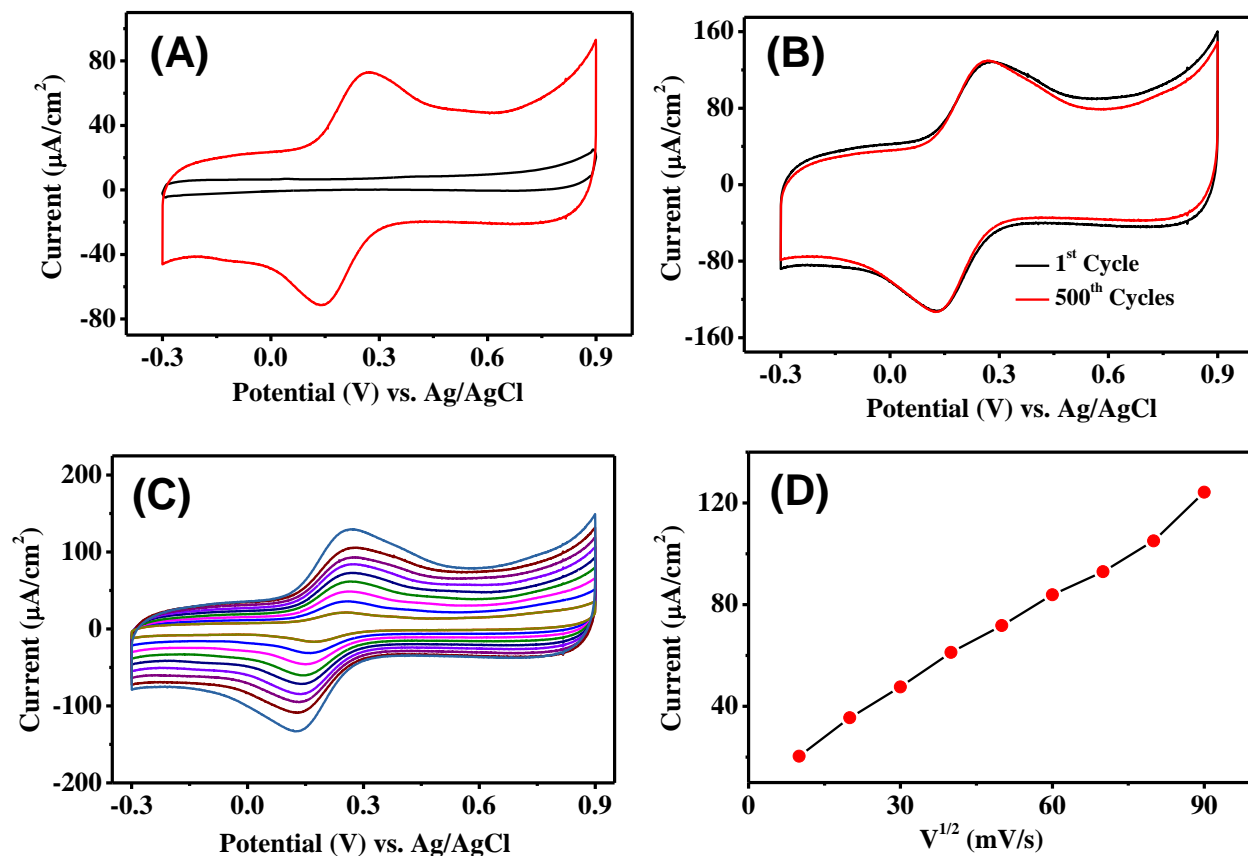
**Figure 6.7**: Cyclic voltammograms of Boc-Phe-Phe-Propyne (**1**) supported on Toray Carbon electrode in 0.1 M potassium phosphate buffer electrolytes at pH = 7.4 and 0.1 M KCl (A) at a scan rate of 50 mV/s; (B) at a scan rate of 100 mV/s of 1$^{st}$ and 500$^{th}$ cycles; (C) and (D) scan rate effect from 10 mV/s to 90 mV/s.
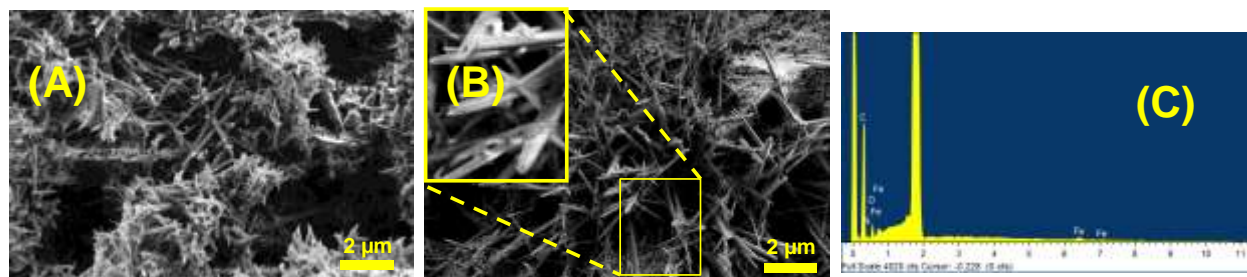


**Figure 6.8**: FESEM and EDX image of Boc-Phe-Phe-Propyne (**1**) after dropcasted on the Toray carbon electrode.
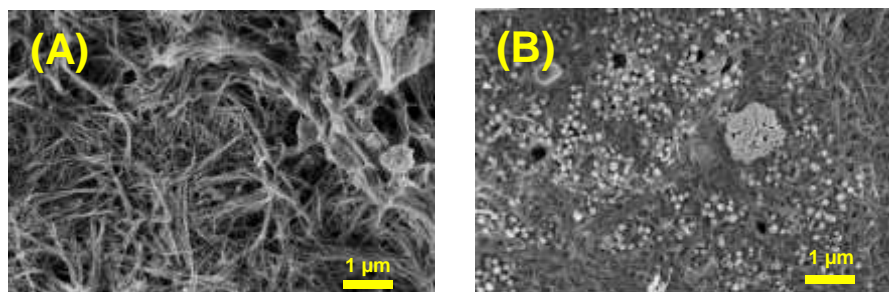
**Figure 6.9**: FESEM images of Boc-Phe-Phe-Propyne (**1**) (A) before and (B) after cyclic voltammetry experiment.

**6.3.2 Synthesis of ferrocene peptides:** Deprotection of Boc group of Boc-Phe-Phe-Propyne (**1**)[36] under acidic condition afforded peptide **2**. This was condensed with ferrocene (Fc) carboxylic acid (**3**) at C-terminus to afford **4** (Scheme 6.1). The alkyne groups of Boc/Fc-Phe-Phe-Propyne (**1** and **4**) were functionalized by 'click' chemistry with the nucleoside azide (**5**) as well as the azide of PNA (**7**) to get the compound **6** [Fc-Phe-Phe-*tz*-A$^{N(Boc)2}$] and **8** [Fc-Phe-Phe-*tz*-*aeg*{A$^{(Boc)2}$}-OEt]. Finally, *N*-(2-azidoethyl)ferrocenyl formamide (**9**) was synthesized through coupling reaction of **3** and 2-azido-ethylamine.[37] Peptide **1** was then clicked with **9** in presence of CuSO$_4$.5H$_2$O and sodium-*L*-(+)-ascorbate to get the peptide **10**, which has ferrocene conjugated at N-terminus. Similarly, peptide **11** was obtained from **4** after clicking ferrocene azide **9** (Scheme 6.2) and has ferrocene unit at both N and C-terminii.
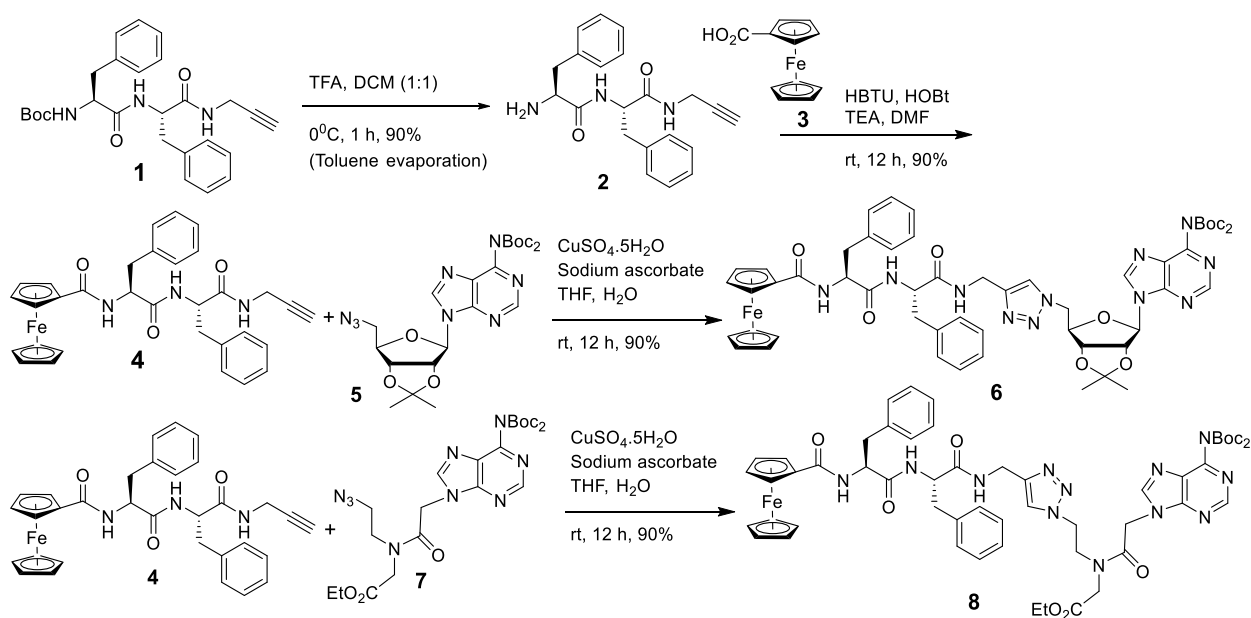


**Scheme 6.1**: Synthesis of ferrocene conjugated triazole linked nucleopeptide **6** and **8**.
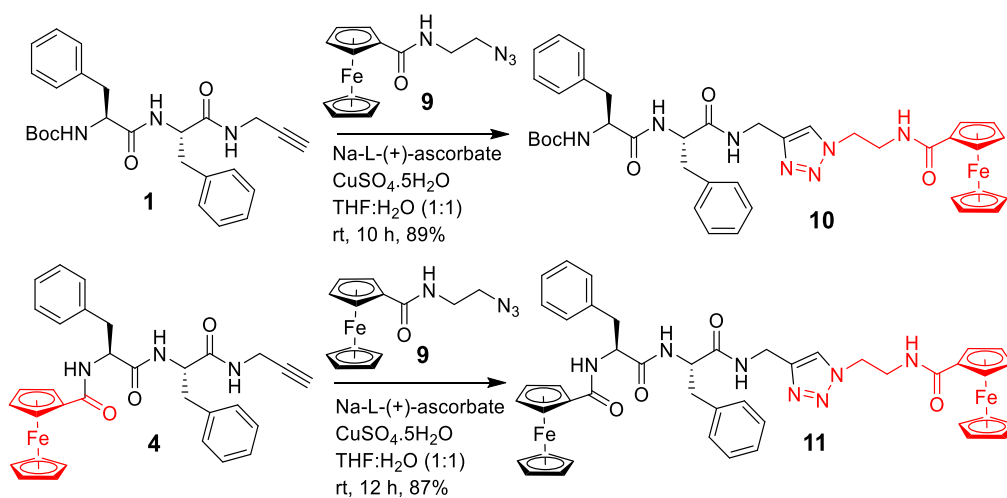
**Scheme 6.2**: Synthesis of ferrocene conjugated triazole linked peptide **10** and **11**.

**6.3.3 Morphology of peptides**: Self-assembly of the five ferrocenyl diphenyl nucleoppeptides was studied through scanning electron microscopy (SEM) and atomic force microscopy (AFM) images after preparation of samples in 1,1,1,3,3,3-hexafluoro-2-propanol (HFIP) and 50% aqueous ethanol. Peptide **4** gave a tubular like structure (Figures 6.10A and 6.11A). The ferrocenyl peptide **6** [Fc-Phe-Phe-*tz*-A$^{N(Boc)_2}$] and **8** [Fc-Phe-Phe-*tz*-*aeg*{A$^{(Boc)_2}$}-OEt] self-assembled into spheres in SEM (Figures 6.10B and C) and confirmed by AFM (Figures 6.11B and C). The peptide **10** (Boc-Phe-Phe-*tz*-Fc) with ferrocenyl unit on N-terminus also gave well-defined spherical nanoparticles. Thus ferrocene conjugation on the N-terminus or on the C-terminus did not have any perceptible effect on the morphology, which remained spheres with a hollow core (Figures 6.10D and 6.11D).

Finally, in order to check the effect of the ferrocene on both the termini (N and C-termini) on the morphology, the FESEM and AFM images of peptide **11** (Fc-Phe-Phe-*tz*-Fc) with ferrocenyl units on both N and C-termini were recorded (Figure 6.10E and 6.11E). These also showed the spherical structure with a hollow core. From the height profile (Figure 6.12A and B) it is clear that the size of the spherical particles vary from 150 to 1500 nm. These observations were further supported by the time-dependent dynamic light scattering (DLS) study where a broad size-distribution of bigger particles of peptide **4** [average size = 1372 nm and polydispersive index (PDI) value: 0.19] (Figure 6.13A), peptide **6** [average size = 701 nm and polydispersive index (PDI) value: 0.25] (Figure 6.13B) and peptide **8** [average size = 675 nm and polydispersive index

(PDI) value: 0.28] (Figure 6.13C) were observed. Elemental composition from energy dispersive spectroscopy (EDX) confirmed peptide composition including iron (Figure 6.14).
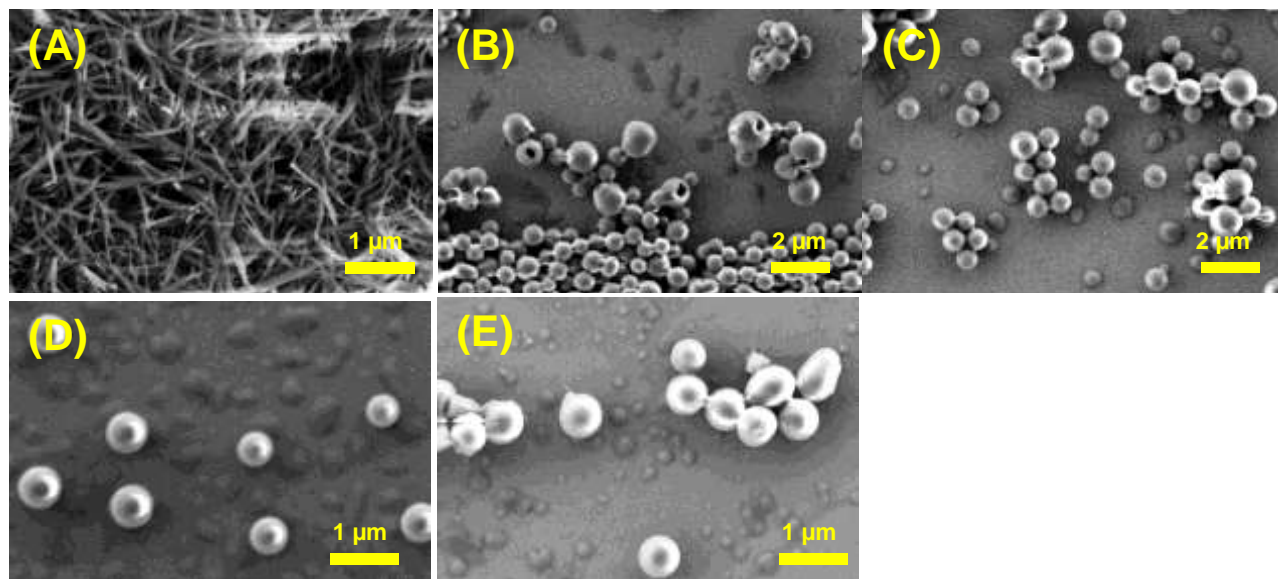


**Figure 6.10**: SEM images of (A) Fc-Phe-Phe-Propyne **(4)**; (B) Fc-Phe-Phe-*tz*-A$^{N(Boc)2}$ **(6)**; (C) Fc-Phe-Phe-*tz-aeg*{A$^{(Boc)2}$}-OEt **(8)**; (D) Boc-Phe-Phe-*tz*-Fc **(10)** and (E) Fc-Phe-Phe-*tz*-Fc **(11)**.
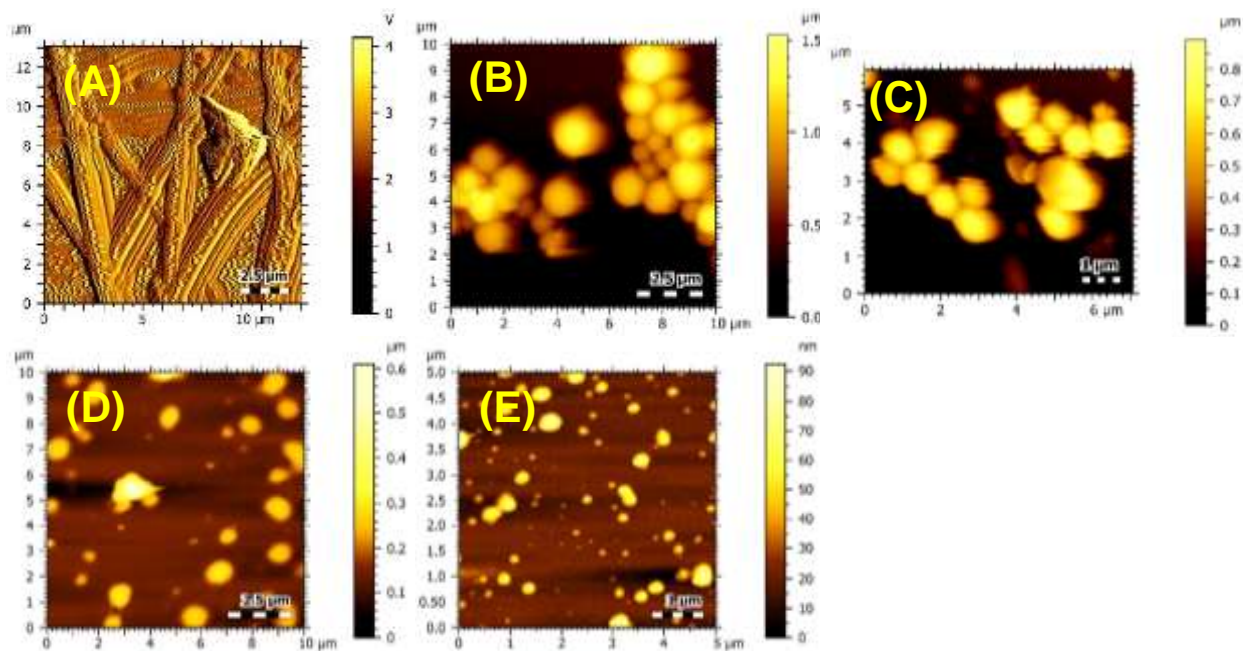


**Figure 6.11**: AFM images of (A) Fc-Phe-Phe-Propyne **(4)**; (B) Fc-Phe-Phe-*tz*-A$^{N(Boc)2}$ **(6)**; (C) Fc-Phe-Phe-*tz-aeg*{A$^{(Boc)2}$}-OEt **(8)**; (D) Boc-Phe-Phe-*tz*-Fc **(10)** and (E) Fc-Phe-Phe-*tz*-Fc **(11)**.
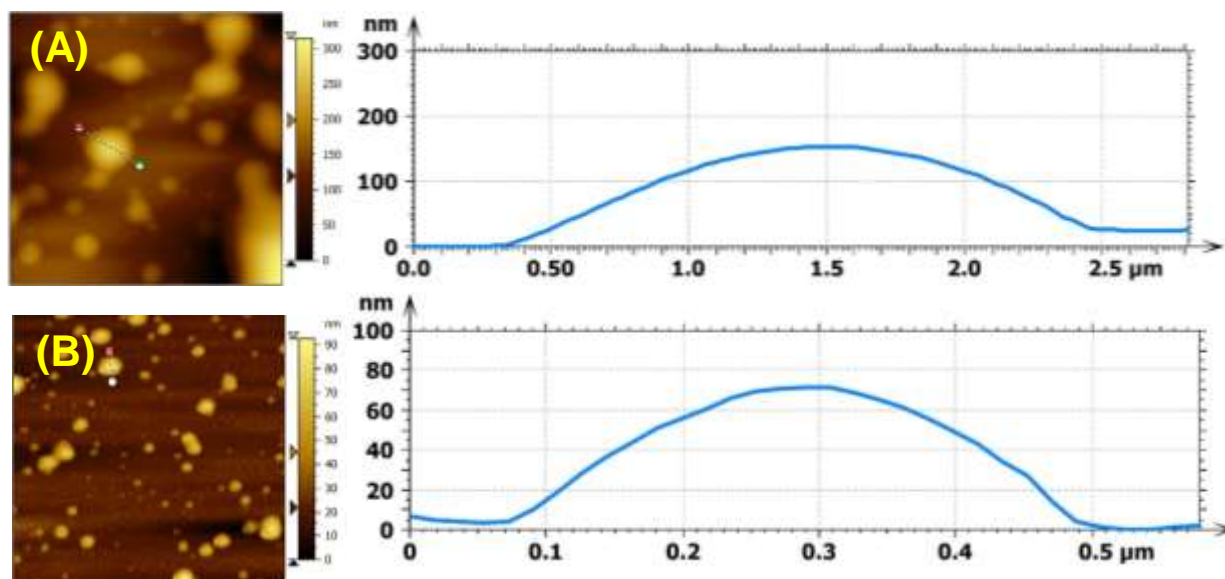
**Figure 6.12**: Height profiles and AFM images of (A) Boc-Phe-Phe-*tz*-Fc (**10**) and (B) Fc-Phe-Phe-*tz*-Fc (**11**).
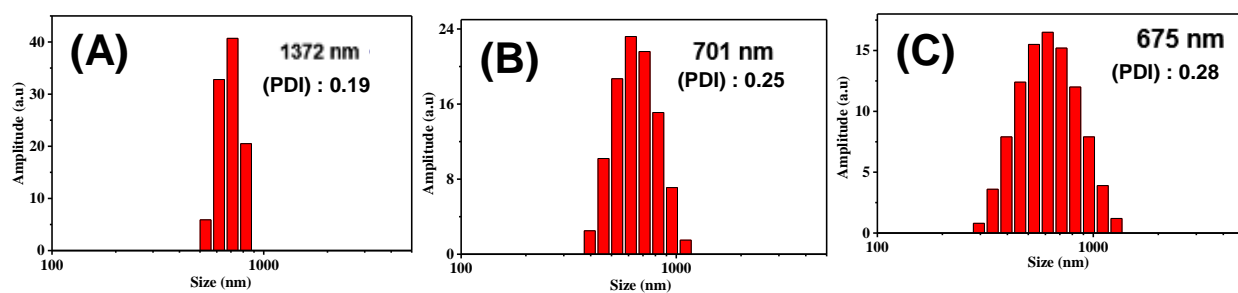


**Figure 6.13**: DLS spectra of (A) Fc-Phe-Phe-Propyne (**4**); (B) Fc-Phe-Phe-*tz*-A$^{N(Boc)2}$ (**6**) and (C) Fc-Phe-Phe-*tz*-*aeg*{A$^{(Boc)2}$}-OEt (**8**).



| Element | Weight% | Atomic% |
|---------|---------|---------|
| C K | 54.44 | 59.90 |
| N K | 27.60 | 26.04 |
| O K | 16.64 | 13.74 |
| Fe K | 1.33 | 0.31 |
| Total | 100 | |
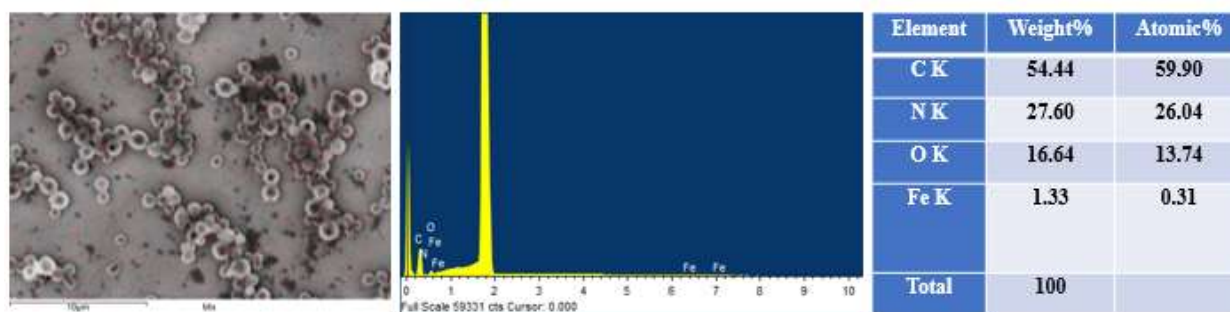
**Figure 6.14**: EDX images of (A) Fc-Phe-Phe-*tz*-A$^{N(Boc)2}$ (**6**).

**6.3.4 Cyclic voltammetry of ferrocene modified electrodes**: The CV study on control ferrocene peptide Fc-Phe-Phe-Propyne (**4**) in the absence of conjugation of the nucleoside showed a clear reversible redox behavior (Figure 6.15). The peak current density was 344.0 µA/cm$^2$ at 100 mV/s scan rate with a half-wave potential of (E$_{redox}$) of 485 mV. The current density response versus voltage for the triazole peptide modified electrode was found to be higher than that of an unmodified-carbon electrode. The CV profiles for all tested electrodes presented reduction as well as oxidation peaks (Figure 6.16), consistent even after 500 cycles. The value of capacitance (Table 6.2) suggests that these peptides can be used as efficient supercapacitors. The capacitance of the unmodified Torey carbon electrode was 72.0 µF/cm$^2$ at 50 mV potential vs. Ag/AgCl. After modification with ferrocene on both sides, the peptide Fc-Phe-Phe-*tz*-Fc (**11**) exhibited a highest capacitance of 2210 µF/cm$^2$ at 50 mV potential vs. Ag/AgCl (so that there is no interference from Faradaic processes), 30 times higher than that for the uncoated carbon electrode and 10 times higher than that without ferrocene conjugated peptide (**P2**). Electrodes coated with ferrocene conjugated nucleoside (**6**), PNA modified peptide (**8**) and peptide with ferrocene conjugated on the C-terminus (**10**) displayed a lower capacitance (Figure 6.17-6.19) than that of G-analogue, probably attributed to morphological features.
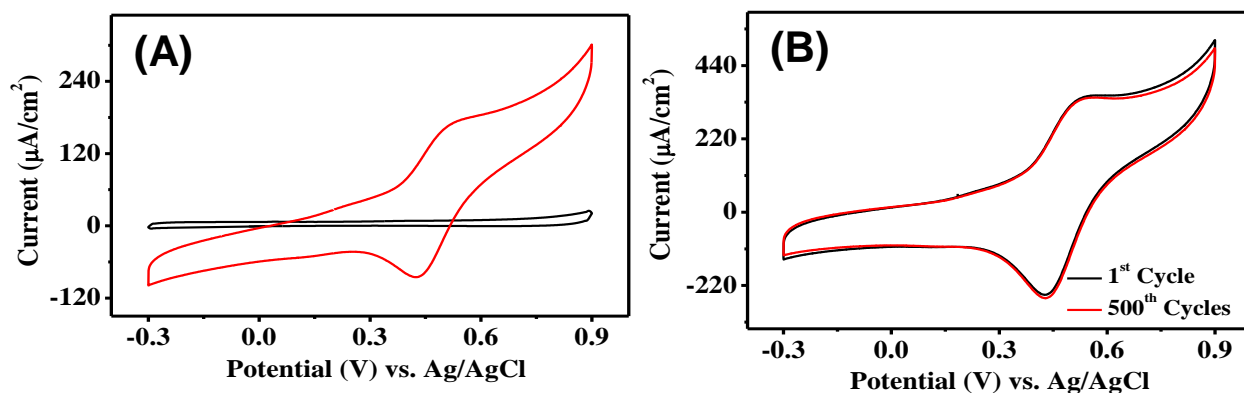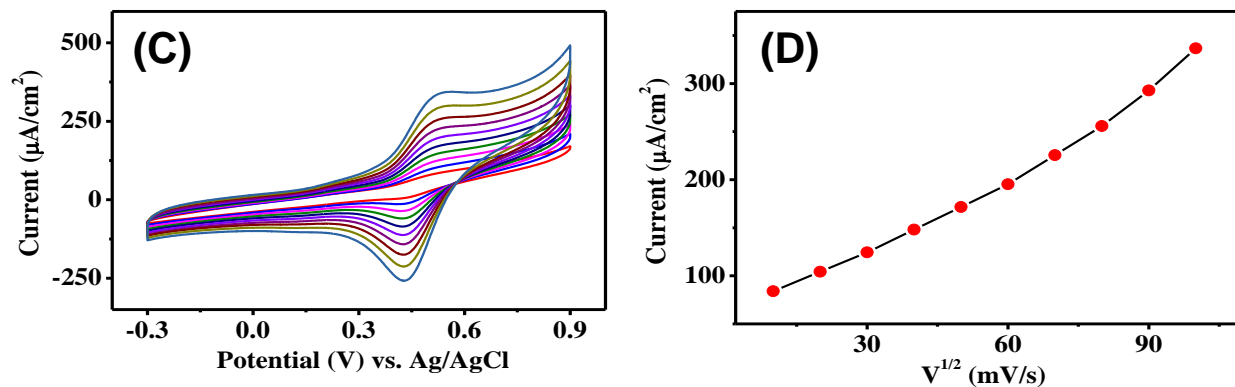
**Figure 6.15**: Cyclic voltammograms of Fc-Phe-Phe-Propyne (**4**) supported on Toray Carbon electrode in 0.1 M potassium phosphate buffer electrolytes at pH = 7.4 and 0.1 M KCl (A) at a scan rate of 50 mV/s; (B) at a scan rate of 100 mV/s of 1st and 500th cycles; (C) and (D) scan rate effect from 10 mV/s to 100 mV/s.
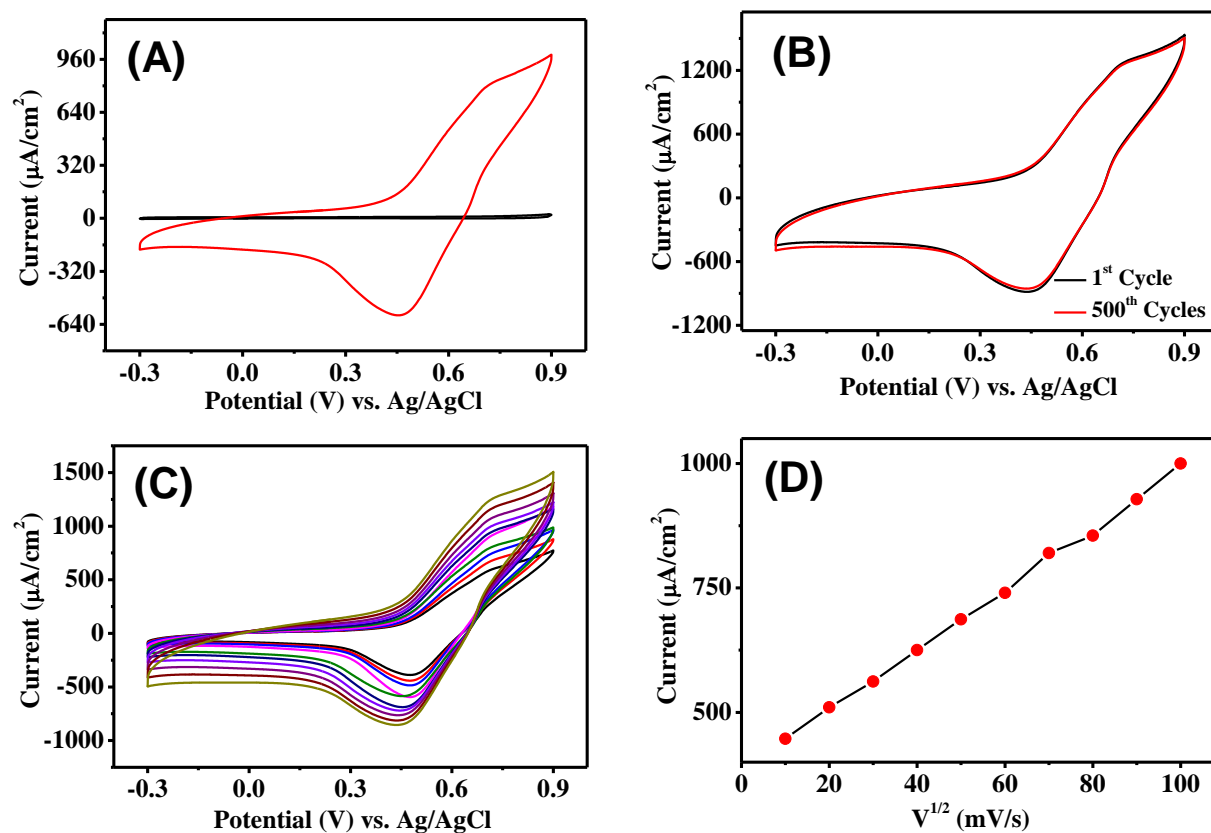


**Figure 6.16**: Cyclic voltammograms of Fc-Phe-Phe-*tz*-Fc (**11**) supported on Toray Carbon electrode in 0.1 M potassium phosphate buffer electrolytes at pH = 7.4 and 0.1 M KCl (A) at a scan rate of 50 mV/s; (B) at a scan rate of 100 mV/s of 1st and 500th cycles; (C) and (D) scan rate effect from 10 mV/s to 100 mV/s.

**Figure 6.17**: Cyclic voltammograms of Fc-Phe-Phe-*tz*-A$^{N(Boc)2}$ **(6)** supported on Toray Carbon electrode in 0.1 M potassium phosphate buffer electrolytes at pH = 7.4 and 0.1 M KCl (A) at a scan rate of 50 mV/s; (B) at a scan rate of 100 mV/s of 1$^{st}$ and 500$^{th}$ cycles; (C) and (D) scan rate effect from 10 mV/s to 100 mV/s.
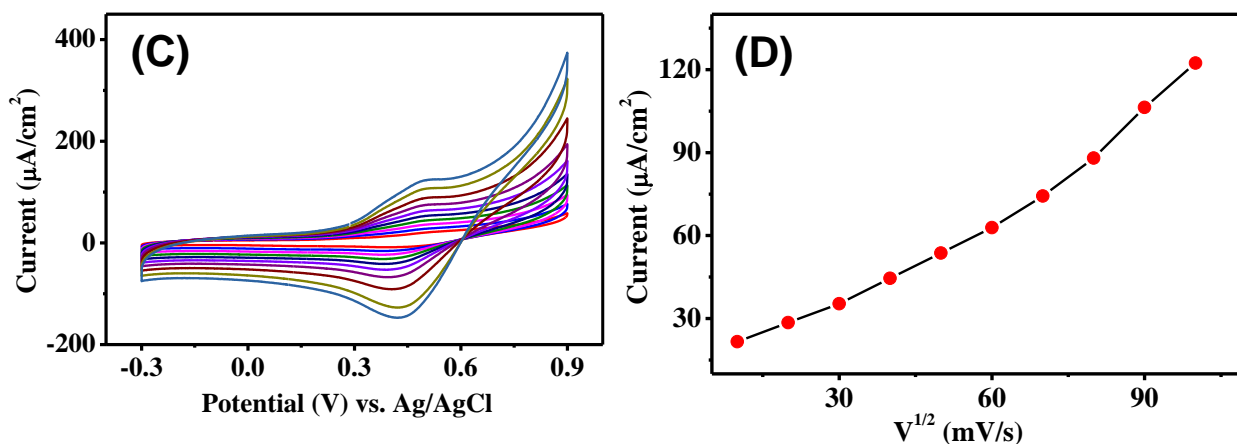
**Figure 6.18**: Cyclic voltammograms of Fc-Phe-Phe-*tz-aeg*{A$^{(Boc)2}$}-OEt (**8**) supported on Toray Carbon electrode in 0.1 M potassium phosphate buffer electrolyte at pH = 7.4 and 0.1 M KCl (A) at a scan rate of 50 mV/s; (B) at a scan rate of 100 mV/s of 1st and 500th cycles; (C) and (D) scan rate effect from 10 mV/s to 100 mV/s.
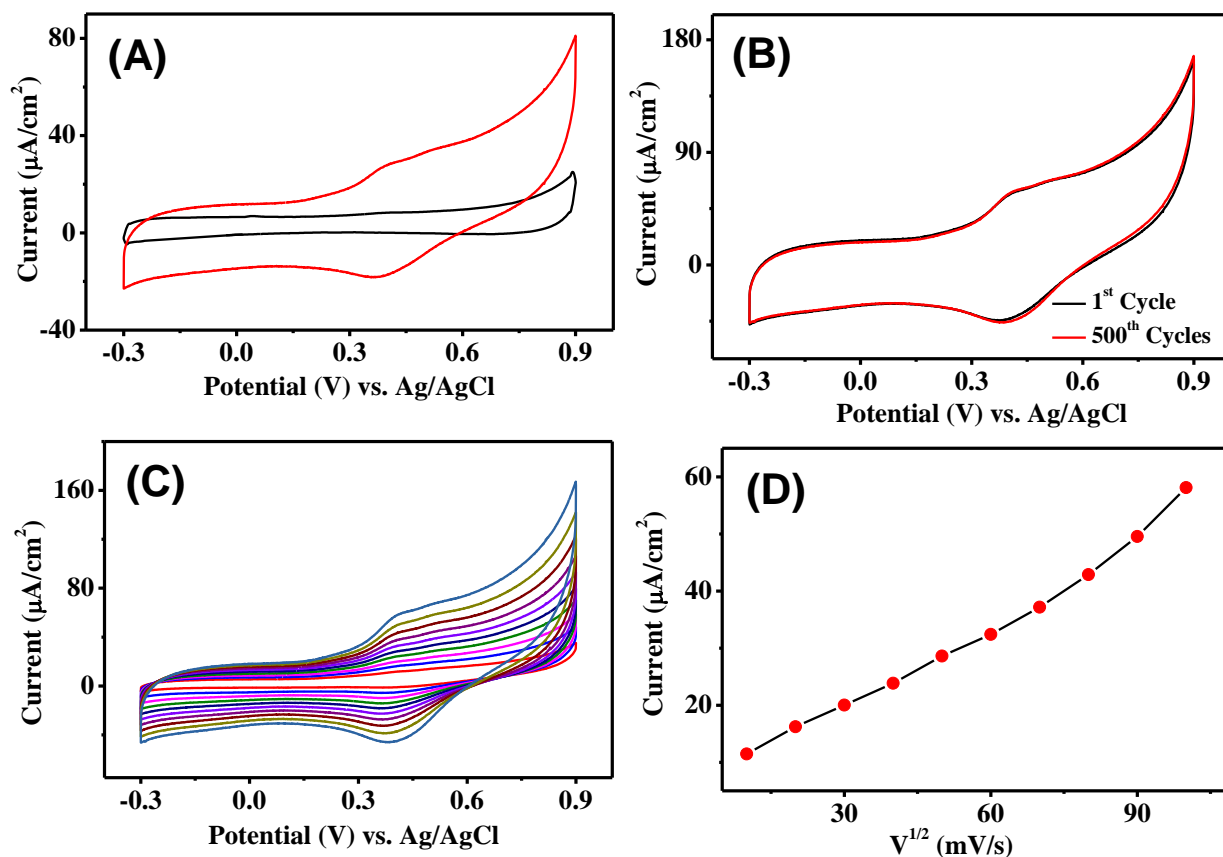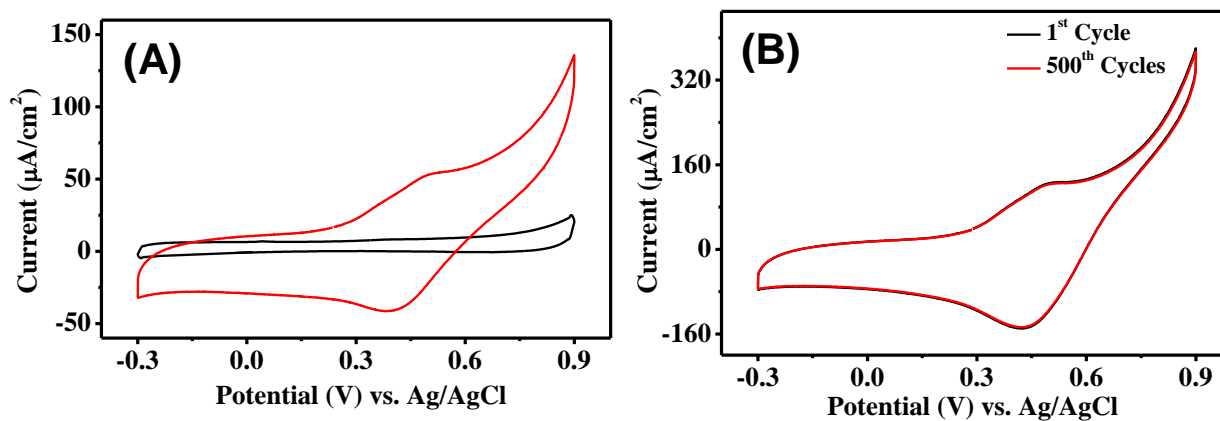


**Figure 6.19**: Cyclic voltammograms of Boc-Phe-Phe-*tz*-Fc (**10**) supported on Toray Carbon electrode in 0.1 M potassium phosphate buffer electrolytes at pH = 7.4 and 0.1 M KCl (A) at a scan rate of 50 mV/s; (B) at a scan rate of 100 mV/s of 1st and 500th cycles; (C) scan rate effect from 10 mV/s to 100 mV/s.
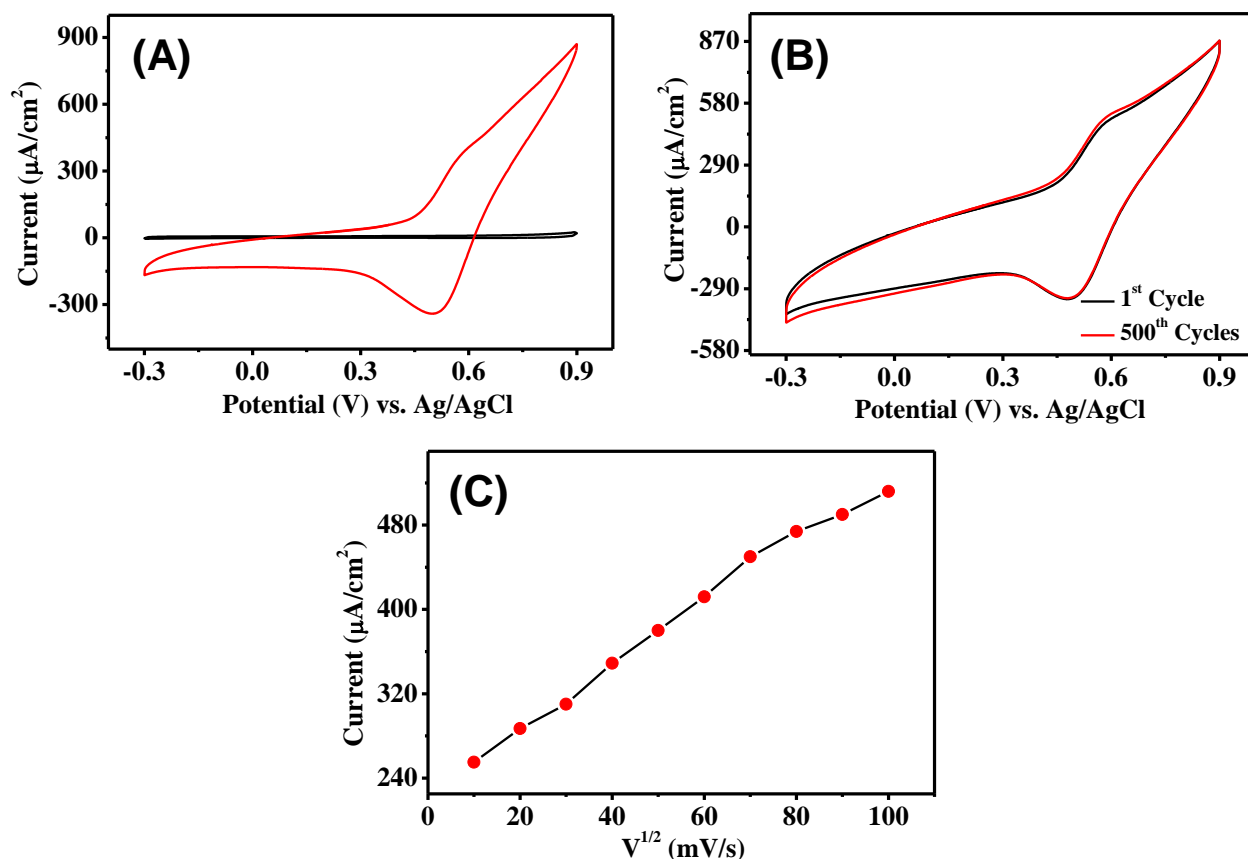
**Table 6.2**: Capacitance values of peptide modified Torey carbon electrodes at scan rate (SR) of 50 mV/s.

| Peptide used for electrode modification | Capacitance ($\mu F/cm^2$) at 50 mV potential vs. Ag/AgCl |
|---|---|
| Fc-Phe-Phe-Propyne **(4)** | 576.0 |
| Fc-Phe-Phe-*tz*-A$^{N(Boc)_2}$ **(6)** | 259.0 |
| Fc-Phe-Phe-*tz*-*aeg*{A$^{N(Boc)_2}$}-OEt **(8)** | 418.0 |
| Boc-Phe-Phe-*tz*-Fc **(10)** | 1359.0 |
| Fc-Phe-Phe-*tz*-Fc **(11)** | 2213.0 |
| None (unmodified electrode) | 72.0 |

## 6.4 Summary

A new class of peptide template consisting of dipeptide *L*-Phe- *L*-Phe and common capping groups elicited either rigid needle like nanorod or spherical morphologies. These morphologies could be controlled well by the selection of capping groups. For example, all triazole containing peptides show hollow or porous morphologies which could be utilized in the field of bioelectronics. Torey carbon electrodes were fabricated with triazole-nucleopeptides and these modified electrodes demonstrated enhanced capacitance. The guanine containing nucleopeptide (P4) furnished the best result with a seven fold increment of the capacitance compared to the bare, unmodifed electrode. Interestingly, both the morphology and the elemental composition remain the same before and after cyclic voltammetry confirming structural stability on the Toray carbon electrode surface. Thus, nucleopeptides consisting of Phe-Phe and PNA motifs can be tuned to engineer hybrid peptides with potential application as biomaterials.

Since, metallocenes are known to have metallic and semiconducting properties, ferrocene was conjugated with Phe-Phe linked to nucleoside as well as the PNA. A change in morphology was noticed from the "needle to sphere" in FESEM, independently confirmed by AFM images and data from DLS measurements. The presence of the iron metal in the structure was confirmed by the elemental analysis (EDX). Finally, Torey carbon electrodes were fabricated with triazole-ferrocene peptides and enhanced capacitance was measured. The both-side ferrocene containing peptide furnished the best result among all the peptides with a 30 fold increment of the capacitance value compared to the bare, unmodified electrode.

An important thing to notice is that Phe-Phe when conjugated with nucleoside or PNA gave the reduction as well as the oxidation peak in the cyclic voltammograms indicating that the redox signature of ferrocene is retained. However, charge storage behavior in potential regions far away from the redox peak indicates enhancement and hence ferrocene conjugated peptides can be used as the supercapacitors.

## 6.5 Experimental section

**6.5.1 Materials and methods**: See the experimental section (**2.5.1**) of chapter **2**.

**6.5.2 Synthesis of Peptides**: Peptide **1** was synthesized in the experimental section of chapter **2**.

**Dipeptide H-Phe-Phe-Propyne (2)**: Peptide **1** (1.0 g, 2.6 mmol) was stirred with TFA in DCM (20%, 15 mL) at room temperature. After 6 hrs, the volatile matters were evaporated under reduced pressure and residual liquid was co-evaporated with chloroform (3 x 15 mL) and toluene (2 x 5 mL). The residue thus obtained was loaded onto silica gel column and purified to obtain peptide **2** (0.7 g, 90%) [Eluent: 0-10% MeOH in CHCl$_3$]. White hygroscopic solid; $^1$H NMR, (400 MHz, CDCl$_3$ 25 °C, TMS) δ = 8.35 (d, *J* = 26.6 Hz, 1H), 7.94 (d, *J* = 56.9 Hz, 1H), 7.18 (dt, *J* = 80.2, 35.3 Hz, 10H), 5.34 (d, *J* = 10.0 Hz, 1H), 4.69 – 4.59 (m, 2H), 3.97 – 3.74 (m, 3H), 3.02 (ddd, *J* = 20.1, 15.5, 6.9 Hz, 3H), 2.83 – 2.62 (m, 1H), 2.28 (d, *J* = 20.9 Hz, 1H); $^{13}$C NMR (100 MHz, CDCl$_3$) δ = 170.2, 136.1, 135.8, 128.8, 128.0, 127.7, 126.3, 126.0, 79.4, 70.6, 54.9, 53.7, 38.5, 37.3, 28.1 ppm. HRMS (ESI$^+$), m/z calculated for (M+H)$^+$ C$_{11}$H$_{23}$N$_3$O$_2$: 350.1868, found: 350.1869.

**Synthesis of dipeptide Fc-Phe-Phe-Propyne (4)**: A mixture of compound ferrocene carboxylic acid **3** (0.5 g, 2.0 mmol), HBTU (0.8 g, 2.0 mmol) and HOBT (0.3 g, 2.0 mmol) was dissolved in dry DMF (10 mL) at 0 °C. To the reaction mixture, DIPEA (0.7 mL, 4.0 mmol) was added. After 0.5 hr, **2** (0.6 g, 2.0 mmol) dissolved in dry DMF (5 mL), was added slowly into the reaction mixture and stirred at room temperature under N$_2$ atmosphere. After 8 hrs brine solution (50 mL) was added into it and aq. layer was washed with ethyl acetate (EtOAc) (3 x 25 mL). Organic layer was washed with satd. NaHCO$_3$, 10% citric acid and brine solutions. The organic layer was separated, dried over anhyd. Na$_2$SO$_4$, filtered and the filtrate was concentrated under reduced

pressure. The crude mass thus obtained, was purified by column chromatography [Eluent: 30-80% of EtOAc in pet ether] to afford peptide **4** (0.8 g, 90% with respect to **1**). Orange solid; m.p. 134-138 °C; $^1$H NMR, 400 MHz (CDCl$_3$, 25 °C, TMS): $\delta$ = 7.37 – 7.27 (m, 3H), 7.24 – 7.18 (m, 2H), 7.17 – 7.03 (m, 4H), 6.87 (d, J = 79.0 Hz, 1H), 6.49 (s, 1H), 6.12 (s, 1H), 4.63 (d, J = 43.7 Hz, 3H), 4.42 (s, 1H), 4.37 – 4.29 (m, 2H), 4.08 – 4.05 (m, 1H), 3.99 (d, J = 20.0 Hz, 5H), 3.94 – 3.85 (m, 1H), 3.19 – 2.90 (m, 4H), 2.18 (t, J = 2.5 Hz, 1H); $^{13}$C NMR, 100 MHz (CDCl$_3$, 25 °C, TMS): $\delta$ = 171.6, 171.4, 170.3, 136.7, 136.4, 129.4, 129.3, 129.2, 129.1, 127.5, 127.1, 79.4, 77.5, 77.2, 76.8, 71.6, 71.6, 71.1, 71.0, 69.9, 69.3, 67.5, 67.5, 54.3, 37.9, 37.8, 29.3 ppm. HRMS (ESI$^+$), m/z calculated for (M+H)$^+$ C$_{32}$H$_{32}$N$_3$O$_3$Fe: 562.1793, found: 562.1794.

**Peptide Fc-Phe-Phe-*tz*-A$^{N(Boc)2}$ (6)**: A mixture of **4** (0.3 g, 0.56 mmol), CuSO$_4$.5H$_2$O (7 mg, 0.03 mmol) and sodium ascorbate (0.1 g, 0.28 mmol) were stirred in tetrahydrofuran (THF) (6.0 mL). To the resulting suspension, azide **5**$^{38}$ (0.6 g, 1.12 mmol) dissolved in THF (6.0 mL) was added. 10 mL distilled water was added to the reaction mixture and stirred at room temperature. After 12 hrs, EtOAc (20 mL) was added into it and aq. layer was further washed with EtOAc (3 x 20 mL). Organic layer was separated, dried over anhyd. Na$_2$SO$_4$, filtered and the filtrate was concentrated under reduced pressure. The crude mass thus obtained, was purified by column chromatography [Eluent: 0-5% of MeOH in DCM] to afford compound **6** (0.5 g, 90% with respect to **4**). Orange hygroscopic solid; m.p. 74-78 °C; $^1$H NMR (400 MHz, CDCl$_3$) $\delta$ = 8.87 (s, 1H), 8.09 (s, 1H), 7.33 (t, J = 7.3 Hz, 3H), 7.28 – 7.22 (m, 4H), 7.20 – 7.09 (m, 3H), 7.07 – 7.02 (m, 1H), 6.92 – 6.77 (m, 2H), 6.14 (d, J = 2.2 Hz, 1H), 6.03 (d, J = 6.4 Hz, 1H), 5.35 (dd, J = 6.4, 2.3 Hz, 1H), 5.19 (dd, J = 6.4, 3.6 Hz, 1H), 4.74 (dd, J = 16.3, 7.0 Hz, 1H), 4.67 – 4.56 (m, 4H), 4.45 (dd, J = 15.3, 5.8 Hz, 1H), 4.40 – 4.21 (m, 5H), 3.99 (d, J = 4.7 Hz, 1H), 3.94 (s, 4H), 3.20 – 3.07 (m, 2H), 3.02 – 2.85 (m, 2H), 1.61 (s, 3H), 1.50 (d, J = 7.1 Hz, 18H), 1.37 (s, 3H); $^{13}$C NMR (100 MHz, CDCl$_3$) $\delta$ = 171.7, 171.4, 170.9, 152.5, 152.4, 150.9, 150.8, 145.1, 144.3, 136.7, 136.7, 129.4, 129.2, 129.2, 128.7, 127.5, 126.9, 123.5, 115.5, 90.5, 85.2, 84.4, 84.0, 71.0, 69.9, 69.2, 67.4, 55.0, 54.5, 51.6, 37.6, 37.5, 28.0, 27.3, 25.5 ppm. HRMS (ESI$^+$), m/z calculated for (M+H)$^+$ C$_{55}$H$_{64}$N$_{11}$O$_{10}$Fe: 1094.4187, found: 1094.4186.

**Peptide Fc-Phe-Phe-*tz-aeg*A<sup>N(Boc)2</sup>-OEt (8)**: A mixture of **4** (0.3 g, 0.56 mmol), $CuSO_4.5H_2O$ (7 mg, 0.03 mmol) and sodium ascorbate (0.1 g, 0.28 mmol) were stirred in tetrahydrofuran (THF) (6.0 mL). To the resulting suspension, azide **7**[38] (0.6 g, 1.12 mmol) dissolved in THF (6.0 mL) was added. 10 mL distilled water was added to the reaction mixture and stirred at room temperature. After 12 hrs, EtOAc (20 mL) was added into it and aq. layer was further washed with EtOAc (3 x 20 mL). Organic layer was separated, dried over anhyd. $Na_2SO_4$, filtered and the filtrate was concentrated under reduced pressure. The crude mass thus obtained, was purified by column chromatography [Eluent: 0-5% of MeOH in DCM] to afford compound **8** (0.5 g, 90% with respect to **4**). Orange hygroscopic solid; m.p. 68-72 °C; $^1H$ NMR (400 MHz, $CDCl_3$) δ = 8.75 (d, J = 9.2 Hz, 1H), 8.27 (s, 1H), 8.12 (s, 0.33H), 7.84 (s, 0.37H), 7.46 (s, 1H), 7.32 (s, 2H), 7.23 (dd, J = 10.4, 5.4 Hz, 4H), 7.15 – 7.01 (m, 5H), 6.33 – 6.19 (m, 1H), 5.15 – 5.07 (m, 1H), 4.65 (s, 3H), 4.51 (d, J = 15.3 Hz, 2H), 4.38 – 4.23 (m, 4H), 4.13 (dd, J = 9.4, 4.5 Hz, 1H), 3.93 (dd, J = 12.8, 6.1 Hz, 5H), 3.83 (s, 1H), 3.14 (d, J = 14.0 Hz, 2H), 3.04 – 2.86 (m, 3H), 2.79 – 2.78 (m, 1H), 2.08 (d, J = 5.2 Hz, 3H), 1.42 (d, J = 13.4 Hz, 15H), 1.25 (d, J = 6.1 Hz, 3H); $^{13}C$ NMR (100 MHz, $CDCl_3$) δ = 172.0, 171.3, 168.9, 167.2, 166.7, 153.7, 153.6, 152.2, 150.6, 146.4, 136.7, 136.5, 129.4, 129.3, 129.2, 128.8, 128.8, 128.4, 127.6, 127.6, 127.2, 124.0, 96.3, 84.0, 74.1, 71.3, 71.1, 69.4, 69.2, 62.6, 62.1, 55.3, 55.0, 50.8, 49.7, 47.9, 44.3, 38.8, 37.5, 37.4, 37.2, 35.4, 35.4, 29.9, 28.1, 28.0, 14.3 ppm. HRMS (ESI⁺), m/z calculated for (M+H)⁺ $C_{55}H_{65}N_{12}O_{10}Fe$: 1109.4296, found: 1109.4298.

**Peptide Boc-Phe-Phe-*tz*-Fc (10)**: A mixture of **1** (0.4 g, 1.0 mmol), $CuSO_4.5H_2O$ (12.5 mg, 0.05 mmol) and sodium ascorbate (0.1 g, 0.5 mmol) were stirred in tetrahydrofuran (THF) (5.0 mL). To the resulting suspension, ferrocene azide **9** (0.5 g, 1.5 mmol) dissolved in THF (5.0 mL) was added. 10 mL distilled water was added to the reaction mixture and stirred at room temperature. After 10 hrs, EtOAc (20 mL) was added into it and aq. layer was further washed with EtOAc (3 x 20 mL). Organic layer was separated, dried over anhyd. $Na_2SO_4$, filtered and the filtrate was concentrated under reduced pressure. The crude mass thus obtained, was purified by column chromatography [Eluent: 0-5% of MeOH in DCM] to afford compound **10** (0.6 g, 89% with respect to **1**). Orange hygroscopic solid; m.p. 119-122 °C; $^1H$ NMR, 400 MHz ($CDCl_3$, 25 °C, TMS): δ 7.48 (s, 1H), 7.29 (dd, J = 6.0, 4.2 Hz, 3H), 7.22 (dd, J = 4.9, 1.7 Hz, 5H), 7.16 – 7.08 (m, 2H),

7.02 (s, 2H), 6.71 (t, J = 5.8 Hz, 2H), 5.03 (s, 1H), 4.75 – 4.65 (m, 3H), 4.55 – 4.43 (m, 3H), 4.40 – 4.24 (m, 4H), 4.16 (d, J = 3.0 Hz, 5H), 3.94 – 3.77 (m, 2H), 3.16 – 2.86 (m, 5H), 1.32 (s, 10H); $^{13}$C NMR, 100 MHz (CDCl$_3$, 25 °C): $\delta$ = 171.5, 171.4, 171.0, 155.9, 145.2, 136.4, 136.3, 129.5, 129.4, 129.0, 128.8, 127.4, 127.2, 123.4, 81.0, 75.5, 70.8, 70.0, 68.5, 56.3, 54.0, 50.0, 39.6, 38.0, 37.6, 35.3, 28.3 ppm; HRMS (ESI$^+$), m/z calculated for (M+H)$^+$ C$_{39}$H$_{46}$N$_7$O$_5$Fe: 748.2910, found: 748.2911.

**Peptide Fc-Phe-Phe-*tz*-Fc (11)**: Peptide **4** (0.3 g, 0.5 mmol) was clicked with azide **9** (0.2 g, 0.8 mmol) following the method described for peptide **10** to afford peptide **11** (0.4 g, 87% with respect to **4**) which was purified by column chromatography [Eluent: 0-7% of MeOH in DCM]. Orange solid; m.p. 81-85 °C; $^1$H NMR, 400 MHz (CDCl$_3$, 25 °C, TMS): $\delta$ = 7.46 (s, 1H), 7.40 – 7.14 (m, 9H), 7.05 (dd, J = 19.1, 2.3 Hz, 5H), 6.86 (s, 1H), 6.39 (s, 1H), 4.70 (d, J = 31.6 Hz, 5H), 4.36 (dd, J = 35.7, 16.2 Hz, 9H), 4.17 (s, 5H), 3.93 (s, 5H), 3.76 (dd, J = 18.7, 12.8 Hz, 2H), 3.10 (dd, J = 19.0, 9.8 Hz, 2H), 2.98 – 2.83 (m, 2H); $^{13}$C NMR, 100 MHz (CDCl$_3$, 25 °C, TMS): $\delta$ = 171.7, 171.4, 171.1, 145.0, 136.8, 136.6, 129.4, 129.2, 129.1, 128.9, 128.6, 127.4, 127.0, 123.5, 75.7, 74.6, 71.2, 71.0, 70.2, 70.0, 69.3, 68.7, 67.6, 60.5, 54.9, 54.6, 49.9, 39.6, 37.9, 37.6, 35.2, 29.8 ppm. HRMS (ESI$^+$), m/z calculated for (M+H)$^+$ C$_{45}$H$_{46}$N$_7$O$_4$Fe$_2$: 860.2310, found: 860.2312.

**Compound 9 [*N*-(2-azidoethyl)ferrocenyl formamide]**: Compound **3** (0.5 g, 2.0 mmol) was coupled with 2-azido-ethylamine[39] (1.1 g, 2.5 mmol) following the method described for **4** to afford **9** which was purified by column chromatography [Eluent: 10-60% of EtOAc in pet ether]. Compound **2** (0.5 g, 90% with respect to **3**) was obtained as brown solid; m.p. 117-120 °C; $^1$H NMR, 400 MHz (CDCl$_3$, 25 °C, TMS): $\delta$ = 6.13 (s, 1H), 4.76 – 4.61 (m, 2H), 4.43 – 4.31 (m, 2H), 4.22 (s, 5H), 3.55 ppm (d, *J* = 4.0 Hz, 4H); $^{13}$C NMR, 100 MHz (CDCl$_3$, 25 °C, TMS): $\delta$ = 170.9, 75.7, 70.7, 69.9, 68.3, 51.4, 39.1 ppm. HRMS (ESI$^+$), m/z calculated for (M+H)$^+$ C$_{13}$H$_{15}$N$_4$OFe: 299.0595, found: 299.0587.

**6.5.3 FT-IR spectroscopy**: See the experimental section **(2.5.3)** of chapter **2**.

**6.5.4 Dynamic light scattering**: See the experimental section **(2.5.6)** of chapter **2**.

**6.5.5 Microscopy studies**: See the experimental section **(2.5.7)** of chapter **2**.

**6.5.6 Electrochemical Analysis:** Electrochemical Analysis was done in the Biologic VMP3 multichannel potentiostat. A standard three-electrode cell consisting of a Toray carbon paper having 1 cm$^2$ as the working electrode, Ag/AgCl (satd. KCl) as the reference electrode and a Pt foil as the counter electrode was used for all electrochemical measurements. The solution was purged with Ar during the experiments and all potential values are expressed in volt (V) vs. Ag/AgCl scale. All working electrodes had an identical geometric area of 1.00 cm$^2$. The capacitance was evaluated from experimental cyclic voltammetric profile, according to the following equation:

$$I_{nF} = C\,\frac{dV}{dt} \quad , \text{Where} \quad I_{nF} = \frac{(I_{pa} + I_{pc})}{2}$$

Where, $C$ = Total capacitance in microfarad per cm$^2$ (or in µF / cm$^2$)

$I_{nF}$ = Non-Faradaic current density (in µA / cm$^2$)

$dV/dt$ = Scan rate (10 mV/s to 100 mV/s)

$I_{pa}$ = Anodic (positive) base line current far away from the anodic peak

$I_{pc}$ = Cathodic (negative) base line current far away from the cathodic peak

All solutions were prepared using triply distilled water and the cell temperature was maintained at 27 °C. Currents are normalized with respect to geometric area (1 cm$^2$). All the electrolytic solutions were prepared by 0.1 M Potassium Phosphate buffer electrolytes at pH = 7.4 and 0.1 M KCl. Working electrodes were made by drop casting a suspension of those peptides (2 mg/400 µL in a 10 wt.% aqueous dispersion of PTFE) on a Toray carbon paper electrode. Also we have calculated the redox potential for the Boc-Phe-Phe-Propyne from the cyclic voltammogram with the help of the given equation:

$$E_{redox} = \frac{(E_{pa} + E_{pc})}{2}$$

Where, $E_{redox}$ = Redox potential (in mV)

$E_{pa}$ = Anodic (positive) peak potential

$I_{pc}$ = Cathodic (negative) peak potential

## 6.6 References

1. Makam, P.; Gazit, E. *Chem. Soc. Rev*. **2018**, *47*, 3406-3420.

2. (a) Subbalakshmi, C.; Manorama, S. V.; Nagaraj, R. *J. Pept. Sci*. **2012**, *18*, 283-292; (b) Subbalakshmi, C.; Nagaraj, R. *ChemPlusChem* **2014**, *79*, 1326-1333.

3. Rica, R. D. L.; Matsui, H. *Chem. Soc. Rev*. **2010**, *39*, 3499-3509.

4. Santis, E. D.; Ryadnov, M. G. *Chem. Soc. Rev*. **2015**, *44*, 8288-8300.

5. Apter, B.; Lapshina, N.; Handelman, A.; Fainberg, B. D.; Rosenman, G. *Small* **2018** (DOI: 10.1002/smll.201801147).

6. Handelman, A.; Natan, A.; Rosenman, G. *J. Pept. Sci*. **2014**, *20*, 487-493.

7. Yemini, M.; Reches, M.; Rishpon, J.; Gazit, E. *Nano Lett*. **2005**, *5*, 183-186.

8. Abramovich, L. A.; Mossberg, M. B.; Gazit, E.; Rishpon, J. *Small* **2010**, *6*, 825-831.

9. Beker, P.; Koren, I.; Amdursky, N.; Gazit, E.; Rosenman, G. *J. Mater. Sci*. **2010**, *45*, 6374-6378.

10. Rosenman, G.; Beker, P.; Koren, I.; Yevnin, M.; Srour, B. B.; Mishina, E.; Semin, S. *J. Pept. Sci*. **2011**, *17*, 75-87.

11. Tao, K.; Makam, P.; Aizen, R.; Gazit, E. *Science* **2017**, *358*, 885.

12. Yan, X.; Zhu, P.; Li, J. *Chem. Soc. Rev*. **2010**, *39*, 1877-1890.

13. Loo, Y.; Zhang, S.; Hauser, C. A. E. *Biotechnol. Adv*. **2012**, *30*, 593-603.

14. Reches, M.; Gazit, E. *Israel J. Chem*. **2005**, *45*, 363-371.

15. Gorbitz, C. H. *Chem. Commun*. **2006**, 2332-2334.

16. Reches, M.; Gazit, E. *Nat. Nanotechnol*. **2006**, *1*, 195-200.

17. Kim, S.; Kim, J. H.; Lee, J. S.; Park, C. B. *Small* **2015**, *11,* 3623-3640.

18. Abramovich, L. A.; Gazit, E. *Chem. Soc. Rev*. **2014**, *43*, 6881-6893.

19. Marchesan, S.; Vargiu, A. V.; Styan, K. E. *Molecules* **2015**, *20*, 19775-19788.

20. Tao, K.; Makam, P.; Aizen, R.; Gazit, E. *Science* **2017**, *358*, 1-7.

21. Reches, M.; Gazit, E. *Science* **2003**, *300*, 625-627.

22. Reches, M.; Gazit, E. *Nano Lett*. **2004**, *4*, 581-585.

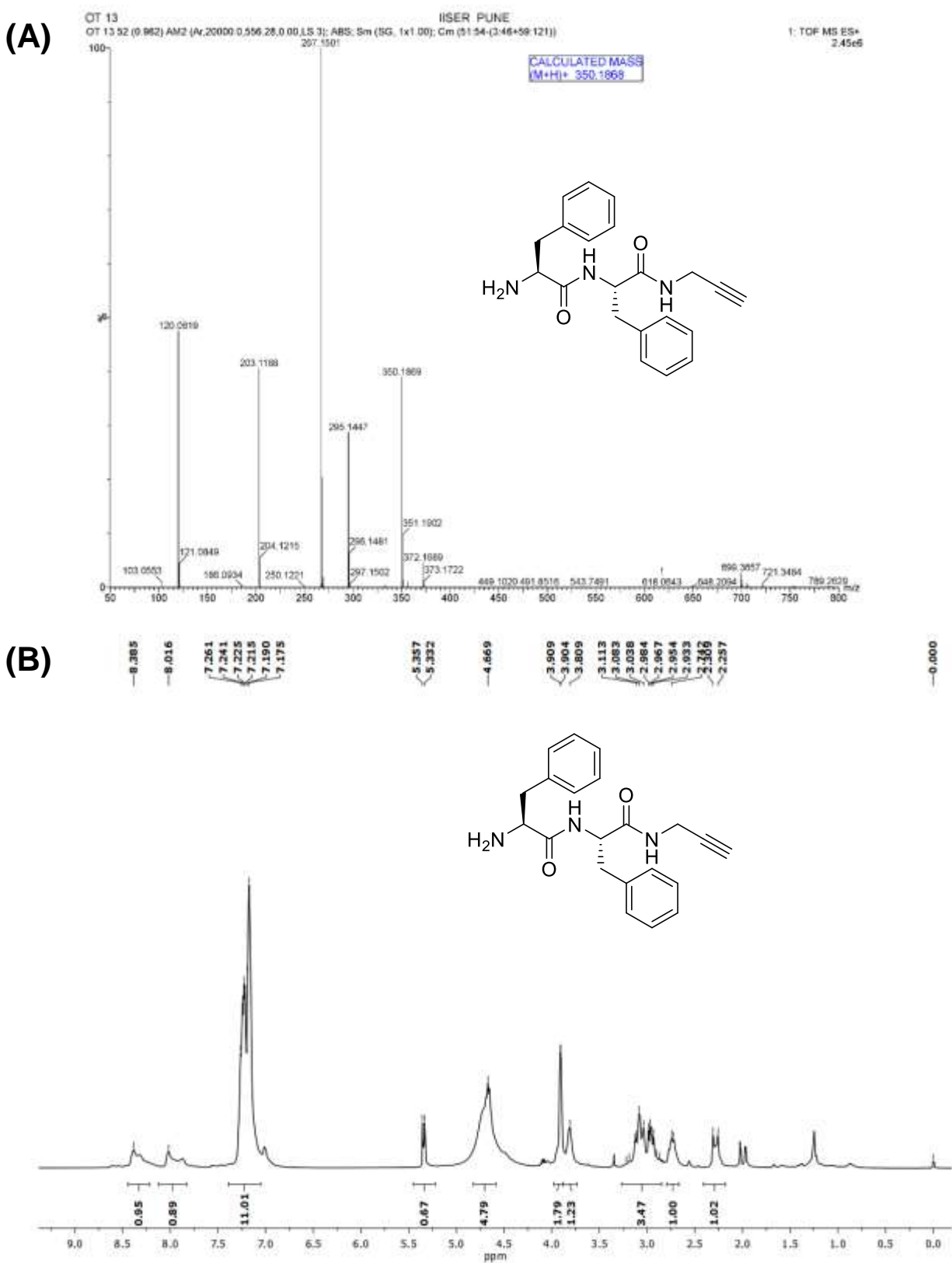23. Reches, M.; Gazit, E. *Nat. Nanotechnol*. **2006**, *1*, 195-200.

24. Abramovich, L. A.; Reches, M.; Sedman, V. L.; Allen, S.; Tendler, S. J. B.; Gazit, E. *Langmuir* **2006**, *22*, 1313-1320.

25. Tamamis, P.; Abramovich, L. A.; Reches, M.; Marshall, K.; Sikorski, P.; Serpell, L.; Gazit E.; Archontis, G. *Biophys. J.* **2009**, *96*, 5020-5029.

26. Azuri, I.; Abramovich, L. A.; Gazit, E.; Hod, O.; Kronik, L. *J. Am. Chem. Soc.* **2014**, *136*, 963-969.

27. Berger, O.; Abramovich, L. A.; Sakin, M. L.; Grunwald, A.; Peer, Y. L.; Bachar, M.; Buzhansky, L.; Mossou, E.; Forsyth, V. T.; Schwartz, T.; Ebenstein, Y.; Frolow, F.; Shimon, L. J. W.; Patolsky, F.; Gazit, E. *Nat. Nanotechnol*. **2015**, *10*, 353-360.

28. Avitabile, C.; Diaferia, C.; della Ventura, B.; Mercurio, F. A.; Leone, M.; Roviello, V.; Saviano, M.; Velotta, R.; Morelli, G.; Accardo, A.; Romanelli, A. *Chem. Eur. J.* **2018**, *24*, 4729-4735.

29. Berger, O.; Yoskovitz, E.; Abramovich, L. A.; Gazit, E. *Adv. Mater.* **2016**, *28*, 2195-2200.

30. (a) Kinoshita, S.; Yoshioka, S. *ChemPhysChem* **2005**, *6*, 1442-1459; (b) Tadepalli, S.; Slocik, J. M.; Gupta, M. K.; Naik, R. R.; Singamaneni, S. *Chem. Rev.* **2017**, *117*, 12705-12763.

31. Nikoloudakis, E.; Karikis, K.; Han, J.; Kokotidou, C.; Charisiadis, A.; Folias, F.; Douvas, A. M.; Mitraki, A.; Charalambidis, G.; Yan, X.; Coutsolelos, A. G. *Nanoscale* **2018**, *11*, 3557-3566.

32. Elgrishi, N.; Rountree, K. J.; Carthy, B. D. M.; Rountree, E. S.; Eisenhart, T. T.; Dempsey, J. L. *J. Chem. Educ.* **2018**, *95*, 197-206.

33. Abramovich, L. A; Aronov, D.; Beker, P.; Yevnin, M.; Stempler, S.; Buzhansky, L.; Rosenman, G.; Gazit, E. *Nat. Nanotechnol*. **2009**, *4*, 849.

34. Beker, P.; Koren, I.; Amdursky, N.; Gazit, E.; Rosenman, G. *J. Mater. Sci*. **2010**, *45*, 6374-6378.

35. Conway B. E. (**1999**) Electrochemical supercapacitors: scientific fundamentals and technological applications. Kluwer Academic / Plenum Publishers, New York.

36. Banerjee, A.; Palui, G.; Banerjee, A. *Soft Matter* **2008**, *4*, 1430-1437.

37. Wang, T.; Wu, Y.; Kuan, S. L.; Dumele, O.; Lamla, M.; Ng, D. Y. W.; Arzt, M.; Thomas, J.; Mueller, J. O.; Kowollik, C. B.; Weil, T. *Chem. Eur. J.* **2015**, *21*, 228-238.

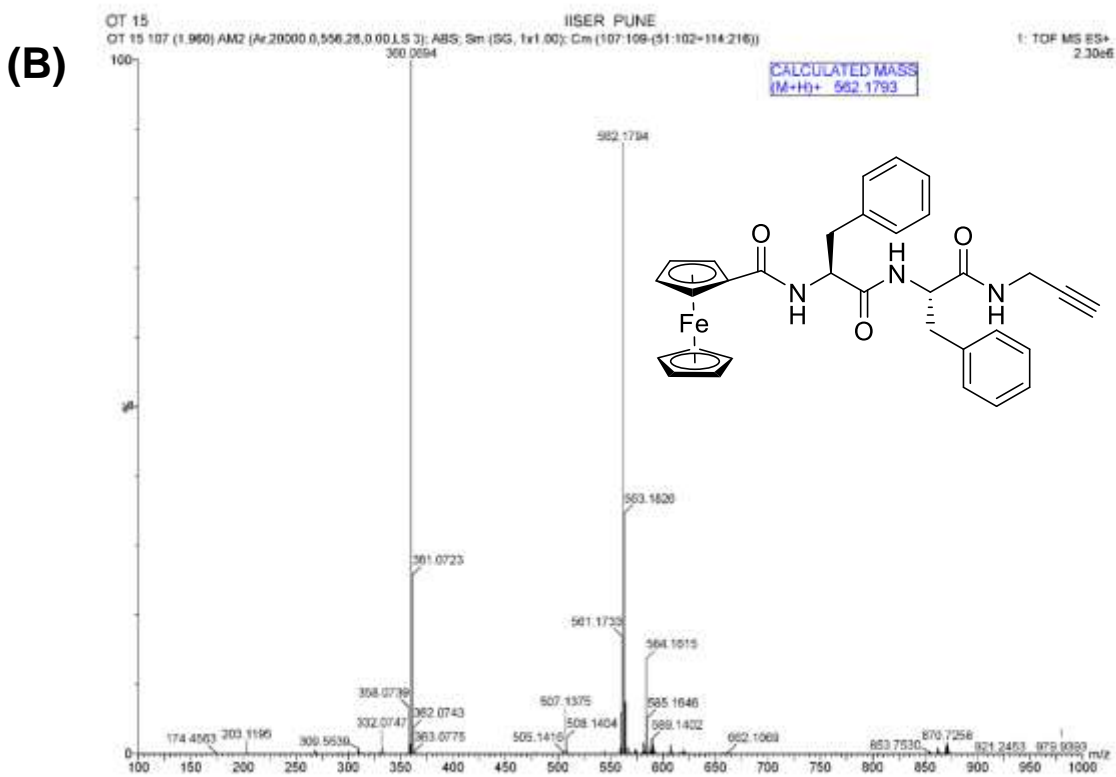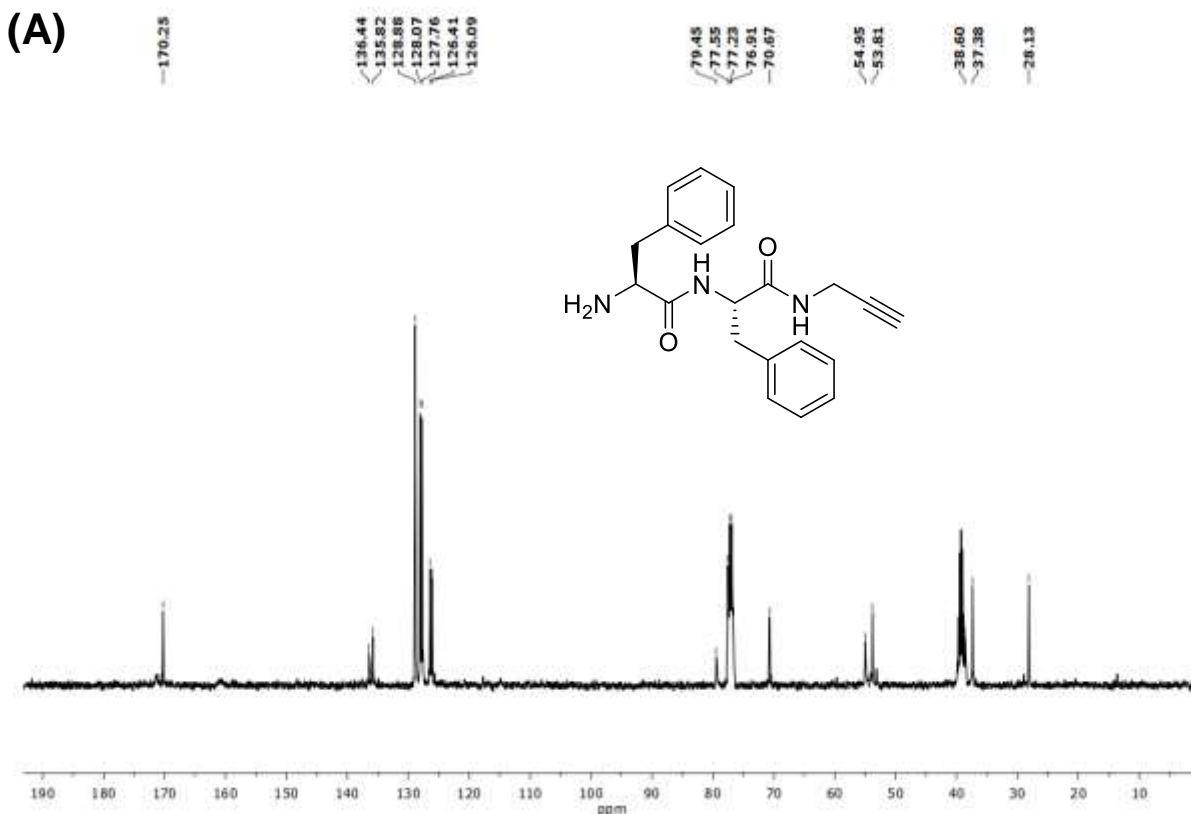38. Liu, F.; Austin, D. J. *Tetrahedron Lett.* **2001**, *42*, 3153-3154.

39. Wang, T.; Wu, T.; Kuan, S. L.; Dumele, O.; Lamla, M.; Ng, D. Y. W.; Arzt, M.; Thomas, J.; Mueller, J. O.; Kowollik, C. B.; Weil, T. *Chem. Eur. J*. **2015**, *21*, 228-238.

## 6.7 Appendix V: Characterization data of synthesized compounds

| Entry | Table of contents | Page No. |
|-------|-------------------|----------|
| 1 | HRMS, $^1$H, $^{13}$C NMR and IR spectra of compounds | 269-279 |

(A) HRMS and (B) ¹H-NMR spectra of **2** (NH₂-Phe-Phe-Propyne).

**(A)**

170.25

136.44
135.82
128.88
128.07
127.76
126.41
126.09

79.45
77.55
77.23
76.91
70.67

54.95
53.81

38.60
37.38

28.13



190  180  170  160  150  140  130  120  110  100  90  80  70  60  50  40  30  20  10
ppm

OT 15
OT 15 107 (1.960) AM2 (Ar,20000.0,556.28,0.00,LS 3); ABS; Sm (SG, 1x1.00); Cm (107:109-(51:102=114:216))

IISER PUNE

1: TOF MS ES+
2.30e6

**(B)**

100

360.0894

CALCULATED MASS
(M+H)+  562.1793

562.1794



563.1828

361.0723

561.1733

564.1815

308.0738

585.1646

507.1375

332.0747

362.0743

508.1404

589.1402

174.4563  203.1195

309.5530

363.0775

505.1416

662.1069

870.7256

863.7530

921.2453  979.9393

m/z

100  150  200  250  300  350  400  450  500  550  600  650  700  750  800  850  900  950  1000

(A) $^{13}$C-**NMR** spectra of **2** (NH$_2$-Phe-Phe-Propyne) and (B) HRMS of **4** (Fc-Phe-Phe-Propyne).

270

**(A)**

**(B)**
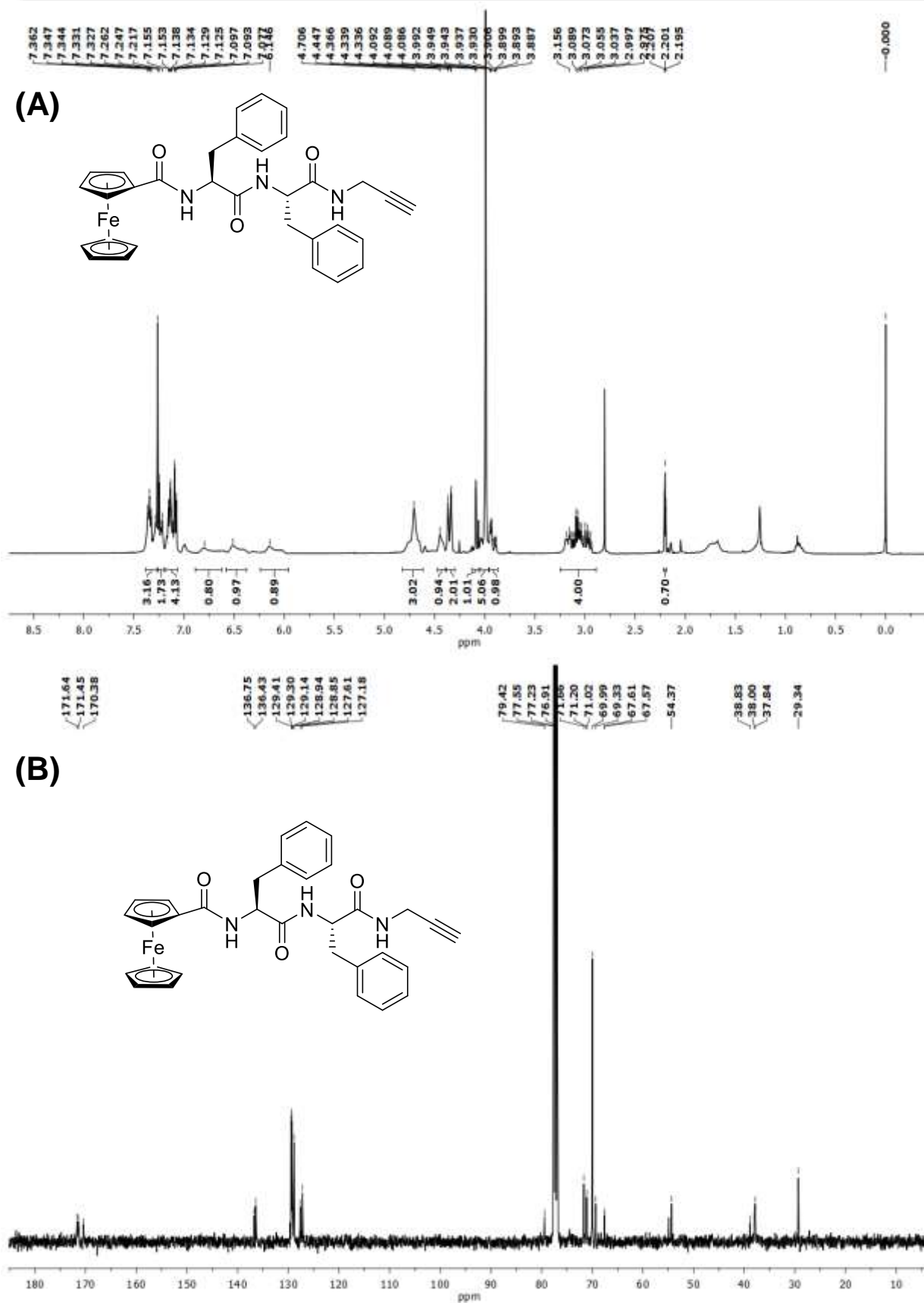
(A) ^{1}H-NMR and (B) ^{13}C-NMR spectra of **4** (Fc-Phe-Phe-Propyne).

**(A)**



**(B)**
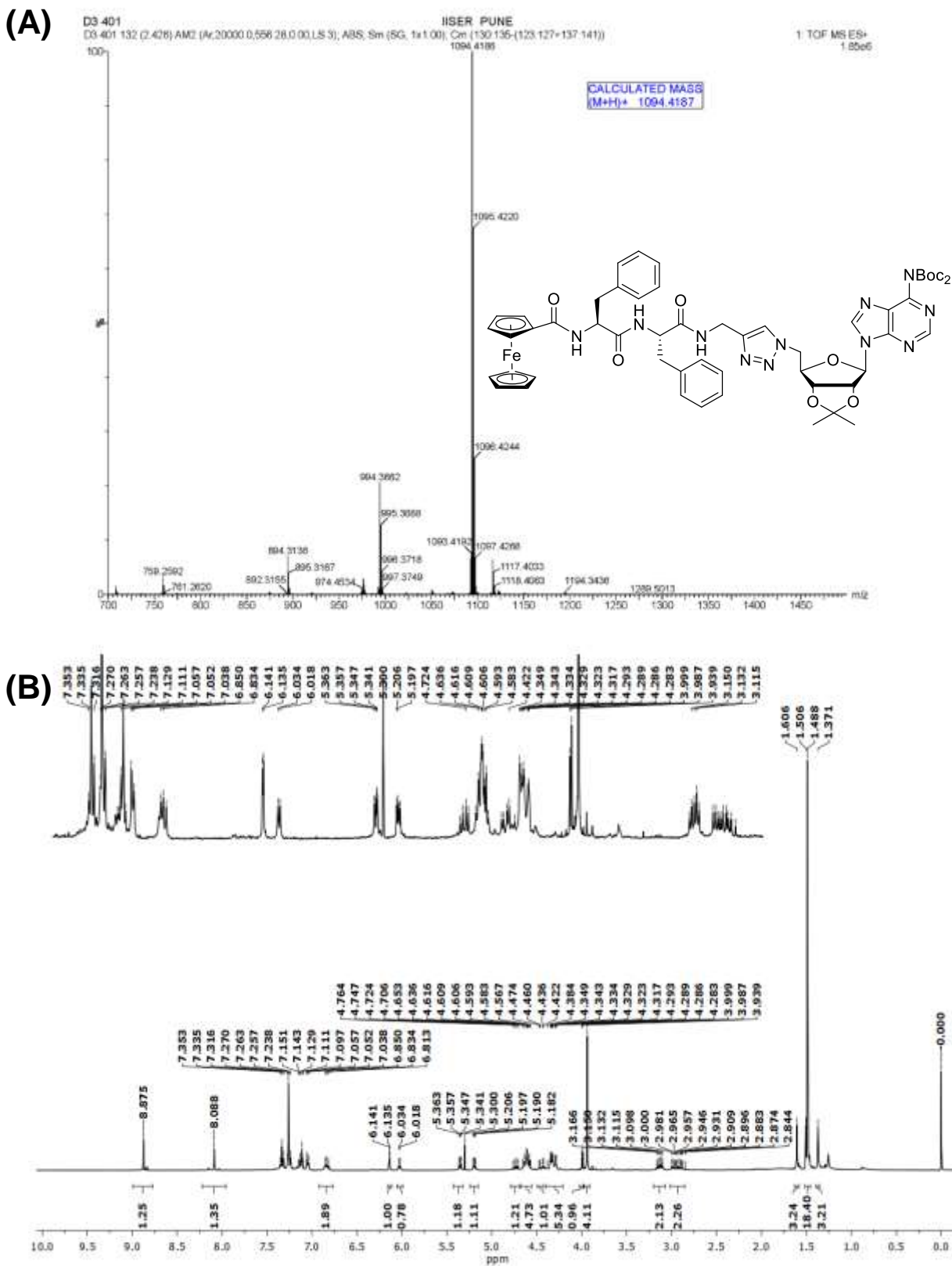


(A) HRMS and (B) $^1$H-NMR spectra of of **6** [Fc-Phe-Phe-*tz*-A$^{N(Boc)2}$].

**(A)**



**(B)**
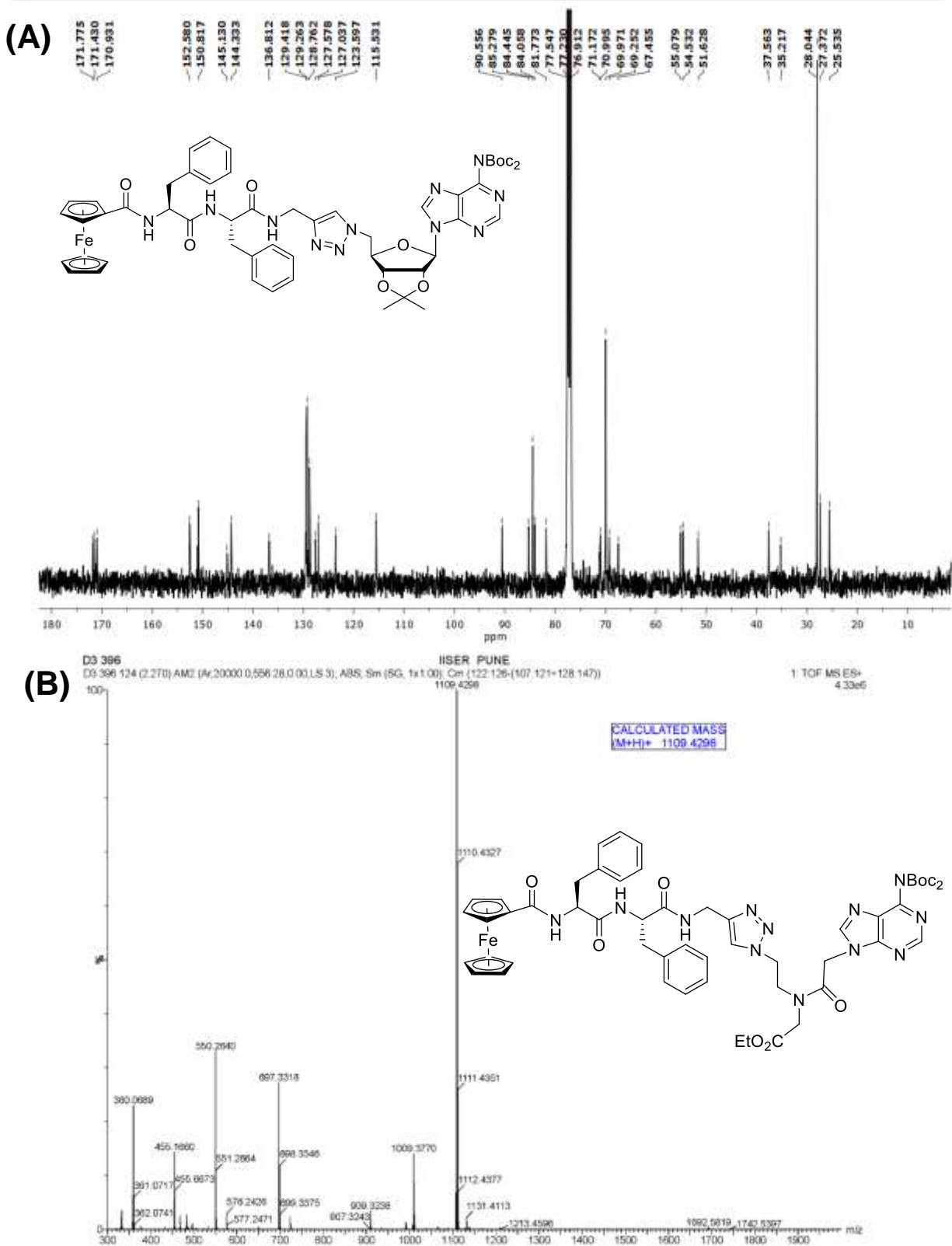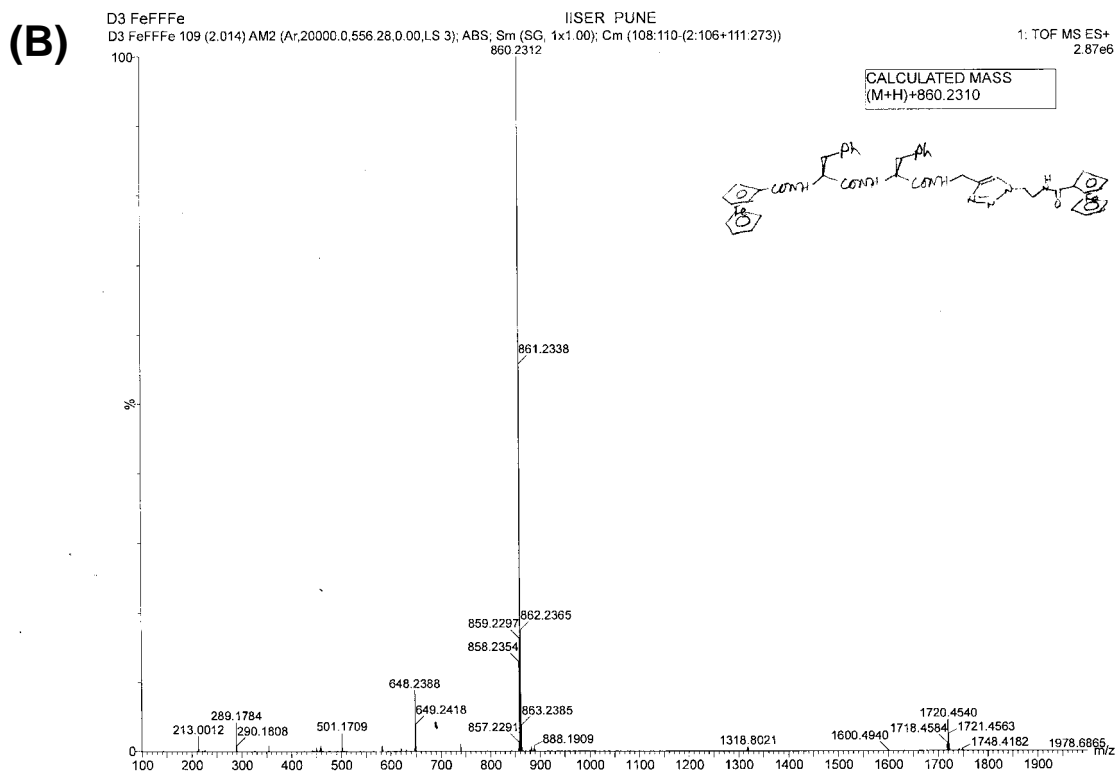

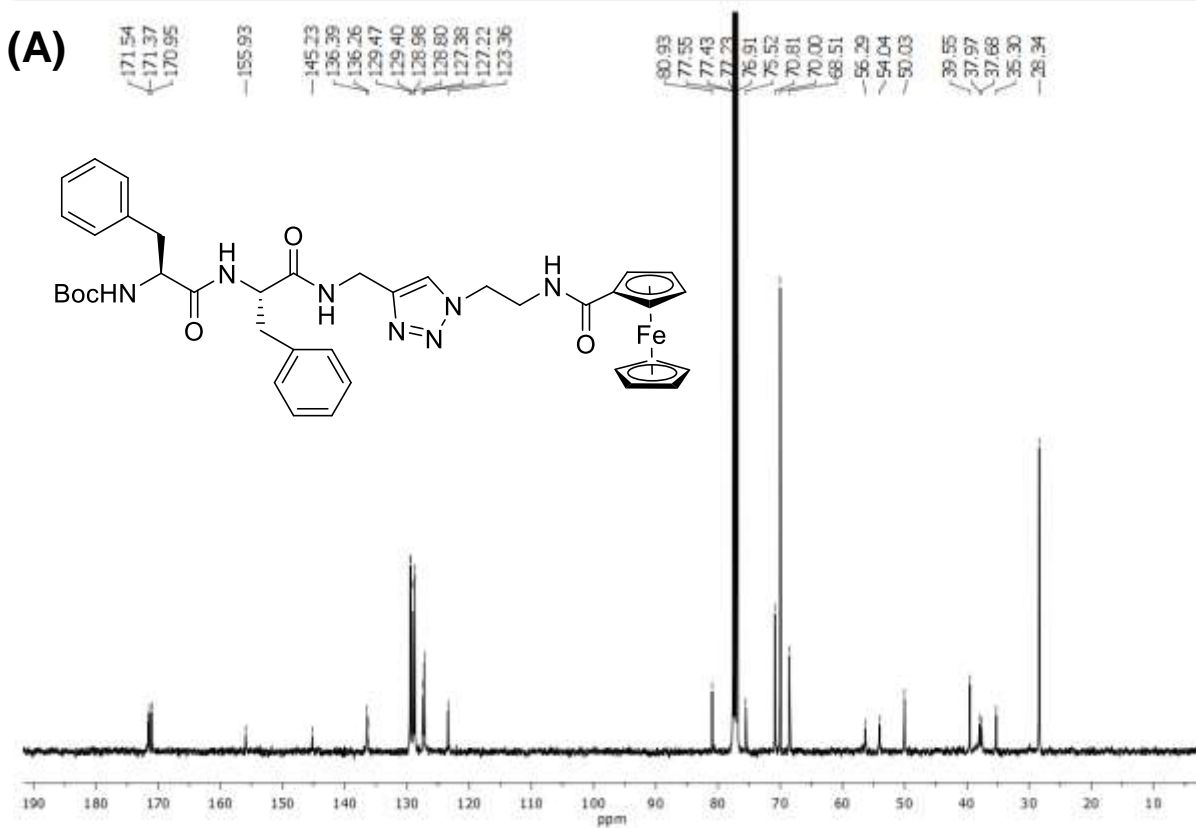
(A) $^{13}$C-NMR spectra of **6** [Fc-Phe-Phe-*tz*-A$^{N(Boc)2}$] and (B) HRMS of **8** [Fc-Phe-Phe-*tz-aeg*{A$^{N(Boc)2}$}-OEt].

**(A)**



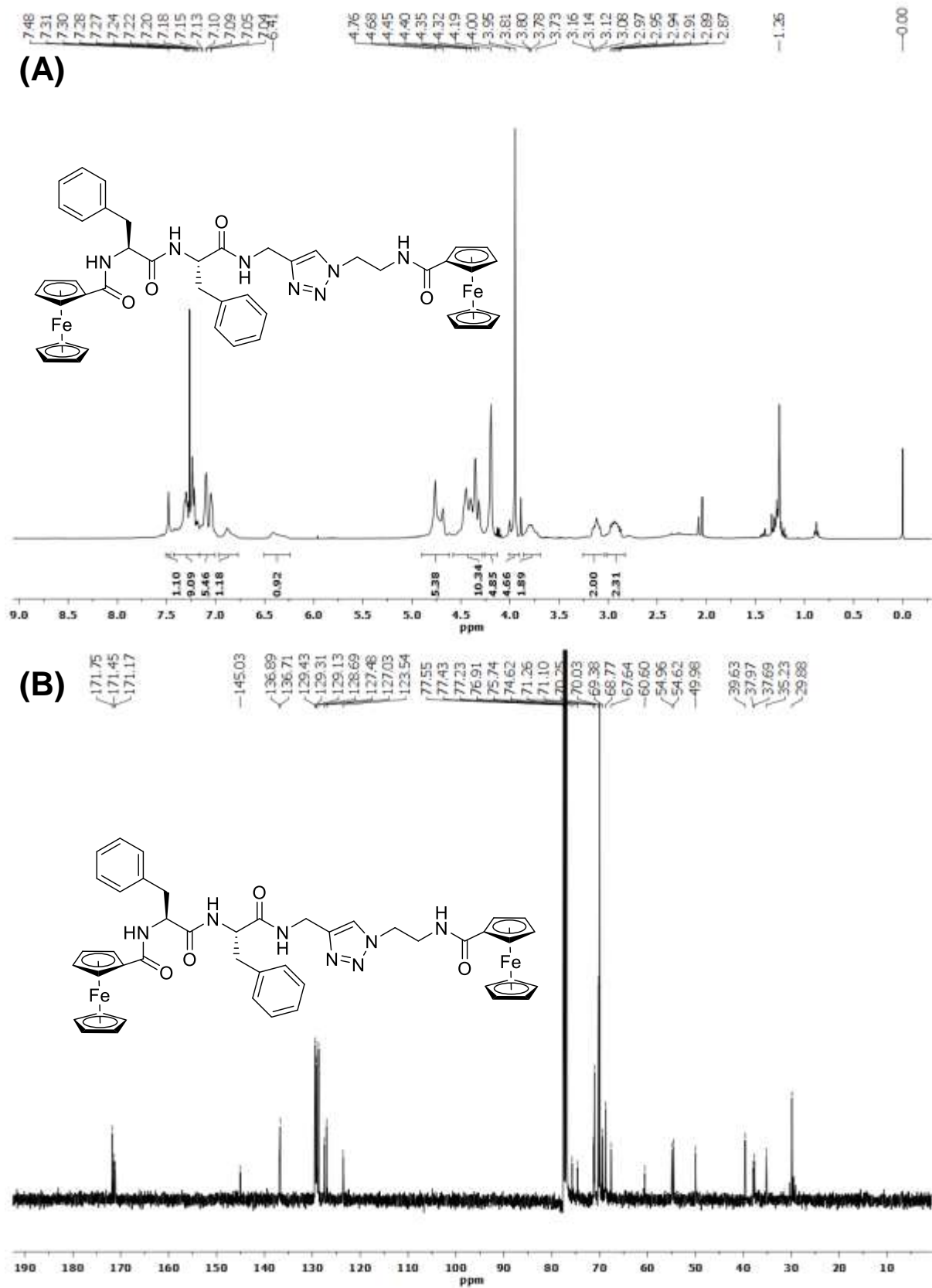**(B)**
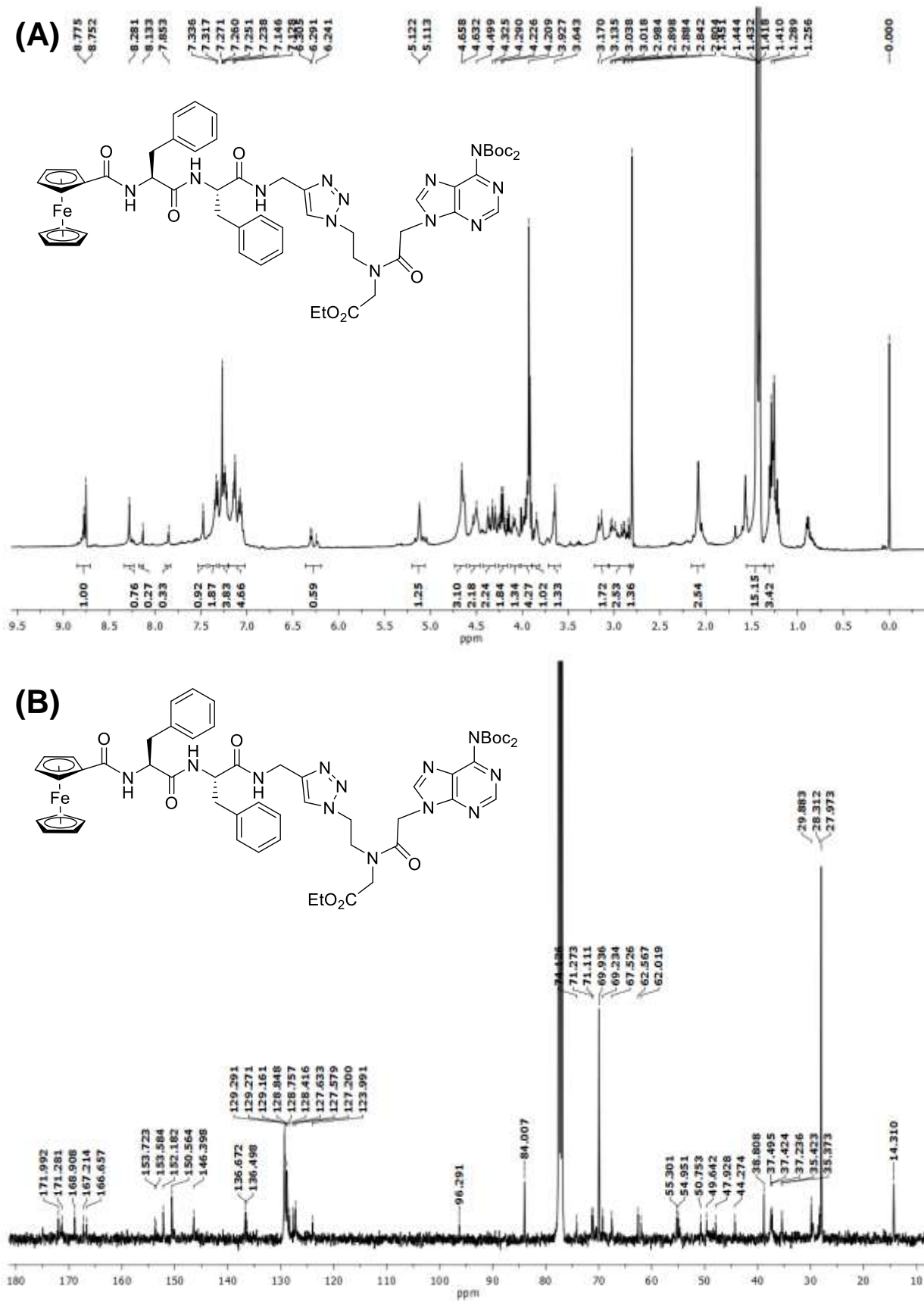


(A) $^1$H-NMR and (B) $^{13}$C-NMR spectra of **8** [Fc-Phe-Phe-*tz-aeg*{A$^{N(Boc)2}$}-OEt].

**(A)**

D3 453
D3 453 106 (1.926) AM2 (Ar,20000.0,556.28,0.00,LS 3); ABS; Sm (SG, 1x1.00); Cm (104:106-(4:101+109.266))

IISER PUNE

1: TOF MS ES+
2.24e6

748.2911

CALCULATED MASS
(M+H)+748.2910

749.2936

648.2386

750.2960

213.0006    436.2462    646.2426    751.2981

289.1782    437.2493    777.7517    1150.3940    1375.6283    1495.5675    1525.5248    1896.1382    m/z

**(B)**



(A) HRMS and (B) $^1$H-NMR spectra of **10** (Boc-Phe-Phe-*tz*-Fc).

**(A)**

171.54
171.37
170.95
155.93
145.23
136.39
136.26
129.47
129.40
128.98
128.80
127.38
127.22
123.36
80.93
77.55
77.43
77.23
76.91
75.52
70.81
70.00
68.51
56.29
54.04
50.03
39.55
37.97
37.68
35.30
28.34



**(B)**

D3 FeFFFe
D3 FeFFFe 109 (2.014) AM2 (Ar,20000.0,556.28,0.00,LS 3); ABS; Sm (SG, 1x1.00); Cm (108:110-(2:106+111:273))

IISER PUNE

1: TOF MS ES+
2.87e6

CALCULATED MASS
(M+H)+860.2310

860.2312

861.2338

862.2365
859.2297
858.2354

648.2388

289.1784
213.0012  290.1808  501.1709
649.2418  863.2385
857.2291
888.1909
1318.8021
1600.4940  1720.4540
1718.4584  1721.4563
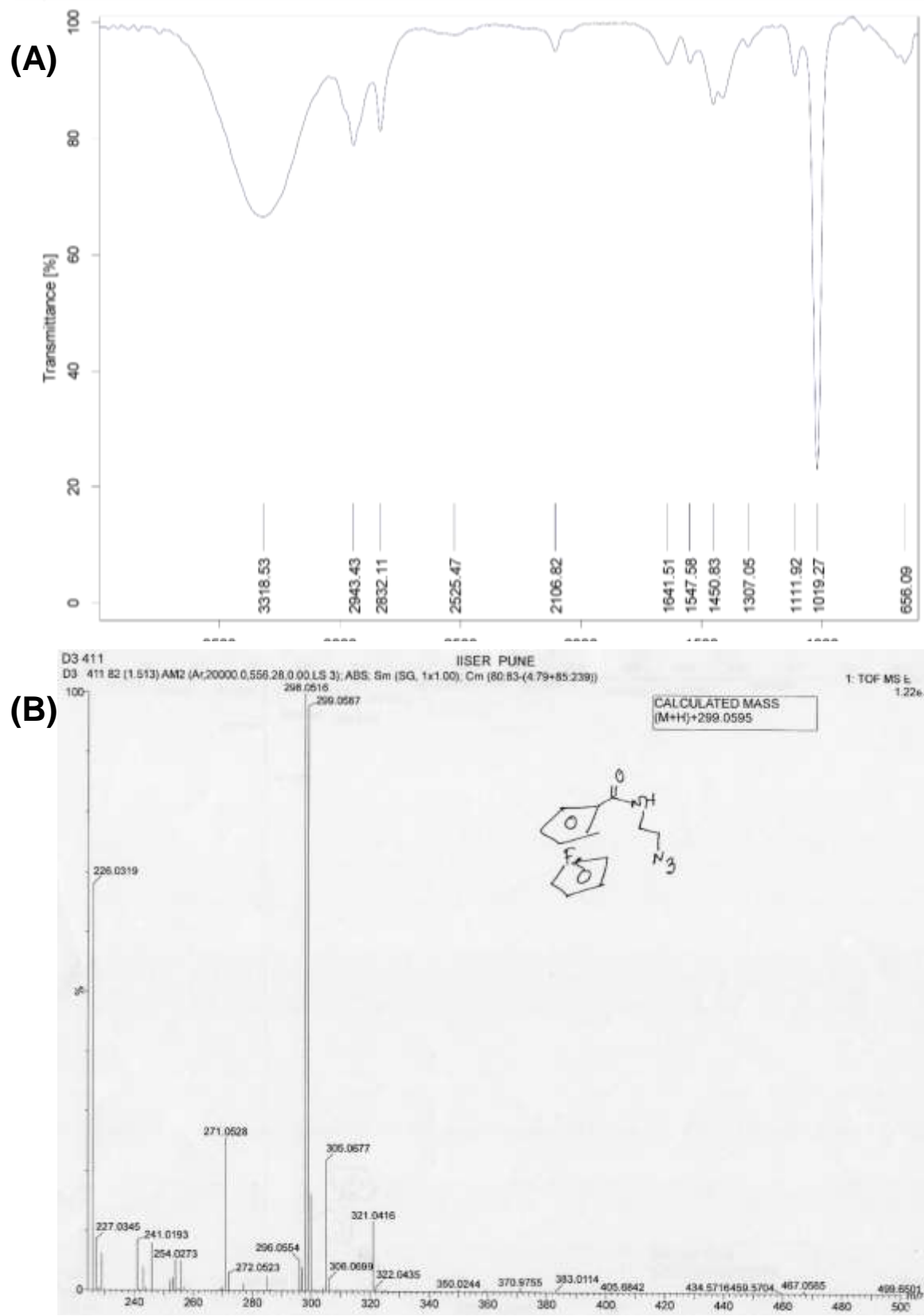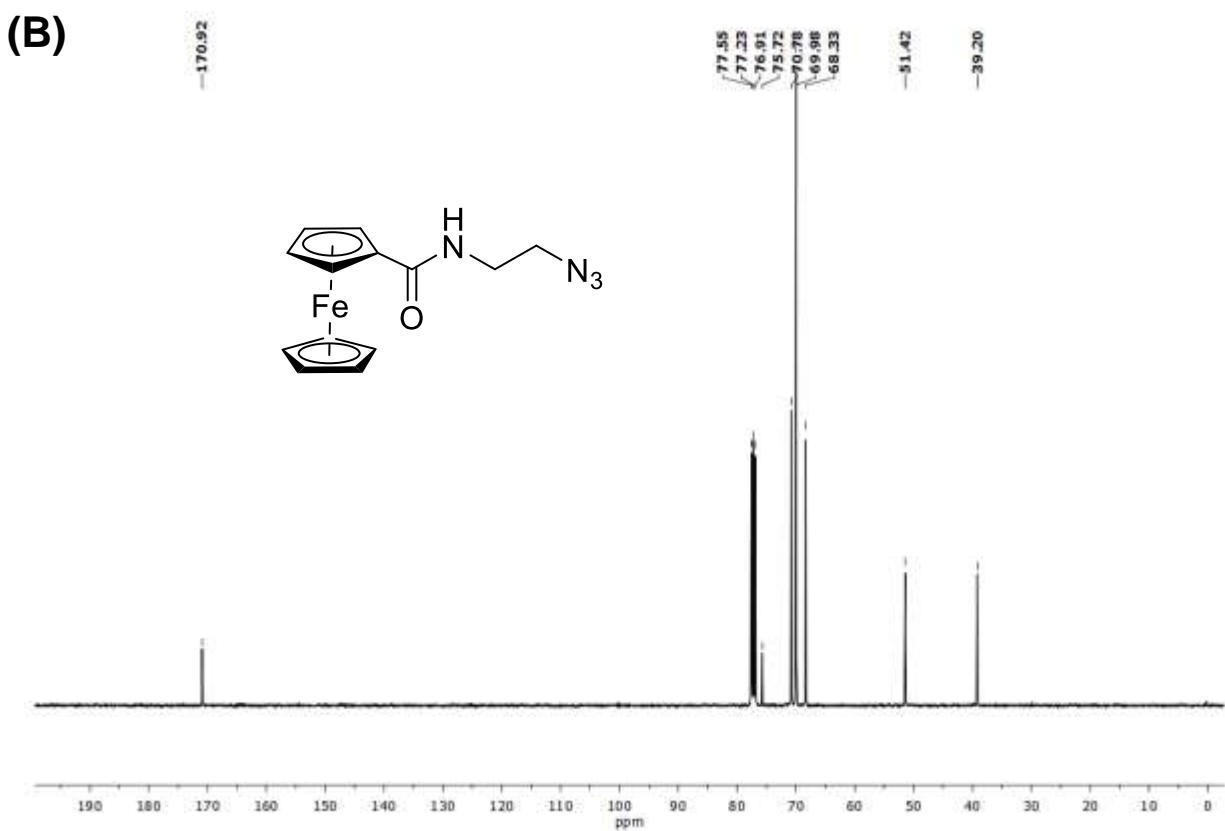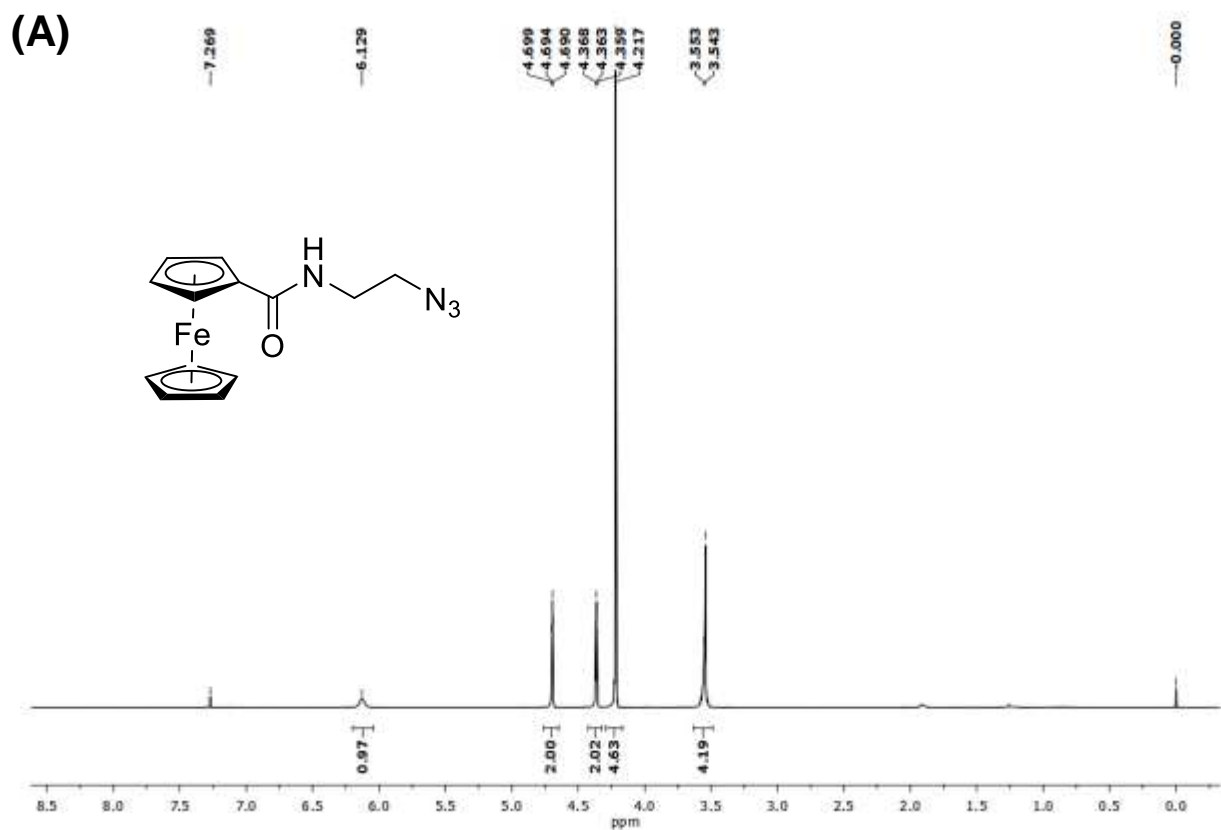1748.4182  1978.6865
m/z



(A) $^{13}$C-NMR spectra of **10** (Boc-Phe-Phe-*tz*-Fc) and (B) HRMS of **11** (Fc-Phe-Phe-*tz*-Fc).

**(A)**



**(B)**



(A) ¹H-NMR and (B) ¹³C-NMR spectra of **11** (Fc-Phe-Phe-*tz*-Fc).

(A) IR spectra and (B) HRMS of **9**.

**(A)**



**(B)**



(A) $^{1}$H-NMR and (B) $^{13}$C-NMR spectra of **9**.